National Science Foundation
WHERE DISCOVERIES BEGIN

SAN FRANCISCO STATE UNIVERSITY

Program and Extended Abstracts

STANFORD UNIVERSITY

USGS science for a changing world

CALIFORNIA ACADEMY OF SCIENCES

UC SANTA CRUZ

25th Himalaya-Karakoram-Tibet Workshop

Important events during the HKT-25 Workshop

Monday

Icebreaker reception

Seven Hills Conference Center - Monday, June 7th, 6:30-10:00pm

Tuesday

Main HKT-25 workshop

Seven Hills and Towers Conference Centers

Tuesday through Thursday, June 8-10th, ending 5:30pm June 10th

Evening reception at the California Academy of Sciences – Tuesday, June 8th, 7:00-10:00pm

Participants will tour through a 4-story living rainforest and explore the Steinhart Aquarium over drinks and hors d'oeuvres.

Buses will leave from the conference center at SF State at 6:30pm and return to campus by 10:30pm

Wednesday

Conference banquet – Wednesday, June 8th, 6:00-8:00pm

Please gather for drinks at 6:00 followed by dinner served at 6:30 at the Seven Hills Conference Center

Evening break-out groups – Wednesday, June 8th, 8:00-9:00

Three thematic break-out groups will meet immediately following the conference banquet in the Seven Hills Conference Center (topics to be announced)

Thursday

HKT-25 conclusion and announcement of HKT-26 – Thursday, June 9th

The HKT-25 Workshop will conclude by 17:30 on Thursday.

Shuttles for NSF workshop participants will depart at 17:45 from the conference center at SF State on Thursday, June 10th

Friday-Saturday

Post-conference NSF workshop –June 11-12th, Romberg Tiburon Center

"Future directions for NSF-sponsored geoscience research in the Himalaya/Tibet"

Presentations

Oral presentations

All oral presentations will take place in the Seven Hills Conference Center. If you were assigned an oral presentation, you received an e-mail giving you details of your allotted time and electronic file formatting.

All contributed talks will be in a 15-minute time-slot, therefore please prepare a talk of no more than 12 minutes, allowing time for one or two quick questions within the 15-minute slot.

Each thematic session of 5 or 6 talks will be followed by a 20-minute discussion session related to all the talks, moderated by the session chairs and by discussants named in the program. Please refer to the detailed workshop program for your presentation time-slot.

We expect that all talks will be presented using .ppt format (Microsoft Powerpoint 2004, not .pptx), using a Macintosh laptop and an LCD projector. All talks (for all days) must be provided to the organizing committee at check-in or during the welcoming event on Monday evening, on a USB drive. You will be able to check your talk on one of the conference computers on Monday after you check-in.

Poster presentations

All posters will be displayed in the Towers Conference Center. All posters will be displayed for three days starting Tuesday afternoon, June 8, with three separate dedicated poster sessions, of 6 hours in total during the workshop. Each poster has been assigned a 2-hour presentation time-slot on Tuesday, Wednesday or Thursday afternoon - Please refer to the detailed workshop program for your poster display location and presentation time-slot. Please set up your posters in the Towers Conference Center (G4 on the campus map) during the lunch break on Tuesday, June 8; posters should be taken down after the afternoon poster session on Thursday, June 10. Each poster may be up to a maximum of 60"x40" (152x102cm).

Poster printing

Posters can be printed on the SF State campus at the Campus Copy Center that is located in the Cesar Chavez Student Center (room M-110; H7 on the campus map). The Campus Copy Center is open 9am to 5pm Monday-Friday and can be reached at 415-338-2434; the cost for printing a 60"x40" poster is $105 plus $15 if you have a "Rush" order.

Extended Abstracts

The extended abstracts included in this volume will be published online as: Leech, M.L., Klemperer, S.L., and Mooney, W.D., eds., online proceedings for the 25th Himalaya-Karakoram-Tibet Workshop: U.S. Geological Survey, Open-File Report 2010-1099, http://pubs.usgs.gov/of2010/1099/

Logistics

Refreshment breaks

Refreshments will be served in the Seven Hills Conference Center during the mid-morning breaks; mid-afternoon refreshments will be served in the Towers Conference Center in the lobby outside of the poster hall.

Meals

Lunches will served in the *City Eats* dining hall adjacent to the Seven Hills Conference Center. At check-in/registration, you will be provided paper tickets for lunches at *City Eats* on Tuesday, Wednesday, and Thursday of the HKT-25 Workshop. *City Eats* is open for lunch from 11:00-1:00 daily and is located adjacent to the Seven Hills Conference Center. *City Eats* offers daily vegetarian options.

Dinners will be provided at the social event planned for the California Academy of Sciences on Tuesday, June 8, and at the conference banquet in the Seven Hills Conference Center on Wednesday, June 9.

On-campus accommodation for the main workshop

On-campus accommodation is located in the Mary Park Residence Hall, the Science & Technology Theme Community, and the Towers at Centennial Square (see campus map in this program). Check-in begins at 4pm on Monday, June 7th and you must check-out by 11am either on Thursday, June 10th or Friday, June 11th (depending on your reservation). Wireless internet access is available in the conference venue (the Seven Hills Conference Center, password: 11111111), but you must supply your own ethernet cable to use a personal computer inside campus accommodation.

All workshop participants staying in on-campus accommodation will be issued a card for use at *City Eats* for breakfast daily. Breakfast is served from 7:00-9:00 daily and *City Eats* offers daily vegetarian options.

Transportation

Parking

Those choosing to drive a personal car to the workshop venue should be aware that street parking is limited but may be available along Lake Merced or Font Boulevards adjacent to the conference venue or other streets surrounding the SF State campus (see campus map in this volume). On-campus parking in Lot 20 (the parking garage) adjacent to the conference venue is available for $5 per day payable at pay stations within the parking structure. Be aware that parking permits are valid until midnight and so you should purchase a two-day permit for $10 if you plan to park overnight. You must use $1 and $5 bills in the permit vending machines and the vending machines do not issue change.

Airport Transportation

There are multiple options for transportation to the San Francisco International Airport at the conclusion of the HKT-25 Workshop, including taxis, door-to-door vans, and public transportation. Please refer to information on the San Francisco International Airport website: http://www.flysfo.com/web/page/tofrom/transp-serv/

Economical shared-ride door-to-door vans can be arranged for individuals or groups:

Bayporter Express	415.467.1800	www.bayporter.com
South & East Bay Shuttle	800.548.4664	www.southandeastbayairportshuttle.com
SuperShuttle	415.558.8500	www.supershuttle.com

San Francisco State University

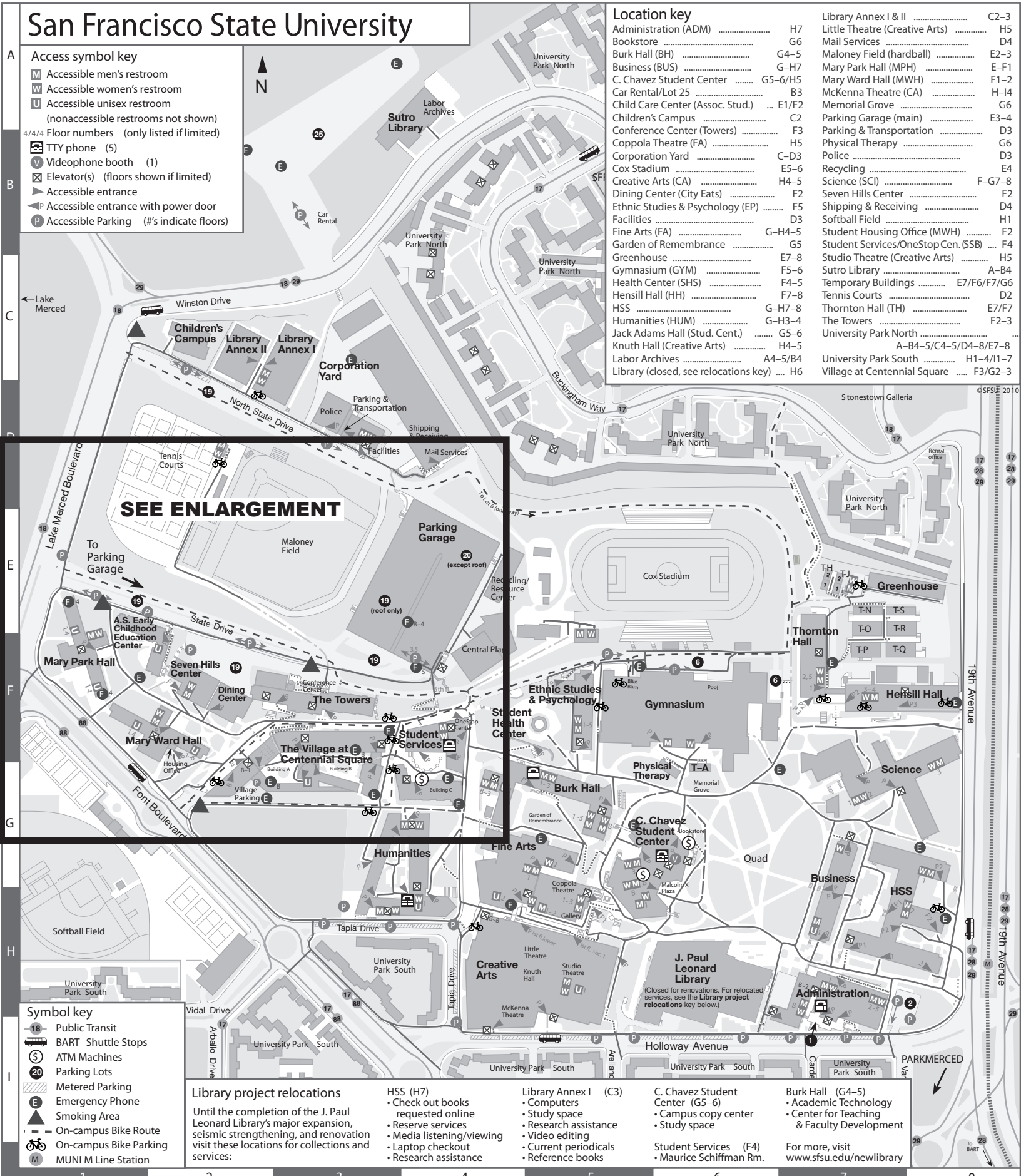

Access symbol key

- M Accessible men's restroom
- W Accessible women's restroom
- U Accessible unisex restroom
- (nonaccessible restrooms not shown)
- 4/4/4 Floor numbers (only listed if limited)
- TTY phone (5)
- V Videophone booth (1)
- Elevator(s) (floors shown if limited)
- Accessible entrance
- Accessible entrance with power door
- P Accessible Parking (#'s indicate floors)

Location key

Symbol key

- 18 Public Transit
- BART Shuttle Stops
- ATM Machines
- 20 Parking Lots
- Metered Parking
- E Emergency Phone
- Smoking Area
- On-campus Bike Route
- On-campus Bike Parking
- M MUNI M Line Station

Library project relocations

Until the completion of the J. Paul Leonard Library's major expansion, seismic strengthening, and renovation visit these locations for collections and services:

HSS (H7)
- Check out books requested online
- Reserve services
- Media listening/viewing
- Laptop checkout
- Research assistance

Library Annex I (C3)
- Computers
- Study space
- Research assistance
- Video editing
- Current periodicals
- Reference books

C. Chavez Student Center (G5–6)
- Campus copy center
- Study space

Student Services (F4)
- Maurice Schiffman Rm.

Burk Hall (G4–5)
- Academic Technology
- Center for Teaching & Faculty Development

For more, visit www.sfsu.edu/newlibrary

Access path key*

- Accessible Route—This path generally conforms to accessibility s tandards.
- Areas that may be a travel hazard (where the slope exceeds the standard maximum ramp slope [8.3%], or the cross-slope is significant [exceeds 4%]).
- Ramp (5%–8.3%)—Complying ramp along the accessible route.
- Partially Accessible Route—This path generally conforms to acces sibility standards, but there may be excessive cross-slope (over 2%) or other irregularities in a portion of the path, often along the path edge. There is usually a 48" wide complying path along these routes, though it may not be a straight or direct line.
- Lighter shade indicates path continues underneath overhang.

*Note: The map and information on pathways are limited by the scale. The accessible route should be clear to a person at a location, while the dashed line is intended to indicate where keener observation may be necessary to locate the accessible route. Pathways are generally asphalt and subject to weathering, erosion, uplifting, and other changes that may create navigational issues. SFSU is committed to maintaining the accessible route. Please report any irregularities to Disability Programs and Resource Center, 415-338-2472 (voice, TTY).

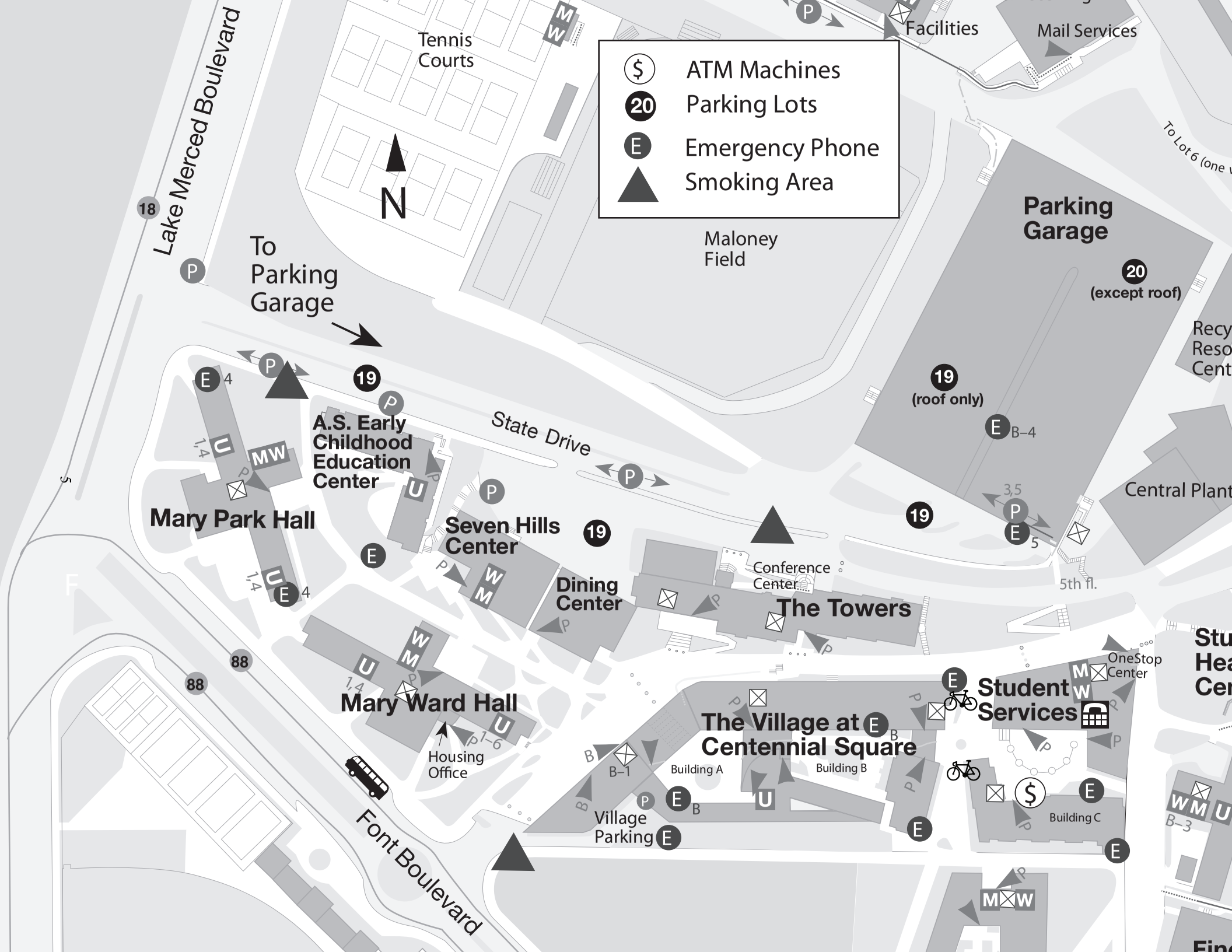
ATM Machines
Parking Lots
Emergency Phone
Smoking Area
N
Lake Merced Boulevard
Tennis Courts
Facilities
Mail Services
Maloney Field
To Parking Garage
Parking Garage
(except roof)
(roof only)
State Drive
A.S. Early Childhood Education Center
Mary Park Hall
Seven Hills Center
Dining Center
Conference Center
The Towers
5th fl.
Central Plant
Mary Ward Hall
Housing Office
The Village at Centennial Square
Building A
Building B
Building C
Village Parking
Student Services
OneStop Center
Font Boulevard

Welcome to the 25th Himalaya-Karakoram-Tibet Workshop

For a quarter of a century the Himalayan-Karakoram-Tibet (HKT) Workshop has provided scientists studying the India-Asia collision system a wonderful opportunity for workshop-style discussion with colleagues working in this region. In 2010, HKT returns to North America for the first time since 1996. The 25th international workshop is held from June 7 to10 at San Francisco State University, California.

The international community was invited to contribute scientific papers to the workshop, on all aspects of geoscience research in the geographic area of the Tibetan Plateau and its bounding ranges and basins, from basic mapping to geochemical and isotopic analyses to large-scale geophysical imaging experiments. In recognition of the involvement of U.S. Geological Survey (USGS) scientists in a wide range of these activities, the USGS agreed to publish the extended abstracts of the numerous components of HKT-25 as an online Open-File Report, thereby ensuring the wide availability and distribution of these abstracts, particularly in the HKT countries from which many active workers are precluded by cost from attending international meetings.

In addition to the workshop characterized by contributed presentations, participants were invited to attend a pre-meeting field trip from the Coast Ranges to the Sierra Nevada, to allow the international group to consider how the tectonic elements of the Pacific margin compare to those of the Himalayan belt. Following the workshop, the National Science Foundation (NSF) sponsored a workshop on the "Future directions for NSF-sponsored geoscience research in the Himalaya/Tibet" intended to provide NSF Program Directors with a clear statement and vision of community goals for the future, including the scientific progress we can expect if NSF continues its support of projects in this geographic region, and to identify which key geoscience problems and processes are best addressed in the Himalaya and Tibet, what key datasets are needed, and how NSF can best support the evolving need for interdisciplinary investigations.

This workshop also has clear societal relevance. Recent earthquakes have brought international attention to active tectonics and earthquake hazards in the HKT region. Prominent examples include the M_w 7.8 Kokoxili (Qinghai, China) earthquake of 2001, the Mw 7.6 Kashmir (Pakistan) earthquake of 2005, the M_w 7.9 Wenchuan (Sichuan, China) earthquake of 2008, and this year the M_w 6.9 Yushu (Qinghai, China) earthquake. Geological and geophysical field work conducted both before these earthquakes, as well as in response to them, has helped to define the active faults and regional tectonics in the HKT region. The research presented at this workshop provides the framework necessary for improved seismic hazard assessments in this region.

The organizers gratefully acknowledge the support of NSF's Continental Dynamics Program and its Office of International Science and Engineering, through award EAR-0965796. We thank San Francisco State University's Sheldon Axler, Dean of the College of Science and Engineering, and Toby Garfield, Director of the Romberg Tiburon Center, for use of their conference facilities; and the Department of Geosciences, particularly Deb Shulman and Miriam Knof, for administrative support. The California Academy of Sciences generously hosted a reception for visiting delegates, and Brad Ritts (Chevron Exploration Technology Company), Todd Greene (California State University, Chico) and John Shervais (Utah State University) together co-led the pre-conference field trip. Technical editing of this volume was led by Roxanne Renedo (U.S. Geological Survey) with assistance from Margaret Milia (Stanford University). We are grateful to the U.S. Geological Survey (USGS) Earthquake Hazards Program and the USGS Menlo Park (California) Publishing Service Center for making this online report possible.

Organizing Committee, HKT-25:

Mary Leech, San Francisco State University;
Walter Mooney, U.S. Geological Survey;
Marty Grove, Stanford University;
Simon Klemperer, Stanford University;
Brad Ritts, Exploration Technology Company;
Xixi Zhao, University of California, Santa Cruz

Summary Program of the 25th Himalaya-Karakoram-Tibet Workshop

SATURDAY-SUNDAY JUNE 5-6th		
Pre-conference field trip	Mesozoic-Cenozoic Convergent Margin of Northern California	*Field trip departs from SFO Travelodge 08:00 Saturday*
MONDAY JUNE 7th		
	Pre-conference field trip ends	*Field trip departs returns to SF State 18:00*
16:00-21:30	Check-in and Conference Registration	*Mary Park, Towers and STTC buildings*
18:30-21:30	Icebreaker party	*Seven Hills Conference Center*
TUESDAY JUNE 8th		*all oral sessions in Seven Hills Conference Center*
08:00-10:00	Oral Session I	Geophysics & Geodynamics of the Tibet Plateau
10:30-12:20	Oral Session II	Pre-collision, Suturing, & Timing of India-Asia Collision
12:20	Lunch	*Lunches served in "City Eats" between Seven Hills and Towers (tickets issued at registration)*
13:50-15:50	Poster Session I	*all poster sessions are in Towers, lower level* Geodynamics and Geophysics of the Tibet Plateau; Pre-collision, Suturing, and Timing of India-Asia collision; Earthquake Hazard & Neotectonics
15:50-18:10	Oral Session III	Earthquake Hazard & Neotectonics
19:00-22:00	Reception at the California Academy of Sciences	*buses leave from in front of Mary Park at 18:30*
WEDNESDAY JUNE 9th		
08:00-09:50	Oral Session IV	Himalayan Belt
10:15-12:20	Oral Session V	Interior Tibet
12:20	Lunch	
13:30-15:30	Oral Session VI	Northern Plateau Margins
15:30-17:45	Poster Session II	Himalayan Belt; Interior Tibet; Northern Plateau Margins
18:00-19:45	Conference Dinner	*Seven Hills Conference Center*
20:00-21:00	Break-Out Sessions	
THURSDAY JUNE 10th		*those leaving Thursday night check-out before lunch*
08:00-10:00	Oral Session VII	Climate & Tectonics
10:30-12:00	Oral Session VIII	Climate, Glaciation, Erosion
12:00	Lunch	
13:30-15:30	Poster Session III	Climate & Tectonics; Glaciation &Erosion; Crustal Flow & Gneiss Domes
15:30-17:20	Oral Session IX	Crustal Flow & Gneiss Domes
17:20-17:30	Conference ends	Announcement of HKT-26
17:45	shuttle buses to Tiburon	*for participants in NSF Workshop*
FRIDAY-SATURDAY JUNE 11-12th		
NSF Workshop	Future directions for NSF-sponsored geoscience research in Himalaya/Tibet	*Bay Conference Center, Romberg-Tiburon Center; accommodation at The Lodge at Tiburon*

Program of the 25th Himalaya-Karakoram-Tibet Workshop

Presenters are shown **bold underline**.
In order to ensure proper citation of the abstracts in the U.S. Geological Survey Open-File Report 2010-1099, online proceedings for the 25th Himalaya-Karakoram-Tibet Workshop, we have attempted to follow the western style of placing the given name before the family name for all scientists; we hope this will also provide consistency with Chinese colleagues working in the USA who have adopted this convention. We apologize if we have made any errors in this.

MONDAY		
16:00-21:30	Check-in to accommodation at Mary Park Hall, Towers, and STTC buildings	
16:00-21:30	Conference Registration at Seven Hills Conference Center	*Speakers should provide, and may test, their .ppt presentations*
18:30-21:30	Icebreaker party	*Seven Hills Conference Center*
TUESDAY MORNING		
08:00-08:10	**Introductory remarks**	*all oral sessions are in the Seven Hills Conference Center*
08:10-10:00	**Oral Session I – GEOPHYSICS AND GEODYNAMICS OF THE TIBET PLATEAU** Chairs: Larry Brown, Lucy Flesch	
08:10	**James Jackson,** Dan McKenzie, Keith Priestley, Alistair Sloan (invited talk)	Earthquake depth distributions in central Asia and lithosphere rheology
08:40	**Kip Hodges**, Kelin Whipple	The Tibet-Himalaya Accommodation Zone and the Nature of Orogenic Plateau Margins
08:55	**Jeffrey Freymueller**, Yuning Fu, Wang Qi, Xu Caijun	Present-Day Vertical Motion of the Tibetan Plateau and Surrounding Area
09:10	**James Mechie**, R. Kind, J. Saul	Crust and mantle structure of the Tibetan Plateau down to 700 km depth as derived from seismological data
09:25	**Keith Priestley**, Jamie Barron, Charlotte Acton, Eric Debayle, Dan McKenzie	State of the Tibetan lithosphere
09:40	**Discussion**	moderated by chairs and discussants Walter Mooney, Zhang Zhongjie
10:00-10:30	**Coffee**	*all morning coffee breaks are in Seven Hills, outside the main auditorium*

10:30-12:20	**Oral Session II – PRE-COLLISION, SUTURING, AND TIMING OF INDIA-ASIA COLLISION** Chairs: Talat Ahmad, Xixi Zhao	
10:30	**Paul Myrow**, Nigel Hughes, John Goodge, Mark Fanning, Ryan McKenzie, Shanchi Peng, Om Bhargava, Suraj Parcha, Kevin Pogue	Implications of Himalayan Detrital Zircon Spectra of Cambrian–Ordovician Strata
10:45	**Chengshan Wang,** Bo Ran, Xixi Zhao	Did the Lhasa Terrane Rift from the Indian Subcontinent?
11:00	**Peter Lippert**, Guilluame Dupont-Nivet, Douwe van Hinsbergen, Xixi Zhao, Robert Coe, Paul Kapp	The Paleogene Latitude of Asia and the Proto-Tibetan Plateau
11:15	**Réjean Hébert,** Carl Guilmette, Rachel Bezard, Jaroslav Dostal, Chengshan Wang, Jingen Dai	Ophiolites Associated with Suture Zones of the Collisional System between India and Eurasia: a Synthesis
11:30	**Lloyd White,** Gordon Lister	The Himalayan Pile-Up: Revised Plate Reconstructions Provide Evidence of Multiple Accretion Events During the Himalayan Orogeny
11:45	**Yani Najman,** Erwin Appel, Marcelle Boudagher-Fadel, Paul Bown, Andy Carter, Eduardo Garzanti, Laurent Godin, Jingtai Han, Ursina Liebke, Grahame Oliver, Randy Parrish, Giovanni Vezzoli	The Age of India-Asia Collision: Biostratigraphic, Sedimentological and Paleomagnetic Constraints
12:00	**Discussion**	moderated by chairs and discussants Joe DiPietro, Nigel Hughes
TUESDAY AFTERNOON		
12:20-13:50	**Lunch**	*Lunches are served in "City Eats" to conference delegates who should present their tickets issued at registration* *(all posters for the entire HKT meeting should be put up during this lunch break)*
13:50-15:50	**POSTER SESSION I**	*All poster sessions are in Towers, lower level*
POSTERS GD	**GEODYNAMICS AND GEOPHYSICS OF THE TIBET PLATEAU**	
1-GD-1	R.Z. Qiu, **Su Zhou**, Y.J. Tan, G.S. Yan, X.F. Chen, Q.H. Xiao, L.L. Wang, Y.L. Lu, Z. Chen, C.H. Yuan, J.X. Han, Y.M. Chen, L. Qiu, K. Sun	A Model for the Tectonic Evolution of the Tethys-Tibetan Plateau System and Implications for Continental Tectonics in China
2-GD-2	**Wayne Thatcher**	Block Versus Continuum Descriptions of Continental Deformation: For Heaven's Sake, how are We Ever Going to Decide Which is Better?

3-GD-3	**Larry Brown,** Wenjin Zhao, Project INDEPTH Team	The INDEPTH Transect: Looking Back from Golmud to Yadong
4-GD-4	**Matthew Agius,** Sergei Lebedev	Shear-Velocity Profiles Across the Tibetan Plateau from Broadband, Surface-Wave, Phase-Velocity Measurements
5-GD-5	**Yingjie Yang,** Yong Zheng, Michael Ritzwoller	Rayleigh-Wave Phase Velocities and Azimuthal Anisotropy in Tibet and Surrounding Regions from Ambient Noise Tomography
6-GD-6	**Sergei Lebedev,** Matthew Agius	Lithospheric Structure and Dynamics of Tibet: Constraints from Shear-Velocity Distribution
12-GD-7	**Eric Sandvol,** John Chen, James Ni, Frederik Tilmann, Shiyong Zhou, Yuhu Ma, Xiaoqing Zhang, Han Yue, Savas Ceylan, Bao Xueyang, Larry Brown	Seismic Velocity Structure From the ASCENT Seismic Array: Implications for Crustal and Mantle Deformation
13-GD-8	**Jingyi Chen**, Zhongjie Zhang, José Badal	The Determination of Anisotropic Parameters from Wide-Angle Seismic Reflection Polarizations: A Model Study
POSTERS PC	**PRE-COLLISION, SUTURING, AND TIMING OF INDIA-ASIA COLLISION**	
14-PC-1	**Shaik Rashid,** Naqeebul Islam, Javid Ganai	Precambrian Granitic Magmatism in the NE Himalaya: Implications for Ancient Tectonics
15-PC-2	**Simon Klemperer,** Rajendra Prasad, V.Vijaya Rao, H.C.Tewari, and Prakash Khare	HIMPROBE Deep Seismic Reflection Profiling of the Sub-Himalayan Fold-Thrust Belt, NW India: Images of a Possible "Ulleri-Wangtu" Paleoproterozoic Accretionary Orogenic Event
16-PC-3	**Ryan McKenzie,** Nigel Hughes, Paul Myrow, Shuhai Xiao, Ganqing Jiang	Chronostratigraphic Constraints on the Inner Lesser Himalayan Sedimentary belt of North India, and Proterozoic Sediment Continuity of the North Indian Margin
22-PC-4	Xuan Feng, **Alexander Webb**, Darrell Henry	Can Detrital Tourmaline Provide Stratigraphic Fingerprints? Initial Tests in the Western Himalaya
23-PC-5	**Bishal Upreti,** George Gehrels, Santa Rai, Masaru Yoshida	Tertiary U-Pb Zircon Ages and Lower Paleozoic Signatures from Leucosomes of the Namche Migmatites, Everest Area, Nepal Himalaya
24-PC-6	**Asif Khan,** R. H. Siddiqui, M. Qasim Jan	Temporal Evolution of Cretaceous to Pleistocene Magmatism in the Chagai Arc, Balochistan, Pakistan
25-PC-7	**Ursina Liebke,** Erwin Appel, Udo Neumann, Borja Antolin, Lin Ding, Qiang Xu	Position of the Lhasa Terrane Prior to India-Asia Collision Derived from Paleomagnetic Inclinations of 53 Ma-Old Dykes of the Linzhou Basin: Constraints on the Age of Collision and Post-Collisional Shortening within the Tibetan Plateau

26-PC-8	**Xixi Zhao**, David Finn, Chengshan Wang, Yalin Li, Lidong Zhu, Wenguang Yang, Jun Meng, Jingen Dai	New Paleomagnetic Result on Tertiary Sediments From NW Qiangtang: Implications for the Cenozoic Tectonic History of the Tibetan Plateau
31-PC-9	**Sunil Bajpai**	Timing of Earliest India-Asia Contact: Evidence of Terrestrial Vertebrates from Cambay Shale, Gujarat, Western Peninsular India
32-PC-10	Anju Pandey, **Mary Leech**, Andy Milton, Preeti Singh, Pramod Varma	Evidence of Former Majoritic Garnet in Himalayan Eclogite Points to 200-km Deep Subduction of Indian Continental Crust
33-PC-11	**Joseph DiPietro,** Alex Pullen	Was There Pre-Collisional Metamorphism in Swat Pakistan?
34-PC-12	Ran Zhang, **Michael Murphy,**Thomas Lapen, Veronica Sanchez, Matthew Heizler	Late Eocene crustal thickening followed by Early-Late Oligocene Extension along the India-Asia suture zone: Evidence for cyclicity in the Himalayan orogen
41-PC-13	**Talat Ahmad**	Geochemical and Isotopic Constraints on the Nature of the Indus and Shyok Suture Zones, Remnants of the Neo-Tethyan Ocean in the Trans-Himalayan Region
42-PC-14	**Rachel Bezard,** Réjean Hébert, Chengshan Wang, Jaroslav Dostal, Jingen Dai	Petrology and geochemistry of the Xiugugabu ophiolitic massif, western Yarlung Zangbo Suture Zone, Tibet
43-PC-15	**Krishnakanta Singh**	Geochemical Constraints on the Origin of the Ophiolites of the Indo-Myanmar Orogenic Belt, North East India

POSTERS EQ	**EARTHQUAKE HAZARD AND NEOTECTONICS**	
44-EQ-1	MonaLisa, **M. Qasim Jan**	Newly Formulated Attenuation Relationship and Seismic Hazard Assessment for Muzaffarabad, Pakistan
45-EQ-2	**Amita Sinvhal,** Ashok Pandey, S. M. Pore	Seismic Performance of the Rural Habitat on the Main Boundary Thrust
40-EQ-3	**Hans Wason**	Post – 1991 Uttarkashi Earthquake Seismicity Pattern in the Garhwal Himalaya Region
51-EQ-4	**Ashok Dubey**	Superposed Folds in the Himalaya Indicating Late Stages of the Himalayan Orogeny: Implications for Seismicity
52-EQ-5	**Laurent Bollinger,** Dili Ram Tiwari, Sudhir Rajaure, Soma Nath Sapkota, Jean-Phillipe Avouac	Simultaneous Earthquake Pulses along the Main Himalayan Thrust
53-EQ-6	**Kristel Chanard**, Jean-Philippe Avouac, Takeo Ito, Jeff Genrich, John Galetzka, Mireille Flouzat, Som Nath Sapkota, Bharat Koirala	Seasonal Variations in Geodetic Strain Induced by Hydrological Surface Loading in the Himalaya and Implications for Shallow Elastic Structure of the Earth

54-EQ-7	**Thomas Ader,** Jean-Philippe Avouac, Sachiko Tanaka	Testing Earthquake Nucleation Models from the Response of Himalayan Seismicity to Secular and Periodic Stress Variations
55-EQ-8	**Bishal Upreti,** M. Yoshida, S.M. Rai, T.N. Bhattarai, P.D. Ulak, A.P. Gajurel, R.K. Dahal, S. Dhakal, M.P. Koirala	Guidebook Series on the Himalayan Geology and Natural Hazards
60-EQ-9	**Qi Wang,** Xuejun Qiao, Qigui Lan, Jeffrey Freymueller, Shaomin Yang, Caijun Xu	Releasing a reservoir of shallow strain as a possible cause of the catastropic Wenchuan earthquake, China
15:20-15:50	**Coffee**	*all afternoon coffee breaks are in Towers, outside the poster hall*
15:50-18:10	**Oral Session III – EARTHQUAKE HAZARD & NEOTECTONICS** Chairs: Laurent Bollinger, Roland Bürgmann	
15:50	**Roger Bilham** (invited talk)	Geodesy and great earthquakes in the Himalaya
16:20	**Soma Nath Sapkota**, Paul Tapponnier, Laurent Bollinger, Yann Klinger, Frederic Perrier, Dilli Ram Tiwari, Surendra Raj Panta, Indira Siwakoti	Probing our understanding of the seismic cycle in the Himalayas of Nepal: Investigating mega-quakes with mega-trenches
16:35	P. Mahesh, **Shyam Rai,** P.R. Sarma, S. Gupta, K. Sivaram, and K. Suryaprakasam	High resolution earthquake location and 3-D velocity imaging of crust beneath the Kumaon Himalaya
16:50	**M. Qasim Jan,** MonaLisa	Seismic Activity and Seismic Hazard Assessment along the Main Boundary Thrust, Northern Pakistan
17:05	**Andrew Meigs,** C. Madden, J.D. Yule, Y. Gavillot, A. Hebeler, A. Hussain, M.I. Bhat, A.B. Kausar, M. Malik, S. Ramzan, M. Sayab, R. Yeats	Distributed Deformation, Distributed Earthquakes in the Northwest Himalaya
17:20	**Peizhen Zhang** (invited talk)	The Uplift of Mountain Chains along the Northern and Eastern Margins of the Tibetan Plateau
17:50	**Discussion**	moderated by chairs and discussants John Nabelek, Wayne Thatcher
TUESDAY EVENING		
18:30	buses depart from Mary Park	
19:00-22:00	**Reception at the California Academy of Sciences**	
21:30, 21:45, 22:00	buses leave California Academy of Sciences for SF State	

WEDNESDAY MORNING		
08:00-09:50	**Oral Session IV – HIMALAYAN BELT** Chairs: Ashok Dubey, Simon Wallis	
08:00	**Delores Robinson**	Correlation of Stratigraphy Along Strike in the Himalaya
08:15	**A. Alexander G. Webb,** Hongjiao Yu	Testing models for the kinematic evolution of the Lesser Himalayan Sequence by balanced reconstruction: Accretion dominant in northwestern India
08:30	**Sandeep Singh,** Th. Nikunja Bihari Singha	Cooling and Exhumation Patterns associated with Tectonometamorphic Evolution of the Himalayan Metamorphic Belt in the Alaknanda and Dhauliganga valleys, Garhwal Himalaya, India
08:45	**Chris Yakymchuk,** Laurent Godin	Metamorphic and Structural Discontinuities in the Greater Himalayan Sequence, Karnali Valley, West Nepal
09:00	**John Cottle,** David Waters, Olivier Beyssac, Micah Jessup	Metamorphic History of the South Tibetan Detachment System, Mt. Everest Region, Revealed by RSCM Thermometry and Phase Equilibria Modeling
09:15	**Djordje Grujic**, Clare Warren, Joseph Wooden	Tertiary Eclogite Facies Metamorphism in the Greater Himalayan Sequence: Evidence from Zircon U-Pb Geochronology and Trace Element Geochemistry
09:30	**Discussion**	moderated by chairs and discussants Yani Najman, Bishal Upreti
09:50-10:15	**Coffee**	*Seven Hills, outside the main auditorium*
10:15-12:20	**ORAL SESSION V – INTERIOR TIBET** Chairs: Eric Sandvol, Chengshan Wang	
10:15	**Mark Harrison,** D.J. DePaolo, X. Mo, Z. Zhao, A. Yin (invited talk)	An Integrated Approach to Determining the Crustal Thickness History of Southern Tibet
10:45	**Anne Meltzer,** Peter Zeitler	Signal or Noise? Significance of Variability in the Himalaya-Tibet System
11:00	**Simon Klemperer,** Mack Kennedy, Siva Sastry, Yizhaq Makovsky, T.Harinarayana	Mantle Helium Signature of the Karakoram fault is that of an Active Plate-Boundary
11:15	**Amy Weislogel,** Delores Robinson	The Impact of Mesozoic Tectonism on Eastern Tibet Plateau Crustal Infrastructure: Implications for Plateau Evolution
11:30	**Peter DeCelles,** P. Kapp, J. Quade, G.E. Gehrels, M. Murphy (invited talk)	Oligo-Miocene Basins in Central Tibet and Along the Indus Suture: Records of Plateau Evolution and Dynamics of Subducting Indian Continental Crust
12:00	**Discussion**	moderated by chairs and discussants Paul Kapp, Brad Hacker

WEDNESDAY AFTERNOON		
12:20-13:30	**Lunch**	Lunches are served in "City Eats" to conference delegates who should present their tickets issued at registration
13:30-15:30	**ORAL SESSION VI – NORTHERN PLATEAU MARGINS** Chairs: Erwin Appel, Xiaomin Fang	
13:30	**Marin Clark,** Alison Duvall, Nora Lewandowski, Eric Hetland, Dewen Zheng, Richard Lease, William Craddock, Eric Kirby, Zhicai Wang (invited talk)	Fault Histories of the Northeastern Tibetan Plateau Margin: Geodynamic Implications of Far-Field Deformation During Continental Collision
14:00	Richard Lease, **Douglas Burbank**	Middle Miocene Reorganization of Faulting and Depositional Patterns in Northeastern Tibet
14:15	**Walter Mooney,** Nihal Okaya, Chungyong Wang, Zhongjie Zhang, Junmeng Zhao	Recent Deep Seismic Refraction/Wide-angle Reflection Profiles in Western China
14:30	**Marianne Karplus,** Simon Klemperer, Zhao Wenjin, Wu Zhenhan, Larry Brown, Shi Danian, James Mechie, Chen Chen, and Jonathan Glen	INDEPTH-IV Seismic Imaging of Channel Flow Outwards from the Kunlun Mountains beneath the Qaidam Basin
14:45	**Isabelle Ryder,** Roland Bürgmann, Zheng-Kang Shen	Lower-Crustal Flow Beneath the Tibetan Plateau: Evidence from the 2001 Kokoxili Earthquake
15:00	**Discussion**	moderated by chairs and discussants Eric Cowgill, Brad Ritts
15:30-16:00	**Coffee**	*Towers, outside the poster hall*
15:30-17:45	**POSTER SESSION II**	*Towers, lower level*
POSTERS HIM	**HIMALAYAN BELT**	
30-HIM-1	**Shah Faisal,** John M. Dixon	Centrifuge Modelling Study of Contrasting Structural Styles in the Salt Range and the Potwar Plateau, Northern Pakistan
39-HIM-2	**Yuning Fu,** Jeffrey Freymueller, Caijun Xu, Qi Wang	Geometry and Slip Patterns of the Main Himalaya Thrust Fault in the India-Eurasia Collistion Zone Constrained by Geodetic Observations
38-HIM-3	**Warren Caldwell,** Simon Klemperer, Jesse Lawrence, Shyam Rai	Receiver function imaging in the western Himalaya
37-HIM-4	**John Nabelek,** Gyorgy Hetenyi, Jerome Vergne, Arnaud Burtin, Jan Baur, Laurent Bollinger, Rodolphe Cattin, Som Sapkota, Heping Su, Project Hi-CLIMB Team	Structure of the Crust and Upper Mantle and Seismic Sources in the Himalaya-Tibet Region: Summary of Results from the Hi-CLIMB Experiment
36-HIM-5	**Ugyen Wangda**	State of geological mapping in the Bhutan Himalaya

35-HIM-6	**Tank Ojha,** P.G. DeCelles, J. Quade, George Gehrels, P. Kapp, Craig Wissler, D.M. Robinson, M.A. Murphy	Role of GIS in Geological Data Interpretation, Map Making and Data Storage: A Case Study from the Nepal Himalaya
50-HIM-7	Michael Doon, **Djordje Grujic**, Isabelle Coutand, Nicholas Whynot	Muscovite
49-HIM-8	Mohammad Sayab, Domingo Aerden, Syed Z. Shah, **Mohammad Asif Khan**	Origin of 'millipede' and 'rotational' inclusion trail microstructures in the NW Himalaya and their tectonic significance
48-HIM-9	**Harsh Sinvhal**, Maibam Rogibala, A.K. Choudhary, A.K. Jain, Sandeep Singh	Two Migmatite Zones within the Himalayan Metamorphic Belt (HMB) of the Sikkim Himalaya, India
47-HIM-10	**Kavita Tripathi**	Magnetic Fabrics, Microstructures and U-Pb Geochronology of the Kinnaur Kailash Granite and Associated leucogranites, Himachal Himalaya: Implications for Extensional Tectonics in the South Tibetan Detachment Zone
46-HIM-11	**Mayumi Mitsuishi**, Simon Wallis, Mutsuki Aoya, Jeffrey Lee, Martin Whitehouse	19 Ma Ductile E–W Extension associated with Normal Faulting in the Kung Co area, Southern Tibet
59-HIM-12	**Alka Tripathy,** Kip Hodges, Matthijs van Soest, Talat Ahmad	Constraining the timing and duration of backthrusting in the Indus Group: a detrital zircon (U-Th)/He approach
58-HIM-13	**A.K. Awasthi,** M.K. Moezabadi, A.K. Jain, S. Singh	Organic Matter Studies for Hydrocarbon Generation in the Argillaceous Sediments of the Ladakh Himalaya, India
57-HIM-14	**Borja Antolín,** Erwin Appel, Richard Gloaguen, István Dunkl, Chiara Montomoli, Lin Ding, Ursina Liebke, Qiang Xu	Clockwise rotation and tilting in the Tethyan Himalaya of SE Tibet deduced from paleomagnetic data: Implications for the Miocene tectonic evolution of the NE Himalaya
POSTERS TIB	**INTERIOR TIBET**	
56-TIB-1	**Wendy Bohon**, Kip Hodges, Ramon Arrowsmith, Alka Tripathy	A New Quaternary Strand of the Karakoram Fault System, Ladakh Himalayas
68-TIB-2	**James Hollingsworth,** Brian Wernicke, Lin Ding	Preliminary Fault Slip-Rate Estimate for the Right-Lateral Beng Co Strike-Slip Fault, based on Quaternary Dating of Displaced Paleo-Lake Shorelines
67-TIB-3	**Su Zhou,** X.X. Mo, Z.D. Zhao, Y.L. Niu, G.G. Xie, L. Qiu, K. Sun	Post-Collisional Leucite Alnoite in South Tibet and its Significance
66-TIB-4	**Genhou Wang**, Xiao Liang	Discovery and Implications of the Qiangtang Indosinian Accretionary Complex Belt in Central Tibet, China
65-TIB-5	**Yuxiu Zhang,** Kaijun Zhang	Structure and Evolution of the Bangong-Nujiang Suture (Gaize, Central Tibet)

64-TIB-6	**Jan Vozar,** Alan Jones, Florian Le Pape, Wei Wenbo, Martyn Unsworth, INDEPTH MT Team	Electromagnetic Studies of Banggong-Nujiang Suture Architecture from INDEPTH Magnetotelluric Profiles and Magnetovariational Data
78-TIB-7	**Rui Gao,** Zhanwu Lu, Xiaosong Xiong, Lingsen Zeng, Wenhui Li, Gong Deng, Simon Klemperer	SINOPROBE Deep Seismic Reflection Profiling across the Bangong-Nujiang Suture, Central Tibet
77-TIB-8	**Yalin Li,** Chengshan Wang, Ganqing Xu, Xixi Zhao, Chao Ma	Crustal Shortening in the Tanggula-Tuotuohe Area, Northern Tibet
76-TIB-9	**Kathryn Snell**, Peter Lippert, John Eiler	Stable and Clumped Isotope Analysis of Eocene Fenghuo Shan Group Sediments: Implications for Paleoelevation Estimates and Carbonate Diagenesis
POSTERS NOR	**NORTHERN PLATEAU MARGINS**	
75-NOR-1	Florian Le Pape, **Alan Jones**, Jan Vozar, Martyn Unsworth, Wei Wenbo, and the INDEPTH MT Team	Evolution of Crustal and Upper-Mantle Structure in Northern Tibet from INDEPTH Magnetotelluric Data
74-NOR-2	**Chen Chen,** Larry Brown, Marianne Karplus, Simon Klemperer	The Golmud Step: New Details of the 15 km Moho Offset Between the Tibet Plateau and Qaidam Basin from INDEPTH IV Seismic Results
89-NOR-3	**Rui Gao,** ChengShan Wang, An Yin, Haiyan Wang, Yuxiu Zhang	Construction of the Tibetan Plateau by Distributed Lithospheric-Scale Shortening: Evidence from Deep Seismic-Reflection Profiling across Northeastern Tibet
88-NOR-4	**Zhongjie Zhang,** Xiaobo Tian, Zhiming Bai, Xi Zhang, Bing Zhao, Jianli Zhang, Shaokun Shi, Tao Xu, Yun Chen, Jiwen Teng	Crustal Structure across the Qilian Orogenic Belt from In-line and Off-line Wide-angle Seismic Profiling in the North-eastern margin of Tibetan plateau
87-NOR-5	Weilin Zhang, **Erwin Appel,** Xiaomin Fang, Chunhui Song, Sihu Hu, Dongliang Liu	Magnetostratigraphy of Core SG-1 in the Western Qaidam Basin and its Tectonic-Environmental Implications
86-NOR-6	**Sam Johnstone,** G. Zhuang, J. K. Hourigan, B. D. Ritts, B. J. Darby	Sedimentary and thermochronologic evidence for Middle to Late Miocene uplift of the Northern Tibetan Plateau
85-NOR-7	**Alison Duvall,** Marin Clark, Ben van der Pluijm, Chuanyou Li	Eocene Faulting in Northeastern Tibet: Insights from Coupled Low-Temperature Thermochronometry and Ar Dating of Fault Gouge along the West Qinling Fault
84-NOR-8	**Eric Cowgill,** Ryan Gold, Ramon Arrowsmith, Xuanhua Chen, Xiao-Feng Wang	Quaternary Slip History for the Central Altyn Tagh Fault Reveals Time-Varying Slip Rate

WEDNESDAY EVENING		*Seven Hills Conference Center*
18:00-18:30	Social gathering	Enjoy a drink with your colleagues
18:30-19:45	Conference Dinner	
19:15-19:45	Dinner talk: Peizhen Zhang on behalf of the China Earthquake Administration	"The Ms 7.1 Yushu earthquake of 4/14/10: a seismological field report"
20:00-21:00	Break-Out Sessions (topics may be volunteered by participants – we are limited to three separate groups by the layout of the Seven Hills Conference Center)	suggestions thus far include: "channel flow, real or imaginary?"; "role of intra-continental strike-slip faults"; "is paleo-altimetry useful?"; and "is lithospheric strength in the crust or the mantle?"
THURSDAY MORNING		*Participants leaving Thursday night must check-out and return keys before noon. Luggage may be brought to Seven Hills*
08:00-08:30	**Break-out Session Chairs provide brief summaries of previous evening's discussions**	*Seven Hills Conference Center*
08:30-10:00	**Oral Session VIII – CLIMATE AND TECTONICS** Chairs: Asif Khan, Kate Snell	
08:30	**Peter Zeitler**	Not Very Old but Not Too Young: Thermochronological Constraints on the Age of Low-Relief Surfaces in the Western Himalaya and Southeastern Tibet
08:45	**Aaron Martin,** Lisa Walsh, Elisabeth Nadin, Tank Ojha, Tom Fedenczuk	Steepness Maxima and Transitions along the Modi Khola do not Correspond to Differences in Apatite Fission Track and (U-Th)/He Ages
09:00	**Seema Singh,** B. Parkash, A. K. Awasthi, S. Kumar	Did the Late Miocene Phase of Himalayan Orogeny Drive a Major Shift in India's Climate and Vegetation?
09:15	**Xiaomin Fang,** Chunhui Song, Weilin Zhang, Erwin Appel, Junping Gao, Maodu Yan	Mid-Miocene Climate-Driven Rapid Erosion of the Northern Tibetan Plateau
09:30	**Malinda Kent-Corson,** Bradley Ritts, Guangsheng Zhuang, Paul Bovet, Julien Charreau, Stephen Graham, Page Chamberlain	Stable Isotopic Constraints on Paleoelevation and Paleoclimate along the Northern Margin of the Tibetan Plateau
09:45	**Discussion**	moderated by chairs and discussants Kevin Furlong, Djordje Grujic
10:00-10:30	**Coffee**	*Seven Hills, outside the main auditorium. Participants leaving SF State today (including those attending the NSF Workshop) must check-out of their accommodation at this time.*

10:30-12:00	**Oral Session VII – CLIMATE, GLACIATION. EROSION** Chairs: Matthias Kühle, C.S. Dubey	
10:30	**Gerard Roe** (invited talk)	The Climate of Asia and Tibet – Not Just a Simple Monsoon
11:00	**Paul Kapp,** Alexander Rohrmann, Richard Heermance, Jon Pelletier, Joellen Russell, Lin Ding	Plio-Quaternary Wind Erosion in the Qaidam Basin, Central Asia: Records, Rates, and Broader Implications
11:15	**Bernard Hallet,** Peter Zeitler, Peter Koons, Noah Finnegan, Adam Barker	Erosion Rates at the Crest of the Himalaya: Slow or Fast?
11:30	**Lewis Owen,** Marc Caffee, Nicole Davis, Jason Dortch, Robert Finkel, Kathyrn Hedrick, Alexander Robinson, Lindsay Schoenbohm, Yeong Bae Seong	Style and Timing of Glaciation along the Karakoram Fault
11:45	**Discussion**	moderated by chairs and discussants Anne Meltzer, Doug Burbank
THURSDAY AFTERNOON		
12:00-13:30	**Lunch**	*Lunches are served in "City Eats" to conference delegates who should present their tickets issued at registration*
13:50-15:30 **POSTERS CL**	**POSTER SESSION III** **CLIMATE & TECTONICS**	*Towers, lower level*
11-CL-1	C.E. Lukens, **Barbara Carrapa**, B.S. Singer, G. Gehrels	Miocene exhumation revealed by detrital minerals of Tajik rivers: Implications for the tectonic evolution of the Pamir
10-CL-2	Erchie Wang, **Xuhua Shi,** Eric Kirby, Kevin Furlong, Ganqing Xu, Peter Kamp, Peter Reiners	Late Cenozoic Exhumation of the Eastern Margin of the Tibetan Plateau: New Constraints from Age-Elevation Transects in the Longmen Shan
9-CL-3	**Yogesh Ray**, Pradeep Srivastava, Y.P. Sundriyal	Aggradation and Incision Phases in the Upper Reaches of the Ganga River System; Timescales and Implications for Hinterland-Foreland Relationships
8-CL-4	**Tejpal Singh,** A.K. Awasthi	Growth of drainage basins and sediment transport in the Dehradun Reentrant and Nahan Salient of the NW Sub-Himalaya: a comparative study
7-CL-5	**C.S. Dubey,** M. Tajbaksh, R. Marston, E.J. Catlos, Sandeep Singh, M. Rogibala	Tectono-Geomorphic and Climatic Controls on Landscape Development in the Lesser Himalaya
21-CL-6	**Itai Haviv,** Jean-Philippe Avouac, Kenneth Farley, Mark Harrison, Matthew Heizler, Neupane Prabhat, Gweltaz Mahéo	Uplift and Exhumation along the Arun River (Eastern Nepal): Implications for the Mechanism of Uplift of the High Himalaya and the Coupling between Erosion and Tectonics

20-CL-7	**Byron Adams,** Matthijs van Soest, Kip Hodges, Kelin Whipple, Arjun Heimsath	Landscape Evolution of the Bhutan Himalaya – Insights from Tectonic Geomorphology and Low-Temperature Thermochronology
19-CL-8	**A.K. Jain,** James Pebam, Nand Lal, Sandeep Singh, Rajeev Kumar	Detrital Apatite Fission-Track Thermochronology of Modern River Sands from the Arunachal Himalaya and its Implications for Exhumation
18-CL-9	**R.C. Patel,** Vikas Adlakha, Paramjeet Singh, Nand Lal	Exhumation of the Higher and Lesser Himalayan Crystallines of the Western Arunachal Himalaya, NE-India: Constraints from Fission-Track Studies
17-CL-10	Dave Mattey, Nigel Harris, **Talat Ahmad,** Bijay Mipun, Andrew Mawlong, Gregory Diengdoh	Speleothem Records of Monsoon Intensity: Evaluating Proxy Fidelity via Cave Process Monitoring in the Shillong Plateau, NE India
29-CL-11	**Adam Barker,** Bernard Hallet	Thinning of Glaciers in the Khumbu Himal from 1955 to 2008
28-CL-12	**Kathryn Hedrick,** Yeong Bae Seong, Lewis Owen, Marc Caffee, Craig Dietsch	Towards Defining the Transition in Style and Timing of Quaternary Glaciation between the Monsoon-Influenced Greater Himalaya and the Semi-Arid Transhimalaya of Northern India
27-CL-13	**Matthias Kühle**	New Indicators of a Former Tibetan Ice Sheet and an Ice Stream Network in the Surrounding Mountain Systems: New Field Observations and Dating on the SE-, S- and W-margin of Tibet from Expeditions in 2004-2009
POSTERS CF	**CRUSTAL FLOW AND GNEISS DOMES**	
61-CF-1	Nicholas Whynot, **Djordje Grujic**, Sean Long, Nadine McQuarrie	Apparent Temperature Gradient across the Lesser Himalayan Sequence: Raman Spectroscopy on Carbonaceous Material in the Eastern Bhutan Himalaya
62-CF-2	**Sean Long,** Nadine McQuarrie, Tobgay Tobgay	Internal Strain and Deformation Temperature of Lesser Himalayan Thrust Sheets, Bhutan
63-CF-3	**Nadine McQuarrie,** Sean Long	Magnitude of Strain in a Low-Grade Greater Himalayan Section, Central Bhutan: Implications for Channel Flow
69-CF-4	**Donald Stahr,** Richard Law, Clayton Loehn, Robert Tracy, Talat Ahmad, Santosh Kumar	Deformation Temperatures and Rapid Exhumation of the Greater Himalayan Series, Sutlej Valley, NW India
70-CF-5	**Christopher Spencer,** Ron Harris	Deformation of the Greater Himalayan Sequence, Garhwal Himalaya via Sheath Folding and Late-Stage Brittle Extension: Implications for Channel Flow
71-CF-6	**Dawn Kellett,** Djordje Grujic, Clare Warren, John Cottle, Rebecca Jamieson	Pressure-Temperature-Time Paths of Tectonites from the South Tibetan Detachment System, Bhutan Himalaya
72-CF-7	**Chie Shirakawa,** Simon Wallis, Kouki Kitajima, Yuji Sano	Cenozoic Emplacement Age of the Kangmar Granite in South Tibet

73-CF-8	**Micah Jessup,** John Cottle, Jackie Langille, Graham Lederer, Talat Ahmad	Contrasting Dome Formation along the Southern Margin of the Tibetan Plateau: Leo Pargil Dome and Ama Drime Massif, India/Tibet
79-CF-9	**Jackie Langille,** Micah Jessup, John Cottle, Graham Lederer, Talat Ahmad	Timing of Metamorphism and Extension in the Western Himalaya: Leo Pargil Dome, NW India
80-CF-10	**Graham Lederer,** John Cottle, Micah Jessup, Jackie Langille, Talat Ahmad	Time-scales of Crustal Melting within the Leo Pargil Dome, NW India
81-CF-11	**William Hassett,** John Sommerfeld, Forrest Horton, Mary Leech	Geochemical comparison of north Himalayan gneiss domes
82-CF-12	**John Sommerfeld,** Forrest Horton, William Hassett, Mary Leech	$^{40}Ar/^{39}Ar$ Thermochronometry of Deformed Muscovite from the Zanskar Shear Zone, NW India
83-CF-13	Forrest Horton, **John Sommerfeld**, William Hassett, Mary Leech	U-Pb SHRIMP geochronology of leucogranites from the Greater Himalayan Sequence in Zanskar and from the Karakoram fault zone, NW India
15:00-15:30	**Coffee**	*Towers, outside the poster hall* *Poster presenters please remove posters starting at 15:15*
15:30-17:30	**Oral Session IX – CRUSTAL FLOW AND GNEISS DOMES** Chairs: A.K. Jain, Nadine McQuarrie	
15:30	**Rebecca Jamieson**, C. Beaumont, J.P. Butler, C.J. Warren (invited talk)	Crustal Structure Linked to Ultra-High-Pressure Rock Exhumation: A "Working" Model for the Tso Morari Complex, Ladakh Himalaya
16:00	Jennifer McGraw, **Brad Hacker,** Lothar Ratschbacher, Konstanze Stübner	The High-Grade Crustal Domes of the Pamir
16:15	**Richard Law,** Donald Stahr, Talat Ahmad, Santosh Kumar	Deformation Temperatures and Flow Vorticities Near the Base of the Greater Himalayan Crystalline Sequence, Sutlej Valley and Shimla Klippe, NW India
16:30	**Erchie Wang,** Dalai Zhong, Jiwen Teng, Eric Kirby	When Did Shortening Cease Within the Tibetan plateau?
16:45	Wei Wenbo, Jin Sheng, Gaofeng Ye, **Alan Jones,** Martyn Unsworth, INDEPTH MT Team	Regional resistivity structure of the Tibetan Plateau
17:00	**Discussion**	moderated by chairs and discussants Jean-Phillipe Avouac, Kip Hodges
17:20-17:30	**Closing Remarks**	**Announcement of HKT-26**
THURSDAY EVENING		
17:45-18:00	shuttle buses depart to Tiburon	*(for participants in NSF Workshop)*

Papers accepted by but not presented at HKT-25, and included among the following abstracts

Hermann Achenbach	Historical (<2000 B.P.) and Recent Glacier Fluctuations in the Inner Himalaya (North of the Annapurna and Dhaulagiri Himalaya)
Irshad Ahmad, Joseph DiPietro, Shuhab Khan, Noor Jehan	Structural Analysis of Swat and the Surrounding Peshawar Basin, North Pakistan: Application of GIS and Remote Sensing
Christopher Beaumont, Rebecca Jamieson	Himalayan-Tibetan Orogeny: Channel Flow versus (Critical) Wedge Models, a False Dichotomy?
Sharat Dutta, N. Suresh, Rohtash Kumar	Pleistocene-Holocene Climate Fluctuations and Fluvial Response in Tectonically Active Yamuna Valley, North-Western Himalaya: Timescales and Source-to-Sink Interlinkage
Noor Jehan, Khalid Durrani	Comparative Analysis of Economic Benefits and Adverse Environmental and Health Impacts of Asbestos Mining and Milling in Behram Dehri, District Charssada, Northern Pakistan
Caijun Xu, Kaihua Ding	Present-Day 3D Crustal Movement in the Qinghai-Tibetan Plateau from GPS Data
Zhu Tongxing, Dong Han, Li Cai, Feng Xintao, Li Zongliang, Yu Yuanshan, Jin Canhai, Zhou Banguo	Late Triassic Tectonic-Sedimentary Paleogeography of the Northern Qiangtang Basin, Tibet Plateau, Western China

Note: the abstracts that follow are listed alphabetically by first-author family name, irrespective of whether they are poster or oral presentations; and irrespective of the presenter.

TOWERS, lower level

POSTER NUMBERING: #1-AB-#2 #1 is location in room, left to right
Letter code is thematic group - see program - #2 is sequence in group
To avoid congestion, each day's allotted posters are on only one side of the aisles

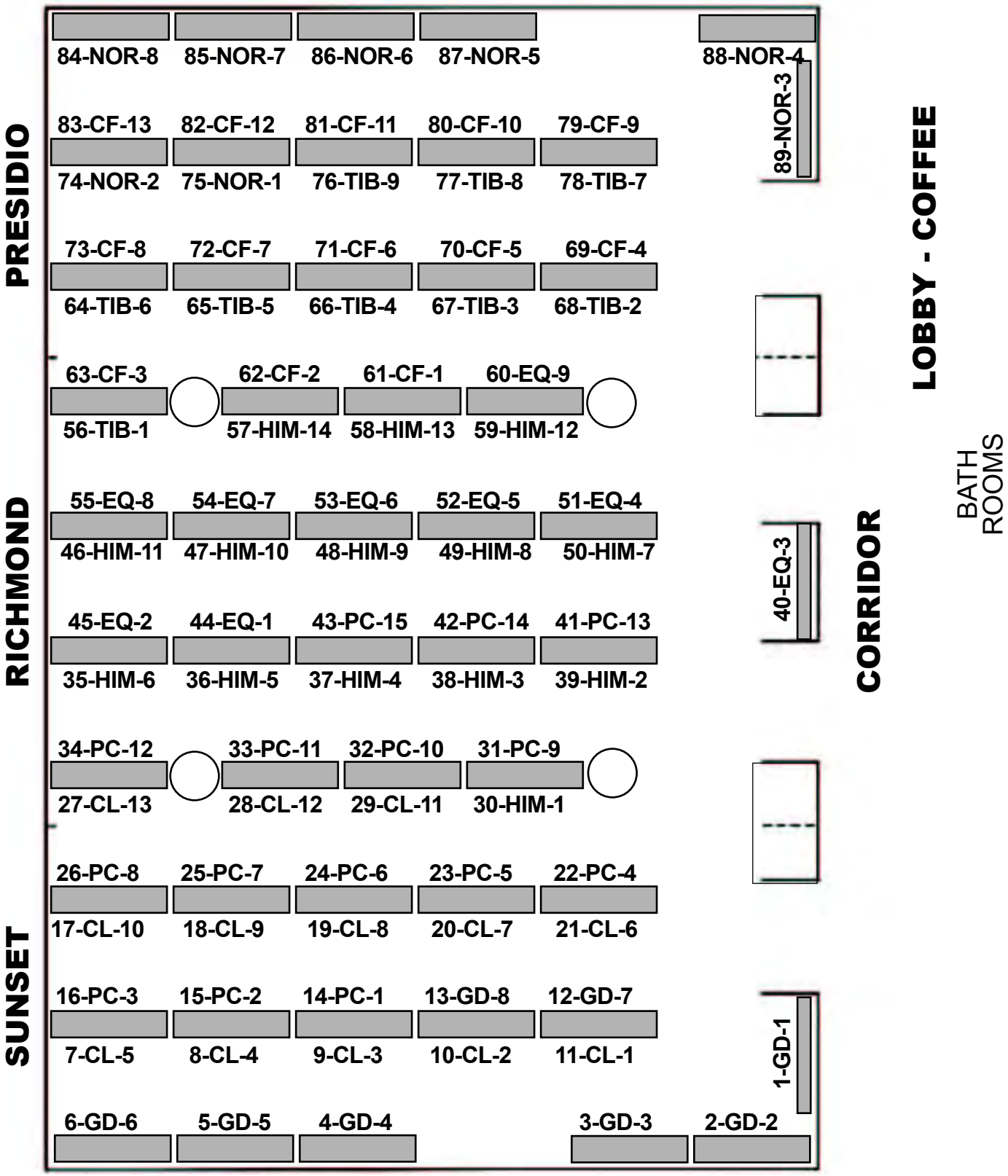

Abstracts

of the

25th Himalaya-Karakoram-Tibet Workshop

The abstracts following this page are published as:

Leech, M.L., Klemperer, S.L., and Mooney, W.D., eds.,
online proceedings for the
25th Himalaya-Karakoram-Tibet Workshop:
U.S. Geological Survey, Open-File Report 2010-1099
http://pubs.usgs.gov/of2010/1099/

The abstracts that follow are listed alphabetically by first-author family name, irrespective of whether they are poster or oral presentations; and irrespective of the presenter.

In order to ensure proper citation of the abstracts in the literature, we have attempted to follow the western style of placing the given name before the family name for all scientists, including our Chinese colleagues for whom this reverses their cultural practice. We apologize if we have made any errors.

Historical (<2000 B.P.) and Recent Glacier Fluctuations in the Inner Himalaya (North of the Annapurna and Dhaulagiri Himalaya)

Hermann Achenbach[1]

[1] Department of Geography and High Mountain Geomorphology, Georg August University, Goettingen, 37077, Germany, hachenb1@gwdg.de

In 2007 and 2008 glacial geomorphological researches were carried out north of the Annapurna and Dhaulagiri Himalaya (28°48'N/83°31'E). Due to climate and relief, the glaciers here are comparatively suitable for setting up a relative glacier chronology. As a consequence of the subtropical location and the rain shadow of the Higher Himalaya, the equilibrium line altitude (ELA) in the study area lies at approximately 5700 m asl. The glaciers under investigation are of subcontinental type. Typically, their ablation zones terminate between 5200 to 5500 m asl and are free of debris or covered with just a thin layer of supraglacial till. The lengths of the glaciers vary from 1 to 8 km. Compared with many huge glaciers in the Higher Himalaya, the ice streams in the Inner Himalaya (north of the Annapurna and Dhaulagiri Himalaya) were less fed by avalanches and their equilibrium lines do not run in high and steep walls surrounding the glaciers. For these reasons it is expected that the snouts of the investigated ice streams north of the Annapurna and Dhaulagiri massifs react more directly to climate signals than huge debris covered glaciers in the Higher Himalaya (e.g. Khumbu Himalaya).

On two expeditions the glacial geomorphological settings of more than 20 glacier forefields were mapped (Figures 1 and 2). In the vicinity of almost all current glacier snouts fresh lateral moraines indicate a youngest glacier stage (stage 4) (mean ELA-depression = 10 m). As can be seen on photos taken by different scientists and mountaineers from 1960 to 1980 these moraine walls and ledges were deposited by the ice margins around the 1970s. Climate measurements as well as proxy data evidence a drop in temperature starting around 1950 A.D. and reaching minimum values around 1970 A.D. (Shrestha and others, 1999, Thompson and others, 2000). After this cooling period the temperatures rose continuously and up to the present the glacier snouts have retreated some decameters to a few hundred meters (Figure 1). The synchronous reactions of the glaciers to these temperature changes prove their sensitivity to such climate signals.

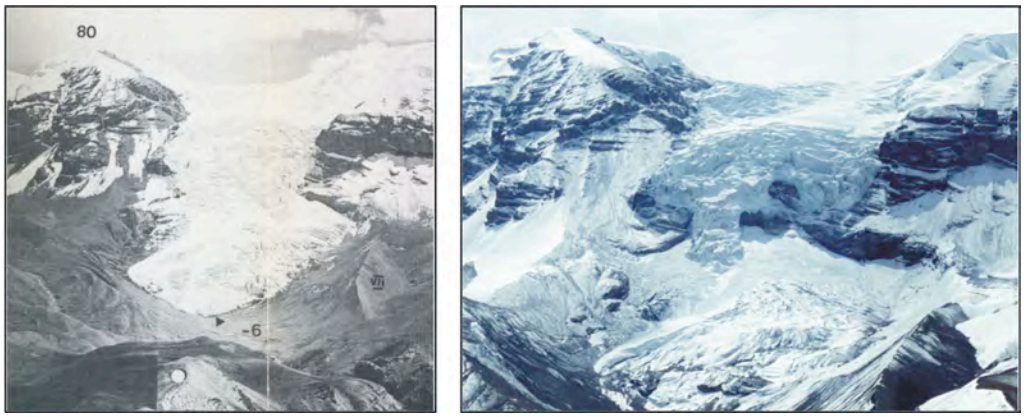

a) 1977 (Kuhle, 1982) b) 2008

Figure 1: Photo a), taken by Kuhle shows the ice front of the Chulu W-Glacier in 1977. Photo b), taken by the author in 2008, shows the interim decrease in volume and the length reduction of the glacier tongue.

For every glacier the maximum historical extension (stage 1) is evidenced by great lateral moraines, which were deposited during several glacier-advances/-stagnations in historical times. These moraine walls border each glacier forefield (Figure 2) and were highly likely built up finally during the "Little Ice Age" (1400 - 1900 A.D.) (mean ELA-depression = 80 m). According to Kuhle (1982) and confirmed by a radiocarbon date, smaller moraine walls downwards the glacier forefields were accumulated before 2000 B.P. Consistently two more glacier stages (stage 2 and 3) could be reconstructed between the moraines of stage 1 (historical maximum) and the lateral moraines deposited around the 1970s (stage 4) (Figure 2).

The lateral moraines of stage 2 (mean ELA-depression = 70 m) indicate a former glacier front just a few decameters inwards of stage 1. The moraines of stage 3 (mean ELA-depression = 40 m) are situated in the middle of the glacier forefields.

The analogue geomorphological settings of the investigated glacier forefields as well as the synchronous glacier stage around the 1970s verify the hypothesis that, in contrast to many glaciers in the Higher Himalaya, the snouts of the glaciers in the Inner Himalaya react relatively directly to climate signals.

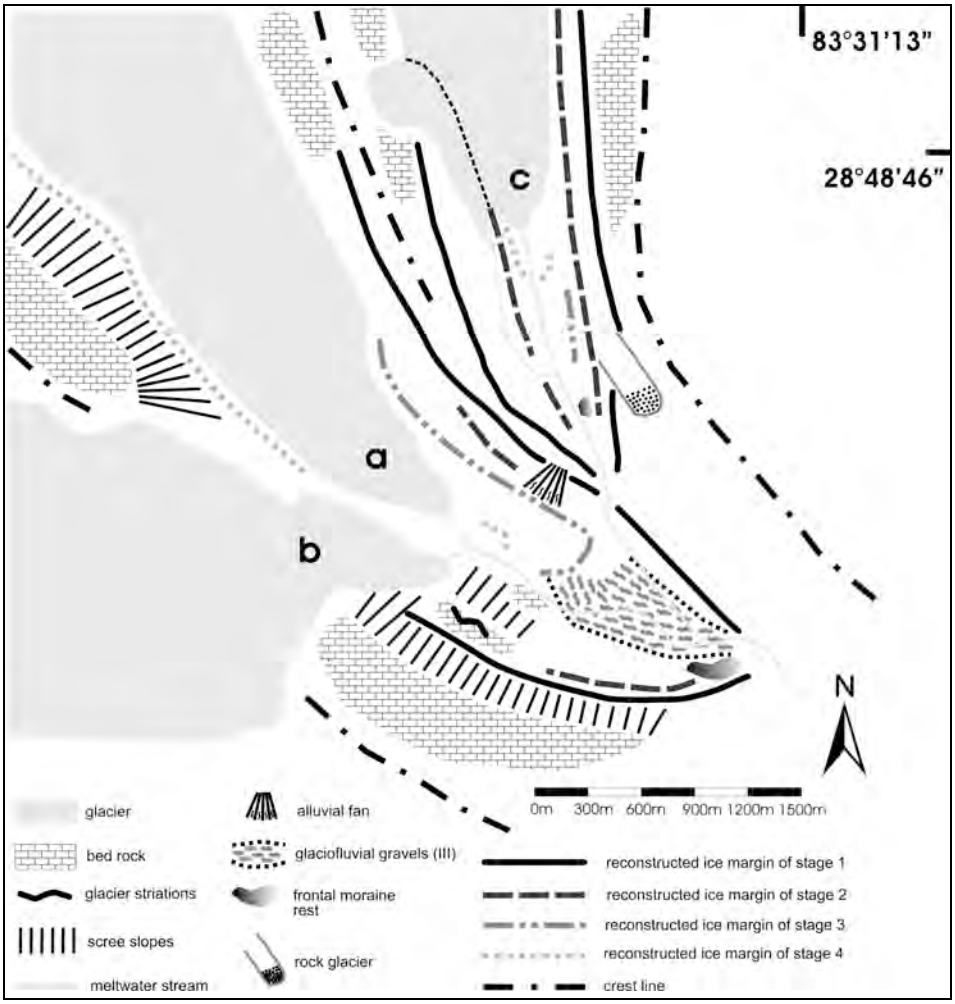

Figure 2: Glacial geomorphological map of the Mukut Glacier (a), the adjacent glacier (b), and the Hongde Himal I-Glacier (c), which are located in the Upper Hidden Valley. The current glacier termini lie in forefields surrounded by great lateral moraines (stage 1) indicating the maximum historical glacier extensions (highly likely LIA-maximum). Between these moraine walls (up to 80 m high) and the glacier snouts, three more stagnations/advances (stage 2; 3; 4) can be reconstructed. The lateral moraines of the youngest stage (stage 4) show the glacier retreat since the 1970s.

References

Kuhle, M., 1982, Der Annapurna und Dhaulagiri Himalaya, Ein Beitrag zur Geomorphologie extremer Hochgebirge, Zeitschrift für Geomorphologie Suppl. Bd., 41, 1-229, 1-183.

Shrestha, A.B., Wake C.P., Mayewski, P.A. and Dibb, J.E, 1999, Maximum temperature trends in the Himalaya and its vicinity: An analysis based on temperature records from Nepal for the period 1971–94, Journal of Climate, 12, 2775-2786.

Thompson, G., Yao, T., Mosley-Thompson, E., Davis, M.E. and Henderson, K.A., 2000, A High-Resolution Millennial Record of the South Asian Monsoon from Himalayan Ice Cores, Science, 289, 1916-1919.

Cite as: Achenbach, H., 2000, Historical (<2000 B.P.) and Recent Glacier Fluctuations in the Inner Himalaya (North of the Annapurna and Dhaulagiri Himalaya), *in* Leech, M.L. and others, eds., Proceedings for the 25th Himalaya-Karakoram-Tibet Workshop: U.S. Geological Survey, Open-File Report 2010-1099, 2 p. [http://pubs.usgs.gov/of/2010/1099/achenbach/].

Landscape Evolution of the Bhutan Himalaya – Insights from Tectonic Geomorphology and Low-Temperature Thermochronology

Byron A. Adams[1], Matthijs C. van Soest[1], Kip V. Hodges[1], Kelin X. Whipple[1], Arjun Heimsath[1]

[1] School of Earth and Space Exploration, Arizona State Unversity, Tempe, AZ, 85287, U.S.A., Byron.A.Adams@asu.edu

In contrast to the steep, rugged terrain that characterizes the southern slopes of the Himalaya in most areas, discontinuous regions of low-relief and shallow-slope occur perched at high elevations (~3500 m) in the middle latitudes of Bhutan. These surfaces are marked by subdued landforms, thick soils and saprolites, massive alluvial and colluvial fills, and presumably slow erosion rates. It is likely that these landscapes were once more continuous east to west across Bhutan and possibly extended south toward the foreland. However, due to active river incision, only isolated patches remain. These enigmatic surfaces pose two problems: (1) how and why did low-relief surfaces develop? and (2) how and why did they become perched at high elevations above rugged mountains and deep river gorges? Although robust answers to these questions require the integration of many modes of investigation, the age of low-relief surface development and the age of its uplift to higher elevations are crucial to our understanding of how climate and tectonics have shaped the Bhutan Himalaya.

Several hypotheses can be proposed to explain the existence of these topographic benches or the escarpments that bound them to the north and south. Plausible hypotheses include either temporal or spatial controls on the evolution of the landforms.

Temporal: The physiographic benches are relict low-relief landscapes perched above rapidly incising canyons.

1) Large regions of subdued landscape were uplifted to their current elevation by decreasing precipitation and maintaining constant uplift. The change in regional precipitation rate was likely a consequence of the uplift of the Shillong Plateau to the south (<3.5 Ma, Worm and others, 1998; 3-4 Ma, Biswas and others, 2007), which produced a rain shadow effect. (Grujic and others, 2006)

2) Large regions of subdued landscape were uplifted to their current elevation by an increase in rock uplift rate.

Spatial: The physiographic benches reflect spatially-variable rock uplift.

3) Fault zones have created the escarpments to the north and south of the low-relief landscapes (Tobgay and Hurtado 2004), as has been proposed for other physiographic transitions in the Himalaya (e.g. Hodges and others, 2001; Wobus and others, 2005).

Our first approach to obtaining quantitative information regarding the timing of uplift of the low-relief surfaces involved sampling an elevation transect beneath the low-relief region in the Bumthang area of eastern Bhutan (Figure 1) for single-crystal apatite (U-Th)/He dating. The cooling ages for most samples decrease with distance below the low-relief surface from 5.94 +/- 0.38 to 4.41 +/- 0.04 Ma (2σ), down to a depth of ~1600 m below the surface (Figure 2). They define a linear array on an apparent-age versus elevation plot suggestive of steady, relatively rapid exhumation at a rate of ~2 mm/yr from around 6 to 5 Ma. However, the lowest sample in the transect is younger than predicted by this exhumation rate. Although more data are needed, this preliminary result implies a deceleration in exhumation rate after ~ 5 Ma, which may suggest establishment of the low-relief surface at about that time. If the surface was established by ~ 5 Ma at low elevations, then uplift of the surface to its current elevation of ~ 3500 m was a Pliocene-Quaternary process.

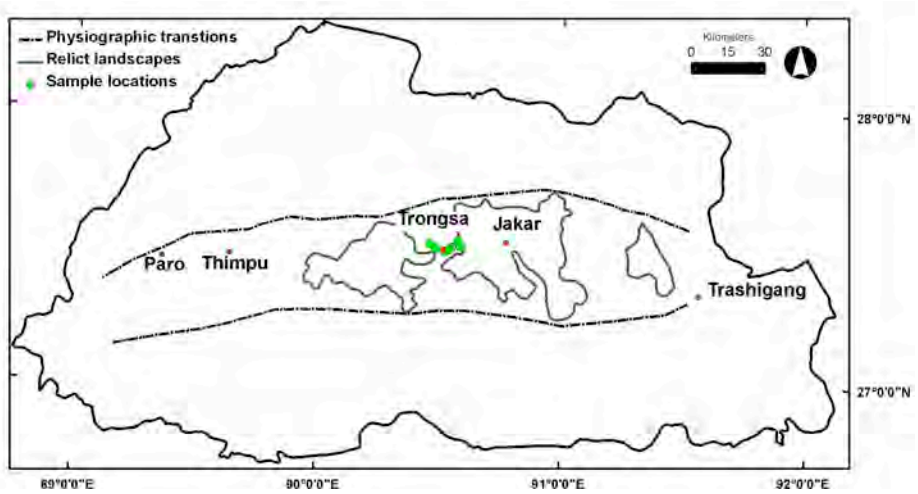

Figure 1. Simplified map of Bhutan showing the proposed relict landscapes of Grujic and others (2006) and physiographic transitions. Apatite (U-Th)/He vertical transect sample locations are denoted in large circles and located in eastern Bhutan near Trongsa. The Bumthang low-relief surface is demarcated with a solid line around Jakar.

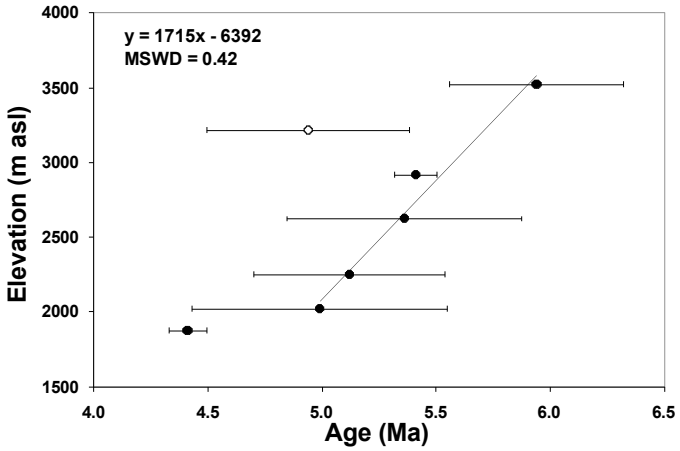

Figure 2. Age-elevation plot of single grain apatite (U-Th)/He samples beneath the Bumthang surface. The cooling ages for most samples decrease with distance below the low-relief surface from 5.94 +/- 0.38 to 4.41 +/- 0.04 Ma (2σ). The data define a linear trend suggestive of exhumation at a rate of ~2 mm/yr from around 6 to 5 Ma. The lowermost sample of the transect has a younger cooling age than predicted by the ~2 mm/yr trend of higher-elevation samples. The sample denoted with a white circle was omitted from the least-squares regression.

References

Biswas, S., and others, 2007, Exhumation and uplift of the Shillong plateau and its influence on the eastern Himalayas: New constraints from apatite and zircon (U-Th-[Sm])/He and apatite fission track analyses, Tectonics, 26, TC6013.

Grujic, D., and others, 2006, Climatic forcing of erosion, landscape, and tectonics in the Bhutan Himalayas, Geology, 34, 801-804.

Hodges, K. V., Hurtado, J. M. and Whipple, K. X., 2001, Southward extrusion of the Tibetan crust and its effect on Himalayan tectonics, Tectonics, 20, 799-809.

Tobgay, T. and Hurtado, J.M., 2004, Field evidence for active uplift in the central Bhutan Himalaya, Eos Trans. Am. Geophys. Un., 85, T53A-0470.

Wobus, C., Heimsath, A., Whipple, K. and Hodges, K., 2005, Active out-of-sequence thrust faulting in the central Nepalese Himalaya, Nature, 434, 1008-1010.

Worm, H.-U., and others, 1998, Large sedimentation rate in the Bengal Delta: Magnetostratigrahpic dating of Cenozoic sediments from northeastern Bangladesh, Geology, 26, 487-490.

Cite as: Adams, B.A., van Soest, M.C., Hodges, K.V., Whipple K.X. and Heimsath, A., 2010, Landscape Evolution of the Bhutan Himalaya, *in* Leech, M.L., and others., eds., Proceedings for the 25th Himalaya-Karakoram-Tibet Workshop: U.S. Geological Survey, Open-File Report 2010-1099, 2 p. [http://pubs.usgs.gov/of/2010/1099/adams/].

Testing Earthquake Nucleation Models from the Response of Himalayan Seismicity to Secular and Periodic Stress Variations

Thomas Ader[1], Jean-Philippe Avouac[1], Sachiko Tanaka[2]

[1] Department of Geological and Planetary Sciences, California Institute of Technology, Pasadena, CA 91125, ader@caltech.edu
[2] National Research Institute for Earth Science and Disaster Prevention, Japan

Shortening across the Nepal Himalaya proceeds at a rate of about 2 cm/yr and is mainly absorbed by one major fault, the Main Himalayan Thrust fault (Lavé and Avouac, 2000). Geodetic measurements show that, over the last few decades, this fault has remained locked from the surface to a depth of about 15-20 km.

The background seismicity is driven by the slow motion of India into Eurasia, responsible for the interseismic stress buildup in the period separating big (M > 8) earthquakes. In addition to this secular motion, strong seasonal variations in the seismicity have been reported (Bettinelli and others, 2008), with the number of events about 30% higher in the winter. Similar seasonal variations have been observed in various contexts and related to factors such as snow load or variations of the water level.

We analyze the relationship between seismicity and temporal stress variations in the Himalaya to constrain earthquake nucleation process. In addition to the secular stress load induced by crustal shortening across the range, the Himalayan arc is also submitted to 2 periodic stress variations of comparable 3-5 kPa amplitudes but different periods: 12.4 hours period variations are induced by earth tides, while 1-year period variations are induced by surface load variations associated with the seasonal hydrological cycle (the monsoon). The seismicity shows no apparent correlation with earth tides, but does show prominent seasonal variations. These observations are used to test models of earthquake nucleation and infer frictional properties of natural faults. We find that the model of Dieterich (1994) can reproduce the correlation between seasonal variations of seismicity and hydrological cycle, but fails at explaining the absence of correlation with earth tides.

References

Bettinelli, P., and others, 2008, Seasonal variations of seismicity and geodetic strain in the Himalaya induced by surface hydrology, Earth Planet. Sci. Letts., 266, 332-334.

Dieterich, J. H., 1994, A constitutive law for rate of earthquakes production and its application to earthquake clustering, Journal of Geophysical Research, 99, 2601-2618.

Lavé, J., and Avouac, J.-P., 2000, Active folding of fluvial terraces across the Siwaliks Hills, Himalayas of central Nepal, Journal of Geophysical Research, 105, 5735-5770.

Cite as: Ader, T. and Avouac, J.P., 2010, Testing earthquakes nucleation models from the response of Himalayan seismicity to secular and periodic stress variations, *in* Leech, M.L., and others, eds., Proceedings for the 25th Himalaya-Karakoram-Tibet Workshop: U.S. Geological Survey, Open-File Report 2010-1099, 1 p., [http://pubs.usgs.gov/of/2010/1099/ader/].

Shear-Velocity Profiles Across the Tibetan Plateau from Broadband, Surface-Wave, Phase-Velocity Measurements

Matthew R. Agius[1], Sergei Lebedev[1]

[1] Geophysics Section, Dublin Institute for Advanced Studies, Dublin, Ireland, matthew@cp.dias.ie

In order to constrain variations in the crustal and lithospheric structure across Tibet, we measure phase velocities of seismic surface waves. The data are seismograms recorded by broadband instruments of permanent and temporary networks within and around the plateau. Phase-velocity measurements are performed in broad period ranges using an elaborate recent implementation of the 2-station method. A combination of the cross-correlation (Meier and others, 2004) and multimode-waveform-inversion (Lebedev and others, 2005) measurements using tens to hundreds of seismograms per station pair produces robust, accurate phase-velocity curves for Rayleigh and Love waves.

We use our new measurements to infer phase-velocity variations and to constrain S-velocity profiles in different parts of the plateau, including radial anisotropy and depths of lithospheric discontinuities. S-velocity profiles are computed using a non-linear gradient search and show a distinct crustal low-velocity zone (LVZ) in the 20–45 km depth range across the plateau, both in the south and in the north. We perform a series of targeted test inversions and show that the dispersion data constrains S velocity in this mid-crust low velocity layer to be within a 3.2–3.5 km/s range. This LVZ coincides with a low-resistivity layer inferred from magnetotelluric studies, interpreted as evidence for partial melting in the middle crust (Nelson and others, 1996, Unsworth and others, 2004). Surface-wave data are, also, consistent with strong radial anisotropy in this layer, indicative of horizontal flow (Royden and others, 2008). At the north-eastern boundary of the plateau, past the Kunlun Fault, S-velocity in the lower middle crust increases, although still relatively low. The mid-crustal LVZ, in the sense of an S-velocity decrease with depth in the 15–25 km depth range, is not required by the surface-wave data outside the plateau.

The mantle-lithosphere structure shows a pronounced contrast between the southern - south-western and central-northern parts of the plateau. The south and south-west are underlain by a thick, high-velocity, craton-like lithospheric mantle. Beneath the north, in contrast, the average S velocity between the Moho and 200 km depth is close to the global continental average (4.5 km/s). In order to investigate the finer detail of the lithospheric structure in the north, and keeping in mind the non-uniqueness of the S-velocity models, we perform an extensive series of test inversions. We find that surface-wave dispersion alone is consistent both with models that have low S velocity just beneath the Moho, increasing with depth below (McKenzie and Priestley, 2008), and with models that display a thin high-velocity mantle lid underlain by a low-velocity zone (asthenosphere). This non-uniqueness implies that a joint analysis of surface-wave data with data of other types may be necessary in order to determine the thickness of the lithosphere in the central and northern Tibet.

We combine our surface-wave measurements in the Qiangtang Block in central Tibet (Hi-Climb experiment area, north of the Banggong-Nujiang suture) with receiver-function constraints on the Moho depth (Tseng and others, 2009) and Sn constraints on the uppermost-mantle S velocities (Pei and others, 2007). We show that the data is matched significantly better with models that contain a thin, high-velocity lithosphere (up to 90 km thick) underlain by a low-velocity zone than by models with no wave-speed decrease between the Moho and ~100 km depth. In the deeper upper mantle (below ~150 km depth), S velocity increases and is likely to exceed the global average value.

References

Lebedev, S., Nolet, G., Meier, T. and van der Hilst, R.D., 2005, Automated multimode inversion of surface and S waveforms, Geophys. J. Int., 162, 951-964.

Meier, T., Dietrich, K., Stöckhert, B. and Harjes, H.P., 2004, One-dimensional model of shear wave velocity for the eastern Mediterranean obtained from the inversion of Rayleigh wave phase velocities and tectonic implications, Geophys. J. Int., 156, 45-58.

McKenzie, D. and Priestley, K., 2008, The influence of lithospheric thickness variations on continental evolution, Lithos, 102, 1-11.

Nelson, K.D., and others, 1996, Partially molten middle crust beneath southern Tibet: a synthesis of Project INDEPTH results, Science, 274, 1684-1688.

Pei, S., and others, 2007, Upper mantle seismic velocities and anisotropy in China determined through Pn and Sn tomography, J. Geophys. Res., 112, B05312.

Royden, L.H., Burchfiel, B.C. and Van der Hilst, R.D., 2008, The geological evolution of the Tibetan plateau, Science, 321,

1054.
Tseng,T.L., Chen, W.P. and Nowack, R.L., 2009, Northward thinning of Tibetan crust revealed by virtual seismic profiles, Geophys. Res. Letters, 36, L24304.
Unsworth, M., and others, 2004, Crustal and upper mantle structure of northern Tibet imaged with magnetotelluric data, J. Geophys. Res., 109, B02403.

Cite as: Agius, M.R. and Lebedev, S., 2010, Shear-Velocity Profiles Across the Tibetan Plateau from Broadband, Surface-Wave, Phase-Velocity Measurements, *in* Leech, M.L., and others, eds., Proceedings for the 25th Himalaya-Karakoram-Tibet Workshop: U.S. Geological Survey, Open-File Report 2010-1099, 2 p. [http://pubs.usgs.gov/of/2010/1099/agius/].

Structural Analysis of Swat and the Surrounding Peshawar Basin, North Pakistan: Application of GIS and Remote Sensing

Irshad Ahmad[1], Joseph A. DiPietro[2], Shuhab D. Khan[3], Noor Jehan[4]

[1] NCE in Geology, University of Peshawar, NWFP, Pakistan, ahmadirshadpk@yahoo.com
[2] Department of Geology, University of Southern Indiana, Evansville, IN 47712, U.S.A.
[3] Deparment of Earth and Atmospheric Sciences, University of Houston, TX 77204, U.S.A
[4] Department of Environmental Sciences, University of Peshawar, NWFP, Pakistan

Remote sensing technology has gained credibility for analyzing the structural and geologic evolution of an area or region. In this regard an attempt has been made to bring out the structural trends in Swat and surrounding of Peshawar basin through satellite imagery. The structural information derived from the satellite imagery was integrated with field observations and existing geologic maps (Ahmad and Jehan, 2005; DiPietro and others, 2008) using GIS software. The integration has given a clear picture of structural trends in Swat and the surrounding Peshawar basin (Fig. 1).

Three major faults, the Kohistan, Kishora and the Khairabad-Panjal thrusts, dominate the structure of the study area. The Kohistan and the Kishora thrusts are the extension of the MMT in the Swat area (Kazmi and others, 1984). The Kohistan thrust dip angle varies from 55° to more than 60° to the northwest and strikes approximately WSW. The map trace of the Kohistan thrust is mostly straight with a few deflections due to topography. The Kishora and the Khairabad-Panjal thrusts are also northwest dipping and strike WSW. These dip less steeply than the Kohistan thrust. Beside the major thrusts, high-angle dip-slip and strike-slip faults oriented north-south dominate the eastern part of the study area. The Swat area and the surrounding Peshawar basin have undergone multiple deformations with at least four periods of folding (DiPietro and Lawrence, 1991; Ahmad and Lawrence, 1992; Ahmad and Jehan, 2005). The northern part of the study area preserves four superposed small-scale folds (F_1 through F_4) whereas in the south only the last two phases are preserved. F_1 and F_2 are primarily small-scale folds that can not be distinguished on the image. These are coaxial and coplanar with isoclinal, recumbent axial surfaces and fold axis that plunge gently toward the NNW. F_3 and F_4 folds describe the map pattern. Large scale F_3 folds are upright folds. Small scale F_3 folds are closed to tight with variably dipping axial surfaces, whereas large scale F_3 axes plunge gently but variably towards the north or less commonly the south or southeast (Fig. 1). F_4 folds are open, E-W trending and asymmetric. These are mostly south vergent but are verging north near Rustam (Fig. 1). The superposition of the east-west trending F_4 folds on the generally north-south trending earlier F_3 folds has created dome and basin structures in the Kot, Kotah and Loe Sar area (Fig. 1).

The fold sequence implies an early period of E-W compression prior to the development of south verging structures. The small scale F_1 and F_2 folds represent a progressive F_1 / F_2 deformation that was associated with a single set of west-southwest vergent large-scale folds (F_2). The large-scale F_3 folds may have developed in intense localized shear strain related to ophiolite emplacement south of the Kohistan fault. F_4 folds may correlate with early doming of the lower Swat sequence and with strike-slip displacement along the Kohistan fault or in the northern part of the MMT.

References

Ahmad, I. and Jehan, N., 2005, Structural analysis south of Malakand and adjoining areas, northern Pakistan, Geol. Bull. Univ. of Peshawar, 38, 31-56.

Ahmad, I. and Lawrence, R. D., 1992, Structure and Metamorphism of the Chakdara area NW of the Swat river, Pakistan, Geol. Bull. Univ. of Peshawar, 25, 95-112.

DiPietro, J.A. and Lawrence, R. D., 1991, Himalayan structure and metamorphism south of the Main Mantle Thrust, lower Swat, Pakistan, J. Met. Geol., 9, 481-495.

DiPietro, J.A., Ahmad, I. and Hussain, A., 2008, Cenozoic kinematic history of the Kohistan fault in the Pakistan Himalaya, Geol. Soc. of Amer. Bull., 120, 1428-1440.

Kazmi, A.H., Lawrence, R.D., Dawood, H., Snee, L.W. and Hussain, S.S., 1984, Geology of the Indus suture zone in the Mingora Shangla area of Swat, N. Pakistan, Geol. Bull. Univ. of Peshawar, 17, 127-144.

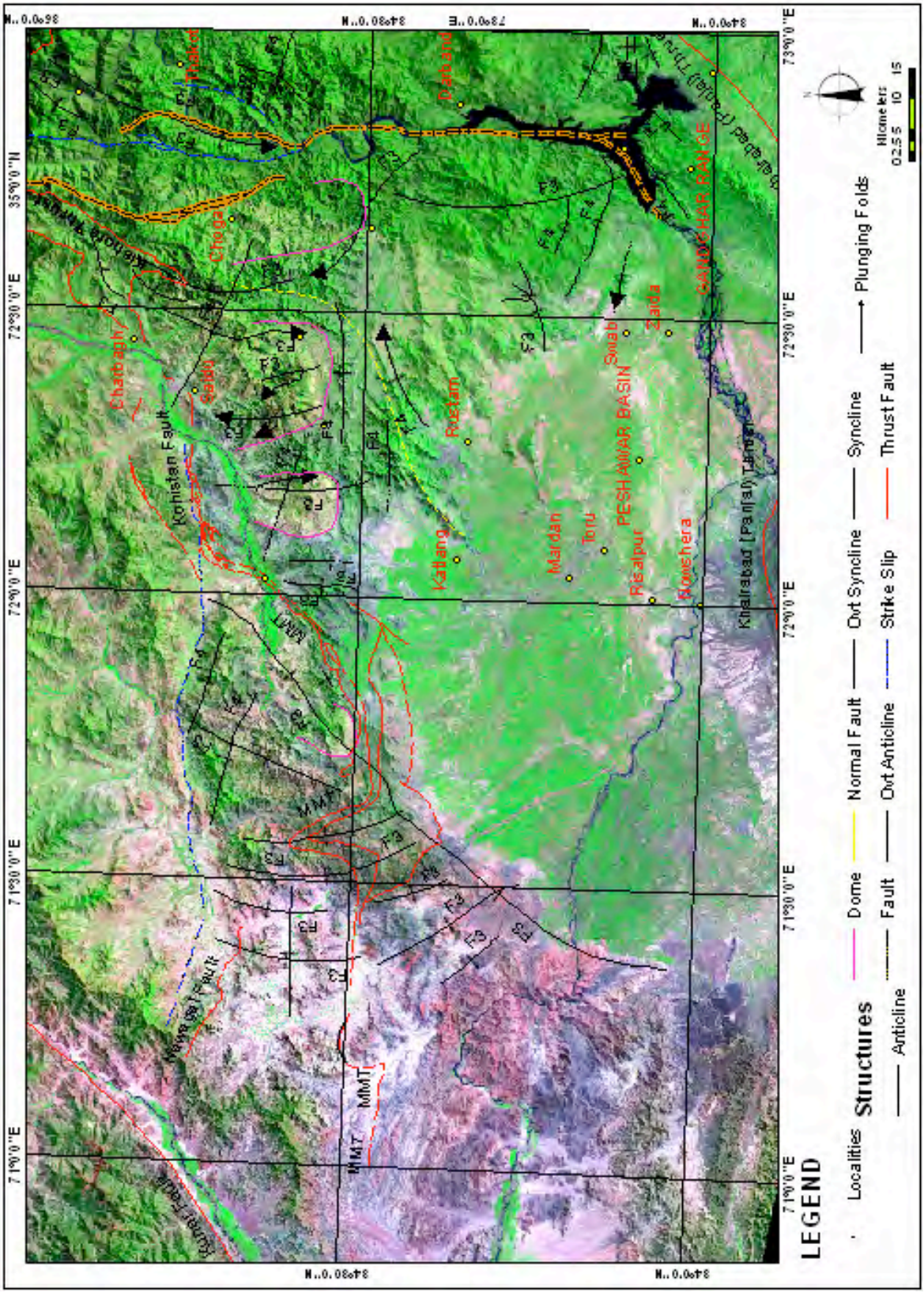

Figure 1. Landsat ETM image showing the structural trends of the Swat and surrounding of Peshawar Basin

Cite as: Ahmad, I., DiPietro, J., Khan, S.D. and Jehan, N., 2010, Structural Analysis of Swat and the Surrounding Peshawar Basin, North Pakistan: Application of GIS and Remote Sensing, *in* Leech, M.L., and others, eds., Proceedings for the 25th Himalaya-Karakoram-Tibet Workshop: U.S. Geological Survey, Open-File Report 2010-1099, 2 p. [http://pubs.usgs.gov/of/2010/1099/ahmadirshad/].

Geochemical and Isotopic Constraints on the Nature of the Indus and Shyok Suture Zones, Remnants of the Neo-Tethyan Ocean in the Trans-Himalayan Region

Talat Ahmad[1]

[1]Department of Geology, University of Delhi, Delhi – 11 00 07, India, tahmad001@yahoo.co.in

The Indus and Shyok suture zones of the Trans-Himalayan region are considered to represent remnants of the Neo-Tethyan ocean that closed via subduction as the Indian plate moved northwards with respect to the Asian plate. Geochemical and isotopic (Sr and Nd) data for the magmatic rocks of the Indus and Shyok sutures reveal important contrasts. The volcanic rocks of the Indus and Shyok suture zones are sub-alkaline basalt, basaltic-andesite, andesite and rhyolite.

The Indus suture rocks have nearly flat to slightly depleted light rare earth and large ion lithophile element (LREE-LILE) characteristics, with strong negative anomalies for the high field strength element (HFSE: Nb, P and Ti). These incompatible elemental characteristics indicate that they probably represent intra-oceanic island arc setting. Shyok suture rocks, on the other hand, have enriched LREE and LILE respectively and depleted HFSE trace element characteristics. They probably represent ocean-continent island arc system.

In addition to the arc component, the Indus suture contains the Zildat ophiolitic mélange with dominant OIB characteristics as evidenced by highly enriched Nb (60 to 130 ppm) and strongly negative values for fSm/Nd (-0.4147 to -0.4676) relative to CHUR. However, these rocks have positive epsilon Ndt=110 Ma of about +3 and +4, like many OIBs, indicating their derivation from isotopically depleted sources that got elementally enriched prior to melting. A minor component of this mélange is characterized by depleted LILE-LREE, highly positive epsilon Ndt=110 Ma of about +9 and initial Sr of 0.70466 to 0.70666, seen in many N-MORBs. The arc component, represented by the Nidar ophiolitic complex, have higher abundances of the LREE-LILE with respect to N-MORB and positive epsilon Ndt=110 Ma of about +8 and +9, similar to Zildat mélange. Initial Sr values for Nidar gabbros vary between 0.70422 and 0.70546 indicating absence of continental crustal component.

Shyok volcanics and Nubra ophiolitic volcanics of the Shyok suture zone have epsilon Ndt=110 Ma of about +5 to -2, fSm/Nd of -0.2553 to -0.2921 and initial Sr values of 0.70376 to 0.70471. Elemental and isotopic characteristics for the rocks of the Shyok suture zone indicate involvement of juvenile crustal component in their genesis.

Thus, the geochemical and isotopic data from Indus and Shyok suture indicate that the Neo-Tethyan ocean in this region was represented by contrasting tectonic scenarios ranging from dominantly OIB to minor MORB on the one hand and from ocean-ocean to ocean-continent arc system on the other.

Cite as: Ahmad, T., 2010, Geochemical and Isotopic Constraints on the Nature of the Indus and Shyok Suture Zones, Remnants of the Neo-Tethyan Ocean in the Trans-Himalayan Region, *in* Leech, M.L., and others, eds., Proceedings for the 25th Himalaya-Karakoram-Tibet Workshop: U.S. Geological Survey, Open-File Report 2010-1099, 1 p. [http://pubs.usgs.gov/of/2010/1099/ahmad/].

Clockwise rotation and tilting in the Tethyan Himalaya of SE Tibet deduced from paleomagnetic data: Implications for the Miocene tectonic evolution of the NE Himalaya

Borja Antolín[1], Erwin Appel[1], Richard Gloaguen[2], István Dunkl[3], Chiara Montomoli[4], Lin Ding[5], Ursina Liebke[1], Qiang Xu[5]

[1]Institute for Geosciences, University of Tübingen, 72076 Tübingen, Germany, borja.antolin@uni-tuebingen.de
[2]Department of Geology, Technical University of Freiberg, 09596 Freiberg, Germany
[3]Sedimentology and Environmental Geology, University of Göttingen, D-37077 Göttingen, Germany
[4]Department of Earth Sciences, University of Pisa, 56126 Pisa, Italy
[5]Institute of Tibetan Plateau Research, Chinese Academy of Sciences, Beijing 100085, China

Crustal movement around and away from the Namche Barwa syntaxis is indicated in the Asian velocity field inferred from GPS data and Quaternary fault slip rates (e.g., Gan and others., 2007; Fig. 1). Nevertheless, there is limited field-based control on the rotational history of the north-eastern Himalayan arc. Exploring the polyphase nature of deformation within the Cretaceous diorite dykes and the Triassic flysch in the eastern Tethyan Himalaya (90°-92°E), combined with new remote sensing data and the existing thermo-geochronological data, allows us to unravel the kinematic relationship between our new paleomagnetic remanence vectors and the deformation phases.

Rock magnetism analyses in the Cretaceous diorite dykes indicate that the characteristic remanent magnetization is mainly carried by pyrrhotite. This is supported by a Hopkinson peak and decay at 325 °C in high-temperature susceptibility curves, SIRM saturation field values > 300 mT, and a sharp decrease of remanent magnetization at ~325 °C during thermal demagnetization of the SIRM. The characteristic remanence magnetization is likely of thermal origin and post Eo-Himalayan folding as suggested by two facts: (i) thermochronological data in the Triassic flysch indicate that a peak metamorphism above the Curie temperature of pyrrhotite was reached for the last time at ~22 Ma at the end of the D2 tectonic phase (Dunkl and others., submitted); (ii) in situ mean declinations are approximately constant in the Qonggyai valley, despite of the double vergence of folds and related axial planar foliation, south-vergent in the southern domain and north-vergent in the northern domain. Therefore the magnetization can be evaluated as a record of the Early Miocene field. Calculated vertical-axis rotations in Nagarze-Yamdrok Lake area and Qonggyai valley indicate a trend from no apparent rotation in the west to 20° clockwise rotation in the east with respect to the stable Indian plate (Fig. 1).

Our data suggest that the strong Miocene strain partitioning between local E-W extension (with unclear influence of reactivation of older structures as strike-slip faults) in an eastward regional motion or extrusion of the upper crust (like show the GPS and rigid rotation velocity field; Gan and others., 2007) around the eastern syntaxis could have been accommodated by the obtained clockwise rotation pattern. Additionally, the observed pattern of tilting around horizontal axis in the Qonggyai valley may reflect concealed North Himalayan doming.

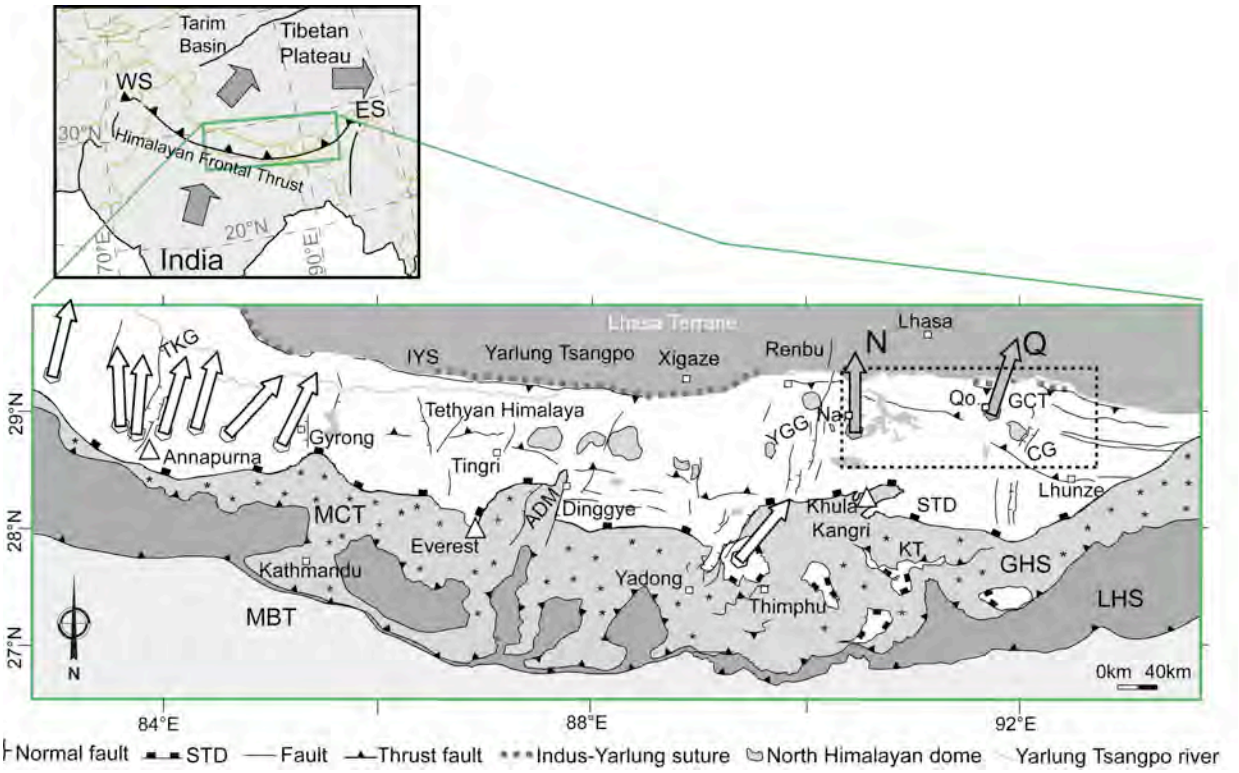

Figure 1. Simplified geological map of the central and eastern Himalaya (after Pan and others, 2004; Kellett and others, 2009). White arrows indicate published paleomagnetic block rotations in the western-central Tethyan Himalaya (age of the remanence is 30-20 Ma; Schill and others, 2004 and references therein) and in NW Bhutan (age of the remanence is ~15 Ma; Baule, 2004) relative to the Indian plate. Study area location within the dashed-line box and corresponding block rotations at Nagarze area (N) and Qonggyai valley (Q) versus India and since ~22 Ma. TKG, Thakkhola Graben; IYS, Indus Yarlung Suture zone; ADM, Ama Drime Massif; YGG, Yadong-Gulu Graben; Na, Nagarze; Qo, Qonggyai; CG, Cona Graben; STD, South Tibetan Detachment; KT, Kakhtang thrust; GHS, Greater Himalayan sequence; MCT, Main Central Thrust; LHS, Lesser Himalayan sequence; MBT, Main Boundary Thrust. Inset map shows location of Western Syntaxis (WS), Eastern Syntaxis (ES) and this vertical-axis block rotation map. Arrows are generalized GPS motions relative to Siberia (Tapponnier and others, 2001).

References

Baule, S., 2004, Clockwise rotation and fold axes distribution in the Tethyan Himalaya of Bhutan: constraints from palaeomagnetic remanences and anisotropy of magnetic susceptibility, Masters Thesis, Tübingen University.

Dunkl, I., and others, submitted, Metamorphic evolution of the Tethyan Himalayan flysch in SE Tibet, in: Gloaguen, R. and Ratschbacher, L., (eds.), Growth and Collapse of the Tibetan Plateau, Geol. Soc. London Spec. Publ.

Gan, W., and others, 2007, Present-day crustal motion within the Tibetan Plateau inferred from GPS measurements, J. Geophys. Res., 112, B08416.

Kellett, D.A., Grujic, D. and Erdmann, S., 2009, Miocene structural reorganization of the South Tibetan detachment, eastern Himalaya: Implications for continental collision, Lithosphere, 1, 259-281.

Schill, E., and others, 2004, Oroclinal bending versus regional significant clockwise rotations in the Himalayan arc-Constrains from secondary pyrrhotite remanences, in: Sussman, A.J. and Weil, A.B. (eds.), Orogenic Curvature: Integrating Paleomagnetic and Structural Analyses, Spec. Pap. Geol. Soc. Am., 383, 73-85.

Pan, G., Ding, J., Yao, D. and Wang, L., 2004, Geological map of Qinghai-Xizang (Tibet) Plateau and Adjacent Areas (1:1,500,000). Chengdu Institute of Geology and Mineral Resources, China Geological Survey. Chengdu Cartographic Publishing House.

Tapponnier, P., and others, Y., 2001, Oblique Stepwise Rise and Growth of the Tibet Plateau, Science, 294, 1671-1677.

Cite as: Antolín, B., Appel, E., Gloaguen, R., Dunkl, I., Montomoli, C., Ding, L., Liebke, U. and Xu, Q., 2010, Clockwise rotation and tilting in the Tethyan Himalaya of SE Tibet deduced from paleomagnetic data: Implications for the Miocene tectonic evolution of the NE Himalaya, *in* Leech, M.L., and others, eds., Proceedings for the 25th Himalaya-Karakoram-Tibet Workshop: U.S. Geological Survey, Open-File Report 2010-1099, 2 p. [http://pubs.usgs.gov/of/2010/1099/Antolin/].

Magnetostratigraphy of Core SG-1 in the Western Qaidam Basin and its Tectonic-Environmental Implications

Weilin Zhang[1,2], Erwin Appel[2], Xiaomin Fang[1], Chunhui Song[3], Sihu Hu[3], Dongliang Liu[1]

[1] Institute of Tibetan Plateau Research, Chinese Academy of Science, Beijing 100085, China
[2] Institut für Geowissenschaften, Universität Tübingen, 72076 Tübingen, Germany, erwin.appel@uni-tuebingen.de
[3] Key Laboratory of Western China's Environmental Systems, Lanzhou University, Gansu 730000, China

The Qaidam basin, the largest intermontane basin on the Tibetan Plateau, contains a continuous long-term Cenozoic sedimentary record providing information on the history of tectonic activity and associated climatic change. We report a magnetostratigraphic study of a 938.5 m deep drill core (SG-1) in the sub-basin depocenter of the Chahansilatu' salt-alkali area between Eboliang anticline and Jianshan anticline in the western Qaidam basin (N38°24′35.3″, E92″30′32.6″) (Figure 1).

The sedimentary sequence comprises clay, clay-silt, and siltstone, intercalated with salt layers (mainly halite) and thin or scattered gypsum, representing long-term paleoclimate trends and fluctuations. From surface to ca. 350 m sedimentary cycles of thick salt and massive-laminated clay-siltstone with a ratio of about 1:3 are observed, while from ca. 350 to 720 m salt layers become much thinner. Below 720 m mainly siltstone/mudstone and intercalated sandstone interbeds dominate, with lesser salt nodules and scattered gypsum crystals.

Palaeomagnetic remanence was measured on 1257 samples from which 1128 samples were accepted for further interpretation, according to quality criteria. The demagnetization behavior is consistent throughout the core and separation of characteristic remanences is straightforward. Magnetite in a relatively hard coercive range is responsible for the magnetic signal. Normal and reverse polarity samples show antipodal inclinations and their numbers and values reflect the polarity distribution of Earth's magnetic field within the last ca. 3 Myr, with some shallowing of inclination. Combining our magnetostratigraphy results with data from previous boreholes and fossil ostracod ages, the age of SG-1 can be determined to the period between ca. 2.7 Ma to 12 ka, including the later Gauss epoch, the complete Matuyama epoch and almost the entire Brunhes epoch (Figure 2a).

The average sediment accumulation rate (SAR) (Figure 2b) and magnetic susceptibility (MS) variation (Figures 2c,d) indicate three major changes at about 2.6 Ma, 2.2 Ma and 0.8 Ma, respectively, correlating well with the changes of lithology and fossil ostracod data. From the trend and spectral characteristics of MS (Figure 2e) and the SAR changes, combined with other available results, we conclude that significant tectonic activity and fluctuating continental aridification were prevailed between 2.6 and 2.2 Ma, followed by ongoing tectonic deformation and strengthening of aridification during the period 2.2 to 0.8 Ma, finally culminating in further intensification of tectonic activity and extreme aridification since the early Brunhes epoch (post-0.8 Ma).

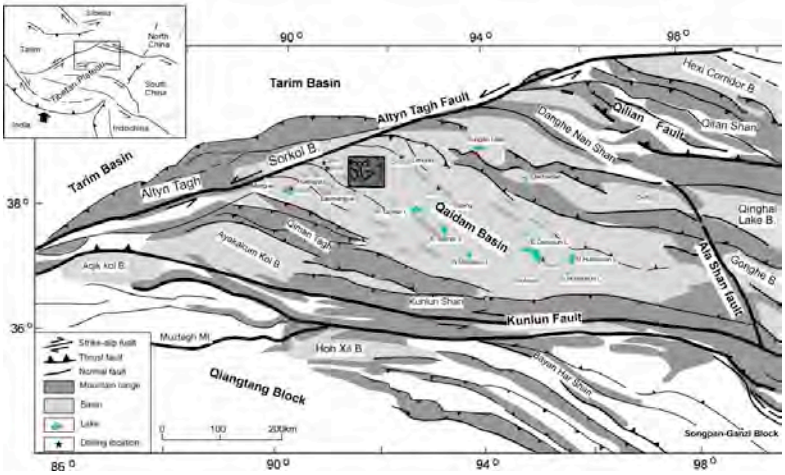

Figure 1. Structural setting of the Qaidam basin and adjacent regions (modified from Meyer et al. 1998). The drilling site SG-1 is indicated by the box.

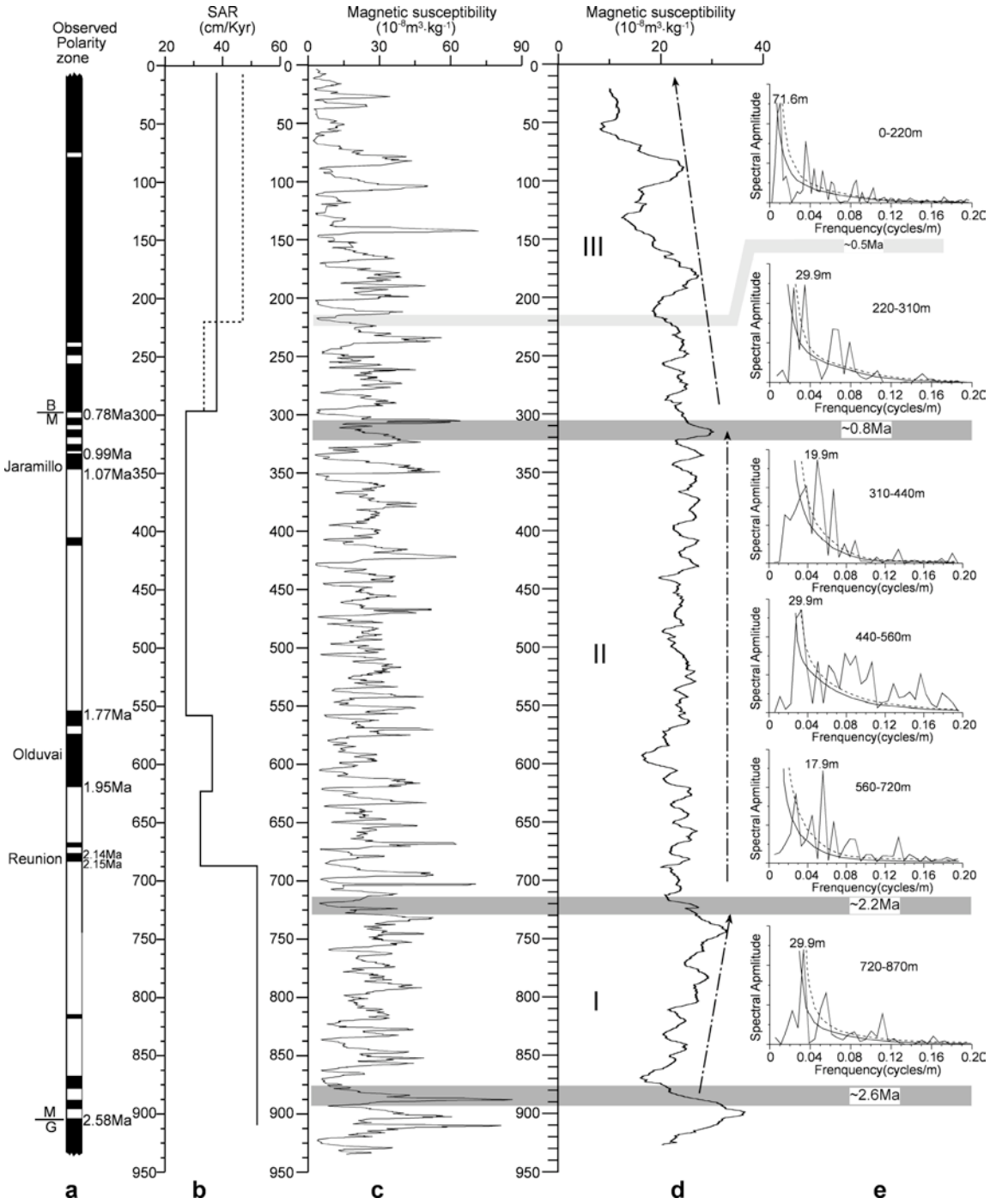

Figure 2. Results from SG-1: (a) observed magnetic polarity zones and interpreted boundaries; (b) sediment accumulation rate (SAR); SAR calculated by the magnetostratigraphic results is shown by solid line, and the dashed line represents a SAR model inferred from spectral analysis; (c-d) 5-point and 101-point running average of magnetic susceptibility; (e) spectral analysis of wavelengths using a smoothed 5-point running average susceptibility from distinct depth windows; full & broken lines denote red noise & 80% confidence level.

Reference

Meyer, B., and others, 1998, Crustal thickening in Gansu-Qinghai, lithospheric mantle subduction, and oblique, strike-slip controlled growth of the Tibetan plateau, Geophys. J. Int., 135, 1-47.

Cite as: Zhang, W., and others, 2010, Magnetostratigraphy of Core SG-1 in the Western Qaidam Basin and its Tectonic-Environmental Implications, *in* Leech, M.L., and others, eds., Proceedings for the 25th Himalaya-Karakoram-Tibet Workshop: U.S. Geological Survey, Open-File Report 2010-1099, 2 p. [http://pubs.usgs.gov/of/2010/1099/zhang/].

Organic Matter Studies for Hydrocarbon Generation in the Argillaceous Sediments of the Ladakh Himalaya, India

A.K.Awasthi[1], M.K.Moezabadi[2], A.K.Jain[1], S.Singh[1]

[1]Dept. of Earth Sciences, Indian Institute of Technology Roorkee, Roorkee-247667, India, prachfes@iitr.ernet.in
[2]Iranian Petroleum Institute, Tehran, Iran

The Indus Suture Zone is a major crustal lineament between the Himalayan range and Tibet. This important tectonic belt covering a lateral stretch of ~2500 km from the Hindukush mountains of Afghanistan to the Mishmi hills of Assam in India, has been interpreted as a collision boundary between the Indian plate in the south to the Eurasian plate in the north and is considered to be the site of Cretaceous subduction zone along which a large portion of pre-Tertiary Tethyan ocean crust was consumed (Gansser, 1977, and many others). The pre-Tertiary Tethys ocean is believed to have an important influence on the accumulation and distribution of petroleum in the world (Bois and others, 1982). Major oil fields of the world are found close to subduction zones (Figure 1) and from this point of view, the Indus Suture Subduction Zone becomes attractive. The present work was therefore taken up to investigate the organic matter and its thermal degradation for generation of petroleum hydrocarbons in the argillaceous sediments of the Ladakh area of the Indus Suture Zone in NW Kashmir Himalaya, India.

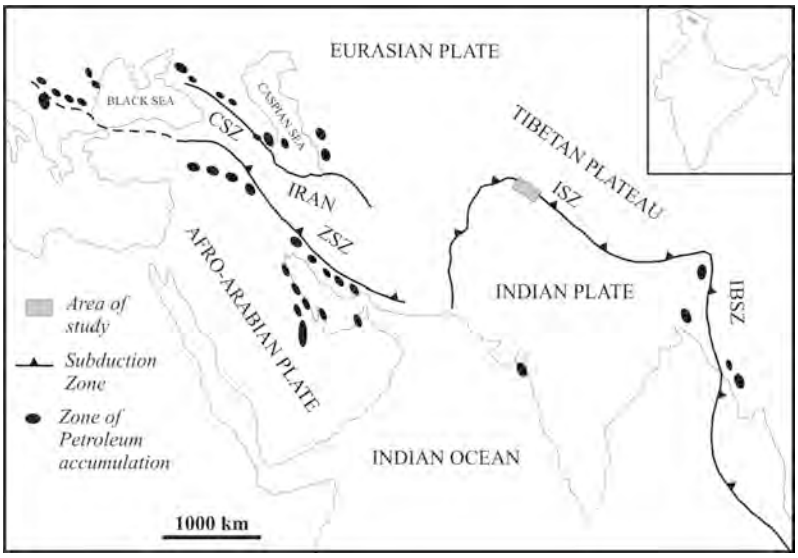

Fig. 1: Association of major oil fields with the subduction zone along Alpine-Zagros-Himalayan tectonic belt (modified after Bois and others, 1982).
ZSZ: Zagros Subduction Zone, ISZ: Indus Subduction Zone, IBSZ: Indo-Burma Subduction Zone, CSZ: Caucasus Subduction Zone.

Based on lithological character, vertical and lateral continuity and lithological associations, various lithostratigraphic units, namely the Lamayuru Formation, Nindum Formation, Indus Formation, Kargil Formation, Ladakh plutonic complex and Khardung Formation, have been identified. Organic matter content in the fine-grained, low-energy sediments such as shales is found to be higher as a rule than that in the coarse-grained high-energy sediments like sandstones and conglomerates. The present study is confined to the argillaceous sediments of the Lamayuru (Triassic-Jurassic), Nindum (Cretaceous) and Indus (Cretaceous-Eocene) formations in the Ladakh area.

The quantity, quality and thermal maturity of the organic matter contained in the shaly sediments of the Lamayuru, Nindum and Indus Formations form the subject of this study. Various geochemical and geooptical techniques have been used for characterization and evaluation of organic matter found in these sediments. A total of 35 shale samples (17 from the Lamayuru, 10 from the Nindum and 8 from the Indus Formation) were studied for this purpose.

Abundance of organic matter has been estimated on the basis of total organic carbon (TOC) content in the argillaceous sediments. The TOC percentage varies between 0.09-3.69 in the Lamayuru, 0.05-3.42 in the

Nindum and 0.03-5.18 in the Indus Formation. The mean TOC contents in the Lamayuru, Nindum and Indus formations are 1.24%, 0.94% and 1.91% by weight respectively. All these values are more than the minimum critical limit of 0.5% TOC, indicating thereby that these sediments have sufficient organic matter to be of importance in the generation of petroleum hydrocarbons in commercial amount.

The nature and type of organic matter has been determined by analysis of extractable organic matter, gas chromatographic analysis of saturate (C 15^{+}), optical examination of organic matter and stable carbon isotopic analysis. Higher percentage of aromatic as compared to saturated hydrocarbons, predominance of odd normal-alkane over even ones (C.P.I more than 1) and the ratio of pristane to phytane (mainly more than 1) indicate land-derived organic matter rich in type III kerogen with a minor amount of type II kerogen. This is further supported by the presence of vitrinite, fusinite, cuticle and woody organic matter found in shales of these formations. Such types of organic matter are prone to generate mainly hydrocarbon gas.

The thermal degradation (thermal maturation) of organic matter was determined on the basis of vitrinite reflectance, thermal alteration index (T.A.I) and gas chromatographic analysis of C 15^{+}. The mean vitrinite reflectance values vary from 0.6-1.7%, 1.44-1.51% and 1.34-1.44% in the Indus, Nindum and Lamayuru formations respectively. These values indicate that organic matter in these formations has undergone sufficient thermal maturation to generate petroleum hydrocarbons. This inference is also corroborated by T.A.I values ranging from 2.25-3.5 in the Indus Formation, 3-3.75 in the Nindum Formation and 3-3.5 in the Lamayuru Formation. Low (< 50mg/g) extractable hydrocarbon to organic carbon ratio and dominance of pristane over phytane further corroborate the deductions that these sediments have undergone sufficient maturity to produce hydrocarbons.

All the three formations have sufficient organic matter of right quality (mainly the kerogen type III with little type II) and have undergone sufficient thermal maturation to generate petroleum hydrocarbons, mainly gas with little oil. The sediments of the Indus formation are more prospective than those of Nindum and Lamayuru formations as petroleum source rocks. Though the studies are based on limited samples, the results encourage us to continue with detailed source-rock studies.

References

Gansser, A., 1977, The great suture zone between Himalaya and Tibet: a preliminary account, In: V.C.Thakur (ed.), Regional framework and geodynamic evolution of the Indus Tsango Suture Zone in the Ladakh Himalayas, Trans. Roy. Soc. Edinburgh: Earth Sciences, 73, 205-219.

Bois, C., Bonche, P. and Pelet, R., 1982, Global geologic history and distribution of hydrocarbon reserves, Am. Assoc. Petrol. Geol. Bulletin, 66, 1248-1270.

Cite as: Awasthi, A.K., Moezabadi, M.K., Jain, A.K. and Singh, S., 2010, Organic Matter Studies for Hydrocarbon Generation in the Argillaceous Sediments of the Ladakh Himalaya, India, *in* Leech, M.L., and others, eds., Proceedings for the 25th Himalaya-Karakoram-Tibet Workshop: U.S. Geological Survey, Open-File Report 2010-1099, 2 p.
[http://pubs.usgs.gov/of/2010/1099/awasthi/].

Timing of Earliest India-Asia Contact: Evidence of Terrestrial Vertebrates from Cambay Shale, Gujarat, Western Peninsular India

Sunil Bajpai[1]

[1]Department of Earth Sciences, Indian Institute of Technology, Roorkee 247 667, India, sunilbajpai2001@yahoo.com

India's physical and biotic links following its break-up from the Gondwana supercontinent continue to be debated in the context of geodynamic plate tectonic models (Ali and Aitchison, 2008). One of the most interesting, though controversial, issues concerns the timing of the collision between India and Asia, for which estimates ranging from approximately 65 to 35 Ma have been proposed. The collision was characterized by major faunal changes that include the origin and radiation of new mammalian communities in the Indian subcontinent, documented in recent years from the Eocene sedimentary sequences of Kutch and Surat (Gujarat) and the Subathu Formation of NW Himalaya in Himachal Pradesh and Jammu & Kashmir. A major recent find is the early Eocene (ca. 54-55 Ma) terrestrial vertebrate fauna which was discovered in a lignite mine at Vastan, District Surat (Gujarat state), western India (Bajpai et al. and others, 2008 a,b; Prasad and Bajpai, 2008). These Vastan mammals constitute the oldest record of the Cenozoic terrestrial mammal fauna of South Asia, and the described taxa include primitive members of several placental land mammal orders including artiodactyls, perissodactyls and primates (APP taxa). Elsewhere, in the holarctic (northern) continents, these mammalian taxa make their first appearance slightly earlier (ca. 55.5 Ma), during the intense warming interval that coincided at the Paleocene-Eocene boundary.

The presence of early Eocene holarctic mammals in India, especially those of medium-to-large size date the earliest Cenozoic faunal exchanges between India and Eurasia, providing independent evidence that subareal contact was established between these landmasses by at least 54 Ma, in response to the initiation of India-Asia collision. The Vastan data also raises the possibility of an Indian origin and subsequent migration to northern continents for some of the modern groups.

References

Ali, J.R. and Aitchison, J.C., 2008, Gondwana to Asia: Plate tectonics, paleogeography and the biological connectivity of the Indian sub-continent from the Middle Jurassic through latest Eocene (166–35 Ma), Earth Sci. Rev., 88 , 145-166.

Bajpai, S., and others, 2008a, The oldest Asian record of Anthropoidea, Proceedings of the National Academy of Sciences, USA, 105, 11093-11098.

Bajpai, S. and Kapur, V.V., 2008b, Earliest Cenozoic frogs from the Indian subcontinent: implications for out-of-India hypothesis, Journal of the Palaeontological Society of India, 53, 65-71.

Prasad, G.V.R. and Bajpai, S., 2008, Agamid lizards from the early Eocene of western India: oldest Cenozoic lizards from South Asia, Palaeontologia Electronica, 11, 4A, 1-19.

Cite as: Bajpai, S., 2010, Timing of Earliest India-Asia Contact: Evidence of Terrestrial Vertebrates from Cambay Shale, Gujarat, Western Peninsular India, *in* Leech, M.L., and others, eds., Proceedings for the 25th Himalaya-Karakoram-Tibet Workshop: U.S. Geological Survey, Open-File Report 2010-1099, 1 p. [http://pubs.usgs.gov/of/2010/1099/bajpai/].

Thinning of Glaciers in the Khumbu Himal from 1955 to 2008

Adam D. Barker[1], Bernard Hallet[1]

[1] Department of Earth and Space Sciences, University of Washington, Seattle, WA 98195, USA, adbarker@uw.edu

The change of Himalayan glaciers is of considerable interest in terms of sea level change and regional climate change impacts including, in particular, altered runoff in Himalayan catchments (Nakawo and others, 1986). Glacial geologic evidence clearly document that glaciers throughout the Himalaya fluctuated during the late Pleistocene and Holocene (Owen and others, 2009). Documentation and understanding of glacier fluctuations are important components in the assessment of climate change consequences at temporal scales relevant to society (Dyurgerov, 2001). Recently, considerable scrutiny, from both scientific and public groups, has shed light on the dearth of measurements characterizing the mass balance of Himalayan glaciers. Clearly, the Himalaya and, in particular, Mt. Everest are extreme elements of topography on our planet, yet they and their glaciated catchments remain some of the least studied and poorly understood places on Earth.

This study on rates of glacier thinning in the Khumbu Himal bypasses the difficult logistics of field work in remote sites through the use of remotely-acquired satellite data. In particular, we focus this study on the Khumbu Glacier, a debris-covered glacier originating on the south face of Everest in the Nepalese Himalaya. We chose the Khumbu not only because large debris-covered glaciers are one of the most striking morphological features on the southern slopes of the higher Himalaya, but because it is one of the very few Himalayan glaciers with a wealth of existing glaciological observations and measurements. Additionally, the glacier's proximity to Mt. Everest and the logistical support that comes with being a large tourist attraction make this site an attractive location to launch a related study to determine rates of erosion and debris flux in a glaciated catchment. The work presented in this study augments this field-based study. Herein, we report estimates of glacier thinning and volume loses for the Khumbu Glacier and surrounding region using a comparison of a suite of satellite derived data and earlier cartographic maps based on photogrammetry.

To calculate glacier thinning rates, we difference the glacier elevation from a digitized and geo-referenced cartographic map made in 1955 and from satellite derived digital elevation models (DEMs). Three different DEMs are used, including two ASTER DEMs and one SRTM DEM. The ASTER DEMs represent a single day in 2003 and an average from 2000-2008 from the recently released global DEM. SRTM DEMs were collected during a single Space Shuttle mission in 2000. A summary of the difference analysis is shown in Figure 1. Below the Khumbu icefall (at ~5400 m), comparison between the ASTER GDEM and 1955 map shows an average thinning of 44 m and thinning rate of 0.8 m/yr. Above the icefall, the glacier continues to thin until ~5900 m. Thickening (34 m average) of the glacier occurs at elevations between 6000 and 6600 m. Overall, we calculate a volume loss of about 0.5 km^3 in 53 years.

In the late 90's, the ice thickness was measured with a ground-based radar system along several transverse transects in the ablation zone of the Khumbu Glacier (elevations < 5400 m). Figure 1, on the left side, shows that this region has the largest fraction of the total area of the glacier. Gades and others (2000) measured thicknesses of about 450 m near the icefall and decreasing to about 20 m near the terminus with an average ice thickness of about 180 m. If we make the simplistic assumption that the thinning rate remains 0.8 m/yr indefinitely, it will take approximately 225 years for the lower portion of this glacier to disappear.

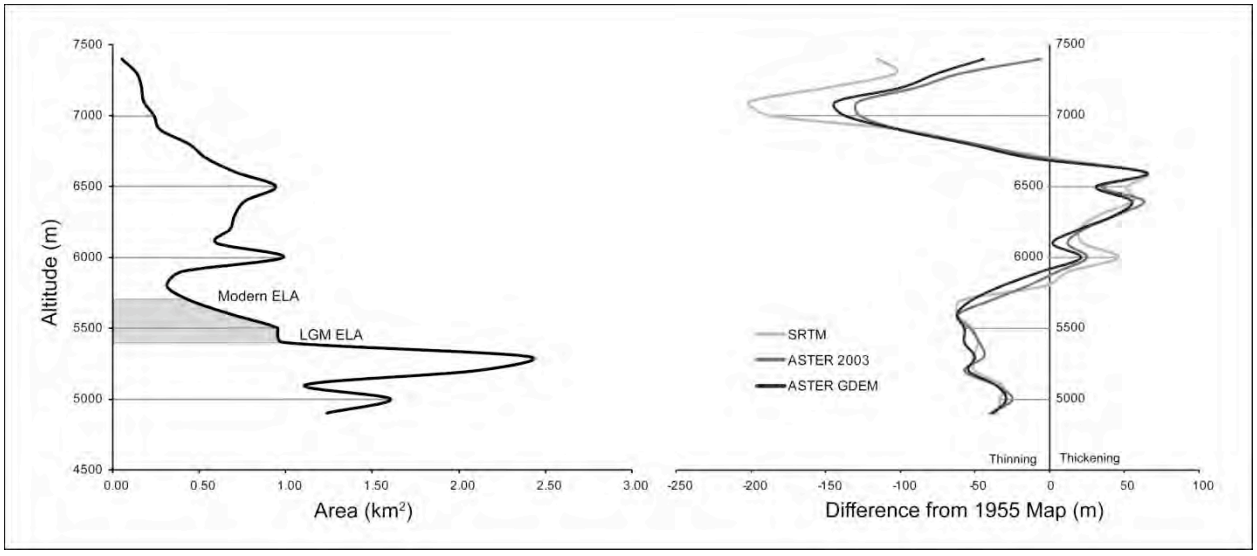

Figure 1. At left, area-altitude distribution of the Khumbu Glacier. The light gray box defines the approximate range of the modern and LGM equilibrium line altitude (ELA) (Owen, 2008). The peak in area just below 5500 m reflects the extensive debris covered ablation zone of the glacier. At right, each curve shows the difference in glacier elevation between one satellite derived DEM and the 1955 map. Below the icefall (at ~5400 m), for example, comparison between the ASTER GDEM and 1955 map shows an average thinning of about 44 m in 53 years, amounting to an average thinning rate of ~0.83 m/yr.

References

Dyurgerov, M.B., 2001, Mountain glaciers at the end of the twentieth century: global analysis in relation to climate and water cycle, Polar Geog., 241-338.

Gades, A., Conway, H., Nereson, N., Naito, N. and Kadota, T., 2000, Radio echo-sounding through supraglacial debris on Lirung and Khumbu Glaciers, Nepal Himalaya, in: Debris-covered Glaciers, IAHS Publ.

Nakawo, M., Iwata, S., Watanabe, O., and Yoshida, M., 1986, Processes which distribute supraglacial debris on the Khumbu Glacier, Nepal Himalaya, Ann. Glac., 8, 129-131.

Owen, L.A., 2008, Latest Pleistocene and Holocene glacier fluctuations in the Himalaya and Tibet, Quaternary Sci. Rev., 1-15.

Owen, L.A., and others, 2009, Quaternary glaciation of Mount Everest, Quaternary Sci. Rev., 28, 1412–1433.

Cite as: Barker, A.D. and Hallet, B., 2010, Thinning of Glaciers in the Khumbu Himal from 1955 to 2008, *in* Leech, M.L., and others, eds., Proceedings for the 25th Himalaya-Karakoram-Tibet Workshop: U.S. Geological Survey, U.S. Geological Survey, Open-File Report 2010-1099, 2 p. [http://pubs.usgs.gov/of/2010/1099/barker/].

Himalayan-Tibetan Orogeny: Channel Flow versus (Critical) Wedge Models, a False Dichotomy?

Christopher Beaumont[1], Rebecca Jamieson[2]

[1]Department of Oceanography, Dalhousie University, Halifax, NS, B3H 4J1, Canada, chris.beaumont@dal.ca
[2]Department of Earth Sciences, Dalhousie University, Halifax, NS, B3H 4J1, Canada

Two classes of hypotheses supported by models, here termed Channel Flow and (Critical) Wedge, have been central to recent discussions concerning the evolution of the Himalayan-Tibetan orogen. The first type, Channel Flow (see Grujic, 2006; Klemperer, 2006; Hodges, 2006; Harris, 2007 for overviews), provides an explanation of the development of the Greater Himalayan Sequence as a consequence of the extrusion of a weak mid-crustal channel at the surface. In the Beaumont and others models (Beaumont and others, 2001, Jamieson and others, 2006) channel flow develops in the thickened orogenic crust by ductile weakening following thermal relaxation and radioactive heating, augmented by a small component of 'melt' weakening. Channel flow is driven outward from beneath the orogen by the pressure difference between the plateau and the foreland, and the channel is interpreted to have been uplifted and exhumed to the surface by climate-enhanced erosion focused on the flank of the plateau. Exhumation occurs between coeval basal thrust-sense, and overlying normal-sense, shear zones. The channel flow model also predicts the formation of a plateau in regions where the strength of the crust is sufficiently low that it will not support topographic gradients. Where not exhumed the channel 'tunnels' beneath the flank of the orogen. In general, crust in this region is too cold and the viscosity too high for the channel to be injected (Medvedev and Beaumont, 2006). Instead, the channel only advances when the adjacent crust has thickened, thermally relaxed, and weakened sufficiently to join the channel flow. The region between the foreland and the active channel, corresponding to the Siwaliks and Lesser Himalaya, develops as a thrust wedge (Beaumont and others, 2001 Fig.4c) and this wedge is more fully developed when there is a weak near-surface decollement layer in the model (Jamieson and others 2006, Fig. 4, model HT111). The foreland is flexed downward to form a foreland basin. These models are thermo-mechanically coupled and they evolve dynamically subject to prescribed basal boundary conditions and surface erosion, which depends on the product of the local surface slope predicted by the model, and an erosion rate coefficient modulated by a climate scale that varies between 0 (no erosion) and 1 (highly erosive).

In the second, (Critical) Wedge class of models, the Himalaya is interpreted to have evolved as a wedge (Kohn, 2008) which may / may not be critical (Dahlen, 1984), or a variant on this approach including reconstruction of wedges using balanced cross sections (e.g. DeCelles and others, 2001; Robinson and others, 2006), or transport of thrust sheets over a basal ramp-flat system. Many models in this class either use thermo-kinematic models to predict the thermal evolution of the system in response to prescribed velocity fields and surface erosion (e.g. Henry and others 1997; Bollinger and others, 2006; Whipp and others, 2007; Robert and others, 2009) or base their interpretations on this type of model (e.g., Kohn, 2008).

The discussion of the relative merits of these models has in some instances portrayed them as mutually exclusive; it was either Channel Flow, or (Critical) Wedge, or possibly another mechanism that accounts for the large-scale tectonic evolution the Himalayan system (e.g., Robinson and others, 2006; Robinson and Pearson, 2006; Kohn, 2008). Here we present the case that the two types of models are not mutually exclusive and that we should expect the corresponding tectonic styles to coexist in nature.

We first present model results that show how an orogenic system evolves through several phases: 1, Bivergent critical wedges (while the system is cold); 2, Plateau bounded by critical wedges (as the interior of the system becomes too weak to sustain topographic gradients); 3,Tunnelling channel flow; 4, Exhuming channel, and; 5, Waning channel exhumation. During Phases 3-5 the part of the orogen external to the channel develops as a critical wedge. This is entirely consistent with this part of the orogen being too cold for the channel to tunnel into it.
We then show that as erosion rates decrease and exhumation of the channel is suppressed, the critical wedge expands into the orogen to encompass the region of the exhumed former channel. Lastly, we

demonstrate reactivation of the Main Central Thrust as an out-of-sequence thrust when significant focused erosion returns to the flank of the plateau. We conclude that there is no real dichotomy between channel flow and critical wedge styles of behaviour in orogen tectonic models, and most likely in nature as well. The interior plateau region of the orogen will be governed by the flow of hot, weak mid- or lower crust and may develop channel flows or other deformation styles (Jamieson and others, 2007). Beneath the flank of the orogen, channel flow will coexist with, and be juxtaposed against, an external critical wedge (foreland-fold-thrust belt). Depending on the rates of surface erosion and basal boundary conditions this part of the system will behave as a tunneling or exhuming channel system with external critical wedge, as a thrust-sense critical wedge, or as an unstable system subject to gravitational spreading. The system is expected to migrate among these behaviours as external conditions vary.

In regard to the Himalayan-Tibetan system we infer:

1) A first phase of Early Miocene channel exhumation coincided with protracted intense erosion focussed on the southern flank of the orogen;
2) As erosion rates progressively waned from Mid-Miocene onward, channel exhumation ceased and the whole flank of the orogen cooled and became a thrust-sense critical wedge with the tip of the channel tunnelling at the edge of the plateau;
3) The return of more aggressive erosion (~3 Ma) has reactivated, or is in the process of reactivating, the Main Central Thrust as an out of sequence thrust; ahead of a channel now situated beneath the plateau;
4) If this aggressive erosion persists for approximately 10 Ma, the modern channel will be exhumed in a similar manner to that of the first Miocene phase.

References

Beaumont, C., Jamieson, R.A., Nguyen, M.H. and Lee, B., 2001, Himalayan tectonics explained by extrusion of a low viscosity crustal channel coupled to focused surface denudation, Nature, 414, 738-742.

Bollinger, L., and others, 2004, Thermal structure and exhumation history of the Lesser Himalaya in central Nepal, Tectonics, 23, TC5015, doi:10.1029/2003TC001564.

Dahlen, F. A., 1984, Noncohesive critical Coulomb wedges: An exact solution, J. Geophys. Res., 89,10125-10133.

DeCelles, P.G., and others, 2001, Stratigraphy, structure, and tectonic evolution of the Himalayan fold-thrust belt in western Nepal, Tectonics, 20, 487-509.

Grujic, D., 2006, Channel flow and continental collision tectonics: an overview, Geol. Soc. Lond. Spec. Pub., 268,25-37.

Harris, N., 2007, Channel flow and the Himalayan-Tibetan orogen: a critical review, J. Geol. Soc. Lond., 164, 511-523.

Henry, P., Le Pichon, X. and Goffe, B., 1997, Kinematic, thermal and petrological model of the Himalayas; constraints related to metamorphism within the underthrust Indian crust and topographic elevation, Tectonophysics, 273, 31-56.

Hodges, K.V.A., 2006, A synthesis of the Channel Flow-Extrusion hypothesis as developed for the Himalayan-Tibetan orogenic system, Geol. Soc. Lond. Spec. Pub., 268, 71-90.

Klemperer, S.L., 2006, Crustal flow in Tibet: geophysical evidence for the physical state of Tibetan lithosphere, and inferred patterns of active flow, Geol. Soc. Lond. Spec. Pub., 268, 39-70.

Kohn, M.J., 2008, P-T-t data from central Nepal support critical taper and repudiate large-scale channel flow of the Greater Himalyan Sequence, Geol. Soc. America Bulletin, 120, 259-273.

Jamieson, R. A., Beaumont, C., Nguyen, M.H. and Culshaw, N.G., 2007, Synconvergent ductile flow in variable-strength continental crust: Numerical models with application to the western Grenville, Tectonics, 26, TC5005, doi:10.1029/2006TC002036.

Jamieson, R.A., Beaumont, C., Nguyen, M.H. and Grujic, D., 2006, Provenance of the Greater Himalayan Sequence and associated rocks; predictions of channel flow models, Geol. Soc. Lond. Spec. Pub., 268, 165-182.

Medvedev, S. and Beaumont, C., 2006, Growth of continental plateaus by channel injection: models designed to address constraints and thermomechanical consistency, Geol. Soc. Lond. Spec. Pub., 147-164.

Robert, X., and others, 2009, Assessing quaternary reactivation of the Main Central thrust zone (central Nepal Himalaya): new thermochronological data and numerical modeling, Geology, 37, 731-734.

Robinson, D. M., DeCelles, P. G. and Copeland, P., 2006, Tectonic evolution of the Himalayan thrust belt in western Nepal: Implications for channel flow models, Geol. Soc. America Bulletin, 118, 865-885.

Robinson, D.M. and Pearson, O.N., 2006, Exhumation of Greater Himalayan rock along the Main Central Thrust in Nepal: implications for channel flow, Geol. Soc. Lond. Spec. Pub., 268, 255-268.

Whipp, D.M. Jr., and others, 2007, Plio-Quaternary exhumation history of the central Nepalese Himalaya: 2 Thermokinematic and thermochronometer age prediction model, Tectonics, 26, TC3003, doi:10.1029/2006TC001991.

Cite as: Beaumont, C. and Jamieson, R.A., 2010, Himalayan-Tibetan orogeny: channel flow versus (critical) wedge models, a false dichotomy, *in* Leech, M.L., and others, eds., Proceedings for the 25th Himalaya-Karakoram-Tibet Workshop : U.S. Geological Survey, Open-File Report 2010-1099, 2 p., [http://pubs.usgs.gov/of/2010/1099/beaumont/].

Petrology and geochemistry of the Xiugugabu ophiolitic massif, western Yarlung Zangbo Suture Zone, Tibet

Rachel Bezard[1], Réjean Hébert[1], Chengshan Wang[2], Jaroslav Dostal[3], Jingen Dai[2]

[1] Département de géologie et de génie géologique, Université Laval, Québec, QC, G1K 7P4, Canada, rachel.bezard.1@ulaval.ca
[2] Research Center for Tibetan Plateau Geology, China University of Geosciences, Beijing 100083, China
[3] Department of Geology, Saint Mary's University, Halifax, NS, B3H 3C3, Canada

The Yarlung Zangbo Suture Zone (YZSZ), southern Tibet, is a more than 2000 km discontinuous belt composed of Neo-Tethyan Mesosoic ocean relics. The Xiugugabu ophiolitic massif is a thrust sheet of more than 260 km^2 overlying the tectonic mélange south of the YZSZ in SW Tibet. Its main lithologies are harzburgites and clinopyroxene(cpx)-harzburgites with porphyroclastic and porphyromylonitic textures. In the southern part of the massif, peridotites are intruded by amphibole(am)-bearing microgabbro and microgabbronorite sills. A diabase unit overlain by a sedimentary sequence crops out on the NE flank of the massif.

The orthopyroxene (Mg# 0.05-0.95, Cr_2O_3 1.03-0.10 wt. %), cpx (Mg# 0.92-0.99, Cr_2O_3 0.31-1.5) and olivine (Fo_{89-92}, NiO 0.35-0.50 wt. %) chemistry in harzburgites and cpx-harzburgites indicate compositions ranging from the abyssal to the forearc fields. The Mg# and Cr# (Cr/(Cr +Al) of the brown to reddish brown spinels range from 0.20-0.80 and 0.15-0.70 respectively, corresponding to 5-35% of partial melting. Non-modal fractional melting modelling shows a similar range of partial melting rate for the whole rock samples. Peridotites are slightly LREE enriched with $[La/Yb]_{CN}$ 0.06-2.8 and $[La/Sm]_{CN}$ 0.34-2.64. These ultramafic rocks are inferred to be the residues of 5-35% of partial melting that have been then percolated by metasomatic fluids in a supra-subduction context.

Am-microgabbro and am-microgabbronorite sills are mostly composed of brown to green amphibole (Mg# 0.72-0.87, TiO_2 0.66-1.64 wt. %), calcic plagioclase (An_{44-80}), cpx (En_{33-50}, Wo_{40-49}, Fs_{8-21}), ilmenite and orthopyroxene in gabbronorite. Textures and compositions of the brown amphiboles indicate a sub-solidus high temperature hydrothermal origin (> 800°C). These rocks are tholeiitic and show N-MORB type REE patterns ($[La/Yb]_{NC}$ 0.35-0.90), a LILE enrichment and noticeable Nb, Ta and Ti negative anomalies. These trace element compositions are similar to the Lau back-arc basin mafic rocks and also fit with the mantle diabase compositions of the central and eastern YZSZ ophiolites interpreted as being of back arc affinity. These mafic sills have suprasubduction affinity and are interpreted to have formed in a back-arc basin setting. The diabase unit cropping out to the NE of the massif has a strong alkalic composition and do not belong to the ophiolite. It suffered from low-grade hydrothermalism with chloritization, sericitization and interstitial quartz crystallisation but shows relics of sodic plagioclase (Or_{0-10}, An_{0-18}, Ab_{99-77}) brown-green amphibole (Mg# 0.49-0.77, TiO_2 0.22-0.43 wt. %) and needles of apatite. It is LREE enriched ($[La/Yb]_{NC}$ 8-8.9) and shows slight Nb, Ta and Ti negative anomalies. No significant crustal assimilation seems to be involved. The diabase is of oceanic intraplate affinity according to its multi-element pattern and may derive from an enriched mantle source. It is similar to the mélange-related alkalic mafic rocks found further east and formed within the Neo-Tethys. The absence of continental crustal contamination indicates that these rocks were emplaced after the Triassic disaggregation of the Indian plate.

Cite as: Bezard, R., and others, 2010, Petrology and geochemistry of the Xiugugabu ophiolitic massif, western Yarlung Zangbo Suture Zone, Tibet, *in* Leech, M.L., and others, eds., Proceedings for the 25th Himalaya-Karakoram-Tibet Workshop: U.S. Geological Survey, Open-File Report 2010-1099, 1 p. [http://pubs.usgs.gov/of/2010/1099/bezard/].

Geodesy and great earthquakes in the Himalaya

Roger Bilham[1]

[1]CIRES and Department of Geological Sciences University of Colorado, Boulder, CO 80309, U.S.A., bilham@colorado.edu

In the past three decades our knowledge of Himalayan collision processes has been changed radically by the application of GPS measurements across the plate boundary, by the clarification of historical accounts of damaging earthquakes, and most recently by the trench excavations across the frontal thrusts of the Himalaya. The single most important discovery is that the past five centuries of earthquakes include only those that are unrepresentative of the megaearthquakes with rupture lengths exceeding 500 km that permit India's northward advance beneath the Tibetan plateau. This is of particular concern when it is realized that populations in the region south of the Himalaya have increased by an order of magnitude in the past century. Perhaps the most important hitherto unresolved question concerns the mechanism that allows large shallow megathrusts to rupture southward over the descending Indian plate.

Early estimates of the convergence rate across the Himalaya were derived by calculating India/EuroAsian plate velocities from a consideration of global plate motions, and then summing cumulative moment release on the various tectonic features between Mongolia and southern Tibet to reveal the velocity across the Himalaya of 20±5 mm/a. Two alternative direct measures of convergence rate were proposed: an estimate for the rate of advance of sedimentary facies south of the frontal thrusts of the Himalaya, and a summation of seismic moment release for known Himalayan earthquakes. The first of these yielded convergence rates of 21±7 mm/a and the second was known to yield an estimate that was too low since less than 30% of the Himalaya has ruptured in the past two centuries, and earthquakes have yet to be observed to repeatedly rupture the same segment of the Himalaya.

Although precise geodetic measurements were introduced throughout India in the mid 19th century the direct measurement of the convergence velocity across the Himalaya was frustrated by the absence of geodetic triangulation crossing the range. In 1913 a line of triangulation points was measured by the Survey of India through Kashmir along what is now the Karakoram highway to Osh in the Pamir. The line was partially remeasured in 1980 with the inconclusive result that convergence of 2±1 m had occurred in this 76 year interval (26±13 mm/a). The estimate was rendered further uncertain by the unknown contribution from unmeasured segments of the line to the north and south. The 1980 measurements, however, were distinguished by being the first to apply space geodesy to the region using the cumbersome and low-precision TRANSIT satellites (Chen and others, 1984).

The application of GPS to the Indian plate was slowed by suspicions on the part of host countries linked to the complex and still unresolved border disputes between the contiguous nations in the region. The first GPS measurements in the Himalaya were undertaken by an Italian team organized by Ardito Desio in 1984 in connection with confirming the relative heights of Everest and K2. With this precedent established Nepal soon followed with a nationwide series of measurements that permitted the velocity field between southern Tibet and the Indian plate (20±3 mm/a) to be determined, a velocity field that serendipitously lacked complexity as was evident from the simple elastic model that could be proposed to explain its essential features - a gently dipping Indian plate locked beneath the Greater Himalaya at depths shallower than 18 km and creeping steadily beneath the southern Tibet at deeper depths (Bilham and others, 1997). Subsequent GPS measurements confirm that this simple geometry prevails throughout most of the central Himalaya, with one or two caveats. The locking depth appears to follow closely the 3.5 km elevation contour as evidenced by a line of microseismicity that follows the transition from the locked to creeping upper surface of the Indian plate throughout the length of the Himalaya (Bollinger and others, 2004). The significance of the locking line is that it represents the northern edge of great ruptures in the Himalaya, and because the distance between the locking line and the frontal thrusts of the Himalaya varies along the arc, so must the steepness of the rupture zone and possibly also the geometric moment release in great earthquakes. The inferred ruptured width narrows from >100 km in the west to <80 km in the east, and is moreover segmented in numerous places along the arc as delineated by small (5 km) abrupt arc-normal offsets in microseismicity.

The second incremental advance of our understanding of earthquakes in the Himalaya followed the reassessment of intensities and sparse geodetic clues describing 19th and 20th century earthquakes. These studies showed that the rupture areas of earthquakes in 1803, 1833, 1897, 1905 and 1934 were smaller than believed hitherto, thereby implying a much greater of the Himalaya remains recently unruptured. Details of the largest and most recent great earthquake in, the 1950 Mw=8.5 event in eastern Assam remain enigmatic. These studies provide unexpectedly, as yet incompletely realized insights into microzonation in the sedimentary plains south of the Himalaya. A recently published compilation of more than 7700 intensity observations in India promises further refinement of estimates of seismic risk.

Perhaps the most important advance in the past decade has been the discovery that the thrust faults fronting the Himalaya, which have not been associated with surface rupture in any of the past 300 years, ruptured in earthquakes with surface slip of 10-24 m in at least two earthquakes between 1150 and 1505 (Lave and others, 2005, Kumar and others, 2006). The estimated magnitudes of these earthquakes depending on the along-arc rupture lengths range from $8.6<Mw<9.0$, releasing 4 to 16 times more energy than the Bihar/Nepal earthquake of 1935. We remain ignorant concerning the recurrence intervals of these megaearthquakes but based on the observed geodetic convergence rate we may infer that they cannot occur more frequently on average than once every 1000-1200 years. The previous occurrence of these megaquakes would have occurred between the time of Buddha (in the eastern Himalaya) and around the time of decline of the Roman Empire (in the central and western Himalaya). Their next recurrence is not anticipated for a few centuries, although megaquakes cannot be excluded from the syntaxial regions where trench studies have yet to find evidence for historical ruptures

GPS geodesy in the western and eastern syntaxis reveals that velocity vectors are not influenced substantially by the curvature of the Himalayan arc. This is unexpected from considerations of the radial mechanisms of moderate and major earthquakes along the arc and requires that slip partitioning occurs near the two syntaxes. This raises an unresolved problem in Kashmir where slip is more than 40° oblique to the range front, and where no active strike-slip fault, other than the Karakoram fault system is known to be seismically active. The low rates of slip on the Karakoram fault are insufficient to accommodate the partitioned sinistral slip deficit in the Pir Pinjal, and it is tempting to conclude that earthquakes rupture obliquely southward beneath the range. The 2005 Kashmir Mw=7.6 earthquake will have advanced a Pir Pinjal earthquake closer to failure. A further unresolved problem in Kashmir concerns the low present rates of oblique convergence across the Pir Pinjal (3-6 mm/yr) and the relatively high rates of convergence (6-12 mm/yr) in the Zanskar ranges of western Ladakh. Although we have no record of historical seismicity in Zanskar the historical record of earthquakes in the Kashmir valley lacks sufficient detail to distinguish between ruptures occurring to its north or to its south. GPS measurements in Zanskar are too sparse as yet to clarify details of the locking line in Zanskar.

References

Bettinelli, P., and others, 2006, Plate motion of India and interseismic strain in the Nepal Himlayan from GPS and DORIS measurements, J. Geod., doi:10.1007/s00190-006-0030-3

Bilham, R., Larson, K., Freymueller, J. and Project Idylhim members, 1997, GPS measurements of present-day convergence across the Nepal Himalaya, Nature, 386, 61-64.

Bollinger, L., Avouac, J. P., Cattin, R. and Pandey, M. R., 2004, Stress buildup in the Himalaya, J. Geophys.Res., 109, doi:10.1029/2003JB002911.

Chen, W.-P. and Molnar, P., 1977, Seismic moments of major earthquakes and the average rate of slip in Central Asia, J. Geophys. Res. 82, 2945-2969.

Chen, J., Crompton, T., Walton, J. and Bilham, R., 1984, survey work of the International Karakorum Project, 1980, International Karakorum Project 1980, 2, Camb. Univ. Press., 124-139.

Kumar, S., and others, 2006, Paleoseismic evidence of great surface rupture earthquakes along the Indian Himalaya, J. Geophys. Res, 111, B03304,

Lave, J., and others, 2005, Evidence for a Great Medieval Earthquake (~1100 A.D.) in the Central Himalayas, Nepal, Science 307, 1302-1305.

Cite as: Bilham, R., 2010, Geodesy and great earthquakes in the Himalaya, *in* Leech, M.L., and others, eds., Proceedings for the 25th Himalaya-Karakoram-Tibet Workshop: U.S. Geological Survey, Open-File Report 2010-1099, 2 p. [http://pubs.usgs.gov/of/2010/1099/bilham/].

A New Quaternary Strand of the Karakoram Fault System, Ladakh Himalayas

Wendy M. Bohon[1], Kip V. Hodges[1], J Ramon Arrowsmith[1], Alka K. Tripathy[1]

[1]School of Earth and Space Exploration, Arizona State University, Tempe, AZ 85287, USA, wendy.bohon@asu.edu

The NW-SE striking, dextral Karakoram fault system stretches for more than 1200 km from the Pamirs of Central Asia at least as far southeast as the Kailas area of Tibet. Estimates for the total lateral displacement along the fault system range from 150-1000 km, and estimated Quaternary rates of slip range from 1 to 30 mm/yr. In the Ladakh region of NW India (~ 33°28'N, 78°45'E), the fault system expresses as northern and southern strands bounding the Pangong Range. Studies of ductile deformation fabrics along these strands suggest that slip began in the Miocene, and Brown and others (2002) documented Quaternary right-lateral slip along the northern strand at ~4 mm/yr on the basis of offset geomorphic features. The lack of documented Quaternary offset along the southern strand has led most researchers to assume that Quaternary slip on the Karakoram fault system in this region was partitioned exclusively to the northern strand.

Our summer 2009 field work in the Pangong Range and adjacent Nubra Valley provides the first documentation of significant Quaternary activity along the southern strand. In the valley between the villages of Tangste (34°01' N, 78°10' E) and Durbuk (34°06' N, 78°07'), the fault is visible high on the northeastern mountain side as a break in slope with offset Quaternary paleosurfaces and beheaded and offset stream channels, the largest of which have been displaced by as much as 250 m. Field mapping north of Durbuk, near the town of Tangyar (34°15'N, 77°52'E), shows that the southern strand continues northwest and cuts across the landscape as a sinuous, continuous trace with shutter ridges, offset alluvial fan surfaces, and sag ponds developed along its length. In this region, the northern and southern strands are linked by a Quaternary, east-directed thrust fault that places high-grade metamorphic rocks over poorly consolidated Quaternary alluvium. The partitioning of dextral slip between two strands of the Karakoram system, rather than one strand, suggests that previous estimates of total Karakoram fault system slip rates in this sector of the Himalaya may be too low. Efforts to determine the slip rate on the newly recognized active strand and to better quantify total slip rates are underway. Determining these rates is essential for answering first-order questions about the evolution and behavior of the Karakoram fault system in this region, the late-stage exhumation kinematics of the Pangong Range, and regional seismic hazard potential.

Cite as: Bohon, W.M., Hodges, K.V., Arrowsmith, J.R. and Tripathy, A.K., 2010, A New Quaternary Strand of the Karakoram Fault System, Ladakh Himalayas, *in* Leech, M.L., and others, eds., Proceedings for the 25th Himalaya-Karakoram-Tibet Workshop: U.S. Geological Survey, Open-File Report 2010-1099, 1 p. [http://pubs.usgs.gov/of/2010/1099/bohon/].

Simultaneous Earthquake Pulses along the Main Himalayan Thrust

Laurent Bollinger[1], Dili Ram Tiwari[2], Sudhir Rajaure[2], Soma Nath Sapkota[2], Jean-Phillipe Avouac[3]

[1] Department Analyse et Surveillance Environnement, CEA/DIF, Arpajon, 91297, FRANCE, laurent.bollinger@cea.fr
[2] Department of Mines and Geology, National Seismological Centre, Lainchaur, Kathmandu, NEPAL
[3] Caltech, Pasadena, California, U.S.A.

The Nepalese Seismological network records a dense midcrustal microseismicity along the front of the high Himalayan topography. Its time structure is complex but mostly dominated by some seasonal oscillations, winter seismicity being twice as dense as summer. Various sources of natural and cultural seismic noises are suspected to affect the detection capacities of the network and therefore cause a large part of this seismic-event rate modulation. Among them, the high-frequency seismic noise generated by debris flow (Burtin and others, 2009) and the sediment transport in the rivers during the summer monsoon (Burtin and others, 2008) have been recognised as major contributors to the noise level in the region. However, a significant part of the seasonality at intermediate magnitude ($2<ML<4$) appear to be genuine and modulated by seasonal stress variations (Bollinger and others, 2007). An important contributor to these stress variations is the hydrological loading-unloading of the India plate, a mechanism evaluated using gravimetrical and continuous GPS time series (Bettinelli and others, 2008). Despite these conclusions, further examinations of the seismic catalogue are required to better constrain the sensitivity of the microseismic midcrustal cluster to spatiotemporal modulations of stresses induced by various forcing.

For this purpose we investigate further the seismic catalogue and focus on the period 1996-1997, encompassing the most dramatic seasonal variations ever recorded. These variations appear dominated by the simultaneous development in December-January of three distinct seismic swarms, located hundreds of kilometres from each other, along the Main Himalayan Thrust (MHT). Their normalised time structures appear very similar, including a pre-swarm decrease in seismic events rate and a pre-mainshocks microseismicity pulse. Another similarity comes from their location at midcrustal depths, at the front of the high topography and within the trace of Southern Tibetan grabens prone, a few months later, to a large seismic crisis. In a Mohr-Coulomb criterion space, these places along the Himalayan arc appear more sensitive than others to small strain perturbations, particularly to slip-rate accelerations on the creeping part of the Main Himalayan Thrust, being sites of the occurrence of subtle transient events.

References

Bettinelli, P., and others, 2008, Seasonal variations of seismicity and geodetic strain in the Himalaya induced by surface hydrology, Earth Planet. Sc. Lett., doi:10.1016/j.epsl.2007.11.02110, 266, 332-344.

Bollinger, L., and others, 2007, Seasonal modulation of seismicity in the Himalaya of Nepal, Geophys. Res. Lett., 34, L08304, doi:10.1029/2006GL029192

Burtin, A., Bollinger, L., Vergne, J., Cattin, R. and Nabelek, J., 2008, Spectral analysis of seismic noise induced by rivers: A new tool to monitor spatiotemporal changes in stream hydrodynamics, J. Geophys. Res., 113, doi:10.1029/2007JB005034

Burtin, A., Bollinger, L., Cattin, R., Vergne, J. and Nábělek, J.L., 2009, Spatiotemporal Sequence of Himalayan Debris Flow from Analysis of High-Frequency Seismic Noise, J. Geophys. Res., doi:10.1029/2008JF001198

Cite as: Bollinger, L., Tiwari, D.L., Rajaure, S., Sapkota, S.N., Avouac, J.P., 2010, Simultaneous Earthquake Pulses along the Main Himalayan Thrust, *in* Leech, M.L., and others., eds., Proceedings for the 25th Himalaya-Karakoram-Tibet Workshop: U.S. Geological Survey, Open-File Report 2010-1099, 1 p. [http://pubs.usgs.gov/of/2010/1099/bollinger/].

The INDEPTH Transect: Looking Back from Golmud to Yadong

Larry D. Brown[1], Wenjin Zhao[2], Project INDEPTH Team

[1] Institute for the Study of the Continents, Cornell University, Ithaca, NY 14853, U.S.A., ldb7@cornell.edu
[2] Chinese Academy of Geological Sciences, Beijing, People's Republic of China

In the summer of 2010, Project INDEPTH will essentially achieve its original vision of a modern geological and geophysical transect across of the Tibetan Plateau. INDEPTH IV, a suite of surveys focussed on the northeastern boundary of the Tibetan Plateau, represents the culmination of an initiative that began in 1992 with a simple multichannel reflection profile in the Himalayas, augmented by a modest wide-angle piggyback experiment (Zhao, Nelson and others, 1993). By the time INDEPTH reached the Qaidam basin, both the techniques for probing, and concepts put forward to explain, the Himalaya-Tibet collision zone had undergone a dramatic evolution. The INDEPTH profiles now stand as but one of a number of major seismic experiments that have probed key aspects of lithospheric structure and process.

Originally intended to focus primarily on the application of the then relatively novel multichannel seismic reflection technique to detail crustal structure, INDEPTH quickly evolved to integrate active (reflection, refraction) and passive (receiver function, tomographic inversion of earthquake recordings) seismology, and to link the seismic results with magnetotelluric observations in a particularly compelling manner. This combination proved critical to the interpretation of crustal melting at the southern margin of the plateau (Nelson and others, 1996). INDEPTH IV, for example, choreographed reflection (P wave), refraction (P and S wave), receiver function and magnetotelluric profiles across the Kunlun Mountains (Zhao and others, 2008), with a regional 2D seismic array (ASCENT) to probe mantle structure from central Tibet to the Qilian Shan northeast of the Qaidam Basin.

INDEPTH's targets have also shifted in response to the evolution of tectonic models emerging to explain the uplift of the plateau, from detailing the geometry of underthrusting of the Indian plate (Zhao, Nelson and others 1993), to the significance of channel flow in plateau uplift (Klemperer, 2006), to defining the mantle suture beneath central Tibet (Tillman and others, 2003) to searching for evidence of southward underthrusting of Asia along the northern boundary of the plateau (Kind and others, 2002). Beyond their initial interpretations, INDEPTH results have served as important components in joint analysis with observations from other major seismic experiments in Tibet (e.g. Li and others, 2008). The latest results from INDEPTH IV and the complementary ASCENT project are the focus of other presentations at this meeting. Here we take this opportunity to look back over the key findings of the INDEPTH traverse with the perspectives provided by subsequent geophysical surveys that have also confronted issues that were the focus of the INDEPTH effort (e.g. Nabelek and others, 2009).

References

Kind, R., and others, 2002, Seismic images of crust and upper mantle beneath Tibet; evidence for Eurasian Plate subduction, Science, 298, 1219-1221.

Klemperer, S.L., 2006, Crustal flow in Tibet: geophysical evidence for the physical state of Tibetan lithosphere, and inferred patters of active flow, in Law R.D., M.P. Searle and L. Godwin (eds), Channel Flow, Ductile Extrusion and Exhumation in Continental Collision Zones, Geological Society, London, Special Publications, 39-70.

Li, C., van der Hilst, R.D., Meltzer, A.S. and Engdahl, E.R., 2008, Subduction of the Indian lithosphere beneath the Tibetan Plateau and Burma, Earth and Planetary Science Letters, 274, 157-168.

Nabelek, J., and others, 2009, Underplating in the Himalaya-Tibet collision zone revealed by the Hi-CLIMB experiment, Science, 325, 1371-1274.

Nelson, K.D., and others, 1996, Partially molten middle crust beneath southern Tibet; synthesis of Project INDEPTH results, Science, 274, 1684-1688.

Tilmann, F., and others, 2003, Seismic imaging of the downwelling Indian lithosphere beneath central Tibet, Science, 300, 1424-1427.

Zhao, W., and others, 1993, Deep seismic reflection evidence for continental underthrusting beneath southern Tibet, Nature, 366, 557-559.

Zhao, W., and others, 2008, Seismology across the northeastern edge of the Tibetan Plateau, Eos Trans. AGU, 89(48).

Cite as: Brown, L.D, Zhao, W.J. and Project INDEPTH Team, 2010, The INDEPTH Transect: Looking Back from Golmud to Yadong, *in* Leech, M.L., and others, eds., Proceedings for the 25th Himalaya-Karakoram-Tibet Workshop: U.S. Geological Survey, Open-File Report 2010-1099, 1 p. [http://pubs.usgs.gov/of/2010/1099/brown/].

Middle Miocene Reorganization of Faulting and Depositional Patterns in Northeastern Tibet

Richard O. Lease[1], Douglas W. Burbank[1]

[1] Department of Earth Science, University of California, Santa Barbara, CA 93117, U.S.A., rlease@crustal.ucsb.edu

Variations in the direction and timing of range growth demonstrate how India-Asia convergence was manifest in northeastern Tibet (near 36°N, 103°E) throughout the Cenozoic. We detect a >45° change in shortening direction in middle Miocene time by examining (i) thermochronological relief transects from contractional ranges in combination with (ii) stratigraphic successions from adjacent foreland basins. Apatite (U-Th)/He and fission-track age-elevation relationships suggest an onset of rapid exhumation in the east-west trending Laji Shan at ~22 Ma. Rapid exhumation of the adjacent north-trending Jishi Shan, however, did not commence until ~13 Ma. Further support for this diachronous Miocene range growth emerges from records of subsidence, provenance, and paleoclimatic change from magnetostratigraphically dated sections in adjacent Xunhua and Linxia basins. Emergence of the east-west trending Laji Shan is highlighted in Xunhua basin by a doubling of sediment-accumulation rates between 24 and 21 Ma and by the introduction at 20 Ma of fluvial facies for which detrital zircon U/Pb age spectra show were sourced from basement terranes within the Laji Shan. In contrast, growth of the north-trending Jishi Shan is expressed by a 50% acceleration in Xunhua accumulation rates between 12 and 9 Ma and a doubling of detrital zircons derived from Jishi Shan sources by 11.5 Ma in the Linxia basin. Additionally, the divergence of Linxia and Xunhua oxygen isotopic values signals topographic isolation of these two basins by surface uplift of the intervening Jishi Shan by 11 Ma. Together these diverse observations document a middle Miocene change in the kinematic style of plateau deformation from initial north-south contraction along a trajectory that mimicked the India-Asia collision to the later onset of east-west contraction. This kinematic shift in northeastern Tibet coincides with expansion of the plateau margin in southeastern Tibet, as well as the onset of normal faulting in the high-elevation plateau interior, and may suggest a common geodynamic cause.

Cite as: Lease, R.O. and Burbank, D.W., 2010, Middle Miocene Reorganization of Faulting and Depositional Patterns in Northeastern Tibet, D.H., *in* Leech, M.L., and others, eds., Proceedings for the 25th Himalaya-Karakoram-Tibet Workshop,: U.S. Geological Survey, Open-File Report 2010-1099, 1 p. [http://pubs.usgs.gov/of/2010/1099/lease/].

Present-Day 3D Crustal Movement in the Qinghai-Tibetan Plateau from GPS Data

Caijun Xu[1], Kaihua Ding[1]

[1] School of Geodesy and Geomatics, Key Laboratory of Geospace Environment and Geodesy, Ministry of Education, Wuhan University, Wuhan, 430079, China, cjxu@sgg.whu.edu.cn

3D displacement rates of GPS monitoring sites in Qinghai-Tibetan Plateau are inferred from seven repeated GPS observation data, which were collected in 1993, 1995, 1997, 2000, 2002, 2007 and 2009 separately. GPS monitoring sites cross the Kunlun faults, the Karakorum-Jiali faults, the Yarlung-Zangbo suture and Yadong-Gulu rift. The movement of sub-blocks within the Plateau is analyzed according to the location of these sites, and the tectonic background of the Plateau.

Adopting previous divisions of the Plateau into sub-blocks, we have sites 0001 (Golmud), 0002 (Budongquan), 0003 (Erdaogou), 0004 (Yanshiping), 0005 (Wenquan), 0006 (Anduo), 0014 (Soxian), 0007 (Naqu) and 0008 (Lhasa) in the Tibetan sub-block, and sites 0009 (Ganzi), 0010 (Lhaze), 0011 (Nyalam), 0012 (Saga), 0013 (Xigaze) and 0015 (Yadong) in the Himalayan sub-block (Liu and others, 2000; Zhang and others, 2004). With reference to the Eurasia plate, the horizontal velocity of site 0008 is 23.3±0.4 mm/a, significantly less than the result of Liu and others (2000) (29.8±1.5 mm/a), but consistent with the result of Zhang and others (2004) (25.1±1.8 mm/a). The reason for the difference may be that only three periods of repeated surveying were processed, with less accurate orbits in early years. Provided that the velocity of the IGS site IISC (Bangalore) represents the subduction velocity of the India plate, the convergence rate of India-Asia collision is 19.0±0.5 mm/a, which is consistent with the results of Liu and others (2000) (19.5±1.7 mm/a) and Zhang and others (2004) (17±3 mm/a) (Zhang and others, 2004), and a result (18±7 mm/a) based on seismic and geological data (Armijo and others, 1986). Similarly, the shortening rate of the Tibetan sub-block in NS direction, represented by the velocity difference of site 0001 and 0008 in NS direction, is 9.1±0.6 mm/a, in agreement with the result of Liu and others (2000) (9.3±4.6 mm/a).

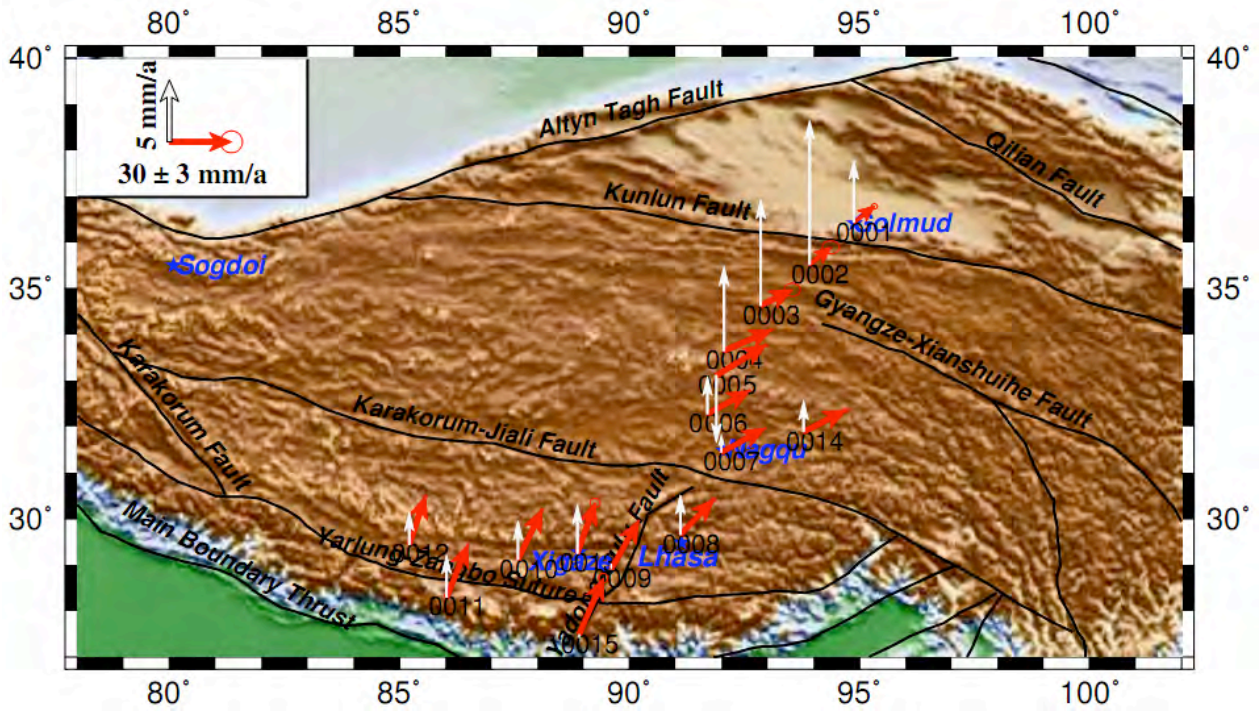

Figure 1. Present-day 3D velocity of GPS monitoring sites in Qinghai-Tibet Plateau. Red and white arrows represent the horizontal and vertical velocity of the sites, respectively.

We also calculated strain rates. The extension and contraction rates of the Himalayan sub-block are 9.4±0.9 nanostrain/yr and 26.6±3.8 nanostrain/yr respectively, less than the results of Chen and others (2004) (11.9±5.4 nanostrain/yr and 41.3±11.6 nanostrain/yr). The difference may be caused by the number and location of the sites. Our extension and contraction rates of the Tibet sub-block are 6.2±1.0 nanostrain/yr and 11.4±2.9 nanostrain/yr respectively, also less than the results of Chen and others (2004) (7.8±2.5 nanostrain/yr and 20.5±2.2 nanostrain/yr), and presumably for the same reason.

The EW extension of the plateau mainly occurs in the central part of the Tibetan sub-block. Relative to site 0001, the average EW extension rate of the other sites in the sub-block is 8.5±0.7 mm/a, consistent with the results of Liu and others (2000) (8.7±6.4 mm/a), Jiang and others (2008) (11.2±0.2 mm/a), and Armijo and others (1986) (10±5 mm/a) that was inferred from the secular average velocity of active faults. The opening rate of the Yadong-Gulu rift, inferred from the velocity difference between sites 0008 and 0009 in the direction $N20^0E$ is 4.9±0.4 mm/a, similar to the result of Chen and others (2004) (5.9±0.7 mm/a), and the dextral strike-slip rate of the Yarlung-Zangbo suture, inferred from the velocity difference between sites 0015 and 0009 in the direction $N20^0E$, is 2.8±0.9 mm/a, consistent with the result of Gan and others (2007) (2.5±1.1 mm/a).

Except for sites 0005 and 0015, the vertical velocities of our sites show ongoing uplift of the Tibetan Plateau. Site 0005 is very close to the Qinghai-Tibet Highway, and may be subsiding with the settlement of the highway. As for 0015, it has been surveyed only three times, and those measurements were early on, so the vertical velocity for this site is not considered reliable. Sites 0002, 0003 and 0013 have similar problems. Except for these sites, the average vertical velocity is 3.2 mm/a, which is less than previously estimated (4-5 mm/a) (Jiang and others, 2008).

In general, the present 3D crustal movement in the Qinghai-Tibet Plateau is characterized by compression in the NS direction, extension in the EW direction, and vertical uplift.

References

Liu J.N., and others, 2000, Present-day crustal movement and deformation in the Qinghai-Tibetan Plateau by GPS, Chinese Science Bulletin, 45, 2,658-2,663.

Zhang P.Z., and others, 2004, Continuous deformation of the Tibetan Plateau from GPS data, Geology, 32, 809-812.

Armijo R., Tapponnier, P., Mercier, J.L. and Tong-Lin, H., 1986, Quaternary extension in southern Tibet: Field observations and tectonic implications, J. Geophys. Res., 91, 13,803-13,872.

Jiang W.P., Zhou, X.H., Liu, J.N. and Xu, C.J., 2008, Present-day crustal movement and strain rate in the Qinghai-Tibetan Plateau from GPS Data, Acta Geodaetica et Cartographica Sinica, 37, 285-292.

Chen Q.Z., and others, 2004, Spatially variable extension in southern Tibet based on GPS measurements, J. Geophys. Res., 109, B09401, doi:10.1029/2002JB002350.

Gan W.J., and others, 2007, Crustal motion within the Tibetan Plateau inferred from GPS measurements, J. Geophys. Res., 112, B08416, doi:10.1029/2005JB004120.

Cite as: Xu, C. and Ding, K., 2010, Present-Day 3D Crustal Movement in the Qinghai-Tibetan Plateau from GPS Data, *in* Leech, M.L., and others, eds., Proceedings for the 25th Himalaya-Karakoram-Tibet Workshop: U.S. Geological Survey, Open-File Report 2010-1099, 2 p. [http://pubs.usgs.gov/of/2010/1099/caijunxu/].

Receiver function imaging in the western Himalaya

Warren B. Caldwell[1], Shyam S. Rai[2], Ashish[2], Simon L. Klemperer[1], Jesse F. Lawrence[1]

[1] Department of Geophysics, Stanford University, Stanford, CA 94305-2215, U.S.A., warrenc@stanford.edu
[2] National Geophysical Research Institute, Hyderabad, India 500 007

Method

The western Himalaya is sparsely studied and imaged compared to the central and eastern portions of the range. In this work, we contribute to the existing body of crustal images of the western Himalaya using an array located at 80°E (Figure 1). The array consists of ~20 stations with ~10 km spacing arranged linearly from SW to NE across the Himalayan thrust belt, from the Main Frontal Thrust (MFT) to the South Tibetan Detachment (STD). The array was active in 2005-2006, and was operated by India's National Geophysical Research Institute (Mahesh and others, 2010).

We generate crustal images using stacking of P-S receiver functions. We calculate receiver functions using an iterative time-domain method and depth-convert them by back propagation in an assumed velocity model, then bin and stack them to obtain two-dimensional images. This method, called common conversion point (CCP) stacking, stacks coherent energy from crustal conversions at the appropriate depths, while simultaneously canceling random noise. This generates a two-dimensional image of converting layers in the crust and mantle, such as abrupt changes in density or lithology caused by faults or other boundaries. Our model has a bin size of 1 km in depth and 10 km horizontally.

Receiver functions were picked using three different Gaussian windows (1, 2.5, 5) and manual time windowing. Spurious receiver functions were discarded by hand, in addition to automated discarding based on signal-to-noise ratio. Of the 23 stations, several had few or zero usable receiver functions. Of the remaining stations, the mean number of quality receiver functions per station was ~40.

The distribution of events is asymmetrical, with a strong concentration of events coming from the northeast (Japan). The remaining events were scattered mainly to the east and southeast, including events from Indonesia. Few events came from the west, and almost none from the south. To account for this azimuthal variability, we weight the receiver functions by backazimuth by binning in 10° increments and scaling the receiver functions in each bin by the number of receiver functions in that bin. Thus each 10° increment (assuming it contains events) has an equal contribution to the final image.

Results

Our results at present (Figure 2) show a Moho conversion at 40-50 km depth in the well-sampled region of our model. This depth is consistent with the Moho depth observed beneath the HiCLIMB array to the east (Nabelek and others, 2009). The Moho is typically the strongest and most continuous conversion in a receiver-function image, but in our image the Moho is not significantly stronger than other conversions, and exhibits some discontinuity. Mafic lower crust and eclogitization of lower-crustal material can be responsible for weak Moho conversions, due to the resulting lessening of the impedance contrast between crust and mantle. These phenomena have been speculated to occur in the subducted Indian lower crust (Nabelek and others, 2009, Schulte-Pelkum and others, 2005), but not in regions as close to the foreland as our study location.

For the HiCLIMB array (85°E, see Figure 1), Nabelek and others (2009) showed a strong azimuthal dependence in Moho visibility, with arrivals from the north illuminating the Himalayan Moho well, and arrivals from the south illuminating it poorly (the former being due to oblique incidence on a northward-dipping Moho and the latter being due to orthogonal incidence, which minimizes P to S conversions). The events recorded on our array were heavily-distributed in the northeast (approximately 5 times more northern events than southern events), so if the Moho in this region exhibits the same dip characteristics as in the nearby HiCLIMB region, our weak Moho is unlikely to be the result of weakly-illuminating southern events.

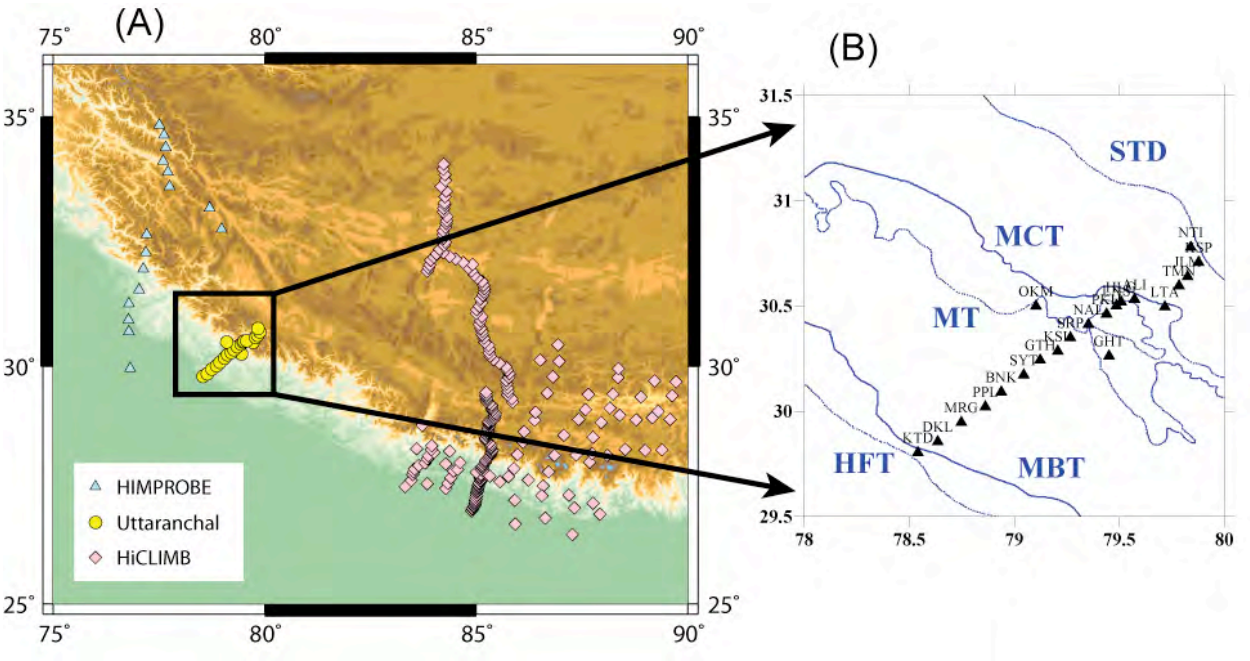

Figure 1. (A) Location of Uttaranchal broadband array used for this study in relation to nearby deployments. (B) Location of stations in relation to tectonic features. The array spans ~200 km and was composed of ~20 stations.

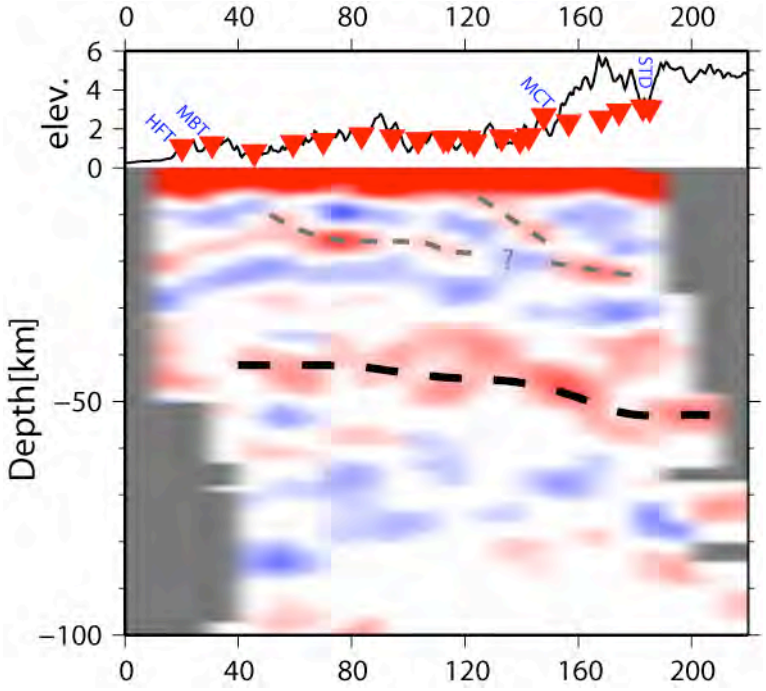

Figure 2. Receiver function CCP image with 10-km horizontal smoothing (red indicates positive impedance contrasts and blue indicates negative impedance contrasts). Bins with fewer than 25 rays are masked to gray. Upper panel shows vertically-exaggerated topography, station locations and approximate locations of the surface expressions of major faults. Approximate Moho shown with black dotted line. Thinner gray lines indicate impedance contrasts within the crust, likely thrust structures.

References

Mahesh, P., Rai, S.S., Sarma, P.R., Gupta, S., Sivaram, K., and Suryaprakasam, K., 2010, High resolution earthquake location and 3-D velocity imaging of crust beneath the Kumaon Himalaya, *in* Leech, M.L., and others, eds., Proceedings for the 25th Himalaya-Karakoram-Tibet Workshop: U.S. Geological Survey, Open-File Report 2010-1099, 2 p.

Nabelek, J., and others, 2009, Underplating in the Himalaya-Tibet Collision Zone Revealed by the Hi-CLIMB Experiment, Science, 325, 1371-1374.

Schulte-Pelkum, V., and others, 2005, Imaging the Indian subcontinent beneath the Himalaya, Nature, 435, 1222-1225.

Cite as: Caldwell, W.B, Klemperer, S.L., Lawrence, J.F. and Rai, S.S., 2010, Receiver function imaging in the western Himalaya, *in* Leech, M.L., and others, eds., Proceedings for the 25th Himalaya-Karakoram-Tibet Workshop: U.S. Geological Survey, Open-File Report 2010-1099, 2 p. [http://pubs.usgs.gov/of/2010/1099/caldwell/].

Miocene exhumation revealed by detrital minerals of Tajik rivers: Implications for the tectonic evolution of the Pamir

C.E. Lukens[1], B. Carrapa[1], B.S. Singer[2], G. Gehrels[3]

[1] Department of Geology and Geophysics, University of Wyoming, Laramie, WY 82071, U.S.A., clukens@uwyo.edu
[2] Department of Geoscience, University of Wisconsin-Madison, Madison, WI 53792, U.S.A.
[3] Department of Geosciences, University of Arizona, Tucson, AZ 85721, U.S.A.

The highest mountains on Earth are located in areas of continent-continent collision, such as the Himalaya, the Alps, and the Pamir of central Asia. Collision-related shortening and crustal thickening are undoubtedly some of the most important processes controlling exhumation in these orogenic systems. Exhumation is recorded by thermochronologic ages in the hinterland and in syn-tectonic detritus shed into adjacent foreland basins. Cenozoic India-Asia collision in the Himalaya has resulted in widespread Eocene-Oligocene exhumation, but it is unclear how the same processes have affected the Pamir Mountains of Central Asia.

New multi-crystal laser total fusion $^{40}Ar/^{39}Ar$ thermochronologic data from detrital white mica in samples from five rivers that drain the western Pamir in Tajikistan (Vanch, Yazgulem, Bartang, Gunt, and Murghab Rivers, Figure 1) give ages significantly younger than previously published thermo- and geo-chronologic data from the magmatic belt (Schwab and others, 2004). Apparent ages range from 14 to 348 Ma with young age peaks at 18 Ma in four samples and 38 Ma in the one sample (Figure 2). These new data suggest 1) the presence of undocumented mid-late Cenozoic plutons within the western Pamirs, and/or 2) deep mid-late Cenozoic exhumation.

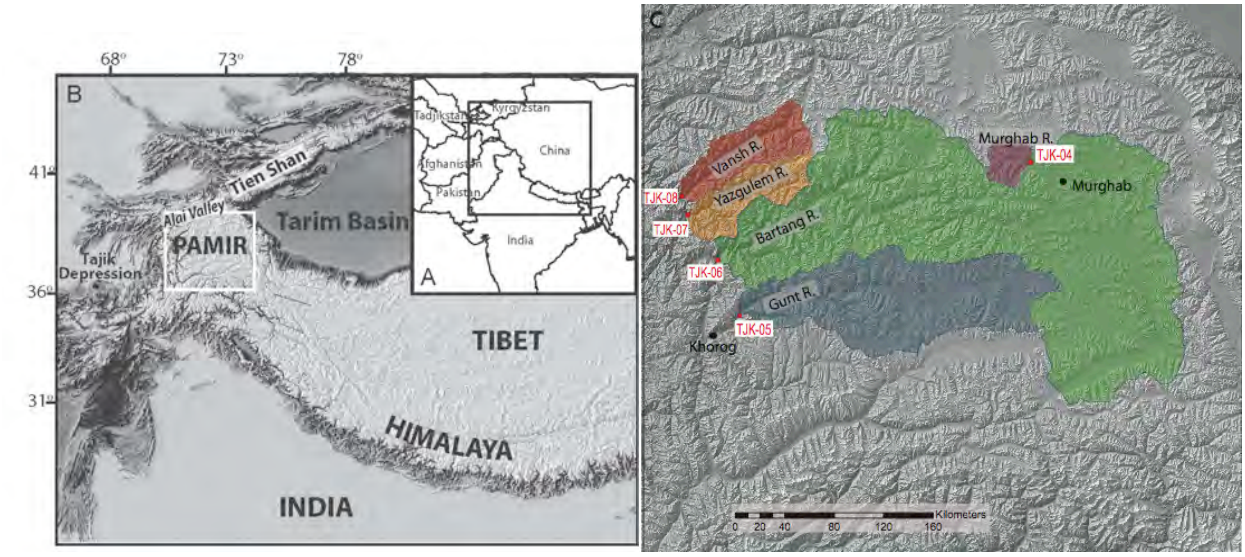

Figure 1. Location maps (A, B) for the Pamir. White box in B is area represented in C. Map C: sampling locations on five major rivers in the western Pamir

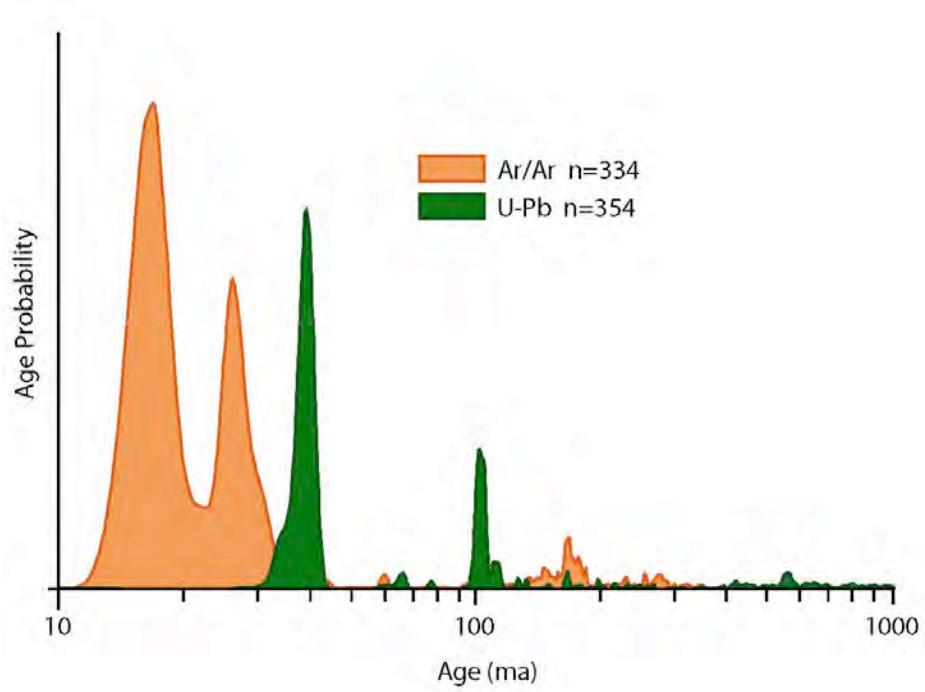

Figure 2. Relative age probability for $^{40}Ar/^{39}Ar$ and U-Pb data for grains younger than 1 Ga. All $^{40}Ar/^{39}Ar$ ages are younger than 1 Ga; a total of 49 grains from all five samples have U-Pb ages older than 1 Ga.

U-Pb dating of zircons from the same sediment samples was also performed, and yielded grains no younger than 33 Ma, suggesting that the Miocene $^{40}Ar/^{39}Ar$ ages reflect exhumation rather than the rapid crystallization of young magmatic bodies (Figure 2). Exhumation at this time is also supported by an increase in foreland basin subsidence and the deposition of > 5 km of coarse alluvial material in the Tajik Depression, west of the Pamir (Nikolaev, 2002).

The regionally uniform exhumation signal documented in our data contrasts with the northward propagation of deformation through time expected from India-Asia collision alone, which should produce exhumation ages that are younger to the north. Though open questions remain on the mechanism responsible for Miocene exhumation, processes related to intra-continental subduction are favored, due largely to support from geophysical data (e.g. Hamburger and others, 1992; Burtman and Molnar, 1993; Negredo, 2007). If this is the case, this process results in high magnitude, regionally-distributed, episodic exhumation, mimicking a 'collisional' signal.

References:

Burtman, V.S. and Molnar, P., 1993, Geological and geophysical evidence for deep subduction of continental crust beneath the Pamir, GSA Special Paper 281, 76 p.

Hamburger, M.W., Sarewitz, D.R., Pavlis, T.L. and Popandopulo, G.A., 1992, Structural and seismic evidence for intercontinental subduction in the Peter the First Range, Central Asia, Geol. Soc. Am. Bull., 104, 397-408.

Negredo, A.M., Replumaz, A., Villaseñor, A. and Guillot, S., 2007, Modeling the evolution of continental subduction processes in the Pamir–Hindu Kush region, Earth Planet. Sci. Lett., 259, 212–225.

Nikolaev, V.G., 2002, Afghan–Tajik depression, Architecture of sedimentary cover and evolution, Russian Jour. of Earth Sci., 4, 399-421.

Schwab, M., and others, 2004, Assembly of the Pamirs: Age and origin of magmatic belts from the Southern Tien Shan to the Southern Pamirs and their relation to Tibet, Tectonics, 23, 31p, TC4002.

Cite as: Lukens, C.E., Carrapa, B., Singer, B.S., Gehrels, G., 2010, Miocene exhumation revealed by detrital minerals of the Tajik rivers: Implications for the tectonic evolution of the Pamir, *in* Leech, M.L., and others, eds., Proceedings for the 25th Himalaya-Karakoram-Tibet Workshop: U.S. Geological Survey, Open-File Report 2010-1099, 2 p. [http://pubs.usgs.gov/of/2010/1099/lukens/].

Seasonal Variations in Geodetic Strain Induced by Hydrological Surface Loading in the Himalaya and Implications for Shallow Elastic Structure of the Earth

Kristel Chanard[1,2], Jean-Philippe Avouac[1], Takeo Ito[1], Jeff Genrich[1], John Galetzka[1], Mireille Flouzat[3], Som Nath Sapkota[4], Bharat Koirala[4]

[1] Department of Geological and Planetary Sciences, California Institute of Technology, Pasadena, CA 91125, kchanard@caltech.edu
[2] Department de Geosciences, Ecole Normale Superieure, Paris, France
[3] Commissariat a l'Energie Atomique, Laboratoire de Detection Geophysique, Bruyeres-le Chatel, France
[2] Department of Mines and Geology, National Seismological Center, Kathmandu, Nepal

Geodetic time series from continuous Global Positioning System (GPS) stations across the Himalaya of Nepal show strong seasonal variations observed on both horizontal and vertical components (Bettinelli and others, 2008). We show here that seasonal variations of surface loading, due to continental water storage (monsoon cycle mostly), is most probably the primary cause for these geodetic seasonal variations and that this effect can be used to constrain the shallow elastic structure of the Earth.

The integrated land-water mass determined from the global time variations of the Earth's gravity field measured by the Gravity Recovery and Climate Experiment (GRACE) is used to estimate surface load variations. To test the proposed model we take advantage of a larger dataset of GPS time series in the India - Nepal area and a longer time period of GRACE water-storage data than previous studies.

We model seasonal variations of geodetic surface displacements using first an elastic half-space approximation (Farrell, 1972) and find that the observed signal at a number of stations in Nepal and India can indeed be predicted reasonably well. The best fit, in the least-squares sense, is obtained for an elastic modulus of 145 GPa. This model is however difficult to assess given that it ignores the spherical and internal structure of the Earth. We therefore show simulations based on a more realistic spherical layered Earth structure (Farrell, 1972; Guo and others, 2004) . We consider an initial model based on the Preliminary Reference Earth Model (PREM), which is found to underestimate seasonal strain amplitude. We next determine a best fitting model, in the Bayesian sense (Fukuda, 2008), by adjusting the distribution of velocities and density with depth to best match the geodetic time series. Variations by up to 10% relative to PREM in the upper 200 km are inferred.

References

Bettinelli, P., and others, 2008, Seasonal variations of seismicity and geodetic strain in the Himalaya induced by surface hydrology, Earth and Planetary Sciences Letters, 266, 332-344.

Farrell, W., 1972, Deformation of the Earth by surface loads, Reviews of Geophysics, 10, 761–797.

Guo, J., and others, 2004, Green's function of the deformation of the Earth as a result of atmospheric loading, Geophysical Journal International, 159, 53–68.

Fukuda, J. and Johnson, K., 2008, A fully Bayesian inversion for spatial distribution of fault slip with objective smoothing, Bulletin of the Seismological Society of America, 98, 1128.

Cite as: Chanard, K., and others, 2010, Seasonal Variations in Geodetic Strain Induced by Hydrological Surface Loading in the Himalaya and Implications for Shallow Elastic Structure of the Earth, *in* Leech, M.L., and others, eds., Proceedings for the 25th Himalaya-Karakoram-Tibet Workshop: U.S. Geological Survey, Open-File Report 2010-1099, 1 p. [http://pubs.usgs.gov/of/2010/1099/chanard/].

The Determination of Anisotropic Parameters from Wide-Angle Seismic Reflection Polarizations: A Model Study

Jingyi Chen[1], Zhongjie Zhang[2], José Badal[3]

[1] Department of Geosciences, The University of Tulsa, Tulsa, OK 74104, U.S.A., jingyi-chen@utulsa.edu
[2] State Key Laboratory of Lithosphere Evolution, Institute of Geology and Geophysics, Chinese Academy of Sciences, Beijing 100029, China, zhangzj@mail.iggcas.ac.cn
[3]Physics of the Earth, Sciences B, University of Zaragoza, Pedro Cerbuna 12, 50009 Zaragoza, Spain, badal@unizar.es

Abstract
As a main anisotropic parameter, generally, S-wave velocity is obtained by S-wave data or the empirical ratio from the P-wave to S-wave velocity (e.g., 1.75). Here, we present a simple inversion method which use seismic P-wave polarizations data to determine vertical SV-wave velocity v_{so} as well as another three anisotropic parameters (vertical P-wave velocity v_{po} and Thomsen's parameters ε and δ) (Thomsen, 1986) in 2D layered transversely isotropic media with a vertical symmetry axis (VTI) (Tsvankin, 1996). The vertical P-wave velocity and Thomsen's parameters are first obtained from the inversion of seismic P-wave reflection traveltimes, and then they are imputed as the corresponding initial parameters for the inversion of seismic P-wave polarizations. A nonlinear global optimization technique named Simulated Annealing (SA) (Rothman, 1985) is applied to both inversions (traveltimes and polarizations). The test results indicate that our inversion strategy is successful in providing favourable constrains to the SV-wave velocity and other anisotropic parameters.

Forward Computation
The shooting two-point ray tracing method is used in our forward computation of seismic P-wave reflection traveltimes and polarizations. Unlike the early paper by Chen and others (2009), we develop a more complex formulation for 2D VTI media and with undulating interfaces. Each layer boundary is specified by an arbitrary number of nodes connected by polynomial linkage and unevenly spaced along the boundary. It is assumed that any layer discontinuity cross the model from left to right without crossing points between boundaries. For some special cases in which the seismic rays can't reach the receivers due to the limitation of shooting two-point ray tracing, we implement cubic spline interpolation to obtain reflection traveltimes and polarization data at stations.

Inversion
For the performance of inversion, the reflection traveltimes and polarizations data (obtained from forward computation) are first reconstructed by adding Gaussian noise with the standard deviation of ±0.1 s and ±0.1°, respectively. The starting model is selected as isotropy model. During SA procedure, the initial temperature is 15^0. The vertical P-wave velocities and Thomsen parameters are obtained from the inversion of P-wave reflection traveltimes, and then are imputed as starting model into the inversion of P-wave reflection polarizations. The initial model, real model, inversion results from traveltimes data and final inversion results from polarizations data are shown in Figure 1. Figure 1a, 1b, 1c and 1d represent curves of vertical P-wave velocity, SV-wave velocity and Thomsen's parameters, respectively. Not only can we obtain SV-wave velocity from polarization inversion, but also we get P-wave velocity and Thomsen's parameters which are much closer to the real model than those from traveltimes inversion.

Conclusions
A simple inversion procedure of seismic P-wave polarizations for determining anisotropic parameters is presented here. Based on the success of the model test, application to real seismic data will be found in the future study.

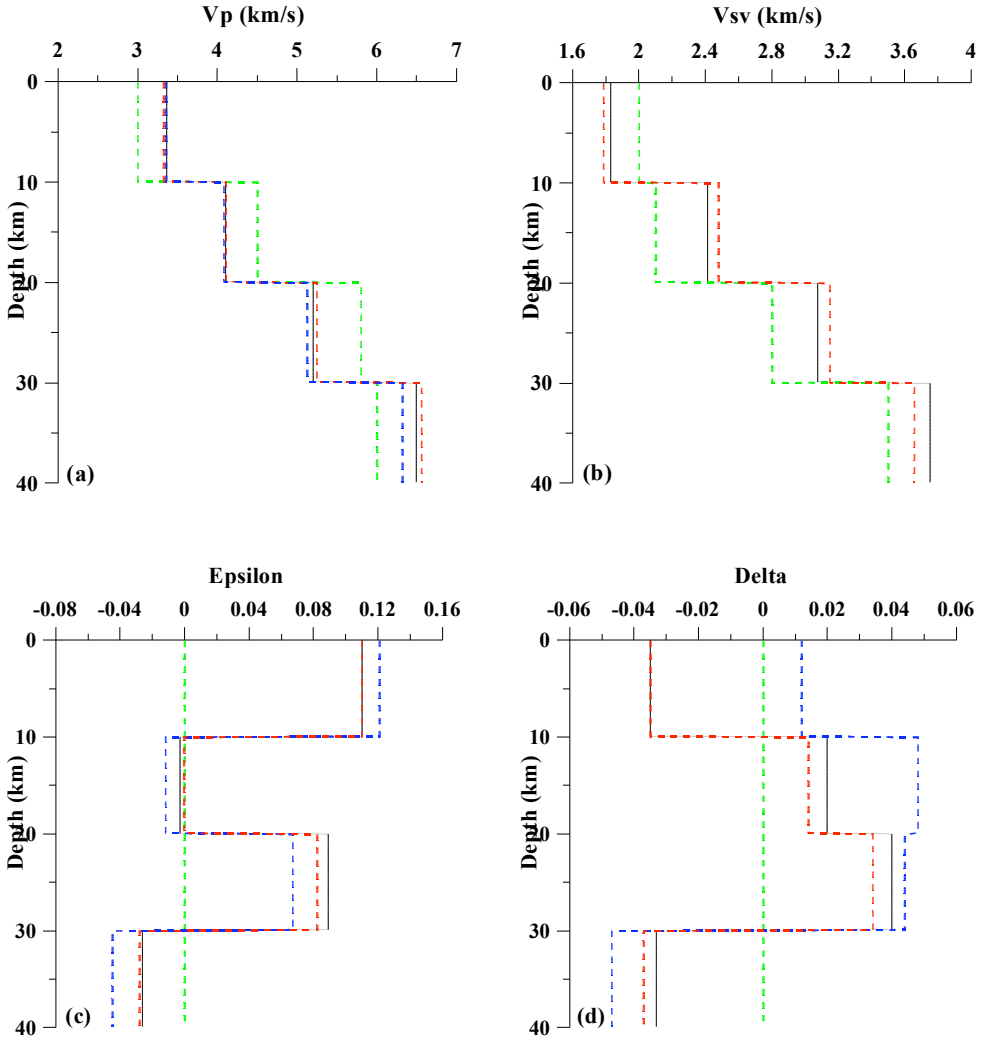

Figure 1. The vertical P-wave velocity (a), vertical SV-wave velocity (b) and Thomsen parameters (c) and (d) as derived by our inversion strategy. The light solid black lines, the solid green lines, the solid dashed blue lines and the solid dashed red lines indicate true model, starting model, inversion results from travel- times and final inversion results from polarizations, respectively.

Acknowledgements

The authors would like to thank the University of Tulsa for its start up funding support. This research was financially supported by the Chinese National Nature Sciences Foundation (grant no. 40604008).

References

Chen, J., Teng, J. and Badal, J., 2009, Constraining the anisotropy structure of the crust by joint inversion of seismic reflection traveltimes and wave polarizations, J. Seismol., 13, 219-240.

Rothman, D.H., 1985, Non-linear inversion, statistical mechanics, and residual statics estimation, Geophysics, 50, 2784-2796.

Thomsen, L., 1986, Weak elastic anisotropy, Geophysics, 51, 1954-1966.

Tsvankin, I., 1996, P-wave signatures and notation for transversely isotropic media, an overview, Geophysics, 61, 467-483.

Cite as: Chen, J., Zhang, Z. and Badal, J., 2010, The determination of anisotropic parameters from wide-angle seismic reflection polarizations: A model study, *in* Leech, M.L., and others, eds., Proceedings for the 25th Himalaya-Karakoram-Tibet Workshop: U.S. Geological Survey, Open-File Report 2010-1099, 2 p. [http://pubs.usgs.gov/of/2010/1099/chenj/].

The Golmud Step: New Details of the 15 km Moho Offset Between the Tibet Plateau and Qaidam Basin from INDEPTH IV Seismic Results

Chen Chen[1], Larry Brown[1], Marianne Karplus[2], Simon Klemperer[2]

[1] Department of Earth and Atmospheric Sciences, Cornell University, Ithaca, NY 14853, U.S.A. cc669@cornell.edu
[2] Department of Geophysics, Stanford University, Stanford, CA 94305, U.S.A.

Zhu and Helmberger (1998) reported a 15-20 km Moho offset over a narrow 5 km range under the northern margin of the Tibetan Plateau near Golmud from anomalous double-pulse teleseismic P-wave arrivals. They proposed a hotter, more-ductile, less-dense lower crust under the Tibetan Plateau in the south abutting a cold, rigid Qaidam Basin crust to the north, the latter serving as a buttress to lower-crustal flow beneath the plateau. A subsequent teleseismic receiver-function profile in the same vicinity by Vergne and others (2002) was interpreted to indicate a similar Moho offset of about 20 km located about 100 km north of the Kunlun fault. Another teleseismic receiver-function study by Shi and others (2009) also reported a 15 km Moho offset at the southern margin of the Qaidam Basin along a transect located about 270 km to the east of Golmud.

In the summer of 2007, a N-S seismic profile was collected as part of INDEPTH IV to extend from the central Qaidam Basin in the north to the Songpan-Ganzi terrane of the Tibetan plateau in the south (Zhao and others, 2008). The 270 km long profile was anchored by 295 PASSCAL "Texan" recorders deployed at 650 km spacing, with a denser deployment of an additional 655 "Texan" at 100 m spacing adjacent to a 1000-channel Sercel multichannel system recording at 50 m spacing in the central part of this profile. This spread recorded 5 large (1-2 ton) explosive shots (KS1-KS5) as well as 100 smaller (60-240 kg) shots for reflection and refraction coverage across the southern margin of the Qaidam Basin and adjacent Kunlun mountains.

Conventional processing of the more numerous smaller shots has yielded little information on deep crustal structure. However, reflection treatment of the wide-angle recordings from the larger shots, especially KS5, provides a fresh perspective on Moho morphology across the Tibet-Qaidam boundary. Figure 1 shows the shot gather for KS5 displayed after applying an NMO correction using an average crustal Vp of 6.2 km/s. There is a clear reflection from a depth of about 48 km (below sea level) beneath the southern Qaidam basin, and a distinctive, albeit weaker and lower frequency (i.e. 2 Hz vs 5 Hz), reflection from about 63 km depth (bsl) beneath the Tibetan plateau to the south. Identifying both events with the Moho implies a 15-km offset about 40 km north of the North Kunlun Thrust along a line about 30 km to the east of Golmud. Close examination suggests that this increase in depth occurs over a zone that may be as narrow 5 km, corresponding to a 72º dip of any linking segment.

The magnitude of the offset implied by this correlation of reflectors, 15 km, is comparable with that estimated by the previous studies. The location of this offset agrees with that of Vergne and others (2002), but lies about 15 km north of the Moho offset calculated by Zhu and Helmberger (1998). We suggest that the abrupt nature of this crustal thickening implies significant strength in the lower crust at this margin of the plateau, and thus represents an important constraint on rheological models used to explain crustal thickening and uplift of the plateau.

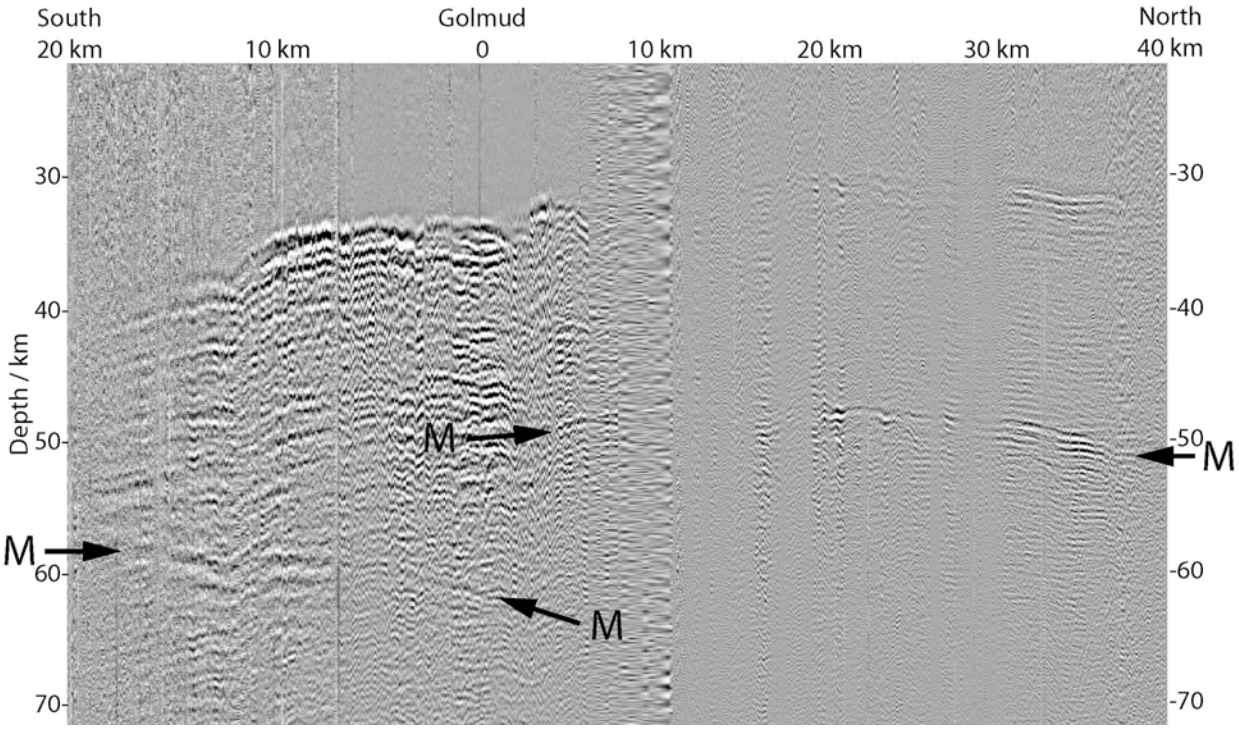

Figure 1. Shot gather for KS5 displayed as depth section. Arrows point to the Moho. Distance of reflection points from Golmud indicated along the top of the section. Energy arriving before the Moho reflections corresponds to direct P phases (Pg) and associated multiples.

References

Shi, D., Shen, Y., Zhao, W. and Li, A., 2009, Seismic evidence for a Moho offset and south-directed thrust at the easternmost Qaidam Kunlun boundary in the Northeast Tibetan plateau, Earth Planet. Sci. Lett. 288, no. 1-2: 329-334. doi:10.1016/j.epsl.2009.09.036.

Vergne, J., and others, 2002, Seismic evidence for stepwise thickening of the crust across the NE Tibetan plateau. Earth Planet. Sci. Lett. 203, 25-53

Zhao, W., and others, 2008, Seismology Across the Northeastern Edge of the Tibetan Plateau, Eos Trans. AGU, 89(48), doi:10.1029/2008EO480002.

Zhu, L. and Helmberger, D.V., 1998, Moho offset across the northern margin of the Tibetan plateau, Science, 281, 1170-1172.

Cite as: Chen, C., Brown, L., Karplus, M. and Klemperer, S., 2010, The Golmud Step: New details of the 15 km Moho offset between the Tibet Plateau and Qaidam Basin from INDEPTH IV Seismic Results, *in* Leech, M.L., and others, eds., Proceedings for the 25th Himalaya-Karakoram-Tibet Workshop: U.S. Geological Survey, Open-File Report 2010-1099, 2 p. [http://pubs.usgs.gov/of/2010/1099/chenchen/].

Fault Histories of the Northeastern Tibetan Plateau Margin: Geodynamic Implications of Far-Field Deformation During Continental Collision

Marin K. Clark[1], Alison R. Duvall[1], Nora Lewandowski[1], Eric A. Hetland[1], Dewen Zheng[2], Richard O. Lease[3], William Craddock[4], Eric Kirby[4], Zhicai Wang[5]

[1] Department of Geological Sciences, University of Michigan, Ann Arbor, MI 48109, U.S.A., marinkc@umich.edu
[2] State Key Laboratory of Earthquake Dynamics, Institute of Geology, China Earthquake Administration, Beijing 100029, China
[3] Department of Earth Science, University of California, Santa Barbara, CA, 93106, U.S.A.
[4] Department of Geosciences, The Pennsylvania State University, University Park, PA, 16802, U.S.A.
[5] Earthquake Engineering Institute of Shandong Province, Jinan 250014, China

The distribution of faulting with respect to the collisional plate boundary provides important geodynamic constraints. First, the "bulk strain rate" of the continental crust or lithosphere can be derived by the plate convergence rate divided by the distance over which faulting is distributed. Second, changes in the type or rate of faulting at the plateau perimeter may indicate how gravitationally-derived stresses originating from the interior of Tibet have evolved as a function of time. We review the chronology of fault histories in northeastern Tibet, largely derived from new and recently published low-temperature thermochronometry data, and with additional resources derived from the published literature. The northeast margin of the plateau is a key locality for understanding the longevity of faulting and subsequent changes to faulting patterns. The strike of this plateau margin is perpendicular to convergence and allows us to consider a two-dimensional model of bulk plateau strain. This margin is also relatively uncomplicated compared to western Tibet where large strength heterogeneities exist and undoubtedly influence the distribution of faulting.

Low-temperature thermochronometry ages from across northeastern Tibet range from Jurassic to late Miocene time, which suggests that the overall erosion magnitude is less than a few kilometres and that entire Cenozoic thermal histories are commonly preserved in vertical elevation sample profiles. Ages from fault blocks show accelerated middle-Eocene to Oligocene erosion rates that are interpreted as thrust fault initiation near collision time (Clark and others, 2010). Collision-age faulting is significant because it demonstrates that the northern perimeter of the plateau has changed little since collision began. A stationary northeastern perimeter to the plateau effectively implies that the orogen has grown smaller in north-south extent with time. By extrapolating the relationship between plate convergence rate and the north-south extent of deformation, we evaluate the bulk strain rate of Tibet that has evolved since collision began. Using recently published plate motions of India with respect to Eurasia over the last 70 Myr, we show that exponentially decreasing convergence rates can be related to the narrowing of the orogen such that the average strain rate across Tibet remains constant and is consistent with modern strain rates derived from geodetic values. Constant strain rate is an unexpected finding that implies a previously unrecognized link between far-field deformation, rheology and plate motions in convergent continental settings.

In addition to thrust faulting occurs within approximately 10 Myr of collision, we also identify a major kinematic change in faulting pattern that develops or evolves by at least mid-Miocene time. In contrast to the few, relatively continuous faults and broad basins that characterize the early Cenozoic fault history, the Miocene and younger period is dominated by the appearance of new faults that are more diverse in strike orientation and sense of slip, and are more closely spaced and discontinuous. These new structures are bound by two major left-lateral strike slip faults (Kunlun and Haiyuan faults) and possibly relate to the transfer of motion between them (Duvall and Clark, 2010). A change in faulting style in northeastern Tibet correlates with a dramatic decrease in fault slip rate of major strike-slip faults (Ritts and others, 2008), initiation of new fault systems (Blisniuk and others, 2001; Wang and others, 1998), expansion of eastern Tibet by lower crustal flow (Kirby and others, 2002; Clark and others, 2005; Ouimet and others, 2010) and propagation of faulting into the eastern Himalayan foreland (Clark and Bilham, 2008). The kinematic change in northeastern Tibet in Miocene time potentially relates to gravitationally derived stresses from central Tibet that initiates lower crustal flow or changes in GPE due to mantle foundering (Lease and others, in review).

Despite a dramatic change in the style and orientation of faults since Miocene time, the northeast perimeter of the plateau changes by only a modest amount. Faulting expands to a region 150 km north and east of where deformation had previously occurred. A stationary boundary that is established at collision time is not easily explained by existing indenter models of continental convergence into a uniform lithosphere and may be better described by considering the role strength heterogeneities in the continental lithosphere (Dayem and others, 2009) or basal tractions induced by small-scale mantle flow resulting from sinking high-density bodies. Under some circumstances, basal tractions may also contribute significantly to plate motion where known contributions from edge tractions are insufficient.

References

Blisniuk, P.M., and others, 2001, Normal faulting in central Tibet since at least 13.5 Myr ago: Nature, 412, 628-632.

Clark, M.K., Farley, K.A., Zheng, D., Wang, Z. and Duvall, A., 2010, Early Cenozoic faulting of the northern Tibetan Plateau margin from apatite (U-Th)/He ages, Earth Plan. Sci. Lett., in press.

Clark M.K. and Bilham R., 2008, Miocene rise of the Shillong Plateau and the beginning of the end for the Eastern Himalaya: Earth Plan. Sci. Lett., 269, 336-350.

Clark M.K., and others, 2005, Late Cenozoic uplift of the southeastern Tibet, Geology, 33, 525 – 528.

Dayem, K., Molnar, P. Clark, M.K. and Houseman, G. A., 2009, Far-field lithospheric deformation in Tibet during continental collision, Tectonics, 28, TC6005, doi:10.1029/2008TC002344.

Duvall, A.R. and Clark, M. K., 2010, Dissipation of fast strike-slip faulting within and beyond northeastern Tibet, Geology, 38, 223–226; doi: 10.1130/G30711.1

Kirby E., and others, 2002, Late Cenozoic evolution of the eastern margin of the Tibetan Plateau: Inferences from $^{40}Ar/^{39}Ar$ and (U-Th)/He thermochronology, Tectonics, 21, doi:10.1029/2000TC001246

Lease, R.O., and others, in review, Middle Miocene reorganization along the northeastern Tibetan Plateau, Geology, in review.

Ouimet, W., and others, 2010, Regional incision of the eastern margin of the Tibetan Plateau, Lithosphere, 2, 50 – 63, doi: 10.1130/L57.1.

Ritts, B.D., and others, 2008, From sea level to high elevation in 15 million years: Uplift history of the northern Tibetan Plateau margin in the Altun Shan, Am. J. Sci., 308, 657 – 678, doi: 10.2475/05.2008.01

Wang, E., and others, 1998, Late Cenozoic Xianshuihe-Xiaojiang, Red River, and Dali fault systems of southwestern Sichuan and central Yunnan, China, Special Paper- Geol. Soc. Am., 327, 108.

Cite as: Clark, M.K., and others, 2010, Fault Histories of the Northeastern Tibetan Plateau Margin: Geodynamic Implications of Far-Field Deformation During Continental Collision, *in* Leech, M.L., and others, eds., Proceedings for the 25th Himalaya-Karakoram-Tibet Workshop: U.S. Geological Survey, Open-File Report 2010-1099, 2 p. [http://pubs.usgs.gov/of/2010/1099/clark/].

Metamorphic History of the South Tibetan Detachment System, Mt. Everest Region, Revealed by RSCM Thermometry and Phase Equilibria Modeling

John M. Cottle[1], David J. Waters[2], Olivier Beyssac[3], Micah J. Jessup[4]

[1] Department of Earth Science, University of California, Santa Barbara, California 93106-9630, U.S.A., cottle@geol.ucsb.edu
[2] Department of Earth Sciences, University of Oxford, Oxford OX1 3PR, U.K.
[3]Institut de Minéralogie et de Physique des Milieux Condensés UMR 7590, CNRS-Paris 6-Paris 7-IPGP, Campus Boucicaut, F-75015 Paris, France
[4]Department of Earth and Planetary Sciences, University of Tennessee, Knoxville, TN 37996, U.S.A.

Understanding the role of large-scale detachment fault systems in the development of collisional orogens is important; their structural history yields insight into the mechanisms by which crustal-scale extension is accommodated within a convergent system whereas their thermal history delineates the extent to which they facilitate the transfer of both heat and mass from the mid to upper crust. Such studies help to elucidate the tectonic evolution of mountain belts and also define important geologic boundary conditions from which large-scale geodynamic simulations can be constructed and to which the results of predictive models must be matched.

A key input into geodynamic models that attempt to explain the evolution of the Himalayan orogen, is knowledge of the structural and thermal history of the South Tibetan Detachment System (STDS). Numerous studies have addressed the kinematic evolution of the STDS, but its thermal structure is less well understood. This is in part due to the relative paucity of index minerals in many sections of the STDS. Exceptions to this include Zanskar (Searle and Rex, 1989), the Sutlej Valley in NW India (Chambers and others, 2009) and the Everest region (e.g. Hodges and others 1992; Jessup and others 2008) and Bhutan (e.g. Kellett and others, 2009). In these areas, detailed work has revealed a complex juxtaposition of Greater Himalayan Series (GHS) rocks with the overlying Tibetan Sedimentary sequence (TSS) during exhumation which progressed from a ductile shear zone into younger and structurally higher brittle detachment(s).

To further refine our understanding of the thermal history of the STD system this study combines micro-structural observations with Raman spectroscopy on carbonaceous material and phase equilibria modeling of rocks from a well-exposed section through the STDS in the Dzakaa Chu valley of Southern Tibet. In the hanging wall of the STDS, undeformed TSS rocks consistently record peak metamorphic temperatures of ~340°C. Peak temperatures increase to ~410°C in the upper 200m and ~630°C at the base of the shear zone. These data document an apparent metamorphic field gradient of ~410ºC/km in the upper 200m of the shear zone and an average field gradient of at least 260ºC/km across the entire structure. The data indicates that this 1-kilometre-thick zone of distributed top-down-to-the northeast ductile shear was responsible for significant and complex juxtaposition of paleo-isotherms and/or excision of material along the upper margin of the GHS during the mid-Miocene. This segment of the shear zone therefore provides a record of the early stages of south-directed exhumation of footwall GHS rocks from beneath the Tibetan plateau that is elsewhere overprinted by later, brittle deformation features including discrete detachment faults.

References

Chambers J.A., and others, 2009, Empirical constraints on extrusion mechanisms from the upper margin of an exhumed high-grade orogenic core, Sutlej valley, NW India, Tectonophysics, doi:10.1016/j.tecto.2008.10.013.

Hodges, K.V., and others, 1992, Simultaneous Miocene extension and shortening in the Himalayan orogen, Science, 258, 1466-1470.

Jessup, M.J., and others, 2008, PT-t-D paths of Everest Series schist, Nepal. J. Met. Geol., 26, 717–739.

Kellett, D., Grujic, D. and Erdmann, S., 2009, Miocene structural reorganization of the South Tibetan detachment, eastern Himalaya: Implications for continental collision, Lithosphere, 1, 259-281.

Searle, M.P. and Rex, A.J., 1989, Thermal model for the Zanskar Himalaya, J. Met. Geol., 7, 127-134.

Cite as: Cottle, J.M., Waters, D.J., Beyssac, O. and Jessup, M.J., 2010, Metamorphic History of the South Tibetan Detachment System, Mt. Everest Region, Revealed by RSCM Thermometry and Phase Equilibria Modeling, *in* Leech, M.L., and others, eds., Proceedings for the 25th Himalaya-Karakoram-Tibet Workshop: U.S. Geological Survey, Open-File Report 2010-1099, 1 p. [http://pubs.usgs.gov/of/2010/1099/cottle/].

Quaternary Slip History for the Central Altyn Tagh Fault Reveals Time-Varying Slip Rate

Eric Cowgill[1], Ryan D. Gold[1,2], J. Ramon Arrowsmith[3], Xuanhua Chen[4], Xiao-Feng Wang[4]

[1] Department of Geology, University of California, Davis, CA 95616, U.S.A., escowgill@ucdavis.edu
[2] now at: Geologic Hazards Science Center, U.S. Geological Survey, Denver, CO 80225, U.S.A.
[3] School of Earth & Space Exploration, Arizona State University, Tempe, AZ 85287, U.S.A.
[4] Inst. of Geomechanics, Chinese Academy of Geological Sciences, Beijing 100081, P.R. China

Although the Tibetan Plateau is cut by a number of major (>1000 km long) strike-slip faults (e.g., Molnar and Tapponnier, 1975), it remains unclear how much deformation is localized along these first-order structures (e.g., Tapponnier and others, 2001) as opposed to distributed within the domains they bound (e.g., England and Molnar, 2005). Disagreements over the rates at which these major faults slip have clouded the debate over the kinematics of deformation within the collision (e.g., Cowgill, 2007; England and Molnar, 2005). Thus, rates and histories of slip on these major faults must be measured accurately before the long-term kinematics within the collision zone can be established (Cowgill, 2007). The largest active major strike-slip fault in Tibet is the left-slip Altyn Tagh fault (ATF), which defines the NW margin of the Tibetan plateau. The latest Quaternary slip rate along the ATF has been disputed for two decades, with reported Quaternary rates varying by almost a factor of three (Peltzer and others, 1989; Mériaux and others, 2004; Bendick and others, 2000; Cowgill, 2007). To address this problem, we have determined the post-16 ka slip history of the central ATF between 86.5° and 88.5°E longitude using morphochronology (i.e., measurement of the age and offset of faulted landforms, Mériaux and others, 2004).

We first evaluated how the determined slip rate varies as a function of epistemic uncertainties in morphochronologic data, including the impact of uncertainties in the age (Cowgill, 2007) and magnitude of lateral erosion (Gold and others, 2009) of a fluvial terrace riser. We then obtained new morphochronologic data from 9 risers at 5 sites (Fig. 1a): Yuemake (Cowgill and others, 2009), Tuzidun (Gold and others, 2009), and Kelutelage, Yukuang, and Keke Qiapu (Gold and others, in review). We also used new field observations to reinterpret the Cherchen He site (Cowgill, 2007). Data are summarized in Figure 1b. To analyze this volume of morphochronologic data, we developed a Monte Carlo approach for determining slip histories from suites of morphochronologic data that allows us to determine both precise average slip rates and evaluate the extent to which such rates have varied over time (Gold and Cowgill, in review). Figures 1c-d show the results of this analysis as applied to the central Altyn Tagh fault. When considered as population, compatibility relationships between age-displacement measurements trims the sizes of individual data boxes, and the grey field on Figure 1d shows the resulting portion of age-displacement that the slip history could occupy. Application of our method of Monte Carlo modelling of such data yields a population of 1000 slip histories that fit the data (space limitations preclude showing the paths here). A Mode II linear regression through these modelled histories yields a preliminary average rate of 9.1 ± 1.1 mm/yr from 16.6 ± 3.9 ka to present, however, this approach forces upon the data an assumption of no temporal variations in slip rate. Thus, a more reasonable approach is to simply contour the slip histories to determine a mean slip history with alpha-95 confidence bounds and thus evaluate the extent to which such an assumption is warranted. Figure 1d shows such a best-fit slip history for the central Altyn Tagh fault, and reveals a phase of accelerated strain release in the mid Holocene. Specifically, from ~6.7 to ~5.9 ka, 20 m of slip was released at a short-term rate (~28 mm/yr) that is 3 times greater than the average rate (~9 mm/yr).

We interpret this pulse to represent a cluster of two to six, Mw > 7.2 earthquakes. It is unlikely that this pulse is due to a single large-magnitude earthquake because slip is too large to have reasonably been released in a single event. To our knowledge, this is the first possible earthquake-cluster detected using morphochronologic techniques. This approach we use here is essential for testing block models of continental tectonics, in which frequent reorganization of the active fault network leads to secular variation in slip along faults at timescales of 10-100 kyr.

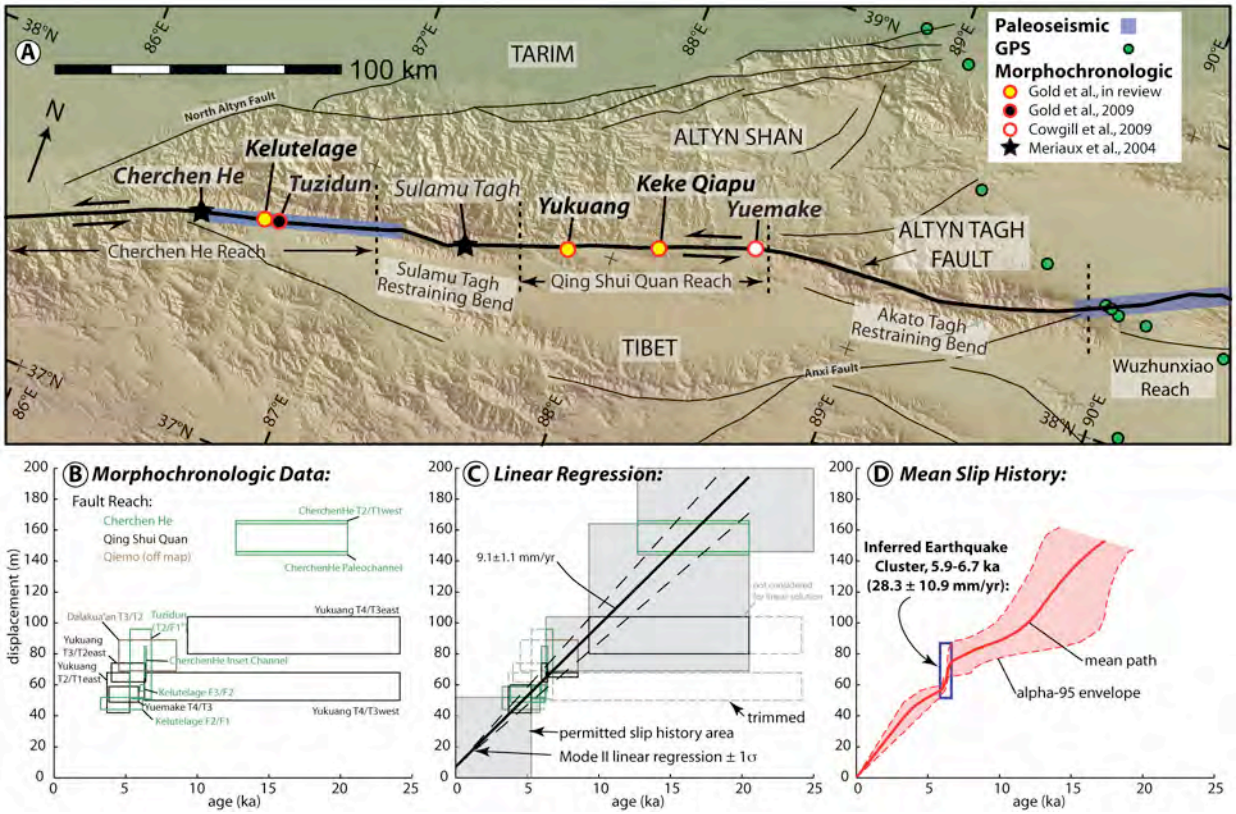

Figure 1. Slip rate sites and summary of slip history analysis. A) Map of the central Altyn Tagh fault showing locations of morphochronologic studies and prior geodetic and paleoseismic investigations. B) Summary of age-displacement measurements along the ATF. Different colors indicate data from different reaches (data from Qiemo reach is from Xu and others, 2005, west of the area shown in part A). C) Considering the data as a population yields compatibility constraints that trim the sizes of individual data boxes and yields the grey field. Monte Carlo modelling of such data then yields a population (not shown) of slip histories fitting the data. D) Contouring the slip histories yields the best-fit slip history and associated confidence interval.

References

Bendick, R., Bilham, R., Freymueller, J., Larson, K. and Yin, G., 2000, Geodetic evidence for a low slip rate in the Altyn Tagh fault system, Nature, 404, 69–72.

Cowgill, E., 2007, Impact of riser reconstructions on estimation of secular variation in rates of strike-slip faulting: Revisiting the Cherchen River site along the Altyn Tagh Fault, NW China, Earth Plan. Sci. Letts., 254, 239-949.

Cowgill, E., and others, 2009, Low Quaternary slip rate reconciles geodetic and geologic rates along the Altyn Tagh fault, northwestern Tibet, Geology, 37, 647-650.

England, P. and Molnar, P., 2005, Late Quaternary to decadal velocity fields in Asia, J. Geoph. Res., 110, doi:10.1029/2004JB003541.

Gold, R.D., and others, 2009, Riser diachroneity, lateral erosion, and uncertainty in rates of strike-slip faulting: A case study from Tuzidun along the Altyn Tagh Fault, NW China, J. Geoph. Res., 114, B04401, doi:10.1029/2008JB005913.

Gold, R.D., and others, in review, Late Quaternary slip rate for the central Altyn Tagh Fault, northwest Tibet, derived from faulted terrace risers at Kelutelage, Yukuang, and Keke Qiapu, Geol. Soc. Am. Bull.

Gold, R.D. and Cowgill, E., in review, Deriving fault-slip histories to test for secular variation in slip, with examples from the Kunlun and Awatere faults, Earth Plan. Sci. Letts.

Mériaux, A.-S., and others, 2004, Rapid slip along the central Altyn Tagh Fault: morphochronologic evidence from Cherchen He and Sulamu Tagh: J. Geoph. Res., 109, B06401, doi: 10/1029/2003jb002558.

Molnar, P. and Tapponnier, P., 1975, Cenozoic tectonics of Asia; effects of a continental collision, Science, 189, 419–426.

Peltzer, G., Tapponnier, P. and Armijo, R., 1989, Magnitude of late Quaternary left-lateral movement along the north edge of Tibet, Science, 246, 1285–1289.

Tapponnier, P., and others, 2001, Oblique stepwise rise and growth of the Tibet Plateau, Science, 294, 1671–1677.

Xu, X., and others, 2005, Late Quaternary sinistral slip rate along the Altyn Tagh fault and its structural transformation model, Science in China, Series D: Earth Sciences, 48, 384-397.

Cite as: Cowgill, E., Gold, R.D., Arrowsmith, J R., Chen, X. and Wang, X.-F., 2010, Quaternary Slip History for the Central Altyn Tagh Fault Reveals Time-Varying Slip Rate, *in* Leech, M.L., and others, eds., Proceedings for the 25th Himalaya-Karakoram-Tibet Workshop: U.S. Geological Survey, Open-File Report 2010-1099, 2 p. [http://pubs.usgs.gov/of/2010/1099/cowgill/].

Oligo-Miocene Basins in Central Tibet and Along the Indus Suture: Records of Plateau Evolution and Dynamics of Subducting Indian Continental Crust

P.G. DeCelles[1], P. Kapp[1], J. Quade[1], G.E. Gehrels[1], M. Murphy[2]

[1] Department of Geosciences, University of Arizona, Tucson, AZ 85721, U.S.A., decelles@email.arizona.edu
[2] Department of Geosciences, University of Houston, Houston, TX 77204-5007, U.S.A.

Mid-Cenozoic sedimentary basins in central Tibet and along the Indus suture zone developed under radically different environmental and tectonic conditions. In the north-central Lhasa terrane directly south of the Bangong suture more than 4 km of Oligo-Miocene fluvial, lacustrine, alluvial fan and fan-delta deposits filled the Nima basin in close association with coeval thrust faults. On the basis of sedimentological features and stable C and O isotope data, Nima basin lakes were shallow and highly evaporative. Carbonate is pervasive: as marls in lacustrine deposits, and as pedogenic carbonates in abundant highly oxidized paleosols. Biotite $^{40}Ar/^{39}Ar$ ages from tuffaceous layers and detrital zircon U-Pb ages indicate that Nima basin was active during the period 27-23 Ma, and probably for several Myr before and after. Oxygen isotope paleoaltimetry indicates that elevation in Nima basin was ~4700 m (equivalent to modern), which is consistent with abundant pollen from cool temperate species.

At the same time (late Oligocene-early Miocene) 400 km to the southwest along the Indus suture zone, the Kailas basin was filled by >2.5 km of alluvial fan, fluvial, and organic-rich deep-lacustrine deposits. The lower alluvial-fan unit lapped northward onto the Kailas magmatic complex, which consists of ~67 Ma andesitic volcanic rocks intruded by ~55 Ma granite of the Gandgese batholith (both ages from U-Pb on zircon). U-Pb zircon ages from interbedded tuffs and minimum age clusters from detrital zircons indicate that the bulk of the Kailas Formation is 26-24 Ma. Phlogopite-bearing basalt/trachyandesite layers are present in the upper half of the Kailas Formation. The southern limit of the preserved Kailas basin is folded and truncated by the north-verging Great Counter thrust (GCT) system, which carries Tethyan Himalayan strata and suture zone rocks in its hanging wall. Kailas basin fill consists of a classic upward fining 'lacustrine sandwich', which we interpret to be the result of deposition in a narrow, E-W elongated extensional basin. Most of the sediment was derived from the Gangdese arc to the north, but southerly-derived Tethyan clasts begin to appear in the upper part of the succession, at about the same level as an abrupt change from organic- and fossil-rich lacustrine facies to highly oxidized and evaporative fluvial and shallow lacustrine deposits. Palynological yields were poor owing to thermal maturity, but the few taxa that are present include tropical ferns and warm weather species; the temperate species so abundant in the Nima record are absent. Individual lacustrine progradational parasequences attain thicknesses >80 m, indicating very deep, large lakes. Lacustrine transgressive lags are littered with fossil fish bones, teeth and turtle scutes. Together with the abundant amorphous kerogen in profundal facies and the absence of cool climate/high elevation palynomorphs, these observations suggest (but by no means prove) that Kailas basin lakes formed at relatively low elevations under humid warm climate. In contrast, the uppermost part of the Kailas Formation is rich in lacustrine marl and paleosol carbonate nodules, similar to Nima basin deposits. The nodules yield $\delta^{18}O$ values of -12 to -16, essentially identical to those from modern-Holocene soil carbonate in the Kailas region. Thus, the Kailas record suggests initial deposition at relatively low elevations, with an abrupt transition to high elevation synchronous with activation of the GCT.

We propose that the Kailas basin formed as a rift coeval with extensional exhumation of Gangdese basement rocks that are now exposed in the footwall of the Ayi Shan detachment. The cause of extension in this region remains uncertain. However, the presence of Oligo-Miocene clastic strata along ~1300 km of the ISZ suggests that this process was regional and not isolated to the SE end of the Karakoram fault. Compilation of ages of volcanic rocks across the entire Tibetan Plateau demonstrates a 500 km northward sweep between ca. 45 and 35 Ma, followed by a southward sweep between ca. 32 and 25 Ma, coeval with opening of the Kailas basin. These magmatic sweeps may provide a rough proxy for the location of the hinge in the subducting/underthrusting Indian plate. Accordingly, the southward sweep represents the velocity of hingeline rollback through the Indian plate, and when added to the ~50 mm/yr convergence rate, would have more than doubled the subduction rate. Increased subduction rate relative to convergence

rate would have driven upper-plate extension, similar to the process operating in many Mediterranean subduction zones. The southward sweep in magmatism culminated in a widespread outburst of 'adakitic' and high-K volcanic rocks, which have been interpreted to represent slab break-off magmatism. This break-off event would have terminated the rollback process, and the tectonic system reverted to hard-collision mode with activation of the GCT, MCT and other shortening structures regionally in Tibet and the Himalaya. Since Eocene time, therefore, there have been two episodes of slab break-off along the Indus suture: the first during Eocene release of the Neotethyan slab, and the second during early Miocene release of a large slab of Greater Indian lithosphere. These break-off events were separated in time by periods of more conventional 'hard collision', during which regional shortening and crustal thickening dominated. Our results hint at the possibility that Indian continental lithosphere has undergone major changes in subduction/underthrusting angle, and large-scale subduction into the mantle, imitating the behaviour of oceanic lithosphere in ocean-continent subduction zones.

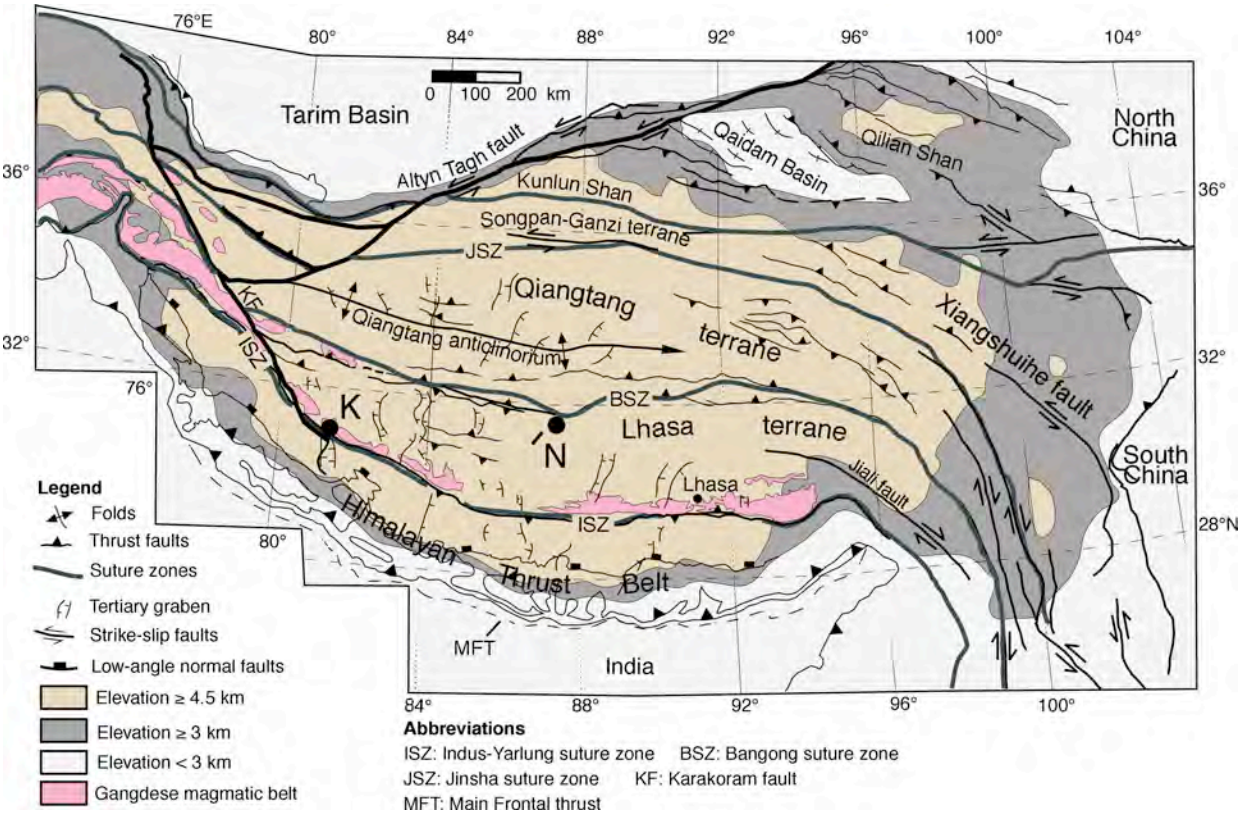

Figure 1. Tectonic and generalized topographic map of the Tibetan Plateau and Himalayan thrust belt, showing major structures and locations of Nima basin (N) and Kailas basin (K). Compiled from multiple sources, most prominently from Yin and Harrison (2000).

References

Yin, A. and Harrison, T.M., 2000, Geologic evolution of the Himalayan-Tibetan orogen, Annu. Rev. Earth Planet. Sci.28, 211-280.

Cite as: DeCelles, P.G., Kapp, P., Quade, J., Gehrels, G.E. and Murphy, M., 2010, Oligo-Miocene Basins in Central Tibet and Along the Indus Suture: Records of Plateau Evolution and Dynamics of Subducting Indian Continental Crust, *in* Leech, M.L., and others, eds., Proceedings for the 25th Himalaya-Karakoram-Tibet Workshop: U.S. Geological Survey, Open-File Report 2010-1099, 2 p. [http://pubs.usgs.gov/of/2010/1099/meltzer/].

Was There Pre-Collisional Metamorphism in Swat Pakistan?

Joseph A. DiPietro[1], Alex Pullen[2]

[1] Department of Geology, University of Southern Indiana, Evansville, IN 47712, U.S.A., dipietro@usi.edu
[2] Department of Geosciences, University of Arizona, Tucson, AZ 85721, U.S.A.

The Pakistan Himalaya in Swat is unusual because; 1) the metamorphic belt lies at the northern edge of the Indian plate in contact with metamorphosed ophiolitic mélange of the Indus suture zone; 2) metamorphism is no younger than middle Eocene; and 3) the primary structures consist of syn-metamorphic west-vergent folds and late-metamorphic N-S plunging open folds yet the metamorphic belt is bound in the south by the E-W trending Panjal-Khairabad thrust and in the north by the E-W trending Kohistan fault. The folds suggest E-W compression throughout metamorphism rather than N-S compression and south-vergence as might be assumed from the orientation of the two bounding faults. The Panjal-Khairabad thrust is post-metamorphic and, therefore, not associated with the syn-metamorphic structures. Instead, syn-metamorphic deformation is attributed to collision between the Indian plate and the Kohistan arc along the Kohistan fault. This collision is commonly assumed to be equivalent with India-Asia collision beginning between 57 and 50 Ma. The Kohistan fault, however, appears to be post-metamorphic and thus, not directly involved with metamorphism. This paper discusses the possibility that metamorphism in Swat began prior to India-Kohistan collision. Regional considerations suggest that the Swat rocks form the lower plate to eclogite-bearing thrust sheets of the Kaghan-Naran region.

West-vergent folds are well displayed in the Kotah and Loe Sar domes. Both consist of Swat augen-flaser gneiss of Middle Permian age (circa 265 Ma) unconformably overlain by Upper Permian-Triassic (and younger?) Marghazar, Kashala, and Saidu formations which, in turn, directly underlie the Indus Suture zone. An unconformity at the Swat gneiss-Marghazar contact is indicated by an absence of intrusive features across the contact, the presence of granitic pebbles in the Marghazar formation, and the large number of detrital zircon ages that cluster around the age of the Swat gneiss. The rock is interpreted as rift-related and correlative with the Panjal formation. A marker unit known as the amphibolite horizon is present everywhere at the top of the Marghazar formation in contact with overlying Kashala formation. It marks the stratigraphically highest position of any amphibolitic rock in Swat. Below the amphibolite horizon the Marghazar formation shows extreme thickness variation from almost zero to more than 300 m. Where it is thin, the Marghazar consists almost entirely of the amphibolite horizon which directly overlies Swat granitic gneiss. Where it is thick it consists of coarse-grained quartz-feldspar schist, schistose marble and amphibolite below the amphibolite horizon. The thickness variations are attributed to a combination of syn-depositional normal faulting (original thickness variations) and subsequent west-vergent recumbent folding. The folds nucleated as shear folds along the faulted, non-planar, Swat gneiss-Marghazar contact.

The Marghazar formation is overlain by marble and schistose marble of the Kashala formation. This rock contains Late Triassic fossils and represents the youngest shelf facies in northern Swat. The overlying Saidu formation consists of fine-grained graphitic phyllite and schist that may represent final drowning of the shelf. Its age is unknown. Regional foliation is continuous from Saidu formation into the overlying Indus suture zone suggesting that mélange matrix rocks were metamorphosed with the Indian plate during development of west-vergent folds and subsequent development of late-metamorphic N-S trending open folds. The Kohistan arc is separated from this deformation by the post-metamorphic Kohistan fault which truncates all structures on the Indian plate.

Northwest of the Kotah dome the Indus suture zone is overlain, not by the Kohistan arc, but by the Malakand fault slice which consists of Indian plate rock with a stratigraphy that is different from the Kotah dome. Another mélange unit, known as the Nawagai mélange, structurally overlies the Malakand slice. Both the Malakand and Nawagai faults are syn-metamorphic ductile contacts. This implies that suture zone mélange was imbricated with Indian plate rock during metamorphism. Regional relationships suggest that both the Malakand and Nawagai thrust sheets where transported toward the southeast in a direction nearly opposite to west-vergent folds exposed in the Kotah and Loe Sar domes. Both the

Malakand and Nawagai thrust sheets were folded across late-metamorphic N-S trending fold axes prior to truncation against the Kohistan fault.

The undeformed and unmetamorphosed Khar diorite intrudes the Nawagai mélange just south of the Kohistan fault near the Afghan border. This rock yielded a weighted mean $^{206}Pb/^{238}U$ age of 48.1 ±0.8 Ma which is interpreted to closely approximate the intrusive age. The circa 48 Ma age is consistent with an average SHRIMP age of 47±3 Ma from zircon rims obtained from the undeformed and unmetamorphosed Malakand granite (Smith and others, 1994) which intrudes across the Malakand slice. This constrains major deformation and metamorphism in both the Nawagai mélange and Indian plate to be 48 Ma or older. A $^{40}Ar/^{39}Ar$ date on hornblende from the Malakand slice gives a well-defined plateau age of 50±3.0 Ma indicating that the rocks had cooled below a maximum temperature of 570 °C by this time. Three somewhat variable pressure-temperature estimates were obtained from garnet-biotite-muscovite-plagioclase-quartz assemblages also from the Malakand slice; 610°C 9.5 kbar, 560°C 8.0 kbar, and 550°C 11.3 kbar. The lower two temperatures imply that the circa 50 Ma argon date records either crystallization of hornblende or cooling closely following crystallization. Peak temperatures close to the argon closure temperature of hornblende for at least part of the Malakand slice are suggested by a second $^{40}Ar/^{39}Ar$ hornblende date of 1040±20 Ma.

The available evidence suggests that major deformation and peak metamorphism in Swat had already occurred by 47-50 Ma and that the Kohistan arc was not directly involved. Instead, the metamorphism is attributed to underthrusting beneath ophiolitic mélange. It is possible that the Swat area is located inland from the buried northern margin of the Indian plate and, by 50 Ma, Kohistan had already collided with the Indian margin such that the arc was acting as a backstop to subduction of Swat rocks beneath ophiolitic mélange. It is equally possible, however, that syn-metamorphic deformation began with subduction or partial subduction beneath ophiolitic mélange prior to collision beginning as early as Late Cretaceous. Evidence for pre-Eocene metamorphism includes hornblende $^{40}Ar/^{39}Ar$ ages of 67±2 and 67±7 Ma from the eastern and western flanks of the Indus syntaxis (Treloar and Rex, 1990) and a concordant U-Pb zircon age of 88.7±0.4 Ma from within the Indus syntaxis (DiPietro and Isachsen, 2001). The data also leave open the possibility that the Kohistan arc collided much earlier than circa 54 Ma or that it collided much later. In all scenarios, final thrusting of Kohistan against Swat rocks was post-metamorphic. Rather than initiate metamorphism in Swat, final thrusting of Kohistan may have caused or initiated the exhumation and cooling of Swat rocks. This implies that the age of metamorphism in Swat and, by extrapolation, in the Kaghan-Naran area, should not be used as a constraint on India-Kohistan (or India-Asia) collision without additional corroborating evidence.

References

DiPietro, J.A. and Isachsen, C.E., 2001, U-Pb zircon ages from the Indian Plate in northwest Pakistan and their significance to Himalayan and pre-Himalayan geologic history, Tectonics, 20, 510-525.

Smith, H.A., Chamberlain, C.P. and Zeitler, P.K., 1994, Timing and duration of Himalayan metamorphism within the Indian plate, northwest Himalaya, Pakistan, Journal of Geology, 102, 493-508.

Treloar, P.J. and Rex, D.C., 1990, Cooling and uplift histories of the crystalline thrust stack of the Indian plate internal zones west of Nanga Parbat, Pakistan Himalaya, Tectonophysics, 180, 323-349.

Cite as: DiPietro, J.A. and Pullen, A., 2010, Was There Pre-Collisional Metamorphism in Swat Pakistan?, *in* Leech, M.L., and others, eds., Proceedings for the 25th Himalaya-Karakoram-Tibet Workshop: U.S. Geological Survey, Open-File Report 2010-1099, 2 p. [http://pubs.usgs.gov/of/2010/1099/dipietro/].

Muscovite

Michael Doon[1], Djordje Grujic[1], Isabelle Coutand[1], Nicholas Whynot[1]

[1] Department of Earth Sciences, Dalhousie University, Halifax, NS B3H 4J1, Canada, dgrujic@dal.ca

Kinematic models for the tectonics of the Lesser Himalayan Sequence (LHS) are primarily based on structural data and balanced cross sections. Thermochronological and metamorphic constraints are however scarce because of the unsuitable mineral assemblages. Here we present $^{40}Ar/^{39}Ar$ ages of detrital muscovite from the Gondwana sequence at the base of the LHS in the Sikkim Himalaya. In this segment of the orogen the LHS is characterised by a complex Rangit duplex system with the Main Boundary thrust (MBT) as the sole thrust and the Ramgarh thrust as the roof thrust (Bhattacharyya and Mitra, 2009). The interference between the Rangit duplex and a NS trending antiform has formed a double tectonic window: the Sikkim half window outlined by the MCT and the inner Rangit window outlined by the Ramgarh thrust. The hinge of this transverse antiform is located along the Tista River, one of the few trans-Himalayan rivers. Study of erosion and rock uplift rates of the window therefore contributes to testing the hypothesis that *Himalayan river antiforms* may be the consequence of focused rock uplift in response to significant differences between net erosion along major rivers and surrounding regions (Montgomery and Stolar, 2006).

Arkose samples from Permian Gondwana sequence were collected at the orogenic front and from the Rangit window in the interior of the orogen. The individual muscovite ages range between 342.5 ± 52.1 and 1783.6 ± 9.5 Ma. All samples yield multiple age-frequency peaks. The dominant peak in all samples is centered at 480-490 Ma, and three smaller peaks are centered at ~800-900 Ma, ~1100 Ma and ~1800 Ma. The closure temperature for the muscovite in our samples is estimated to be ca. 425 °C. The Tertiary burial of Gondwana sediments therefore did not exceed this temperature.

Furthermore, we have performed Raman spectroscopy on carbonaceous material (RSCM) on slates in the hanging wall of the Ramgarh thrust to determine their peak metamorphic temperatures. The RSCM data yield temperatures of ~440 °C. This is consistent with the findings in the eastern Bhutan (Whynot and others, this volume) which indicate RSCM temperatures of ca 350 °C in the hanging wall of the MBT jumping to > 450 °C in the hanging wall of the Shumar thrust, which is the lateral equivalent of the Ramgarh thrust.

The most likely source for Cambrian-Ordovician muscovite grains are the granites of similar age observed along the entire Himalaya orogen (Cawood and others, 2007) but also at a few locations in the Indian basement in the Himalayan foreland. At this time, our preferred model to explain the provenance of sediments invokes a Permian northward-flowing river system supplying the detritus to the Gondwanan basins. Considering peak metamorphic temperatures, maximum burial estimated from NS and EW cross sections, and a likely geothermal gradient, we conclude that the Tertiary peak-temperature distribution in the LHS of Sikkim is compatible with the river incision and concomitant transverse antiform amplification.

References

Bhattacharyya, K. and, Mitra, G., 2009, A new kinematic evolutionary model for the growth of a duplex — an example from the Rangit duplex, Sikkim Himalaya, India, Gondwana Research, 16, 697-715.

Cawood, P. A., Johnson, M. R. W. and Nemchin, A. A., 2007, Early Paleozoic orogenesis along the Indian margin of Gondwana: Tectonic response to Gondwana assembly, Earth and Planetary Science Letters, 255, 70-84.

Montgomery, D. R. and Stolar, D. B., 2006, Reconsidering Himalayan river anticlines, Geomorphology, 82, 4-15.

Whynot, N., Grujic, D., Long, S. and McQuarrie, N., 2010, Apparent temperature gradient across the Leasser Himalayan Sequence: Raman spectroscopy on carbonaceous material in the eastern Bhutan Himalaya, *in* Leech, M.L., and others, eds., Proceedings for the 25th Himalaya-Karakoram-Tibet Workshop: U.S. Geological Survey, Open-File Report 2010-1099.

Cite as: Doon, M., Grujic, D., Coutand, I. and Whynot, N., 2010, Muscovite, *in* Leech, M.L., and others, eds., Proceedings for the 25th Himalaya-Karakoram-Tibet Workshop: U.S. Geological Survey, Open-File Report 2010-1099, 2 p. [http://pubs.usgs.gov/of/2010/1099/doon/].

Superposed Folds in the Himalaya Indicating Late Stages of the Himalayan Orogeny: Implications for Seismicity

Ashok Kumar Dubey[1]

[1]Wadia Institute of Himalayan Geology, 33 GMS Road, Dehradun – 248 001, India, akdubey@wihg.res.in

The present stage of the Himalayan orogeny is characterized by simultaneous development of contrasting structural features that include early folds, superposed folds, thrust, normal, and strike-slip faults. The early folds have initiated simultaneously with the prominent Himalayan thrusts. The fold geometries are characterized by asymmetric folds in the vicinity of the thrusts, and symmetric folds at a distance from the thrusts. Development of superposed folds at late stages of deformation is shown in Figure 1. A positive listric fault (gradual decrease in dip amounts towards the basal décollement) in the basement is shown in Figure 1a. The fault terminates at the front face into a transfer fault (TF), and into an oblique ramp (OR) at the back face. The gray shade denotes an overlying layer prior to deformation. Thrusting along the basement fault during early deformation results in development of an asymmetric fault-propagation fold above the thrust and upright buckle folds at a distance from the thrust (Figure 1b). The fold hinge lines are parallel to strike of the fault. The deformation has also resulted in steepening of the thrust as a result of rotation of the fault surface with progressive deformation. The thrust locks at a steep dip and the folds also acquire rotation hardening at low inter-limb angles (Figure 1c). The locked fault tends to extend parallel to its strike resulting in formation of a conjugate set of strike-slip faults. The fold hinge lines also extended parallel to the hinge line. However the horizontal extension was restricted by the boundary condition imposed by the transfer fault and the oblique ramp. Hence the restriction has resulted in curvature of the fold hinge lines and formation of superposed folds. At lower structural levels where the thrust dip is gentle (because of listric geometry), the thrust may not lock simultaneously with the upper horizons. Hence the superposed deformation may remain absent at deeper levels as shown in Figure 1d. In the Himalaya these superposed fold hinge lines trend N-S to NE-SW, i.e. nearly orthogonal to the early fold hinge lines and parallel to the axis of maximum compression imposed by the movement of the Indian plate.

Apart from the development of superposed folds, the superposed deformation is also responsible for formation of the following structures.

1. Reactivation of thrust faults as normal faults along the oblique fault ramps.
2. Initiation of normal faults at higher topographic levels.

The study is important to understand the seismicity of the Himalayan orogenic belt.

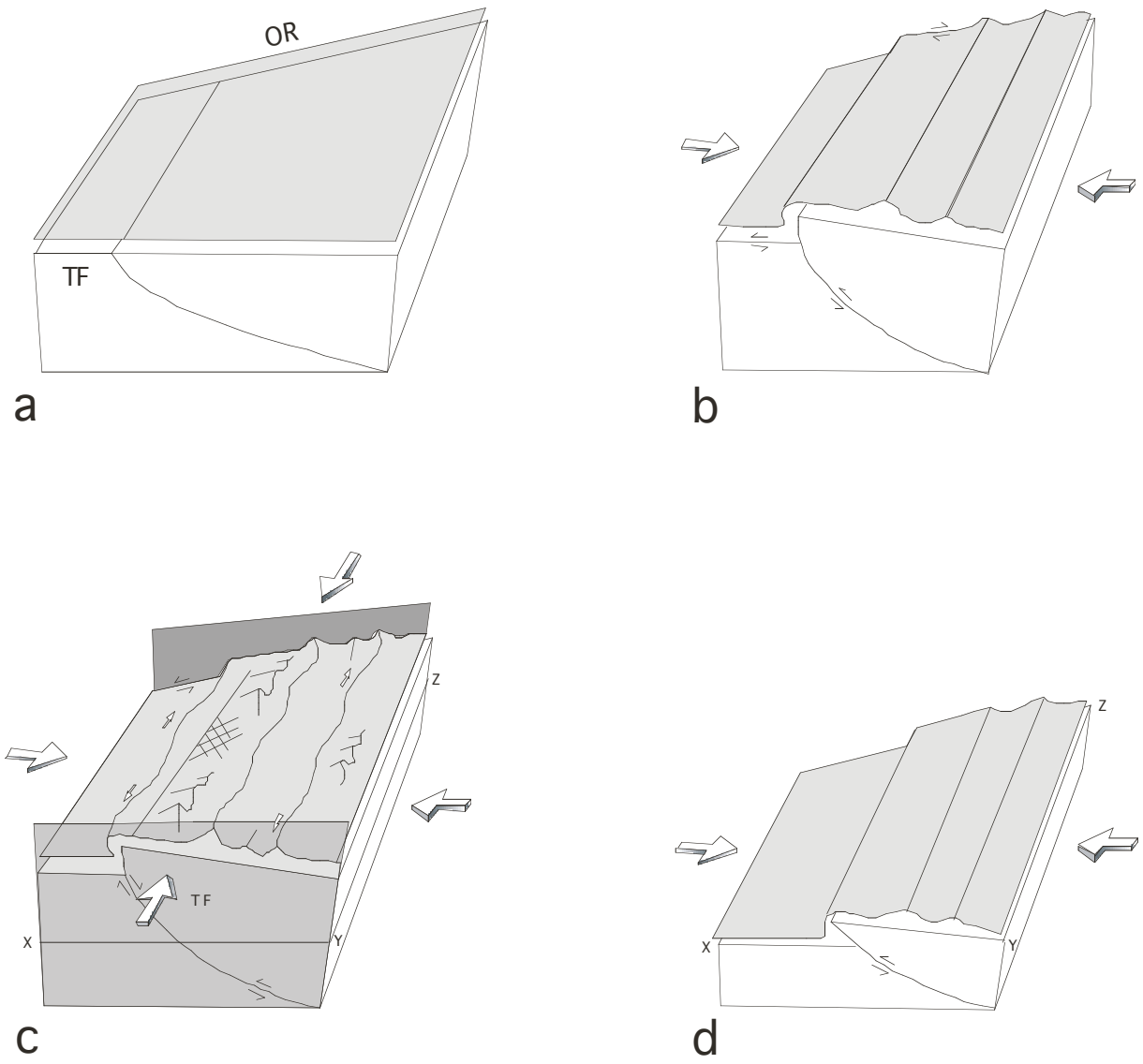

Figure 1. Simultaneous development of strike-slip and thrust faults at different structural levels.
a. A positive listric fault in the basement and an overlying undeformed layer shown in gray. OR, oblique ramp; TF, transfer fault.
b. Thrusting in the basement fault and folding of the cover layer. The oblique ramp and the transfer fault show a component of horizontal displacement as well.
c. Locking of the folds and thrust at late stages of deformation, extension of the fold surface parallel to hinge lines and extension of the hanging wall parallel to strike of the thrust. Obstruction of the extensions as a result of restriction provided by boundary conditions provided by the oblique ramp and the transfer fault thereby resulting in formation of conjugate set of strike-slip faults, curvature of the early fold hinge lines, and initiation of superposed folds. The curvature of the fold hinge lines along with the superposed folds gave the impression that the maximum compression direction is parallel to the early fold hinge lines.

Cite as: Dubey, A.K., 2010, Superposed folds in the Himalaya Indicating Late Stages of the Himalayan Orogeny: Implications for Seismicity, *in* Leech, M.L., and others, eds., Proceedings of the 25th Himalaya-Karakoram-Tibet Workshop: U.S. Geological Survey, Open-File Report 2010-1099, 2 p. [http://pubs.usgs.gov/of/2010/1099/dubey/].

Tectono-Geomorphic and Climatic Controls on Landscape Development in the Lesser Himalaya

C. S. Dubey[1], M. Tajbaksh[1], R. Marston[2], E.J. Catlos[3], Sandeep Singh[4], M. Rogibala[4]

[1] Department of Geology, Centre for Advanced Studies, University of Delhi, Delhi - 110007 India, csdubey@gmail.com
[2] Department of Geography, 118 Seaton Hall, Kansas State University, Manhattan, KS 66506-2904, U.S.A.
[3] Department of Geological Sciences, University of Texas at Austin, 1 University Station C1100, Austin, TX 78712-0254
[4] Department of Earth Sciences, Indian Institute of Technology Roorkee, Roorkee - 247 667, India

Large annual precipitation, fluvial erosion and high sediment flux cause sensitivity to interactions and possible feedbacks between tectonic, geomorphic and climatic processes, leading to along-strike variations and asymmetric development of the Himalaya. This paper discusses the formation of antiformal/domal structure in Sikkim and the role of complex out-of-sequence thrusting (OST) and normal and strike-slip faulting in the Main Central Thrust (MCT) zone, and related neotectonic activity from Garhwal to Sikkim and into the Eastern Himalaya. GIS-based geomorphotectonic study indicates that there is high tectonic activity and uplift in the study area especially along the MCT-III and that OST and normal and strike-slip faulting in the area are the main factors for developing the current landscape morphology, organization and formation of the drainage network. The EPM model (Erosion Potential Method, Gavrilovic, 1988) depicted areas of high or low sediment yield and its relation with tectonic activity. On the other hand, along the thrusts and faults, sediment yield estimated pixel-by-pixel showed that the tectonic zone around the MCT-II is highly active. The erosion rate for the Sikkim area is twice that of the Garhwal area (2.2mm/yr for Sikkim and 0.9 mm/yr for Garhwal). Incision/erosion rates are highest around the out-of-sequence MCT-III as calculated by the SPL model (Stream Power Law, Whipple and Tucker, 1999 and 2002). Active tectonic regions and major knickpoints of the rivers lie on the hanging wall of the out-of-sequence and near MCT-III, supporting the view that this stretch of valley is undergoing rapid exhumation. It is possible that the knickpoints along the rivers have been produced by differential uplift corresponding to movement of the thrusts.

The exhumation rates derived by from available P-T-t data indicate that the Garhwal area between MCT-I (Vaikrita Thrust) and MCT-II (Munsiari Thrust) was active up to ~10 Ma (exhumation <1 mm/yr) whereas the area between the Munsiari Thrust (MCT II) and MCT III (Srinagar Thrust/Ramgarh Thrust) was active between ~2.65 to 1 Ma (exhumation >1 mm/yr). Incision rates obtained from by ^{10}Be dating indicate that out-of-sequence MCT-III areas are very active, with exhumation rates about 6–10 mm/y.

The relation between linear factors and areal factors shows the real-time changes in landforms that are caused due to active tectonics in and around Gangtok and the out-of-sequence thrusts. Ratios of valley floor width to valley height (V_f) values, being one of the best morphometric parameters for tectonic studies, were calculated along the Gangtok river and its tributaries, especially in the vicinity of thrusts. V_f values at the intersection of the OST/ MCT-III are 12 to 18 times less than for the MCT-I. Fission-track ages and Rb/Sr ages of biotite and muscovite confirm the exhumation data.

Along the Himalayan range, the interplay between topography and the Indian summer monsoon circulation profoundly controls precipitation distribution, erosion, sediment transport, and river discharge. In the study area the amount and trend of precipitation is controlled by the tectonic settings and topography of the area.

References

Gavrilovic, Z., 1988, The use of an empirical method (erosion potential method) for calculating sediment production and transportation in unstudied or torrential streams, International Conference of River Regime, 18–20 May, Wallingford, England, 411–422.

Whipple, K. X. and Tucker, G.E., 1999, Dynamics of the stream-power river incision model: implications for height limits of mountain ranges, landscape response timescales, and research needs, Journal of Geophysical Research, 104, 17661–17674.

Whipple, K. X. and Tucker, G.E., 2002, Implications of sediment-flux dependent river incision models for landscape evolution. Journal of Geophysical Research, 107, 2039.

Cite as: Dubey, C.S., and others, 2010, Tectono-Geomorphic and Climatic Controls on Landscape Development in the Lesser Himalaya, *in* Leech, M.L., and others, eds., Proceedings for the 25th Himalaya-Karakoram-Tibet Workshop: U.S. Geological Survey, Open-File Report 2010-1099, 1 p. [http://pubs.usgs.gov/of/2010/1099/dubey/].

Pleistocene-Holocene Climate Fluctuations and Fluvial Response in the Tectonically Active Yamuna Valley, North-Western Himalaya: Timescales and Source-to-Sink Interlinkage

Sharat Dutta[1], N. Suresh[1], Rohtash Kumar[1]

[1]Wadia Institute of Himalayan Geology, Dehra Dun, India, sharatdutta@gmail.com

The present study focus on aggradation and incision history of late Quaternary terrace staircases of Yamuna River and its tributaries in the Sub-Himalaya, between the Main Boundary Thrust (MBT) and the Himalayan Frontal Thrust (HFT) (Fig. 1) to understand the control of tectonics and climate in their genesis. We documented five levels of terraces (T-1 to T-5), cutting across numerous tectonic plains (MBT and its imbricate thrusts), maintaining similar elevations ranging from 65-80, 40-44, 26-28, 8-12 and 3-4 m from the present-day river bed, deposited by both high mountain-fed perennial and piedmont-fed ephemeral streams.

Geomorphological and sedimentological attributes coupled with absolute ages based on optically stimulated luminescence (OSL) chronology of terrace deposits sugggest that fluvial accretion in the area took place in five phases between Marine Isotope Stage-3 (MIS-3) and MIS-1, separated by incision phases, with two major aggradational phases in late Pleistocene (>37 to 24ka and >15 to 11ka) and three minor phases in Mid- to late Holocene (7- 4ka; 3 -2ka; and younger than 2ka). During phase-I (>37 to 24ka), the aggradation was dominantly controlled by ephemeral streams, and occurs as alluvial fill in a pre-existing valley, whereas younger accretion sequences are deposited by both perennial and ephemeral streams after lateral erosion and are deposited on remnants of Phase-1 deposits. The late Pleistocene incision occurred after 24ka under relatively wet to drier climatic conditions prior to the global Last Glacial Maximum (LGM) and weakened ISM whereas after 11ka, incision is in response to increased ISM strength. The multiple minor aggradation-incision phases since mid-Holocene are coeval with ISM dynamics that resulted in the development of three levels of terraces (T-3 to T-5).

The present data is correlated with previous reported aggradation and incision events in the Ganga River system from its upper reaches (north of MBT; Srivastava and others, 2008; Figure 2), Sub Himalaya (Sinha and others, 2010; Figure 2) and south of HFT (southern Ganga Plain; Sinha and others, 2010; Gibling and others, 2005; Figure 2) and other Sub Himalayan basins (Suresh and others, 2007; Phillip and others, 2009; Figure 2) confirms the close linkage of fluvial accretion and incision with Pleistocene-Holocene Indian Summer Monsoon (ISM) oscillations, and in turn, profound climatic control on the terrace genesis in the tectonically active Himalaya on the scale of 10^3 - 10^4 years guided by source to sink sediment dispersal system through Enhanced hillslope erosion in the catchment via glacial fluctuations and precipitation gradient (dry and wet transitions).

References

Gibling, M.R., Tandon, S.K., Sinha, R. and Jain, M., 2005, Discontinuity bounded alluvial sequences of the southern Gangetic plains, India: aggradation and degradation in response to monsoonal strength, Journal of Sedimentary Research 75, 369–385.

Philip, G., Virdi, N.S. and Suresh, N., 2009, Morphotectonic evolution of Parduni basin: An intra dun piggyback basin in western Doon Valley, NW Outer Himalaya, Journal of Geological Society of India 74, 189-199.

Prell, W. L. and Kutzbach, J. E., 1987, Monsoon Variability over past 150000 years, J. Geophys. Res. 92, 8411-8425.

Sinha, S., Suresh, N., Kumar, R., Dutta, S. and Arora, B.R., 2010, Sedimentologic and geomorphic studies on the quaternary alluvial fan and terrace deposits along the Ganga exit, Quaternary International, doi: 10.1016/j.quaint.2009.09.015

Srivastava, P., Tripathi, J. K., Islam, R. and Jaiswal, M. K., 2008, Fashion and phases of late Pleistocene aggradation and incision in the Alaknanda River Valley, western Himalaya, India, Quaternary Research 70, 68–80.

Suresh, N., Bagati, T.N., Kumar, R. and Thakur, V.C., 2007, Evolution of Quaternary alluvial fans and terraces in the intramontane Pinjaur Dun, Sub-Himalaya, NW India: interaction between tectonics and climate change, Sedimentology 54, 809–833.

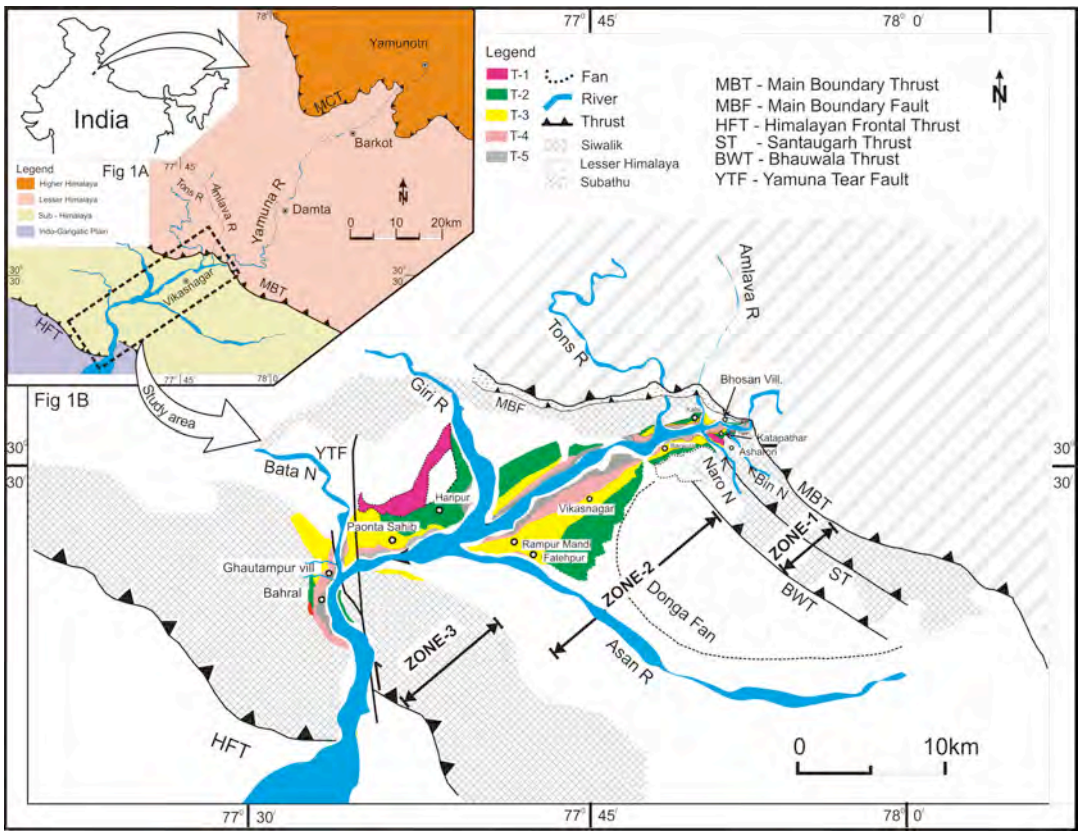

Fig.1. (A) Regional geological map of Yamuna Valley showing major lithotectonic units of Himalaya. (B) Tectonic and geomorphic map of Yamuna Valley between the Main Boundary Thrust and Himalayan Frontal Thrust showing various landforms and intervening thrusts.

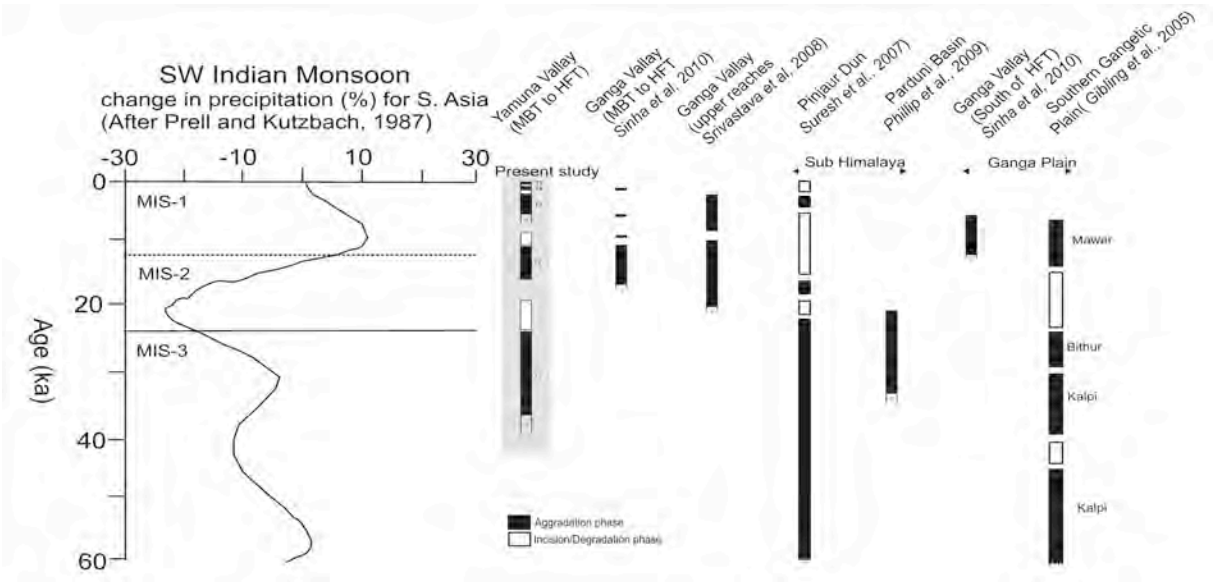

Fig.2. Distribution of late Pleistocene-Holocene aggradation and incision phases in the Yamuna Valley in relation to South-West Indian Monsoon strength and its comparison with various part of Sub-Himalaya and the upper reaches of the Ganga Valley to the Ganga Plain.

Cite as: Dutta, S., Suresh, N., Kumar, R., 2010, Pleistocene-Holocene Fluctuations and Fluvial Response in the Tectonically Active Yamuna Valley, North-Western Himalaya: Timescales and Source-to-Sink Interlinkage, *in* Leech, M.L., and others, eds., Proceedings for the 25th Himalaya-Karakoram-Tibet Workshop: U.S. Geological Survey Open-File Report 2010-1099, 2 p. [http://pubs.usgs.gov/of/2010/1099/dutta/].

Eocene Faulting in Northeastern Tibet: Insights from Coupled Low-Temperature Thermochronometry and Ar Dating of Fault Gouge along the West Qinling Fault

Alison R. Duvall[1], Marin K. Clark[1], Ben van der Pluijm[1], Chuanyou Li[2]

[1] Department of Geological Sciences, University of Michigan, Ann Arbor, MI 48109-1005, U.S.A., duvall@umich.edu
[2]Institute of Geology, China Earthquake Administration, Beijing, China

According to the most widely-cited models of Tibetan Plateau evolution, plateau perimeters likely represent the youngest deformation fronts in the expanding orogen (Tapponnier et al., 2001; England and Houseman, 1986). Thus, studies focused along the margins of the Tibetan Plateau offer important tests for models of orogenic growth. In this study, we focus on the West Qinling fault, which is among the longest and most continuous reverse faults within the northeastern margin of Tibet (Figure 1). In general, timing of brittle fault activity is difficult to assess because the low temperatures typical in the shallow crust prevent dateable syntectonic mineral recrystallization that occurs during deeper faulting. Therefore, indirect means, such as erosion studies in hanging wall rocks using low-temperature thermochronometry, are commonly relied upon to constrain reverse fault timing in the near surface (Ehlers and Farley, 2003). Increased rates of erosion, however, can occur solely with increased precipitation (Reiners and others, 2003) thereby complicating unique correlation of erosion events with fault motion. A separate technique, Ar-dating of clays in fault gouge (van der Pluijm, 2001), provides direct timing of fault activity. However, results from this method are limited because they represent a single event in both space and time.

Here we establish the history of West Qinling faulting by pairing Apatite (U-Th)/He cooling ages within the hanging wall rocks with fault gouge dating of illite polytypes along the fault proper in order to provide a more complete and unambiguous interpretation of faulting. Fault-gouge dating results indicate a Middle Eocene age of faulting and a Middle Triassic age of the source area of wall rocks (Duvall and others, in prep). Helium analysis shows little exhumation in the Jurassic and early Cenozoic followed by an increase in apparent erosion rate at 45 – 50 Ma (Clark and others, in press) that was sustained through the Middle-Miocene. Thus, results from the two datasets are in good agreement and support the interpretation that the West Qinling fault initiated at ~ 45 Ma and continued until at least Middle Miocene time. Contrary to the widely accepted models that emphasize northward Tibetan Plateau growth through time, our results indicate that deformation occurred in northeastern Tibet at approximately the same time that the Indo-Asian collision initiated (Rowley, 1996) >3000 km away. Results from this study also emphasize the value of a coupled approach to assessing brittle fault activity.

References

Clark, M.K., Farley, K.A., Zheng, D., Zhicai, W. and Duvall, A.R., in press, Early Cenozoic faulting of the northern Tibetan Plateau margin from (U-Th)/He ages, Earth Planet Sci Lett..

Duvall, A.R., Clark, M.K., van der Pluijm, B. and Li, C., in prep, Syntectonic fault motion and accelerated erosion in northeastern Tibet circa the onset of Indo-Asia collision.

Ehlers, T. E. and Farley, K. A., 2003, Apatite (U-Th)/He thermochronometry: methods and applications to problems in tectonics and surface processes, Earth Planet Sci Lett., 206, 1-14.

England, P. and Houseman, G., 1986, Finite strain calculations of continental deformation II: comparison with the India-Asia collision zone, J. Geophys, Res., 91, 3664-3676.

Qinghai BGMR (Bureau of Geology and Mineral Resources of Qinghai Province), 1991, Regional geology of Qinghai province: Beijing, China, Geological Publishing House (in Chinese with English abstract).

Reiners, P.W., Ehlers, T.A., Mitchell, S.G. and Montgomery, D.R., 2003, Coupled spatial variation in precipitation and long term erosion rates across the Washington Cascades, Nature, 426, 645 – 647.

Rowley, D., 1998, Age of initiation of collision between India and Asia: A review of stratigraphic data, Earth Planet Sci Lett., 145, 1 – 13.

Tapponnier, P., and others, 2001, Oblique stepwise rise and growth of the Tibet Plateau, Science, 294, 1671-1677.

van der Pluijm, B., Hall, C., Vrolijk, P., Pevear, D., and Covey, M., The dating of shallow faults in the Earth's crust, Nature, 412, 172-175.

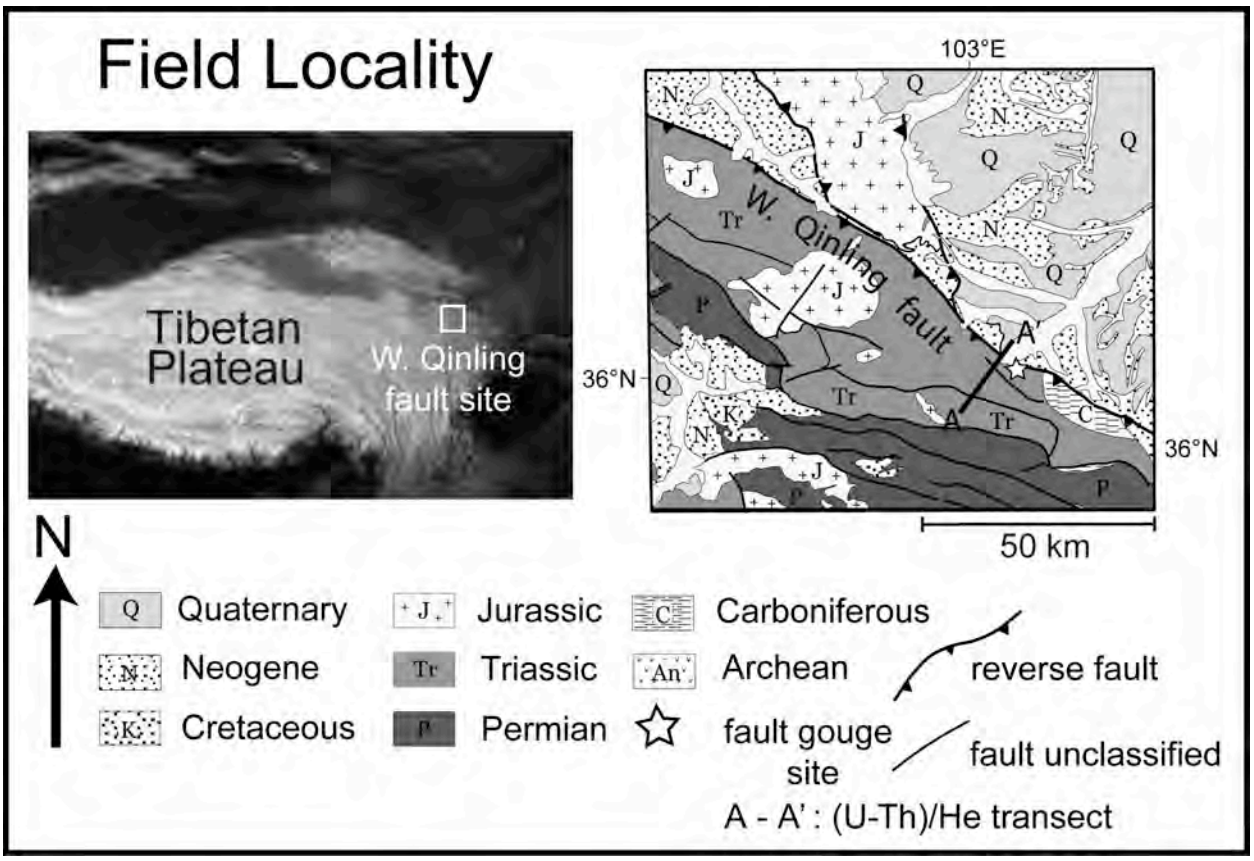

Figure 1. Study location and generalized geology for the West Qinling fault site in northeastern Tibet. Generalized geologic map adapted from 1:200,000 Chinese geologic mapping (Qinghai BGMR, 1991). Q-quaternary deposits, N-Neogene sandstones and shales of the Linxia basin, K-Cretaceous sandstones and shales, Tr-Triassic flysch deposits (Songpan Ganzi complex), P-Permian rocks, C-Carboniferous rocks, An-Archean rocks. A-A' line shows the location of the (U-Th)/He vertical transect (Clark and others, in press).

Cite as: Duvall, A.R., Clark, M.K., van der Pluijm, B. and Li, C., 2010, Eocene Faulting in Northeastern Tibet: Insights from Coupled Low-Temperature Thermochronometry and Ar Dating of Fault Gouge along the West Qinling Fault, *in* Leech, M.L., and others, eds., Proceedings for the 25th Himalaya-Karakoram-Tibet Workshop,: U.S. Geological Survey, Open-File Report 2010-1099, 2 p. [http://pubs.usgs.gov/of/2010/1099/duvall/].

Centrifuge Modelling Study of Contrasting Structural Styles in the Salt Range and the Potwar Plateau, Northern Pakistan

Shah Faisal[1], John M. Dixon[1]

[1]Department of Geological Sciences and Geological Engineering, Queen's University, Kingston, Ontario, Canada, faisal@geoladm.geol.queensu.ca

The ENE-trending Himalayan fold-thrust belt in Pakistan exhibits contrasting deformation styles along strike. The central Salt Range and Potwar Plateau (SR/PP) are gently deformed, but deformation become more complex in the eastern SR/PP. The emergent Salt Range Thrust transforms into a blind thrust in the east. This drastic change in the deformation style in two adjacent areas has been suggested to be caused by the presence of a north-dipping frontal ramp in the center, connected to the east by an east-dipping lateral ramp. Centrifuge modelling is used to replicate the variations in the structural style. For the purpose of modelling, the SR/PP stratigraphy has been grouped into four mechanical units, the lower Salt Range Formation, carapace (Cambrian-Eocene platform sequences), the Rawalpindi Group, and the Siwalik Group. These stratigraphic units of alternating competence, composed of thin layers of plasticine and silicon putty, rest on a rigid base plate. The models are built at a linear scale ratio of ~10^{-6} (1mm = 1km) and deformed in a centrifuge at 4000g. Matched models are serially sectioned transversely and longitudinally to constrain the structure in 3-D.

The thrust sheet models develop a prominent culmination structure over the frontal ramp with a fault-bend fold geometry. The main ramp, localized by a basement normal fault, is responsible for the deflection of the roof sequence to the surface and repetition of the whole stratigraphic sequence. In the presence of a basement warp, deformation readily transferred to the ramp region. As a result the fault-bend fold over the ramp will form out-of-sequence. Although the main décollement remained in the Salt Range Formation, the eastern SR/PP is more internally deformed by detachment folds, fault-propagation folds and pop-up and pop-down structures. The transition from fault-bend fold to detachment and fault-propagation fold geometry takes place in a transfer zone marked by an S-bend (Chambal Ridge and Jogi Tilla) structure on the surface and a lateral ramp in the subsurface.

Cite as: Faisal, S. and Dixon, J.M., 2010, Centrifuge Modelling Study of Contrasting Structural Styles in the Salt Range and the Potwar Plateau, Northern Pakistan, *in* Leech, M.L., and others, eds., Proceedings for the 25th Himalaya-Karakoram-Tibet Workshop,: U.S. Geological Survey, Open-File Report 2010-1099, 1 p. [http://pubs.usgs.gov/of/2010/1099/faisal/].

Mid-Miocene Climate-Driven Rapid Erosion of the Northern Tibetan Plateau

Xiaomin Fang[1], Chunhui Song[2], Weilin Zhang[1], Erwin Appel[3], Junping Gao[2], Maodu Yan[1]

[1] Institute of Tibetan Plateau Research, Chinese Academy of Sciences, Beijing 100085, China, fangxm@itpcas.ac.cn
[2] Key Laboratory of Western China's Environmental Systems, Ministry of Education of China, and College of Resources and Environment, Lanzhou University, Lanzhou 730000, China
[3] Institut für Geowissenschaften, Zentrum für Angewandte Geowissenschaften, Arbeitsbereich Geophysik, Universitaet of Tübingen, 72076 Tübingen

The northeastern Tibetan Plateau is an area of active interaction between tectonics and the Asian monsoon. Both tectonic uplift and climatic change can cause intense erosion of the plateau and sedimentation in intermontane basins. High resolution paleomagnetism has been carried out to date 15 sections of Cenozoic stratigraphy in six basins in the Altyn Tagh and Qilian Shan. Detailed seismostratigraphic and tectonosedimentary investigations and balanced-section restoration were carried out to constrain deformation and uplift. The results show that the Cenozoic sediments in the northern Tibetan Plateau span about 54 Ma to present, and a permanent rapid stepwise increase of erosion and filling of basins was observed to occur at about 15-14 Ma. This increased erosion caused rapid change of the detritus composition in source areas, coarsening of sediments, increased sedimentation rate, and progradation of sediments unconformably upon former raised and eroded areas in basin margins and around the base of mountains. Since deformation at about 15-14 Ma was less strong than at earlier and later times, we suggest that this erosion event was driven by the global Mid-Miocene rapid cooling due to rapid expansion of Southeast Antarctic ice cap.

Cite as: Fang, X., and others, 2010, Mid-Miocene Climate Driven Rapid Erosion of the Northern Tibetan Plateau, *in* Leech, M.L., and others, eds., Proceedings for the 25th Himalaya-Karakoram-Tibet Workshop: U.S. Geological Survey, Open-File Report 2010-1099, 1 p. [http://pubs.usgs.gov/of/2010/1099/fang/].

Can Detrital Tourmaline Provide Stratigraphic Fingerprints? Initial Tests in the Western Himalaya

Xuan Feng[1], A. Alexander G. Webb[1], Darrell J. Henry[1]

[1]Department of Geology and Geophysics, Louisiana State University, Baton Rouge, LA 70803, U.S.A., xfeng5@lsu.edu

The locations and definitions of stratigraphic units in the western Himalaya are controversial. This limits our ability to identify and to reconstruct slip upon the major structures. We investigated the use of the chemistry populations of detrital tourmaline as signatures to correlate and discriminate stratigraphic units in the western Himalaya.

Detrital tourmaline has been used as a provenance indicator because of its chemical variations and stability. Previous studies examined the molecular proportions of Al, Fe, Mg and Ca in tourmalines and showed that different source-rock types have different major-element chemistry (Henry and Guidotti, 1985). Other elements (Na, Mn, K, and Ti) can also be used. We tested if this tool could (1) correlate the Haimanta Group with the Shimla Group and the Greater Himalaya Crystalline complex (GHC); (2) discriminate these late Proterozoic sequences from Early Proterozoic sequences in the western Himalaya. Our results are mixed, showing some promise and indicating some limits for the application of this tool in Himalayan studies.

We obtained electron-microprobe analyses of tourmaline chemistry of samples from the Shimla Group, the Berinag Group, the Damtha Group, the Haimanta Group, and the Greater Himalaya Crystalline. We attempted to separate tourmalines from three Shimla Group samples, two Berinag Group samples, three Damtha Group samples, four Haimanta Group samples and four Greater Himalaya Crystalline samples. Among those samples, one Shimla sample, one Berinag sample, one Damtha sample, three Haimanta samples and two Greater Himalaya Crystalline samples yield tourmalines. The analyzed Berinag Group sample is recrystallized orthoquartzite. The tourmalines are euhedral and observing zoning under cross-polarized light and backscatter imaging does not reveal detrital cores. The analyzed Shimla Group and Damtha Group samples are sandstones dominated by detrital quartz grains with minor micas. Tourmalines are rounded and show cores and thin-overgrowth rim zoning. The Haimanta Group samples are phyllite and garnet mica schist. Out of ~100 tourmaline grains, 25 of them show rounded detrital cores under cross-polarized light and on backscatter images. One Greater Himalaya Crystalline complex sample is schist with quartz, plagioclase, kyanite, garnet and mica. The tourmalines are euhedral and homogenous. They do not show rounded detrital cores under cross-polarized light. The other Greater Himalaya Crystalline complex sample is gneiss with quartz, plagioclase, garnet and mica. The tourmalines in this sample are heterogeneous and show rounded detrital cores with overgrowth-rim zoning.

We plot data from the detrital tourmalines (as determined by textural and zoning evidence described above) in Figure 1. This x-y plot shows Al-Fe-Mg composition in molecular proportions of detrital tourmaline (modified after Henry and Guidotti, 1985). Eight different zones are defined on the basis of different source rock types (see figure caption for specific zone definition). 96 detrital tourmalines from the Shimla Group sample have populations concentrated in zones B and D, 25 Haimanta detrital tourmalines distribute in zones D, E and F, 90 detrital tourmalines from the Damtha Group sample spread evenly across zones B, D, E and F. The Greater Himalaya Crystalline only has 10 detrital tourmaline analyses; these plot in zones B, D, F and G. The analyzed Berinag tourmalines have a very distinctive pattern with two highly concentrated clusters in Al-Fe-Mg and Ca-Fe-Mg binary diagrams. The metamorphic GHC tourmalines show one concentrated cluster in both diagrams.

The chemistry patterns of the Berinag Group tourmalines and most GHC tourmalines likely represent metamorphic growth phases. The analyses of Shimla, Haimanta, and Damtha detrital tourmalines appear sufficient to meaningfully distinguish these populations. Only the Damtha Group and Shimla Group feature low-Mg tourmalines. The Shimla Group and the Damtha Group are distinct, because the Damtha Group tourmaline compositions define a more significant presence in zones E and F (22 vs. 5), with a near absence of Shimla results in zone F (13 vs. 1). Interestingly, the high-temperature (~650-700 °C) Greater Himalaya Crystalline sample preserves detrital tourmalines, while the lower-temperature (~450 °C) Berinag Group sample does not. Finding detrital tourmalines and using their chemistry to establish signatures are the keys to fully apply this tool in differentiating and correlating stratigraphic units.

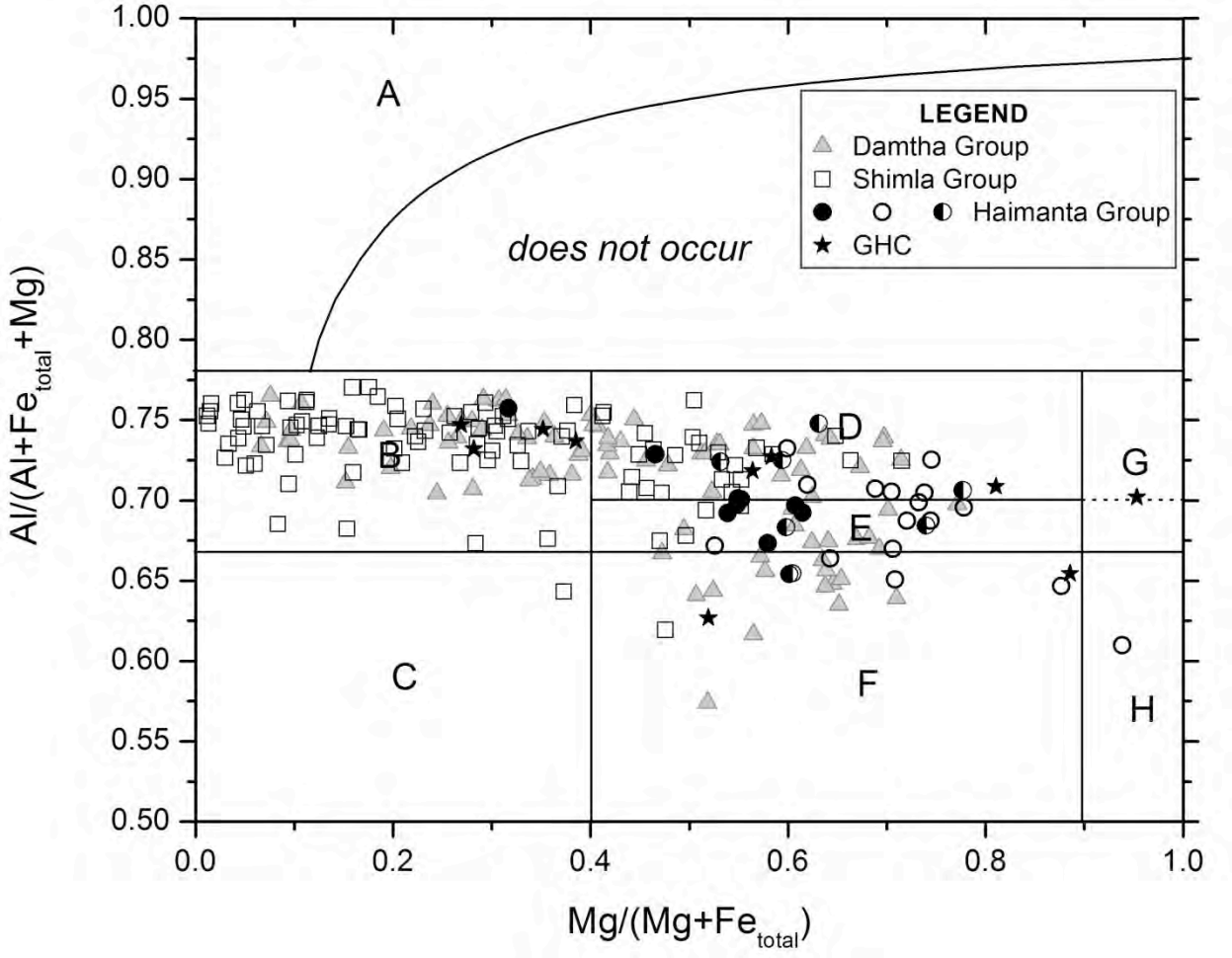

Figure 1. Al-Fe-Mg diagram (in molecular proportions) for detrital tourmalines from Damtha Group, Shimla Group, Haimanta Group and GHC. Zone A—Li-rich granitoids, pegmatites and aplites. Zone B—Li-poor granitoids, pegmatites and aplites. Zone C—hydrothermally altered granitic rocks. Zone D—Aluminous metapelites and metapsammites. Zone E—Al-poor metapelites and metapsammites. Zone F—Fe^{3+}-rich quartz–tourmaline rocks, calc–silicates and metapelites. Zone G—Low Ca ultramafics. Zone H—metacarbonates and metapyroxenites (plot and zones modified after Henry and Guidotti, 1985)

References

Henry D. J. and Guidotti C. V., 1985, Tourmaline as a petrogenetic indicator mineral: an example from the staurolite-grade metapelites of NW Maine, American Mineralogist, 70, 1-15,

Cite as: Feng, X., Webb, A.A.G. and Henry, D.J., 2010, Can Detrital Tourmaline Provide Stratigraphic Fingerprints? Initial Tests in the Western Himalaya, *in* Leech, M.L., and others, eds., Proceedings for the 25th Himalaya-Karakoram-Tibet Workshop,: U.S. Geological Survey, Open-File Report 2010-1099, 2 p. [http://pubs.usgs.gov/of/2010/1099/feng/].

Present-Day Vertical Motion of the Tibetan Plateau and Surrounding Area

Jeffrey T. Freymueller[1], Yuning Fu[1], Wang Qi[2], Xu Caijun[3]

[1] Geophysical Institute, Unversity of Alaska Fairbanks, Fairbanks, AK 99775, U.S.A., jeff.freymueller@gi.alaska.edu
[2] Institute of Seismology, China Seismological Bureau, Wuhan, China
[3] School of Geodesy and Geomatics, Key Laboratory of Geospace Environment and Geodesy, Wuhan University, Wuhan, China

The Tibetan Plateau is by far the largest area of high topography on the planet, and it deforms actively today. Is it growing taller due to ongoing contraction as India continues to collide with Eurasia? Is it collapsing due to extension driven by its excess gravitational potential energy? Is it in a rough state of balance, no longer growing higher, but simply changing shape? Or are different parts of the Plateau evolving in different ways? GPS measurements from the Tibetan Plateau and its surroundings are dense enough and precise enough to make meaningful measurements of vertical motions in Tibet and the rest of the India-Eurasia collision zone, but this data resource has not yet been exploited. We are estimating the vertical motions of hundreds of geodetic sites in the Tibetan Plateau and its surroundings in order to map out the pattern of vertical motions, and construct models to explain the uplift rates and their variation.

Chen and others (2004) showed that if tectonic blocks are defined based on the known major strike-slip faults, there is nearly as much deformation within the blocks as on their boundaries. However, the net areal dilatation in the region studied by Chen and others (2004) is small, because NNE-SSW shortening is nearly balanced by ENE-WSW extension. Later studies have shown similar results based on the horizontal GPS velocities. Vertical motions were ignored in these studies, but careful reprocessing of all the data using the latest GPS analysis methods, models, orbits, and reference frame makes it possible to characterize vertical motions as well as horizontal.

Figure 1 shows a preliminary map of vertical motions, based on a reprocessed version of the Chen and others (2004) data set. The general trend is toward uplift, although the sites with the smallest uncertainties tend to have uplift rates <4 mm/yr except within the Himalaya. We are now reprocessing the data set again taking advantage of a number of significant model improvement and bug fixes, including using a newly-reprocessed and homogeneous series of GPS orbits, improved GPS antenna calibration models, improved ocean tidal loading models, improved atmospheric models, and a more accurate reference frame model. Initial tests show that the scatter of vertical position estimates over a few days has been reduced by nearly a factor of 2 over previous solutions. We will use this improved vertical velocity field to evaluate tectonic and non-tectonic (i.e., changes in surface loads) causes of vertical motion, and then expand the data set to include all of the more recent data now available in China.

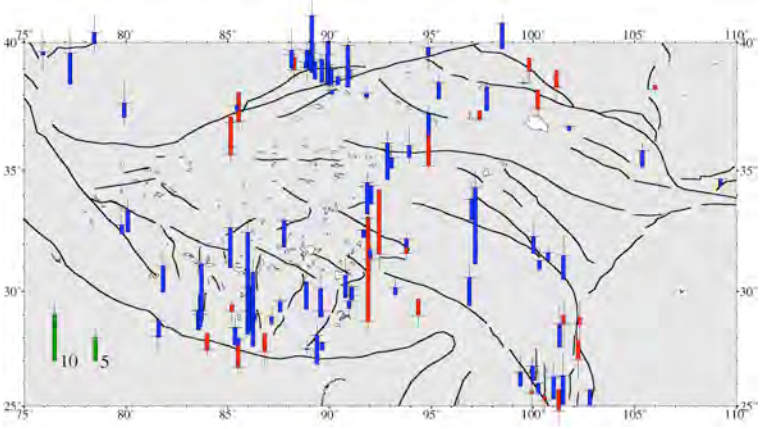

Figure 1. Preliminary estimated vertical velocities for Tibet and the surrounding area. Blue (dark) bars indicate uplift, whereas red (light) bars indicate subsidence, and a horizontal line is drawn at the end of each velocity vector. Error bars are 2σ. The general trend is toward uplift, although the sites with the smallest uncertainties tend to have uplift rates <4 mm/yr except within the Himalaya. Sites displaying large subsidence rates may reflect subsidence if groundwater is being pumped.

Reference

Chen, Q., and others, 2004, A deforming block model for the present-day tectonics of Tibet, J. Geophys. Res., 109, B01403, doi:10.1029/2002JB002151.

Cite as: Freymueller, J.T., Fu, Y., Wang, Q. and Xu, C., 2010, Present-day vertical motion of the Tibetan Plateau and surrounding area, *in* Leech, M.L., and others, eds., Proceedings for the 25th Himalaya-Karakoram-Tibet Workshop: U.S. Geological Survey, Open-File Report 2010-1099, 1 p. [http://pubs.usgs.gov/of/2010/1099/freymueller/].

Geometry and Slip Patterns of the Main Himalaya Thrust Fault in the India-Eurasia Collistion Zone Constrained by Geodetic Observations

Yuning Fu[1], Jeffrey T. Freymueller[1], Caijun Xu[2], Qi Wang[3]

[1] Geophysical Institute, University of Alaska Fairbanks, Fairbanks, AK 99775, U.S.A., yuning@gi.alaska.edu
[2] Wuhan University, Wuhan, China
[3] Institute of Seismology, China Seismological Bureau, Wuhan, China

Like a subduction trench where oceanic lithosphere moves beneath a continental plate, the Indian continental lithosphere, in the India-Eurasia collision zone, is subthrusting beneath another continent (Asia) along the Main Himalaya Thrust (MHT) fault. The sudden significant slips along this thrust fault due to accumulated strain are accommodated by strong earthquakes. Hence, the investigations for the geometry and slip patters of the main thrust fault are essential for both scientific study and geo-hazard research.

Seismic data can be used to image the detailed underthrusting structures beneath Himalaya and southern Tibet (Zhao and others, 1993). However, the seismic-derived cross section is not sensitive to lateral structure variation. In addition, seismic data alone can not offer information about ongoing interseismic slip of the MHT. In contrast geodetic observations, such as GPS and levelling, are able to provide precise constrains for both slip pattern and geometric character of the subthrusting fault (Jackson and Bilham, 1994; Chen and others, 1999). Especially for inferring interseismic slip, geodetic measurements play an irreplaceable role. Consequently, seismic data and geodetic observations can complement each other to better understand the geometry and slip patterns of the main thrust fault in the collision zone.

We therefore assemble published geodetic measurements for the Himalaya and southern Tibet, map out comprehensive velocity fields for the India-Eurasia collision zone, and investigate the present detailed slip pattern of the main thrust fault based on the geometry information constrained from seismic study.

References

Chen, Q., and others, 2004, Spatially variable extension in southern Tibet based on GPS measurements, J. Geophys. Res., 109, B09401, doi:10.1029/2002JB002350.

Jackson, M. and R. Bilham, 1994, Constraints on Himalayan deformation inferred from vertical velocity fields in Nepal and Tibet, J. Geophys. Res., 99, 12,897-13912.

Zhao W., Nelson, K. D. and Project INDEPTH Team, 1993, Deep seismic reflection evidence for continental underthrusting beneath southern Tibet, Nature, 366, 557-559.

Cite as: Fu, Y., Freymueller, J.T., Xu, C. and Wang, Q., 2010, Geometry and slip patterns of the Main Himalaya Thrust fault in the India-Eurasia collision zone constrained by geodetic observations, *in* Leech, M.L., and others, eds., Proceedings for the 25th Himalaya-Karakoram-Tibet Workshop: U.S. Geological Survey, Open-File Report 2010-1099, 1 p. [http://pubs.usgs.gov/of/2010/1099/fu/].

SINOPROBE Deep Seismic Reflection Profiling across the Bangong-Nujiang Suture, Central Tibet

Rui Gao[1], Zhanwu Lu[1], Xiong Xiaosong[1], Lingsen Zeng[1], Wenhui Li[1], Gong Deng[1], Simon L. Klemperer[2]

[1] Institute of Geology, Chinese Academy of Geological Sciences, 100037, Beijing, China, gaorui@cags.net.cn
[2] Department of Geophysics, Stanford University, CA94305-2215, U.S.A.

Exploring the composition and structure of the overthickened crust of the Tibetan plateau is fundamental to unravelling the mechanisms of uplift of the Tibetan plateau. Deep seismic reflection profiling is a well recognized technique to reveal the fine structure of continental lithosphere. INDEPTH deep reflection profiling in the southern Tibetan plateau imaged the Main Himalayan Thrust beneath which the Indian plate underthrusts beneath the Himalaya (Zhao and others, 1993), and also the Moho beneath the great crustal thickness of the Himalyan orogen. However, deep reflection profiling within the interior of the Tibetan plateau was too limited to image lower-crustal structure across the Bangong-Nujiang suture (BNS) (Ross and otheres, 2004), perhaps due to partial melting in the lower crust of the Lhasa Block (LB) (Nelson and others, 1996). The BNS resulted from collision of the LB and Qiangtang block (QB) in the late Jurassic, but may have been reactivated by subsequent strike-slip faulting (Meissner and others, 2004). The QB may be the location of the boundary between the Indian plate and Eurasian plate at lithospheric depths down to 200 km (Zheng and others, 2007). Thermal effects of mantle upwelling maybe the primary cause of the low Pn velocity and the shallower Moho depth in this region. The E-W trending Qiangtang central uplift in the interior of the QB and the convergent structure beneath the west Kunlun orogenic belt (Gao and others, 2000) suggest that the Qiangtang central uplift may be associated with continent-continent collision.

With funding from project "SINOPROBE-02" and the China NSF (40830316), we are currently acquiring a 300-km long deep seismic reflection profile across the BNS and the Qiangtang central uplift (Fig. 1). The reflection profile is a nominal 72-fold common-midpoint (CMP) stack profile, recorded with a 720-channel Sercel 408 XL. The seismic sources are nominal 50-kg charges in boreholes ~30 m deep at intervals of 250 m, and additional charges of 200 kg every 1 km and 1000 kg every 50 km, in boreholes ~50 m deep. All data was recorded to 30 seconds (60s for the 1000 kg shots) using a geophone group interval of 50 m. A maximum far offset of 48 km was used to record the 1000-kg shots.

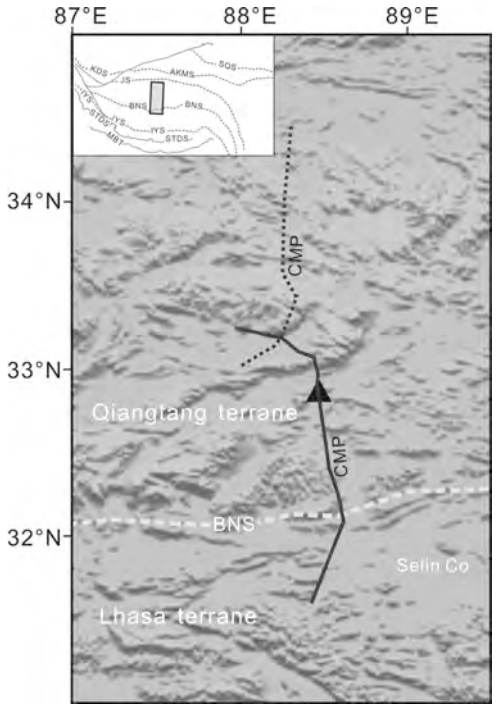

Compared to previous profiles in the QB (Lu and others, 2009), this SINOPROBE profiling achieved deeper shot holes (~50 m), used larger charges (1000 kg), and recorded to longer offsets (~ 50 km). These measures clearly improved the quality of the acquired data, and allowed reflections to be recorded from the lower crust. Figure 2 shows raw data from a single large shot, with a reflection at 22s presumed to be the Moho.

After initial processing, including elevation (statics) corrections, de-noising to improve signal-to-noise ratio, filtering of surface waves, surface-consistent deconvolution, velocity analysis and residual static corrections, a preliminary 93-km long stack-section shows that: (1) beneath the

Figure 1. Location of the Sinoprobe seismic reflection profile (CMP) from the west side of Selin Co northward into the Qiangtang terrane. Tectonic setting after Yin and Harison (2000) . Solid black line: acquired data; dotted line: acquisition in progress. BNS: Banggong-Nujiang suture. ▲ locates shot 626 (Fig. 2).

southernmost part of the profile, there are two sets of strong northward-dipping reflectors at 10 s and 19 s TWT respectively, which suggest that the LB may underthrust beneath the BNS; (2) there is a well-developed northward thrust beneath the shallow part of the BNS; (3) a broad, open fold is imaged south of the BNS at 10 s that shallows to ~ 7 s beneath the BNS; (4) the Moho reflector at 22 s indicates little change in Moho depth across the BNS. As our experiment proceeds, new data further north in the QB will provide an improved crustal image of the collision between the LB and the QB.

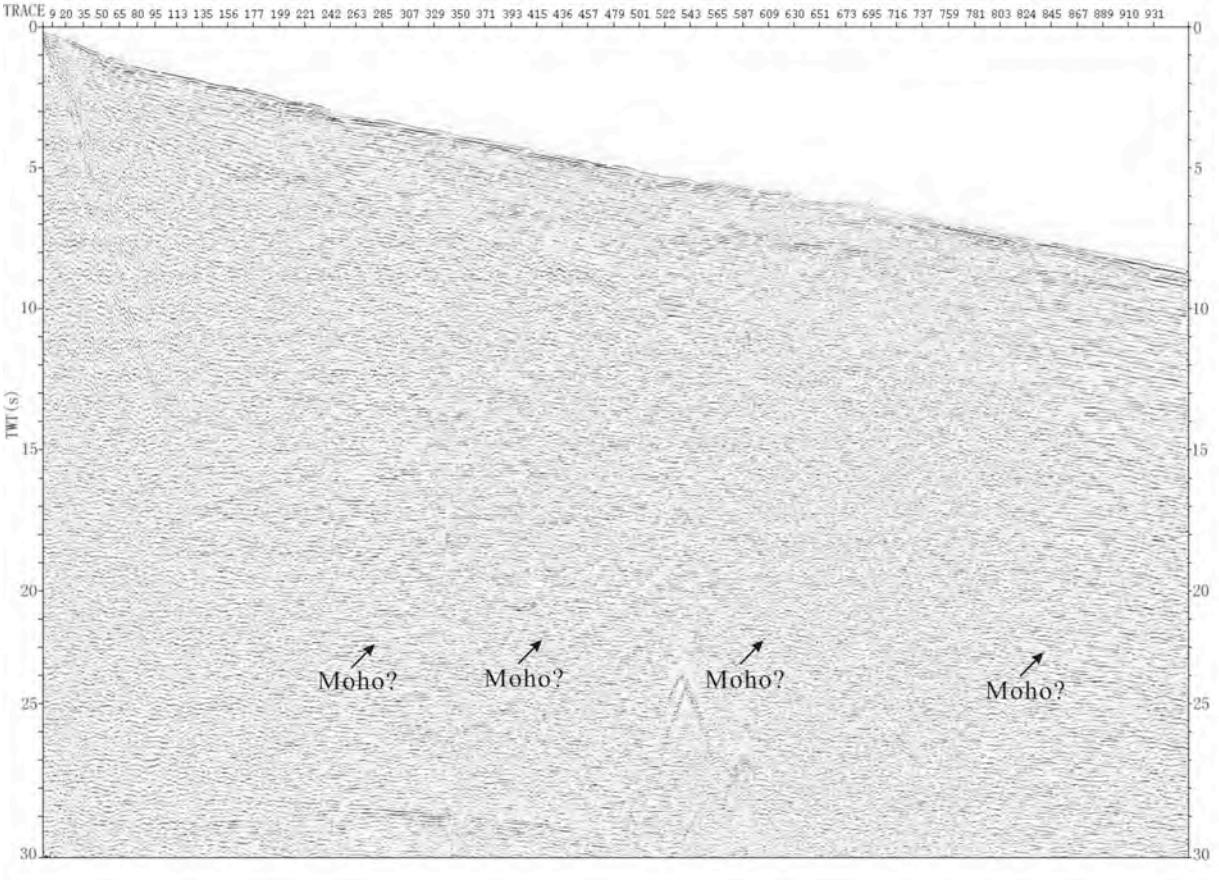

Figure 2. Shot 626 (1000 kg explosive) Moho reflection at 22s TWT. The record was filtered from 3Hz to 15Hz.

References

Gao R., and others, 2000, Deep seismic reflection profile across the juncture zone between the Tarim Basin and the West Kunlun Mountains, Chinese Science Bulletin, 45, 2281-2286.

Lu Z., and others, 2009, Test of deep seismic reflection profiling across central uplift of Qiangtang terrane in Tibetan plateau, Journal of Earth Science, 20, 438-447.

Meissner R., Tilmann F. and Haines S., 2004, About the lithospheric structure of central Tibet, based on seismic data from the INDEPTH III profile, Tectonophysics, 380, 1-25.

Nelson K.D., and others, 1996, Partially molten middle crust beneath southern Tibet: synthesis of project INDEPTH results, Science, 274, 1684-1688.

Ross A., and others, 2004, Deep reflection surveying in central Tibet: lower-crustal layering and crustal flow, Geophys. J. Internat., 156, 115-128.

Yin A. and Harrison T. M., 2000, Geologic evolution of the Himalayan-Tibetan orogen, Ann. Rev. Earth Planet. Sci., 28, 211-280.

Zhao W., and others, 1993, Deep seismic reflection evidence for continental underthrusting beneath southern Tibet, Nature, 366, 557-559.

Zheng H., Li T., Gao R., Zhao D. and He R., 2007, Teleseismic P-wave tomography evidence for the Indian lithospheric mantle subducting northward beneath the Qiangtang terrane, Chinese J Geophys, 50, 1418-1426.

Cite as: Rui, G., and others, 2010, SINOPROBE Deep Seismic Reflection Profiling across the Bangong-Nujiang Suture, Central Tibet, *in* Leech, M.L., and others, eds., Proceedings for the 25th Himalaya-Karakoram-Tibet Workshop: U.S. Geological Survey, Open-File Report 2010-1099, 2 p. [http://pubs.usgs.gov/of/2010/1099/rui/].

Construction of the Tibetan Plateau by Distributed Lithospheric-Scale Shortening: Evidence from Deep Seismic-Reflection Profiling across Northeastern Tibet

Rui Gao[1], Cheng-Shan Wang[2], An Yin[2,3], Haiyan Wang[1], Yuxiu Zhang[3]

[1] Institute of Geology, Chinese Academy of Geological Science, Beijing 100037, China
[2] Research Center for Tibetan Plateau Geology, China University of Geosciences (Beijing), Beijing 100083, China
[3] Dept of Earth and Space Sciences and Institute of Geophysics and Plantary Physics, University of California, Los Angeles, CA 90095-1678, U.S.A., yin@ess.ucla.edu

The northeastern corner of the Tibetan plateau south of Lanzhou has been interpreted as one of outlets of middle-crustal flow sourced from the high-altitude central Tibetan plateau. To test this hypothesis, a 240-km long north-south deep seismic-reflection profile was obtained from Tonggor to Hezuo along longitude of ~103°E across northeastern Tibet. The profile traverses the Songpan-Ganze terrane, the eastern segment of the active left-slip Kunlun fault, and the Kunlun-Qaidam terrane. Major structures in the Songpan-Ganze terrane are isoclinal folds in Triassic strata formed during the latest Triassic closure of the Paleo-Tethys ocean(s) and younger Cenozoic thrusts (mostly south-directed) placing Triassic strata over Tertiary basin fill. The structures in the Kunlun Qaidam terrane north of the Kunlun fault are marked by the appearance of two large anticlinoria cored by Paleozoic and locally Proterozoic units flanked by Paleogene strata. This relationship indicates that their formation occurred in Cenozoic. The Kunlun fault marks the boundary between the two terranes and has developed via reactivation of the Paleo-Tethys suture zone. Our detailed examination of the seismic profile assisted by deep-well data (> 6 km in the Songpan-Ganze terrane) has revealed that the Moho is offset by the vertical Kunlun fault zone for ~10 km. The Moho is also offset by a series of low-angle thrusts with total shortening on the order of at least 10s km along the profile. The Songpan-Ganze terrane consists of four structurally distinctive sequences bounded by major low-angle thrusts. They are from the bottom to the top (1) a highly reflected and well laminated lower crust that exhibits three prominent hanging-wall cutoffs, indicating that the section has been duplicated by discrete thrust shear zones, (2) a thickly laminated but internally folded section in the middle crust, (3) a thrust triangle zone tapering southward lies in the lower part of the upper crust, and (4) a highly folded section corresponding to surface exposure of Triassic flysch complexes is observed in the uppermost part of the section. We interpret sequence (3) as Proterozoic-Paleozoic passive margin sequence of the South China block and sequences (1) and (2) as its basement equivalent to the Pengguan high-grade metamorphic complex in the Longmen Shan to the east. For the Kunlun-Qaidam terrane, two main lithologic units can be recognized in the seismic reflection profile: the relatively transparent basement with short and discontinuous reflectors and its cover sequence with well-laminated and continuous reflectors. The main structures across this terrane are two large wedge systems cored by the two large anticlinoria exposed the northern and southern margins of the terrane along our traverse. The southern thrust wedge tapers northward whereas the north thrust wedge tapers southward. As a result of this structural configuration, a large synclinorium is developed between the two wedges. Internally, each thrust wedge comprises multiple thrust duplex systems and smaller wedges.

The total amount of shortening across the 130-km segment of the profile is at least 90 km. We tentatively suggest that this amount of shortening was entirely created in the Cenozoic rather than in the Triassic, as the style of Triassic deformation is distinctively different from that of the Cenozoic: the former is characterized by tight to isoclinal folds whereas the latter by flat-ramp thrusts that cut and duplicate the older folded sequences. The presence of discrete shear zones offsetting the Moho and duplicating lower-crustal sections on both sides of the Kunlun fault suggests that channel flow and continental subduction are implausible mechanisms for the development of the northeastern Tibetan plateau. Instead, distributed shortening of the entire lithosphere during Cenozoic India-Asia collision is the most likely process that has generated the northeastern Tibetan plateau.

Cite as: Gao, R., Wang, C.S., Yin, A., Wang, H., and Zhang, Y., 2010, Construction of the Tibetan Plateau by Distributed Lithospheric-Scale Shortening: Evidence from Deep Seismic-Reflection Profiling across Northeastern Tibet, *in* Leech, M.L., and others, eds., Proceedings for the 25th Himalaya-Karakoram-Tibet Workshop: U.S. Geological Survey, Open-File Report 2010-1099, 1 p. [http://pubs.usgs.gov/of/2010/1099/gaorui1/].

Tertiary Eclogite Facies Metamorphism in the Greater Himalayan Sequence: Evidence from Zircon U-Pb Geochronology and Trace Element Geochemistry

Djordje Grujic[1], Clare Warren[2], Joseph L. Wooden[3]

[1] Department of Earth Sciences, Dalhousie University, Halifax, NS B3H 4J1, Canada, dgrujic@dal.ca
[2] Earth and Environmental Sciences, The Open University, Milton Keynes MK7 6AA, England
[3] Department of Geological and Environmental Science, Stanford University, Stanford, CA 94305, U.S.A.

Mafic and pelitic granulites exposed in the Greater Himalayan Sequence (GHS) in the eastern Himalayan kingdom of Bhutan preserve textural evidence for a precursor high-pressure metamorphic event, the precise conditions of which are generally unrecoverable due to the later high-temperature overprint (Groppo and others, 2007). As high pressure metamorphism is rare in the Himalayas, especially in the eastern parts of the orogen, their thermobarometrical and geochronological evolution place important constraints on the geodynamic evolution of the Himalaya in particular, and continental collisions in general. We report SHRIMP-RG trace element (REE) and U–Pb zircon geochronological data, collected by the same instrument and on adjacent spots of the same crystal. These data suggest that zircons crystallized at 14-15 Ma over a temperature range of ca. 705-815 °C. This age is interpreted to indicate the timing of HP metamorphism due to the lack of negative Eu anomaly, the depleted heavy REE signature and the temperatures of crystallization.

U-Th-Pb Monazite ages indicate that the near-peak T conditions in this area were attained shortly after the somewhat lower grade area underneath separated by a ductile shear zone. Ti-in-zircon and Zr-in-rutile geothermometry further help to establish links between accessory mineral crystallization and metamorphism. Finally, crystallization ages of deformed leucogranites suggest a concomitant shift of deformation along the roof normal-geometry shear zone towards the interior of the orogen (Kellett and others, 2009). These data are consistent with multiple pulses of GHS exhumation in Bhutan from south to north (Hollister and Grujic, 2006), possibly by tectonic forcing over an incoming Indian crustal ramp.

We suggest that rocks in GHS in the eastern Himalaya were buried to greater depths and subjected to greater temperatures than in the central parts of the orogen, and were exhumed rapidly during the later stages of orogenic evolution. The formation of the Himalaya is currently explained by two contrasting tectonic models that differ in their predictions for the sequence of deformation along the main structures. We conclude that deformation and metamorphism distribution in the Bhutan Himalaya is compatible with the predictions of geodynamic models of Himalaya applying concepts of the channel flow hypothesis (Jamieson and others, 2006).

References

Hollister, L. S. and Grujic, D., 2006, Pulsed channel flow in Bhutan, in: Law, R. D., Searle, M. P. & Godin, L. (eds) Channel Flow, Extrusion, and Exhumation in Continental Collision Zones, Geological Society, London, Special Publications, 268, 415–423.

Groppo, C., Lombardo, B., Rolfo, F. and Pertusati, P., 2007, Clockwise exhumation path of granulitized eclogites from the Ama Drime range (Eastern Himalayas), Journal of Metamorphic Geology, 25, 51-75.

Jamieson, R.A., Beaumont, C., Nguyen, M.H. and Grujic, D., 2006, Provenance of the Greater Himalayan Sequence and associated rocks: Predictions of channel flow models, in: Law, R. D., Searle, M. P. & Godin, L. (eds) Channel Flow, Extrusion, and Exhumation in Continental Collision Zones, Geological Society, London, Special Publications, 268, 165–182.

Kellett, D., Grujic, D. and Erdman, S., 2009, Miocene structural reorganization of the South Tibetan detachment, eastern Himalaya: Implications for continental collision, Lithosphere, 1, 259-281.

Cite as: Grujic, D., Warren, C. and Wooden, J.L., 2010, Tertiary Eclogite Facies Metamorphism in the Greater Himalayan Sequence: Evidence from Zircon U-Pb Geochronology and Trace Element Geochemistry, *in* Leech, M.L., and others, eds., Proceedings for the 25th Himalaya-Karakoram-Tibet Workshop: U.S. Geological Survey, Open-File Report 2010-1099, 1 p. [http://pubs.usgs.gov/of/2010/1099/grujic/].

The High-Grade Crustal Domes of the Pamir

Jennifer McGraw[1], Bradley R. Hacker[1], Lothar Ratschbacher[2], Konstanze Stübner[2]

[1] Department of Earth Science, University of California, Santa Barbara, CA 93106, U.S.A., hacker@geol.ucsb.edu
[2] Geowissenschaften, Technische Universität Bergakademie Freiberg, Freiberg, 09599, Germany

In contrast to Tibet, the Pamir expose multiple domes of Cenozoic high-grade lower crustal rocks. The Pamir thus present an opportunity for understanding the role of the lower crust in continent collisions, in plateaux formation and in the exchange of material between the crust and mantle. These roles can be evaluated by measuring the distribution in space and time of ages of magmatism, ages of crustal thickening, ages of exhumation, depths of exhumation, and deformation associated with formation and exhumation of the domes. Here we report on the depths, temperatures, and exhumation histories of several key domes of the Pamir.

Quantitative constraints on P-T conditions were obtained by 1) assessing mineral parageneses via optical and electron microscopy, 2) measuring mineral compositions by electron microprobe, 3) using *Perple_X* and bulk-rock compositions to calculate pseudosections and mineral compositions, and 4) using *Thermocalc* to calculate positions of equilibria. The most easily interpretable rocks are pelites with garnet ± kyanite ± staurolite + biotite + muscovite + oligoclase + quartz + rutile or ilmenite, but information was also extracted from semi-pelites with garnet + biotite + muscovite + oligoclase + quartz + rutile or ilmenite, and mafic rocks with garnet + hornblende + clinopyroxene + oligoclase–andesine + quartz + rutile or ilmenite. Intrusion, recrystallization, and cooling histories were determined by SIMS and LA-ICP-MS U-Pb zircon and monazite, Rb/Sr mica, $^{40}Ar/^{39}Ar$ hornblende and mica, fission-track and (U-Th)/He apatite dating.

For the northern Pamir Kurgovat dome we find peak conditions of ~600°C and 6 kbar. Hornblende and biotite ages indicate that this metamorphism is Jurassic–early Cretaceous, overprinting Devonian arc intrusions. The central Pamir Yazgulem and Muskol–Sares domes yield similar P-T conditions. Magmatism is late Eocene and early Miocene; the domes show rapid cooling from metamorphic zircon crystallization to near-surface conditions at ~15 Ma. The southwestern Pamir Shakhdara dome gives higher peak metamorphic conditions at ~700°C and 10 kbar; metamorphism, migmatization, and leucogranite intrusion is variable in age but mostly early–mid Miocene. Cooling ages depend on position of the samples to the dome bounding normal shear zone in the south; rapid cooling is mid-Miocene and younger. Robinson and others (2007) reported similar peak metamorphic conditions and mid-Miocene and younger rapid cooling for the Kongur Shan dome.

These data, combined with those of earlier studies (e.g., Hubbard, 1989; Schwab and others, 2004), indicate that the bulk of the Pamir high-grade crystalline rocks were at ~35 km depth in the early Miocene and then exhumed to shallow crustal levels over ~10 Myr. The similar metamorphic and cooling histories of the Kongur Shan, close to the active front of the Pamir, and the Shakhdara dome, in the Pamir hinterland, might reflect the dual intra-continental subduction of the Pamir and the Hindu–Kush slabs.

References

Hubbard, M. S., 1989, Thermobarometric constraints on the thermal history of the Main Central Thrust zone and Tibetan Slab, eastern Nepal Himalaya, Journal of Metamorphic Geology, v. 7, p. 19–30.

Robinson, A. C., and others, 2007, Cenozoic evolution of the eastern Pamir: Implications for strain-accommodation mechanisms at the western end of the Himalayan-Tibetan orogen. Geological Society of America Bulletin, v. 119, p. 882-896.

Schwab, M., and others, 2004, Assembly of the Pamirs. Age and origin of magmatic belts from the southern Tien Shan to the southern Pamirs and their relation to Tibet, Tectonics, v. 23, p. TC4002, doi:10.1029/2003TC001583.

Cite as: McGraw, J., Hacker, B.R., Ratschbacher, L.R. and Stübner, K., 2010, The High-Grade Crustal Domes of the Pamir, *in* Leech, M.L., and others, eds., Proceedings for the 25th Himalaya-Karakoram-Tibet Workshop: U.S. Geological Survey, Open-File Report 2010-1099, 1 p. [http://pubs.usgs.gov/of/2010/1099/mcgraw/].

Erosion Rates at the Crest of the Himalaya: Slow or Fast?

Bernard Hallet[1], Peter K. Zeitler[2], Peter O. Koons[3], Noah J. Finnegan[4], Adam D. Barker[1]

[1] Department of Earth and Space Sciences, University of Washington, Seattle, WA 98195, U.S.A., hallet@uw.edu
[2] Department of Earth and Environmental Sciences, Lehigh University, Bethlehem, PA 18015, U.S.A.
[3] Department of Earth Sciences, University of Maine, Orono, ME 04669, U.S.A.
[4] Department of Earth & Planetary Sciences, University of California, Santa Cruz, CA 95064, U.S.A.

The tempo of erosion in the Himalaya has been studied extensively because of the broad interest in the rich interactions between tectonics, topography and climate that govern the development of this and other mountain ranges. Rates of exhumation at lower elevations have been examined in a multitude of studies by a number of research groups using diverse approaches. For example, Thiede and Ehlers (work in progress) have compiled from these studies ~950 mineral cooling ages obtained from in-situ samples across the entire Himalaya. They include the syntaxial regions at both ends of the range where erosion is clearly linked to the spatial pattern and rate of crustal deformation (e.g., Zeitler and others, 2001a; Koons and others, 2002; Sol and others, 2007; Finnegan and others, 2008).

Little is known, however, about contemporary rates of erosion at the crest of the Himalaya where glacial and periglacial processes dominate. Currently, there is not even consensus in the most recent literature on whether glaciers accelerate or impede erosion in the Himalaya, and contradictory assumptions are being made in the current literature about the role of glaciers and glaciations in shaping the range, and by inference, other mountain belts that are or were glaciated. For example, Rahaman and others (2009), who report on climate control on the distribution of erosion over the Himalaya during the past ~100 ka, claim that sediment yields decreased during periods of more extensive glacial cover in the Higher Himalaya. On the other hand, Gabet and others (2008) reporting on their work in the northern Marsyandi catchment make the common assumption that glacial erosion is, in general, relatively fast and argue that high rates of erosion during periods of glaciation compensate for the low rates during interglacials. Actual data on glacial erosion rates for the Himalaya are indeed very sparse, consisting of only two studies, one of Raikot Glacier,in the Nanga Parbat region (Gardner and Jones, 1993) and another in the Annapurna Range (Heimsath and McGlynn, 2008). This sets the stage for our impending research on erosion rates in the Mt. Everest area.

Are the high peaks eroding fast or are they relatively immune to erosion? The well known occurrence of marine sediments on Mount Everest shows clearly that the amount of exhumation at the crest of the range has been small relative to many areas where igneous and high grade metamorphic rocks have been exhumed from great depth (e.g. Burg and others, 1997; Zeitler and others, 2001b). This does not require erosion to be slow, however, because the Everest massif may be rising and eroding rapidly, but has only done so in the recent geologic past; little is known about the exhumation and uplift history of the region.

Slow erosion is consistent with the notion, which emerged early in the literature (Griffiths, 1952), that high peaks could be relatively resistant to erosion. Indeed, the high peaks and great relief characteristic of the core of high mountain ranges suggest that glacial and periglacial processes are relatively ineffective at the highest elevations. Contributing factors include the limited moisture carried in cold air, increased snow armoring of slopes, snow avalanching off the steep slopes of the "Teflon peaks" (Anderson, 2005), as well as high rock strength of the crystalline-cored peaks and the extremely low temperatures that impede freeze-thaw processes as well as glacial erosion (Koons, 1989; Foster and others, 2008).

Erosion is fast, however, for at least one major mountain in the Himalaya in the eastern most Himalaya (Figure 1). Detrital zircons from a stream draining the cirque glacier incising the north flank of Namche Barwa, analyzed by R.S. Stewart (sample #NB0904), yielded a population of extremely young ages characterized by a number of peaks, the youngest of which is 0.3 Ma and accounts for 35% of the 81 grains analyzed; the oldest grain in this entire sample is 3.6 Ma. The cooling ages for Namche Barwa

north-west flank samples indicate extremely rapid erosion; they are comparable to those found in the Siang river at Pasighat, India (dotted line with beige infilling) that most probably originate from a ~3300 km^2 area where exhumation rates by fluvial incision by the Tsangpo/Siang River (Brahmaputra) range from 7 to 21 mm yr^{-1} (Stewart and others, 2008).

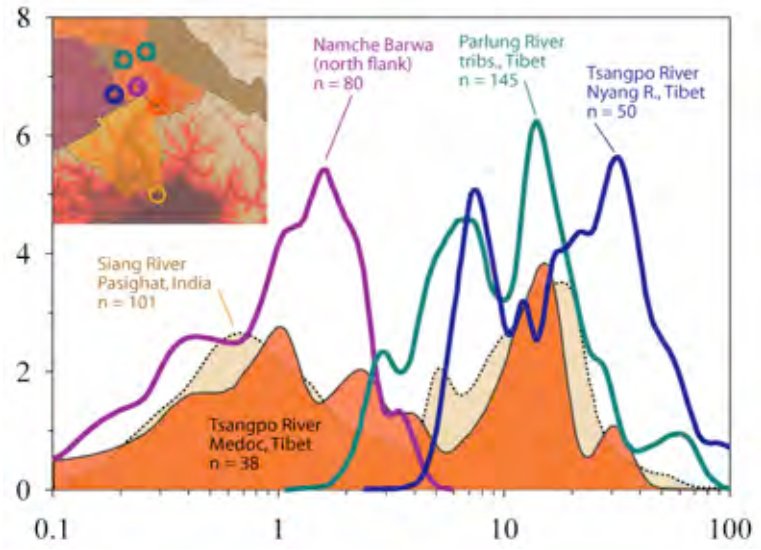

Figure 1. Frequency (vertical axis, in %) of cooling ages (horizontal axis, in Ma) from fission tracks in detrital zircon grains from the easternmost Himalaya. Zircons from the north flank of Namche Barwa (magenta color) have cooled as quickly, and by inference have been exhumed as rapidly, as those from Brahmaputra River as it slices through the Himalaya (labelled by the regional name of the river: the Siang and Tsangpo shown with the beige and orange infilling, respectively). The green and blue curves delineate frequency distributions of material for more slowly eroding drainages of SE Tibet.

References

Anderson, R.S., 2005, Teflon Peaks: the Evolution of High Local Relief in Glaciated Mountain Ranges, EOS Transactions AGU, 86(52), Fall Meeting Supplement, Abstract H33F-04.

Burg, J-P., and others, 1997, Exhumation during crustal folding in the Namche-Barwa syntaxis, Terra Nova, 9(2), 53-56.

Finnegan, N.J., and others, 2008, Coupling of rock uplift and river incision in the Namche Barwa-Gyala Peri massif, Tibet, GSA Bulletin, 120, 142-155.

Foster, D., S.H. Brocklehurst and R.L. Gawthorpe, 2008, Small valley glaciers and the effectiveness of the glacial buzzsaw in the northern Basin And Range, USA, Geomorphology, 102, 624-639.

Gabet, E.J., D.W. Burbank, B. Pratt-Sitaula, J. Putkonen and B. Bookhagen, 2008, Modern erosion rates in the High Himalayas of Nepal, Earth and Planetary Science Letters, 267, 482-494.

Gardner, J.S. and N.K. Jones, 1993, Sediment transport and yield at the Raikot glacier, Nanga Parbat, Punjab Himalaya, In: Himalaya to the Sea: Geology, Geomorphology and the Quaternary, Shroder Jr., J.F., Routledge, eds., London, 184-197.

Griffiths, T.M., 1952, Glacial geomorphology on the Mt. McKinley massif, Alaska, in: Proceedings, eighth General Assembly and seventeenth International Congress, International Geographical Union, Washington, D.C., 331-336.

Heimsath, A.M. and R. McGlynn, 2008, Quantifying periglacial erosion in the Nepal high Himalaya, Geomorphology, 97, 5-23.

Koons, P.O., 1989, The topographic evolution of collisional mountain belts: A numerical look at the Southern Alps, New Zealand, American Journal of Science, 289, 1041-1069.

Koons, P.O., P.K. Zeitler, C.P. Chamberlain, D. Craw, and A.S. Meltzer, 2002, Mechanical links between erosion and metamorphism in Nanga Parbat, Pakistan Himalaya, American Journal of Science, 302, 749-773.

Rahaman, W., S.K. Singh, R. Sinha, and S.K. Tandon, 2009, Climate control on erosion distribution over the Himalaya during the past ~100 ka, Geology, 37, 559-562.

Sol, S., and others, 2007, Geodynamics of the southeastern Tibetan Plateau from seismic anisotropy and geodesy, Geology, 35, 563-566.

Stewart, R.J., and others, 2008, Brahmaputra sediment flux dominated by highly localized rapid erosion from the easternmost Himalaya, Geology, 36(9), 711-714, doi: 10.1130/G24890A.1.

Zeitler, P.K., and others, 2001a, Erosion, Himalayan geodynamics, and the geomorphology of metamorphism, GSA Today, 11, 4-9.

Zeitler, P.K., and others, 2001b. Crustal Reworking at Nanga Parbat, Pakistan: Evidence for erosional focusing of crustal strain. Tectonics, 20, 712-728.

Cite as: Hallet, B., Zeitler, P., Koons, P., Finnegan, N. and Barker, A.D., 2010, Erosion rates at the crest of the Himalaya: slow or fast?, *in* Leech, M.L., and others, eds., Proceedings for the 25th Himalaya-Karakoram-Tibet Workshop: U.S. Geological Survey, Open-File Report 2010-1099, 2 p. [http://pubs.usgs.gov/of/2010/1099/hallet/].

An Integrated Approach to Determining the Crustal Thickness History of Southern Tibet

T.M. Harrison[1], D.J. DePaolo[2], X. Mo[3], Z. Zhao[3], A. Yin[1]

[1]Institute of Geophysics and Planetary Physics and ESS, UCLA, Los Angeles, CA 90095, U.S.A., tmark.harrison@gmail.com
[2]Department of Earth and Planetary Science, University of California, Berkeley, CA 94720, U.S.A.
[3]School of Earth Science and Mineral Resources, China University of Geosciences, Beijing, 100083 PRC

A full understanding of the evolution of a plate margin through the transition from convergence to collision requires knowledge of time-dependent boundary conditions at both the surface and depth. Remote imaging via geophysical studies can tell us about the present structure of the lithosphere but few strategies have been advanced to assess crustal-thickness variations through time. Indeed, post-collisional thrusting and strike-slip faulting typically modify suture zones to such an extent that little can be learned about syn-collisional crustal structure from direct observation.

The Lhasa Block offers the opportunity to combine results from seismology, isotope geochemistry, and thermochronology to gauge crustal thickness variations through time. High-resolution receiver-function analyses are providing an increasingly accurate image of present variations in crustal thickness and structure across southern Tibet. Using a combination of thermochronometry and isotope geochemistry, we have obtained preliminary model crustal thickness estimates for a series of snapshots in time from 120 Ma to present. For example, Nd isotopic data from ca. 50 Ma granitoids along a N-S traverse near Lhasa show a pronounced gradient in ε_{Nd}, with mantle-like values adjacent to the suture zone (+5) rising to $\varepsilon_{Nd} \approx$ -12 at ~120 km north of the suture. This spatial gradient in ε_{Nd} is interpreted as reflecting decreasing mantle input/increasing crustal assimilation due to progressively thickened crust continentward (i.e., higher lower-crustal temperatures enhance crustal assimilation). Using a calibrated crustal thermal model, our initial results suggest that this strong northward gradient in assimilation is due to gradually decreasing northward mantle magma flux coupled with increasing crustal thickness, from ≤20 km immediately north of the suture to ≥50 km in the northern portion of the Gangdese Batholith where the granitoids are essentially pure crustal melts. Exhumation studies using continuous thermochronology applied to pre-120 Ma plutons document the quantity and timing of removal of material from the surface boundary of the Lhasa Block and record time-varying paleo-geothermal gradients. Thus, projecting back from the present reference, we can in principle use these three data sets to determine crustal thickness, exhumation, and petrogenesis through time and possibly assess potential feedbacks between tectonics and topography.

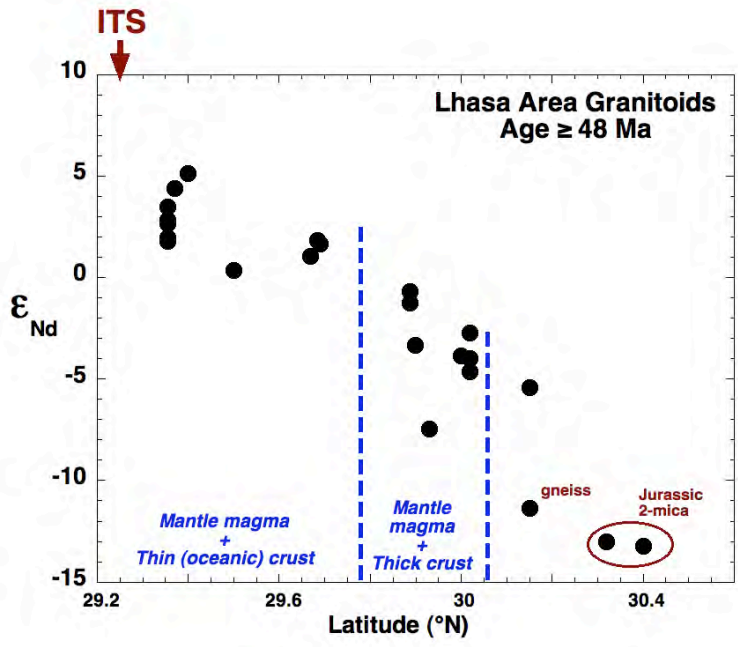

Figure 1. Plot of ε_{Nd} of SE Tibetan granitic rocks vs. latitude. (left) Pre-collisional (>48 Ma) granitoids show a classic continentward decrease in ε_{Nd}. High ε_{Nd} values south of ~29.8°N suggest that this area was underlain by oceanic crust at the time of magmatism. Between 29.8° and 30.1°N there may have been thicker Precambrian basement. North of 30.1°N, melting appears to have been intracrustal. Crustal thickness can be related to wallrock temperature, basement Sm-Nd model ages, and young granitoid initial ε_{Nd} through heat flow models.

Understanding the evolution of southern Tibet has significance well beyond its key role in recording events of the Indo-Asian collision. Knowledge of the pre-collisional geometries of India and Asia is vital to assessing when collision began and how much convergence was accommodated by thickening, extrusion, lower crustal flow, or delamination. The integrated approach described here offers a way to 'image' the pre- and syn-collisional crustal structure of southern Tibet to help address these fundamental issues.

Cite as: Harrison, T.M., DePaolo, D.J., Mo, X., Zhao, Z. and Yin, A., 2010, An Integrated Approach to Determining the Crustal Thickness History of Southern Tibet, *in* Leech, M.L., and others, eds., Proceedings for the 25th Himalaya-Karakoram-Tibet Workshop: U.S. Geological Survey, Open-File Report 2010-1099, 2 p. [http://pubs.usgs.gov/of/2010/1099/harrison/].

Geochemical comparison of north Himalayan gneiss domes

William C. Hassett[1], John W. Sommerfeld[1], Forrest M. Horton[1], Mary L. Leech[1]

[1] Department of Geosciences, San Francisco State University, San Francisco, CA 94132, U.S.A., whassett@sfsu.edu

The Leo Pargil, and Renbu and Yalashangbo gneiss domes are among the western- and easternmost in the chain of north Himalayan gneiss domes, respectively (Figure 1). The processes of gneiss dome formation are still debated, but there is a growing consensus that they result from the diapiric rise of pooled melt from a mid-crustal, ductile channel (Beaumont and others, 2004; Whitney and others, 2004). In the channel-flow model, the ductile channel is exhumed towards the southern Himalayan range front and is exposed as the Greater Himalayan Sequence (GHS). Gneiss domes should be petrogenetically-related to the GHS if the channel flow theory is correct. Geochemical investigation of these granitic gneiss domes can therefore help to determine their origin and mode of development.

Leo Pargil is composed of amphibolite-facies schists, phyllites, metagraywacke, and subordinate quartzites, with numerous cm- to m-scale two-mica granite, tourmaline granite, and leucogranite dikes that constitute between 10% and 50% of the host rock (Thiede and others, 2006). The Renbu dome consists of an ~undeformed two-mica tourmaline granite intruded into upper amphibolite-facies schists, and lies on the west side of a north-south trending graben that is part of the Yadong-Gulu rift system (Leech, 2008). The Yalashangbo gneiss dome consists of a muscovite-biotite granite pluton, intruded into high-grade schists and gneisses (Zhang and others, 2007).

Leo Pargil contains relict U-Pb zircon core ages ranging from Late Archean to Middle Paleozoic (2.8 Ga to 400 Ma) and Middle Eocene to Middle Miocene ages (49 to 15 Ma) for zircon rims, with a weighted mean age of 24.4 Ma (Figure 2; Hassett and Leech, 2007). The Renbu dome has relict U-Pb zircon core ages ranging from Late Archean to Late Triassic (2.5 Ga to 200 Ma) and Late Eocene to Late Miocene ages (39 to 7 Ma) for zircon rims, with a weighted mean age of 9.4 Ma (Figure 2; Hassett and Leech, 2008). Yalashangbo has relict U-Pb zircon core ages ranging from Late Paleoproterozoic to Middle Cretaceous (1.8 Ga to 115 Ma), but zircon rims were too small for analysis and we therefore do not have a record of the timing of most recent magmatism. These results show that broadly, gneiss domes young towards the east, and support the idea that melts feeding gneiss-dome formation may have been truncated in the west by the Karakoram fault (Leech, 2009).

Statistical comparison of granitic zircon cores and country rock zircons for Leo Pargil show that 9 out of 10 REE are statistically indistinguishable, with only Pr showing significant variation in mean relative abundance (Figure 3). Similar results are found for analysis of host rock zircon from the Renbu gneiss dome, in which 8 out of 10 REE are statistically indistinguishable (Figure 3). There is little agreement between granitic zircon rims and cores, suggesting that fractionation occurred during the last magmatic event and zircon rims became enriched in HREE relative to zircon cores. These results indicate that the granitic and host rock zircon share a common protolith, that leucogranites within gneiss domes are most likely anatectic melts of the host rock, and that gneiss domes across the entire Himalayan orogen share a common origin.

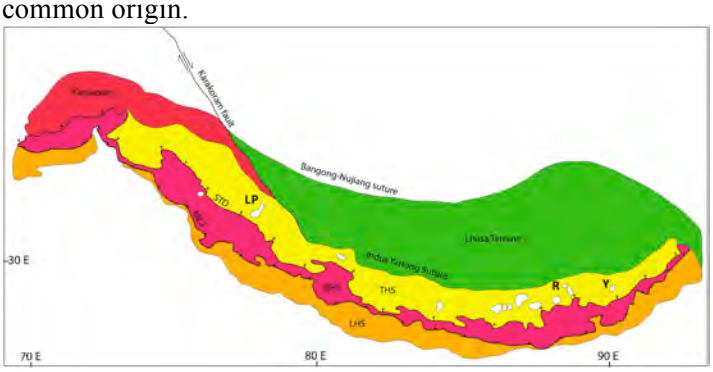

Fig. 1. Simplified geologic map of the Himalayas. Gneiss domes are shown in white, and occur within the THS, between the Indus Yarlung Suture Zone, and the South Tibetan Detachment zone. LHS, Lesser Himalayan Sequence; LP, Leo Pargil; MCT, Main Central thrust; R, Renbu; STD, South Tibetan Detachment; THS, Tethyan Himalaya Sequence; Y, Yalashangbo.

U-Pb SHRIMP age data from zircon cores indicate that the common source for anatectic granites cannot be the Lesser Himalayan Sequence as this unit contains no ages younger than 1.5 Ga (Richards and others, 2005), but ages are consistent with either the GHS or the Tethyan Himalayan Sequence. Future Pb and Nd isotopic analyses will identify the source of the gneiss-dome granites, and may strengthen arguments in favor of the channel flow model.

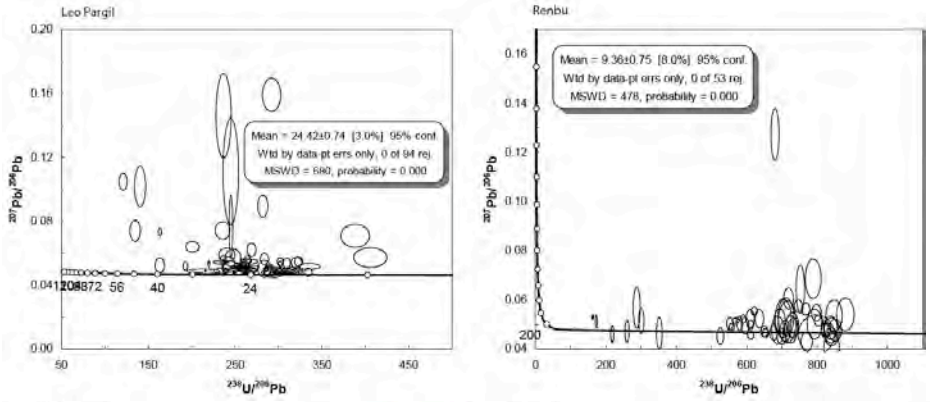

Fig. 2. Tera-Wasserberg Concordia diagrams for Leo Pargil and Renbu gneiss domes, showing ages of most recent magmatism.

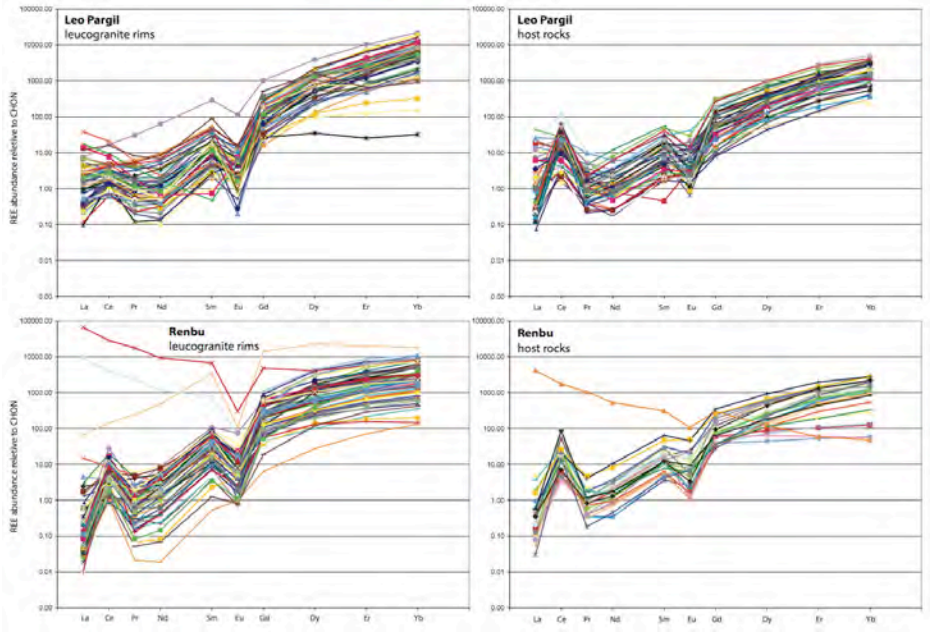

Fig. 3. REE spider plots for Leo Pargil and Renbu gneiss domes, showing HREE-enrichment for granitic zircon rims compared to country rock zircon.

References

Beaumont, C., Jamieson, R.A., Nguyen, M.H. and Medvedev, S., 2004, Crustal channel flows: 1. Numerical models with applications to the tectonics of the Himalayan-Tibetan orogen, Journal of Geophysical Research, 109, B06406.

Hassett, W.C. and Leech, M.L., 2007, Early Miocene granitoids from the Leo Pargil gneiss dome, northwest Himalaya, Eos Trans., Am. Geophys. Union, 88, Fall Meeting Supplement, Abstract T34C-08.

Hassett, W.C. and Leech, M.L., 2008, U-Pb and Trace Element Data From the Renbu Gneiss Dome, Southeast Tibet, Eos Trans., Am. Geophys. Union, 88, Fall Meeting Supplement, Abstract T33B-2049.

Leech, M.L., 2008, Petrology and structure of the Renbu gneiss dome, southeast Tibet, Eos Trans., Am. Geophys. Union, 88, Fall Meeting Supplement, Abstract T33B-2048.

Leech, M.L., 2008, Does the Karakoram fault interrupt mid-crustal channel flow in the western Himalaya?, Earth and Planetary Science Letters, 276, 314–322.

Richards, A., and others, 2005, Himalayan architecture constrained by isotopic tracers from clastic sediments, Earth and Planetary Science Letters, 236, 773–796.

Thiede, R. C., and others, 2006, Dome formation and extension in the Tethyan Himalaya, Leo Pargil, northwest India, Geological Society of America Bulletin, 118, 635.

Whitney, D. L., Teyssier, C. and Vanderhaeghe, O., 2004, Gneiss domes and crustal flow, in: Gneiss Domes in Orogeny (eds. D.L. Whitney, C. Teyssier, C.S. Siddoway), Geological Society of America Special Paper 380, 15–33.

Zhang, J., Guo, L. and Zhang, B., 2007, Structure and kinematics of the Yalashangbo dome in the northern Himalayan dome belt, China, Dizhi Kexue/Chinese Journal of Geology, 42, 16–30.

Cite as: Hassett, W.C., Sommerfeld, J.W., Horton, F.M. and Leech, M.L., 2010, Geochemical investigation of north Himalayan gneiss domes, *in* Leech, M.L., and others, eds., Proceedings for the 25th Himalaya-Karakoram-Tibet Workshop: U.S. Geological Survey, Open-File Report 2010-1099, 2 p. [http://pubs.usgs.gov/of/2010/1099/hassett/].

Uplift and Exhumation along the Arun River (Eastern Nepal): Implications for the Mechanism of Uplift of the High Himalaya and the Coupling between Erosion and Tectonics

Itai Haviv[1], Jean-Philippe Avouac[1], Kenneth A. Farley[1], Mark T. Harrison[2], Matthew T. Heizler[3], Neupane C. Prabhat[4], Gweltaz Mahéo[5]

[1]Division of Geology and Planetary Sciences, California Institute of Technology, Pasadena, CA, U.S.A., haviv@gps.caltech.edu
[2]Department of Earth and Space Sciences, UCLA, Los Angeles, CA, U.S.A.
[3]NM Bureau of Geology and Mineral Resources, NM Tech, Socorro, NM, U.S.A.
[4]Department of Earth and Environmental Sciences, The University of New Orleans, New Orleans, LA, U.S.A.
[5]Laboratoire des Sciences de la Terre, UCB-ENS Lyon, France

The Arun River is one of the largest rivers across the Himalayan arch. Its deep valley is flanked by the >8 km peak of Mt. Everest and its ridge-to-valley relief exceeds 6 km. We combine (U-Th)/He and $^{40}Ar/^{39}Ar$ thermochronology, geomorphic analysis and thermo-kinematic modelling to decipher the mechanism of uplift across the High Himalaya of eastern Nepal and to examine possible tectonic, climatic and erosional interactions along the Arun deep gorge and the parallel Arun-Ama Drime antiformal structure.

Three different thermochronometers depict a pattern of decreasing valley-bottom cooling ages to the north. $^{40}Ar/^{39}Ar$ muscovite ages decrease from 16 Ma near the Main Boundary Thrust to 6 Ma north of the Himalaya topographic front. Zircon (U-Th)/He ages decrease from 6 Ma south of the topographic front to 2 Ma and apatite (U-Th)/He ages decrease from 3 to 0.8 Ma. The decrease in cooling ages across the topographic front is gradual, rather than abrupt. Farther to the north, across the transition to the Tibetan plateau, the increase in the ages is also gradual. At both of these transitions, the increase in exhumation rates towards the core of the range is apparently not a reflection of significant active faulting and more likely reflects mechanisms such as transport over a ramp and uplift due to duplex growth. The observed pattern limits the permissible duration and magnitude of out-of-sequence thrusting as well the possibility for significant, recent, normal faulting parallel to the south Tibetan detachment.

A 3D thermo-kinematic model which includes overthrusting over a flat-ramp-flat geometry and underplating, matches well the observed trends in the cooling ages while respecting geophysical constraints. The inferred spatial pattern of exhumation rates is in agreement with erosion rate proxies including relief, hillslope gradients, tributaries steepness, and specific stream power.

Exhumation rates along the Arun valley are higher than along the Everest (Rongbuk) valley and the Dudh Kosi upper reach, ~ 50 km to the west. This pattern seems to require some differential uplift with higher uplift rates along the Arun valley. Utilizing two thermochronologic transects perpendicular to the axis of the Arun antiform we discuss the possible activity of this structure and place constraints on accommodation of differential uplift.

To examine possible tectonic-climatic interactions, we characterize the north-to-south orographic rainfall gradient along the Arun valley using the Topical Rainfall Measuring Mission data (TRMM), rainfall measurement stations, and discharge gauges. Specific stream power (SSP), calculated using field-measured river width and the TRMM precipitation data, increases considerably across the topographic front of the Himalaya and delineates a ~50 km strip of rapid incision rate. The SSP remains high along this stretch despite more than a 3-fold decrease in precipitation. In addition, the (U-Th)/He cooling ages for apatite and zircon and $^{40}Ar/^{39}Ar$ muscovite ages keep decreasing at least 25 km north of the precipitation maximum. Considered in conjunction with previously published studies along the Marsyandi River this data suggests that the belt of rapid uplift within central and eastern Nepal is not a simple reflection of the spatial pattern of monsoon precipitation. We use the data to discuss the coupling between climate and tectonic deformation in the Himalaya and highlight other mechanisms which could localize strain.

Cite as: Haviv, I., and others, 2010, Uplift and Exhumation along the Arun River (Eastern Nepal): Implications for the Mechanism of Uplift of the High Himalaya and the Coupling between Erosion and Tectonics, *in* Leech, M.L., and others, eds., Proceedings for the 25th Himalaya-Karakoram-Tibet Workshop: U.S. Geological Survey, Open-File Report 2010-1099, 1 p. [http://pubs.usgs.gov/of/2010/1099/haviv/].

Ophiolites Associated with Suture Zones of the Collisional System between India and Eurasia: a Synthesis

Réjean Hébert[1], Carl Guilmette[1], Rachel Bezard[1], Jarosalv Dostal[2], Chengshan Wang[3], Jingen Dai[3]

[1] Département de Géologie et de Génie Géologique, Université Laval, Québec, QC G1V 0A6, Canada
rejean.hebert@ggl.ulaval.ca
[2] Department of Geology, St.Mary's University, Halifax, NS B3H 3C3, Canada
[3]Research Center for Tibetan Plateau Geology, China University of Geosciences, Beijing, 100083, China

Reinvestigation of the Yarlung Zangbo Suture Zone (YZSZ) and other similar sutures occurring within the India-Eurasia collisional system has shown that they are very complex in terms of geochronology and metamorphic and igneous history. YZSZ comprises rocks from as old as Late Devonian to rocks as young as mid-Miocene. Metamorphic facies vary from high-grade to very-low grade. Late Devonian rocks (363.7 ± 1.7 Ma) are alkalic gabbros resulting from activity of a plume active within the Paleo-Tethys. The Permian and Triassic rocks are limestone associated with radiolarite showing affinities with Indian continental margin and deep Tethyan ocean floor, respectively. Two ophiolite sub-groups are recognized. Sub-group I is mid- to late Jurassic (150-177 Ma) in age and ill-defined because only few sequences have been found and studied so far. It is probably derived from the destruction of a marginal basin comprising intra-oceanic arc and fore-arc settings. The Spontang and Zedong sequences are type-examples. Sub-group II is Lower Cretaceous in age (120-130 Ma) and represents the destruction of a large-scale suprasubduction environment comprising marginal basins, arcs, and back-arc systems. These ophiolites are spatially associated with ophiolitic mélanges and flysch respectively representing the reworking of the Cretaceous ophiolites and Indian continental margin and part of the Neo-Tethyan ocean floor. Most ophiolitic sequences found in suture zones belong to sub-group II such as Yungbwa, Xiugubagu, Saga, Xigaze, etc... Amphibolite and garnet amphibolite blocks (123-130 Ma) found within the ophiolitic mélange share the same geochemical attributes with sub-group 2 ophiolites. Their protoliths were probably generated within a back-arc spreading center and metamorphosed in a nascent subduction zone at around 50 km depth. Some radiometric ages suggest events at 80 Ma and 90 Ma represent the entry of Indian continental margin into the intra-oceanic subduction zone and/or obduction of ophiolites. However these ages seem to be very rare throughout the whole suture zone and are therefore considered as resulting from local metamorphic events. Some alkalic igneous rocks (131-144 Ma) within the flysch could represent Kerguelen OIB plume products. The study of igneous blocks and the sedimentary matrix suggests a continuous passive-margin model. The Miocene (11-17 Ma) post-collisional ultrapotassic rocks discovered in 2006-2007 result from the collapse of the Tibet Plateau accommodated by the E-W extensional regime. They carry crustal xenoliths of metamorphic origin representing a window through the deep crustal section underlying the YZSZ. The geochemistry of these shoshonitic intrusives shows strong subduction components resulting from metasomatism of the mantle wedge over the subduction zones accommodating the closure of the Neo-Tethys basin. εNd values suggest the source reservoir for these magmatic rocks has mostly Asian late-Precambrian affinity.

The YZSZ contains features related to the interplay between India and Eurasian plates formerly separated by the Tethys Ocean or associated smaller marginal basins such as the Neo-Tethys basin. However, the complexity of the YZSZ and the diversity of rock types call for a redefinition of the suture zone to include the mosaic of terranes now tectonically juxtaposed within this narrow orogenic collisional zone.

Cite as: Hébert, R., and others, 2010, Ophiolites associated with suture zones of the collisional system between India and Eurasia: a synthesis, *in* Leech, M.L., and others, eds., Proceedings for the 25th Himalaya-Karakoram-Tibet Workshop: U.S. Geological Survey, Open-File Report 2010-1099, 1 p. [http://pubs.usgs.gov/of/2010/1099/hebert/].

Towards Defining the Transition in Style and Timing of Quaternary Glaciation between the Monsoon-Influenced Greater Himalaya and the Semi-Arid Transhimalaya of Northern India

Kathryn A. Hedrick[1], Yeong Bae Seong[2], Lewis A. Owen[1], Marc W. Caffee[3], Craig Dietsch[1]

[1] Department of Geology, University of Cincinnati, P.O. Box 0013, Cincinnati, OH 45221-0013, U.S.A., hedricka@mail.uc.edu
[2] Department of Geography Education, Korea University, Anam-Dong, Seongbuk-Gu, Seoul 136-701, Korea
[3] Department of Physics/PRIME Laboratory, Purdue University, West Lafayette, IN 47906, U.S.A.

Himalayan glaciation is heavily influenced by variable input from competing climate systems: the South Asian summer monsoon and the mid-latitude westerlies (Benn and Owen, 1998). To delineate the transition in climatic glacial forcing between two regions with contrasting glacial history—Lahul to the south and Ladakh to the north—moraines in Puga and Karzok valleys, located in the intermediate Zanskar region of the Transhimalaya, were mapped and moraine boulders dated using ^{10}Be terrestrial cosmogenic nuclide exposure age dating. In Lahul, Late Quaternary glaciation was extensive; glaciers advanced >100 km from the modern ice margin, whereas glaciation in Ladakh has been comparatively restricted as advances reached only ~30 km from the contemporary glacial margins during the last 200 ka (Owen and others, 1997, 2001, 2006).

In the Puga valley, glaciers advanced >10 km at ~115 ka and <10 km at ~40 ka, ~3.3 ka, and ~0.5 ka, while in the Karzok valley glaciers advanced <2 km at ~3.6 ka. Boulder exposure ages from a large moraine complex in Karzok indicate a possible glacial advance at ~80 ka of <5 km. The oldest moraine in Karzok is ~310 ka, indicating that glaciers advanced >10 km during MIS-9 or older.

The glacial chronology of the Puga and Karzok valleys shows generally asynchronous glaciation despite the proximity of the valleys (~25 km). Moraine ages in the Puga and Karzok valleys broadly correlate with previous studies in the Zanskar Range (Taylor and Mitchell, 2000) but the paucity of data for many of the glacial stages across the Zanskar region makes these correlations tentative. The lack of early Holocene glaciation in the Puga and Karzok valleys is in stark contrast to many regions of the Himalaya, including the Lahul and Garhwal ranges to the south, the Karakoram to the north, and in Nanga Parbat and the Swat valley in the Greater Himalaya to the west (Benn and Owen, 1998). The restricted glacial extent in Puga and Karzok valleys is more similar in style to glaciations in Ladakh, however, moraines in both valleys have ^{10}Be ages similar to the northern ranges; well-established advances in the Karakoram and Ladakh range at ~20 and ~80 ka may match Karzok valley glacial records, whereas advances at ~100 and ~40 ka match the Puga valley records (Owen and others, 1997, 2001, 2006). The dissimilarity between the glacial records in the Puga and Karzok study areas suggests a possible relatively sharp transition from southern monsoon to westerly-controlled glacial advances.

References

Benn, D.I. and Owen, L.A., 1998, The role of the Indian summer monsoon and the mid-latitude westerlies in Himalayan glaciation: review and speculative discussion, Journal of the Geological Society of London 155, 353–363.

Owen, L.A., Mitchell, W., Bailey, R.M., Coxon, P. and Rhodes, E., 1997, Style and timing of glaciation in the Lahul Himalaya, Northern India: a framework for reconstructing late Quaternary palaeoclimatic change in the western Himalayas, Journal of Quaternary Science 12, 83–109.

Owen, L.A., and others, 2001, Cosmogenic radionuclide dating of glacial landforms in the Lahul Himalaya, Northern India: defining the timing of Late Quaternary glaciation, Journal of Quaternary Science 16, 555–563.

Owen, L.A., Caffee, M.W., Bovard, K.R., Finkel, R.C. and Sharma, M.C., 2006, Terrestrial cosmogenic nuclide surface exposure dating of the oldest glacial successions in the Himalayan orogen: Ladakh Range, northern India, Geological Society of America Bulletin 118, 383-392.

Taylor, P.J. and Mitchell, W.A., 2000, The Quaternary glacial history of the Zanskar Range, northwest Indian Himalaya, Quaternary International 65/66, 81-99.

Cite as: Hedrick, K.A., Seong, Y.B., Owen, L.A., Caffee, M.W. and Dietsch, C., 2010, Towards defining the transition in style and timing between the monsoon-influenced Greater Himalaya and the semi-arid Transhimalaya of northern India, *in* Leech, M.L., and others, eds., Proceedings for the 25th Himalaya-Karakoram-Tibet Workshop: U.S. Geological Survey, Open-File Report 2010-1099, 1 p. [http://pubs.usgs.gov/of/2010/1099/hedrick/].

The Tibet-Himalaya Accommodation Zone and the Nature of Orogenic Plateau Margins

K.V. Hodges[1], K.X. Whipple[1]

[1] School of Earth and Space Exploration, Arizona State University, Tempe, AZ 85287, U.S.A., kvhodges@asu.edu

Geodetic studies have established the existence of a profound discontinuity in modern surface strain between the Tibetan Plateau and the Himalaya. To the north, the surface strain field of southern Tibet is one of essentially E-W extension expressed as N-S–striking normal fault systems and NW-SE–striking and NE-SW–striking transcurrent fault systems. To the south, the modern surface strain of the Himalaya is characterized by N-S contraction by deformation on active, N-S–striking, S-vergent thrust fault systems. This discontinuity persists at least as far back in time as the initiation of N-S graben systems of southern Tibet in Middle-Late Miocene time.

Precisely how these two surface strain fields interact is one of the most poorly understood facets of the active tectonics of the Himalayan-Tibetan orogenic systems. In a 2001 *Tectonics* paper with José Hurtado (Hodges et al., 2001), we hypothesized that active, discrete, N-dipping detachments of the South Tibetan fault system (STFS) may maintain strain compatibility between the Himalayan and Tibetan Plateau regimes. In our model, these detachments projected northward into the middle crust beneath southern Tibet and served as modern manifestations of the upper bounding faults of a Miocene-Recent, southward extruding channel of reprocessed crust of Indian Plate affinity (see also Beaumont and others, 2001; Hodges, 2006). This idea derived from geologic observations in the Kali Gandaki drainage in the Annapurna-Dhaulagiri Himalaya of central Nepal (~28˚40'N; 83˚36'E), where the N-S–trending Thakkhola graben appears to truncate abruptly at the surface trace of a prominent STFS detachment (Hurtado et al., 2001). While few other segments of the STFS had been scrutinized by 2001 for evidence of neotectonic activity, we also noted that the strain transition from southern Tibet to the Himalaya was roughly coincident with mapped traces of the STFS, with a major physiographic transition from the plateau to the main Himalayan ranges, and with knick points and drainage divides on large trans-Himalayan rivers as they flowed off the plateau. To us, these provided additional (albeit indirect) evidence of recent slip on the STFS.

Since 2001, our research group has conducted additional studies along the southern boundary of the Tibetan Plateau in Bhutan, Nepal, and Tibet and it is now clear that the transition between the Himalayan and Tibetan strain fields – which we refer to here as the *Tibet-Himalaya Accommodation Zone* (THAZ) – is more complicated than a single array of detachments along the trace of the STFS. In detail, THAZ (most easily defined as the southern limit of N-S–striking normal faults) sometimes lies near the trace of major Miocene detachments of the STFS or the Himalayan range crest but sometimes does not. For example, in the Dhaulagiri Himalaya (~28˚37'N; 83˚15'E), it is marked by a series of oblique-slip faults that express as N-dipping fault scarps and lineaments cropping out south of the trace of the STFS and not far north of the trace of the Main Central thrust. In the upper Arun drainage (~28˚06'N; 87˚22'E) and at the Yadong cross-structure (~27˚48'N; 89˚12'E), THAZ corresponds in part to ~N-S–striking normal faults that bound major transverse ranges or extensional graben. In some poorly mapped regions, the position of THAZ can be estimated only approximately and is not marked by faults that are obvious in remote sensing imagery. Thus, it appears that the southern boundary of the Tibetan Plateau is marked by active, surface-breaking faults in some places and a steep topographic gradient, presumably developed over blind structures, in others.

We hypothesize that active structures of THAZ root northward to form a décollement at the top of the modern seismic low-velocity zone in the middle crust of southern Tibet (e.g., Nelson et al., 1996). In this model, THAZ is a detachment separating the upper crust of southern Tibet (which is undergoing E-W extension) from deeper structural levels that experience N-S contraction directly related to the continued northward subduction of the Indian Plate. If correct, this implies that the upper crust of southern Tibet is essentially delaminated from the middle crust and that the observed surface strain field in southern Tibet may be quite different from the strain field in the middle and lower crust below.

The nature of the southern boundary of the Tibetan Plateau, characterized by a strain accommodation zone that dips toward the plateau and in the same direction as the main subduction zone of the Himalayan-Tibetan orogen (currently the Main Himalayan thrust system), is markedly different from the western boundary of the Andean Plateau in South America. The boundary there is marked instead by a combination of steep homoclines, minor thrust faults, and – at least in Southern Peru (~16˚S; 72-73W; Schildgen and others, 2009) – steep normal faults that dip away from the plateau and in the opposite direction as the main subduction zone of the Andean orogen (the Peru-Chile trench). The differences in these margins are interesting because the western Andean Plateau and the southern Tibetan Plateau share a variety of physiographic and geodynamic characteristics, including the likelihood of there being a fluid middle crust beneath each that is susceptible to lateral flow under the influence of gravity. Unlike the southern margin of the Tibetan Plateau, where channel flow may be responsible for recycling of accreted Indian crust to the Himalayan range front, the western margin of the Andean Plateau exhibits no evidence for the return flow of lower plate material toward the range front by an extruding channel. This may simply be a difference between continent-continent convergence and ocean-continent convergence, but it is noteworthy that the western Andean front has an arid to hyperarid climate whereas the Himalayan front experiences a monsoon climate with up to 5m/yr rainfall. Comparative studies of the much wetter (Amazonian) eastern margin of the Andean Plateau with the southern margin of the Tibetan Plateau, as well as the dry northern margins of the Tibetan Plateau with the dry western margin of the Andean Plateau, may yield a better understanding of the role of climate in the evolution of plateau margins.

References

Beaumont, C., Jamieson, R. A., Nguyen, M. H. and Lee, B., 2001, Himalayan tectonics explained by extrusion of a low-viscosity crustal channel coupled to focused surface denudation, Nature, 414, 738-742.

Hodges, K. V., 2006, A synthesis of the Channel Flow-Extrusion hypothesis as developed for the Himalayan-Tibetan orogenic system, in Law, R., Searle, M., and Godin, L., eds., Channel Flow, Ductile Extrusion, and Exhumation of Lower-Middle Crust in Continental Collision Zones, London, Geological Society Special Publication 268, p. 71-90.

Hodges, K. V., Hurtado, J. M. and Whipple, K. X., 2001, Southward extrusion of Tibetan crust and its effect on Himalayan tectonics, Tectonics, 20, 799-809.

Hurtado, J. M., Hodges, K. V. and Whipple, K. X., 2001, Neotectonics of the Thakkhola Graben and implications for Recent activity on the South Tibetan Fault System in the central Nepalese Himalaya, Geological Society of America Bulletin, 113, 222-240.

Nelson, K. D., and others, 1996, Partially molten middle crust beneath southern Tibet: Synthesis of Project INDEPTH Results, Science, 274, 1684-1688.

Schildgen, T. F., and others, 2009, Late Cenozoic structural and tectonic development of the western margin of the Central Andean Plateau in southwest Peru, Tectonics, 28, doi:10.1029/2008TC002403.

Cite as: Hodges, K.V. and Whipple, K.X. 2010, The Tibet-Himalaya Accommodation Zone and the Nature of Orogenic Plateau Margins, *in* Leech, M.L., and others, eds., Proceedings for the 25th Himalaya-Karakoram-Tibet Workshop: U.S. Geological Survey, Open-File Report 2010-1099, 2 p. [http://pubs.usgs.gov/of/2010/1099/hodges/].

Preliminary Fault Slip-Rate Estimate for the Right-Lateral Beng Co Strike-Slip Fault, based on Quaternary Dating of Displaced Paleo-Lake Shorelines

James Hollingsworth[1], Brian Wernicke[1], Lin Ding[2]

[1] Division of GPS, Caltech, MC 100-23, Pasadena, CA 91125, U.S.A., james@gps.caltech.edu
[2] Institute of Tibetan Plateau Research, Chinese Academy of Sciences, Beijing 100029, China

GPS data indicate that eastward extrusion of material across the Tibetan Plateau accommodates some of the northward motion of India, with respect to Eurasia (Zhang and others, 2004). The Beng Co fault is a major right-lateral strike-slip fault, which strikes ESE for a distance of 150+ km across the eastern Central Tibetan plateau. Armijo and others (1989) suggested the Beng Co fault is one of a small number of important strike-slip faults in Central Tibet which accommodate the eastward extrusion of material. However, such a kinematic model requires the Beng Co fault slip-rate to be relatively high (~10 mm/yr), compared to the relatively slow rate (~1 mm/yr) expected if eastward motion is accommodated in a more distributed way across many active structures throughout the region.

Unfortunately, existing GPS data or measurements from Satellite Radar Interferometry (InSAR) collected over the decadal timescales are not currently able to resolve the slip-rate for the Beng Co fault with enough precision to resolve this issue (e.g. Zhang and others, 2004; Taylor and Peltzer, 2006). In this study, we use a variety of Quaternary dating techniques to determine the age of geomorphic markers which are displaced across the Beng Co fault. From this we calculate a slip-rate for this fault, averaged over the late Quaternary period, which allows us to test if a distributed or block model approach is more appropriate for describing active deformation in Central Tibet.

The Beng Co fault cuts across a number of paleo-lake shorelines around the southern margin of the Peng Co Lake, Central Tibet. Three main sequences of beach berms are present around the present lake shoreline (1 being the oldest, 3 being the youngest), with each sequence comprising as many as 5 individual beach berms. At 31.389°N 90.426°E, the fault displaces sequence 2 beach berms in a pure right-lateral sense by ~15 m. These beach berms can be clearly traced 6 km eastwards around the lake, where they become incised and exposed by a river which drains into the Peng Co Lake. We collected shells for radiocarbon dating, and fine sand samples for OSL dating from beach berms within shoreline sequences 1,2 and 3, as well as samples for ^{36}Cl exposure dating from profiles through each beach berm. Dating of these samples is ongoing. However, we present the initial results from carbon dating of snail shells found within each berm, thereby allowing us to bracket the age of the 15 m displacement on the Beng Co fault, and calculate a preliminary fault slip-rate for this section of the fault.

References

Armijo, R., Tapponnier, P. and Tonglin, H., 1989, Late Cenozoic right-lateral strike-slip faulting in southern Tibet, J. Geophys. Res., 94, 2787 – 2838.

Taylor, M. and G. Peltzer, 2006, Current slip rates of conjugate strike slip faults in central Tibet using Synthetic Aperture Radar Interferometry, Journal of Geophysical Research, 111, B12402, doi:10.1029/2005JB004014

Zhang, P.Z., and others, 2004, Continuous deformation of the Tibetan plateau from global positioning system data, Geology, 32, 809-812.

Cite as: Hollingsworth, J., Wernicke, B. and Ding, L., 2010, Preliminary Fault Slip-Rate Estimate for the Right-Lateral Beng Co Strike-Slip Fault, based on Quaternary Dating of Displaced Paleo-Lake Shorelines, *in* Leech, M.L., and others, eds., Proceedings for the 25th Himalaya-Karakoram-Tibet Workshop: U.S. Geological Survey, Open-File Report 2010-1099, 1 p. [http://pubs.usgs.gov/of/2010/1099/hollingsworth/].

U-Pb SHRIMP geochronology of leucogranites from the Greater Himalayan Sequence in Zanskar and from the Karakoram fault zone, NW India

Forrest M. Horton[1], John W. Sommerfeld[1], William C. Hassett[1], Mary L. Leech[1]

[1] Department of Geosciences, San Francisco State University, San Francisco, CA 94132, U.S.A.

New U-Pb SHRIMP ages have been obtained along the westernmost limb of the South Tibetan Detachment in northwest India, locally known as the Zanskar Shear Zone (ZSZ), and from the dextral strike-slip Karakoram fault zone. This research investigates the extent of ductile mid-crustal exhumation and anatexis in the westernmost part of the Greater Himalaya Sequence (GHS), and explores a possible relationship between leucogranites in Zanskar and the Karakoram fault zone. All ages presented here are ^{204}Pb-corrected ^{238}U/^{206}Pb ages.

Leucogranite from the lowest structurally-exposed GHS near the Suru dome in the Zanskar region (Z45, 34°3.69' N, 75°56.07' E; Figure 1) yields an average monazite age of 19.2±0.4 Ma, which correlates with the previously-determined U-Pb TIMS age of 20.8±0.3 Ma for a leucogranite to the east (Noble and Searle, 1995); both leucogranite ages are appreciably younger than the 25.1±0.6 Ma monazite age of pelitic schist from the Nun-Kun valley (Z40, 34°3.09' N, 76°14.67' E). Approximately 100 km to the southeast in the Haptal valley, a migmatite yields an average monazite age of 20.7±0.4 Ma (Z1, 33°26.60' N, 76°46.59' E), while an adjacent late-stage pegmatite dike in a small leucogranite pluton yields monazite ages ranging from 25.9±1.3 to 19.0±0.9 Ma (Z5, 33°27.07' N, 76°46.11' E; Figure 2). Leucogranite samples Z23 and Z4 yielded inherited monazite ages of ~470 Ma and ~450 Ma, respectively, indicating that Cambro-Ordovician Pan-African granites were a partial source for Zanskar leucocratic melts.

Oligocene−Miocene ages suggest that units near the ZSZ reached monazite closure temperatures (~750–720 C; Copeland and others, 1988) earlier than deeper GHS units. In the Haptal valley, ductile shear along the ZSZ juxtaposed Miocene migmatites, associated leucogranites and older metapelites while telescoping the metamorphic isograds (Searle and others, 1999). Haptal leucogranites can be traced in the field to migmatite zones, indicating that locally-generated melt ponded below the ZSZ; this is consistent with observations made by Dezes and others (1999) to the east near the Gumburanjun dome. In the Nun-Kun valley, less extensional offset occured along the ZSZ than in the Haptal valley (Inger, 1998) and leucogranites are hosted by schists and gneisses rather than migmatite, suggesting that leucogranite melts migrated further from their source in northwest Zanskar. Also, there is a significant structural transition near Pensi La, where extensional shear zones in the northwest, distributed among imbricated thrust sheets, converge into the compact ZSZ in the east (Kundig, 1989). These observations suggest that the Pensi La segment of the ZSZ may represent the northwesternmost limit of ductile, melt-facilitated exhumation of the GHS.

In the Nubra Valley, a leucogranite from the Karakoram fault zone yielded an average U-Pb zircon age of 15.0±0.2 Ma (KF19, 34°37.99' N, 77°38.18' E). In the Pangong range, leucogranite intruded into a psammite host from the northern end of Tangste gorge gave a zircon age range from 19.8±0.1 to 12.7±0.5 Ma (PT10, 34°03.65' N, 78°13.877' E). A two-mica leucogranite from the southern end of Tangste gorge yielded zircon core ages ranging from 69.0±0.3 to 35.7±0.2 Ma and zircon rim ages that cluster at ~20 Ma (PT22, 34°02.23' N, 78°12.70' E; Figure 2). Whereas Karakoram and Zanskar leucogranite crystallization ages appear coeval, the inherited Paleocene—Eocene cores from the Karakoram zircons indicate that fault zone leucogranites are at least partially related to Neo-Tethyan oceanic subduction. Anomalously low zircon εHf(t) values for leucogranites in the Pangong range reported by Ravikant and others (2009) suggest that Indian crust may have been an additional melt source. Hf isotope analysis of Zanskar and Karakoram zircon cores may determine whether Karakoram fault zone leucogranites are related to GHS units to the south.

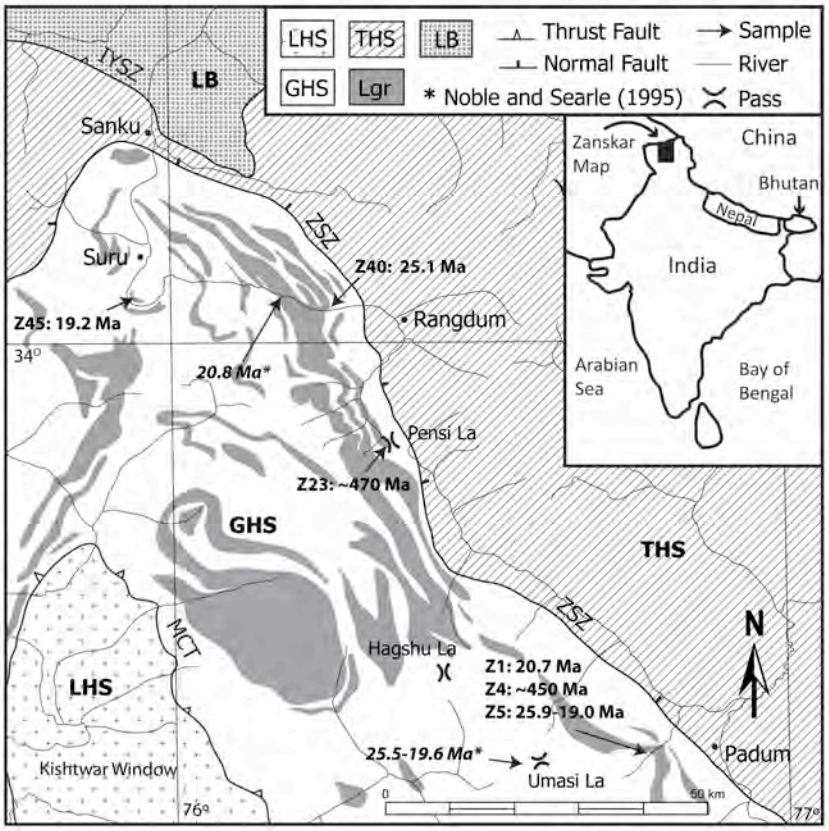

Figure 1. Simplified geological map of the Zanskar region delineating major lithotectonic units and showing sample locations. LHS, Lesser Himalaya Sequence; GHS, Greater Himalaya Sequence; THS, Tethyan Himalaya Sequence; IYSZ, Indus Yarlung Suture Zone; ZSZ, Zanskar Shear Zone; MCT, Main Central Thrust; LB, Ladakh Batholith. Modified from Steck (2003).

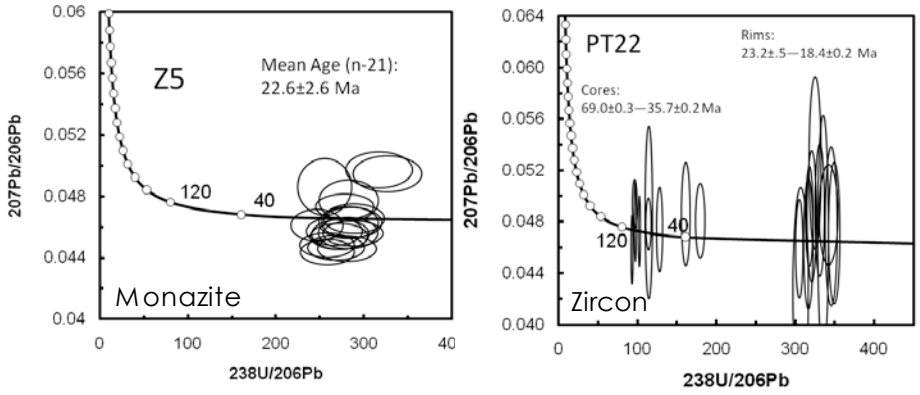

Figure 2. Tera-Wasserburg concordia diagrams for A) sample Z5, leucogranite from the Haptal Valley in Zanskar, and B) sample PT22, a 2-mica leucogranite from Tangste Gorge in the Karakoram fault zone. Data-point error ellipses are 2σ.

References

Copeland, P., Parrish, R.R. and Harrison, T.M., 1988, Identification of inherited radiogenic Pb in monazite and its implications for U-Pb systematic, Nature, 333, 760-763.

Dezes, P.J., Vannay, J.C., Steck, A., Bussy, F. and Cosca, M., 1999, Synorogenic extension: Quantitative constraints on the age and displacement of the Zanskar shear zone (northwest Himalaya), Geological Society of America Bulletin, 111, 364-374.

Inger, S., 1998, Timing of an extensional detachment during convergent orogeny: New Rb-Sr geochronological data from the Zanskar shear zone, northwestern Himalaya, Geology, 26, 223-226.

Kundig, R., 1989, Domal structures and high-grade metamorphism in the Higher Himalayan Crystalline, Zanskar region, North-west Himalaya, India, Journal of Metamorphic Geology, 7, 43-55.

Noble, S.R. and Searle, M.P., 1995, Age of crustal melting and leucogranite formation from U-Pb zircon and monazite dating in the western Himalaya, Zanskar, India, Geology, 23, 1135-1138.

Ravikant, V., Wu, F. and Ji, W., 2009, Zircon U-Pb and Hf isotopic constraints on petrogenesis of the Cretaceous-Tertiary granites in eastern Karakoram and Ladakh, India, Lithos, 110, 153-166.

Searle, M.P., and others, 1999, Thermal and mechanical models for the structural and metamorphic evolution of the Zanskar High Himalaya, Geological Society London Special Publications, 164, 139-156.

Steck, A., 2003, Geology of the NW Indian Himalaya, Eclogae Geologicae Helvetiae, 96, 147-196.

Cite as: Horton, F.M., Sommerfeld, J.W., Hassett, W.C. and Leech, M.L., 2010, U-Pb SHRIMP Geochronology of Leucogranites from the Greater Himalayan Sequence in Zanskar and from the Karakoram fault zone, NW India, *in* Leech, M.L., and others, eds., Proceedings for the 25th Himalaya-Karakoram-Tibet Workshop: U.S. Geological Survey, Open-File Report 2010-1099, 2 p. [http://pubs.usgs.gov/of/2010/1099/horton/].

Earthquake depth distributions in central Asia and lithosphere rheology

James Jackson[1], Dan McKenzie[1], Keith Priestley[1], Alistair Sloan[1]

[1] Bullard Laboratories, Madingley Road, Cambridge CB3 0EZ, UK, jaj2@cam.ac

This talk will examine the depth distribution of earthquakes in the greater Tibetan region in the context of our current understanding of lithosphere strength, composition and structure. Much has changed since the early studies of McKenzie & Fairhead (1997) and Maggi and others (2000) showed that accepted views which had remained unchallenged for 20 years needed some modification. In particular, a single generic view of the continental lithosphere is unable to account for the differences in earthquake depths, elastic thicknesses and geological histories commonly observed between ancient shields (or cratons) and younger orogenic belts.

An important conclusion of the studies by McKenzie & Fairhead (1997) and Maggi and others (2000) was that the long-term strength of the continental lithosphere resides only in its upper part, which was contained wholly within the crust, and that there was little evidence for substantial long-term strength in the continental mantle, contrary to previously accepted views. The effort to understand the physical mechanisms responsible led quickly to a series of developments in related subjects, including: (1) a re-examination of geotherms and thermal structure in both oceans and continents; (2) connections between seismic velocity and temperature; (3) relations between mechanical properties and the metastability of lower crustal rocks in mountain roots; (4) causes of the variations between the ancient continental shields (or 'cratons') and younger Phanerozoic orogenic belts; and, (5) the issue of how the continental cratons were created.

A recent review by Jackson and others (2008) summarised the developments above, in order to demonstrate that a coherent picture is emerging which reconciles observations from fields as diverse as seismology, gravity, heat flow, rock mechanics, metamorphic petrology and geochemistry. Furthermore, the insights, and agreement, that these widely differing disciplines offer on the same subject produce an overall view that is more robust than any obtained from just one of those disciplines alone. A relatively simple view of the distribution of lithosphere seismicity and its implications for rheology is now emerging, which can be summarized as follows:

1. Earthquakes in the mantle, in both oceans and continents, are confined to regions colder than about 600°C (McKenzie and others, 2005). In most places on the continents the uppermost mantle is expected to be at 600°C or more, and hence aseismic. But there are some circumstances in which the continental mantle might be colder, and experience some earthquakes (e.g. Priestley and others, 2008), one example of which is in the Himalaya (below).

2. With very few exceptions, earthquakes everywhere are confined to a single seismogenic layer, which in the oceans is limited by the 600°C isotherm, in young orogenic belts is typically limited to the upper crust (less than about 350°C), and in some regions, often in or adjacent to ancient shields, may include the whole crust. An important exception is in the Himalaya, where the seismogenic lower crust of India underthrusts the seismogenic upper crust of Tibet, giving an apparent bimodal depth distribution, but one that is not in steady-state and has no generic significance for continental rheology. In this particular example of the Himalaya, where the underthrusting Indian crust is unusually thin (~35 km) for a Precambrian shield and the Moho temperature is correspondingly unusually cold (~500°C rather than ~600°C), earthquakes extend from the lower crust into the uppermost 15–20 km of the mantle (Monsalve and others, 2006; Priestley and others, 2008).

3. The great strength of some of the ancient shields is associated with lower-crustal earthquakes and larger elastic thickness than in younger continental lithosphere. In such shields two effects are likely to be responsible: (a) the crust may be relatively cold because of a thick low-density mantle root, and (b) the composition of the lower continental crust is probably dominated by a dry

granulite-facies mineral assemblage.

4. Lateral strength contrasts in the continents between ancient shields and young orogenic regions are important, and cannot be represented by a laterally uniform continental rheology or composition. In spite of the lower-than-average Moho temperatures in shields, lower-crustal earthquakes within them occur in material up to 600°C, much hotter than the normal cut-off temperature of ~350°C for earthquakes in younger regions; a situation which probably requires the hotter seismogenic lower crust to be dry. These lateral strength contrasts allow mountains to be supported by their adjacent forelands without requiring the mantle beneath the forelands to be strong.

5. The stability and survival of the ancient shields and cratons over Ga of geological time is related to both their strength and buoyancy, neither of which can easily be changed.

References

Jackson, J., McKenzie, D., Priestley, K. and Emmerson, B., 2008, New views on the structure and rheology of the lithosphere, Journal of the Geological Society, London, 165, 453-465.

Maggi, A., Jackson, J., McKenzie, D. and Priestley, K., 2000, Earthquake focal depths, effective elastic thickness, and the strength of the continental lithosphere, Geology, 28, 495−498.

McKenzie, D., Jackson, J., and Priestley, K., 2005, Thermal structure of oceanic and continental lithosphere, Earth & Planetary Science Letters, 233, 337−349.

McKenzie, D. and Fairhead, D., 1997, Estimates of the effective elastic thickness of the continental lithosphere from Bouguer and free air gravity anomalies, Journal of Geophysical Research, 102, 27,523−27,552.

Monsalve, G., and others, 2006, Seismicity and one-dimensional velocity structure of the Himalayan collision zone: earthquakes in the crust and upper mantle, Journal of Geophysical Research, 111, B10301.

Priestley, K., Jackson, J. and McKenzie, D., 2008, Lithospheric structure and deep earthquakes beneath India, the Himalaya and southern Tibet, Geophysical Journal International, 172, 345-362.

Cite as: Jackson, J., McKenzie, D., Priestley, K. and Sloan, A., 2010, Earthquake depth distributions in Central Asia and lithosphere rheology, *in* Leech, M.L., and others, eds., Proceedings for the 25th Himalaya-Karakoram-Tibet Workshop: U.S. Geological Survey, Open-File Report 2010/1099, 2 p. [http://pubs.usgs.gov/of/2010/1099/jackson/].

Detrital Apatite Fission-Track Thermochronology of Modern River Sands from the Arunachal Himalaya and its Implications for Exhumation

A.K. Jain[1], James Pebam[1], Nand Lal[2], Sandeep Singh[1], Rajeev Kumar[3]

[1] Department of Earth Sciences, Indian Institute of Technology Roorkee, Roorkee-247667 India, himalfes@gmail.com
[2] Department of Geophysics, Kurukshetra University, Kurukshetra, India
[3] Department of Earth Sciences, University of Bergen, Bergen 5007, Norway

The Eastern Himalayan Syntaxis (EHS) is characterized by (i) a northern large strike-slip region, and (ii) fold- and thrust-controlled tectonics in the southern parts. The main syntaxial sequence of highly deformed Namcha Barwa Group felsic gneiss and high-pressure granulite reveals extremely localized erosion and an intense phase of very young and fast fold-controlled exhumation rates up to 10 mm/yr in the core (Booth and others, 2008; Seward and Burg, 2008; Stewart and others, 2008; Cina and others, 2009). Further south, in the Arunachal Himalaya, the Cenozoic foreland Siwalik belt abruptly rises over the Holocene Brahmaputra alluvium along the Main Frontal Thrust (MFT), and is overridden by the pre-Cenozoic Lesser Himalayan sedimentary sequence along the Main Boundary Thrust (MBT). Two windows at Menga and Nacho reveal its extension beneath the Himalayan Metamorphic belt (HMB), which is thrust southeastwards along the folded Main Central Thrust (MCT). The southern metamorphic belt dominantly contains mylonitized Daporijo Gneiss, whereas the inner metamorphics are medium to high grade garnetiferous-kyanite-sillimanite schist/gneiss and granulite of the Higher Himalayan Crystallines (HHC). These are overlain by the low grade or unmetamorphosed Tethyan Sedimentary Zone (TSZ) in the extreme northwest, while the Indus-Tsangpo/Tidding Suture Zone rocks separate this belt/HHC from the Lohit Batholith around the EHS. Many of these tectonic belts may be physically traced around the EHS into the northeastern Mishmi Hills, which dominantly expose the batholith.

Apatite FT detrital thermochronology of the Subansiri, Siang, Dibang and Lohit rivers sands and their tributaries as well as the Siwalik Group (Miocene-Pleistocene) on 1028 grains from 20 samples have been undertaken to decipher the source rocks of these modern sands. Individual AFT grain ages range from 0.2 to 99.3 Ma and reveal the time elapsed since it attained its closure temperature of ~135^{o} C. These mixed population of different ages were reduced to individual peaks between 0.2 to 33.4 Ma, using the BINOMFIT software (Brandon and others, 2002), and have been assigned to different sources in the Himalaya, and compared with the bedrock AFT ages from some of the units falling in catchment area of each sample.

In the westernmost parts, the smallest Ranga River drains the Siwalik, the LH sedimentary belt including the Gondwanas, and overthrust Daporijo Gneiss. Sample Z155 from the Ranga Dam has sediments coming from the Daporijo Gneiss and the LH Sedimentary Zone with a P1 Peak of 6.4 Ma from the latter sources, while the 10.7 Ma P2 Peak has a mixed source of the Daporijo Gneiss and the Lesser Himalaya. However, a new P1 Peak of 2.2 Ma in the foothill sand sample Z145 is likely to be derived from the youngest Pliocene Kimin Formation of the Siwalik Group or the reworked older terraces.

The main Subansiri River valley drains a very large area of Tibet covered by the Tethyan Sedimentary Zone. The HHC bedrock within Arunachal has the AFT ages from 2.6 to 2.9 Ma, whereas those of the Daporijo Gneiss are between 6.2 and 7.4 Ma. The 1.9 Ma P1 Peak in sand sample Z93 in the extreme northwest matches approximately that of the bedrock AFT ages from the HHC. It is likely that the 3.7 Ma P2 Peak has a source in the leucogranite intrusion within the HHC as well as the Tethyan sediments; a few older AFT ages are also sourced within this belt. The picture of sediment source in this river is clearer when we compare peak ages of sample Z80(S), where the 1.9 Ma P1 Peak is certainly coming from the HHC and the LH windows, whereas the 4.9 Ma P2 Peak grains are contributed from the Daporijo Gneiss and Lesser Himalayan Sedimentary belt. In the sand sample Z185, collected from Gaurkamukh, the youngest P1 Peak is diluted to 3.7 Ma, possibly due to an admixture of youngest apatite ages from different sources and various tributaries of the Subansiri River. The 7.9 Ma P2 Peak grains might have apatite contributed by the Daporijo Gneiss. Although there is no exposed bedrock with ~20 Ma age, it is likely that 19.5 Ma peak is from un-reset Cenozoic foreland-basin Siwalik sediments.

In the Kurung-Kamla Rivers, the important tributaries of the Subansiri, the bedrock AFT ages range from 2.2 to 3.5 Ma for the HHC. However, the river sand sample Z169 from Kurung, having inputs from the HHC and the TSZ, has two peaks: P1 and P2 of 2.4 and 8.9 Ma, respectively. The P1 Peak may have its source from the HHC, while the P2 Peak is presumably from the TSZ. Bedrock AFT ages from the Daporijo Gneiss of the LH metamorphic belt range from 5.0 to 8.0 Ma. A single sample from the LH window has an AFT age of 2.0 Ma, however these ages vary from 4.7 to 8.5 Ma in the LH sedimentary belt. Sand sample Z113 from the Kamala River has two peaks, with P1 of 5.0 Ma containing 88.8% of the bulk population, and a P2 Peak of 12.0 Ma. This means that majority of the grains are coming from the Daporijo Gneiss but have a mixed population. The 12.0 Ma P2 Peak may be assigned to the Lesser Himalaya.

The Siang River, the main tributary of the Brahmaputra River, has the largest drainage system in Tibet and Arunachal Himalaya, and drains the EHS. The northernmost sand sample SP43 from Tuting has an AFT age range between 0.2 and 28.0 Ma with a P1 Peak of 1.2 Ma (88.1%, n=46), which is likely to be derived from the HHC complex of the EHS, whereas the older P2 Peak of 10.8 Ma possibly has its source in the Lohit Batholith. Sand sample SP 34, collected downstream from the Siyom-Siang confluence, has an AFT P1 Peak of 1.7 Ma with its source in the HHC, as is evident from four bedrock ages between 1.3 and 1.8 Ma; the P2 Peak is 14.1 Ma with a possible source within the batholith. Sand from Rotung along the Siang has only one peak of 1.9 Ma (Sample SP 87), whereas sample SP 86 from Pasighat has P1 and P2 Peaks of 2.1 and 31.5 Ma; the latter bears strong similarity to the AFT peak from the Middle Siwalik Formation (sample SP86A) from Pasighat, whose youngest P1 Peak of 8.0 Ma constrains its minimum depositional age and is distinctly older than the Upper Siwalik peak of 4.3 Ma from Kimin in the Ranga valley (Sample Z 143).

In the Siyom River valley, a tributary of the Siang River, the 4.4 Ma single P1 Peak of sample Z30 in the westernmost parts (100%, n=36) may have a mixed source of the HHC as well as the TSZ. This argument is based on the bedrock AFT age of ~2.9 Ma from the HHC. Sand sample Z62 from the middle stretch did not yield any peak but individual grain ages range from 2.1 to 12.9 Ma. This implies that the sample has a mixed source of different units including the Lesser Himalayan package.

Two mighty rivers, the Dibang and Lohit, mainly drain the Lohit Batholith in Mishmi Hills, besides the Tidding Suture Zone, the HHC and other tectonic units of adjoining Tibetan region in the northeast. Two sand samples from Amboli and Etalin along the Dibang have P1 Peaks of 2.9 and 2.6 Ma respectively, whereas the older peaks between 8.2 and 15.4 Ma are sourced from the Lohit Batholith. Along the Lohit, the northernmost sample SIV has grains as young as 0.7 Ma with a P1 Peak of 0.00 Ma and others between 5.7 and 26.3 Ma, indicating recent fault activity within the source area. In two samples further south (samples SIII and SV), older peaks between 7.8 and 33.4 Ma appear to be derived from the Lohit/Gangdese Batholith, while the 0.2 Ma Peak in the southernmost sample at Parasuram indicates Holocene movements along the frontal Mishmi Thrust.

References

Booth, A.L., Chamberlain, C.P., Kidd, W.S.F. and Zeitler, P.K., 2008, Metamorphic and geochronologic constraints on the tectonic evolution of the eastern Himalayan syntaxis, Namche Barwa, Geol. Soc. Amer. Bull., 121(3-4), 385–407.

Brandon, M.T., 2002, Decomposition of mixed grain-age distributions using BINOMFIT, On Track, 24, 13–18.

Cina, S.E., and others, 2009, Gangdese arc detritus within the eastern Himalayan Neogene foreland basin: Implications for the Neogene evolution of the Yalu–Brahmaputra River system, Earth Planet. Sci. Letts., 285, 150–162.

Seward, D. and Burg, J.P., 2008, Growth of the Namche-Barwa Syntaxis and associated evolution of the Tsangpo Gorge: Constraints from structural and thermochronological data, Tectonophysics, 451, 282–289.

Stewart, R.J., and others, 2008, Brahmaputra sediment flux dominated by highly localized rapid erosion from the easternmost Himalaya, Geology, 36, 711–714.

Cite as: Jain, A.K., Pebarn, J., Lal, N., Singh, S. and Kumar, R., 2010, Detrital Apatite Fission-Track Thermochronology of Modern River Sands from the Arunachal Himalaya and its Implications for Exhumation, *in* Leech, M.L., and others, eds., Proceedings for the 25th Himalaya-Karakoram-Tibet Workshop: U.S. Geological Survey, Open-File Report 2010-1099, 2 p. [http://pubs.usgs.gov/of/2010/1099/jain/]

Crustal Structure Linked to Ultra-High-Pressure Rock Exhumation: A "Working" Model for the Tso Morari Complex, Ladakh Himalaya

Rebecca A. Jamieson[1], C. Beaumont[2], J.P. Butler[1], C.J. Warren[3]

[1] Department of Earth Sciences, Dalhousie University, Halifax, NS, Canada, B3H 4J1, beckyj@dal.ca
[2] Department of Oceanography, Dalhousie University, Halifax, NS, Canada, B3H 4J1
[3] Department of Earth and Environmental Science, The Open University, Walton Hall, Milton Keynes, UK, MK7 6AA

The distribution of ultra-high-pressure (UHP) metamorphic rocks in the Himalayan-Tibetan orogen and elsewhere demonstrates that burial (to >100 km) and rapid exhumation (>1 cm.a^{-1}) of continental crust is a normal part of early (~10 Ma) continental collision. Until recently, there has been no comprehensive model for this fundamental tectonic process that also satisfactorily explains the upper-crustal structures resulting from early collisional UHP rock exhumation. Among the characteristic features requiring explanation are: structural domes that are cored by UHP nappes; associated medium- to high-pressure nappes displaying a distinct "pressure gap"; overlying lower-grade rocks, including suture zone ophiolites; and, coeval foreland-directed thrust-faults and syn-exhumation normal faults (numbers 1-6, Figure 1).

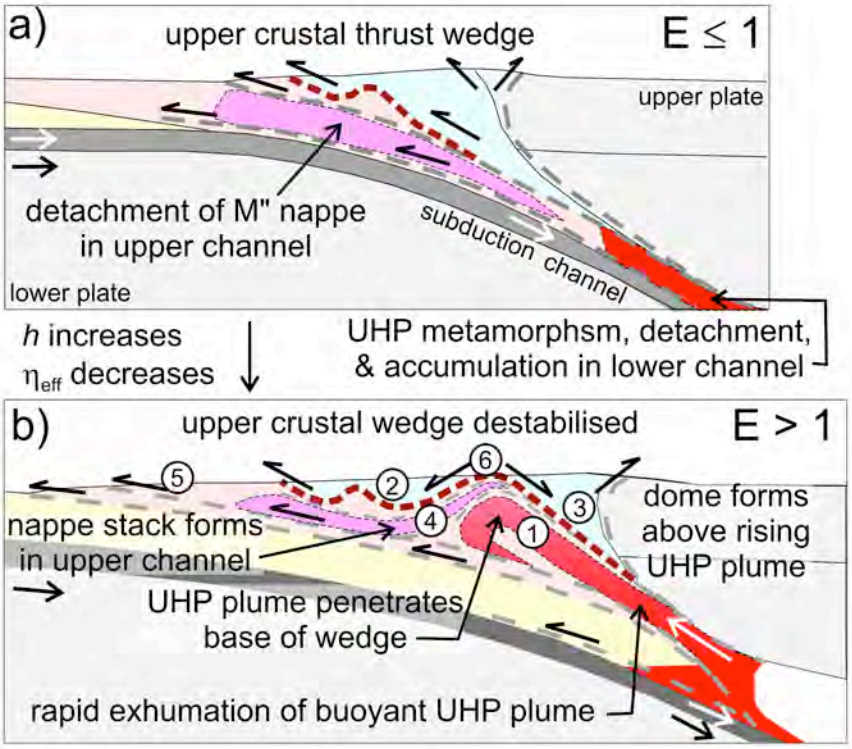

Figure 1. Processes involved in formation and exhumation of UHP metamorphic rocks, including the Tso Morari complex. a) Formation of UHP material in lower channel and detachment of M″ nappe in upper channel. Increasing channel thickness (h) and decreasing effective viscosity (η_{eff}), combined with inherent buoyancy of subducted crust, increase exhumation number (E) above critical threshold value (E>1). b) Formation of upper-crustal structures in response to rapid exhumation of a buoyant UHP plume (E>>1) that penetrates and destabilizes the overlying thrust wedge, leading to extension above the dome and coeval foreland-directed thrusting. 1) structural dome cored by UHP nappe; 2) overlying lower grade rocks; 3) suture zone ophiolites; 4) medium- to high-pressure (M") nappes; 5) foreland-directed thrust-faults; 6) syn-exhumation normal faults.

We present a geodynamical model involving crustal burial and exhumation in a subduction channel below an accretionary wedge and upper plate (e.g., Beaumont et al., 2009). Competition between down-channel shear traction and up-channel buoyancy forces, expressed as the exhumation number, E, controls burial and exhumation, leading to rapid up-channel flow when E >1 (Figure 1; e.g., Warren and others, 2008). Exhuming UHP material forms a nappe stack and structural dome as it penetrates and destabilises the overlying wedge, driving thrusting and extension. This solution is compelling because it explains both the

geology and the petrology of UHP complexes, and because it demonstrates that pulse-like buoyant exhumation from deep in the subduction channel creates observed upper-crustal structures. This places constraints on the exhumation mechanism and provides a test of alternative models. Other proposed mechanisms, such as continuous circulation in a lithospheric-scale wedge or overpressured subduction channel, predict different types of upper-crustal structures and are therefore unsatisfactory explanations for early collisional exhumation of UHP terranes.

Model feasibility has been tested against observations from the Tso Morari Complex, Ladakh Himalaya (e.g., de Sigoyer and others, 2004; Leech and others, 2005; Epard and Steck, 2008, and references therein). Peak UHP metamorphic conditions have been estimated at >2.8 GPa and 600-650°C. Geochronological data suggest that UHP conditions were achieved at ca. 50-55 Ma, within 1-5 Ma of collision. UHP rocks were exhumed to crustal levels (<1.2 GPa) by ca. 48 Ma, followed by cooling to <300°C by ca. 40 Ma. The immediately overlying Tetraogal nappe, which lacks evidence for UHP metamorphism, was affected by amphibolite facies metamorphism (ca. 550-700°C, 0.8-1.2 GPa) with top-to-the-south fabrics formed at ca. 48-45 Ma. The nappe stack now occupies the core of a dome developed between 47-30 Ma, coeval with SW-directed thrusting in the frontal part of the North Himalayan nappes. The complex is separated from ophiolitic rocks of the Indus Suture Zone by a late normal fault, and dismembered ophiolitic rocks are also present at mid-structural levels within the nappe stack.

These observations are compared with Model V_P15-5, in which convergence velocity, V_P, is initially 15 cm.a^{-1}, representing the high convergence rate at the onset of the India-Asia collision, followed at 5.5 Ma by a decline to V_P = 5 cm.a^{-1}. Collision begins at 3.3 Ma (0 Ma-pc) and exhumation begins at 4.3 Ma-pc. The overlying accretionary wedge and M″ nappe are deformed into a structural dome above the exhuming UHP plume (Figure 1), and by 6.7 Ma-pc, UHP material lies in the core of the dome within 10 km of the model surface. The geometry of the model upper crust corresponds very well to the Tso Morari cross-section (Epard and Steck, 2008). Within uncertainties, the model is also consistent with available age constraints, and model *PTt* paths reproduce observed peak *PT* conditions, duration of UHP metamorphism (<1 Ma), and most of the exhumation path (Beaumont et al., 2009). We therefore consider this a good "working" model for the formation and exhumation of the UHP Tso Morari complex.
In addition, we consider the fate of (U)HP rocks formed during the early stages of collision that are not exhumed to the upper crust, but instead become entrained in a mid-crustal channel. Finally, we offer an explanation for the formation and exhumation of relatively young (< 20 Ma), strongly overprinted, eclogitic rocks exposed in the eastern Himalaya (e.g., Corrie and others, 2010) in terms of deep burial of a footwall ramp followed by transfer to and exhumation within the overriding channel (e.g., Jamieson and others, 2006).

References

Beaumont, C., Jamieson, R.A., Butler, J.P. and Warren, C.J., 2009, Crustal structure: A key constraint on the mechanism of ultra-high-pressure rock exhumation, Earth Planet. Sci. Lett. 287, 116-129.

Corrie, S. L., Kohn, M.J. and Vervoort, J.D., 2010, Young eclogite from the Greater Himalayan Sequence, Arun Valley, eastern Nepal: P–T–t path and tectonic implications, Earth Planet. Sci. Lett. 289, 406-416.

de Sigoyer, J., Guillot, S. and Dick, P., 2004, Exhumation of the ultrahigh-pressure Tso Morari Unit in eastern Ladakh (NW Himalaya); a case study, Tectonics 23, 18, doi: 10.1029/2002TC001492.

Epard, J-L. and Steck, A., 2008, Structural development of the Tso Morari ultra-high pressure nappe of the Ladakh Himalaya, Tectonophysics 451, 242-264.

Jamieson, R.A., Beaumont, C., Nguyen, M.H. and Grujic, D., 2006, Provenance of the Greater Himalayan Sequence and associated rocks; predictions of channel flow models; Channel flow, ductile extrusion and exhumation in continental collision zones, Geological Society Special Publications, 268, 165-182.

Leech, M.L., Sing, S., Jain, A.K., Klemperer, S. and Manickavasagam, R.M., 2005, The onset of the India-Asia continental collision: early, steep subduction required by the timing of UHP metamorphism in the western Himalaya, Earth Planet. Sci. Lett. 234, 83-97.

Warren, C.J., Beaumont, C. and Jamieson, R.A., 2008, Formation and exhumation of ultra-high pressure rocks during continental collision: Role of detachment in the subduction channel. Geochemistry, Geophysics, Geosystems 9, Q04019, doi:10.1029/2007GC001839.

Cite as: Jamieson, R.A., Beaumont, C., Butler, J.P. and Warren, C.J., 2010, Crustal structure linked to ultra-high-pressure rock exhumation: A "working" model for the Tso Morari Complex, Ladakh Himalaya, *in* Leech, M.L., and others, eds., Proceedings for the 25th Himalaya-Karakoram-Tibet Workshop: U.S. Geological Survey, Open-File Report 2010-1099, 2 p. [http://pubs.usgs.gov/of/2010/1099/jamieson/].

Seismic Activity and Seismic Hazard Assessment along the Main Boundary Thrust, Northern Pakistan

M. Qasim Jan[1], MonaLisa[2]

[1]National Centre of Excellence in Geology, University of Peshawar, Pakistan, mqjan@yahoo.com
[2]Department of Earth Sciences, Quaid-i-Azam University, Islamabad, Pakistan

The seismicity of the northwestern Himalayan syntaxial bend, including that of the Main Boundary Thrust (MBT), is examined in a wider tectonic context by using about 2000 microearthquakes and 100 macroevents obtained from a telemetered seismic network in northern Pakistan centered at Tarbela dam on the Indus River for the period 1971-1993. The seismicity map (1904-2004) prepared for the purpose indicates that a branch of the MBT traverses the region as a straight northwesterly extension of the Murree Thrust, the mapped section of the MBT southeast of the Hazara-Kashmir Syntaxis (HKS). The HKS and MBT are microseismically inactive at present but are associated with recent and historical microseismicity, and overprint the northwesterly seismic blind zone, i.e. the Hazara Lower Seismic Zone.

Ten fault plane solutions (1965-1993) show the dominance of strike-slip over the thrusting with north-south compressional stresses, as six events out of ten are strike-slip and four are thrusts. Seismic Hazard Assessment (SHA) has also been incorporated on three selected sites of Islamabad, Kohat and Muzaffarabad, using both the deterministic and probabilistic approaches. Deterministic Seismic Hazard Assessment (DSHA) suggests MBT as the most critical tectonic feature for the three sites, with a maximum potential magnitude of 7.8 for all the three sites.

Cite as: Jan, M.Q. and MonaLisa, 2010, Seismic activity and seismic hazard assessment along the Main Boundary Thrust, northern Pakistan, *in* Leech, M.L., and others, eds., Proceedings for the 25th Himalaya-Karakoram-Tibet Workshop: U.S. Geological Survey, Open-File Report 2010-1099, 1 p. [http://pubs.usgs.gov/of/2010/1099/jan/].

Comparative Analysis of Economic Benefits and Adverse Environmental and Health Impacts of Asbestos Mining and Milling in Behram Dehri, District Charssada, Northern Pakistan

Noor Jehan[1], Khalid Durrani[2]

[1]Department of Environmental Sciences, University of Peshawar, noorjpk1984@yahoo.com
[2]California Regional Water Quality Board Fresno, CA, 93706, U.S.A., durranikp@gmail.com

Asbestos is not a mineralogical term but rather a commercial term applied to highly fibrous minerals including serpentine and amphibole asbestos. The principal varieties most commonly used in commerce are chrysotile, crocidolite, amosite, tremolite, actinolite and anthophyllite, all being used since the beginning of the industrial era around the globe. Presently asbestos is used in more than 3000 products including in the construction and textile industries, as heat-resistant material, special filters for industrial chemicals, thermal insulation products, friction material, gaskets, floor tiles, roofing materials, packing materials, paints and protective paper and as sprayed insulation and binding material for buildings and other structures (Shirde, 1973; Jehan, 1996). Apart from this it was also identified that asbestos is being used in detergent and talcum powder and soap and furniture in Pakistan.

Beside the commercial and economic importance, the exposure to all types of asbestos including chrysotile, tremolite, amosite, anthophyllite, crocidollite and mixture of all these have resulted in a high incidences of various cancers (lungs, larynx, gastrointestinal, ovarian) and malignant mesothelioma among humans (IARC, 1987).

This study highlighted the economic benefits and the environmental and health impacts posed by the asbestos mining and milling carried out in Behram Dehri District Charssada, northern Pakistan. Twenty small scale asbestos mines and 5 milling units were selected for sampling purposes. A total of 15 samples including raw and airborne were collected and analysed. The type of asbestos was identified as chrysotile tremolite using X-Ray Diffraction (XRD). The exposure level to asbestiform asbestos fibers was found beyond the permissible exposure limit in all samples using Scanning Electron Microscope (SEM).

A detailed survey was conducted to identify the economic benefits and the adverse health impacts in the area under consideration. The total production capacity from all mines was recorded as 200 metric tonnes per day, worth of US$5 per tonne. The overall total income generated from asbestos mining was calculated as US$1,000 per day in the target area. Similarly the production capacity of 5 milling units was recorded as 200 metric tonnes per day, worth of US$1,200 per day. The total income generated as a result of the asbestos business was calculated as US$2,200 per day.

Despite being an economic mineral, the environmental consequences and the premature deaths and chronic illness among the asbestos miners and millers in the area require investigation. The mortality and morbidity rate among the miners and millers indicated that almost 50% of the total employees were suffering from asbestos-related diseases including lung cancer and malignant mesothelioma and skin allergies. The overall comparative analysis of this study concluded that the unaware and poor people are highly exposed around the clock to asbestos fibres and thus at high risk to asbestos related diseases at the cost of only US$, 2,200/ per day in the study area. The unsustainable management of asbestos business created a considerable environmental chaos among the miners and the general public in the target area.

References

Jehan, N., 1996, Geology, Economics and Environmental impacts of asbestos from Mohmand and Malakand agencies and district Charsadda, Unpublished M.Phil Thesis, University of Peshawar.

IARC, 1987, Silica and some silicates. Lyon, France, International Agency for Research on Cancer, (IARC) Monographs on the Evaluation of the Carcinogenic Risk of Chemicals to Humans, 42, 33-143.

Shride, A.F., 1973, Asbestos, in: Brobst, D. and Part, W.P., eds., United States mineral resources. U.S. Geol. Surv. Prof. Paper, 820, 63-72.

Cite as: Jehan, N. and Durrani, K., 2010, Comparative Analysis of Economic Benefits and Adverse Environmental and Health Impacts of Asbestos Mining and Milling in Behram Dehri, District Charssada, Northern Pakistan, *in* Leech, M.L., and others, eds., Proceedings for the 25th Himalaya-Karakoram-Tibet Workshop: U.S. Geological Survey, Open-File Report 2010-1099, 1 p. [http://pubs.usgs.gov/of/2010/1099/jehan/].

Contrasting Dome Formation along the Southern Margin of the Tibetan Plateau: Leo Pargil Dome and Ama Drime Massif, India/Tibet

Micah Jessup[1], John Cottle[2], Jackie Langille[1], Graham Lederer[2], Talat Ahmad[3]

[1]University of Tennessee, Knoxville, TN 37996, U.S.A., mjessup@utk.edu
[2]University of California, Santa Barbara, CA 93106, U.S.A.
[3]University of Delhi, Delhi -110007, India

Domes that record the onset of orogen-parallel extension (e.g. Murphy and others, 2002) along the southern margin of the Tibetan plateau were exhumed in different kinematic settings and provide windows into processes at various depths in the middle-crust. Exposure of mid-crustal rocks provided by these domes enables detailed field and lab-based investigations to test the role of melting and strain partitioning during mid-crustal flow and exhumation. Data from these domes are critical for deriving kinematic and thermomechanical models for dome formation and evolving mid-crustal flow along the southern margin of the plateau. To test for along strike variability in mechanisms of dome formation and extent of mid-crustal flow we integrate kinematic analysis, P-T paths and geothermochronology on samples from the Ama Drime Massif (ADM), Tibet, and the Leo Pargil dome (LPD), NW India (Thiede and others, 2006).

The ADM and LPD were both exhumed by oppositely dipping, normal-sense shear zones. The NNE-striking shear zones bounding the ADM record a progression in deformation mechanisms from early distributed shear zones to discrete detachments. The Ama Drime detachment juxtaposes upper amphibolite facies Greater Himalayan series in the hanging wall with granulite facies orthogneiss and paragneiss in the footwall and records at least 21-42 km down-dip displacement (Langille and others, in review). In contrast, the NE-striking Leo Pargil shear zone records top-down-to-the-northwest sense of shear (Thiede and others, 2006) at high temperature (>550ºC), does not develop a discrete detachment, and juxtaposes an injection complex in the footwall with greenschist facies Tibetan Sedimentary series in the hanging wall.

Our data suggest that in the ADM and LPD, in-situ anatexis and mobilization of melt into dikes and sills plays a major role in controlling the effective viscosity of the crust by weakening different structural positions in the mid-crust. Melting at granulite facies (0.7-0.8 GPa; 750ºC) in the ADM initiated at 12-13 Ma and was followed by post-kinematic dikes at 11-12 Ma in a kinematic setting that was dominated by orogen-parallel extension. Injection of multiple generations of leucogranites in the footwall of the Leo Pargil shear zone occurred during a protracted event ~26-16 Ma (Lederer and others, 2010) at intermediate structural positions. Toward deeper structural positions the injection complex transitions into migmatitic gneiss. Both domes record a transition between melt-present deformation in the core to solid-state fabric development on the margins.

References

Langille, J., Jessup, M. J., Cottle, J. M. and Newell, D. L., in review, Kinematic evolution of the of the Ama Drime Detachment: Insights into orogen-parallel extension and exhumation of the Ama Drime Massif, Tibet-Nepal, Journal of Strucutral Geology.

Lederer, G., Cottle, J., Jessup, M., Langille, J. and Ahmad, T., 2010, Petrochronologic constraints on partial melting in the Leo Pargil Dome, NW India, Geochimica et Cosmochimica Acta, Annual Goldschmidt conference, Knoxville, TN.

Thiede, R.C., Arrowsmith, J.R., Bookhagen, B., McWilliams, M., Sobel, R. and Strecker, M., 2006, Dome formation and extension in the Tethyan Himalaya, Leo Pargil, northwest India, Geol. Soc. Am. Bulletin, 118, 635−650.

Murphy, M.A., Yin, A., Kapp, P., Harrison, T.M. and Manning, C.E., 2002, Structural evolution of the Gurla Mandhata detachment system, southwest Tibet: implications for the eastward extent of the Karakoram fault system, Geol. Soc. Am. Bulletin, 114, 428−447.

Cite as: Jessup, M., Cottle, J., Langille, J. Lederer, G. and Ahmad, T., 2010, Contrasting dome formation along the southern margin of the Tibetan plateau: Leo Pargil dome and Ama Drime Massif, India/Tibet, *in* Leech, M.L., and others, eds., Proceedings for the 25th Himalaya-Karakoram-Tibet Workshop: U.S. Geological Survey, Open-File Report 2010-1099, 1 p. [http://pubs.usgs.gov/of/2010/1099/jessup/].

Sedimentary and thermochronologic evidence for Middle to Late Miocene uplift of the Northern Tibetan Plateau

S. A. Johnstone[1], G. Zhuang[1], J. K. Hourigan[1], B. D. Ritts[2], B. J. Darby[3]

[1]Earth and Planetary Sci., UC Santa Cruz, CA 95064, U.S.A., Johnstone@ucsc.edu
[2]Chevron Corporation, San Ramon, CA 94583, U.S.A.
[3]Exxon Mobil Corporation, Houston, TX 77002, U.S.A.

The Altyn Tagh Fault (ATF) plays a central role in accommodating strain related to the India-Asia collision. Previous work has documented 375 ± 50 km of Cenozoic sinistral offset on the ATF, which is in turn fundamental to crustal thickening in the northern Tibetan Plateau (Yue and others, 2003). However, questions regarding the timing and extent of deformation and associated uplift of the northern Plateau remain unanswered. Two end-member models, the "two-stage" and "continuum" models, exist to characterize the coupled evolution of the ATF and the Northern Plateau (Yue and Liou, 1999; Yin and others, 2002). Both of these models yield distinct and readily testable predictions for the basin evolution, exhumation history, and structural growth of the northern Tibetan Plateau. Here we present sedimentary sequences from the northern Qaidam basin and Hexi corridor as well as low-temperature thermochronology cooling ages from the North and South Qilian Shan.

Upward coarsening sequences within the Qaidam Basin and Hexi Corridor and rapid cooling throughout the Qilian Shan suggest rapid uplift and attendant exhumation in the Late to Middle Miocene. These events are nearly synchronous with a decline in slip rate along the ATF and suggest a shift from strike-slip dominated deformation to distributed crustal thickening. Additionally these events coincide with tectonic reorganizations along the south China and Pacific plate margins during the mid-Miocene that resulted in a relatively confined margin (Northrup and others, 1995), potentially favoring crustal thickening within the orogen over lateral escape.

References:

Northrup, C.J., Royden, L.H. and Burchfiel, B.C., 1995, Motion of the Pacific plate relative to Eurasia and its potential relation to Cenozoic extension along the eastern margin of Eurasia, Geology, v. 23, p. 719–722.

Yin, A., and others, 2002, Tectonic his tory of the Altyn Tagh fault system in northern Tibet inferred from Cenozoic sedimentation, Geological Society of America Bulletin, v. 114, p. 1257-1295.

Yue, Y.J. and Liou, J.G., 1999, Two-stage evolution model for the Altyn Tagh fault, China, Geology, v. 27, p. 227-230.

Yue, Y., and others, 2003, Slowing extrusion tectonics: lowered estimate of post-Early Miocene long-term slip rate for the Altyn Tagh fault, China, Earth Planet. Sci. Lett., v. 217, p. 111–122.

Cite as: Johnstone, S.A., Zhuang, G., Jourigan, J.K., Ritts, B.D. and Darby, B.J., 2010, Sedimentary and thermochronologic evidence for Middle to Late Miocene uplift of the Northern Tibetan Plateau, in Leech, M.L., and others, eds., Proceedings for the 25th Himalaya-Karakoram-Tibet Workshop: U.S. Geological Survey, Open-File Report 2010-1099, 1 p. [http://pubs.usgs.gov/of/2010/1099/johnstone/].

Plio-Quaternary Wind Erosion in the Qaidam Basin, Central Asia: Records, Rates, and Broader Implications

Paul Kapp[1], Alexander Rohrmann[2], Richard Heermance[3], Jon D. Pelletier[1], Joellen Russell[1], Lin Ding[4]

[1] Department of Geosciences, University of Arizona, Tucson, AZ 85721, U.S.A., pkapp@email.arizona.edu
[2] Institut für Geowissenschaften, Universität Potsdam, 14476 Potsdam, Germany
[3] Department of Geological Sciences, California State University Northridge, Northridge, CA 91330, U.S.A.
[4] Institute of Tibetan Plateau Research, and Institute of Geology and Geophysics, Chinese Academy of Sciences, Beijing 100085, China

Liquid water and ice are the dominant agents of erosion and sediment transport in most actively growing mountain belts. An exception is in the western Qaidam Basin along the northeastern margin of the Tibetan Plateau. Here, northwesterly to westerly winds and wind-blown sand have sculpted enormous fields of mega-yardangs, with up to 60 m of relief, in actively folding sedimentary strata (Figure 1). Located downwind of the Qaidam Basin is the Loess Plateau, one of the most voluminous and best exposed accumulations of Plio-Quaternary loess on Earth. Here, loess accumulation occurred primarily during glacial and stadial periods when climatic conditions were colder and drier in central Asia and alternated with episodes of paleosol development during wetter interglacial and interstadial periods (e.g., Porter, 2007).

Figure 1. Mega-yardangs with up to 60 m of relief sculpted into mainly lacustrine, Pleistocene strata within the west-central Qaidam Basin.

We speculate that the Qaidam Basin experienced alternating episodes of sediment accumulation and wind erosion in phase with Loess Plateau paleosol development and loess accumulation, respectively. A supporting preliminary investigation of Plio-Pleistocene basin fill in the west-central Qaidam Basin shows that lacustrine sedimentation was punctuated by periodic episodes of sub-aerial exposure and wind erosion. The latter is evidenced by the presence of salt paleosols/crusts, deflation lag deposits, wind-storm deposits, paleopans filled with lacustrine and/or eolian deposits, and paleoyardangs separating meter-scale lacustrine parasequences. Except for perhaps along the crests of large anticlines, which parallel topographic highs in the basin, sediment accumulation during periods of lacustrine deposition must have exceeded the thickness of material removed when wind erosion was active in order to lead to the observed, positive net Plio-Pleistocene sediment accumulation in the region. The ongoing folding in the Qaidam Basin coupled with the most recent episode of severe wind erosion led to the preservation and exposure of this stratigraphic record of episodic wind erosion.

Rates of wind erosion have not been quantified in the Qaidam Basin, but must be significant. The modern Qaidam yardangs must have developed since the basin was largely occupied by lakes ~200,000 years ago

(Mischke and others, 2006) and possibly as recently as ~25,000 years ago. The development of mega-yardangs with 50 m of relief since these times yields time-averaged erosion rates in the 0.25-2.0 mm/yr range in the troughs between the yardangs, assuming an initial flat surface into which the yardangs were sculpted. Time-averaged erosion rates can also be estimated over a longer time scale. Seismic-reflection profiles show that sediment accumulation was continuous across the entire Qaidam Basin until ~2.8 Ma, when fold growth accelerated based on growth strata (Zhou and others, 2006). This suggests that the erosion of Qaidam Basin folds has occurred since 2.8 Ma. Geometric constraints provided by published regional cross sections and our own, more local cross sections show that hundreds of meters to thousands of meters of strata have been eroded from above the Qaidam Basin folds since 2.8 Ma. Given stratigraphic evidence for closed-basin conditions since 2.8 Ma, this material could only have been removed from the basin by wind. We estimate that the average erosion rate across the sandblasted part of the Qaidam Basin is ~0.29 mm/yr, with localized erosion hotspots above the crests of large anticlines (~1.4 mm/yr). These estimates are minima for when wind erosion was active, as they are averaged over a time interval when erosion was not continuously active (excluding perhaps along the crests of the largest anticlines) but alternated with episodes of sediment accumulation.

Our estimates of wind-erosion rates are comparable to rates of fluvial and glacial erosion in tectonically-active mountain ranges, and at least locally above anticline crests, comparable to those in other orogens where positive tectonic-climate feedback relationships have been suggested. The possibility that wind erosion may have exerted a positive feedback relationship with fold growth in the Qaidam Basin is intriguing. An observation supporting this hypothesis is the presumably not coincidental, coeval acceleration of wind erosion in central Asia (based on the Loess Plateau record) and fold growth in the Qaidam Basin (based on imaged/mapped growth strata) at 2.8-2.5 Ma.

The Qaidam Basin is presently not thought to be a major source of Loess Plateau deposits, despite its proximity, upwind geographic position, and vast exposure of wind-eroded landforms. Rather, and strongly influencing popular thinking, in the modern climatic conditions the Gobi and adjacent sand deserts are the locus of major northwesterly wind storms that transport dust over the Loess Plateau. In the modern winter-to-spring climate, the main axis of the polar jet stream is located over the Gobi region- the locus of modern dust storms. During glacial and stadial periods, global climate models suggest that the main axes of the high-level westerlies in both hemispheres shift ≥10° in latitude toward the equator (e.g., Toggweiler and Russell, 2008). This places the main axis of the jet stream directly over the Qaidam Basin during glacial and stadial periods, when wind erosion was most severe. A corollary of this hypothesis is that the strong winds that produced the exposed Qaidam yardangs are not active during the modern interglacial climate. This is consistent with the relative scarcity of major, documented dust storms in the Qaidam and our observations that in many places, the Qaidam yardangs are armored with a decimeter-scale-thick crust/soil of strongly indurated salt, indicating landform stability. A testable prediction is that the provenance of Loess Plateau deposits should shift back-and-forth between the Gobi Desert and Qaidam regions, with the bulk of the accumulated loess being sourced from the Qaidam during glacial and stadial episodes.

References

Mischke, S., Herzschuh, U., Sun, N., Qiao, Z. and Sun, Z., 2006, A large Middle Pleistocene freshwater to oligohaline lake in the contemporary hyperarid Qaidam Basin (China), Episodes, 29, 34-38.

Porter, S.C., 2007, Loess Records / China, Encyclopedia of Quaternary Science, Elsevier B.V., 1429-1440.

Toggweiler, J.R. and Russell, J., 2008, Ocean circulation in a warming climate, Nature, 451, 286-288.

Zhou, J., Xu, F., Wang, T., Cao, A. and Yin, C., 2006, Cenozoic deformation history of the Qaidam Basin, NW China: Results from cross-section restoration and implications for Qinghai-Tibet Plateau tectonics, Earth and Planetary Science Letters, 243, 195-210.

Cite as: Kapp, P., and others, 2010, Plio-Quaternary wind erosion in the Qaidam Basin, central Asia: records, rates, and broader implications, *in* Leech, M.L., and others, eds., Proceedings for the 25th Himalaya-Karakoram-Tibet Workshop: U.S. Geological Survey, Open-File Report 2010-1099, 2 p. [http://pubs.usgs.gov/of/2010/1099/kapp/].

INDEPTH-IV Seismic Imaging of Channel Flow Outwards from the Kunlun Mountains Beneath the Qaidam Basin

Marianne S. Karplus[1], Simon L. Klemperer[1], Zhao Wenjin[2], Wu Zhenhan[2], Larry D. Brown[3], Shi Danian[2], James Mechie[4], Chen Chen[3], Jonathan Glen[5]

[1] Department of Geophysics, Stanford University, Stanford, CA 94305, U.S.A., mkarplus@stanford.edu
[2] Chinese Academy of Geological Sciences (CAGS), Beijing 100037, China
[3]Department of Earth and Atmospheric Sciences, Cornell University, Ithaca, NY 14853, U.S.A.
[4]Deutsches GeoForschungsZentrum – GFZ, Telegrafenberg, 14473 Potsdam, Germany
[5]U. S. Geological Survey, Menlo Park, CA 94025, U.S.A.

The INDEPTH IV active-source seismic experiment illuminated continued growth and deformation of the Tibetan Plateau with a high resolution, 270-km wide-angle refraction profile in Northeast Tibet (Fig. 1*A*). The Kunlun Suture (collinear with the North Kunlun Fault, NKF) is the boundary along which the Songpan-Ganzi (SG) terrane and the Kunlun Mountains (KM) accreted (see, for example, Yin and Harrison, 2000). Our new seismic data suggest that the North Kunlun Thrust system (NKT) bounds an indenting Qaidam crustal wedge, beneath which a lowermost-crustal channel extrudes outwards from the Tibetan Plateau.

The INDEPTH IV refraction profile incorporated 5 large (>1,000 kg) and 105 small (60-100 kg) explosions and more than 2,000 seismometers with 650-m spacing at the profile ends and 50- to 100-m spacing across the central 100-km of the profile. Two off-end earthquakes also provided valuable constraints. First-arrival refraction ray tracing and least-squares inversion yielded a crustal p-wave velocity model for the top 15 km of the crust. Ray tracing of deeper reflections shows considerable differences between the Qaidam Basin (QB) and the SG, including higher crustal velocities beneath the QB and an 18-km deepening of the Moho from 52 km to 70 km located beneath the southern QB (Fig. 1*C*) (see also Chen and others, this vol.). The 18-km offset occurs 30-50 km north of the NKT, farther north than inferred from previous seismic studies (Vergne and others, 2002; Zhu and Helmberger, 1998). A 50-52 km deep reflector beneath the SG and KM may represent an older, shallower Moho. The shallow QB Moho at 52 km depth is underlain by crustal material near the northernmost extent of the deeper Moho.

We tested our seismic velocity model by developing a two-dimensional gravity model. The gravity profile (Fig. 1*B*) roughly follows the Golmud-to-Lhasa highway and was extracted from Bouguer anomaly maps of the Yadong-to-Golmud and Golmud-to-Ejin Qi segments of the Tibet Geoscience transect (Meng and others, 1995). This gravity profile follows the INDEPTH IV profile north of large shot KS3 and then deviates from the INDEPTH IV profile south of KS3 to follow the highway up to 165 km west of the profile. We converted our model velocities (Fig. 1*C*) to densities, simplified the model into density layers, modeled gravity predicted for those densities, and then simplified the model to highlight the main density anomalies (Fig. 1*D*). Our velocity model is consistent with the gravity data and the existence of the Moho step (Fig. 1*B*).

Our preferred tectonic model, which accounts for the main features of the velocity and density model, incorporates a channel of lower-crustal material flowing northward from the Kunlun Mountains (KM) beneath the Qaidam Basin. Surface geologic mapping shows both south- and north-directed thrust faults in the KM (Wu and others, 2009), but we favor a north-vergent NKT based on the south-dipping velocity contrast, and consistent with the topographic step at the north margin of the Tibetan Plateau. The middle and upper QB crust has faster velocities than the KM and SG crust and may form a rigid wedge over which the KM crust is thrust and beneath which the Tibetan lower crust is extruding.

References

Chen, C., Brown, L., Karplus, M. and Klemperer, S., 2010, The Golmud Step: New details of the 15 km Moho offset between the Tibet Plateau and the Qaidam Basin from INDEPTH IV seismic results, *in* Leech, M.L., and others, eds., Proceedings for the 25th Himalaya-Karakoram-Tibet Workshop, U.S. Geological Survey Open-File Report 2010-1099,.

Meng, L.S., Guan, Y., Qi, L. and Gao, R., 1995, Gravity field and deep crustal structure in Golmud-Ejin Qi geoscience transect and nearby area, Chinese Journal of Geophysics (in Chinese), 38, 36-45.

Vergne, J., and others, 2002, Seismic evidence for stepwise thickening of the crust across the NE Tibetan plateau, Earth Planet. Sci. Letts., 203, 25-33.

Wu, Z., and others, 2009, Late Oligocene early Miocene thrusting in southern East Kunlun Mountains, northern Tibetan Plateau, Journal of Earth Science, 20, 381-390.
Yin, A. and Harrison, T.M., 2000, Geologic evolution of the Himalayan-Tibetan orogen, Ann. Rev. Earth Planet. Sci., 28, 211-280.
Zhu, L. and Helmberger, D.V., 1998, Moho offset across the northern margin of the Tibetan Plateau, Science, 281, 1170-1172.

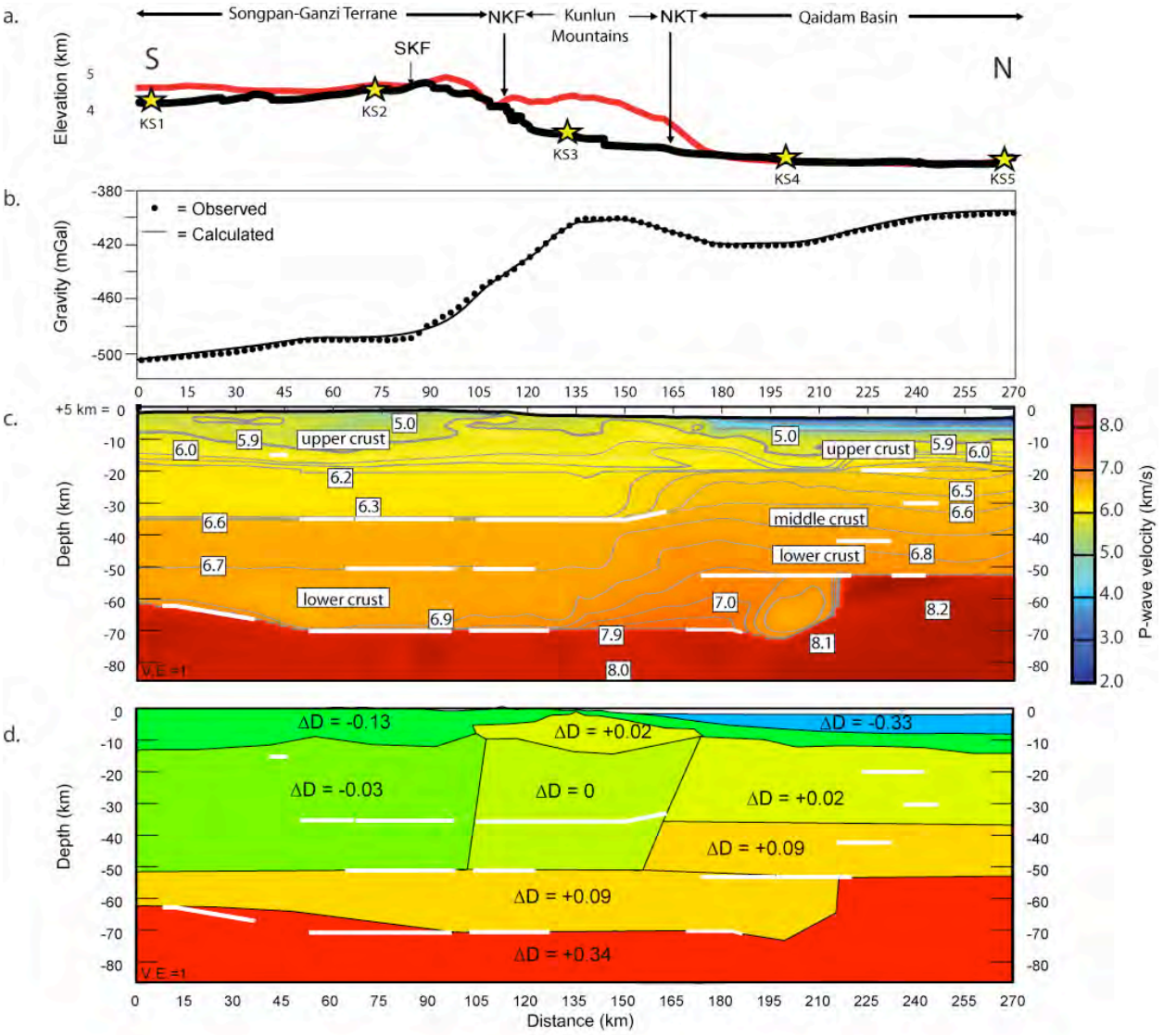

Figure 1. (*A*) Elevation along INDEPTH IV active source profile (black curve) and TOPO1 elevation along the profile averaged over longitudes 94 to 96°E (red curve). South Kunlun Fault (SKF), North Kunlun Fault (NKF), and North Kunlun Thrusts (NKT) are indicated by arrows. Yellow stars show locations of large shots KS1 through KS5. (*B*) Bouguer anomaly data extracted from the gravity map of the Tibet Global Geoscience Transect (Meng and others, 1995) plotted with gravity calculated for the model shown in d. (*C*) Composite shallow and deep crustal velocity model from ray tracing the INDEPTH IV controlled source profile. Major reflectors shown as white lines. (*D*) Simplified density model based on major velocity anomalies shown in c. Density anomalies are given relative to the density of the QB middle crust. Major reflectors shown as white lines. Poor fit of gravity Moho to seismic Moho south of the SKF may be due to the 100 km west-east separation of the gravity and seismic data.

Cite as: Karplus, M.S., and others, 2010, INDEPTH-IV seismic imaging of channel flow outwards from the Kunlun Mountains beneath the Qaidam Basin, *in* Leech, M.L., and others, eds., Proceedings for the 25th Himalaya-Karakoram-Tibet Workshop: U.S. Geological Survey, Open-File Report 2010-1099, 2 p. [http://pubs.usgs.gov/of/2010/1099/karplus/].

Pressure-Temperature-Time Paths of Tectonites from the South Tibetan Detachment System, Bhutan Himalaya

Dawn A. Kellett[1], Djordje Grujic[1], Clare Warren[2], John Cottle[3,4], Rebecca Jamieson[1]

[1] Department of Earth Sciences, Dalhousie University, Halifax, NS, B3H 4J1, Canada, dawn.kellett@dal.ca
[2] Department of Earth and Environmental Sciences, The Open University, Milton Keynes, MK7 6AA, United Kingdom.
[3]Natural Environment Research Council Isotope Geosciences Laboratory, British Geological Survey, Keyworth, NG125GG, United Kingdom.
[4]Now at: Department of Earth Sciences, University of California, Santa Barbara, California, 93106-9630, U.S.A.

The South Tibetan detachment system (STDS) in the Himalayan orogen is an example of normal-sense displacement on an orogen-parallel shear zone during lithospheric contraction. *In situ* monazite U(-Th)-Pb geochronology, textural observations and metamorphic pressure and temperature estimates constrain pressure-temperature-time (P-T-t) paths for both the hanging wall and footwall rocks of a Miocene ductile component of the STDS (outer STDS) now exposed in the Bhutan Himalaya. The outer STDS is located south of a younger, ductile/brittle component of the STDS (inner STDS), and is characterized by structurally-upward decreasing metamorphic grade corresponding to a transition from sillimanite-bearing Greater Himalayan sequence (GHS) rocks in the footwall with garnets that preserve diffusive chemical zoning to staurolite-bearing Chekha Group rocks in the hanging wall with garnets that record prograde chemical zoning. Monazite ages indicate that garnet growth in GHS footwall rocks occurred prior to 22.6 ± 0.4 Ma, and that peak temperatures were reached following ca. 20.5 Ma. In contrast, peak temperatures were reached in the Chekha Group hanging wall by ca. 22 Ma. Normal-sense (top-to-the-north) shearing in both the hanging wall and footwall followed peak metamorphism and continued until at least ca. 16 Ma. Retrograde P-T-t paths are compatible with modeled P-T-t paths for an outer STDS analogue that is isolated from the inner STDS by intervening extrusion of a dome of mid-crustal material.

Cite as: Kellett, D.A., Grujic, D., Warren, C., Cottle, J. and Jamieson, R., 2010, Pressure-temperature-time paths of tectonites from the South Tibetan Detachment System, Bhutan Himalaya, *in* Leech, M.L., and others, eds., Proceedings for the 25th Himalaya-Karakoram-Tibet Workshop: U.S. Geological Survey, Open-File Report 2010-1099, 1 p. [http://pubs.usgs.gov/of/2010/1099/kellett/].

Stable Isotopic Constraints on Paleoelevation and Paleoclimate along the Northern Margin of the Tibetan Plateau

Malinda L. Kent-Corson[1], Bradley D. Ritts[2], Guangsheng Zhuang[3], Paul M. Bovet[4], Julien Charreau[5], Stephen A. Graham[6], C. Page Chamberlain[7]

[1] Department of Earth Sciences, Bridgewater State College, Bridgewater, MA 02325, U.S.A., mkentcorson@bridgew.edu
[2] Chevron Energy Technology Company, San Ramon, CA 94582, U.S.A.
[3]Department of Earth and Planetary Sciences, University of California Santa Cruz, Santa Cruz, CA 95060, U.S.A.
[4]Chevron Energy Technology Company, Sugar Land, TX 77478, U.S.A.
[5]Centre de Recherches Petrographiques et Geochimique, Vandoeuvre-Les-Nancy Cedex, France
[6]Department of Geological and Environmental Sciences, Stanford University, Stanford 94305, U.S.A.
[7]Department of Environmental Earth System Science, Stanford University, Stanford 94305, U.S.A.

In this study we present oxygen isotope data from thirteen terrestrial records that span the northern margin of the Tibetan Plateau, including Tarim and Qaidam Basins, Hexi Corridor, and the Altun Shan. Oxygen isotope values from the analysis of 1475 samples of paleosol, lacustrine, fluvial, and alluvial carbonate, yield $\delta^{18}O$ values that range from 13.1 to 38.9‰ (SMOW). In these data we identify a Paleogene decrease in oxygen isotope values and a Neogene increase in oxygen isotope values (Fig. 1).

We interpret the Paleogene trend, in which oxygen-isotope values become less variable and decrease 1-3‰, to result from a change from disorganized, low-gradient depositional environments with diverse water sources, to more integrated and mountainous source areas. In most sections, this isotopic shift occurs in conjunction with a lithologic transition from mostly finer-grained mudstone, siltstone, and sandstone to coarser-grained sandstone and conglomerate. The finer-grained sediments were deposited in playa, lacustrine, and meandering fluvial depositional environments, where oxygen-isotope compositions of waters may reflect a variety of water sources in absence of a single major integrated drainage system. Waters in these types of environments are likely to further evolve with evaporative effects, evidenced in the study areas by the formation of evaporite minerals. As grain sizes increase upsection to sandstone and conglomerate deposited in braided fluvial and alluvial fan environments, oxygen-isotope average values and variability decrease. Because the isotopic change is associated with a sedimentological change to higher energy deposits, we believe that the isotopic change most likely occurs with the transition to a more regionally integrated drainage system with less-variable source waters, that may record an isotopic signal of uplift south of the study area itself, probably in the region of the northern Qiangtang terrane and Fenghuoshan (Wang and others, 2008). Furthermore, with the transition to fluvial depositional environments, we expect there to be less extreme evaporation than in the playa and lacustrine facies downsection. This decrease in oxygen isotope variability causes mean oxygen isotope values to decrease.

We interpret the Neogene isotopic trend, in which both oxygen and carbon isotopic values increase through time, to result from the uplift of basin-bounding ranges in the study region itself, with ranges blocking moisture sources to the region and increasing aridity and evaporative effects. The uplift of basin bounding ranges in this region is supported by a change to depositional environments that include high-energy braided fluvial and alluvial fan deposits, with paleocurrents showing the establishment of strong unimodal drainage systems from adjacent ranges, similar to the modern drainage systems. Uplift at this time is also shown by an increase in elevation in some Tarim study areas from sea level to their current elevations (~1400 m), beginning as late as the early middle Miocene in the Miran River section (Ritts and others, 2008). The contribution of evaporative effects to the isotopic record is indicated by the presence of aeolian and evaporite deposits, extreme oxygen and carbon isotope values ($\delta^{18}O$ up to 39‰ in Lenghu), and covariation between oxygen and carbon isotope values (Kent-Corson and others, 2009)

The isotopic data presented in this study provides additional evidence for a transition in tectonic style along the northern margin of the Tibetan Plateau in the early to middle Miocene from accommodation of convergence through plate-like escape along the Altyn Tagh Fault to accommodation of convergence through distributed shortening and crustal thickening (Yue and others, 2003; Ritts and others, 2008). The early to middle Miocene initiation of mountain building in this region also significantly postdates isotopic predictions for the attainment of high elevations on the central Tibetan Plateau (e.g. Rowley and Currie,

2006; DeCelles and others, 2007), and predates isotopic evidence for the contribution of high elevation waters to study areas along the Tian Shan to the north (Graham and others, 2005; Charreau and others, in review), consistent with differential uplift of the Tibetan Plateau.

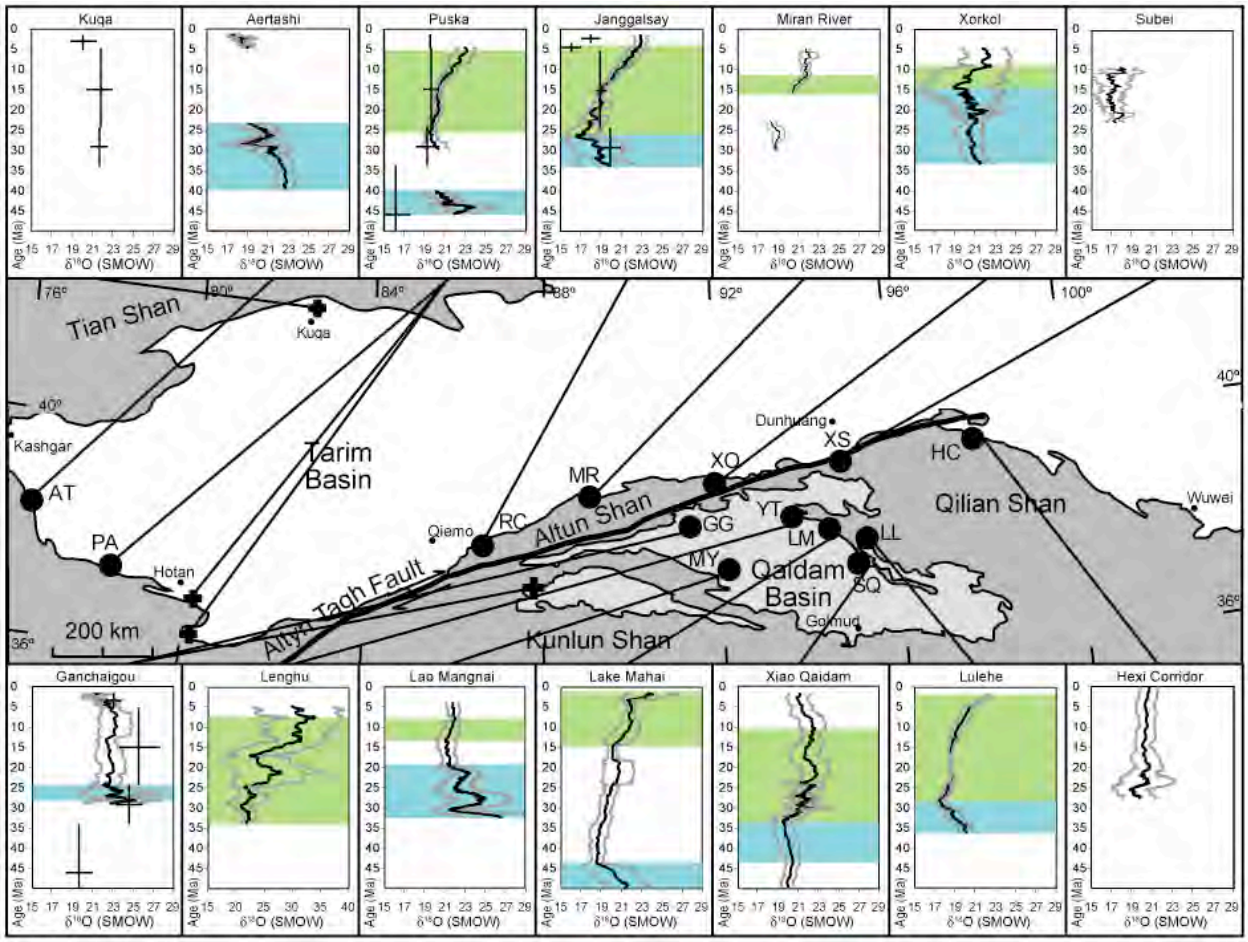

Figure 1. Oxygen isotope data plotted with age. Nine-point running average is shown by black line, and running standard deviation is shown by gray lines. The two trends are shaded, with the "Paleogene" trend shown in blue, and the "Neogene" trend shown in green. Data from Graham and others (2005) are shown with crosses.

References

Charreau, J., and others, in review, High resolution stable isotopic record from the Junggar Basin (NW China): Implications for the paleotopography of the Tian Shan Mountains, Geology.

DeCelles, P.G., and others, 2007, High and dry in central Tibet during the Late Oligocene, Earth and Planetary Science Letters, 253, 389-401.

Graham, S.A., and others, 2005, Stable isotope records of Cenozoic climate and topography, Tibetan Plateau and Tarim Basin, American Journal of Science, 305, 101-118.

Kent-Corson, M.L., and others, 2009, Stable isotopic constraints on the tectonic, topographic, and climatic evolution of the northern margin of the Tibetan Plateau, Earth and Planetary Science Letters, 282, 158-166.

Ritts, B.D., and others, 2008, From Sea Level to High Elevation in 15 Million Years: Uplift History of the Northern Tibetan Plateau Margin in the Altun Shan, American Journal of Science, 308, 657-678.

Rowley, D.B. and Currie, B.S., 2006, Palaeo-altimetry of the late Eocene to Miocene Lunpola basin, central Tibet, Nature, 439, 677-681.

Yue, Y., and others, 2003, Slowing extrusion tectonics: lowered estimate of post-Early Miocene slip rate for the Altyn Tagh fault, Earth and Planetary Science Letters, 217, 111-122.

Wang, C., and others, 2008, Constraints on the early uplift history of the Tibetan Plateau, Proceedings of the National Academy of Science, 105, 4987-4992.

Cite as: Kent-Corson, M.L., and others, 2010, Stable isotopic constraints on paleoelevation and paleoclimate along the northern margin of the Tibetan Plateau, *in* Leech, M.L., and others, eds., Proceedings for the 25th Himalaya-Karakoram-Tibet Workshop: U.S. Geological Survey, Open-File Report 2010-1099, 2 p. [http://pubs.usgs.gov/of/2010/1099/kentcorson/].

Temporal Evolution of Cretaceous to Pleistocene Magmatism in the Chagai Arc, Balochistan, Pakistan

M. Asif Khan[1], R. H. Siddiqui[2], M. Qasim Jan[1]

[1] National Centre of Excellence in Geology, University of Peshawar, Peswar 25120, Pakistan, masifk@upesh.edu.pk
[2]Geoscience Laboratory, Geological Survey of Pakistan, Shahzad Town, Islamabad, Pakistan

The Chagai arc is part of the southern Afghan block, a microcontinent of Gondwanan affinity accreted at the southern margin of Eurasia (Jacob and Quittmeyer, 1979). The arc, together with an over 300 km wide classic accretionary prism to its south (Platt and others, 1986), overrides the active Makran subduction zone (MSZ). The Gulf of Oman (and associated Makran trench) represents a unique living remnant of the Neotethys, which has elsewhere been consumed in India-Arabia and Eurasia collision (e.g., Zagros Ranges, Iran and the Kirthar-Sulaiman Ranges, Pakistan). The longstanding activity on the MSZ is manifested in intermittent magmatism in the Chagai Arc spanning about 70 Ma from the Late Cretaceous to the Pleistocene, which is unmatched in Neotethyan arcs preserved elsewhere in the Himalaya and Zagros Ranges.

The Chagai arc exposes a >10,000 m stratigraphic succession from Late Cretaceous to Pliocene-Pleistocene, comprising volcanic, volcano-sedimentary and sedimentary rocks. A thick (~2,500 m) succession of massive basaltic-andesite lava flows (associated with lapilli tuff, volcanoclastic sediments and minor felsic lavas) dominates the Late Cretaceous Sinjarani Group (Ahmed and others, 1972; Siddiqui, 1996, 2004), the oldest unit exposed in the Chagai Arc. Volcanic rocks abundantly occur in younger stratigraphic units including the Paleocene Juzzak Formation, Eocene Saindak Formation, Oligocene Amlaf Formation, Miocene Buz Mashi Koh Formation, and Pliocene-Pleistocene Koh-i-Sultan Formation (Siddiqui, 2004). The Late Cretaceous-Paleocene volcanism is dominated by basalts and basaltic andesites. In comparison, Eocene and younger volcanism is dominantly andesitic to dacitic with minor basalts.

Detailed major, trace, and rare-earth geochemistry classifies the temporal volcanism in the Chagai Arc into three groups; 1) Late Cretaceous-Paleocene, 2) Eocene, and 3) Oligocene and younger. Trace element characteristics like LILE and LREE enrichment and HFSE and HREE depletion relative to mid-oceanic ridge basalts (MORB), positive anomalies for LILE (K, Sr, and Ba) and marked negative anomalies for Nb (in mantle normalized trace-element patterns) are common to all the three groups, conforming to their origin in subduction-related settings. However, there are distinct geochemical differences between the three groups, suggesting temporal changes in their tectonic setting of origin. The Late Cretaceous-Paleocene volcanic rocks are typical low-K island-arc tholeiites formed in an intra-oceanic island-arc setting. The Eocene volcanic rocks are transitional from low-K tholeiites to calc-alkaline and suggest formation in a transitional island-arc/continental-margin setting. The Oligocene and younger rocks are typically calc-alkaline (with some trachy-andesite alkaline facies in the Miocene rocks) formed in a mature continental-margin setting.

The information from geochemistry and tectonic setting of origin from the Chagai volcanic rocks enables revising the tectonic models for the evolution of the southern margin of the Afghan block. Whereas previous workers (Sillitoe, 1978; Arthurton and others, 1979, 1982; Kazmi and Jan, 1997) considered the modern-day continental-margin setting to have been maintained since the Late Cretaceous, our study suggests a two-stage evolution. We propose that the Chagai Arc formed as an intra-oceanic island arc in the Neotethys (coeval with the better known Kohistan island arc to the NE in the Western Himalayas), which collided with the Eurasian margin (Central Afghan block) in the latest Palaeocene. Through a transitional evolution during the Eocene, the arc evolved into a mature Andean-type continental margin by Oligocene and continues as such to the present day.

The northern margin of the E-W oriented Chagai arc is covered by superficial sediments of the Sistan basin at Pakistan-Afghan border, which conceal the contact between the Chagai arc and the Central Afghanistan block. Indirect information about this contact zone is available from the Kandahar region of

SE Afghanistan, which occupies the NW side of the Chaman Fault analogous to the Chagai Arc at Naushki, Baluchistan. Two tectonic blocks are recognized in the Kandahar region to the immediate NW of the Chaman Fault; 1) Spin-Boldak, and 2) Kandahar (Debon and others, 1986). The abundance of continental-margin intrusive and volcanic rocks in the Kandahar Block led previous workers to suggest equivalence with the Chagai Arc. However, the presence of Precambrian basement rocks in the Kandahar block negates this possibility. A better candidate for a NE extension of the Chagai arc is the Spin Boldak block, which hosts temporally and compositionally equivalent rocks and, like the Chagai arc, is built on an oceanic basement rather than a continental basement (Debon and others, 1986). We propose that the late Paleocene Kandahar suture zone (Benham and others, 2009), separating the Spin Boldak block from the Kandahar block, extends SW and separates the Chagai arc from the Central Afghan block, a situation analogous to the Kohistan-Karakoram suture separating Kohistan arc from the Karakoram block in the NW Himalayas (Heuberger and others, 2007).

References

Ahmed, W., Khan, S.N. and Schmidt, R.G., 1972, Geology and copper mineralization of the Saindak Quadrangle, Chagai District, West Pakistan, U.S. Geological Survey Professional Paper, 716-A, 21 p.

Arthurton, R.S., Alam, G.S., Ahmed, S.A. and Iqbal, S., 1979, Geological history of Alam Reg-Mashki Chah area, Chagai District, Balochistan, in Farah, A. and DeJong, K.A., eds., Geodynamics of Pakistan, Geological Survey of Pakistan, 325-331.

Arthurton, R.S., Farah, A. and Ahmed, W., 1982, The Late Cretaceous-Cenozoic history of western Balochistan, Pakistan - the northern margin of the Makran subduction complex, in Leggett, J.K., ed., Trench Fore-Arc Geology, Geological Society of London, Special Publication, 10, 343-385.

Benham, A.J., Kováč, P., Petterson, M.G., Rojkovic, I., Styles, M.T., Gunn, A.G., McKervey, J.A. and Wasy, A., 2009, Chromite and PGE in the Logar Ophiolite Complex, Afghanistan, Applied Earth Science, IMM Transactions Section B, 118, 45-58.

Debon, F., Afzali, H., Le Fort, P. and Sonet, J., 1986, Plutonic belts in Afghanistan: typology, age and geodynamic setting, Sciences de la Terre, 47, 129-153.

Heuberger, S., and others, 2007, Age and isotopic constraints on magmatism along the Karakoram-Kohistan suture zone, NW-Pakistan: Evidence for subduction and continued convergence after India-Asia collision, Eclogae Geologicae Helvetiae, 1, 1–24.

Jacob, K.H. and Quittmeyer, R.L., 1979, The Makran region of Pakistan and Iran: Trench-arc system with active plate subduction, Geodynamics , in Farah, A. and DeJong, K.A., eds., Geodynamics of Pakistan, Geological Survey of Pakistan, 305–317.

Kazmi, A.H. and Jan, M.Q., 1997, Geology and tectonics of Pakistan, Graphic Publishers, Karachi, 554 p.

Platt, J.P., Leggett, J.K., Young, J., Raza, H. and Alam, S., 1986, Large-scale sediment underplating in the Makran accretionary prism, southwest Pakistan, Geology, 13, 507-511.

Siddiqui, R.H., 1996, Magmatic evolution of Chagai-Raskoh arc terrane and its implication for porphyry copper mineralization, Geologica, 2, 87-119.

Siddiqui, R.H., 2004, Crustal evolution of the Chagai-Raskoh Arc Terrane, Balochistan, Pakistan, Unpublished PhD. Thesis, University of Peshawar, Pakistan, pp. 352.

Sillitoe, R.H., 1978, Metallogenic evolution of a collision mountain belt in Pakistan: a preliminary analysis, Journal of Geological Society, London, 125, 377-387.

Cite as: Khan, M.A., Siddiqui, R.H. and Jan, M.Q., 2010, Temporal evolution of Cretaceous to Pleistocene magmatism in the Chagai Arc, Balochistan, Pakistan, *in* Leech, M.L., and others, eds., Proceedings for the 25th Himalaya-Karakoram-Tibet Workshop: U.S. Geological Survey, Open-File Report 2010-1099, 2 p. [http://pubs.usgs.gov/of/2010/1099/khan/].

HIMPROBE Deep Seismic Reflection Profiling of the Sub-Himalayan Fold-Thrust Belt, NW India: Images of a Possible "Ulleri-Wangtu" Paleoproterozoic Accretionary Orogenic Event

Simon L. Klemperer[1], B. Rajendra Prasad[2], V.Vijaya Rao[2], H.C.Tewari[2], Prakash Khare[2]

[1] Department of Geophysics, Stanford University, CA 94305-2215, U.S.A., sklemp@stanford.edu
[2] National Geophysical Research Institute, Hyderabad - 500 606, India

NGRI has acquired and processed the first deep seismic reflection study from the Sub-Himalaya (Fig. 1). Previous shallow (4.5 s) oil-industry profiles (e.g. Powers and others, 1998) show complex fold-and-thrust structures within the Tertiary sequence that our HIMPROBE profiles did not target or image. HIMPROBE profiles (Fig. 2) are dominated by a bright reflection band at 3.0–3.5 s two-way-time (TWT) (6–8 km). We follow Powers and others (1998) in interpreting the bright reflections as representing Neoproterozoic (Lesser Himalayan Series-equivalent) Vindhyan strata that have been drilled immediately beneath the décollement. The planar top to the bright reflections is therefore the Main Himalayan Thrust (MHT). Below 3.5 s, reflectivity is far more prominent than above 3 s, and has apparent dips of c. 15° down to c. 12 s TWT on the west-east Profile H2, and (less clearly) as much as 30° on the SW-trending Profile H1 to at least 8 s TWT. These unmigrated dips imply a true dip of the imaged geological fabric of c. 35° WSW. Limited evidence from shallow hydrocarbon-exploration profiles suggest the WSW-dipping reflections exist for at least 150 km NW-SE along strike. The WSW-dipping reflections appear to be truncated upwards by the sub-horizontal bright reflections, so must be older than these interpreted Neoproterozoic strata. We consider the dipping reflections as a single tectonic element forming the major part, 25–30 km, of the Indian basement thickness. The WSW-dipping reflectivity is underlain or overprinted by sub-horizontal reflections, locally bright, that continue to ~16 s TWT ("reflection Moho", c. 51 km), consistent with teleseismic data (Rai and others, 2006). The 42–49 km cratonic basement on our profiles (and at teleseismic stations from CHD to KUL) is 10–30% thicker than directly to the south.

Possible origins for the WSW-dipping reflectivity include: (1) original Archean fabric of the Mewar-Aravalli craton – but this craton has thinner crust and a NE-SW structural trend orthogonal to the reflectivity; (2) a Meso-Neoproterozoic (meta-)sedimentary basin – but the thickness of dipping reflectors is double reported stratigraphic thicknesses in this region, and should not show dips of 35° without subsequent deformation; (3) a "Pan-African" Cambro-Ordovician accretion of the Greater Himalayan terrane to cratonic India or a "Himalayan" Cenozoic tectonic fabric – but Phanerozoic events seem precluded by the apparent truncation of the WSW-dipping reflectivity by overlying Vindhyan strata.

In contrast, a Paleoproterozoic compressional orogeny is consistent with the 35° dip and upward Neoproterozoic truncation of the reflectivity, with 10–30% crustal thickening, and with the widespread occurrence of 1.8–1.9 Ga granitoids in the Lesser Himalaya (Kohn and others, 2010), including Ulleri orthogneisses throughout Nepal. We suggest that an orogenic event thickened the crust between 1.86 Ga deformation of the Wangtu partially-mylonitized augen gneisses and 1.8 Ga eruption of the low-grade Rampur volcanics. The WSW dip of the reflectivity may imply an underthrusting or subduction direction to the (modern) southwest, consistent with an "Andean-type" arc forming along the northern margin of India and the Columbia super-continent (Kohn and others, 2010). The deepest horizontal reflectivity on our profiles and a possible velocity increase above the Moho (Rai and others, 2006) could mark mafic sills related to a rifting episode correlated with the 1.8 Ga Rampur basalt. Crust thickened by the "Ulleri-Wangtu" orogenic event may extend 100–150 km NE of our profiles to the pre-Himalayan location of the Wangtu gneisses, and would first have been subducted beneath the Himalayan thrust front at about 10 Ma, with possible concomitant changes in structural evolution of the Himalayan thrust belt.

References

Kohn, M.J., Paul, S.K. and Corrie, S.L., 2010, The lower Lesser Himalayan Sequence: a Paleoproterozoic arc on the northern margin of the Indian Plate, Geol. Soc. Am. Bull., 122, 323–335, doi: 10.1130/B26587.1.

Powers, P.M., Lillie, R.J. and Yeats, R.S., 1998, Structure and shortening of the Kangra and Dehra Dun reentrants, Sub-Himalaya, India, Geol. Soc. Am. Bull., v.110, 1010-1027.

Rai, S.S., Priestley, K., Gaur, V.K., Mitra, S., Singh, M.P. and Searle, M., 2006, Configuration of the Indian Moho beneath the NW Himalaya and Ladakh, Geophys. Res. Letts., 33, L15308, doi:10.1029/2006GL026076, pp. 5.

Figure 1. Location of HIMPROBE deep profiles H1 and H2, and shallow exploration profiles (K2–Kangra 2 and N1–Nahan 1) possibly showing WSW-dipping reflectivity. MFT–Main Frontal Thrust; MBT–Main Boundary Thrust; MCT–Main Central Thrust. Broadband seismic stations: black triangles with 3-letter codes (Rai and others, 2006).

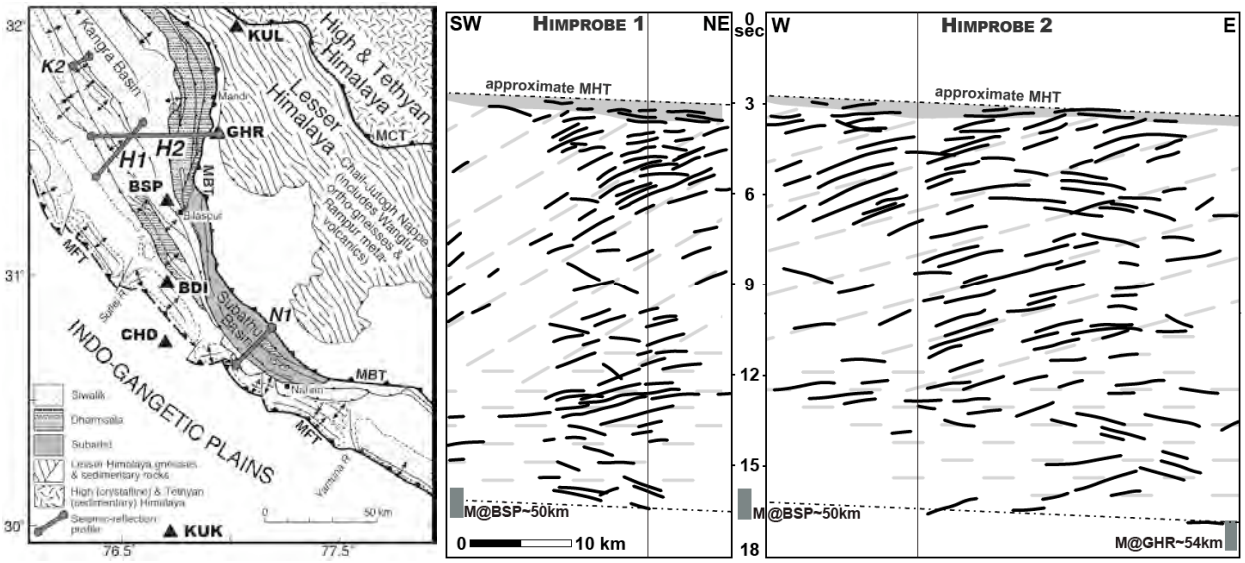

Figure 2. (above right) Line drawings (thick black lines) and interpretive cartoons (grey) of HIMPROBE 1 and 2 stack sections (shown below), all true scale for a velocity of 6 km/s. Thin vertical line: profile intersection. Dot-dash lines at MHT and Moho dip 2.5° (dip of Himalayan décollement, Powers and others, 1998). Grey rectangles: Moho travel-times from teleseismic data (Rai and others, 2006). Grey shading: region of region of bright sub-horizontal reflections inferred to be Proterozoic sedimentary rocks. Dashed grey lines, dipping 30° on H1 and 15° on H2: region of WSW dipping reflectivity. Horizontal dashed grey lines: region of sub-horizontal reflectivity.

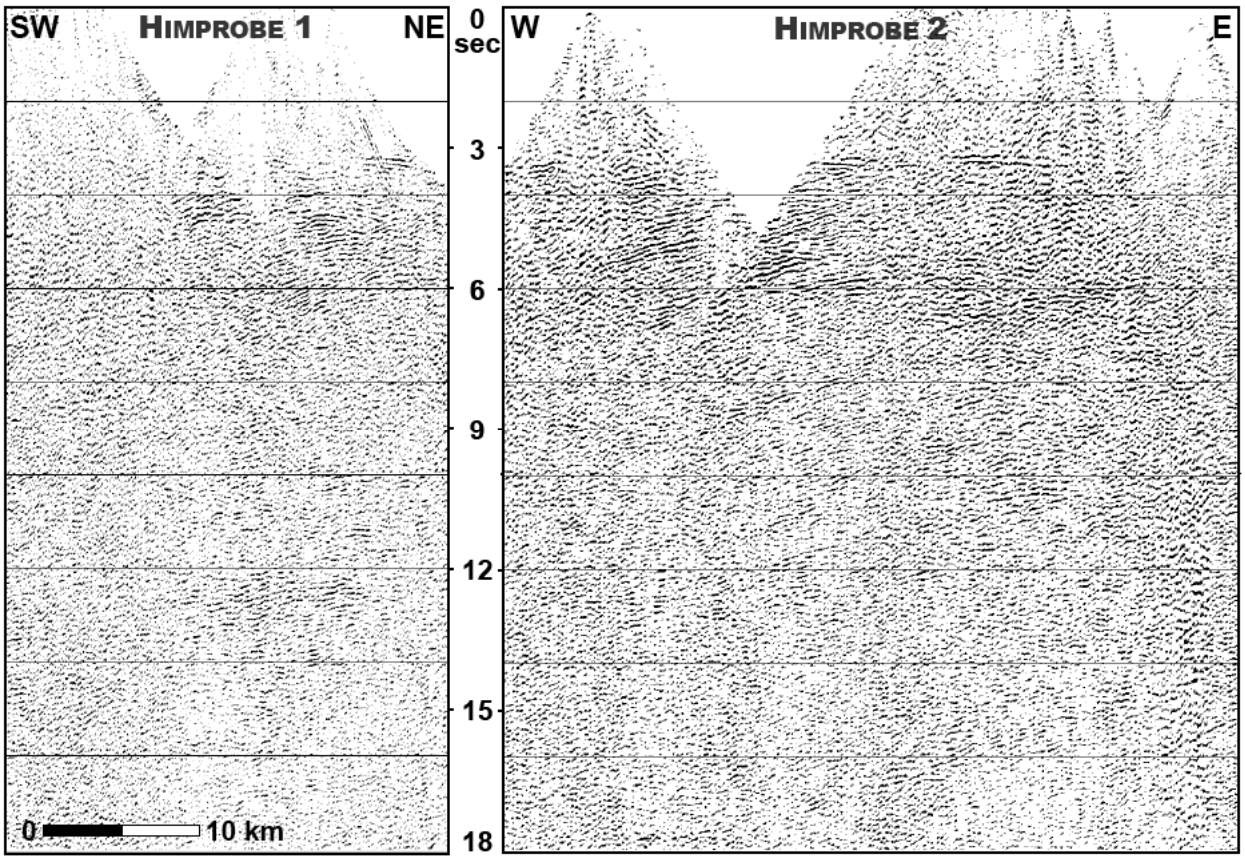

Cite as: Klemperer, S.L., Rajendra Prasad, B., Vijaya Rao, V., Tewari, H.C., and Khare, P., 2010, HIMPROBE Deep Seismic Reflection Profiling of the Sub-Himalayan Fold-Thrust Belt, NW India: Images of a Possible "Ulleri-Wangtu" Paleoproterozoic Accretionary Orogenic Event, *in* Leech, M.L., and others, eds., online proceedings for the 25th Himalaya-Karakoram-Tibet Workshop: U.S. Geological Survey, Open-File Report 2010-1099, 2p. [http://pubs.usgs.gov/of/2010/1099/klemperer1/].

Mantle Helium Signature of the Karakoram fault is that of an Active Plate-Boundary

Simon L. Klemperer[1], B. Mack Kennedy[2], Siva R. Sastry[3], Yizhaq Makovsky[4], T.Harinarayana[3]

[1] Department of Geophysics, Stanford University, CA 94305-2215, U.S.A., sklemp@stanford.edu
[2] Center for Isotope Geochemistry, Lawrence Berkeley National Laboratory, CA 94720, U.S.A.
[3] National Geophysical Research Institute, Hyderabad - 500 007, India
[4] Department of Marine Geosciences, CSMS, University of Haifa, Haifa, 31905, Israel

The Karakoram fault (KKF) of southwest Tibet has been argued, from geologic and geodetic data, either to function as a lithosphere-penetrating plate boundary with ~1000 km of offset at ~30 mm/yr, or to be essentially locked (motion ~1±3 mm/yr; total offset only a few tens of km) and be just the near-surface localization of distributed deformation at depth. Various seismic data have been claimed to preclude direct penetration of the KKF into the mantle, including the similarity of Moho depth immediately south and north of the KKF that has been used to argue for continuity of the Indian plate beneath the KKF, and the transition from efficient to inefficient high-frequency Sn propagation over 200 km NE of the KKF that has been used to argue for underthrusting of Indian crust beneath Tibet to that location.

We tested the depth of penetration of the KKF by measuring $^3He/^4He$ ratios (R) in springs within and away from the KKF (Fig. 1). Helium from atmospheric, crustal and mantle sources is characterized by unique $^3He/^4He$ ratios, respectively Ra, Rc ≈ 0.02 Ra, and ≈ 8 Ra. Plate-boundary strike-slip faults that penetrate from earth's surface to the mantle are obvious pathways for migration of mantle fluids. Helium studies measured R/Rc > 200 close to the San Andreas fault (SAF) (Kennedy and others, 1997) and North Anatolian fault (NAF) (Dogan and others, 2009), with minimum values of R/Rc ≈ 5 just a few 10s of km distant indicative of mantle fluids penetrating the thin, warm and ductile lithosphere of these areas in a process now well-established across the western USA. The ratio (≈ 40) of the highest-to-lowest observed $^3He/^4He$ values is a strong argument that the SAF and NAF penetrate through the whole crust or the whole lithosphere. Previous studies of helium isotopes in eastern Tibet (Fig. 2) have identified a "crustal helium domain" (R/Rc < 2.5) and a "mantle helium domain" (R/Rc > 5) separated by a transition ≈ 90 km north of the Indus suture zone that is considered to mark the mantle suture (Hoke and others, 2000). $^3He/^4He$ ratios up to R/Rc ≈ 10 may represent degassing of Quaternary mantle-derived melts intruded deep into the crust (Hoke and others, 1999) with pathways to the surface enabled by diffuse deformation of a very weak, albeit very thick crust. Our new measurements from hot springs and a fumarole within 50 km of the KKF show a significant influx of mantle helium along the KKF, up to 25 Rc, more than double the highest values observed elsewhere in Tibet. The ratio of highest-to-lowest observed $^3He/^4He$ values is ≈ 60 across the KKF, comparable with the equivalent ratios across the SAF and NAF. The lower absolute values than in California and Turkey are consistent with the three-times thicker thick crust in Tibet that – at least to the south of the KKF – includes subducting Indian craton. The very rapid transition from "crustal" to "mantle" helium values over < 40 km suggests that the upward transport is more focused in the NW Himalaya, presumably by the KKF. In contrast, the 50% smaller increase over three times the distance in southern Tibet is presumably controlled by widely distributed deformation facilitating an active upward migration of aqueous fluids through the crust, as imaged by Makovsky and Klemperer (1999). The lack of enhanced $^3He/^4He$ ratios at orogen-normal rift valleys (Tso Morari fault) shows that these are only an upper-crustal feature, not the lithospheric-scale rifts suggested by Yin (2000).

Our observations provide unequivocal evidence for the presence of mantle-derived fluids transported through the crust to the surface along the KKF. These mantle fluids are not widely disseminated through a fractured, continuously deforming crust, because the Indus suture zone just tens of kilometers southwest of the KKF does not show any evidence of mantle helium. The KKF must be accessing sub-continental or asthenospheric mantle. Our observations imply unbroken Indian crust does not underthrust and underly Asian crust for any significant distance north of the KKF.

References

Dogan, T., and others, 2009, Adjacent releases of mantle helium and soil CO_2 from active faults: Observations from the Marmara region of the North Anatolian Fault zone, Turkey, Geochem., Geophys., Geosyst., 10, Q11009, doi:10.1029/2009GC002745

Giggenbach, W.F., Gonfiantini, R., Jangi, B.L. and Truesdell, A.H., 1983, Isotopic and chemical composition of Parbati Valley

geothermal discharges, North-West Himalaya, India, Geothermics, 12, 199-222.
Hoke, L., Lamb, S., Hilton, D.R. and Poreda, R.J., 2000, Southern limit of mantle-derived geothermal helium emissions in Tibet: Implications for lithospheric structure, Earth Planet. Sci. Letts., 180, 297-308.
Kennedy, B.M., and others, 1997, Mantle fluids in the San Andreas fault system, California, Science, 278, 1278–1281.
Makovsky, Y. and Klemperer, S.L., 1999, Measuring the seismic properties of Tibetan bright-spots: Evidence for free aqueous fluids in the Tibetan middle crust, J. Geophys. Res., 104, 10,795-10,825.
McNamara, D.E., Owens, T.J. and Walter, W.R., 1995, Observations of regional phase propagation across the Tibetan Plateau, J. Geophys. Res., 100, 22,215– 22,229.
Nábelek, J., and others, 2009, Underplating in the Himalaya-Tibet collision zone revealed by the Hi-CLIMB experiment, Science, 325, 1371-1374.
Priestley, K., Jackson, J. and McKenzie, D., 2007 Lithospheric structure and deep earthquakes beneath India, the Himalaya and southern Tibet, Geophys. J. Int., doi: 10.1111/j.1365-246X.2007.03636.x, pp 18.
Yin, A., 2000, Mode of Cenozoic east-west extension in Tibet suggesting a common origin of rifts in Asia during the India-Asia collision, J. Geophys. Res., 105, 21,745-21,579.

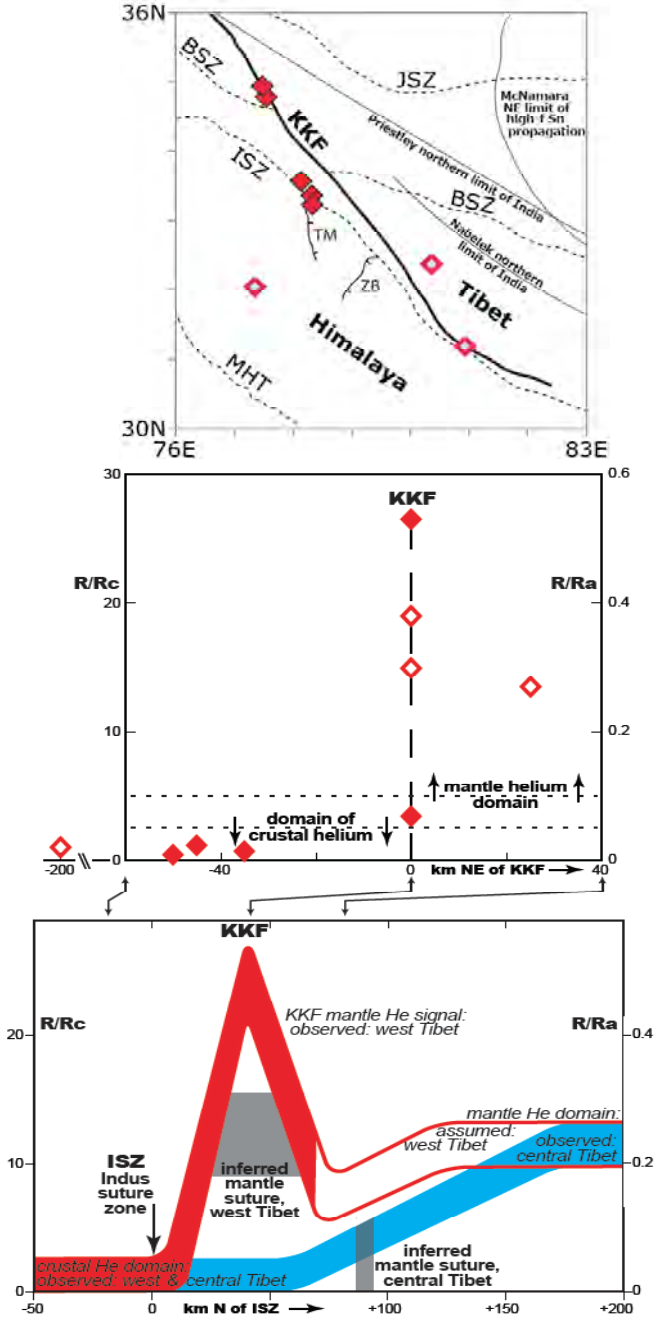

Figure 1. Location of $^{3}He/^{4}He$ samples along the Karakoram Fault (KKF) and Indus Suture Zone (ISZ). Solid diamonds: our new data; open diamonds: data of Hoke and others (1999) and Giggenbach and others (1983). Dashed lines: Main Himalayan Thrust (MHT), Banggong Suture Zone (BSZ), and Jinsha Suture Zone (JSZ). TM and ZB: Tso Morari and Zada Basin (LeoPargil) normal faults. Northern limit of Indian crust inferred by Nabelek and others (2009) from interpretations of receiver function images, and by Priestley and others (2007) from the northern limit of supposed deep-crustal earthquakes; northeastern limit of propagation of high-frequency Sn (seismic phase propagating just beneath the Moho) (McNamara and others, 1995) has been taken to be the northern limit of Indian cratonic mantle.

Figure 2a. $^{3}He/^{4}He$ values measured in hot springs, expressed as ratios of standard continental crustal and atmospheric ratios (respectively R/Rc and R/Ra), plotted as a function of distance NE of the Karakoram Fault (KKF). Atmospheric helium has a $^{3}He/^{4}He$ ratio, Ra, of $1.4\ 10^{-6}$, whereas crustal helium (dominated by radiogenic ^{4}He), is characterized by a $^{3}He/^{4}He$ ratio Rc of ~0.02 Ra. Definition of "crustal" and "mantle" domains, and open symbols at and NE of the KKF from Hoke and others (1999); open symbol SW of the KKF from Giggenbach and others (1983).

Figure 2b. Schematic results from south-central Tibet (blue, R/Rc ≤ 10, from Hoke and others (1999)) and new results from western Tibet (red, R/Rc ≥ 25 at the KKF: this paper) aligned with respect to the Indus suture zone (ISZ), to show the very different spatial gradients in each region. Grey boxes show the inferred mantle suture (the northward limit of penetration of Indian lithosphere in contact with Asian crust) of Hoke and others (1999) 90km north of the ISZ, and our inferred mantle suture just 30–60 km north of the ISZ, and essentially at the KKF.

Cite as: Klemperer, S.L., Kennedy, B.M., Sastry, S.R., Makovsky, Y., and Harinarayana, T., 2010, Mantle helium signature implies the Karakoram fault is an active plate-boundary, *in* Leech, M.L., and others, eds., Proceedings for the 25th Himalaya-Karakoram-Tibet Workshop: U.S. Geological Survey, Open-File Report 2010-1099, 2 p. [http://pubs.usgs.gov/of/2010/1099/klemperer2/].

New Indicators of a Former Tibetan Ice Sheet and an Ice Stream Network in the Surrounding Mountain Systems: New Field Observations and Dating on the SE-, S- and W-margin of Tibet from Expeditions in 2004-2009

Matthias Kuhle[1]

[1]Geography and High Mountain Geomorphology, University 37077 Göttingen, Goldschmidtstr.5, Germany, mkuhle@gwdg.de

Great Karakoram: South side

In 2006 detailed researches between the Skardu basin and the source branches of the Hushe valley showed that 600 up to 2500m above the current gravel floors of the main valley and the present glacier surfaces, ground moraine covers on the valley flanks and even glacier polishings (35°30'52"N 76°20'20"E) are preserved up to abrasion and polish lines. In the left flank of the Ghondokhoro glacier valley sedimentary remnants of ground moraine (35°33'30"N/76°25'E) are preserved up to 4480 m, whilst flank polishings occurred up to at least 5000 m; trough profile lines were found even higher. In the confluence area of the Charakusa glacier valley, on the flanks of the Masherbrum and Aling glacier valley (35°29'15"N 76°19'E), corresponding findings prove a maximum former valley glacier level. Down-valley of the Hushe settlement key glacigenic forms (35°24'10"N/76°21'30"E) up to c. 5400 m document an ice thickness of 2000 m. 30 km down the Hushe valley, in the confluence area with the Saltoro- and Shyok valley, ground moraines with erratics and polishings (35°16'N/76°24'E) on all valley flanks evidence an ice thickness of c. 1700 m above the 5 km wide gravel floor of the river during the last glacial period (LGP), plus a valley bottom filled with loose sediments more than 500 m-thick. 20 km down the Shyok main valley there was the Ice Age inflow of the Thalle glacier branch near the Bragar settlement. 33 km further down the past Shyok glacier a confluence occurred with the largest main glacier, the Indus glacier. Coming from the SE, it flowed down from the valley chamber of Kargil, where the Suru glacier joined from the S, from the Zanskar (Kuhle 1998). Glaciogeomorphological evidence (34°38'N/74°58'E) suggests a c. 1500 m thick, 25 km long Indus parent glacier from this Shyok glacier confluence up to the Indus valley near Skardu. With that, the S-side of the Masherbrum-range has been reconstructed as one part of the c. 125,000 km² extended Karakoram-ice stream network. Near Skardu there was inflow of the 2000 m-thick Shigar glacier with the feeding areas of the Braldu (LGP-Baltoro) and Basna (LGP-Chogolungma) glaciers (Kuhle 2001). The comparison of glacial-geological and glaciological relative dating with cosmogenic nuclide (CN)-tests and of ^{14}C- with OSL-data prove an LGP-ice-stream-network during the Marine Isotope Stage (MIS) 3-2 (Kuhle 2010, Hewitt 2009).

Dolpo

Research in the Bheri Khola began in 1995 (Kuhle, 1998) and ended in the Barbung Khola, N of the Dhaulagiri Himal and Dolpo (Kanjiroba, Do Tarap). Up-valley of Tripurakot (29°02'N/82°46'E), with a minimum ice thickness of 400 m and a height of the thalweg of 1900 m (Kuhle 1998), the valley flanks of the Bheri Khola that to the E passes into the Barbung Khola and those of its side valleys (Suli Gad, Tarap Chu etc.) are mantled by large-scale ground moraine covers with erratic material up to 4400 m (e.g. in the Barbung Khola above Seri) (28°53'N/83°21'30"E). In the middle Suri Gad (3200 m) there are more than 100 m-thick ground moraines. Below the Poksundo Tso they are dovetailed with Late Glacial end moraines of Stages III and IV. The Poksundo Tso itself has been dammed up by such an end moraine. In the Chhura Khola between Bagla and Numla and in the upper Tarap Chu, in the wide S-Tibetan valley of Dho, large-scale ground moraine covers may derive from a relief-filling glaciation. The Tarap gorge up to Khanigau (inflow of the Barbung Khola) was filled with ground moraine more than 100 m thick. The accompanying LGP- ice level runs up to 4800 m. From the valley of Kakkot down the Barbung Khola, as far as the Tarap Chu, over 200 m-thick ground moraine does occur. Lake sediments 500 m above the thalweg (28°52'50"N/83°09'20"E) prove a Late Glacial lateral valley (Stage IV) at 3700 m. Near Kakkot LGP-ground moraine covers and polish bands reach c. 4600 m. Thus, a further section of the S-Tibetan ice stream network - here W of the upper Thak Khola - is reconstructed in detail.

Damodar Himal

Research started in 2004 between Mustang (in the W) and Dhud Khola (Manaslu) and in 2007 in all main valleys and their catchment areas. On both sides of the Pangri glacier remnants of ground moraine covers

were mapped at high slope positions. The same applies to the upper Phu Khola - today a large-scale non-glaciated region - with its plane S-Tibetan morphology. Abrasion forms (e.g. at 28°48'50"N/84°19'E) prove that the LGP-glaciers of both the valleys must have had a connected ice level at over 5400 m asl. A more than 1000 m-thick main valley glaciation down the Phu Khola as far as Metagau is evidenced by moraines, flank abrasions and glacier polishings. Erratic material, ground moraines and abrasion forms on the flanks of the Labse- and Kangla Khola confirm an Ice Age ice infilling up to c. 4800 m asl in the confluence area of all three main valleys between Kanguru and Jong Ri (Pisang Peak). The valley head of the Kangla Khola, a truncated valley at 5350 m, shows all characteristics of a transfluence pass. Here, an ice transfluence into the Marsyandi Khola or from there into the Kangla Khola has taken place (Kuhle 1998). The gorge between Metagau and Koto was filled with ground moraine up to 300 m above the current thalweg, so that in the Late Glacial the Naur Khola-parent glacier must have flowed down on a trough-shaped ground moraine layer, the surface of which continues without any steps on that one of the Marsyandi Khola parent glacier (Kuhle, 1998) down-valley between Chame and Thonche.

SE-Tibet between Tsangpo- and Yalong River

In 1989 glaciological investigations started on Namche Bawar in the area of the Tsangpo transverse gorge; in 2000 they continued from the E, from the Dadu- up to the Yalong- and Litang River (Kuhle 1998, 2001) and ended between Namche Bawar and Litang River in 2009. They led to the following glacier reconstruction as to the LGP: in the left side valley of the Jangtsekiang from Yidun down to Yarwa ground moraines have been mapped on the slopes between c. 3000 and 3600 m. In the right side valley (Lanzang River) from Mangkam down to the Jangtsekiang at 2530 m (level of the thalweg), ground moraine and flank polishings on phyllites were mapped 300 m above the thalweg (29°43'N/98°58'E). A subglacial-glacigenic ravine in the valley ground at c. 2550 m and ground moraines on the slopes near Rongme prove an LGM-outlet glacier tongue in the Langcang valley (Mekong) down to at least 2000 m. The corresponding ELA was recorded by cirque bottoms facing S at 3500 m (29°34'N/98°18'E), i.e. below the heights of the Tibetan plateau. In this cross profile the huge, deeply incised western parallel valley with the Saluen River (Nu Jiang) at 2600 m shows enormous deposits of ground moraine up to over 1000 m up the valley slopes (30°03'N/97°22'E), so that a former outlet glacier terminus must have existed up to at least 2000 m. The watersheds between these valleys were locally glaciated with their catchment area being the Tibetan plateau that wascovered by ice above 3500 m (Kuhle 1998). N of Namche Bawar ground moraines are situated down to at least 2000 m (30°01'30"N/ 95°04'E) showing a connected ice-stream network for the steeply cut marginal mountains. These new field findings and laboratory results provide further evidence as to the existence of the Tibetan inland ice (Tibetan Ice Sheet) and its outlet glaciers during MIS 3-2 in places down to 1000 m asl.

Calibration of TCN-data

Quaternary-geological and glaciological (ELA-calculations) assessment of CN (TCN)-data and their control by ^{14}C-datings on the S-margin of Tibet (Khumbu) showed that the CN (TCN)-datings carried out at a height of more than 4000 m are overestimated by a factor of 6.5, so that moraines formerly classified as belonging to the LGM are of neoglacial origin.

References

Hewitt, K., 2009, Catastrophic rock slope failures and late Quaternary developments in the Nanga Parbat – Haramosh Massif, Upper Indus basin, northern Pakistan, Quaternary Science Reviews, doi: 10.1016/j.quascirev.2008.12019.

Kuhle, M., 1998, Reconstruction of the 2.4 Million km² Late Pleistocene Ice Sheet on the Tibetan Plateau and its Impact on the Global Climate, Quaternary International 45/46, 71-108 (Erratum: Vol. 47/48:173-182 (1998) included).

Kuhle, M., 2001, The maximum ice age (LGM) glaciation of the Central- and South Karakorum: an investigation of the heights of its glacier levels and ice thicknesses as well as lowest prehistoric ice margin positions in the Hindukush, Himalaya and in East-Tibet on the Minya Konka-massif, GeoJournal 54 (2–4), 55 (1), Tibet & High Asia (VI): Boston/London, 109–396.

Kuhle, M. and Kuhle, S., 2010, Review on Dating Methods: Numerical Dating in the Quaternary Geology of High Asia, Journal of Mountain Science, 7, 1-18, Science Press, Beijing, Springer, in press.

Cite as: Kuhle, M., 2010, New Indicators of a Former Tibetan Ice Sheet and an Ice Stream Network in the Surrounding Mountain Systems: New Field Observations and Dating on the SE-, S- and W-margin of Tibet from Expeditions in 2004-2009, *in* Leech, M.L., and others, eds., Proceedings for the 25th Himalaya-Karakoram-Tibet Workshop: U.S. Geological Survey, Open-File Report 2010-1099, 2 p. [http://pubs.usgs.gov/of/2010/1099/kuhle/].

Timing of Metamorphism and Extension in the Western Himalaya: Leo Pargil Dome, NW India

Jackie Langille[1], Micah Jessup[1], John Cottle[2], Graham Lederer[2], Talat Ahmad[3]

[1]University of Tennessee, Knoxville, TN 37996, U.S.A., jlangill@utk.edu
[2]University of California, Santa Barbara, CA 93106, U.S.A.
[3]University of Delhi, Delhi -110007, India

Background

The Himalayan orogen is the product of significant crustal shortening and thickening that has occurred since the Eocene and has resulted in generally east-west trending major fault systems, such as the Main Central thrust zone and South Tibetan detachment system that accommodated displacement since the Eocene (e.g. Searle and others, 2003; Cottle and others, 2007). In contrast to these older structures, the Leo Pargil dome, NW India, is a 30-km-wide, northeast-southwest trending antiformal structure bound by normal faults (Thiede and others, 2006) that are interpreted to record the onset of orogen-parallel extension in this region.

The Leo Pargil dome is composed of amphibolite facies rocks intruded by multiple generations of deformed and undeformed leucogranite dikes and sills. In the deepest structural positions, the injection complex transitions into migmatitic gneiss. The northwest-dipping, ~300-m-thick Leo Pargil shear zone bounds the western limb of the dome and records top-to-the-northwest normal-sense shear and separates the footwall rocks on the western side of the dome from the low-grade Tethyan Sedimentary sequence (Thiede and others, 2006) and Upper Hiamanta sequence in the hanging wall.

Metamorphism

New pressure-temperature data from the Leo Pargil shear zone and the hanging wall were calculated using THERMOCALC. These data suggest that Barrovian-style metamorphism occurred at ~640 ºC and 0.7 GPa in the staurolite-grade Upper Hiamanta sequence in the hanging wall of the Leo Pargil shear zone. Syn-kinematic staurolite growth during top-to-the-northwest shear on the Leo Pargil shear zone occurred at ~590 ºC and 0.8 GPa. This data suggests that the rocks exposed within the Leo Pargil shear zone were exhumed from mid-crustal levels by significant displacement on the shear zone during orogen-parallel extension.

Geochronology

In situ U-Th-Pb dating of monazite from hanging wall rocks suggest that Barrovian-style metamorphism occurred during the late Eocene to early Oligocene, similar to other studies of the Upper Hiamanta group in the Sutlej valley (Chambers and others, 2008). Staurolite growth during top-to-the-northwest shear on the Leo Pargil shear zone occurred during the late Oligocene. This was followed by injection of multiple generations of leucogranite in the footwall during the early Miocene (Lederer and others, 2010). These data provide new constraints on the transition from crustal thickening to melting and extensional exhumation in the NW Himalaya.

References

Chambers, J.A., and others, 2008, Empirical constraints on extrusion mechanisms from the upper margin of an exhumed high-grade metamorphic core, Sutlej valley, NW India, Tectonophysics, 477, 77–92.

Cottle, J.M., and others, 2007, Structural insights into the early stages of exhumation along an orogen-scale detachment: the South Tibetan Detachment system, Dzakaa Chu section, eastern Himalaya, Journal of Structural Geology, 29, 1781−1797.

Lederer, G., Cottle, J., Jessup, M., Langille, J., Ahmad, T., 2010, Petrochronologic constraints on partial melting in the Leo Pargil Dome, NW India, Geochimica et Cosmochimica Acta, Annual Goldschmidt conference, Knoxville, TN.

Searle, M.P., Simpson, R.L., Law, R.D., Parrish, R.R., and Waters, D.J., 2003, The structural geometry, metamorphic and magmatic evolution of the Everest massif, High Himalaya of Nepal-South Tibet, Journal of the Geological Society, London, 160, 345–366.

Thiede, R.C., and others, M., 2006, Dome formation and extension in the Tethyan Himalaya, Leo Pargil, northwest India, Geol. Soc. Am. Bull., 118, 635−650.

Cite as: Langille, J., Jessup, M., Cottle, J., Lederer, G. and Ahmad, T., 2010, Timing of metamorphism and extension in the western Himalaya: Leo Pargil dome, NW India, *in* Leech, M.L., and others, eds., Proceedings for the 25th Himalaya-Karakoram-Tibet Workshop: U.S. Geological Survey, Open-File Report 2010-1099, 2 p., [http://pubs.usgs.gov/of/2010/1099/langille/].

Deformation Temperatures and Flow Vorticities Near the Base of the Greater Himalayan Crystalline Sequence, Sutlej Valley and Shimla Klippe, NW India

Richard D. Law[1], Donald W. Stahr III[1], Talat Ahmad[2], Santosh Kumar[2]

[1] Department of Geosciences, Virginia Tech., Blacksburg, VA 24061, U.S.A., rdlaw@vt.edu
[2] Department of Geology, University of Delhi, Delhi 110007, India

We report new flow-vorticity and deformation-temperature data from near the base of the Greater Himalayan Series (GHS) exposed in the Sutlej River section and Shimla klippe of NW India (Figure 1), focusing on variation in these parameters traced from foreland to hinterland positions.

The Sutlej River section trends approximately WSW-ENE and in map view extends for approximately 100 km between the westernmost map position of the Main Central thrust (MCT) and the Sangla Detachment (a strand of the South Tibetan Detachment System). The section is oriented oblique to the pervasive NNE-SSW to NE-SW trending mineral stretching lineation in the GHS, assumed to indicate transport direction, and, traced from WSW to ENE, more hinterland structural positions are progressively exposed. However, regional scale NW-SE trending folding and subsequent erosion has resulted in formation of a structural window in the center of the Sutlej River section with low-grade Lesser Himalayan Sedimentary Series rocks and higher-grade Lesser Himalayan Crystalline Sequence rocks being exposed beneath the antiformally folded MCT (Figure 1). This allows us to examine exposures of the GHS that are at similar structural distances above the mapped position of the MCT, but in progressively more hinterland positions traced from WSW to ENE. Additionally, the Shimla klippe, located to the SW of the Sutlej River section, allows us to examine outcrops of the GHS that occupy a more foreland position than those exposed along the Sutlej.

At the western end of the Sutlej River section exposures of mylonitic granite and quartzite located at structural distances of 350-900 m above the MCT were described by Grasemann and others (1999) in the first quantitative study of flow vorticities reported from the Himalaya. This study, which employed the

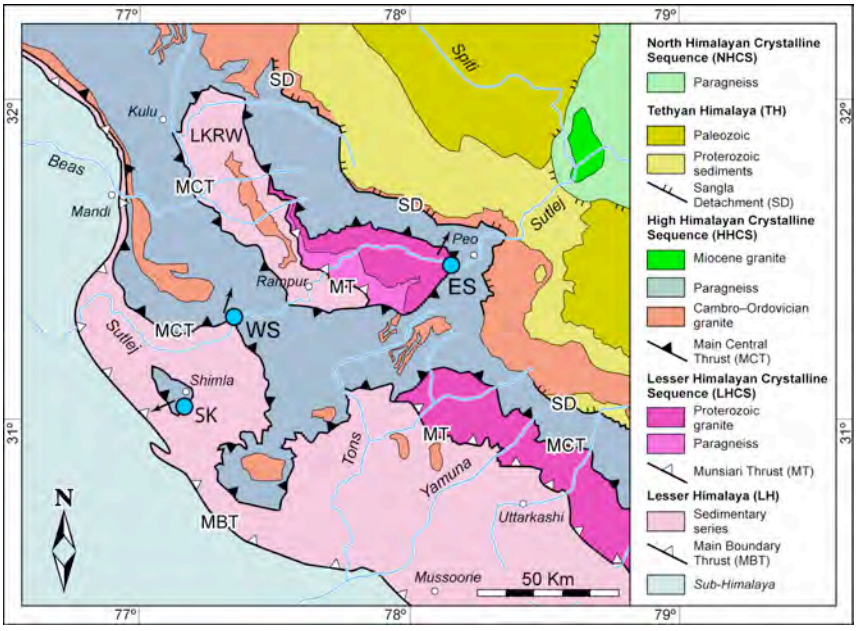

Figure 1. Geologic map of the structural units in the Sutlej River area; circles indicate the three areas referred to in text: WS – western Sutlej section, ES – eastern Sutlej section, SK – Shimla klippe. Average trend of mineral stretching lineation for the three localities indicated by arrows. LKRW – Larji-Kullu-Rampur Window. Modified from Wiesmayr and Grasemann (2002).

Rxz strain ratio / quartz c-axis method of Wallis (1992), indicated that penetrative deformation close to the base of the GHS involved a general shear (combined pure and simple shear, where pure shear has mean kinematic vorticity number Wm = 0 and simple shear has Wm = 1). However, due to uncertainty in

the strain values employed, only semi-quantitative estimates of flow vorticity could be made. We have re-examined some of these exposures using the rigid grain and oblique grain shape / quartz c-axis fabric methods of Wallis (1992). Our rigid-grain data indicate flow vorticities in the Wm = 0.73–0.81 range (47-40% pure shear; 53-60% simple shear component), confirming the basic conclusion of a general shear reached by Grasemann and others (1999) in their pioneering study. Our oblique grain shape / quartz c-axis fabric data indicate higher Wm values and hence higher simple-shear components. The data from the western Sutlej section indicate higher simple-shear components than generally recorded close to the base of the GHS in the Everest and Annapurna regions of eastern-central Nepal (Jessup and others, 2006; Larson and others, 2009), but are similar to Wm estimates recorded by Carosi and others (2007) from western Nepal.

Deformation temperatures of the mylonitic granite and quartzite located close to the underlying MCT at the western end of the Sutlej section are estimated at c. 525 °C based on the quartz c-axis fabric opening angle thermometer of Kruhl (1998) and Law and others (2004). These temperature estimates are in good agreement with the observed quartz recrystallization regime (limited grain-boundary migration) in these tectonites. However, both crystallographic fabrics (this study, and Grasemann and others, 1999) and recrystallization microstructures indicate that deformation temperatures increase structurally upwards, reflecting the inversion of metamorphic isograds at the base of the GHS.

Close to the base of the GHS preserved in the Shimla klippe (Figure 1), which occupies a more foreland position than the exposures at the western end of the Sutlej section, quartz fabrics and recrystallization mechanisms (subgrain rotation with minor grain boundary migration) indicate lower deformation temperatures than those recorded in the western Sutlej mylonites. In contrast, plastically deformed and recrystallized quartz-rich tectonites located immediately (< 300 m) above the mapped position of the MCT in the eastern part of the Sutlej River section, and occupying a more hinterland position than the western Sutlej exposures, record the highest deformation temperatures. Deformation temperatures of c. 625 °C are indicated by quartz c-axis fabric opening angles and this is confirmed by microstructural evidence for widespread grain-boundary migration recrystallization. Identical temperatures are estimated by phase-equilibria methods in these tectonites, indicating that penetrative deformation occurred at close to peak temperature and that the high-temperature fabrics have not been pervasively overprinted by later lower-temperature events associated with exhumation. Microstructures needed for quantitative vorticity analysis do not develop, however, at such elevated deformation temperatures.

The tectonic implications of these vorticity and thermal data for internal flow and extrusion/exhumation of the GHS will be discussed.

References

Carosi, R., Montomoli, C. and Visona, D., 2007, A structural transect in the Lower Dolpo: Insights on the tectonic evolution of Western Nepal, Journal of Asian Earth Sciences, 29, 407-423.

Grasemann, B., Fritz, H. and Vannay, J-C., 1999, Quantitative kinematic flow analysis from the Main Central Thrust zone, (NW Himalaya): implications for a decelerating strain path and the extrusion of orogenic wedges, J. Struct. Geol., 21, 837-53.

Jessup, M., Law, R.D., Searle, M.P. and Hubbard, M., 2006, Structural evolution and vorticity of flow during extrusion and exhumation of the Greater Himalayan Slab, Mount Everest Massif, Tibet/Nepal: implications for orogen-scale flow partitioning, in: Law, R.D., Searle, M.P and Godin, L. (eds) *Channel Flow, Ductile Extrusion and Exhumation in Continental Collision Zones*, Geological Society of London Special Publication, 268, 379-413.

Krul, J.H., 1998, Reply: Prism- and basal-plane parallel subgrain boundaries in quartz: a microstructural geothermobarometer, Journal of Metamorphic Geology, 16, 142-146.

Larson, K.P. and Godin, L., 2009, Kinematics of the Greater Himalayan Sequence, Dhaulagiri Himal: implications for the structural framework of eastern Nepal, Journal of the Geological Society, London, 166, 25-43.

Law, R.D., Searle, M.P. and Simpson, R.L., 2004, Strain, deformation temperatures and vorticity of flow at the top of the Greater Himalayan Slab, Everest Massif, Tibet, Journal of the Geological Society, London 161, 305-320.

Wallis, S., 1992, Vorticity analysis in a metachert from the Sanbagawa Belt, SW Japan, J. Struct. Geol., 14, 271-280.

Wiesmayr, G. and Grasemann, B., 2002, Eohimalayan fold and thrust belt: Implications for the geodynamic evolution of the NW-Himalaya (India), Tectonics, 21(6), 1058, doi:10.1029/2002TC001363.

Cite as: Law, R.D., Stahr III, D.W., Ahmad, T. and Kumar, S., 2010, Deformation Temperatures and Flow Vorticities Near the Base of the Greater Himalayan Crystalline Sequence, Sutlej Valley and Shimla Klippe, NW India, *in* Leech, M.L., and others., eds., Proceedings for the 25th Himalaya-Karakoram-Tibet Workshop: U.S. Geological Survey, Open-File Report 2010-1099, 2 p. [http://pubs.usgs.gov/of/2010/1099/law/].

Lithospheric Structure and Dynamics of Tibet: Constraints from Shear-Velocity Distribution

Sergei Lebedev[1], Matthew R. Agius[1]

[1] Geophysics Section, Dublin Institute for Advanced Studies, Dublin 2, Ireland, sergei@cp.dias.ie

Seismic-velocity structure of the crust and underlying upper mantle of Tibet reflects the physical state of the rock at depth and can offer essential constraints on the dynamics and evolution of the plateau. Data from a number of broad-band seismic experiments conducted in recent years, together with data from permanent stations in the region, produce dense coverage of the plateau and its surroundings. In spite of the intensive seismic study, however, even the basic elements of the lithospheric structure of Tibet are still disputed. The mid-crustal low-viscosity layer is thought to play a key role in the dynamics of the plateau (e.g., Royden and others, 2008), but both its lateral extent and its depth range in different parts of the plateau still need to be mapped in detail. Thick, cold mantle lithosphere is present beneath the Himalaya and southern Tibet but not in northern Tibet, according to a number of recent studies. The nature of the lithosphere, however, in particular in the north, has been debated.

We study seismic-velocity structure of Tibet using primarily surface waves and combine two main approaches: regional-scale multimode tomography (Lebedev and others, 2006, Lebedev and van der Hilst, 2008) and broadband inter-station analysis (Meier and others, 2004, Lebedev and others, 2005, Lebedev and others, 2009). We detect strong north-south variations in the seismic-velocity (and, by inference, thermal) structure of the lithosphere. Whereas the south-southwestern part of the plateau is underlain by thick, seismically fast, craton-like mantle lithosphere, the central-northern part, in contrast, displays *S* velocities that are close to the global continental mean, when averaged over the depth range from the Moho to ~200 km.

The north-south contrast in the lithospheric wavespeeds is a clear first-order feature, and can be seen in published tomographic models (e.g., Friederich, 2003, Priestley and others, 2006, Li and others, 2008). The finer seismic-velocity layering within the top 100-200 km of the mantle is more difficult to resolve, however. A series of targeted test inversions of our broadband phase-velocity curves shows that surface-wave dispersion data can be fit equally well with substantially different shear-velocity profiles. In particular, the models with a thin high-velocity lid (and a moderate low-velocity zone beneath it) and the models with a low-velocity layer just below the Moho (and an increase in shear velocity beneath it) can fit surface-wave data equally well. By combining the surface-wave data with additional constraints on the Moho depth and on the uppermost-mantle seismic velocities from receiver functions and *S*n mapping, respectively (e.g., Pei and others, 2007; Tseng and others, 2009), we are able to resolve the ambiguity, at least in some locations. For example, in the central Qiangtang Block in west-central Tibet (north of the Banggong-Nujiang suture in the Hi-Climb experiment area), the joint seismic data set can be matched significantly better with models with thin (<100 km) seismic lithosphere underlain by a low-velocity asthenosphere, compared to models without a low-velocity zone at 100-150 km. Our analysis can reconcile published tomographic models and other seismic evidence. It suggests that the lithosphere is, indeed, substantially thinner in the middle than it is in the south of Tibet.

Regional tomography and broadband dispersion data also agree regarding the presence of a mid-crustal low-velocity layer across the plateau. We show that the layer, with isotropic-average shear speeds in the range of 3.2-3.5 km/s between 20 and 45 km depths, is present both in the South and in the North of Tibet. Our results have important implications relating to the geodynamic evolution of the Tibetan Plateau.

References

Friederich, W., 2003, The S-velocity structure of the East Asian mantle from inversion of shear and surface waveforms, Geophys. J. Int., 153, 88-102.

Lebedev, S., Boonen, J. and Trampert, J., 2009, Seismic structure of Precambrian lithosphere: New constraints from broadband surface-wave dispersion, Lithos Special Issue, 109, 96-111.

Lebedev, S., Meier, T. and van der Hilst, R.D., 2006, Asthenospheric flow and origin of volcanism in the Baikal Rift area, Earth Planet. Sci. Lett., 249, 415–424.

Lebedev, S., Nolet, G., Meier, T. and van der Hilst, R.D., 2005, Automated multimode inversion of surface and S waveforms, Geophys. J. Int., 162, 951-964.

Lebedev, S. and van der Hilst, R.D., 2008, Global upper-mantle tomography with the automated multimode inversion of surface and S-wave forms, Geophys. J. Int., 173, 505–518.

Li, C., van der Hilst, R.D., Meltzer, A.S. and Engdahl, E.R., 2008, Subduction of the Indian lithosphere beneath the Tibetan Plateau and Burma, Earth Planet. Sci. Lett., 274, 157-168.

Meier, T., Dietrich, K., Stöckhert, B. and Harjes, H.P., 2004, One-dimensional model of shear wave velocity for the eastern Mediterranean obtained from the inversion of Rayleigh wave phase velocities and tectonic implications, Geophys. J. Int., 156, 45-58.

Pei, S., and others, 2007, Upper mantle seismic velocities and anisotropy in China determined through Pn and Sn tomography, J. Geophys. Res., 112, B05312.

Priestley, K., Debayle. E., McKenzie, D. and Pilidou, S., 2006, Upper mantle structure of eastern Asia from multimode surface waveform tomography, J. Geophys. Res., 111, B10304, doi:10.1029/2005JB004082.

Royden, L. H., Burchfiel, B. C. and van der Hilst, R. D., 2008, The Geological Evolution of the Tibetan Plateau. Science, 321, 1054-1058.

Tseng, T.L., Chen, W.P. and Nowack, R.L., 2009, Northward thinning of Tibetan crust revealed by virtual seismic profiles, Geophys. Res. Lett., 36, L24304.

Cite as: Lebedev, S. and Agius, M.R., 2010, Lithospheric structure and dynamics of Tibet: Constraints from shear-velocity distributions, *in* Leech, M.L., and others, eds., Proceedings for the 25th Himalaya-Karakoram-Tibet Workshop: U.S. Geological Survey, Open-File Report 2010-1099, 2 p. [http://pubs.usgs.gov/of/2010/1099/lebedev/].

Time-scales of Crustal Melting within the Leo Pargil Dome, NW India

Graham Lederer[1], John Cottle[1], Micah Jessup[2], Jackie Langille[2], Talat Ahmad[3]

[1] Department of Earth Science, University of California, Santa Barbara, CA 93106, U.S.A., grahamlederer@umail.ucsb.edu
[2] Department of Earth and Planetary Sciences, University of Tennessee, Knoxville, TN 37996, U.S.A.
[3] Department of Geology, University of Delhi, Delhi - 110007, India

Dome complexes within the Himalayan orogen are dominantly composed of amphibolite-facies metapelites intruded by dikes and sills of leucogranite resulting from mobilization and amalgamation of batches of in-situ partial melt. These exposures provide an exceptional opportunity to study the time-scales of melt generation in the mid-crust and the mechanisms of melt transport and emplacement within a well-defined structural framework. Knowledge of the dynamics of crustal-melting and the inter-relationships between metamorphism, melting, and exhumation play a key role in evaluating competing models of dome formation within the Himalaya, and potentially have important implications for understanding the rheologic evolution of the mid-crust during collision.

Located in the northwestern Himalaya, the northeast-striking Leo Pargil dome (LPD) consists of a high-grade metamorphic and anatectic core surrounded by low-grade Tibetan metasedimentary rocks. Exhumation of the LPD has previously been ascribed to extensional unroofing processes controlled by a large-scale detachment fault system, the Leo Pargil shear zone (LPSZ) (Thiede and others, 2006). Normal-sense displacement on this structure has resulted in juxtaposition of kyanite-bearing gneiss in the footwall beneath lower-grade rocks in the hanging wall.

Leucogranitic dikes and sills pervasively intrude the footwall of the LPSZ and, while less abundant, are also present in the hanging wall of the LPSZ. Individual intrusions are relatively small in volume and extent, ranging from 5 cm to 2 m wide by 20 cm to >100 m long, and form a complex network of cross-cutting bodies distinguishable by differences in mineralogy and chemistry. Solid-state fabric development in the leucogranites varies from moderately and weakly foliated to isotropic, indicating both syn- and post-kinematic emplacement with respect to the dominant tectonic fabric in the host gneisses. Deformed and undeformed leucogranites found within the LPSZ provide minimum age constraints for movement along the LPSZ.

U-Th-Pb monazite ages from the leucogranites range from ~26-16 Ma, with individual samples exhibiting discrete age populations consistent with cross-cutting relationships. The majority of individual melt batches appear to be relatively short-lived, forming on the sub million-year time-scale. Field relationships and detailed geochronology suggest that, in contrast to other domes (e.g. Cottle and others, 2009), melting within the LPD occurred over a protracted period (>10 Ma). Melt production and mobilization into dikes and sills likely resulted from semi-continuous production of melt by in-situ partial melting of the metamorphic host rock at different structural positions immediately prior to, and/or during, exhumation of the LPD. Transects examined thus far indicate strong evidence of a temporal link between magmatic events and exhumation of the dome. Further geochronologic work currently underway will attempt to document the scale of along-strike temporal variability in leucogranite formation with the goal of developing a 4-D model for melt generation within the LPD.

References

Cottle, J. M., and others, 2009, Geochronology of granulitized eclogite from the Ama Drime Massif: Implications for the tectonic evolution of the South Tibetan Himalaya, Tectonics, 28, TC1002.

Thiede, R.C., and others, 2006, Dome formation and extension in the Tethyan Himalaya, Leo Pargil, northwest India, Geol. Soc. Am. Bull., 118, 635−650.

Cite as: Lederer, G., Cottle, J., Jessup, M., Langille, J. and Ahmad, T., 2010, Timing and duration of anatexis within the Leo Pargil Dome, NW India, *in* Leech, M.L., and others, eds., Proceedings for the 25th Himalaya-Karakoram-Tibet Workshop: U.S. Geological Survey, Open-File Report 2010-1099, 1 p. [http://pubs.usgs.gov/of/2010/1099/lederer/].

Evolution of Crustal and Upper-Mantle Structure in Northern Tibet from INDEPTH Magnetotelluric Data

Florian Le Pape[1], Alan G. Jones[1], Jan Vozar[1], Martyn J. Unsworth[2], Wei Wenbo[3], the INDEPTH MT Team

[1] Dublin Institute for Advanced Studies, Dublin, Ireland, flepape@cp.dias.ie
[2] Department of Physics, University of Alberta, Edmonton, AB, T6G 2J1, Canada
[3] China University of Geosciences Bejing, Beijing, 100083, China

The overall goal of the INDEPTH (International Deep Profiling of Tibet and Himalaya) Phase IV is to develop a better understanding of the structure and evolution of the northern margins of the Tibetan plateau. During Phase III in 1999, broadband and long-period magnetotelluric data were collected in Northern Tibet across the Kunlun Shan. The MT stations, placed along the northern part of the Lhasa to Golmud highway, defined the so-called 600-line profile extending from the middle of the Qiangtang Terrane to the southern edge of the Qaidam Basin. Previous inversions of the data from the 600-line used the MT TE-mode, TM-mode and vertical magnetic field data to derive minimally smooth models (Unsworth and others, 2004). The final model obtained is characterized by a uniform mid-crustal conductor extending from the Kunlun Shan to the south end of the 600 profile and ending abruptly at the Kunlun Fault. The high conductivity of the middle lower crust south of the Kunlun Shan was previously identified as due to partial melting.

As part of Phase IV, seismic data crossing again the Kunlun Shan are being acquired east of the 600 line. In Spring 2010 the long-period MT (LMT) acquisition of INDEPTH Phase IV will commence, including a profile east of the 600 line to complement the seismic data. In anticipation of the upcoming survey, the existing MT 600-line data were re-analysed and re-modelled. As found previously, south of the Kunlun Shan the middle and lower crust are conductive, and north of the Kunlun fault the crust and the upper mantle are resistive. However, the new models are geometrically more complex, exhibiting greater lateral variability. Although in general the dominant features are the same as the prior models, in detail, spatial correlation with surface thrusting implies structural and/or lithological control on the enhanced conductivity. This particular behaviour of the crust may be linked to the thrusting history of the north part of the plateau and the high thickness of the crust leading to particular conditions of pressure and temperature.

The Kunlun Fault can be characterized as a rheological boundary in the middle and lower crust of northern Tibet, between a crust weakened by partial melting and a more stable (dry, cold) crust north of the fault. The lateral resistivity changes along the profile are representative of changing conditions, such as lithology, temperature, water content variability or dehydration processes affecting the crustal rheology.

Reference

Unsworth, M., and others, 2004, Crustal and upper mantle structure of northern Tibet imaged with magnetotelluric exploration, J. Geophys. Res., 109, B02403-1 - B02403-18, doi: 10.1029/2002JB002305.

Cite as: Le Pape, F., Jones, A.G., Vozar, J., Unsworth, M.J., Wei W., and the INDEPTH MT Team, 2010, Evolution of Crustal and Upper-Mantle Structure in Northern Tibet from INDEPTH Magnetotelluric Data, *in* Leech, M.L., and others, eds., Proceedings for the 25th Himalaya-Karakoram-Tibet Workshop: U.S. Geological Survey, Open-File Report 2010-1099, 1 p. [http://pubs.usgs.gov/of/2010/1099/lepape/].

Crustal Shortening in the Tanggula-Tuotuohe Area, Northern Tibet

Yalin Li[1], Chengshan Wang[1], Ganqing Xu[2], Xixi Zhao[3], Chao Ma[1]

[1] Research Center for Tibetan Plateau Geology, China University of Geosciences, Beijing, 100083, China, liyalin@cugb.edu.cn
[2] Department of Earth and Ocean Science, University of Waikato, Hamilton, New Zealand
[3] Institute of Geophysics and Planetary Physics, University of California, Santa Cruz, CA 95064, U.S.A.

Indo-Asian collision and intracontinental deformation resulted in large crustal shortening and uplift of the Tibetan Plateau, and much attention has been paid to determine the deformation, crustal shortening, and the uplift of the plateau（Patriat and others, 1984; Besse and others, 1984; Dewey and others, 1989; Harrison and others, 1992; Ratschbacher and others, 1994; Wang and others, 2002, 2008; Molnar and Tapponnier, 1975; Tapponnier and Molnar 1977; DeCelles and others, 1998, 2002). Previous research has indicated that the Tanggula-Tuotuohe area has undergone intensive deformation during the Cenozoic (Leeder and others, 1988; Yin and Harrison, 2000; Wang and others, 2002), and that the Tuotuohe basin was formed as a result of the Early Tertiary Tanggula thrust system (Li and others, 2006). However, compared to the Himalayas and other areas, the Cenozoic evolution and upper-crustal shortening in this area is almost unknown.

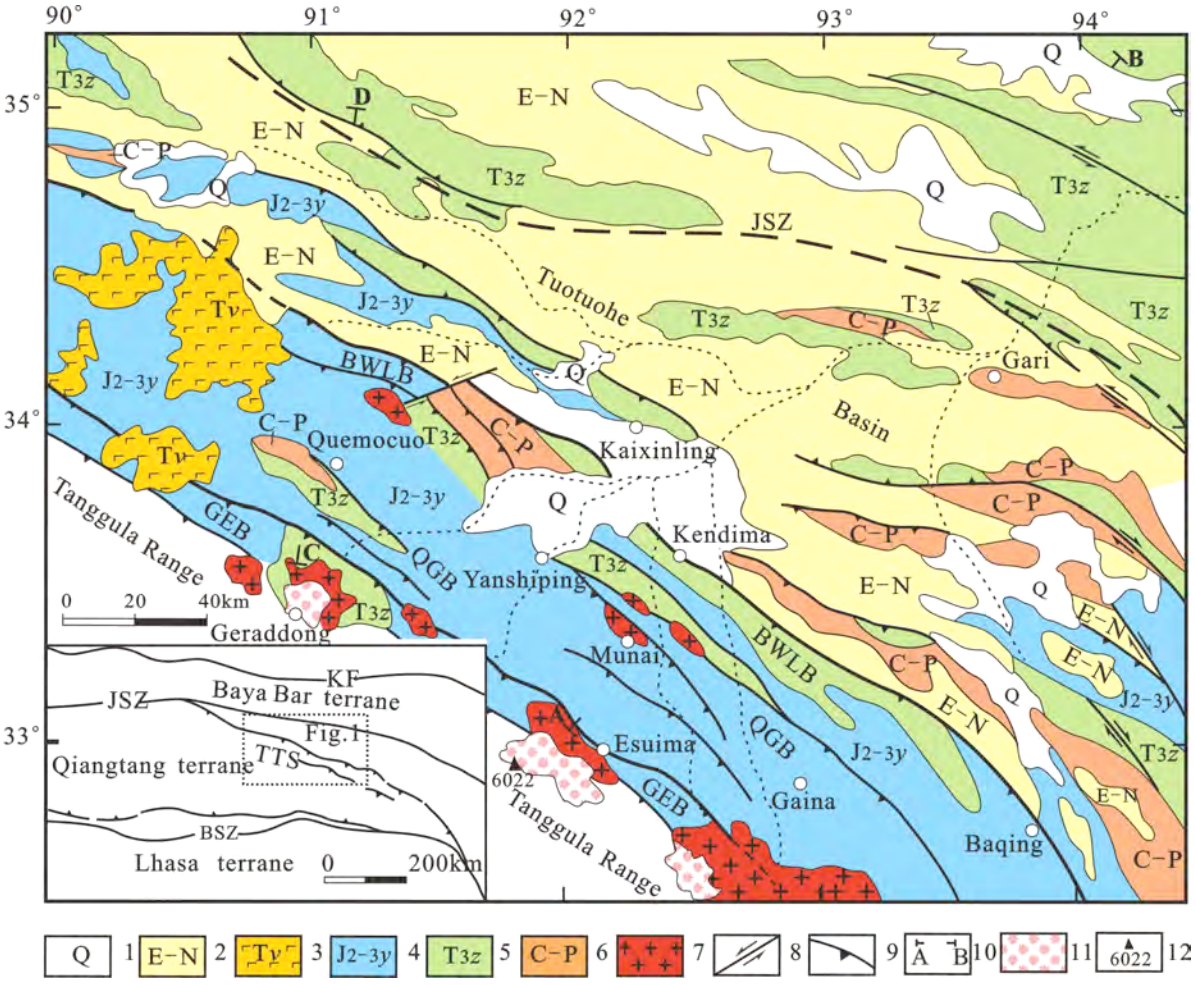

Figure 1. Simplified geological map of Tanggula Mountain and the Tuotuohe area. 1. Quaternary alluvial deposits; 2. Eocene-Miocene deposits; 3. Cenozoic volcanic rocks; 4. Middle-Upper Jurassic Yanshiping group; 5. Late Triassic Jieza Group; 6. Carboniferous-Permian strata; 7. Cenozoic granite; 8. strike-slip fault; 9. thrust; 10. location of balanced cross-section; 12. Glacier or year round snow; 13. mountain peak and elevation; JSZ: Jinshajiang Suture; BWLB-Baqing-Wulwl Lake thrust belt；QGB-Quemocuo-Gaina fold-thrust belt; GEB -Geraddong-Esuima thrust belt.

Our investigation shows that the Tanggula thrust system, south to Geladandong-Esuima area and north to the Wulwl Lake-Kendima-Baqing area, runs parallel to the Tanggula Range. In the study area the Tanggula thrust system extends more than 320 km to the northwest with a width of 60-80 km (Figure 1). On the basis of the balanced cross-section laws, two routes were chosen for reconstructing balanced sections (AB and CD). Based on the restoration of balanced cross-sections, we calculated crustal-shortening ratios using line-length balancing techniques. The results show that: 1/ the Jurassic strata in two sections are presently 55.6 km and 72.2km long, while the original lengths were 156 km and 147 km respectively, indicating that the shortening is 100.4 km and 74.8 km and the shortening ratios are 64.4% and 50.9%; 2/ the Tertiary strata in Tuotuohe basin are currently 128 km and 76.4 km long in the two sections. Compared to the original lengths of the Tertiary strata, this suggests that the shortening is 114.4 km and 54.6 km and the shortening ratios are 47.2% and 41.7%. Consequently, the crustal shortening in the Tanggula-Tuotuohe area is 214.8 km and 132.4 km with shortening ratios of 53.9% and 47.0%.

Previous studies suggest that the Tanggula range has been uplifted and became the northern boundary of Paleo-Tibetan Plateau in the Paleogene (Wang and others, 2008, and others, 2006). Comparison of the Jurassic and Tertiary shortening in the two sections shows that the Jurassic strata have undergone only little shortening before the Tertiary, implying that the early Tertiary is the main period with intensive shortening in the study area. Our comprehensive analysis indicates that the age of the Tanggula thrust system can be confirmed as 67-23 Ma (Li and others, 2006), and that the age of the Tuotuohe and Yaxicuo Formations which is overlain by undeformed Wudaoliang Formation (Wang and others, 2002) is 52-23.8 Ma (Yi and others, 2004; Liu and others, 2005). This suggests that the main stage of crustal shortening was during the Paleocene-Oligocene in the Tanggula-Tuotuohe area.

Reference

Besse, J., Courtillou, V., Possi, J.P., Westphal, M. and Zhou, Y.X., 1984, Paleomagnetic estimates of crustal shortening in the Himalayan thrusts and Zangbo suture, Nature, 311, 621–626.

DeCelles, P.G., Robinson, D.M. and Zandt, G., 2002, Implications of shortening in the Himalayan fold-thrust belt for uplift of the Tibetan Plateau, Tectonics, 21, 1062, doi:10.1029/2001TC001322.

DeCelles, P.G., and others, 1998, Neogene foreland basin deposits, erosional unroofing, and the kinematic history of the Himalayan fold-thrust belt, western Nepal, Geol. Soc. Am. Bull., 110, 2 –21.

Dewey, J.F., Cande, S. and Pitman, W.C., 1989, Tectonic evolution of the India-Eurasia collision zone, Ecol. Geol. Helv. 82, 717–734.

Harrison, T.M., Copeland, P., Kidd, W.S.F. and Yin, A., 1992, Raising Tibet, Science, 255, 1663–1670.

Leeder, M. R., Smith, A.B. and Y. Jixiang, 1988, Sedimentology and palaeoenvironmental evolution of the 1985 Lhasa to Golmud geotraverse, Philos. Trans. R. Soc. London, Ser. A, 327, 107 – 143.

Li, Y., Wang, C., Yi, H., Liu, Z. and Li, Y., 2006, Cenozoic thrust system and uplifting of the Tanggula Mountain, Northern Tibet, Acta Geologica Sinica, 80, 1118-1130 (in Chinese with English Abstract).

Liu, Z.F., and others, 2005, Oligo-Miocene Depositional Environment of the Tuotuohe Basin, Central Tibetan Plateau, Acta Sedimentologica Sinica, 23, 210–217 (in Chinese with English Abstract).

Molnar, P. and Tapponnier, P., 1975, Cenozoic tectonics of Asia effects of a continental collision, Science, 189, 419–426.

Patriat, P. and Achache, J., 1984. India-Eurasia collision chronology has implications for crustal shortening and driving mechanism of plates, Nature, 311, 615–621.

Ratschbacher, L., Frisch, W., Liu, G. and Chen, C.C., 1994, Distributed deformation in southern and western Tibet during and after the India-Asian collision, J. Geophys. Res., 99, 19917–19945.

Tapponnier, P. and Molnar, P.J., 1977, Active faulting and tectonics of China, J. Geophys. Res., 82, 2905–2930.

Wang, C.S., Liu Z.F., Yi H.S., Zhao, X.X., and Liu, S., 2002, Tertiary crustal shortening and peneplanation in the Hoh Xil region: implications for the tectonic history of the northern Tibetan Plateau, J. Asian Earth Sci., 20, 211–223.

Wang, C.S., and others, 2008, Constraints on the early uplift history of the Tibetan Plateau. Proc. Natl. Acad. Sci., 105, 4987–4992.

Yi, H.S, and others, 2004, Magnetostratigraphic Studies of Tertiary Continental Redbeds in Wulanwula Lake Area of Northern Tibetan Plateau and Their Geologic Significance, Acta Geosicientia Sinica, 25, 633–638 (in Chinese with English Abstract).

Yin, A. and Harrison, T. M., 2000, Geologic Evolution of the Himalayan-Tibetan Orogen, Ann. Rev. Earth Planet Sci., 28, 211–280.

Cite as: Li, Y., Wang, C., Xu, G., Zhao, X., Ma, C., 2010, Crustal Shortening in the Tanggula-Tuotuohe Area, Northern Tibet, *in* Leech, M.L., and others, eds., Proceedings for the 25th Himalaya-Karakoram-Tibet Workshop: U.S. Geological Survey, Open-File Report 2010-1099, 2 p. [http://pubs.usgs.gov/of/2010/1099/li/].

Position of the Lhasa Terrane Prior to India-Asia Collision Derived from Paleomagnetic Inclinations of 53 Ma-Old Dykes of the Linzhou Basin: Constraints on the Age of Collision and Post-Collisional Shortening within the Tibetan Plateau

Ursina Liebke[1], Erwin Appel[1], Udo Neumann[1], Borja Antolin[1], Lin Ding[2], Qiang Xu[2]

[1] Institute for Applied Geosciences, University of Tuebingen, 72076 Tuebingen, Germany, ursina.liebke@uni-tuebingen.de
[2] Institute of Tibetan Plateau Research, Chinese Academy of Sciences, Beijing 100085, China

The Lhasa terrane comprises the southern Eurasian margin since at least mid-Cretaceous. Therefore paleomagnetic data from the Lhasa terrane are crucial to reconstruct the pre-collisional southern margin of Eurasia. Previous paleomagnetic data from the Cretaceous Takena Formation provide a rough constraint on the pre-collisional paleolatitudinal position of the southern Eurasian margin. However, Paleogene paleomagnetic data from the Lhasa terrane, which can provide more direct constraints, are very limited. In addition, reliability of the existing data is ambiguous because of a possible later overprint. In our new study 17 sites were drilled from mafic dykes intruded in the T1 unit of the Linzizong Formation of the Linzhou Basin near Lhasa for paleomagnetic studies (Figure 1). The dykes were Ar^{40}/Ar^{39} dated to c. 53 Ma by Yue and Ding (2006). From ten sites a higher coercivity component demagnetized between 20 and 100 mT could be isolated. Detailed rock-magnetic analyses reveal Ti-rich titanomagnetite as the remanence carrier, which suggests that the rock is not much altered and the remanent magnetization is likely of primary origin. This is supported by a positive fold test. The occurrence of normal and reverse polarity directions within single sites, the subvolcanic character of the dykes, and the within-site scatter, as well as the scatter between site mean directions, indicate that paleosecular variation is recorded within sites. Tilt correction was performed using the bedding of overlying fluvial- lacustrine sediments and tilt angles of ignimbrite columns postdating the dyke emplacement.

Bedding-corrected directions give an overall mean direction of D/I = 12.3°/27.2° (α_{95} = 10.6°, k = 21.7, N = 10) corresponding to a paleolatitude of 13.2° ± 5.8°N at a reference location on the suture zone (20°N/90°E). Comparison with previous Cretaceous data mainly from the Takena Formation yields a stable position of the Lhasa terrane during Cretaceous and Early Eocene. This indicates that no large north-south crustal shortening occurred along the southern Eurasian margin between Late Cretaceous and Early Eocene. The difference between expected paleolatitudes determined from the APWP of Eurasia and observed paleolatitudes reveals relative northward movement of the Lhasa block of ca. 1847±763 km since Early Eocene. This is attributed to indentation of India into Asia and implies a considerable amount of north-south crustal shortening. Two models of "Greater India" were used to determine the extended northern margin of India: Ali and Aitchison (2005) proposed a Greater India based on bathymetric features in the Eastern Indian Ocean and Patzelt and others (1996) determined the paleolatitude of northern India using paleomagnetic investigations on Paleocene sediments of the Zongpu Formation at Gamba and Duela. Intersection of the pre-collisional southern Eurasian margin and the northern margin of India yields a collision age of the Indian and Eurasian continents of c. 53-49 Ma. An initial collision within this time range is in accordance with previous studies based on paleomagnetic or geologic data (e.g. Patriat and Achache 1984, Klootwijk and others, 1992, Guillot and others, 2003). A significantly later collision age at the Eocene/Oligocene boundary as proposed by Aitchison and others (2007) is not in agreement with our new and previous paleomagnetic data from the Lhasa Block.

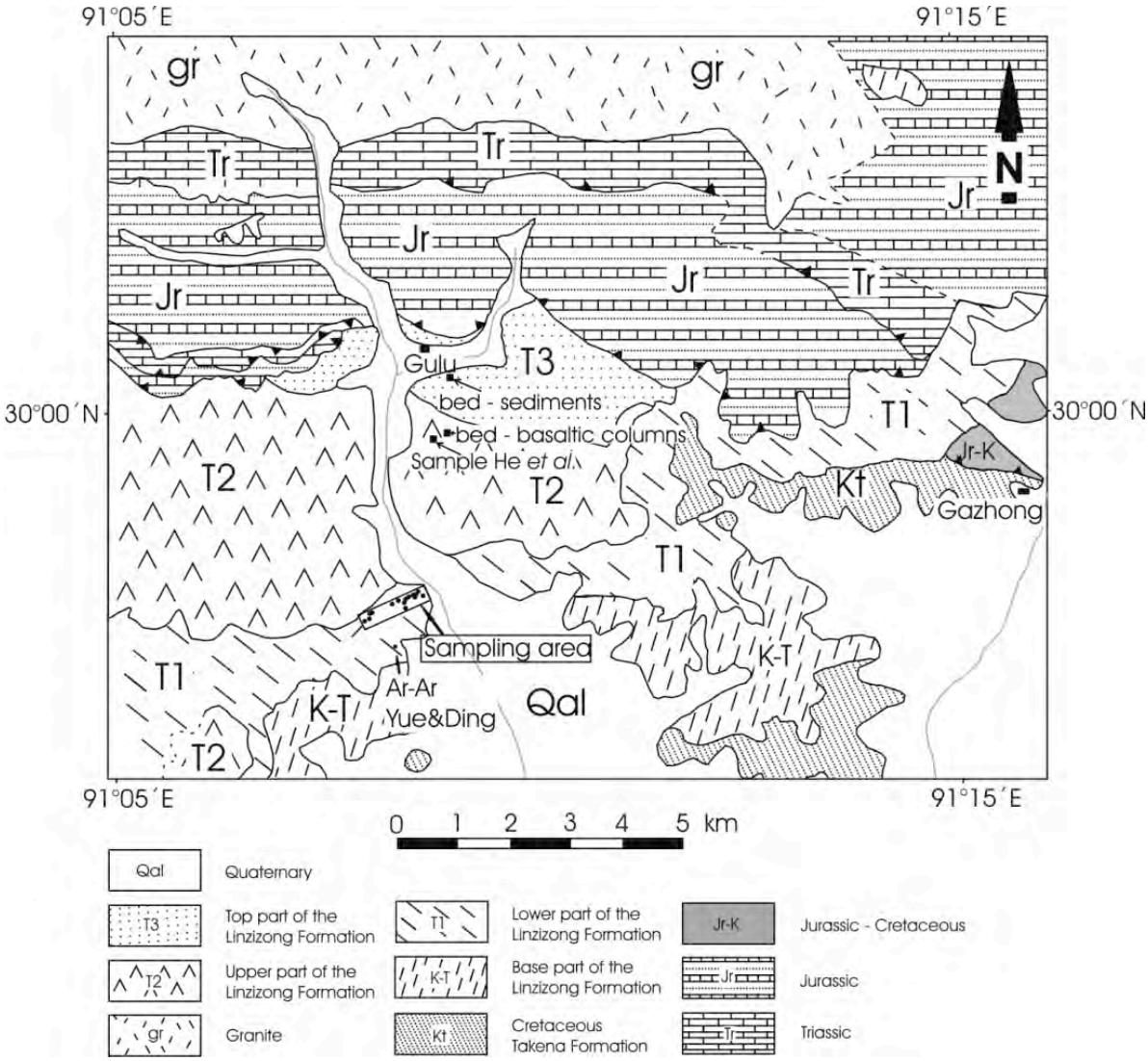

Figure 1. Geological map of the Linzhou area (modified after He and others, 2007) showing our site locations.

References

Aitchison, J. C., Ali, J. R. and Davis, A. M., 2007, When and where did India and Asia collide?, J. Geophys. Res., 112, B0523, doi: 10.1029/2006JB004706.

Ali, J. R. and Aitchison, J. C., 2005, Greater India, Earth Sci. Rev., 72, 169-188.

Guillot, S., Garzanti, E., Baratoux, D., Marquer, D., Mahéo, G. and de Sigoyer, J., 2003, Reconstructing the total shortening history of the NW Himalaya, Geochem. Geophys. Geosys., 4, doi: 10.1029/2002GC000484.

Klootwijk, C. T., Gee, J. S., Peirce, J. W., Smith, G. M. and McFadden, P. L., 1992, An early India – Asia contact: paleomagnetic constraints from Ninetyeast Ridge, ODP Leg 121, Geology, 20, 395-398.

Patriat, P. and Achache, J., 1984, India-Eurasia collision chronology has implications for crustal shortening and driving mechanism of plates, Nature, 311, 615-621.

Patzelt A., Li, H., Wang, J. and Appel E., 1996, Palaeomagnetism of Cretaceous to Tertiary sediments from southern Tibet: evidence for the extent of the northern margin of India prior to the collision with Eurasia, Tectonophysics, 259, 259-284.

Yue, Y. H. and Ding, L., 2006, $^{40}Ar/^{39}Ar$ Geochronology, geochemical characteristics and genesis of the Linzhou basic dikes, Tibet, Acta Petrologica Sinica, 22, 855-866.

Cite as: Liebke, and others, 2010, Position of the Lhasa Terrane Prior to India-Asia Collision Derived from Paleomagnetic Inclinations of 53 Ma-Old Dykes of the Linzhou Basin: Constraints on the Age of Collision and Post-Collisional Shortening within the Tibetan Plateau, in Leech, M.L., and others, eds., Proceedings for the 25th Himalaya-Karakoram-Tibet Workshop: U.S. Geological Survey, Open-File Report 2010-1099, 2 p. [http://pubs.usgs.gov/of/2010/1099/liebke/].

The Paleogene Latitude of Asia and the Proto-Tibetan Plateau

Peter C. Lippert[1], Guilluame Dupont-Nivet[2], Douwe J.J. van Hinsbergen[3], Xixi Zhao[1], Robert S. Coe[1], Paul Kapp[4]

[1] Department of Earth & Planetary Sciences, University of California, Santa Cruz, CA 95064, U.S.A., plippert@pmc.ucsc.edu
[2] Paleomagnetic Laboratory "Fort Hoofddijk", Utrecht University, Budapestlaan 17, 3584 CD Utrecht, The Netherlands
[3] Physics of Geological Processes, University of Oslo, Sem Sælands vei 24, NO-0316 Oslo, Norway
[4] Department of Geosciences, University of Arizona, Tucson, AZ 85721, U.S.A.

The Himalayan-Tibetan orogen is one of the most distinctive topographic features on Earth, yet just how it is the product of intracontinental deformation caused by the India-Asia collision remains poorly understood. Importantly, how, where, and when the >1500 km of post-Early Eocene convergence between India and Asia is distributed throughout the orogen is crucial for determining the processes responsible for the remarkably high elevation, low relief, and thick crust of the Tibetan plateau. Most tectonic models for the surface uplift of the Tibetan plateau assume that crustal thickening began after the onset of India-Asia collision. Therefore, the age of collision between Indian and Asian crustal units, as well as the latitude of Asian crustal units throughout the Cenozoic, provide fundamental first-order constraints on tectonic development of the Tibetan Plateau.

The age at which collision began is currently debated, however. Here collision is defined as when Asian or ophiolitic detritus first appears in Tethyan Himalayan sediments, by the last marine deposition in the Himalaya, and when the paleolatitude of Greater India and Southern Tibet are statistically indistinguishable from each other. Paleogeographic reconstructions based on plate velocities determined from marine magnetic anomalies and geologic data are consistent with the interpretation that the leading edge of the Indian subcontinent (i.e., Greater India and the Tethyan Himalaya) collided with the southern margin of Asia at approximately 55±10 Ma. Previous paleomagnetic-based reconstructions, however, have led to estimated collision ages that range from 70 to 30 Ma. The large disparity between paleomagnetic-based collision ages is due largely to the poor quality or large uncertainty of existing paleomagnetic data from Asia, which typically are not corrected for sedimentary inclination shallowing, are poorly dated, and, in the case of volcanic rocks, do not sufficiently characterize the time-averaged behavior of the geomagnetic field (secular variation). Thus, the paleolatitude of Asian crustal units, from Southern Tibet to Central Asia, is poorly defined.

Here we present paleomagnetic data from well-dated Paleogene volcanic rocks from Southern Tibet, Central Tibet, and southern Mongolia to calculate the latitude of these Asian crustal blocks. We then use these paleolatitude calculations to refine the paleomagnetically-determined age of the collision between Greater Indian units and southern Asia, as well as Cenozoic upper-crustal shortening budgets for Asia. The paleomagnetic results presented here are free of inclination shallowing-biases and are the first Cenozoic volcanic data from the Tibetan Plateau and Central Asia with enough sampling units to average secular variation well enough to yield reliable paleolatitude estimates. In southern Tibet, 54-47 Ma lavas and tuffs from the Linzizong Formation ~50 km north of Lhasa indicate that the southern margin of Asia was 22.8±3.3°N latitude at approximately 50 Ma. Late Paleogene (~37 Ma) lavas from Central Tibet record a paleolatitude of 25.9±5.6°N, consistent with the paleomagnetic results from the Linzizong Formation and the structural record of upper-crustal shortening between Southern and Central Tibet. In southern Mongolia, 40-30 Ma lavas record a paleolatitude of 38.5±3.0°N. These paleomagnetic data from Mongolia indicate that stable Asia was located ~10° of latitude farther south in the late Paleogene than predicted from the Eurasian reference poles traditionally used to reconstruct the paleogeography of Asia. The geophysical mechanism for the discrepancy between the predicted and observed paleolatitudes for Mongolia is presently debated, but may be due to non-rigid behavior of the Eurasian lithosphere, small non-dipole geomagnetic fields, or a combination of these processes. Importantly, the paleomagnetic data from Mongolia suggest that the Eurasian reference poles do not correctly predict the Cenozoic paleogeography of Asia, and therefore are not suitable for reconstructing the Asian side of the India-Asia collision.

Paleolatitudes calculated from the 54-47 Ma Linzizong Formation and inclination-shallowing-corrected marine limestones from the Tethyan Himalaya imply that the paleomagnetically-determined age of collision between Southern Tibet and Greater Indian units occurred at approximately 48 Ma (95% confidence interval between 57 Ma and 40 Ma) at ~20±5°N latitude. These results are consistent with tomographic anomalies locating the India-Asia collision at 15-25°N latitude, and with independent 56-46 Ma collision age estimates inferred from the plate-velocity record for the Indian plate and from the age of a) high pressure metamorphism, b) end of marine sedimentation, and c) first occurrence of Asian detritus on the Greater Indian margin.

Moreover, the volcanic-based paleolatitude calculations for Tibet and Mongolia presented here suggest that there has been less than 700 km of convergence, or lithospheric shortening, between Central Tibet and Stable Asia since 40 Ma. Structural studies of mountain belts separating Central Tibet and Southern Mongolia indicate at least 360 km but probably not more than 500 km of upper crustal shortening between these regions. Thus, shortening budgets for the Tibetan orogen calculated from geologic and high-quality paleomagnetic studies are consistent and together suggest that intra-continental shortening of Asian lithosphere is on the order of a few 100s of km since 40 Ma, and not 1000s of km.

Furthermore, the southern margin of Asia is the late-stage product of plate convergence and terrane accretion throughout Central Asia that began in the Paleozoic. It is expected, then, that convergence-related intracontinental deformation and surface uplift of the Tibetan plateau may have begun much earlier than the India-Asia collision. Indeed, the last marine facies are replaced by non-marine deposystems throughout Southern and Central Tibet beginning in the Cretaceous (~120 Ma). The development of the Gangdese volcanic arc and associated retro-arc fold-and-thrust belt on the southern margin of Asia is the most likely cause for this pre-India-Asia collision phase of crustal thickening and surface uplift. Collectively, recent geological observations from the plateau interior and our new paleomagnetic-determined latitudes suggest that the southern margin of Asia may have been characterized by a high elevation, subtropical, continental plateau prior to the onset of the India-Asia collision.

Cite as: Lippert, P.C., and others, 2010, The Paleogene Latitude of Asia and the Proto-Tibetan Plateau, *in* Leech, M.L., and others, eds., Proceedings for the 25th Himalaya-Karakoram-Tibet Workshop: U.S. Geological Survey, Open-File Report 2010-1099, 2 p. [http://pubs.usgs.gov/of/2010/1099/lippert/].

Internal Strain and Deformation Temperature of Lesser Himalayan Thrust Sheets, Bhutan

Sean P. Long[1], Nadine McQuarrie[1], Tobgay Tobgay[1]

[1] Department of Geosciences, Princeton University, Princeton, NJ 08544, U.S.A., slong@princeton.edu

Analysis of quartz deformation microstructure in concert with quantification of crystal-plastic strain of quartz clasts constrains deformation temperature ranges and internal strain magnitude and orientation within thrust sheets of Subhimalayan (SH) and Lesser Himalayan (LH) rocks in eastern and central Bhutan. Quantifying strain geometry and magnitude provides a better understanding of the 3-D evolution of deformation, allows assessment of the relative contribution of internal strain to large-scale deformation, and illuminates the sequential development of strain patterns.

The LH zone displays an inverted gradient in metamorphic grade (Gansser, 1983) and deformation temperature between the MBT and MCT (Fig. 1A). From foreland to hinterland, deformation temperatures constrained by quartz recrystallization microstructure (e.g. Stipp et al., 2002) show that: 1) thrust sheets of the Permian Diuri Formation and Permian Gondwana succession were deformed at ca. 250-310ºC (transition to bulging recrystallization); 2) multiple horses of the Neoproterozoic-Cambrian(?) Baxa Group in the upper LH duplex were deformed at temperatures between ca. 280º-400ºC (bulging recrystallization), with Baxa strata just under the Shumar Thrust (ST) recording deformation temperatures up to ca. 450 ºC (subgrain rotation recrystallization); 3) deformation temperatures of horses of the Paleoproterozoic Daling-Shumar Group and Neoproterozoic-Ordovician(?) Jaishidanda Formation in the lower LH duplex increase from ca. 400-450ºC (subgrain rotation recrystallization) at the ST to ca. 500-670ºC (grain-boundary migration recrystallization, combined with ca. 640-670ºC garnet peak temperatures; Daniel et al. [2003]) at the MCT, with the majority of the change (ca. 140-170ºC) occurring within ca. 350 m of the MCT. Thus, the LH inverted deformation temperature gradient can be attributed to: A) stacking of discrete thrust sheets of upper LH rocks below the ST that were deformed at progressively higher temperatures (and presumably depths) toward the hinterland, and B) the 'hot-iron' effect of the MCT hanging wall, which only affected thrust sheets of the lower LH duplex above the ST. The repetition of stratigraphy (Long and others, in press), metamorphic isograds, and inverted temperatures emphasizes the discrete stacking of thrust sheets of lower LH rocks between the ST and the MCT.

3D strain ellipsoids were determined by quantifying the elongation and orientation of strained sand-size quartz clasts for 68 SH and upper LH samples, using the Rf-φ and Normalized Fry methods. In general, two bedding- or foliation-perpendicular oriented thin sections were analyzed from each sample, with the XZ thin section cut parallel to lineation (~N-S trending) and the YZ thin section cut perpendicular to lineation (~E-W trending). In eastern Bhutan, the XY strain plane of ellipsoids from foreland thrust sheets of the Baxa Group, Gondwana succession, and Siwalik Group are oriented at moderate to high angles (θ', the angle between the X direction and bedding/foliation, ~45-90º) to bedding, and exhibit Rs (tectonic ellipticity) values between ~1.1-1.2 (n=7). This is indicative of low-magnitude (~7%) layer-parallel shortening (LPS) strain. Further to the hinterland, upper LH map units, including the Diuri Formation thrust sheet and multiple horses of the Baxa Group in the upper LH duplex, exhibit layer-normal flattening (LNF) strain, with the XY strain plane oriented subparallel to bedding or tectonic foliation. Baxa Group quartzite and phyllite show similar strain magnitude.

We propose the following sequential development of strain patterns. First, low-magnitude (7%) LPS strain developed foreland-ward of the thrust deformation front (Fig. 1B-D) as seen in frontal thrust sheets in eastern Bhutan. Previous studies have suggested that LPS strain initiates from an increase in burial depth (and corresponding temperature) from subsidence and sedimentation in the foreland basin, and/or an increase in deviatoric stress near the leading edge of the approaching thrust wedge (e.g. Yonkee and Weil, 2009). We interpret the transition from LPS to LNF strain observed further to the hinterland as the result of tectonic loading due to emplacement of thick overriding thrust sheets (Fig. 1B, C). As deformation propagated toward the foreland, the record of early LPS fabrics in hinterland units, if it was ever present, was overprinted by higher-magnitude LNF fabrics when units were tectonically buried (Fig

1B-D). The transition between low-magnitude (Rs~1.1-1.2) LPS and higher-magnitude (Rs~1.8-2.0) LNF strain occurs approximately at the lower temperature limits for crystal-plastic quartz deformation (ca. 250-270ºC), which illustrates the strong control of deformation temperature on strain magnitude and orientation. Thrust sheets comprised of quartz- or mica-rich rocks above this temperature range were sufficiently weak enough due to loss of shear strength to cause far-field tectonic stresses oriented at a low angle to layering to rotate into a layer-normal orientation (e.g. Means, 1989). The bedding/foliation-subparallel orientation of the XY strain plane for the LNF ellipsoids persists regardless of dip angle and dip direction at any given location. The orientations of the LNF ellipsoids are folded to the same degree as the thrust sheets in which they lie, which indicates that LNF strain preceded thrust imbrication and southward translation. LNF strain observed in Baxa Group horses (upper LH duplex) is attributed to burial and loading from emplacement of lower LH thrust sheets (lower LH duplex), which in turn were loaded by the GH-TH section (Fig. 1C). Subsequently, deformation became localized along thrust faults, as these previously-strained rocks were imbricated and translated in thrust sheets separated by discrete fault zones (Fig. 1C, D). After thrust emplacement, strata retaining older LNF fabrics were then passively folded and translated as thrusting propagated toward the foreland, creating the upper LH duplex (Fig. 1C, D). A lack of increase in Rs with decreasing structural distance above thrusts in the upper LH duplex supports the interpretation that LNF strain pre-dated thrust imbrication and translation. This indicates that significant internal strain did not extend outside of fault zones during thrusting, which requires that fault zones were significantly weaker than the previously-strained rocks carried in their hanging wall. This supports the existence of discrete faults with large translations, as generally depicted in balanced cross-sections, even when the rocks within the thrust sheets have undergone significant internal strain.

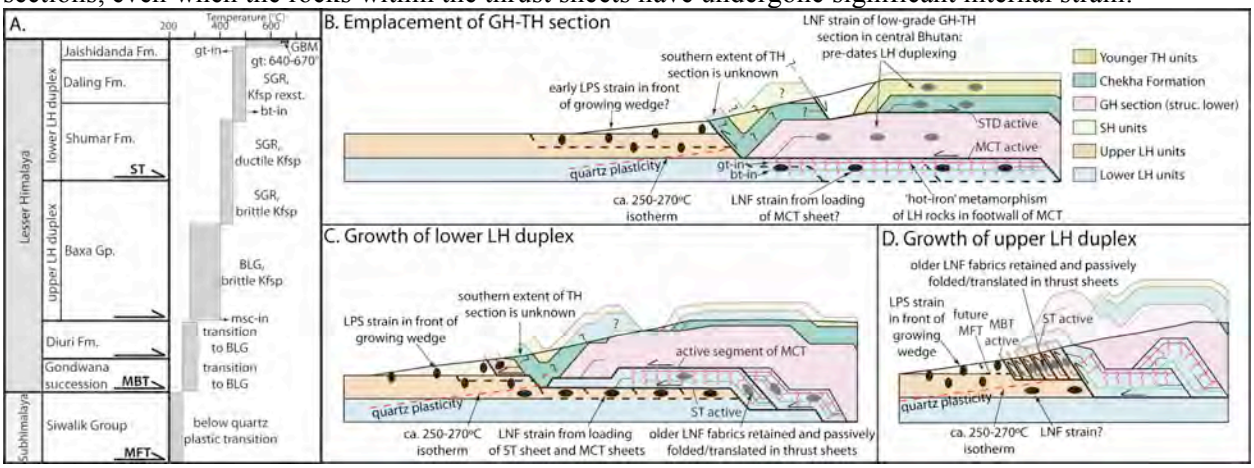

Figure 1. A) Deformation temperature profile through Bhutan SH and LH zones. Quartz recrystallization abbreviations: BLG - bulging, SGR – subgrain rotation, GBM – grain-boundary migration. B-D) Schematic cross-sections illustrating sequential development of strain patterns during specific deformation increments. Layer-parallel shortening (LPS) strain in SH and upper LH units in front of the growing wedge preceded layer-normal flattening (LNF) strain of LH units that accompanied tectonic burial. LNF strain occurred at temperatures above ca. 250-270ºC (quartz plastic transition). LH thrust sheets retaining LNF fabrics were then translated, folded and exhumed by motion along discrete thrust faults.

References

Daniel, C.G., Hollister, L.S., Parrish, R.R., and Grujic, D., 2003, Exhumation of the Main Central Thrust from Lower Crustal Depths, Eastern Bhutan Himalaya, Journal of Metamorphic Geology, 21, 317-334.

Gansser, A., 1983, Geology of the Bhutan Himalaya, Birkhauser Verlag, Boston, 181 pp.

Long, S., McQuarrie, N., Tobgay, T., and Grujic, D., in press, Geometry and crustal shortening of the Himalayan fold-thrust belt, eastern and central Bhutan, Geological Society of America Bulletin.

Means, W.D., 1989, Stretching faults, Geology 17, 893-896.

Stipp, M., Stunitz, H., Heilbronner, R., and Schmid, S.M., 2002, The eastern Tonale fault zone: a 'natural laboratory' for crystal plastic deformation over a temperature range from 250° to 700°C, Journal of Structural Geology, 24, 1861-1884.

Yonkee, A., and Weil, A.B., 2009, Reconstructing the kinematic evolution of curved mountain belts: Internal strain patterns in the Wyoming salient, Sevier thrust belt, U.S.A., Geological Society of America Bulletin, 122, 24-49.

Cite as: Long, S.P., McQuarrie, N., and Tobgay, T., 2010, Internal strain and deformation temperature of Lesser Himalayan thrust sheets, Bhutan, *in* Leech, M.L., and others, eds., Proceedings for the 25th Himalaya-Karakoram-Tibet Workshop: U.S. Geological Survey, Open-File Report 2010-1099, 2 p. [http://pubs.usgs.gov/of/2010/1099/long/].

Steepness Maxima and Transitions along the Modi Khola do not Correspond to Differences in Apatite Fission Track and (U-Th)/He Ages

Aaron J. Martin[1], Lisa S. Walsh[1], Elisabeth S. Nadin[2], Tank P. Ojha[3], Tom Fedenczuk[4]

[1] Department of Geology, University of Maryland, College Park, MD 20742, U.S.A. martinaj@geol.umd.edu
[2] Department of Geology and Geophysics, University of Alaska Fairbanks, Fairbanks, AK 99775, U.S.A.
[3] Department of Geosciences, University of Arizona, Tucson, AZ, 85721, U.S.A.
[4] National Center for Island, Maritime, & Extreme Environment Security, University of Hawaii, Honolulu, HI 96822, U.S.A.

Two of the classical foci of studies in tectonic geomorphology are steepness changes and maxima on major bedrock river systems. These studies typically identify multiple such features in large bedrock streams (recent examples from central Nepal include Kirby and Whipple, 2001; Wobus and others, 2003; 2005; and Hodges and others, 2004). Bedrock river systems are thought to respond quickly to even small-magnitude rock uplift, making steepness studies using them more sensitive indicators of rock uplift than most other techniques. Thus one of the main goals of many such studies is detection of active faults. However, several other processes can cause steepness changes on streams, including along-stream changes in lithology and precipitation, tributary junctions, and glacial or landslide damming of the river. In the absence of other data, generally it is not possible to discriminate among these possibilities.

We studied the Modi Khola, located in the western Annapurna Range of central Nepal, near and below the high elevations in the range because other workers, using data from other rivers in central Nepal, have suggested recent motion on faults at this position (Fig. 1; Wobus and others, 2003; 2005; and Hodges and others, 2004). We started with elevation contour lines digitized from topographic maps and interpolated using a multiquadric radial basis function to obtain a digital elevation model with 25 meter resolution (Hardy, 1990; Buhmann, 2003). Using freely available software (Whipple and others, 2007), we identified a high concavity zone on the river and steepness transitions and maxima within this high concavity zone. The steepest reach of the river is located near or directly downstream from the Bhanuwa fault, a normal fault within Greater Himalayan rocks. The largest change in steepness overlaps spatially with the Romi fault, a normal fault within Lesser Himalayan rocks.

In order to assess whether any of these steepness features may be caused by active faults, we obtained apatite fission-track and (U-Th)/He (AHe) ages from fifteen Greater and Lesser Himalayan pelites and quartzites at nearly constant elevation, 2220 meters above sea level. Fission track ages are mostly c. 0.8 Ma, and large uncertainties mean outliers cannot be distinguished with confidence to have a different age. AHe ages are mostly near 0.5 Ma, also with large uncertainties. Neither type of age shows any apparent difference between the fifteen samples. We modeled cooling paths of the samples using AHe ages and fission track ages and lengths and likewise find no statistically robust difference in cooling histories between any of the samples. Thus at the temporal resolution of the apatite fission-track and He data, we find no support for motion on faults in this region of the Modi Khola valley in the past c. 1 million years, and suggest that the steepness maxima and transitions on the river likely result from other causes.

Figure 1 (following page). Geologic map of part of the Modi Khola valley showing the study area. The detailed geologic map allowed comparison of structural and lithologic features with steepness maxima and changes on the river. Modified from Martin and others (2010).

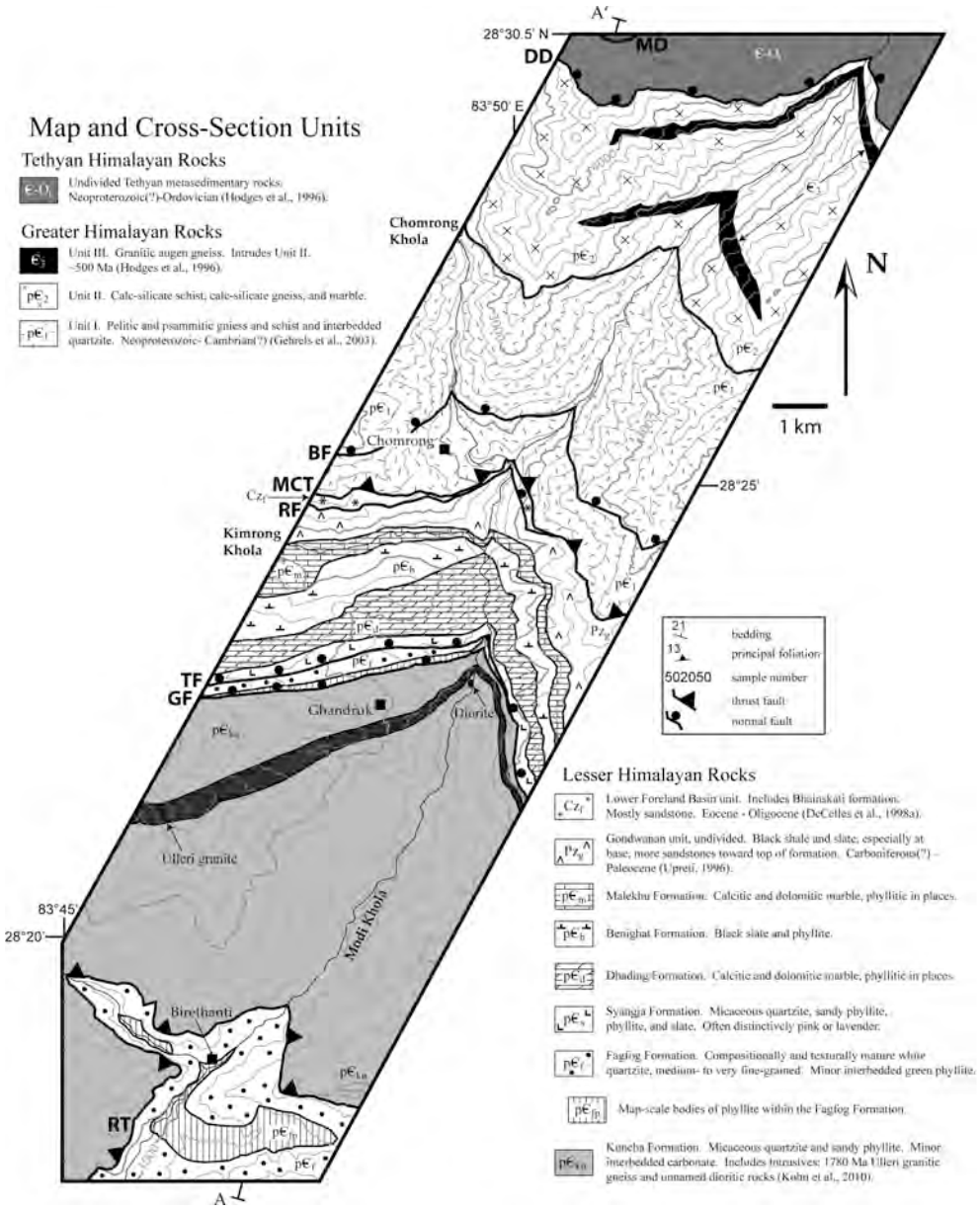

References

Buhmann, M.D., 2003, Radial Basis Functions: Theory and Implementations, Cambridge Univ. Press, Cambridge, UK, 259 p.

Hardy, R.L., 1990, Theory and applications of the multiquadric biharmonic method, Computers and mathematics with applications, 19, 163-208.

Hodges, K.V., Wobus, C., Ruhl, K., Schildgen, T. and Whipple, K., 2004, Quaternary deformation, river steepening, and heavy precipitation at the front of the Higher Himalayan ranges, Earth Planet. Sci. Let., 220, 379-389.

Kirby, E. and Whipple, K.X., 2001, Quantifying differential rock-uplift rates via stream profile analysis, Geology, 29, 415-418.

Martin, A.J., Ganguly, J. and DeCelles, P.G., 2010, Metamorphism of Greater and Lesser Himalayan rocks exposed in the Modi Khola valley, central Nepal, Contrib. Min. Pet., 159, 203-223, doi: 10.1007/s00410-009-0424-3.

Whipple, K., Wobus, C., Crosby, B., Kirby, E. and Sheehan, D., 2007, New tools for quantitative geomorphology: Extraction and interpretation of stream profiles from digital topographic data, http://www.geomorphtools.org/Tools/StPro/Tutorials/StPro_UserGuidees_Final.pdf

Wobus, C.W., Hodges, K.V. and Whipple, K.X., 2003, Has focused denundation sustained active thrusting and the Himalayan topographic front?, Geology, 31, 861-864.

Wobus, C., Heimsath, A., Whipple, K. and Hodges, K., 2005, Active out-of-sequence thrust faulting in central Nepalese Himalaya, Nature, 434, 1008-1011.

Cite as: Martin, A.J., Walsh, L.S., Nadin, E.S., Ojha, T.P., Fedenczuk, T., 2010, Steepness Maxima and Transitions along the Modi Khola do not Correspond to Differences in Apatite Fission Track and (U-Th)/He Ages, *in* Leech, M.L., and others, eds., Proceedings for the 25th Himalaya-Karakoram-Tibet Workshop: U.S. Geological Survey, Open-File Report 2010-1099, 2 p. [http://pubs.usgs.gov/of/2010/1099/martin/].

Speleothem Records of Monsoon Intensity: Evaluating Proxy Fidelity via Cave Process Monitoring in the Shillong Plateau, NE India

Dave P. Mattey[1], Nigel B. W. Harris[2], Talat Ahmad[3], Bijay S. Mipun[4], Andrew Mawlong[4], Gregory Diengdoh[5]

[1] Department of Earth Sciences, Royal Holloway University of London, Egham, Surrey TW20 OEX, U.K.
[2] Department of Earth and Environmental Sciences, Open University, Milton Keynes MK7 6AA, U.K.
[3] Department of Geology, University of Delhi, Delhi 110 007, India, tahmad001@yahoo.co.in
[4] Department of Geography, North-Eastern Hill University, Shillong 793 022, India
[5] Meghalaya Adventure Tours, Shillong 793 001, India

The Indian monsoon delivers intense summer rainfall to southern Asia and so affects the survival of many millions of people, yet the underlying causes that determine its intensity on interannual to decadal timescales remain poorly understood. Climate modellers require a knowledge of how the distribution and intensity of the Indian summer monsoon (ISM) has varied through a range of timescales and to compare these variations with known astronomical and terrestrial cycles in order to identify the mechanisms that drive monsoon evolution.

Geochemical records of atmospheric processes, primarily rainfall and temperature, are preserved in carbonate formations formed within caves (speleothems); for example variations in oxygen isotopes provide a memory of the original oxygen-isotope composition of rainfall. Annual variations in speleothem growth, like those of tree rings, provide a record of temperature and rainfall, but interpretation of their oxygen-isotope record in terms of real climatic processes requires detailed knowledge of how the climate signal is passed from rainfall through the soil and groundwater system and into the cave, to be recorded as a stalagmite grows from the dripwater. Our primary objective is to obtain pilot data to improve understanding of processes that transfer and modify the $\delta^{18}O$ climate signal via the precipitation-soil-karst-speleothem system. Using proven cave monitoring techniques developed in Gibraltar (Mattey and others, 2008) we are employing both oxygen- and carbon-isotope proxies that reflect climatic variations and we hope to decipher profiles of trace-elements such as Mg, Sr and P that record processes in the soil and bedrock.

The Shillong plateau of NE India captures the early rainout of the ISM air mass moving north from the Bay of Bengal. The plateau is a fragment of Indian crystalline basement overlain by a Late Proterozoic-Cambrian cover sequence, uplifted as a rigid pop-up structure between 8-14 Ma, in response to the India-Asian collision and continued convergence (Clark and Bilham, 2008). Tertiary deposits from the southern plateau include the Late Paleocene Lakadong carbonates, a 200-m sequence of hard nummulitic limestone that hosts a labyrinth of speleothem-rich caves distributed in an E-W sequence along the southern plateau (Jauhri and Agarwal, 2001). A recent study of Shillong rainfall (Breitenbach and others, 2010) has established a strong seasonal variation in $\delta^{18}O$ reflecting changing water-vapour source dynamics. During the summer monsoon, depleted $\delta^{18}O$ (average = -7.16) reflect marine sources from the Arabian Sea and Bay of Bengal, whereas pre-monsoon values ($\delta^{18}O$ = -2.41) reflect recycled continental moisture. Post-monsoon values are extremely depleted ($\delta^{18}O$ = -11.78) indicating an increased runoff component from the flooded Ganges-Brahmaputra catchments. This strong seasonal variation provides a geochemical signature for assessing changing monsoon intensity through time.

Since this study exploits the potential of speleothems for proxy-mapping past precipitation intensity in the core of the South Asian Summer monsoon it requires close monitoring of the relationship between the cave environment, groundwater chemistry and surface climate in order to quantify atmospheric processes back through time. During a field campaign in January 2010 we have identified a promising site for climate research near Cherrapunjee (Krem Mawmluh) from which we have recovered suitable speleothem deposits and dripwater samples and have installed monitoring equipment within the cave to record diurnal temperature and humidity changes, established strategies for monitoring variations in air composition on a monthly basis and, on the surface, have installed a soil-sampling site and weather station with a view to providing robust linkage between underground and surface conditions throughout the year. Currently we

are establishing isotopic profiles through the speleothems and are embarking on a U-series dating programme to identify the time period represented by the proxy.

Our study will generate new information on tropical carbonate processes, fundamental to the quantitative interpretation of speleothem climate records, leading to the development of reliable geochemical proxies as a measure of the changing temperatures and intensities of the monsoon. Depending on the time interval recorded by speleothem growth we believe that this work will provide precisely dated quantitative meteorological records over centennial timescales and so provide a vital land-based record of variations in the Indian monsoon during the Holocene.

References

Breitenbach, S.F.M., Adkins, J.F., Meyer, H., Marwan, N., Kumar, K.K. and Haug, G.H., 2010, Strong influence of water vapor source dynamics on stable isotopes in precipitation observed in Southern Meghalaya, NE India, Earth and Planetary Science Letters, 292, 212-220.

Clark, M.K. and Bilham, R., 2008, Miocene rise of the Shillong Plateau and the beginning of the end for the Eastern Himalaya, Earth and Planetary Science Letters, 269, 336-350.

Jauhri, A.K. and Agarwal, K.K., 2001, Early Palaeogene in the south Shillong Plateau, NE India: local biostratigraphic signals of global tectonic and oceanic changes, Palaeogeography, Paleoclimatology and Palaeoecology, 168, 187-203.

Mattey, D., and others, 2008, A 53 year seasonally resolved oxygen and carbon isotope record from a modern Gibraltar speleothem: Reconstructed drip water and relationship to local precipitation, Earth and Planetary Science Letters, 269, 80-95.

Cite as: Mattey, D.P., 2010, Speleothem Records of Monsoon Intensity: Evaluating Proxy Fidelity via Cave Process Monitoring in the Shillong Plateau, NE India, *in* Leech, M.L., and others, eds., Proceedings for the 25th Himalaya-Karakoram-Tibet Workshop: U.S. Geological Survey, Open-File Report 2010-1099, 2 p. [http://pubs.usgs.gov/of/2010/1099/mattey/].

Chronostratigraphic Constraints on the Inner Lesser Himalayan Sedimentary belt of North India, and Proterozoic Sediment Continuity of the North Indian Margin

N. Ryan McKenzie[1], Nigel C. Hughes[1], Paul M. Myrow[2], Shuhai Xiao[3], Ganqing Jiang[4]

[1] Department of Earth Sciences, University of California Riverside, Riverside, CA 92521, U.S.A., neil.mckenzie@email.ucr.edu
[2] Department of Geology, Colorado College, Colorado Springs, CO 80903, U.S.A.
[3] Department of Geosciences, Virginia Tech, VA 24061, U.S.A.
[4] Department of Geoscience, University of Nevada, Las Vegas, NV 89154, U.S.A.

In northern India the Lesser Himalaya lithotectonic unit is divided into two sedimentary belts referred to as the "inner" and "outer" Lesser Himalaya (iLH & oLH, respectively). However, the relationship between these units is problematic, primarily due to a poor understanding of the stratigraphic architecture and age of the iLH. The chronostratigraphy of the majority of oLH strata is well established and the system can be broadly divided into four major units, in ascending order, the Neoproterozoic Jaunsur/Simla Group, the Cryogenian Blaini Formation, the Ediacaran Krol Group, and the Cambrian Tal Group. The Blaini diamictite has been correlated to the Marinoan Glaciation (ca. 635 Ma) with base of the carbonate-dominated Krol Group marked by the corresponding cap-carbonate, and both the chemostratigraphy and lithostratigraphy of the Krol are remarkably similar to the Ediacaran Yangtze Platform of South China (Jiang and others, 2003). The siliciclastic dominated Tal Group contains Cambrian metazoan macrofossils (Hughes and others, 2005). The iLH can be broadly divided into three major units, the quartzite dominated Berinag, the mixed siliciclastic Damtha, and the carbonated dominated Deoban Groups, although the ages and stratigraphic relationships of these strata are currently unconstrained. The Deoban Group is well known to overlie the Damtha Group, but the Berinag Group has been suggested to sit either below the Damtha Group as the lowermost unit of the iLH (Richards and others, 2005), or above the Deoban Group as the uppermost unit of the iLH (Valdiya, 1980). This issue is greatly complicated by a lack of geochronologic data. For instance, the Deoban Group was originally assigned a "Riphean" (Mesoproterozoic) age (Valdyia, 1980), an age broadly supported by geochemical data (Ahmad and others, 2000), yet recent reports of Ediacaran-Cambrian fossils have been used to argue for significantly younger ages for these strata (e.g., Tiwari & Pant 2009).

Our investigations of new U-Pb detrital zircon geochronology, sedimentology, and microfossil paleobiology of iLH strata in the Gahwal-Kumaon regions of northern India helps resolve some of these issues. Strata from the Berinag Group yielded distinctive detrital zircon spectra with a single dominant peak at ~1880 Ma and no grains younger than ~1800 Ma, similar to the results from the Berinag-Rampur Formation from the Sutlej Valley to the west (Richards and others, 2005). Damtha Group strata yielded broader spectra with peaks at 1600-1700 Ma, 1880 Ma, and 2500 Ma, with the youngest grain ~1600 Ma. These contrasts with a spectrum from the definitive Neoproterozoic Blaini Diamictite that shows similar peaks to Damtha Group, but includes a large number of younger grains around ~900 Ma and a youngest grain ~770 Ma. Given that all recent spectra from Cambrian siliciclastic rocks from the Himalaya contain high concentrations of relatively young material (Myrow and others, in press), the Berinag-Damtha groups are likely significantly older than the Blaini Diamictite. The Berinag-Damtha zircon spectra are remarkably similar to that from the Kuncha Formation and overlying strata of the Lower Nawakot Unit of Nepal (Martin and others, 2005). Damtha spectra are also similar to the Shumar Formation of Bhutan (McQuarrie and others, 2008), which suggests that these strata were all part of the laterally contiguous late Paleoproterozoic north Indian margin. The spectra also support a model in which the Berinag Group is the lowermost unit of the iLH, in agreement with the Richards and others (2005) model. K-S statistical analysis of Blaini Diamictite grains older than 1600 Ma and the Damtha Group showed no significant differences between these populations, suggesting both the oLH and iLH were deposited in a single continuous margin with the Blaini receiving more ancient sediment from either reworked Damtha strata, similar primary sources, or a combination of the two.

Reviews of published material and our independent research of fossiliferous material from the Deoban Group show no evidence for an Ediacaran–Cambrian age assignment. Phosphatic *Baicalia* stromatolites in the Gangolihat Dolomite (i.e., Deoban Group) yielded three-dimensionally preserved organic-walled microfossils and microbial textured intraclasts with gas bubbles preserved within the microbial fabrics.

This lithologically distinct deposit is identical to those in the Tirohan Dolomite in the Vindhyan Basin from central India, which have been dated at ~1600 Ma (Bengtson and others, 2009). The lithological similarity between these units, and the fact that the youngest detrital zircon from strata directly underlying the Gangolihat Dolomite is ~1600 Ma, suggest these are age-equivalent deposits that were part of a large epicontinental platform that covered the north Indian margin during the late Paleoproterozoic to early Mesoproterozoic. The potential continuity between the Vindhyan Basin and the Himalayan margin contrasts with the current view that Vindhyan sediment was deposited in an intracratonic basin isolated from the rest of the north Indian margin (e.g., Bose and others, 2001).

References

Amhad, T., and others, 2000, Isotopic constraints on the structural relationships between the Lesser Himalayan Series and the High Himalayan Crystalline Series, Garhwal Himalaya, Geol. Soc. Am. Bulletin, 112, 467-477.

Bengtson, S., Belivanova, V., Rasmussen, B. and Whitehouse, M., 2009, The controversial "Cambrian" fossils of the Vindhyan are real, but more than a billion years older, Proc. Nat. Acad. Sci., 106, 7729-7734.

Bose, P.K., Sarkar, S., Chakrabarty, S. and Banerjee, S., 2001, Overview of the meso- to Neoproterozoic evolution of the Vindhyan Basin, central India, Sedimentary Geology, 141, 395-419.

Hughes, N.C., and others, 2005, Cambrian biostratigraphy of the Tal Group, Lesser Himalaya, India, and early Tsanglangpuan (late early Cambrian) trilobites from the Nigali Dhar syncline, Geol. Mag., 142, 57-80.

Jiang, G., Sohl, L.E. and Christie-Blick, N., 2003, Neoproterozoic stratigraphic comparison of the Lesser Himalaya (India) and Yangtze block (south China): Paleogeographic implications, Geology, 31, 917-920.

Martin, A.J., DeCelles, P.G., Gehrels, G.E., Patchett, P.J. and Isachsen, C., 2005, Isotopic and structural constraints on the location of the Main Central thrust in the Annapurna Range, central Nepal Himalaya, Geol. Soc. Am. Bulletin, 117, 926-944.

McQuarrie, N., and others, 2008, Preliminary stratigraphic and structural architecture of Bhutan: Implications for the along strike architecture of the Himalayan system, Earth Planet Sci. Letts., 272, 105-117.

Myrow, P.M., and others, in press, Extraordinary transport and mixing of sediment across Himalayan central Gondwana during the Cambrian-Ordovician, Geol. Soc. Am. Bulletin.

Richards, A., and others, 2005, Himalayan architecture constrained by isotopic tracers from clastic sediments, Earth Planet Sci. Letts., 236, 773-796.

Tiwari, M. and Pant, I., 2009, Microfossils from the Neoproterozoic Gangolihat Formation, Kumaun Lesser Himalaya: Their stratigraphic and evolutionary significance, J. Asian Earth Sci., 35, 137-149.

Valdiya, K.S., 1980, Geology of Kumaun Lesser Himalaya, Wadia Institute of Himalayan Geology Dehra Dun, India, p. 291.

Cite as: McKenzie, N.R., Hughes, N.C., Myrow, P.M., Xiao, S. and Jiang, G., 2010, Chronostratigraphic constraints on the inner Lesser Himalayan sedimentary belt of north India and Proterzoic sediment continuity of the north Indian margin, *in* Leech, M.L., and others, eds., Proceedings for the 25th Himalaya-Karakoram-Tibet Workshop: U.S. Geological Survey, Open-File Report 2010-1099, 2 p. [http://pubs.usgs.gov/of/2010/1099/mckenzie/].

Magnitude of Strain in a Low-Grade Greater Himalayan Section, Central Bhutan: Implications for Channel Flow

Nadine McQuarrie[1], Sean P. Long[1]

[1] Department of Geosciences, Princeton University, Princeton, NJ 08544, U.S.A., nmcq@princeton.edu

The recognition of potential crustal melt under the Tibetan plateau, in conjunction with ubiquitous partial melt textures and shear indicators within the Greater Himalayan (GH) sequence has led to the development of kinematic and numerical models that argue for the southward extrusion of weak crust between the Main Central Thrust (MCT; top-to-south) and the Southern Tibetan Detachment (STD; top-to-north). This ductile extrusion of the GH section driven by gravitational potential energy of the Tibetan plateau and focused erosion along the topographic front, may be as great as 400-600 km (e.g. Jamieson and others, 2006), implying coeval and roughly equal displacements across the MCT and STD. However, seemingly pervasive ductile deformation within GH rocks and a lack of exposed cut-offs for the MCT and STD have hindered efforts of evaluating the magnitude of extrusion through field studies. We present geologic mapping, stratigraphic columns, metamorphic mineral assemblages, and structural and strain data from GH and TH rocks in central Bhutan, which allow us to quantify the magnitude, direction and temperature of deformation. These data collectively argue for: 1) a depositional contact between the TH and GH sections in central Bhutan, and 2) the presence of a low-grade GH section in central Bhutan that exhibits the kinematic profile of a channel. Our observations contribute to the channel flow debate by 1) placing constraints on the magnitude of displacement on a portion of the STD, and 2) quantifying the maximum top-to-the-north component of channel flow through the upper part of the GH and TH section. While these data support a kinematic model of channel flow in central Bhutan, the magnitude of ductile extrusion of the GH section is minor (Long and McQuarrie, 2010).

In central Bhutan, the GH section is 5-10 km thick, and consists of a lower granitic orthogneiss unit and an upper metasedimentary unit, comprised of quartzite, schist, phyllite, and paragneiss (Fig. 1). The overlying TH section consists of quartzite and schist of the Chekha Formation, and phyllite of the Maneting Formation (Long and McQuarrie, 2010). Kyanite and partial melt textures are only observed in the lower-mid parts of the GH orthogneiss unit, and the overlying parts of the GH and TH sections are dominated by a melt-free, biotite-muscovite-garnet mineral assemblage (Long and McQuarrie, 2010). The basal-mid GH orthogneiss unit section was deformed at ~500°-700°C (grain-boundary migration quartz recrystallization; Stipp and others, 2002). An upsection transition to subgrain rotation quartz recrystallization, accompanied by K-feldspar recrystallization, indicates that the higher part of the GH section and full exposed TH section underwent deformation at temperatures between ~450°-500°C. Similar mineral assemblages and deformation temperatures that persist for several km structural distance across both sides of the GH-TH contact, combined with interfingering of distinct biotite-porphyroblast schist and quartzite across a significant structural thickness at the GH-TH contact, indicate that TH strata are in depositional contact above GH strata in central Bhutan (Long and McQuarrie, 2010). This stratigraphic contact is in contrast to observations in eastern Bhutan, where melt-free TH rocks are separated from GH rocks displaying partial melt textures by a top-to-the-north sense shear zone correlated with the STD (Grujic and others, 2002). Peak temperature conditions for GH rocks in eastern Bhutan are estimated at 750-800°C (Daniel and others, 2003). These data indicate a ca. 250°-300°C along-strike decrease in GH deformation temperature from eastern to central Bhutan (Long and McQuarrie, 2010). In central Bhutan, thin-section scale kinematic indicators in the composite GH-TH section fit the profile of an asymmetric channel, with a 2-3 km-thick section exhibiting a top-to-the-south shear sense at the base overlain by an ~11-km thick section exhibiting a top-to-the-north shear sense (Long and McQuarrie, 2010). Using the Rf-φ method, we quantified crystal-plastic strain of sand-size quartz porphyroclasts for 41 GH and TH samples. Two bedding- or foliation-perpendicular oriented thin sections were analyzed from each sample, with the XZ thin section cut parallel to lineation (~N-S trending) and the YZ thin section cut perpendicular to lineation (~E-W trending), allowing us to calculate 3-D strain ellipsoids (Fig. 1B). GH and TH rocks in central Bhutan show evidence for heterogeneous layer-normal flattening strain, with the XY strain plane deviating from bedding/foliation by median values of only 6° (N-S; Fig 1B) and 8° (E-W). We observe significant lithologic control on strain magnitude, with XZ and YZ elongations

varying between 1.2-4.1 and 1.1-2.8 for quartzite, and between 1.6-8.5 and 1.4-3.8 for phyllite and schist. Layer-normal flattening strain can be approximated with median strain ellipsoids of 3.0:2.2:1.0 for phyllite/schist, 1.6:1.5:1.0 for quartzite, and 2.1:1.8:1.0 for all lithologies, with the X direction trending approximately N-S. Assuming only simple shear, integrating these median strain values across the 11-km thick section indicates that the top-to-the-north component of channel flow was between ~23-34 km. However, kinematic vorticity numbers range between ca. 0.0-0.7, with over half of analyses ≤0.4, indicating that pure-shear was the dominant strain mechanism with a simple shear component of only ~8-11 km. The stratigraphically-continuous GH-TH section discussed here limits slip on a portion of the STD system to ~20 km. A low-offset STD combined with a low-displacement channel have implications for the role of channel-flow processes in the Himalaya. We document a dramatic along-strike gradient in metamorphic grade from cool in central Bhutan to hot in eastern Bhutan. If these temperature gradients were matched by comparable changes in viscosity, there would be potential for significant along-strike differences in flow velocity and material transport. If the melt rich, potentially low-viscosity region experienced large magnitudes of flow, GH rock would have been emplaced on LH rocks as much as ~300 km south of its modern southern extent, or similar magnitudes of material would have to had been removed via erosion at the same time as extrusion. For erosion to keep pace requires rates of ~30-50 mm/yr and erosion to vary spatially with displacement gradients. We conclude that, when present, the magnitude of channel flow must be small with respect to the total mass balance of material in the system. In central Bhutan, the top-to-the-north component of channel flow represents <5% of the mass added by shortening within the Himalayan orogenic belt (Long and McQuarrie, 2010; Long and others, in press).

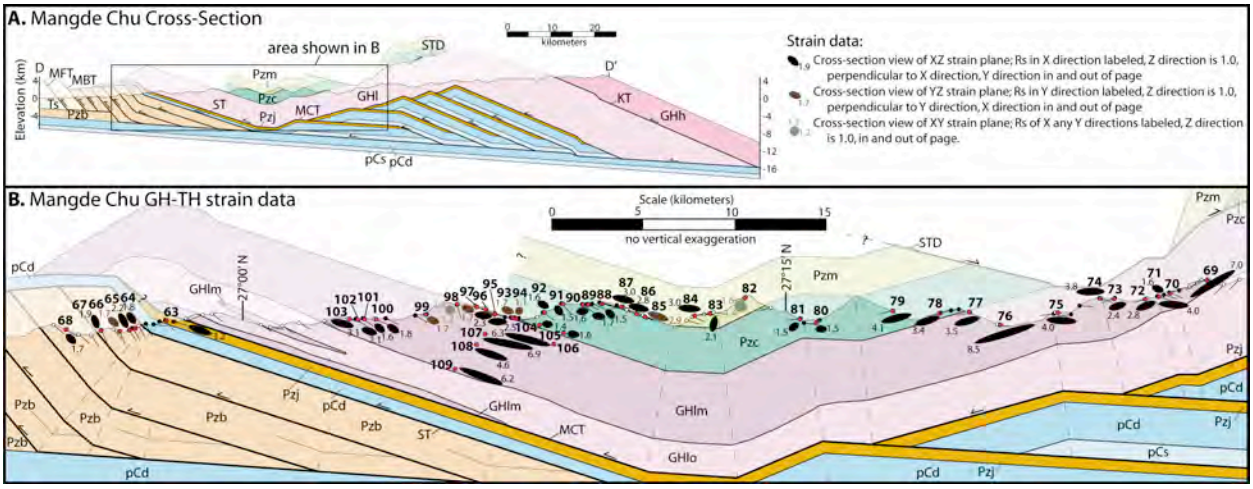

Figure 1. A) Mandge Chu cross-section, simplified from Long and others (in press). Unit abbreviations: pCs – Shumar Formation, pCd – Daling Formation, Pzb – Baxa Group, Pzj – Jaishidanda Formation, Ts – Siwalik Group, GHlm – Greater Himalayan metasedimentary unit, GHlo – orthogneiss unit, Pzc – Chekha Formation, Pzm – Maneting Formation. B) Inset showing strain data from GH and TH rocks on the Mandge Chu cross-section. Strain ellipses from N-S (generally XZ) thin sections are projected directly onto the cross-section.

References

Daniel, C.G., Hollister, L.S., Parrish, R.R. and Grujic, D., 2003, Exhumation of the Main Central Thrust from Lower Crustal Depths, Eastern Bhutan Himalaya, J. Metamorphic Geol., 21, 317-334.

Grujic, D., Hollister, L.S. and Parrish, R.R., 2002, Himalayan metamorphic sequence as an orogenic channel: insight from Bhutan, Earth Planet. Sci. Letts., 198, 177-191.

Jamieson, R.A., Beaumont, C., Nguyen, M.H. and Grujic, D., 2006, Provenance of the Greater Himalayan Sequence and associated rocks: predictions of channel flow models, Geol. Soc. London Spec. Pub. 268, 165-182.

Long, S., McQuarrie, N., Tobgay, T. and Grujic, D., in press, Geometry and crustal shortening of the Himalayan fold-thrust belt, eastern and central Bhutan, Geol. Soc. Am. Bull.

Long, S. and McQuarrie, N., 2010, Placing limits on channel flow: insights from the Bhutan Himalaya, Earth Planet. Sci. Letts., 290, 375-390.

Stipp, M., Stunitz, H., Heilbronner, R. and Schmid, S.M., 2002, The eastern Tonale fault zone: a 'natural laboratory' for crystal plastic deformation over a temperature range from 250° to 700°C, J. Struct. Geol., 24, 1861-1884.

Cite as: McQuarrie, N. and Long, S.P., 2010, Magnitude of strain in a low-grade Greater Himalayan section, central Bhutan: implications for channel flow, *in* Leech, M.L., and others, eds., Proceedings for the 25th Himalaya-Karakoram-Tibet Workshop: U.S. Geological Survey, Open-File Report 2010-1099, 2 p. [http://pubs.usgs.gov/of/2010/1099/mcquarrie/].

Crust and Mantle Structure of the Tibetan Plateau Down to 700 km Depth as Derived from Seismological Data

J. Mechie[1], R. Kind[1], J. Saul[1]

[1] Deutsches GeoForschungsZentrum – GFZ, Sections "Geophysical Deep Sounding" and "Seismology", Telegrafenberg, 14473 Potsdam, Germany, jimmy@gfz-potsdam.de

We have constructed a seismic velocity cross-section of the crust and mantle down to 700 km depth beneath the Tibetan plateau. The cross-section is based on the many controlled and passive source seismological experiments and studies which have reported results within an 800-km swath centered on the main Lhasa-Golmud transect. Beneath the 2.5-7 km thick cover layer, the upper crust down to 15-25 km depth has compressional (P) wave velocities of 5.8-6.1 km/s and low Poisson's ratios of 0.21-0.23, indicative of felsic rocks rich in quartz in the α state. There are many observations e.g. bright spots in seismic reflection records, low-velocity regions in shear (S) wave models derived from receiver-function analysis, seismicity drop off and high electrical conductivity which indicate that below 15-25 km depth, temperatures are high enough such that ductile flow and partial melting can occur.

One of the main results of our study is the recognition of a boundary at 30-40 km depth. From the velocity values above and below this boundary it is suggested that it marks the interface between the felsic upper crust and the more mafic lower crust. Within the swath, crustal thickness is greatest (approx. 74 km) beneath the southern part of the plateau south of about 31.5°N, where Indian lower crust forms the basal crustal layer. To the north crustal thickness decreases to about 66 km beneath the southern Qiangtang terrane around 33°N, before again increasing to about 70 km beneath the northern part of the plateau south of the Kunlun mountains. As the Kunlun mountains are crossed the crust thins dramatically to about 54 km beneath the Qaidam basin.

Beneath the crust, high-velocity, dense and cold Indian lithospheric mantle extends northwards within the swath until about the Banggong-Nujiang suture, where it downwells to at least 350-400 km depth in a zone about 100-200 km wide centred at about 31.2°N. To the north, low-velocity, less dense and warm Asian lithospheric mantle is present. The lithosphere-asthenosphere boundary occurs at 160-225 km depth under the plateau.

The 410 and 660 km discontinuities, at the top and base of the mantle transition zone respectively, produce prominent seismic phases beneath the whole plateau in receiver-function images, implying that no subducting slab penetrates the mantle transition zone under the plateau. This is, however, at variance with a recent tomographic image which suggests that Indian lithospheric mantle does penetrate into the mantle transition zone. The observation that the 410 and 660 km discontinuities run parallel to each other implies that temperature variations in the mantle transition zone are negligible. On the other hand, the apparent northwards deepening by about 20 km of both discontinuities implies that the upper mantle beneath north Tibet is slower, less dense and warmer than under south Tibet, in agreement with the observed uppermost mantle velocities. This, in turn, could provide some of the isostatic support for the high elevations in the northern part of the plateau where the crust is somewhat thinner than in the southern portion of the plateau.

Cite as: Mechie, J., Kind, R. and Saul, J., 2010, Crust and mantle structure of the Tibetan Plateau down to 700 km depth as derived from seismological data, *in* Leech, M.L., and others, eds., Proceedings for the 25th Himalaya-Karakoram-Tibet Workshop: U.S. Geological Survey, Open-File Report 2010-1099, 1 p. [http://pubs.usgs.gov/of/2010/1099/mechie/].

Distributed Deformation, Distributed Earthquakes in the Northwest Himalaya

Andrew Meigs[1], C. Madden[1], J.D. Yule[2], Y. Gavillot[1], A. Hebeler[2], A. Hussain[3], M. I. Bhat[4], A. B. Kausar[3], M. Malik[5], S. Ramzan[2,3], M. Sayab[6], R. Yeats[1]

[1] Department of Geosciences, Oregon State University, Corvallis, OR, 97331, USA, meigsa@geo.oregonstate.edu
[2] Department of Geological Sciences, California State Uinversity, Northridge, Northridge, CA,
[3]Geological Survey of Pakistan, Islamabad and Peshawar, Pakistan
[4]Department of Geology and Geophysics, Univeristy of Kashmir, Srinagar, India
[5]Department of Geology, University of Jammu, Jammu, India
[6]National Centre of Excellence in Geology, University of Peshawar, Peshawar, Pakistan

An elegant model sensibly links interseismic strain accumulation, historic and paleoseismic earthquakes, and intermediate- to long-term shortening in the central Himalaya. Records of historic and paleoseismic earthquakes include more frequent, blind earthquakes (M_w<8.4) and less frequent, emergent earthquakes (M_w>8.5) on the Himalayan Frontal thrust (HFT). These earthquakes relieve the majority of interseismic strain accumulation, and faults *within* the central Himalayan accommodate little strain (Bettinelli and others, 2006; Kumar and others, 2006; Larson and others, 1999; Lavé and others, 2005). Active deformation of the northwestern Himalaya reveals a different story. An asymmetric anticline marks the deformation front in Kashmir and the HFT is inferred to be blind. The Salt Range thrust system (SRT) defines the thrust front in Pakistan to the west, which includes active folds in the footwall of the SRT proper (Yeats and Thakur, 2008). Within the orogenic wedge to the north of the deformation front, active shortening occurs along a system of emergent reverse faults, including the Reasi fault in Indian Kashmir and the Balakot-Bagh fault, source of the Mw=7.6 Kashmir earthquake of 2005 in Pakistani Kashmir (Gavillot, 2010; Hebeler, 2010; Hussain and others, 2009). Farther north, faults in the Kashmir Valley cut Quaternary deposits (Madden, 2010; Nakata, 1989). Active deformation is thus distributed more than 120 km across the orogen from the deformation front to the internides of the northwest Himalayan orogen.

Northwest Himalayan thrust front

It has been clear since the publication of the Salt Range maps of Gee (1989) that the SRT deforms young surficial deposits and is an active fault. New mapping and preliminary OSL dates from deformed Holocene sediments exposed along the westernmost SRT reveal that the last surface rupture on this fault occurred at least several thousand years ago. Our observations suggest that surface rupturing events occur on the SRT on millennial timescales, consistent with low shortening rates (4 to 13 mm/yr). It is simply unknown whether the HFT ruptures to the surface in the Kashmir Himalaya. Tilted fluvial strath terraces across the frontal structure imply that a fold defines the deformation front. However, ~20 m-high escarpments oriented perpendicular to rivers suggest that unrecognized thrust fault(s) reach the surface locally. Contact relations within the Siwalik sediments on the limb of the frontal anticline imply fold growth initiated after 0.78 Ma (Ranga Rao and others, 1988).

Active faults at intermediate distances from the thrust front

A seismically active emergent thrust fault system extends stepwise from the Balakot-Bagh fault (BB; source of the Mw=7.6, 2005 Kashmir earthquake (Kaneda, 2008; Kumahara and Nakata, 2006)) southeast more than 200 km to the Reasi fault (RF) (Hussain and others, 2009). Both the BB and RF are reverse faults; the BB locally cuts the 17 – 12 Ma Kamlial Formation. A balanced cross-section indicates a minimum of 20 km fault displacement on the BB, yielding a minimum 1.2-1.7 mm/yr long-term slip rate, lower than the 1.4 -4.1 mm/yr slip rate inferred from faulted Quaternary fluvial terraces (Kaneda, 2008). The penultimate earthquake occurred between 500 and 2200 yr b.p. (Kondo and others, 2008). The RF is a ~70 km-long, ~50° northeast-dipping reverse fault system, which lies ~40 km north of the deformation front in the Kashmir Himalaya (Gavillot, 2010). Two strands define the Reasi fault. The northern strand, Main Reasi fault (MRF), places Precambrian Sirban Limestone on folded unconsolidated conglomerates. Younger alluvial deposits cover the MRF. A preliminary OSL age of 80 ± 6 ka from a 350 m-high Bidda terrace in the upper plate of the MRF, yields a minimum long-term uplift rate of 4.4±0.3 mm/yr, a slip rate of 5.7±0.4 mm/yr, and a shortening rate of 3.7±0.3 mm/yr for the RF. To the south, the Reasi frontal

fault (RFF) includes a fault scarp that offsets Holocene deposits. Trenches excavated across the RFF reveal a distinct angular unconformity, steeply dipping strata cut by low-angle thrusts, and an unconformity below relatively undeformed strata (Hebeler, 2010). The trench relations can be explained by surface rupture of the RF ~4,500 yrs ago. The age of this unconformity is constrained to be ~4,500 yrs old based on calibrated calendar C-14 ages from detrital charcoal. These results and those from the BB (Kondo and others, 2008) imply long recurrence intervals ($\geq$2,000 yrs) for the faults.

Active faults in the hinterland

Active faulting also occurs within the Kashmir Valley (KV) (Madden, 2010), an intermontane basin ~ 100 km north of the deformation front. Three northeast-dipping reverse faults cut Quaternary terraces on the southwest side of the KV. Overbank deposits in a Rambira River terrace exhibit ~13 m of vertical separation across one of the faults (the 40-km-long Balapora fault (BF)). Weakly developed soils and the lack of loess suggest deposition after the last glacial maximum (22-17 ka), possibly as young as 10-6 ka. Given the 60° fault dip, we estimate a preliminary BF shortening rate of 0.3 to 1.3 mm/yr. Fault and stratal relations in trenches suggest at least 2 surface rupturing events in the latest Quaternary, consistent with the low fault slip rate.

Given a ~34 mm/yr India-Asia convergence rate in the NW Himalaya (Bettinelli and others, 2006), active structures within the NW Himalaya absorb roughly 15 to 50% of that convergence. In contrast to the central Himalaya where deformation is focused at the HFT, up to ~20% of the shortening occurs on structures north of the HFF, *within* the NW Himalayan orogenic belt. Discovery of internal surface-rupturing reverse faults indicates that moderate to great earthquakes have occurred on the Main Himalayan thrust (the basal décollement) and upper plate faults within the NW Himalaya.

References

Bettinelli, P., and others, 2006, Plate motion of India and interseismic strain in the Nepal Himalaya from GPS and DORIS measurements, J. Geod., 80, 567-589.

Gavillot, Y., and others, 2010, Active thrusting within the Himalayan orogenic wedge in the Kashmiri Himalaya, Seis. Res. Letts., 81 (2), p. 325.

Gee, E. R., 1989, Overview of the geology and structure of the Salt Range, with observations on relted areas of northern Pakistan, Geol. Soc. Amer. Spec. Pap., 232, 95-112, Boulder, CO.

Hebeler, A., C., and others, 2010, Middle Holocene surface rupture of the Reasi thrust, Kashmir, India , Seis. Res. Letts., 81(2), p. 346.

Hussain, A., Yeats, R. S., and MonaLisa, 2009, Geological setting of the 8 October 2005 Kashmir earthquake, J. Seism., 13, 315-325.

Kaneda, H., and others, 2008, Surface rupture of the 2005 Kashmir, Pakistan, earthquake, and its active tectonic implications, Bull. Seis. Soc. Amer., 98, 521-557.

Kondo, H., and others, 2008, Long recurrence interval of faulting beyond the 2005 Kashmir earthquake around the northwestern margin of the Indo-Asian collision zone, Geology, 36, 731-734.

Kumahara, Y. and Nakata, T., 2006, Active faults in the epicentral area of the 2005 Pakistan earthquake, 54 pp., Hiroshima University Research Center for Regional Geography, Hiroshima.

Kumar, S., and others, 2006, Paleoseismic evidence of great surface rupture earthquakes along the Indian Himalaya, J. Geophys. Res., 111, doi:10.1029/2004JB003309.

Larson, K. M., Bürgmann, R., Bilham, R. and Freymueller, J. T., 1999, Kinematics of the India-Eurasia collision zone from GPS measurements, J. Geophys. Res., 104, 1077-1093.

Lavé, J., and others, 2005, Evidence for a Great Medieval Earthquake (~A.D. 1100) in Central Himalaya, Nepal, Science, 307, 1302-1305.

Madden, C., and others, 2010, Late Quaternary Shortening and Earthquake Chronology of an Active Fault in the Kashmir Basin, Northwest Himalaya, Seis. Res. Letts., 81(2), p. 346.

Nakata, T., 1989, Active faults of the Himalaya of India and Nepal, in Tectonics of the Western Himalaya, edited by L. L. Malinconico and R. J. Lillie, pp. 243-264, Geol. Soc. Amer. Spec. Pap., 232, Boulder, CO.

Ranga Rao, A., Agarwal, R.P., Sharma, U.N., Bhalla, M.S. and Nanda, A.C., 1988, Magnetic polarity stratigraphy and vertebrate paleontology of the Upper Siwalik Subgroup of Jammu Hills, India, J. Geol. Soc. India, 31, 361-385.

Yeats, R. S. and Thakur, V., 2008, Active faulting south of the Himalayan front: Establishing a new plate boundary, Tectonophys., 453, 63-73.

Cite as: Meigs, A., and others, R., 2010, Distributed deformation, distributed earthquakes in the northwest Himalaya, *in* Leech, M.L., and others, eds., Proceedings for the 25th Himalaya-Karakoram-Tibet Workshop: U.S. Geological Survey, Open-File Report 2010-1099, 2 p. [http://pubs.usgs.gov/of/2010/1099/meigs/].

Signal or Noise? Significance of Variability in the Himalaya-Tibet System

Anne S. Meltzer[1], Peter K. Zeitler[1]

[1] Department of Earth and Environmental Sciences, Lehigh University, Bethlehem, PA 18015, U.S.A., ameltzer@lehigh.edu

Over the past several decades, numerous research projects have used the Himalaya and Tibet as a natural laboratory to investigate the process of continental collision. Much has been learned about the orogen, including the remarkable along-strike continuity of many features, such as the orogen's basic geology and zonation, structures such as the MFT, MBT, MCT, and STD, the morphology and drainages of the Himalayan arc and adjacent regions, and the apparent symmetry of the syntaxes that cap the orogen. At the same time, and not surprising for an orogen as large as the Himalaya-Tibet system, studies have also identified considerable spatial variability in such elements as the divergent GPS field, the apparent presence of eclogite in the lower crust at locations in southern Tibet, variations in Moho depth, possible differences in inferred lower-crustal and mantle lithosphere strain, significant lateral variations in the magnitude and timing of exhumation in southern Tibet and the Himalaya, and localized exposure of both high-pressure and anatectic metamorphic terranes. To first order and better, synthesis of these observations has led to general geodynamical models that do well at linking solid-Earth and surface processes, for example the aneurysm model at local scales and the channel-flow model at broader scales.

However, significant questions about the Himalaya and Tibet remain. In particular, the early history of the orogen, the nature of initial boundary conditions, and the importance of these features in controlling the evolution of the orogen are not well understood. This includes such factors and phenomena as the diversity in arc terranes that faced incoming India before collision, the prehistory of Gondwanan blocks that make up Tibet, the rheology of the deeper lithosphere in southern Tibet, and the intact nature and persistence of the Lhasa Block. An interesting question is whether this lateral variability represents minor geological noise, or whether these features are telling us something about initial conditions, their impact on the current and future dynamics of the orogen, and which orogenic records ultimately will have preservation potential.

The Lhasa Block is an interesting case to consider in this context. Little deformed, the terrane sits in the midst of the actively deforming Himalayan-Tibet system, and shows little evidence of the intense deformation that took place not far to its south: the lithosphere of incoming India, often presumed to be old-and cold, was intensely shortened during collision, whereas in comparison, the presumed warm-and-soft crustal portions of the Lhasa Block have remained enigmatically unscathed. Elevations throughout much of the central and eastern block are high and fairly uniform although in contrast to the remarkably small degrees of exhumation evident in the central and western Lhasa Block, the block's eastern portions have been significantly exhumed. This exhumation has occurred over the region where crustal thicknesses decrease. At depth, the Lhasa Block currently appears to be underlain in places by eclogitized lower crust, and the timing and modification of this eclogite formation or retrogression could have significant geodynamic consequences. The widespread granites in the block contain a petrologic and isotopic record that spans the transition from Andean-margin convergence to collision. This record of transition from convergence to collision should also exist in many of the structures, rocks and landscapes of the Lhasa Block, and integrated work on this terrane could provide important constraints on the dynamics of the Himalaya-Tibet system.

Cite as: Meltzer, A.S. and Zeitler, P.K., 2010, Lhasa Block: signal or noise? The importance of initial conditions and variability in the Himalaya-Tibet system, *in* Leech, M.L., and others, eds., Proceedings for the 25th Himalaya-Karakoram-Tibet Workshop: U.S. Geological Survey, Open-File Report 2010-1099, 1 p. [http://pubs.usgs.gov/of/2010/1099/meltzer/].

Regional resistivity structure of the Tibetan Plateau

Wei Wenbo[1], Jin Sheng[1], Gaofeng Ye[1], Alan G. Menzel-Jones[2], Martyn J. Unsworth[3], the INDEPTH MT Team

[1] China University of Geosciences Bejing, Beijing, 100083, China
[2] Dublin Institute for Advanced Studies, Dublin 2, Ireland, alan@cp.dias.ie
[3] Department of Department of Physics, University of Alberta, Edmonton, AB T6G 2J1, Canada

Modern magnetotelluric measurements have been made on the Tibetan Plateau since INDEPTH's Phase II in 1995 (Chen and others, 1996), using both broadband MT (BBMT) and long period MT (LMT) instrumentation. The MT interpretations of the data from the 1995 Yarlung-Zangbo suture profile on those 100 and 200 lines (Chen and others, 1996) were the definitive results that led to the influential Nelson and others (1996) interpretation of partial melt north of the suture. Field campaigns during Phase III resulted in MT acquisition from southern Tibet across the top of the Plateau to the Qaidam Basin north of the Kunlun Fault (Wei and others, 2001; Unsworth and others, 2004). Optimally smooth models of the MT data from these profiles showed pervasive mid-crustal low resistivity, taken as evidence of extensive partial melting (Li and others, 2003) across the whole central plateau from the Yarlung-Zangbo suture to the Kunlun Fault. Detailed analyses and modelling of the data across the Yarlung-Zangbo suture (Spratt and others, 2005) and the Bangong-Nujiang suture (Solon and others, 2005) demonstrated the geometrical complexity and lateral variation of the mid-crustal conductive layer, indicating strong structural control.

Optimally smooth models from four profiles crossing the Yarlung-Zangbo suture from the Northwestern Himalaya at 77° E to the INDEPTH profiles at 92° E along over 1,000 km of the southern margin of the Tibetan plateau show remarkable similarity (Unsworth and others, 2005), testifying to the uniformity of regional-scale processes.

Recently, the INDEPTH MT data (Fig. 1, blue squares) have been augmented by BBMT measurements by the China University of Geosciences Bejing (CUGB). These MT measurements have been made across the central part of the plateau west of the INDEPTH 400 and 600 profiles essentially along the Bangong-Nujiang suture, and along the Yarlung-Zangbo suture both to the west and east of the INDEPTH 100 and 700 profiles with two additional suture-crossing profiles (Fig. 1, red circles). Images at various depths have been generated from these INDEPTH+CUGB data of the regional resistivity variations across the Plateau. The crust exhibits lateral variations on rather small wavelengths, whereas the mantle exhibits strikingly strong east-west and north-south variation, with resistive mantle to the east and north, and more conducting mantle in the centre and west.

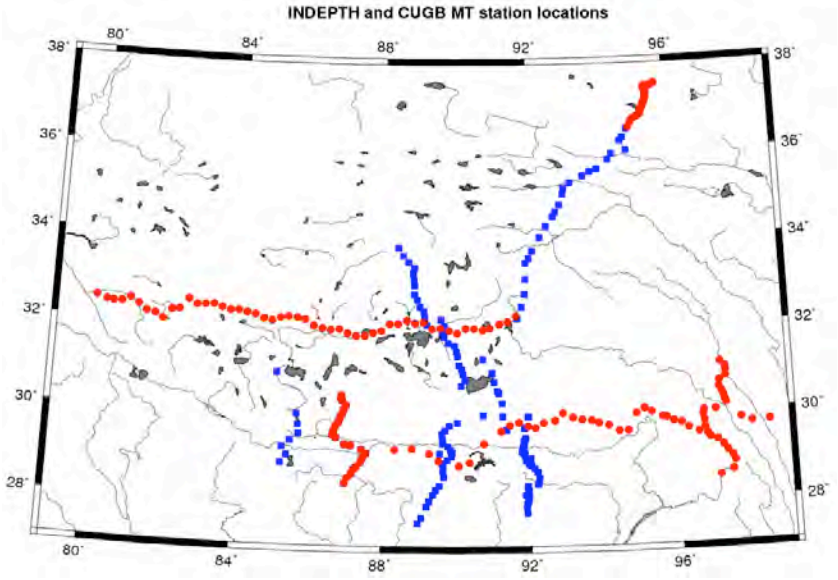

Figure 1. Modern MT site locations on the Tibetan Plateau. **Blue squares** are those of INDEPTH, and are a mixture of BBMT-only and BBMT+LMT. **Red circles** are those of CUGB, and are BBMT-only.

References

Chen, L., and others, 1996, Electrically conductive crust in southern Tibet from INDEPTH magnetotelluric surveying, Science, 274, 1694-1696.

Li, S., and others, 2003, Partial melt or aqueous fluid in the mid-crust of southern Tibet? Constraints from INDEPTH magnetotelluric data, Geophys. J. Internat., 153, 289-304.

Nelson, K.D., and others, 1996, Partially molten middle crust beneath southern Tibet: an initial synthesis of Project INDEPTH results, Science, 274, 1684-1688.

Solon, K., and others, 2005, Structure of the crust in the vicinity of the Banggong-Nujiang suture, central Tibet from INDEPTH magnetotelluric data, J. Geophys. Res., 110, B10102, doi: 10.1029/2003JB002405.

Unsworth, M., and others, 2004, Crustal and upper mantle structure of northern Tibet imaged with magnetotelluric exploration, J. Geophys. Res., 109, B02403-1 - B02403-18, doi:10.1029/2002JB002305.

Unsworth, M.J., and others, 2005, Crustal rheology of the Himalaya and Southern Tibet inferred from magnetotelluric data, Nature, 438, 78-81, doi:10.1038/nature04154.

Wei, W., and others, 2001, Widespread fluids in the Tibetan crust, Science, 292, 716-718.

Cite as: Wei W., Jin S., Ye G., Menzel-Jones, A.G., Unsworth, M.J. and the INDEPTH MT Team, 2010, Regional resistivity structure of the Tibetan Plateau, 2010, *in* Leech, M.L., and others, eds., Proceedings for the 25th Himalaya-Karakoram-Tibet Workshop: U.S. Geological Survey, Open-File Report 2010-1099, 2 p. [http://pubs.usgs.gov/of/2010/1099/wei/].

19 Ma Ductile E–W Extension associated with Normal Faulting in the Kung Co area, Southern Tibet

Mayumi Mitsuishi[1], Simon R. Wallis[1], Mutsuki Aoya[2], Jeffrey Lee[3], Martin Whitehouse[4]

[1] Department of Earth & Planetary Sciences, Graduate School of Environmental Studies, Nagoya University, Nagoya 464-8601, Japan, mitsuishi.mayumi@f.mbox.nagoya-u.ac.jp
[2] Institute of Geology and Geoinformation, National Institute of Advanced Industrial Science and Technology (AIST), Central 7, Tsukuba 305-8567, Japan
[3] Department of Geological Sciences, Central Washington University, Ellensburg, U.S.A.
[4] Laboratory for Isotope Geology, Swedish Museum of Natural History, Box 50007, SE-104 05, Stockholm, Sweden

Active tectonics in the central part of Tibet is dominated by a linked set of strike-slip and N–S trending normal faults. The normal faulting acts to reduce the overall height of the plateau despite the ongoing convergence of India with Asia. The age at which N–S normal faulting began marks the time when the horizontal deviatoric stresses changed from compressional to extensional and many workers relate this to the time at which the Plateau reached its maximum elevation (e.g. Molnar and others, 1993). Obtaining age constraints for the onset of N–S trending normal faulting is therefore an important topic in understanding the evolution of the region. Dates for the initiation of movement on the major N–S normal faults are generally around 10–14 Ma (Coleman and Hodges, 1995, Garzione and others, 2000). The presence of N–S oriented dykes with intrusion ages of around 18 Ma (Williams and others, 2001) suggests extension may have begun earlier. In this contribution we present evidence for E-W ductile extension at around 19 Ma associated with a major normal fault in the Kung Co area. This ranks with the oldest previously known examples of extension and is a rare documented example of ductile flow associated with E–W extension in this region.

The Kung Co region is located to the north of the Mt Everest and contains a well-developed N–S trending fault (Figure 1). This fault cuts a granite body—the Kung Co granite—that intrudes metasediments (Fig. 2). In this study, we combine ASTER remote-sensing analysis, field studies, microstructural observations and the results of U–Pb dating to determine the relationship between granite intrusion, deformation structures, and normal faulting and constrain the age of the onset of E–W extension in this area.

ASTER remote-sensing data and field studies shows that the Kung Co normal fault trends roughly NNW-SSE but also bends and locally trends both N-S and NW-SE (Figure 2). The lowermost parts of the facets dip 50° to 60° W. Slickenline data suggest a dip-slip movement compatible with the distribution of bedding suggested by ASTER images. Moreover, in the Kung Co area two stages of widespread penetrative ductile deformation, D1 and D2, can be defined. Foliation S2 associated with D2 trends NW to SW and dips at a high angle. The flow direction associated with D2 is roughly E-W and the shear sense is dominantly top-to-the-W to NW. Therefore, the kinematics of D2 ductile deformation is close to the brittle normal faulting.

Field studies and microstructural observations were used to determine the relative timing of granite intrusion and ductile deformations. The granite intrusion cross-cuts D1 deformation fabrics showing D1 was complete at the time of intrusion. In contrast, dyking associated with the granite is locally folded by D2 deformation suggesting intrusion predates D2. However, dykes locally cut D2 fabrics without clear deformation. In addition, andalusite formed in the contact metamorphic aureole shows synkinematic growth during D2 deformation. These observations show the granite intrusion was synchronous with D2 deformation.
U-Pb zircon spot ages show the Kung Co granite crystallized at 19.1 ± 0.5 Ma suggesting D2 ductile deformation representing E–W to NW–SE extension was already active at 19 Ma. The similarities of kinematics between D2 ductile deformation and brittle normal faulting indicate that the two styles of deformation may represent a continuous process. The age for the onset of E–W extension in the Kung Co area overlaps with the age of N–S extension in Everest area (i.e., 19-22 Ma; Hodges and others, 1992). Therefore, a tectonic model is needed that can explain N–S movements occurring at the same time as E–W movements.

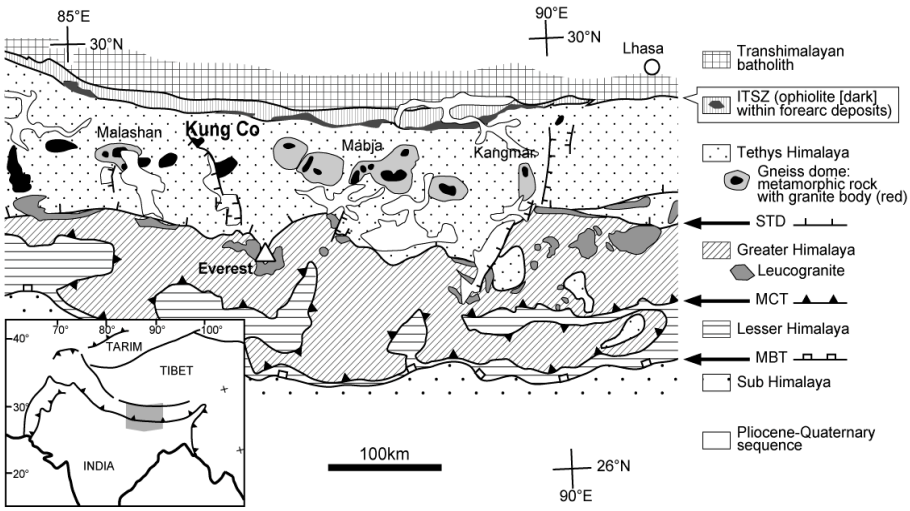

Figure 1. Tectonic map of southern Tibet (modified from Burchfiel and others, 1992) showing Kung Co area. ITSZ = Indus Tsangpo Suture Zone; STD = South Tibetan Detachment system; MCT = Main Central Thrust; MBT = Main Boundary Thrust.

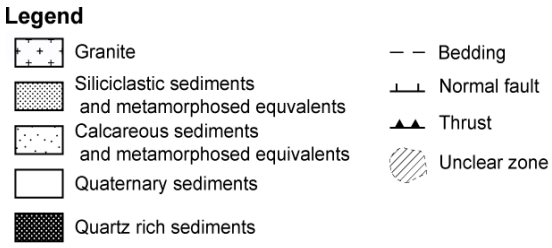

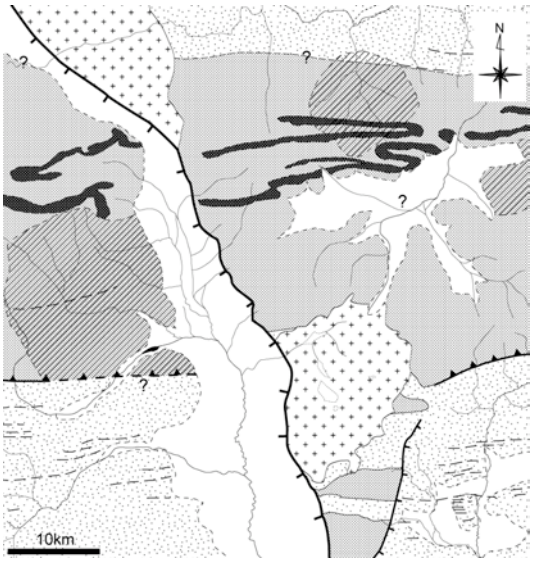

Figure 2. Geological map of Southern Tibet, Kung Co area.

References

Coleman, M. and Hodges, K., 1995, Evidence for Tibetan Plateau Uplift before 14-Myr Ago from a New Minimum Age for East-West Extension, Nature, 372, 49-52.

Garzione, N. C., and others, 2000, High times on the Tibetan Plateau: Paleoelevation of the Thakkhola graben, Nepal, Geology, 28, 339-342.

Hodges, K. V., and others, 1992, Simultaneous Miocene extension and shortening in the Himalayan orogen, Science, 258, 1466-1470.

Molnar, P., and others, 1993, Mantle dynamics, uplift of the Tibetan Plateau, and the Indian Monsoon, Rev. Geophys, 31, 357-396.

Williams, H., and others, 2001, Age and composition of dikes in Southern Tibet: new constraints on the timing of east-west extension and its relationship to postcollisional volcanism, Geology, 29, 339-342.

Cite as: Mitsuishi, M., Wallis, S.R., Aoya, M., Lee, J. and Whitehouse, M., 2010, 19 Ma Ductile E-W Extension associated with Normal Faulting in the Kung Co area, Southern Tibet, *in* Leech, M.L., and others, eds., Proceedings for the 25th Himalaya-Karakoram-Tibet Workshop: U.S. Geological Survey, Open-File Report 2010-1099, 2 p. [http://pubs.usgs.gov/of/2010/1099/mitsuishi/].

Newly Formulated Attenuation Relationship and Seismic Hazard Assessment for Muzaffarabad, Pakistan

MonaLisa[1], M. Qasim Jan[2]

[1]Department of Earth Sciences, Quaid-i-Azam University, Islamabad, Pakistan, lisa_qau@yahoo.com
[2]National Centre of Excellence in Geology, university of Peshawar, Pakistan

The region/site-specific attenuation equation has been established for the site of Muzaffarabad, using the global data bank of accelerograms and local strong-motion data (already existing data and the data generated in the present study). A comprehensive database has been compiled using the global data bank (i.e. strong motion records from on-line data banks of European Strong-motion Data, and the COSMOS Virtual Data Center); and the local data bank (i.e. the strong motion data of WAPDA, Nilore and PMD). We removed uncertainties involved in this attenuation equation for Muzaffarabad.

Peak ground accelerations using a catalogue containing instrumentally recorded events of magnitude 4 and greater have been calculated. Seismic source regions are modelled to establish relationships between earthquake magnitude and earthquake frequency. Seismic hazard curves have been generated based on probable Peak Ground Acceleration (PGA) for 10% probability of exceedance for time-spans of 50 years (return period of 475 years) using the EZ FRISK software. The newly formulated attenuation equation has been used for the purpose. Twelve faults have been selected as the critical seismogenic features and their maximum potential magnitudes determined using four regression relations. The MBT with a maximum potential magnitude of 8.1 and PGA value of 0.25g is designated as the most critical tectonic feature for the site of Muzaffarabad.

Cite as: MonaLisa and Jan, M.Q., 2010, Newly formulated attenuation relationship and seismic hazard assessment for Muzaffarabad, Pakistan, in Leech, M.L., and others, eds., Proceedings for the 25th Himalaya-Karakoram-Tibet Workshop,: U.S. Geological Survey, Open-File Report 2010-1099, 1 p. [http://pubs.usgs.gov/of/2010/1099/monalisa/].

Recent Deep Seismic Refraction/Wide-angle Reflection Profiles in Western China

Walter D. Mooney[1], Nihal Okaya[1] , Chungyong Wang[2] , Zhongjie Zhang[3], Junmeng Zhao[4]

[1] Earthquake Science Center, U.S.Geological Survey, Menlo Park, CA 94025, U.S.A., mooney@usgs.gov
[2] Institute of Geophysics, China Earthquake Administration, Beijing, China
[3] Institute of Geology and Geophysics, Chinese Academy of Sciences, Beijing, China
[4] Institute of Tibetan Research, Chinese Academy of Sciences, Beijing, China

The deep crustal structure of western China has been investigated in the past several decades with multiple geophysical techniques, including gravity, magnetic, magnetotellurics, seismic surface waves and receiver functions, seismic reflection profiles, and seismic refraction/wide-angle reflection profiles. Here we review new results obtained by the last technique, compare them with previous results, and discuss the implications for the tectonic evolution of western China (Liu and others, 2006; Li and others, 2006; Mooney, 2007; Zhang and others, 2009; Wang and others, 2009).

Northern Margin of the Tibetan Plateau

We examined the northern margin of the plateau with a seismic refraction/wide-angle reflection profile across the Altyn Tagh Range and its adjacent basins and found that the crustal velocity structure and compositional interpretation sharply change beneath the Cherchen Fault, that is, ~100 km north of the northern margin of the Tibetan Plateau. North of the Cherchen Fault, beneath the Tarim Basin, a platform-type crust is evident. South of the Cherchen Fault, the crust is characterized by a missing high-velocity, lower-crustal layer. The high topography (~3 km) of the Altyn Tagh Range is supported by a wedge-shaped region of 7.6-7.8 km/s that we interpret as a zone of crust-mantle mix. Our seismic velocity structure supports the viscous sheet model for the origin of the Altyn Tagh Range (England and McKenzie, 2007). The Altyn Tagh Range formed by crustal-scale strike-slip motion along the North Altyn Tagh Fault and by northeastward extrusion. Contraction across the Altyn Tagh Range is accommodated by (1) crustal thickening via upper-crustal thrusting and lower-crustal flow and (2) slip-parallel (SW-directed) underthrusting of only the lower crust and mantle of the eastern Tarim Basin.

The central Qaidam Basin, the largest basin within the Qinghai-Tibetan plateau, was investigated with a detailed seismic wide-angle reflection/refraction profile. The 350-km-long profile extends from the northern margin of the East-Kunlun Shan to the southern margin of the Qilian Shan. The P- and S-wave velocity structure and Poisson's ratio data provide constraints on composition. The crust here consists of a near-surface sedimentary layer and a four-layered crystalline crust having several significant features: (1) The sedimentary fill of the Qaidam Basin reaches a maximum thickness of 8 km, and the basin shape mirrors the uplifted Moho. (2) Within the four layers of the crystalline crust, P- (S-) wave velocities increase with depth and fall within the following velocity ranges: 5.9-6.3 km/s (3.45-3.65 km/s), 6.45-6.55 km/s (3.7 km/s), 6.65 km/s (3.8 km/s), and 6.7-6.9 km/s (3.8-3.9 km/s), respectively. (3) Low-velocity zones with a 3 to 5 percent reduction in seismic velocity are detected in the lower half of the crust beneath the Qaidam Basin and its transition to the Qilian Shan. (4) The crystalline crust is thickest beneath the northern margin of the basin towards the Qilian Shan (58-62 km) and thinnest beneath the center of the basin (52 km). Variations in crustal thickness are mostly due to thickness variations in the lowermost layer of the crust. (5) Poisson's ratio and P-wave velocity values suggest that the Qaidam crust has an essentially felsic composition with an intermediate layer at its base. Based on the crustal structure reported here, we suggest that late Cenozoic convergence is accommodated by thick-skinned tectonic deformation with thickening involving the entire crust across the Kunlun-Qaidam-Qilian system.

The Northeastern Tibetan Plateau (Tarim Basin to Sichuan Basin)

We obtained a deep crustal section across the northeastern Tibetan Plateau based on active-source seismic data. Our profile was recorded along a 1,600-km-long profile crossing the southern Tarim Basin, the western flank of the South-Qilian Shan, the northeastern margin of Qaidam basin, East-Kunlun Shan, Songpan-Ganzi terrane, and Sichuan Basin. The crustal P- and S-wave velocity structure and Poisson's ratio outline the seismic characteristics of the crust and provide constraints on the crustal composition. The resultant crustal cross-section shows several significant features: (1) The crustal thickness varies considerably along this profile. North of the Kunlun Fault, variations in crustal thickness and topography correlate well. The crust thickens from 48 km below the Tarim Basin to 70 km beneath the northeastern

margin of the Qaidam Basin, and then thins to 56 km beneath the eastern flank of the Qaidam Basin. The crust thickens to 70 km beneath the East-Kunlun Shan. Across the Songpan-Ganzi terrane, the crust steadily thins from 70 km just south of the Kunlun Fault to 48 km beneath the Sichuan Basin, despite the fact the topography remains constant across the Songpan-Ganzi terrane and then abruptly drops by 3.5 km from the elevated Longmen Shan into the low-lying Sichuan Basin. (2) North of the Kunlun Fault, variations in crustal thickness are mainly caused by variations in lower-crustal thickness, whereas south of the Kunlun Fault they are caused by variations in upper-, middle- and lower-crustal thickness. (3) North of the Kunlun Fault we detect a mid-crustal low-velocity zone that is not apparent south of the fault. (4) Across the NE Tibetan Plateau, Poisson's ratio has a nearly constant value of 0.24-0.25 in the upper and middle crust, indicating a felsic bulk composition. However, the Kunlun Fault seems to act as a compositional boundary for the lower crust, with a Poisson's ratio of 0.29 north of the fault (Kunlun-Qaidam terranes) and 0.26 south of the fault (Songpan-Ganzi terranes). Measured Poisson's ratio and P-wave velocity values suggest that the lower crust throughout the Tibetan Plateau (South-Qilian Shan, margins of the Qaidam Basin, East-Kunlun Shan, Songpan-Ganzi terrane) is of intermediate composition. Thus the NE Tibetan Plateau along our profile is missing a mafic lower crustal layer. The Tarim Basin, which borders the Tibetan Plateau to the north, shows a typical platform-like crustal structure with a felsic upper and middle, and a mafic lower crust. The Sichuan Basin, which borders the Tibetan Plateau to the east, also has a felsic upper and middle crust, and an intermediate or mafic lower crust.

References

England, P. and McKenzie, D., 2007, A thin viscous sheet model for continental deformation, Geophysical Journal of the Royal Astronomical Society, 70, 2, 295 – 321.

Li, S.-L., Mooney, W.D. and Fan, J.C., 2006, Crustal structure of mainland China from Deep Seismic Sounding Data, Tectonophysics, 420, 239-252.

Liu, M.J., Mooney, W.D., Li, S.L., Okaya, N. and Detweiler, S., 2006, Crustal structure of the northeastern margin of the Tibetan plateau from the Songpan-Ganzi terrane to the Ordos basin, Tectonophysics, 420, 253-266.

Mooney, W.D., 2007, Global Crustal Structure, in The Treatise of Geophysics, Vol. 1, Crust and Mantle, B. Romanowicz and A. Dziewonski, volume editors, G. Schubert, Treatise editor-in-Chief, Elsevier, Netherlands, 361-417.

Wang, C.Y., and others, 2009, Detailed shallow structure of the Kunlun fault zone of the northern Tibetan plateau, China: implications for the Ms 8.1 Kunlun Earthquake, Geophysical Journal International, 177, 978-1000.

Zhang, J.J., and others, 2009, Crustal structure across the Three Gorges area of the Yangtze platform, central China, from seismic refraction/wide-angle reflection data, Tectonophysics, 475, 423-437.

Cite as: Mooney, W.D., Okaya, N., Wang, C., Zhang, Z. and Zhao, J., 2010, Recent Deep Seismic Refraction/Wide-angle Reflection Profiles in Western China, *in* Leech, M.L., and others, eds., Proceedings for the 25th Himalaya-Karakoram-Tibet Workshop: U.S. Geological Survey, Open-File Report 2010-1099, 2 p. [http://pubs.usgs.gov/of/2010/1099/mooney/].

Implications of Himalayan Detrital Zircon Spectra of Cambrian–Ordovician Strata

Paul M. Myrow[1], Nigel C. Hughes[2], John W. Goodge[3], C. Mark Fanning[4], N. Ryan McKenzie[2], Shanchi Peng[5], Om N. Bhargava[6], Suraj K. Parcha[7], Kevin R. Pogue[8]

[1]Department of Geology, Colorado College, Colorado Springs, CO 80903, U.S.A., pmyrow@coloradocollege.edu
[2]Department of Earth Sciences, University of California, Riverside, CA 92521, U.S.A., nigel.hughes@ucr.edu
[3]Department of Geological Sciences, University of Minnesota-Duluth, Duluth, MN 55812, U.S.A.
[4]Research School of Earth Sciences, The Australian National University, Canberra, ACT 0200, Australia
[5]State Key Laboratory on Paleobiology and Stratigraphy, Nanjing Institute of Geology and Paleontology, Nanjing 210008, China
[6]103 Sector 7, Panchkula, Harayana 160020, India
[7]Wadia Institute of Himalayan Geology, Dehra Dun, Uttranchal 248001, India
[8]Department of Geology, Whitman College, Walla Walla, WA 99362, U.S.A.

We present detrital zircon U-Pb age data for eleven Cambrian and Ordovician sandstone samples taken across and along the strike of the Himalaya in Bhutan, Tibet, northern India, and Pakistan, as well as one sample from Cambrian strata of the Indian craton. Detrital zircon age spectra for Cambrian samples of the Himalaya are of particular interest because the Cambrian Period witnessed the final amalgamation of core Gondwana (Cawood and Buchan, 2007). In addition, they are also the only rocks of Phanerozoic age known to occur in all three of the northernmost lithotectonic zones of the Himalaya, comprising sedimentary strata in the Lesser Himalaya (LH) to the south and the Tethyan Himalaya (TH) to the north, as well as protolith for part of the high-grade metamorphic assemblage of the intervening Greater Himalaya (GH). The biostratigraphically constrained depositional ages of the Himalayan strata sampled in this study range from terminal Early Cambrian to Ordovician. Tethyan sample names, ages and locations are as follows. Batal, PV, and Thango: Lower(?) Cambrian, Middle Cambrian, and Ordovician, respectively, Spiti Valley, northern India. MS-2 and MS-5: Cambrian and Ordovician, respectively, Kumaon region, northern India. NY-11: Middle Cambrian, Nyalam region, Tibet. WL-270: Upper Cambrian, Black Mountains, Bhutan. KU2: Middle Cambrian, Zanskar Valley, northern India. MBQ: Ordovician, Nowshera, Pakistan. Lesser Himalaya samples are Tal and Tal–GKM: Lower and Middle/Late Cambrian, northern India.

Eight of the eleven samples show very high p values of paired comparisons (Kolmogorov-Smirnov test). The p values range up to 0.976, and average a high value of 0.418. These very high p values strongly support the assertion of Myrow and others (2009) concerning the detailed correlation of Cambrian strata across the Himalaya to unfossiliferous, relatively high-grade rocks on the slopes of Mt. Everest and adjacent regions. More importantly, the uniformity of the age spectra from the northern Indian margin is remarkable, particularly given the broad geographic range of our samples over a distance of more than 2,000 km.

Myrow and others (2003) presented detrital zircon data from two samples that demonstrated a similarity in age spectra of these lower Paleozoic samples from the LH and TH, with grain ages that span from Archean to Cambrian in both. The data help refute the claim that pre-Permian deposits of the LH contain only Mesoproterozoic and older detritus (DeCelles and others, 2000; DeCelles and others, 2004; Martin and others, 2005; Richards and others, 2005), and instead support the hypothesis that the LH, GH and TH were part of a continuous northern passive margin of the Indian craton from the Neoproterozoic through the Cambrian (e.g., Searle, 1996). Continuity of the three zones is also supported by Cambrian stratigraphy, paleocurrent data and sedimentary facies relationships (Myrow and others, 2003; Hughes and others, 2005; Myrow and others, 2009). A detrital-zircon age spectrum from a Cambrian deposit of cratonic India, sample NAG-2 from the Nagaur Group of Rajasthan, shows large peaks from 0.7 to 1.3 Ga, accompanied by peaks at 1.6–1.7, 1.8, and 2.4–2.7 Ga. The sample lacks grains younger than 737 +/- 9 Ma, but the overall age distribution matches those of Cambrian samples across the Himalaya, including a large proportion of younger (< 1.6 Ga) grains (Myrow and others, 2003; in press).

The presence of the younger grains (< 1.6 Ga) in all these rocks has important implications for tectonic reconstructions and for characterization and mapping of the lithotectonic zones of the Himalaya in general. Specifically, a large fraction of bedrock exposed in the Lesser Himalaya (LH) has depositional ages that are >1.6 Ga, and the old geochronological and geochemical signatures of these rocks have been linked to sediment sources within the Indian craton (DeCelles and others, 2000; Najman, 2006). It is widely accepted that these signatures represent the LH zone, and can thus be used to distinguish it from other zones (e.g., Richards and others, 2005). Greater Himalayan (GH) and Tethyan Himalayan (TH) rocks with younger detrital zircon ages (0.5-1.6 Ga) and less negative ε_{Nd} values are generally considered to have sources in more distal Gondwanan orogenic belts. The younger grains (< 1.6 Ga) of our cratonic sample contradict the idea of a uniquely Indian geochronological signature (> 1.6 Ga grains) for the craton and the hypothesis that the GH and TH are exotic to the LH and the rest of India, and were accreted to the Indian margin during the Cambrian–Ordovician boundary interval (DeCelles and others, 2000; Yoshida and Upreti (2006). A detrital age spectrum from the Tal Formation of the Outer LH suggests continuity of the northern Indian margin and thus rejection of this hypothesis. Recent interpretations of the Krol-Tal Belt as a far-transported unmetamorphosed thrust sheet that roots into the GH or TH (Richards and others, 2005; Yoshida and Upreti, 2006; Célérier and others, 2009) are consistent with the general view that the entire LH consists of strata derived from older (> 1.6 Ga) source rock. However, our stratigraphic and geochronologic data clearly demonstrates that that the Outer LH was part of a proximal facies realm, distinct from the TH zone, and that it was part of a Neoproterozoic–Cambrian succession that would have overlain the older inner LH and extended south onto the Indian craton and north across the Tethyan realm.

References

Cawood, P.A. and Buchan, C., 2007, Linking accretionary orogenesis with supercontinent assembly, Earth-Science Reviews, v. 82, p. 217-256.

Célérier, J., Harrison, T.M., Webb, A.A. and Yin, A., 2009, The Kumaun and Garwhal Lesser Himalaya, India. Part 1: Structure and stratigraphy, Geological Society of America Bulletin 121, 1281-1297.

DeCelles, P.G., and others, 2004, Detrital geochronology and geochemistry of Cretaceous–Early Miocene strata of Nepal: implications for timing and diachroneity of initial Himalayan orogenesis, Earth and Planetary Science Letters, v. 227, p. 313-330.

DeCelles, P.G., Gehrels, G.E., Quade, J., LaReau, B. and Spurlin, M., 2000, Tectonic implications of U-Pb zircon ages of the Himalayan orogenic belt in Nepal, Science, v. 288, p. 497-499.

Hughes, N.C., and others, 2005, The Cambrian biostratigraphy of the Tal Group, Lesser Himalaya, India, and early Tsanglangpuan (late early Cambrian) trilobites from the Nigali Dhar syncline, Geological Magazine, v. 142, p. 57-80.

Myrow, P.M., Hughes, and others, 2003, Integrated tectonostratigraphic reconstruction of the Himalaya and implications for its tectonic reconstruction, Earth and Planetary Science Letters, v. 212, p. 433-441.

Myrow, P.M., and others, 2009, Stratigraphic correlation of Cambrian–Ordovician deposits along the Himalaya: implications for the age and nature of rocks in the Mt. Everest region: Geological Society of America Bulletin, v. 120, p. 323-332.

Myrow, P.M., and others, in press, 2010, Extraordinary transport and mixing of sediment across Himalayan central Gondwanaland during the Cambrian-Ordovician, Geological Society of America Bulletin.

Najman, Y., 2006, The detrital record of orogenesis: a review of approaches and techniques used in Himalayan sedimentary basins, Earth-Science Reviews 74, 1-72.

Richards, A., and others, 2005, Himalayan architecture constrained by isotopic markers from clastic sediments, Earth and Planetary Science Letters 236, 773-796.

Searle, M.P., 1996, Cooling history, erosion, exhumation, and kinematics of the Himalaya–Karakoram–Tibet orogenic belt, in Yin, A., and Harrison, T. M., eds., Tectonics of Asia: Cambridge, England, Cambridge University Press (Rubey Volume), p. 110-137.

Yoshida, M. and Upreti, B.N., 2006, Neoproterozoic India within east Gondwana: constraints from recent geochronological data from Himalaya, Gondwana Research, v. 10, p. 349-356.

Cite as: Myrow, P.M., and others, 2010, Implications of Himalayan Detrital Zircon Spectra of Cambrian–Ordovician Strata, *in* Leech, M.L., and others, eds., Proceedings for the 25th Himalaya-Karakoram-Tibet Workshop: U.S. Geological Survey, Open-File Report 2010-1099, 2 p. [http://pubs.usgs.gov/of/2010/1099/myrow/].

Structure of the Crust and Upper Mantle and Seismic Sources in the Himalaya-Tibet Region: Summary of Results from the Hi-CLIMB Experiment

John Nabelek[1], Gyorgy Hetenyi[2], Jerome Vergne[3], Arnaud Burtin[4], Jan Baur[1], Laurent Bollinger[4], Rodolphe Cattin[5], Som Sapkota[6], Heping Su[7], Project Hi-CLIMB Team

[1] College of Oceanic and Atmospheric Sciences, Oregon State University, Corvallis, OR 97331, U.S.A.
[2] Earth Sciences Department, ETH Zurich, 8092 Zurich, Switzerland
[3] Ecole et Observatoire des Sciences de la Terre, CNRS–UMR7516, 67084 Strasbourg, France
[4] CEA/DAM/DIF 91297 Arpa jon Cedex, France
[5] Laboratoire de Geologie, Ecole Normale Superieure de Paris-CNRS, F-75231, Paris Cedex 05, France
[6] National Seismological Center, Department of Mines and Geology, Lainchaur, Kathmandu, Nepal
[7] Institute of Geology, Chinese Academy of Geological Sciences, Beijing, People's Republic of China

The 2002-2005 Hi-CLIMB (Himalayan-Tibetan Continental Lithosphere during Mountain Building) field experiment deployed 233 broadband seismic stations in the Himalaya-Tibet region. The centrepiece of the project was a closely spaced, 800-km-long linear array of broadband seismometers extending northward from the Ganges Basin (27°N), across the Himalayas, the Yarlung Tsangpo Suture (YTS), and the Banggong-Nujiang Suture (BNS) to the central Tibet (34°N). A sparser network of stations in Nepal and southern Tibet flanked the main linear array. By now, various studies have been published by different groups based on the Hi-CLIMB data set. Here we present a summary of the results related to crustal and upper-mantle structure and seismic sources, both conventional and non-conventional.

Using the linear seismic array we have constructed images of the crust and upper mantle beneath the Himalaya and the southern Tibetan Plateau (Nábělek and others, 2009; Vergne and others, 2005; Wittlinger and others, 2009). The images reveals in a continuous fashion the Main Himalayan thrust fault as it extends from a shallow depth under Nepal to the mid-crust under southern Tibet. Indian crust can be traced to 31°N. The crust-mantle interface beneath Tibet is anisotropic, indicating shearing during its formation. The dipping mantle fabric suggests that the Indian mantle is subducting in a diffuse fashion along several evolving sub-parallel structures. Reverse south-verging processes appear to have formed the lower crust and upper mantle north of 31°N.

The Main Himalayan thrust (MHT) fault, the detachment along which the India plate descends beneath the Himalaya and southern Tibet, is characterized by a velocity decrease, extending from shallow depths under Nepal to mid-crustal depths in the Lhasa Block. Beneath Nepal, the MHT partially underthrusts low-velocity sediments from the Ganges Basin under the Lesser Himalaya formations (Vergne and others, 2005). The sharp velocity decrease associated with this part of the MHT possibly reflects the presence of water released from the underthrust sediments and trapped beneath by clay-bearing fault gauge. The induced over-pressure of the trapped fluid decreases the fault strength and enables low-angle thrusting in this zone characterized by large earthquakes. In contrast, the velocity decrease associated with the deeper, creeping section of the MHT is probably caused by increased ductility and local partial melting.

The Moho is a prominent conversion seen along the entire profile. In the south, it dips gently from a depth of 40 km beneath the Ganges Basin on the Indian Plate to 50 km beneath the Himalayas. North of the Great Himalaya, the Moho deepens more rapidly, reaching a depth of 70 km north of the YTS. From this point, in the Lhasa Block, the Moho signal is at a constant depth over the next 200 km. The Moho becomes less clearly defined in the Northern Lhasa Block. It reappears as a strong interface north of the BNS, under the Qiangtang Block, but at a shallower depth of about 65 km.

These changes in crustal thickness do not correlate with the topography in the region between the Greater Himalaya and the YTS. This lack of relation indicates that the region is in regional isostatic compensation involving high density (high velocity) lower crust and mantle and support from flexural strength of the Indian plate. The thinner crust of the Qiangtang Block appears to be compensated by a lower density and lower velocity mantle and thus is distinctly different from the southern Lhasa Block.

The lowermost crust in the southern Lhasa Block is characterized by strong velocity-depth gradient and can be traced, albeit much less clearly, to shallower depths under Nepal. On the basis of gravity anomalies, this lower-crustal layer, probably of amphibolitic composition beneath Nepal, has been at least partially transformed into eclogite due to high-grade metamorphic reactions (Hetényi and others, 2007).

Modelling gravity and the shape of the subducted Indian crust (Hetényi and others, 2006) shows that (1) the effective elastic thickness (EET) of the India Plate decreases northwards from 60–80 to 20–30 km as it is flexed down beneath Himalaya and Tibet; (2) the only resistant layer of the India Plate beneath southern Tibet is the upper mantle, which serves as a support for the topographic load and (3) the most abrupt drop in the EET, located around 200 km south of the MFT, is associated with a gradual decoupling between the crust and the mantle.

Continuous seismic data recorded along the steep, narrow and deeply incised channel of the Trisuli River show clear seismic noise amplitude correlation with both regional meteorological and hydrological data along the river (Burtin and others, 2008). Seasonal increase in river-induced noise coincides with the strong monsoon rainfall and the rapid melting of snow and ice in the high elevations. The seismic noise exhibits a time hysteresis of the noise amplitude versus the water level suggesting that vibrations generated by bed-load transport are the main mechanism for the noise generation. This suggests that, if calibrated, seismic noise may be used to monitor the river bed load in a continuous fashion.

The Hi-CLIMB data have been also use to locate debris flows (Burtin and others, 2008), unusual low-frequency events (Vergne and others, 2008) and regional earthquakes (Baur and others, 2008).

References

Baur, J., and others, 2008, Correlation of topography and earthquakes along the Himalayan arc, Eos Trans. AGU, 89(52), Fall Meet. Suppl., Abstract T53E-2005.

Burtin, A., Bollinger, L., Vergne, J., Cattin, R. and Hetényi, J.L., 2008, Spectral analysis of seismic noise induced by rivers: A new tool to monitor spatiotemporal changes in stream hydrodynamics, Journal of Geophysical Research, VOL. 113, B05301, doi:10.1029/2007JB005034.

Burtin, A., Bollinger, L., Cattin, R., Vergne, J. and Nábělek, J.L., 2009, Spatiotemporal sequence of Himalayan debris flow from analysis of high-frequency seismic noise, J. Geophys. Res., 114, F04009, doi:10.1029/2008JF001198.

Hetényi G., Cattin, R., Vergne, J. and Hetényi, J.L., 2006,The Effective Elastic Thickness of the India Plate from Receiver Function Imaging, Gravity Anomalies and Thermo-mechanical Modeling, Geophysical Journal International, 167 (3), 1106-1118, doi: 10.1111/j.1365-246X.2006.03198.x .

Hetényi, G., and others, 2007, Density distribution of the India plate beneath the Tibetan plateau: Geophysical and petrological constraints on the kinetics of lower-crustal eclogitization, EPSL, doi:10.1016/j.epsl.2007.09.036.

Nábělek, J., and others, 2009, Underplating in the Himalaya-Tibet collision zone revealed by the Hi-CLIMB experiment, Science, 325, 1371-1374.

Vergne, J., Nábělek, J.L. and the Hi-CLIMB Team, 2005, Geometry and Characteristics of the Main Himalayan Thrust in Nepal/Tibet Revealed by the Hi-CLIMB Seismological Experiment, Eos Trans. AGU, 86, Fall Meet. Suppl..

Vergne J., Nábělek, J.L., Rivera, L., Bollinger, L. and Burtin, A., 2008, Non Conventional Seismic Events Along the Himalayan Arc Detected in the Hi-Climb Dataset, Eos Trans. AGU, 89(53), Fall Meet. Suppl., Abstract S41C-1857.

Wittlinger, G., Farra, V., Hetényi, G., Vergne, J. and Nábělek, J.L., 2009, Seismic velocities in Southern Tibet lower crust: a receiver function approach for eclogite detection, Geophysical Journal International, 177, 1037–1049, doi: 10.1111/j.1365-246X.2008.04084.x.

Cite as: Nabelek, J., and others, 2010, Structure of the crust and upper mantle and seismic sources in the Himalaya-Tibet region: Results summary from the Hi-CLIMB, *in* Leech, M.L., and others, eds., Proceedings for the 25th Himalaya-Karakoram-Tibet Workshop: U.S. Geological Survey, Open-File Report 2010-1099, 2 p. [http://pubs.usgs.gov/of/2010/1099/nabelek/].

The Age of India-Asia Collision: Biostratigraphic, Sedimentological and Paleomagnetic Constraints

Yani Najman[1], Erwin Appel[2], Marcelle Boudagher-Fadel[3], Paul Bown[3], Andy Carter[4], Eduardo Garzanti[5], Laurent Godin[6], Jingtai Han[7], Ursina Liebke[2], Grahame Oliver[8], Randy Parrish[9], Giovanni Vezzoli[5]

[1] Lancaster Environment Centre, Lancaster University, Lancaster, LA1 4YQ, UK. y.najman@lancs.ac.uk
[2] Institut für Geowissenschaften, Zentrum für Angewandte Geowissenschaften Arbeitsbereich Geophysik, Universität Tuebingen, 72076 Tübingen, Germany
[3] Department of Earth Sciences, University College London, London, WC1E 6BT, UK
[4] Department of Earth Sciences, Birkbeck College, University of London, London, WC1E 6BT, UK
[5] Dipartimento di Scienze Geologiche e Geotecnologie, Universita Di Milano-Bicocca, Milano 20126, Italy
[6] Dept Geological Sciences & Geological Engineering, Queen's University, Kingston, Ontario, K7L 3N6, Canada
[7] School of Geography and Geology, University of St Andrews, North Street, St Andrews, Fife KY16, UK
[8] Institute of Geology and Geophysics, Chinese Academy of Sciences, 100029, Beijing, PR China
[9] NERC Isotope Geosciences Laboratories, BGS Keyworth, Nottingham, NG12 5GG, UK

Determining the timing of India-Asia collision is critical for understanding crustal deformation processes, and for evaluating the potential influence of Himalayan orogenesis on global climate and ocean geochemistry (e.g. Raymo and Ruddiman, 1998; Richter and others, 1992). The majority of published work dates collision between ~55-50 Ma, with some younger and some older ages proposed (e.g. Garzanti and others, 1987; Jaeger and others, 1989; Klootwijk and others, 1992; De Sigoyer and others, 2000; Aitchison and others, 2007, to quote just a few of the numerous references), the range to some extent being the result of different definitions of collision and methods used to date it. In this paper we use three approaches to date collision: the time of cessation of marine facies in the suture zone; the time of first arrival of Asian detritus on the Indian plate; and paleomagnetic constraints on the positions of Indian and Asian continents through time. In the Qumiba sedimentary section in southern Tibet, our biostratigraphic data indicates the youngest marine facies preserved at this locality to be of 50.6-52.8 Ma age. First arrival of Asian material on the Indian plate occurs at this time at this location, as determined by petrography, U-Pb and fission-track dating of detrital zircons. Our reconstructions of the relative positions of India and Asia using a compilation of published paleomagnetic data indicates initial contact between the continents at 55-50 Ma. Both our biostratigraphic data and our paleomagnetic interpretations contradict a recent assertion that proposes that collision could not have occurred before ~34 Ma (Aitchison and others, 2007), based on the view that paleomagnetic data show the continents to be a considerable distance apart at 55 Ma, that marine facies at the Qumiba section persisted until ca. 35 Ma and that these data, coupled with a number of other lines of geological evidence, “demand” that collision occurred no earlier than the Oligocene. We discuss each of these lines of evidence and conclude that the assertion that geological and paleomagnetic evidence “demand” an Oligocene age of collision is overstated: whilst it may be a viable theory, the quoted evidence is not incompatible with collision at 55-50 Ma as Aitchison and others (2007) propose.

References

Aitchison, J. C., Ali, J.R. and Davis, A.M., 2007, When and where did India and Asia collide?, Journal of Geophysical Research, 112, B05423, doi:05410.01029/02006JB004706.

de Sigoyer, J., and others, 2000, Dating the Indian continental subduction and collisional thickening in the northwest Himalaya: Multichronology of the Tso Morari eclogites, Geology, 28, 487-490.

Garzanti, E., Baud, A. and Mascl, G., 1987, Sedimentary Record of the Northward Flight of India and Its Collision with Eurasia (Ladakh Himalaya, India), Geodin. Acta, 1(4-5), 297-312.

Jaeger, J. J., Courtillot, V. and Tapponnier, P., 1989, Paleontological View of the Ages of the Deccan Traps, the Cretaceous Tertiary Boundary, and the India-Asia Collision, Geology, 17, 316-319.

Klootwijk, C. T., and others, 1992, An Early India-Asia Contact - Paleomagnetic Constraints from Ninetyeast Ridge, ODP Leg 121, Geology, 20, 395-398.

Raymo, M. E. and Ruddiman, W. F., 1988, Influence of late Cenozoic mountain building on ocean geochemical cycles., Geology, 16, 649-653.

Richter, F. M., Rowley, D.B and DePaulo, D.J., 1992, Sr Isotope Evolution of Seawater - the Role of Tectonics, Earth Planet. Sci. Lett., 109(1-2), 11-23.

Cite as: Najman, Y., and others, 2010, The Age of India-Asia Collision: Biostratigraphic, Sedimentological and Paleomagnetic Constraints, *in* Leech, M.L., and others, eds., Proceedings for the 25th Himalaya-Karakoram-Tibet Workshop: U.S. Geological Survey, Open-File Report 2010-1099, 1 p. [http://pubs.usgs.gov/of/2010/1099/najman/].

Role of GIS in Geological Data Interpretation, Map Making and Data Storage: A Case Study from the Nepal Himalaya

T. Ojha[1], P.G. DeCelles[1], J. Quade[1], George Gehrels[1], P. Kapp[1], Craig Wissler[2], D.M. Robinson[3], M. A. Murphy[4]

[1] Department of Geosciences, University of Arizona, Tucson, AZ 85721, U.S.A., ojha@email.arizona.edu
[2] School of Natural Resources, University of Arizona, Tucson, AZ 85721, U.S.A.
[3] Department of Geological Sciences, University of Alabama, Tuscaloosa, AL 35487, U.S.A.
[4] Department of Geosciences, University of Houston, Houston, TX 77204, U.S.A.

The use of GIS in petroleum, mining, and geo-environmental industries has long been recognized, but examples of GIS-based geospatial database development for small-scale structural analysis, geological mapping, and map compilation are relatively few. The power of GIS for spatial data analysis makes it a very important tool to compile and enhance geological maps. Using this technique we have compiled a new geological map of the far west Nepal Himalaya. This region contains exemplary geological features related to the ongoing collision between India and Asia. Although geological mapping has been underway in the Nepal Himalaya since the mid 18th century, systematic geological mapping did not start until the 1970s. Geological mapping conducted by Nepalese geologists in far western Nepal is based on regional geological correlation without the advantage of geochronology and systematic structural analysis. Geological investigations in far west Nepal since 1994 by a team of students and researchers from the University of Arizona involved geological mapping followed by detailed geochronological, geochemical, petrologic, and structural analytical work. Our new map combines results of this recent work with the earlier work by Nepal Government geologists. Himalayan tectonostratigraphy is complicated and involves numerous, thrust-bounded units ranging in age from Mio-Pliocene foreland basin deposits to Paleoproterozoic metasedimentary and meta-plutonic rocks. Major structures include active frontal and possibly out-of-sequence thrusts, a regional-scale duplex, major thrust faults with >100 km of displacement, and imbricate thrusts and related folds.

This project is focused on building a geospatial data model by integrating geochronological, geological, seismological, petrographic, and geochemical datasets from far west Nepal. The large data set integrated in this model may lead to better understanding of Himalayan geological history. The stepwise process includes the collection of all available geological, topographical, seismic, geochronological and geochemical information in the form of vector and raster spatial data, tables, and reports. With the available information a new geological map of far west Nepal was compiled in GIS using ESRI ArcMap 9.3. Several data layers were developed and hyperlinked with the newly revised geological map; this will allow users to access supporting data from the map directly. In general this study describes the process of geological data compilation, query, visualization, and analysis for map compilation and data storage in the GIS platform for the better understanding of regional structural and kinematic history of far western Nepal Himalaya. Ongoing work involves updating and overlaying geological mapping from all of Nepal onto our seamless topographic base for the entire country.

Cite as: Ojha, T., and others, 2010, Role of GIS in Geological Data Interpretation, Map Making and Data Storage: A Case Study from the Nepal Himalaya, *in* Leech, M.L., and others, eds., Proceedings for the 25th Himalaya-Karakoram-Tibet Workshop: U.S. Geological Survey, Open-File Report 2010-1099, 1 p. [http://pubs.usgs.gov/of/2010/1099/ojha/].

Style and Timing of Glaciation along the Karakoram Fault

Lewis A. Owen[1], Marc W. Caffee[2], Nicole Davis[1], Jason Dortch[1], Robert C. Finkel[3], Kathyrn Hedrick[1], Alexander C. Robinson[4], Lindsay Schoenbohm[5], Yeong Bae Seong[6]

[1] Department of Geology, University of Cincinnati, Cincinnati, OH 45221, U.S.A., lewis.owen@uc.edu
[2] Department of Physics/PRIME Laboratory, Purdue University, West Lafayette, IN 47906, USA
Institute for Tibetan Plateau Research, Chinese Academy of Sciences, Beijing, 100085, China
[3] Department of Earth and Planetary Sciences, University of California, Berkeley, CA 95064, U.S.A. and Centre Européen de Recherche et d'Enseignement des Géosciences de l'Environnement, 13545 Aix en Provence Cedex 4 France
[4] Department of Earth and Atmospheric Science, University of Houston, Houston, TX 77204, USA
[5] Department of Geology, University of Toronto Mississauga, South Building 4051, Mississauga, ON, L5L 1C6, Canada
[6] Department of Geography Education, Korea University, Anam-Dong, Seongbuk-Gu, Seoul, 136-701, Korea

The Karakorum fault system extends for ~ 1000 km from southwestern Tibet into the Pamir along the western margin of the Tibetan Plateau separating it from the Pamir-Karakorum region. Although it is one of the most prominent structures in the Himalayan-Tibetan orogen, nearly every aspect about the evolution and role of this fault is actively debated including its initiation age, magnitude of displacement, and current slip rate. In recent years, displaced Quaternary landforms, commonly moraines, have been used to help define geomorphic rates (10^1 to 10^6 years) of displacement along this fault zone, and to aid in understanding the landscape evolution of this region. However, determining the ages of Quaternary landforms in order to determie the geomorphic history of this region is challenging because of the general lack of organic material needed to date landforms and sediments by the standard Quaternary geochronological technique of radiocarbon dating and the inaccessibility of the region. Terrestrial cosmogenic nuclide (TCN) surface exposure methods are now allowing many of the landforms to be dated, which are providing new insights into the evolution of this fault system and the associated landscape. In particular, with regard to the style and timing of glaciation throughout the region are beginning to be defined. Defining the nature of glaciation is important since glaciation likely controls much of the erosion and sediment transfer along the fault system, and glacial and associated landforms are used to define the timing and rates of faulting. To define the style of glaciation and to examine regional correlation and variations, four main study areas along the length of the fault system have been examined. These include: Mustaga Ata and Kongur Shan; the Taskorgan and Wuqa valleys; the Nubra and Shyok valleys; and Gurla Mandata. Glacial and associated landforms were mapped in these regions and dated using ^{10}Be TCN methods (including >250 ^{10}Be dates). In each region, glacial landforms have been dated back to several glacial cycles, the oldest being >400 ka. Later glacial advances are progressively less extensive, changing from expanded ice cap glaciation to valley glaciation in style. The glacial story that is emerging is complex due to sharp contrasts in the timing and extent of glaciation across mountain ranges along the fault system, which are controlled by strong topographic and climatic gradients. This intricate picture of glaciation highlights the need to be cautious when assigning ages to landforms on the basis of morphostratigraphy in the region without adequate numerical dating to determine tectonic and geomorphic histories.

Cite as: Owen, L.A, and others, 2010, Style and Timing of Glaciation along the Karakoram Fault, *in* Leech, M.L., and others, eds., Proceedings for the 25th Himalaya-Karakoram-Tibet Workshop: U.S. Geological Survey, Open-File Report 2010-1099, 1 p. [http://pubs.usgs.gov/of/2010/1099/owen/].

Evidence of Former Majoritic Garnet in Himalayan Eclogite Points to 200-km Deep Subduction of Indian Continental Crust

Anju Pandey[1], Mary L. Leech[2], Andy Milton[1], Preeti Singh[3], Pramod K. Varma[3]

[1] National Ocenaography Centre, Southampton, SO14 3ZH, U.K., anju.pandey@noc.soton.ac.uk
[2] Department of Geosciences, San Francisco State University, 1600 Holloway Avenue, San Francisco, CA 94132, U.S.A.
[3] Department of Geology, University of Delhi, Delhi-110007, India

Relict majorite, recognized petrographically and confirmed by *in situ* laser-ablation microprobe analyses, is reported from eclogites from near Kiagar Tso in the central part of the Tso Morari Complex (TMC), India. This is the first record of relict majorite in the Himalaya (Pandey and others, 2010). Previous studies established that the Tso Morari Complex eclogites represent metamorphosed basic continental rocks within a sequence of paragneisses and metapelites interbedded with granitic gneisses. Our study provides evidence for subduction of the Indian continental crust to majorite-forming depths (≥200 km).

Relict majorite microtexture and LA-ICPMS analyses

The two eclogite samples with relict majorite textures are composed mainly of garnet and omphacite with associated rutile, quartz, and apatite. These eclogites contain an older generation of coarse-grained garnet (grt1) that occurs as plastically-deformed porphyroblasts in the matrix of later medium-grained garnet (grt2), omphacite (cpx2), rutile, and apatite. Grt1 exhibits abundant fine-grained euhedral needles of clinopyroxene (cpx1) and rutile that are 2-3μm wide and 100-200 μm long (Fig. 1a). Needle concentration increases with distance from a needle-free rim zone to a maximum of 4-7 vol.% for clinopyroxene, and 1-1.5% vol.% for rutile in the core. Clinopyroxene needles occur in parallel groups, oriented in one of the four directions corresponding to the isometric form {111} (i.e., octahedral planes), that form a distinct equilateral triangle pattern (Fig. 1b). The regular distribution of needles with respect to crystallographic planes suggest that the needles of clinopyroxene in porphyroblastic garnets were generated by decompression-induced exsolution.

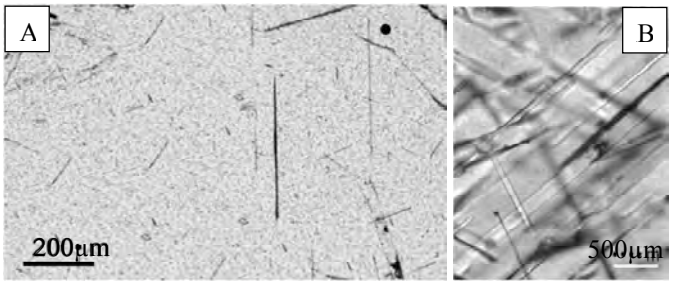

Figure 1. Exsolved pyroxene needles (lighter) and rutile (dark) in different garnet domains in eclogite.

Clinopyroxene needles in grt1 cores show light rare-earth element (LREE)-enriched and heavy rare-earth element (HREE)-depleted profiles (Fig. 2a). Grt1 grains show very different REE profiles in their rims and cores. There is a significant LREE-enrichment in the pyroxene needle-rich cores compared to the needle-free rims, while HREEs are similar (Fig. 2a). REE profiles of grt1 cores, that represent garnet plus exsolved clinopyroxene, yield an unusual flat REE pattern for garnet, indicating that REE for the original majorite partitioned into the exsolved clinopyroxene plus grt1 core, confirming the exsolution nature of clinopyroxene needles in grt1 cores (Scambelluri and others, 2008). Because the flat REE pattern in grt1 cores represents garnet plus exsolved clinopyroxene, it provides a combined concentration for the original bulk majorite. The consistent REE patterns of grt1 cores in different grt1 grains reflect uniform REE composition of the pre-exsolution majoritic garnet. The REE chemistry of grt2 shows HREE-enriched and LREE-depleted profiles while matrix omphacite grains (cpx2) show LREE-enriched and HREE-depleted patterns (Fig. 3b). Such complementary REE patterns for co-existing garnet and clinopyroxene indicate their co-crystallization (Malaspina and others, 2006). In terms of total REE abundance, cpx2 and grt2 have REE contents about one order of magnitude higher than phases exsolved from majoritic garnet, although inter-element fractionation remains constant (Fig. 2). This aspect can be explained in terms of fluid-deformation activity: during eclogitization, deformation creates textural and mineralogical microdomains. Consequently, fluid circulation favors the development of heterogeneities by transport of

elements in excess toward areas protected from deformation where grt2 and cpx2 may have crystallized. Texturally, grt2 and cpx2 grain boundaries show triple junctions (Fig. 1a), hence we concluded that grt2 and cpx2 grew synchronously after exsolution of clinopyroxene needles in grt1. Cpx2 shows exsolved quartz rods (Fig. 2a), suggesting persistence of UHP conditions during their growth.

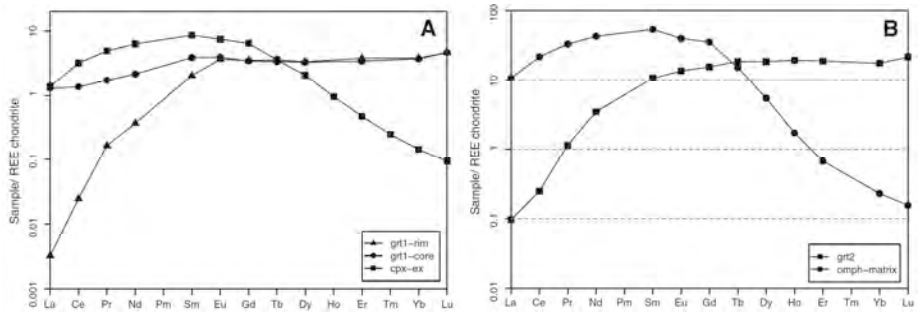

Fig. 2. Chrondrite-normalized representative REE compositions (in ppm) of a) grt1 with cpx1 needles, and b) grt 2 and cpx2 in the matrix of relict marjorite-bearing eclogites.

Pressure estimate

Crystallization conditions for majorite in TMC eclogites were derived by re-calculating the original composition of the majorite garnet. Averaged mineral compositions of grt1, cpx1, and rutile with the relative mineral volume percentage ($grt_{91.5}cpx_7rut_{1.5}$) were used to calculate the original majorite composition, following the method detailed in Sautter and others (1991).

The calculated original garnet exhibits high Na_2O (0.34 wt%) and is depleted in Al compared to normal garnet stoichiometry, consistent with garnet formed at ultrahigh pressures (Moore and Gurney, 1985). In the absence of a suitable pressure indicator, the calculated major-element composition of original garnet is compared with experimentally-synthesized garnet compositions from experimental data on basaltic systems at subduction conditions. The calculated Na_2O content (0.34 wt%) and octahedral-silicon values (0.04) of the original TMC garnet are consistent with garnet synthesized at 70.6 kbar and 1,200°C in an olivine tholeiite system (Irifune and others, 1986). Thus, we conclude that the original garnet in the TMC eclogites was formed at pressures >70 kbar placing TMC eclogites at depths >200 km.

Conclusions

UHP metamorphic conditions have been identified in the TMC, and interpreted as subduction of the Indian continental crust to coesite-formation depths during the collision between India and Asia (Mukherjee and Sachan, 2001). This study provides evidence for the existence of majoritic garnets in eclogites of the TMC that we interpret as an indication of subduction of the Indian plate to a minimum depth of 185-200 km during the Himalayan collision, nearly double previous depth estimates for Indian plate subduction in the TMC or anywhere within the Himalaya. The presence of relict majorite in the TMC requires major revision of tectono-metamorphic models for the India-Asia collision.

References

Irifune, T., Sekine, T., Ringwood, A.E. and Hibberson, W.O., 1986, The eclogite-garnet transformation at high pressure and some geographical implications, Earth and Planetary Sciences Letters, 77, 245-256.

Malaspina, N., Hermann, J., Scambelluri, M. and Compagnoni, R., 2006, Polyphase inclusions in garnet-orthopyroxenite (Dabie-Shan, China) as monitors for metasomatism and fluid related trace element transfer in subduction zone peridotite, Earth and Planetary Science Letters, 249, 173-187, doi: 10.1016/j.epsl.2006.07.017.

Moore, R.O. and Gurney, J.J., 1985, Pyroxene solid solution in garnets included in diamond, Nature, 318, 553-555.

Mukherjee, B.K. and Sachan, H.K., 2004, Garnet response diamond pressure metamorphism from Two-Morari region, Ladakh, India, Himalayan Journal of Science, 2, p. 209.

Pandey, A., Leech, M., Milton, A., Singh, P. and Pramod, K.V., 2010, Evidence of former majoritic garnet in Himalayan eclogite points to 200-km-deep subduction of Indian continental crust, Geology, 38, 399-402.

Sautter, V., Haggerty, S.E. and Field, F., 1991, Ultra-deep (>300 kilometers) ultramafic xenoliths: Petrological evidence from the transition zone, Science, 252, 827-830.

Scambelluri, M., Pettke, T. and van Roermund, H.L.M., 2008, Majoritic garnets monitor deep subduction fluid flow and mantle dynamics, Geology, 36, 59-62.

Cite as: Pandey, A., Leech, M.L., Milton, A., Singh, P. and Verma, P.K., 2010, Evidence of former majoritic garnet in Himalayan eclogite points to 200-km-deep subduction of Indian continental crust, *in* Leech, M.L., and others, eds., online proceedings for the 25th Himalaya-Karakoram-Tibet Workshop: U.S. Geological Survey, Open-File Report 2010-1099, 2 p. [http://pubs.usgs.gov/of/2010/1099/pandey/].

Exhumation of the Higher and Lesser Himalayan Crystallines of the Western Arunachal Himalaya, NE-India: Constraints from Fission-Track Studies

R.C. Patel[1], Vikas Adlakha[1], Paramjeet Singh[1], Nand Lal[1]

[1]Department of Geophysics, Kurukshetra University, Kurukshetra-136 119, India patelramesh_chandra@rediffmail.com

The active topography and extrusion of the ductilely deformed and highly metamorphosed rocks of the high peaks of the Himalaya have attracted many geoscientists from different parts of the world to study the growth mechanism of the Himalaya. Despite many studies from the NW- and Nepal Himalayas, the growth mechanism is still not completely understood in the absence of geological and geochronological data from the eastern segment of the Himalaya. Current debate has focused on the role of dynamic interaction between tectonics and climate. To address this issue, we conducted detailed field studies and apatite and zircon fission-track (AFT and ZFT) thermochronology of the Higher Himalayan Crystallines (HHC) and the Lesser Himalayan Sequence (LHS) along the Bhalukpong-BomdiLa-Tawang-BumLa/LumLa traverse in western Arunachal Himalaya, NE-India (Figure 1)

AFT and ZFT data collected from western Arunachal Himalaya across the HHC and LHS has been used to understand the exhumation of the region. AFT results from both the HHC and LHS show no change in ages in each tectonic zone with respect to distance from the Main Central Thrust (MCT), whereas ZFT ages show a well-developed correlation with respect to their distance from the HHC to the LHS through the MCT. Ages within the HHC gradually increase from the location close to the Jimithang Thrust to the LHS with a break along the MCT (Figure 2). AFT ages range between 1.4±0.2 to 2.6±0.4 Ma with ages clustering around 2.1 Ma whereas ZFT ages range between 4.5±0.5 and 8.9±1.3 Ma with clustering around 7 Ma. No AFT ages > 5 Ma have been found from this part of the HHC, despite being reported by Grujic and others (2006) from the adjacent eastern Bhutan Himalaya (separated by only ~50 km) (3.0± 0.7 to 8.6±0.8 Ma with weighted mean 5.08±0.09 Ma) although both the regions share similar ectonic structures, rock types and rainfall. It reflects rapid exhumation of the HHC in the western Arunachal Himalaya as compared to the eastern Bhutan Himalaya in spite of their similar location in the shadow zone of the Shillong plateau, a topographic high in front of the Himalaya.

The FT data of the LHS are significantly older than the HHC. The AFT ages in the LHS range between 5.6±0.6 and 12.4±1.3 Ma with ages clustering around 7.9 Ma and ZFT ages range between 10.9±0.6 and 14.1±1.1 Ma with ages clustering around 12.5 Ma. This indicates slow exhumation of the LHS in comparison to the HHC.

Analysis of FT data from both the HHC and LHS indicates that: 1. the MCT is not only a structural boundary separating the HHC and the LHS but also a break in exhumation pattern i.e. a rapidly exhuming zone in the hanging-wall HHC rocks but a slowly exhuming zone in the footwall LHS rocks. Reactivation of the MCT might be mainly responsible for accelerating the exhumation rate in the hanging wall i.e the HHC zone. 2. Ages are poorly correlated with the present-day rainfall. There is a major difference in exhumation of the HHC and LHS zone despite their similar rainfall pattern. 3. Despite the location of the western Arunachal Himalaya adjacent to the eastern Bhutan Himalaya and in the same rain-shadow zone of the Shillong plateau in the Himalayan foreland, there is significant difference in AFT age data sets between the eastern Bhutan and western Arunachal Himalayas. This neither supports any spatial correlation between long-term erosion and precipitation rates nor a climatically driven erosion rate change on the scale of the eastern Himalaya as described by Grujic and others (2006) in the Bhutan Himalaya. It is likely that the tectonic structures such as large-scale folding and thrusting along the MCT in the eastern Himalaya are responsible for the change in erosion rate.

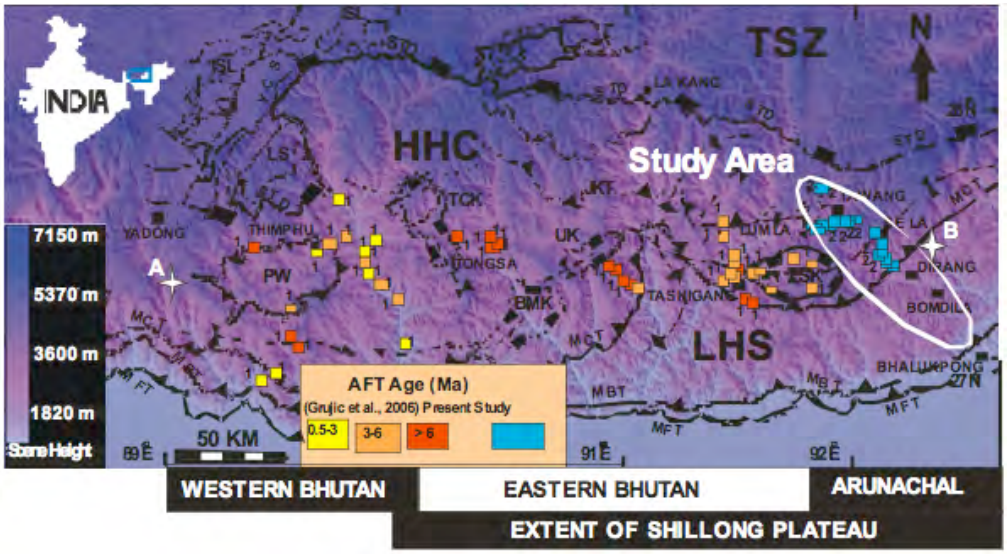

Figure 1. Digital elevation model of Bhutan and western Arunachal Himalaya. MFT: Main Frontal Thrust, MBT: Main Boundary Thrust, MCT: Main Central thrust, JKT: Jimithang-Kakhtang Thrust, STD: South Tibet Detachment, PW: Parro Window, SK: Skteng Klippen, UK: Ura Klippen, BMK: Black Mountain Klippen, TCK: TangChu Klippen.

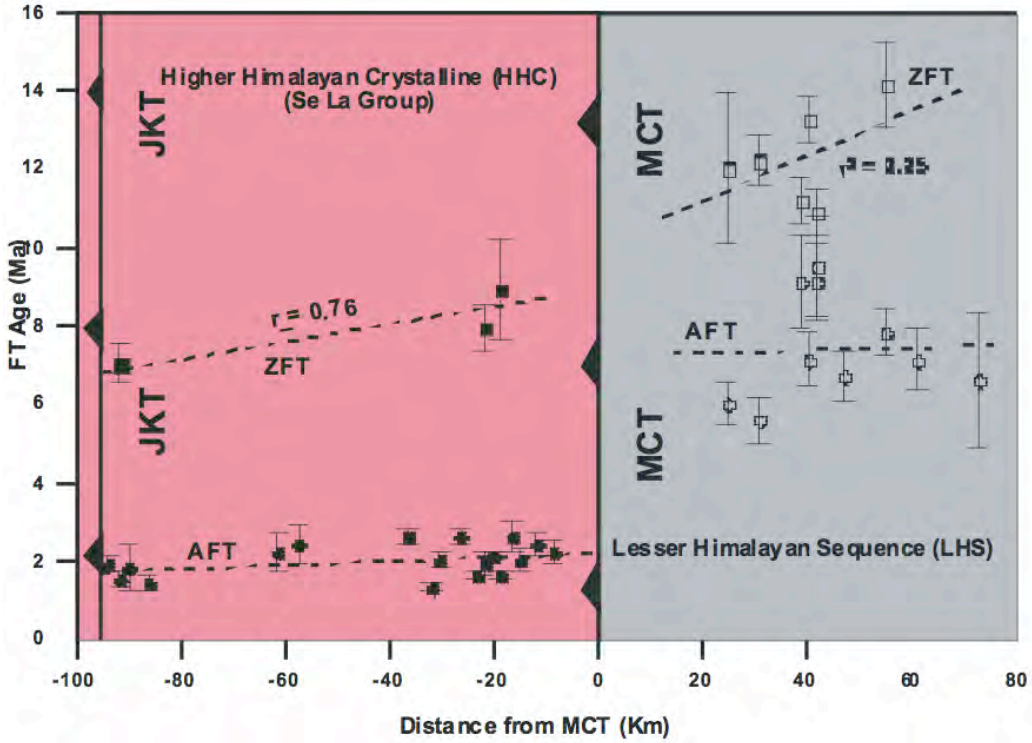

Figure 2: FT age plotted against distance from MCT to test for thrusting along the MCT. Solid and open circles represent AFT ages, and solid and empty squares represent ZFT ages.

Reference

Grujic, D., and others, 2006, Climatic forcing of erosion, landscape, and tectonics in the Bhutan Himalayas, Geol. Soc. Am. Bull., 34, 801-804.

Cite as: Patel, R.C., Adlakha, V., Singh, P., Lal, N., 2010, Exhumation of the Higher and Lesser Himalayan Crystallines of the Western Arunachal Himalaya, NE-India: Constraints from Fission Track Studies, *in* Leech, M.L., and others, eds., Proceedings for the 25th Himalaya-Karakoram-Tibet Workshop: U.S. Geological Survey, Open-File Report 2010-1099, 2 p. [http://pubs.usgs.gov/of/2010/1099/patel/].

State of the Tibetan lithosphere

Keith Priestley[1], Jamie Barron[1], Charlotte Acton[1], Eric Debayle[2], Dan McKenzie[1]

[1] Bullard Laboratories, Dept. Earth Sciences, University of Cambridge, Cambridge, CB30EZ, UK, KFP10@cam.ac.uk
[2] Ecole et Observatiore des Sciences de la Terre, Universite Louis Pasteur, Strasbourg, 67084 France

Although it has long been accepted that the uplift of the Himalaya and Tibet result from the collision of India with Eurasia, there is still no agreement on the details of the geodynamical processes involved. This lack of consensus arises primarily from uncertainties in the Tibetan upper mantle structure. The prevalent, but not universally accepted explanation has been that the uplift of Tibet was associated with delamination of at least part of the Tibetan lithosphere. We use a variety of seismic observations to assess the state of the Tibetan upper mantle. Waveform inversion of more than 50,000 low frequency multi-mode surface waveforms recorded in Asia for paths crossing the plateau show the existence of a high velocity lid extending at depths of 150-250 km across the entire plateau. At shallow depths (~130 km or less) the mantle velocity is slow beneath northern Tibet but fast beneath southern Tibet. However, the low-frequency surface waves have a lateral resolution of about 400 km.

We have analyzed a number of other seismic data which better resolve the structure of the Tibet crust and uppermost mantle. We have measured shorter-period (10-70 s) fundamental-mode Rayleigh-wave group-velocity dispersion for more than 4000 paths recorded in Tibet and India. The dispersion data are inverted with receiver-function data for lateral Vs variations of the crust and uppermost mantle. The interesting feature of this result is that while the sub-Moho mantle beneath southern and western Tibet is fast, that below central and northeastern Tibetan Plateau is slow at shallow depths (<125 km) but fast at deeper depths. In addition, fundamental mode Rayleigh wave phase velocities for paths confined to the northern part of the plateau are only 1-2 % slow in the 70-120 s period range compared to paths confined to the southern part of the plateau. These surface-wave observations from measurements largely confined to the plateau have higher resolution than the large-scale low-frequency surface-wave analysis but support the low-frequency surface-wave tomographic model.

Other seismic observations support this picture. Analysis of frequency-dependent Sn propagation in Tibet shows that at high frequency (~1 Hz) Sn is blocked for paths across the northern plateau but not for paths confined to the southern part of the plateau, a feature first noted more than 25 years ago. In contrast, low frequency (~0.2 Hz) Sn is observed to propagate across the whole of the plateau, consistent with the surface-wave results. Relative teleseismic S-wave delays measured for sites in the northern part of Tibet are delayed 0.5-1.0 s with respect to sites in southern Tibet. The magnitudes of the teleseismic S-wave delays are incompatible with complete removal of the Tibetan high-velocity lid and lithosphere.

These seismic observations indicate that the Tibetan high-velocity lid and lithosphere are still largely, if not completely intact. The seismic model suggests that most of the plateau has been underthrust by high wave speed Indian mantle from the south and possibly to a lesser extent, high wave speed Asian mantle from the north. Low velocities in the upper mantle beneath northern Tibet have previously been noted and these, along with the recent volcanism in northern Tibet, have been cited as evidence for lithospheric delamination beneath the plateau. However, the seismic studies reported here suggest that the low wave speeds in the upper mantle below central and northeast Tibet are a relatively a shallow feature and not the result of lithospheric delamination. We propose that the low velocity sub-Moho mantle beneath central and northeast Tibet result from radioactive heating of the thickened Tibetan crust. With increasing time, this heating results in a temperature inversion which heats the uppermost mantle lowering the sub-Moho shear velocity.

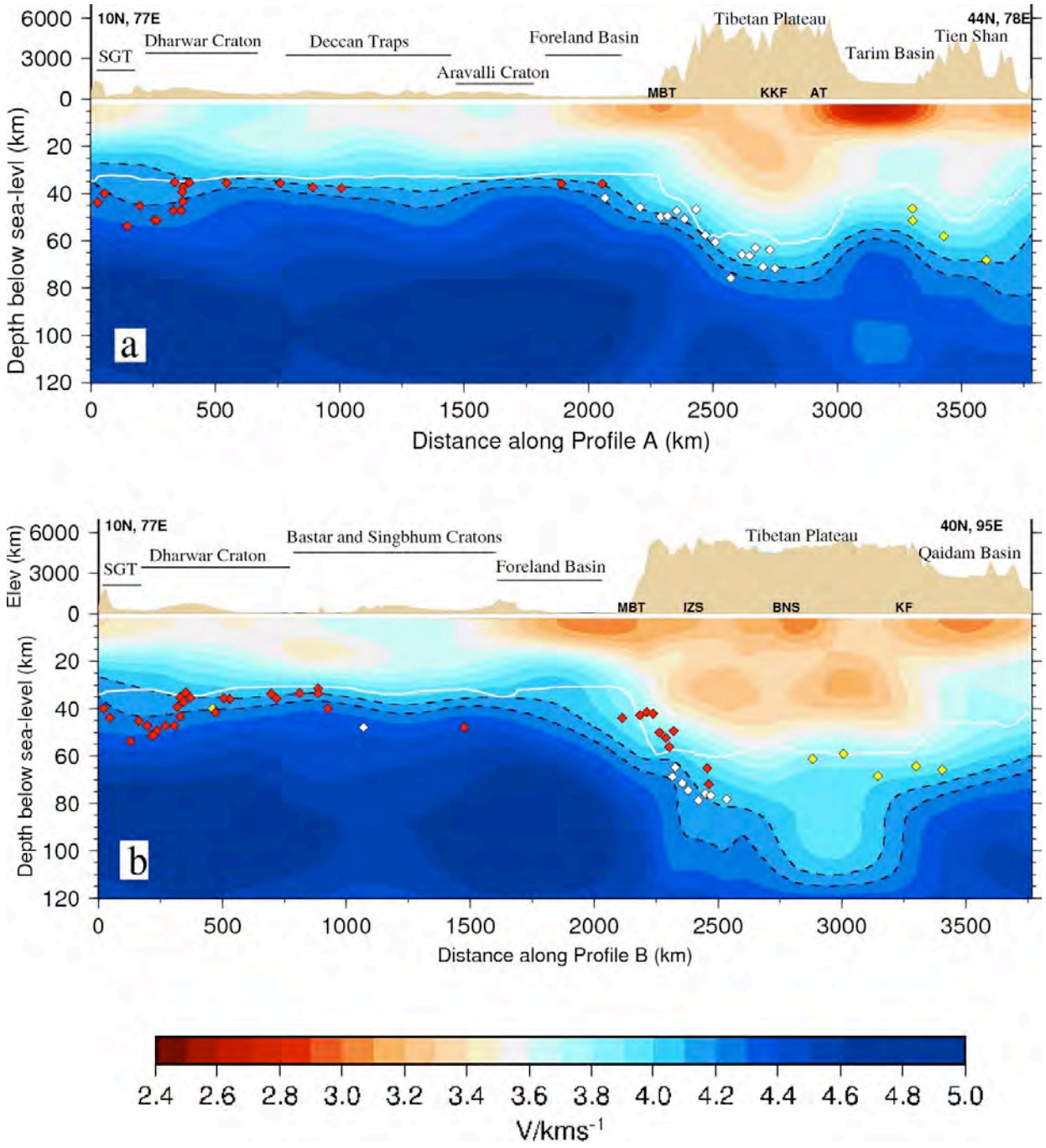

Figure 1. Velocity section through the Sv wave-speed model derived from inversion of the fundamental-mode Rayleigh-wave group-velocity data with receiver-function Moho depths superimposed. Profile (a) crosses India and western Tibet and profile (b) crosses India and eastern Tibet. The surface waves are sensitive to the crustal structure but because of their depth-averaging properties and frequency, are not sensitive to the details of the Moho discontinuity. Comparison of the surface-wave velocity model and the receiver-function results show the depth of the 4.1 km/s contour in the surface-wave model correlates, with a few exceptions, to the receiver-function Moho position for most of the Tibet-Indian region. Low sub-Moho shear velocities occur in the uppermost mantle beneath northeastern Tibet but not western Tibet.

Cite as: Priestley, K., Barron, J., Acton, C., Debayle, E. and McKenzie, D., 2010, State of the Tibetan lithosphere, *in* Leech, M.L., and others, eds., Proceedings for the 25th Himalaya-Karakoram-Tibet Workshop: U.S. Geological Survey, Open-File Report 2010-1099, 2 p. [http://pubs.usgs.gov/of/2010/1099/priestley/].

A Model for the Tectonic Evolution of the Tethys-Tibetan Plateau System and Implications for Continental Tectonics in China

R.Z. Qiu[1], S. Zhou[2], Y.J. Tan[1], G.S. Yan[3], X.F. Chen[1], Q.H. Xiao[4], L.L. Wang[1,2], Y.L. Lu[1], Z. Chen[1], C.H. Yuan[1,2], J.X. Han[1], Y.M. Chen[1], L. Qiu[2], K. Sun[2]

[1] Development and Research Center, China Geological Survey, Beijing 100037, China
[2] China University of Geosciences, Beijing 100083, China, zhousu62@yahoo.cn
[3] China Geological Survey, Beijing 100037, China
[4] Information Center of Ministry of Land and Resources, Beijing 100812, China

An integrated petrologic, geochemical and geochronological study of magmatic-tectonic-assemblages (volcanic and plutonic rocks and ophiolite suites) from the Greater Tibetan Plateau has led to a new model for the tectonic evolution of the Tethys-Tibetan Plateau system: opening of the Tethyan oceans followed by initial subduction, subduction/collision, post-collision and uplifting. The evidence for this comprehensive model comes from (1) Sm-Nd and ^{40}Ar-^{39}Ar ages of gabbros in ophiolite suites (180–204 Ma) from both Yarlung Zangpo and Bangong-Nujiang sutures reflecting the timing of the opening of the two ocean basins at J_1, probably under the influence of a super-plume. (2) Ages of subduction-related lavas: ~140–170Ma in the Bangong-Nujiang suture and ~ 65–170Ma in the Yarlung Zangpo suture. Among these lavas, boninite and boninite series, which are generally regarded as the indicating an early state of subduction initiation, have been recognized at both the northern and southern edges of the Gangdese block (Zhang, 1985; Qiu, 2004, 2007). The harzburgite-IAT-boninite association indicates that both Bangong-Nujiang and Yarlung Zangpo are SSZ ophiolites (Qiu, 2007). (3) O-type adakite rocks, among the igneous rocks next to the ophiolite belts with the ages of about 75~139Ma in Bangong-Nujiang and of about 40~110Ma in Yarlung Zangpo with low (^{87}Sr/^{86}Sr)i (0.7041~0.7064), positive ε Nd(t) (+2.5 ~ +5.7) and young T_{DM} ages (312–562Ma) show their subduction origin. (4) Collision of the continental mass with the island-arc systems in the Bangong-Nujiang ocean basin indicates its closure by the end of K_1, and the India-Asia collision at K_2/E (~65Ma; Mo, 2003; Zhou, 2004) is consistent with the closure of the Yarlung Zangpo ocean basin. These explain the large-scale magmatism at the northern (75–95Ma) and southern (65–40Ma) Gangdese. (5)With the continuous northward subduction of Indian plate, a lithospheric root was formed. C-type adakites can be regarded as the orogenic lithosphere delamination episode (Qiu, 2006). The occurrences of C-type adakite of 45–9.4Ma in the Qiangtang (Lai, 2003) and 10–18Ma in the Gangdese (Cai, 2004; Hou, 2004) suggest that the delamination happened first in the Qiangtang, before in the Gangdese. At the same period of delamination in the Gangdese, intra-continental subduction occurred in the Himalayas to form the muscovite-biotite granite belt of 20–10Ma. In brief, the above tectonic evolution model is shown in Figure 1.

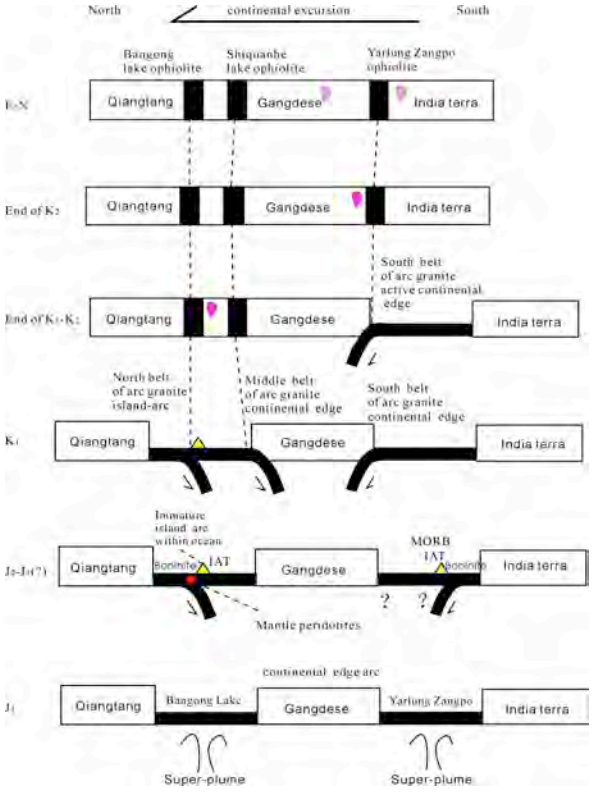

Figure 1. Tectonic evolution of the Greater Tibetan Plateau

Figure 2 (after Qiu, 2006) shows the five types of lithosphere in continental China, whose characteristics are consistent with being produced by processes described above for the Tethyan-Tibetan Plateau system.

Since the Triassic, the dominantly N-S compressional regime in continental China changed to an E-W dominated compressional regime. In western China, the Tethys Ocean opened in the Mesozoic and underwent compressional orogenies in the Cenozoic, forming the Tethys-Himalaya orogenic-type lithosphere. In the Cenozoic, due to bi-directional (north- and south-directed) compression in western China and extension in eastern China, the Qinghai-Tibet Plateau expanded and evolved into the western segment (Qilian and Kunlun) of the Qinling-Qilian-Kunlun orogenic belt, thus forming the Cenozoic orogenic-type lithosphere with "old material and new structure", while in Xinjiang the Paleozoic orogenic belts, such as Tianshan and Altay, "rose again" and became the Cenozoic orogenic-type lithosphere with "old material and new structure", with only the Paleozoic Central Asian orogenic-type lithosphere represented by that of Ejin Qi remaining. The east part of continental China underwent compressional orogenies in the Mesozoic and extensional rifting in the Cenozoic. The Cenozoic rifting gave rise to the rift-type lithosphere in the Songliao plain, North China plain and sea areas off Fujian and Guangdong and only in Northeast China, North China and North China did the Yanshanian lithospheres represented by those in the Da Hinggan and Yanshan-Taihang mountains and central segment of the Nanling Mountains remain. In the Late Cenozoic, the oceanic type lithospheres represented by the Central basin of the South China Sea formed with further expansion of the rift-type lithosphere in eastern China. After undergoing rifting in the Cenozoic, the pre-Cenozoic continental margins in eastern China were separated and interacted with the Pacific plate, thus forming the island arc-type lithosphere represented by that of Taiwan.

The above observations and interpretations suggest that the evolutional process of the Tethyan system in Qinghai-Tibetan Plateau is one of the most importance factors for the dynamic process of continental China and for the formation of different lithosphere types. The coexistence and formation of the different types of lithosphere in continental China also indicate that Qinghai-Tibetan Plateau is one of the best sites to study continental dynamics in China, and is perhaps of global significance.

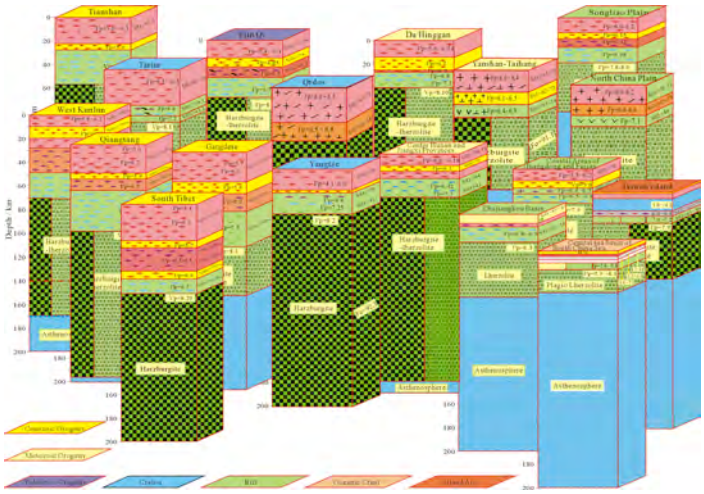

Figure 2. Present lithosphere types in continental China.

References

Cai, Z.Y., Qiu, R.Z. and Xiong, X.L., 2004, Geochemical characteristics and geological significance of the adakites from west Tibet, 19th HKT workshop special issue, Himalayan Journal of Science, 2, 291.

Hou, Z.Q., and others, 2004, Origin of adakitic intrusives generated during mid-Miocene east-west extension in southern Tibet, Earth and Planetary Science Letters, 220, 139-155.

Lai, S.C., 2003, Identification of the Cenozoic adakitic rock association from Tibetan plateau and its tectonic significance, Earth Science Frontiers, 10, 407-415.

Mo, X.X., and others, 2003, Response of volcanism to the India-Asia collision, Earth Science Frontiers, 10, 135-148.

Qiu, R.Z, Cai, Z.Y. and Li, J.F., 2004, Boninite of Ophiolite Belts in Western Qinghai-Tibet Plateau and its Geological Implication, Geoscience, 18, 305-308.

Qiu, R.Z., and others, 2006, The composition and evolution of lithosphere in China continent. Beijing: Geological Publishing House, 1-308.

Qiu, R.Z., and others, 2007, The Ophiolite Forming Tectonic-setting in Western Qinghai-Tibetan, China—Evidences from Geology, Petrology and Geochemistry, Journal of Asia Earth Sciences, 29, 215-228.

Zhang, Q. and Yang, R.Y., 1985, The plutonite of High-Mg-andesite types in Dingqing ophiolite and its geological significance, Chinese Science Bulletin, 30, 1243-1245.

Zhou, S., 2002, Study on the Geochronology of several key regions of Gangdese magmatic and Yarlung Zangpo ophiolite belts, Tibet, China University of Geosciences, Beijing.

Zhou, S., and others, 2004, ^{40}Ar-^{39}Ar geochronology of Cenozoic Linzizong volcanic rocks from Linzhou Basin, Tibet, China, and their geological implications, Chinese Science Bulletin, 49, 1970-1979.

Qiu, R.Z,, and others., 2010, A model for the tectonic evolution of the Tethys-Tibetan Plateau system and its Implication for Continental tectonics in China, in Leech, M.L., and others, eds., Proceedings for the 25th Himalaya-Karakoram-Tibet Workshop: U.S. Geological Survey, Open-File Report 2010-1099, 2 p. [http://pubs.usgs.gov/of/2010/1099/qiu/].

High resolution earthquake location and 3-D velocity imaging of crust beneath the Kumaon Himalaya

P. Mahesh[1], Shyam S. Rai[1], P.R. Sarma[1], S. Gupta[1], K. Sivaram[1], K. Suryaprakasam[1]

[1] National Geophysical Research Institute (CSIR), Hyderabad, India, shyamsrai@gmail.com

The seismological record and recent space-geodetic measurements suggest a significant seismic potential for the Kumaon-Garhwal Himalayan region. The region has several recent, deadly, moderate earthquakes, the most prominent being the Uttarkashi (1991 Oct 20, 30.75ºN 78.86ºE, M 6.6) and Chamoli (1999 March 29, 30.41ºN 79.42ºE, M 6.8) earthquakes. The major Himalayan faults are the Southern Tibetan Detachment (STD), the Main Central Thrust (MCT), the Main Boundary Thrust (MBT) and the Main Frontal Thrust (MFT). The Main Central Thrust in this region is a zone bounded by the Munsiari thrust (MT) in the south and the Vaikrita thrust (VT) in the north. Existing knowledge suggests that apart from sporadic outliers, most of the seismicity in the Himalaya is very well clustered in a narrow zone of MCT.

We operated a network of 46 broadband digital seismographs from April 2005 to June 2008 (Figure 1) in the Kumaon-Garhwal Himalaya region, in order to study the seismicity pattern, earth structure, fault geometry, earthquake mechanics and dynamics of the earthquake system. These stations were operated in two phases: (i) a NE-SW directed linear array of 20 stations for an initial period of 18 months from April 2005 with a couple of stations off the profile, and (ii) a laterally distributed network operating for around 18 months. We used 350 local earthquakes with at least 8 P and 5 S phase readings and an azimuth gap <180° to generate a 1-D reference velocity model for the region using VELEST. Using this velocity model, we relocated 1400 earthquakes recorded by at least 5 network stations. The geographical distribution of seismicity is shown in Figure 1. While the majority of earthquakes follow the trend of the MCT zone, we also observed earthquakes beneath the Ganga basin, the Lesser Himalaya, and the Higher Himalaya, continuing north of the STD. Figure 2 shows the depth distribution of earthquakes along a NE-SW section. Though the majority of earthquakes have their hypocenter in the upper crust (above 20 km), a significant number of them are located in the middle and lower crust. This pattern has been further verified by joint hypocenter and 3-D velocity imaging. Figure 3 shows the velocity-depth section along the profile with earthquakes plotted on it. Unlike in the Nepal Himalaya, we have no reliable observations of earthquakes in the mantle suggesting a lateral diversity in the rheological properties of Indian lithosphere underthrusting the Himalaya. We discuss the implication of the imaged velocity pattern in seismogenesis in the region.

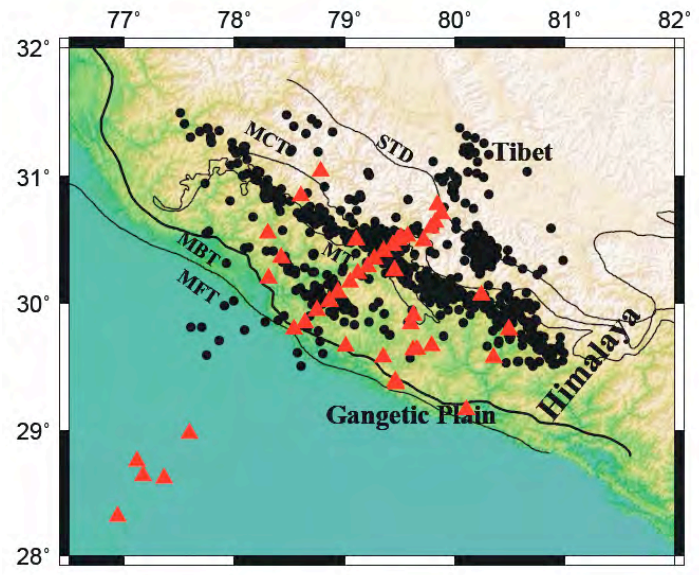

Figure 1: Location of broadband seismographs (red triangles) and distribution of earthquakes (filled circles) in the Kumaon Himalaya region. Major tectonic features are identified in the text.

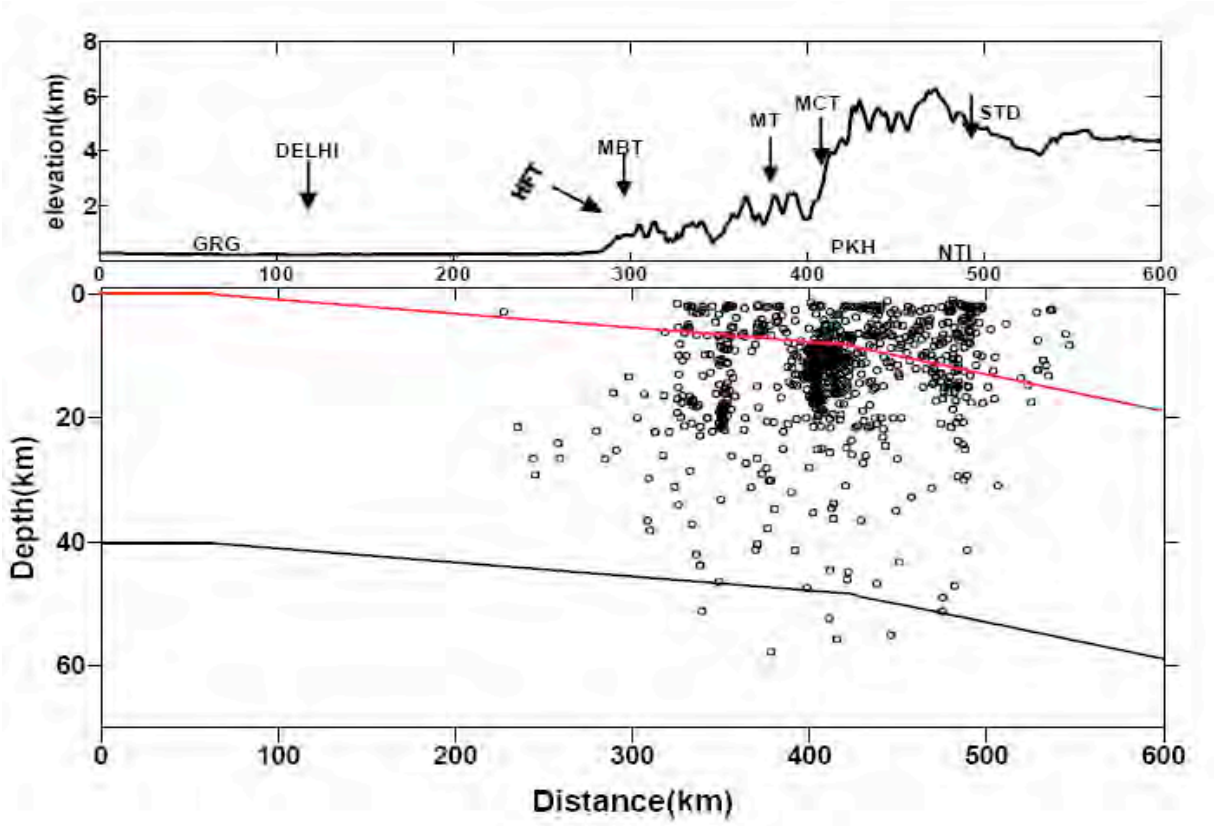

Figure 2. Earthquake locations in arc-normal cross-section for 1400 earthquakes recorded by the network. Earthquakes with at least 5 P and 3 S phase reading were relocated. Moho is mapped using receiver-function modeling. Also shown are the topography and the location of selected stations.

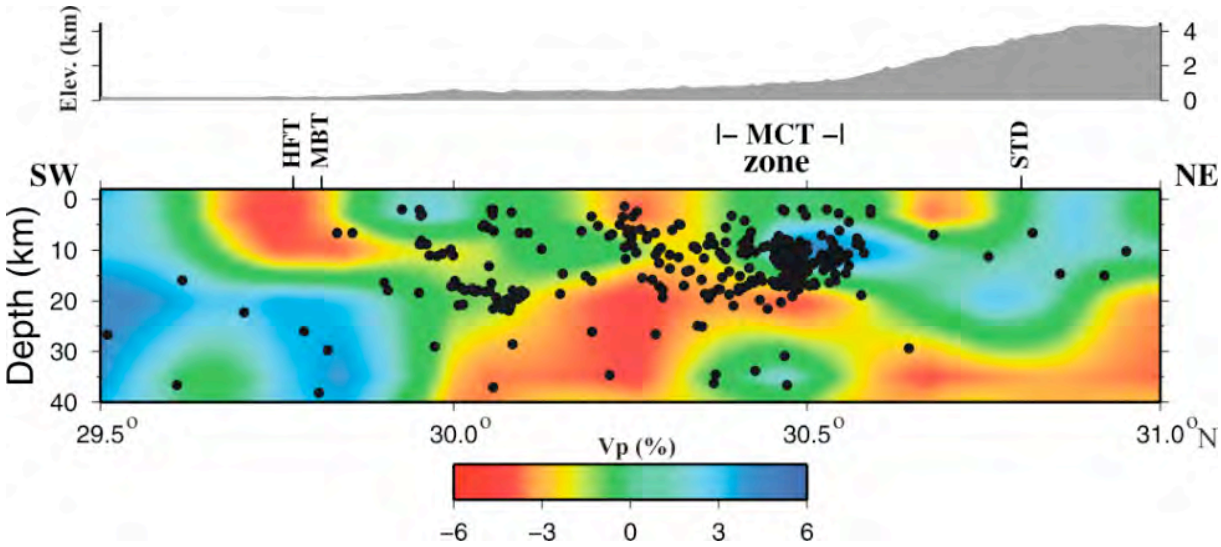

Figure 3. P wave velocity-depth section along a NE-SW profile aligned with the array of seismic stations. Also plotted is the location of earthquakes on the velocity image.

Cite as: Mahesh, P., Rai, S.S., Sarma, P.R., Gupta, S., Sivaram, K., and Suryaprakasam, K., 2010, High resolution earthquake location and 3-D velocity imaging of crust beneath the Kumaon Himalaya, *in* Leech, M.L., and others, eds., online proceedings for the 25th Himalaya-Karakoram-Tibet Workshop: U.S. Geological Survey, Open-File Report 2010-1099, 2 p. [http://pubs.usgs.gov/of2010/1099/rai].

Precambrian Granitic Magmatism in the NE Himalaya: Implications for Ancient Tectonics

Shaik A. Rashid[1], Naqeebul Islam[1], Javid Ganai[1]

[1]Department of Geology, Aligarh Muslim University, Aligarh, India, rashidamu@hotmail.com

The Paleoproterozoic Bomdila granites (metamorphosed to orthogneisses) are developed close to the Main Central Thrust in the amphibolite-grade metasedimentary rocks in Arunachal Pradesh, northeast Lesser Himalaya. On the basis of field and petrographical observations, two principle types of granites have been distinguished: porphyritic biotite-muscovite (two-mica) granites and tourmaline-bearing leucogranites. Both types are subalkaline, strongly peraluminous (A/CNK > 1.1) and have >70% SiO_2, Na_2O+K_2O = 5.5–8.5%, and K_2O/Na_2O = 0.8–2.9. The Bomdila orthogneisses are enriched in incompatible elements such as Rb, Ba, K and Th, and depleted in high field strength elements (HFSE) like Zr, Hf, Ta, Y and Nb. The enrichment of the Bomdila samples in the incompatible elements and their depletion in HFSE strongly supports their postulated crustal source. Both the granite suites are characterized by high incompatible elements/HFSE ratios, which is similar to many intra-crustally derived granites. Tourmaline granites are clearly distinguished by their low Sr and Ba contents compared with the two-mica granites and are generally depleted in Sc, Y and Nb. The discriminant Rb vs. (Nb+Y) diagram shows that the tourmaline granite generally lies within the syn-collision field (as do other Himalayan leucogranites), whereas the two-mica granites straddle the field boundary between collision granite and volcanic-arc granite. Extensive studies on Himalayan leucogranites by Harris and others (1986) suggest that the granites that form in the syn-collision zones are generally peraluminous leucogranites and may be derived from the hydrated bases of continental thrust sheets. Primitive-mantle normalized spidergrams for the Bomdila rocks, like most crustal granitoids, show negative Ti, Sr and Nb anomalies, reflecting the influence of some accessory phases such as rutile as a residual phase in high-pressure melting during the event that formed juvenile sialic crust (Gill, 1981).

In contrast with other Himalayan leucogranites that are generally characterized by unusually low REE contents, the Bomdila rocks show higher concentrations of all REEs than published averages from other such leucogranites (Vidal and others, 1982; Scaillet and others, 1990). The two-mica granites show higher REE concentrations (up to 294 ppm) than the tourmaline granites (sum = 67 ppm). The REE contents of two suites indicate light REE (LREE) enrichment over heavy REE (HREE) and have variable LREE/HREE ratios [$(La/Yb)_N$ = 3–23]. The patterns show steeply inclined LREEs with flatter and little-fractionated HREEs resulting in overall concave patterns. The REE abundances of the Bomdila granites coincide with typically crustally derived granites (i.e. La = 20–100X chondritic, Yb = 0.5–8X chondritic, Holtz, 1989) and show consistent fractionation patterns within the LREE group [$(La/Sm)_N$ = 3–5]. Negative Eu anomalies are pronounced in both the suites and reveal a very narrow range of difference (Eu/Eu* = 0.35–4) indicating that plagioclase fractionation has been essential in their petrogenesis.

Although experimental studies suggest that leucogranites can be generated by a variety of processes, both the major and trace element characteristics of the Bomdila leucogranites are better explained by varying degrees of partial melting and fractionation. An overlap in the wide concentration ranges of oxides, such as SiO_2, CaO, MgO, $Fe_2O_3^t$ and Sr of the two-mica and tourmaline granite suites, with no discernable differentiation trends on a Harker variation diagram, precludes the derivation of one suite from the other by differentiation following emplacement. This, in turn, suggests that both suites may have been derived from different sources. In order to determine the phase-equilibria conditions of the Bomdila granites, the samples were projected onto the Q-Ab-Or phase diagram which also contains 2 and 5 kbar minima and eutectics of the haplogranite system with varying aH_2O in the melt (Holtz and others, 1991). It can be noticed in the diagram that the two-mica granites do not cluster about a minimum-melt composition characteristic of water-saturated haplogranite phase relations (Tuttle and Bowen, 1958). Instead, they form a spread of compositions with a trend defined by variable quartz/orthoclase and orthoclase/albite ratios. Experimental work by Johannes and Holtz (1990) has demonstrated that quartz/orthoclase ratios increase as pressure decreases in water-undersaturated melts. Further studies indicate that

orthoclase/albite ratios of granite minimum-melt compositions are greatly increased at decreased water activities (Ebadi and Johannes, 1991). Experimental studies on crystallization of leucogranite magmas (Scaillet and others, 1995) suggest that two-mica granites and tourmaline granites can be generated at low (between 5 and 7.5 wt %) and high (>7 wt. %) initial water contents, respectively. Therefore, the Bomdila two-mica granites with quartz-rich compositions and plotting at decreased pressures (< 5 kbars) and low water activities in the diagram, suggest their derivation from an alumina-saturated source under water-undersaturated condition at temperatures >800^{0}C. In contrast the tourmaline-granite samples cluster around a composition corresponding to minimum melt at ~3 kbar, a$H_2O \approx 0.5$. These values are consistent with thermobarometric studies of the many well-studied leucogranites from the Himalaya such as Manaslu (Guillot and others, 1991), Langtang (Inger and Harris, 1993), etc.

From the above discussion, it can be convincingly argued that the two suites of the peraluminous Bomdila orthogneiss were predominantly formed by partial melting and fractional crystallization (in the case of two-mica granites) of pelitic rocks from the upper crust. Presence of metasedimentary enclaves (pelitic schists) in the two-mica granites and the crystallization of magmatic tourmaline in tourmaline granites are also consistent with a metasedimentary source (Bernard and others, 1985). An attempt is made in this paper to explore the possible source rocks for these granites. In this perspective, the mica schists with which the granites are associated offer potential source lithologies. A striking similarity between the composition of proposed source lithology and the average Bomdila orthogneiss is clearly evident in the diagram, supporting the assumption that metasedimentary rock (similar to the micaschists) exposed along with granites are the most likely source for the Bomdila orthogneisses.

These studies show that the granites formed in a syn-collisional tectonic environment, suggesting that collision of two continental blocks might have occurred during the Proterozoic period along this linear belt, similar to the already established Paleozoic Lesser Himalayan granitoid belt (Le Fort and others, 1986) related to Pan-African orogeny. This further implies an episode of significant Proterozoic orogenic events in the Lesser Himalaya. Subsequent tectonics exposed these granites to weathering and provided detritus to the newly formed large Proterozoic sedimentary basins in the Lesser Himalaya.

References

Bernard, F., Moutou, P. and Pichavant, M., 1985, Phase relations of tourmaline leucogranites and the significance of tourmaline in silicic magmas, Jour. Geol., 93, 271-291.

Ebadi, A. and Johannes, W., 1991, Beginning of melting and composition of first melts in the system Qz-Ab-Or-H_2O-CO_2, Contrib. Mineral. Petrol., 106, 286-295.

Gill, J.B., 1981, Orogenic andesites and plate tectonics, Springer-Verlag, Berlin. 358 pp.

Guillot, S., Le Fort, P. and Pecher A., 1991, Contact metamorphism of the Manaslu leucogranite: an emplacement within a thickened upper crust. Geol. Alp. Mem. H.s., 16, 47.

Harris, N.B.W., Pearce, T.A. and Tindle, A.G., 1986, Geochemical characteristics of collision zone magmatism, in: Coward, M.P. and Ries, A.C., eds., Collision Tectonics. Geol. Soc. London Spec. Pub. 19, 67-81.

Holtz, F., 1989, Importance of melt fraction and source rock composition in crustal genesis- the example of two granitic suites of northern Portugal, Lithos, 24, 21-35.

Holtz, F., Johannes, W. and Pichavant, M., 1991, Effects of excess alumina on phase relations and composition of granitic melts, Terra abst., 3, 29.

Inger, S. and Harris, N.B.W., 1993, Geochemical constraints on leucogranite magmatism in the Langtang Valley, Nepal, Himalaya, Jour. Petrol., 34, 345-368.

Johannes, W. and Holtz, F., 1990, Formation and composition of H_2O under-saturated granitic melts, in: Ashworth, J.R. and Brown, M., eds., High temperature metamorphism and crustal anatexis, Unwin Hyman, 87-104.

Le Fort, P., Debon, F., Pecher, A., Sonet, J. and Vidal, P., 1986, The 500 Ma magmatic event in Alpine Southern Asia, a thermal episode at Gondwana scale, Sciences de la Terre, Memoire 47, 191-209.

Scaillet, B., France-Lanord, C. and Le Fort, P., 1990, Badrinath-Gangotri plutons (Garhwal, India): petrological and geochemical evidence for fractionation processes in a High Himalayan leucogranite, Jour. Volc. Geotherm. Res., 44, 163-188.

Scaillet, B., Pichavant, M. and Roux, J., 1995, Experimental crystallization of leucogranite magmas, Jour. Petrol., 36, 663-705.

Vidal, P., Cocherie, A. and Le Fort, P., 1982, Geochemical investigations of the origin of the Manaslu leucogranite (Nepal Himalaya), Geochim. et Cosmochim. Acta, 46, 2279-2292.

Cite as: Rashid, S.A., Islam, N. and Ganai, J., 2010, Precambrian Granitic Magmatism in the NE Himalaya: Implications for Ancient Tectonics, *in* Leech, M.L., and others, eds., Proceedings for the 25th Himalaya-Karakoram-Tibet Workshop: U.S. Geological Survey, Open-File Report 2010-1099, 2 p. [http://pubs.usgs.gov/of/2010/1099/rashid/].

Aggradation and Incision Phases in the Upper Reaches of the Ganga River System; Timescales and Implications for Hinterland-Foreland Relationships

Yogesh Ray[1], Pradeep Srivastava[1], Y.P. Sundriyal[2]

[1] Wadia Institute of Himalayan Geology, 33 GMS Road, Dehradun 248001, India, yogeshwihg@gmail.com
[2] Department of Geology, HNB Garhwal University, Srinagar 246174, India

The Ganga (Ganges) river system originates in the Himalaya and debouches into its foreland after cutting thorough all the major morpho-tectonic units of the orogen. The river traverses vast alluvial plains before falling into its ultimate sink, the Bay of Bengal. The upper reach of the Ganga river system comprises two major tributaries i.e. the Alaknanda and Bhagirathi rivers that drain out through the major litho-tectonic units of the Himalayan orogen. This region also shows a varied climatic regime where precipitation ranges from ~3000 mm/year at the mountain front of the Higher Himalaya to 1200 mm/year at the foothills. Thus the river system provides a natural laboratory to study the generation of fluvial landforms in response to climatic perturbations and tectonic pulsation, the two major forcing factors for the development of river terraces during the Late Pleistocene-Holocene in the mountainous catchment of the Himalaya.

The geomorphic study, in terms of the total height of the bedrock steps and overlying alluvial cover records three types of fluvial terraces in this valley: (i) Cut-and-fill terraces with thick alluvial cover over a thin bedrock step; (ii) terraces with almost equal thickness of alluvial cover and underlying bedrock step; and (iii) terraces with thicker bedrock steps and thin alluvial cover. Sedimentologically the alluvial cover is composed of clast-supported massive gravel (Gcm), matrix-supported gravel (Gmg), clast-supported horizontally stratified gravel (Gh) and horizontally stratified sand (Sh). These deposits are formed by (a) the aggrading channel bars, (b) episodic flash floods and (c) by the local landslides (Srivastava and others, 2008).

The luminescence chronology shows that the aggradational events are in two major phases; first from 49-25 ka and secondly from 18-11 ka. These phases are in coherence with global climatic oscillations. The Aggradation in these valleys is focused at Marine Isotope Stage 3 (MIS 3) and during the transition phase of MIS 2 and MIS 1. Glaciation-deglaciation processes in the upper reaches produced copious sediment during 63-11 ka, which were deposited by these rivers in several cycles and lead to extensive aggradation. The climatic changes at ~11 ka and then the completion of deglaciation process lead to increased fluvial discharge and decreased sediment supply, a condition favorable for incision of alluvial fills. Available literature from the Ganga plain and from the Ganga delta shows that the phase of aggradation is regional but the incision in the foreland initiated at least 2-3 ka later, after 7 ka (Srivastava and others, 2003 a, b; Tandon and others, 2006).

References

Srivastava, P., Singh, I.B., Sharma, M. and Singhvi, A.K., 2003a, Luminescence chronometry and Late Quaternary geomorphic history of the Ganga Plain, India, Palaegeography, Palaeoclimatology, Palaeoecology 197, 15–41.

Srivastava, P., Sharma, M. and Singhvi, A.K., 2003b, Luminescence chronology of incision and channel pattern changes in the River Ganga, India. Geomorphology 51, 259-268.

Srivastava, P., Tripathi, J.K., Islam, R. and Jaiswal, M.K., 2008, Fashion and phases of Late Pleistocene aggradation and incision in Alaknanda River, western Himalaya, India, Quaternary Research 70, 68-80.

Tandon, S.K., and others, 2006, Alluvial valleys of the Gangetic Plains, India: causes and timing of incision. Incised Valleys in Time and Space, SEPM Special Publication 85, 15–35.

Cite as: Ray, Y., Srivastava, P, Sundriyal, Y.P., 2010, Aggradation and Incision Phases in the Upper Reaches of the Ganga River System; Timescales and Implications for Hinterland-Foreland Relationships, *in* Leech, M.L., and others, eds., Proceedings for the 25th Himalaya-Karakoram-Tibet Workshop: U.S. Geological Survey, Open-File Report 2010-1099, 2 p. [http://pubs.usgs.gov/of/2010/1099/ray/].

Correlation of Stratigraphy Along Strike in the Himalaya

Delores M. Robinson[1]

[1]Department of Geological Sciences, The University of Alabama, Tuscaloosa, AL 35473, U.S.A., dmr@geo.ua.edu

Incorrect correlation of the stratigraphic units along strike in the Himalaya is currently causing a communication breakdown amongst researchers. For example, researchers who work in Nepal view the Lesser Himalayan sequence as a group of Paleo- and Mesoproterozoic rocks. Above these units and separated by a billion-year unconformity and completing the Lesser Himalayan rock group are the Gondawanan and Foreland Basin sequences. In Northwest India, Lesser Himalayan sequence rocks have terms which refer to their position in relation to the Indian craton – Inner and Outer, and includes Proterozoic rock as well as rock that is as young as Cambrian in age, the Tal Group (Hughes and others, 2005). Rocks unconformably on top of the older Lesser Himalayan sequence and completing the Lesser Himalayan rock group correlate to the Gondawanan and Foreland Basin sequences. This Cambrian-aged Tal Group is referred to as Lesser Himalayan sequence rock but what makes these rocks Lesser Himalayan sequence rock as opposed to Tethyan (or Tibetan) Himalaya rock? Tethyan Himalayan rock deposition also began in early Paleozoic and may extend back into Precambrian time. Some researchers advocate that because of the geographic location of the Cambrian rock toward the Indian craton, they should be called Lesser Himalayan rocks. Some researchers advocate that because of the age of the units, they should be called Tethyan Himalayan rocks. However, are age and/or geographic location the proper way to define a unit? If that is true, than all rocks of a certain age should have the same name which is not sensible if the origins are different. In Nepal, the Lesser Himalayan region is still sometimes referred to as that geographic area between the highlands, Greater Himalaya rock, and the lowlands, Siwalik Group rock. However, Lesser Himalaya should not be referred to as a geographic location, rather, the name should be reserved for the Lesser Himalayan rock group. Age and geographic location are not viable ways to group rocks in the Himalaya; thus, the only plausible correlation that remains is to group rocks that have a similar origin together.

However, this is a difficult idea because researchers can not agree as to the origin of each of these units. In general, across the Himalayan arc, Lesser Himalayan rocks are referred to as those units which are derived from the Indian craton. Thus, the isotopic signatures and detrital zircons should look similar to those of the Indian craton. This is true until one examines the Cambrian "Lesser Himalayan" rocks. These signatures have characteristics which span across the Lesser, Greater, and Tethyan Himalayan rocks (e.g. Richards and others, 2005). This occurs in India, as previously stated, and also in Bhutan. The Baxa Formation has a stratigraphic position that suggests it is part of the Lesser Himalayan sequence but certain samples yield detrital zircons which suggests more similarity to Tethyan Himalayan rocks and ages that are Cambrian-Ordovician in age. Should these units still be referred to as Lesser Himalayan? Or should there be a different name for these units?

In addition, lower Tethyan Himalayan rocks that are Cambrian-Ordovician in age such as the Haimantas Group in Northwest India and Chekha Formation in Bhutan are the same age as the "Lesser Himalaya" units mentioned above, and occupy the geographic region in which rocks are usually referred to as Lesser Himalayan, south of the Greater Himalayan rocks. Are these units more similar than different? Is it possible that the Haimantas Group and Chekha Formation are the units more proximal to the erosion of Greater Himalayan rocks and that the Tal Group and Baxa Formation may be more proximal to the Indian craton? Because of their position as rocks which are eroded from and overlap both older Lesser and Greater Himalayan rocks, both groups of rocks are cover sequences shed into an intervening basin between older Lesser Himalayan rocks and the outer (with respect to India) Greater Himalayan rocks. Thus, these units would contain overlapping ages and isotopic signatures that make them neither "Lesser Himalaya" nor "Tethyan Himalaya". Perhaps a new stratigraphic architecture should be developed or at least a nomenclature that does not cause confusion.

Greater (or Higher) Himalayan rocks are not without difficulty and nomenclature confusion. A subdivision was developed in central Nepal for defining the units formally as Formations I, II, and III and informally as units I, II, and III. However, the system breaks down when attempting to span across the entire arc. In Bhutan, this system is not appropriate. Rocks are not only high-medium grade but include schist and quartzite with primary bedding and do not include a simple tripartite system. In far-western Nepal, unit 2, which is primarily composed of calcsilicate, is not present (Robinson and others, 2006). In northwest India, I have observed that the tripartite system is also not appropriate. In central Nepal, rock that is related to Greater Himalayan rocks in the crystalline klippe do not adhere to this system. Clearly, more work needs to be done understanding how Greater Himalayan rocks, which span an age from ~900 to 480 Ma, are related to the other systems. Because Greater Himalayan rocks can have an age range that overlaps the ages of both Tethyan and Lesser Himalayan rock, more work needs to be done in order to understand the original nature of the contacts between these units.

References

Hughes, N.C., and others, 2005, Early Tsanglangpuan (late early Cambrian) trilobites from the Nigali Dhar syncline and the Cambrian biostratigraphy of the Tal Group, Lesser Himalaya, India, Geological Magazine, v. 142, p. 57-80.

Richards, A., and others, 2005, Himalayan architecture constrained by isotopic tracers from clastic sediments, Earth and Planetary Science Letters, 236, 773-796.

Robinson, D.M., DeCelles, P.G. and Copeland, P., 2006, Tectonic evolution of the Himalayan thrust belt in western Nepal: Implications for channel flow models, Geological Society of America Bulletin, v. 118, p. 865-885, doi: 10.1130/B25911.1.

Cite as: Robinson, D.M., 2010, Correlation of Stratigraphy Along Strike in the Himalaya, *in* Leech, M.L., and others, eds., Proceedings for the 25th Himalaya-Karakoram-Tibet Workshop: U.S. Geological Survey, Open-File Report 2010-1099, 2 p. [http://pubs.usgs.gov/of/2010/1099/robinson/].

The Climate of Asia and Tibet – Not Just a Simple Monsoon

Gerard H. Roe[1]

[1] Department of Earth and Space Sciences, University of Washington, Seattle, WA 98195, USA, gerard@ess.washington.edu

Asia, the largest continuous landmass, experiences the greatest seasonality and climate gradients on Earth, and induces an atmospheric circulation that each year draws more than half the air mass of a hemisphere across the equator. Tibet, the largest topographic feature outside of the poles, sits square in the middle of the jet stream and induces atmospheric circulation patterns that affect climate around the globe.

Within Earth Sciences, and also many textbooks, the climate of Asia is often deconstructed into two semi-annual components: a wintertime, dry cold monsoon, associated with the Siberian high-pressure system; and a summertime, warm wet monsoon associated with a thermal low-pressure system over the continent. In the extreme of this cartoon, the whole Indian-Asian monsoon system is depicted as a single dynamical system, driven by the thermal contrast between land and ocean.

In actuality, this vast tract of real estate experiences a rich spatial structure of atmospheric circulation and related weather. In many cases these varied phenomena have largely independent causes. Moreover some of the most interesting features of the climate dynamics defy a simple deconstruction into two monsoonal seasons.

Some examples of this: in fall, northern Asia experiences the greatest circulation variability anywhere in the hemisphere; year-round coastal and orographic precipitation dominates in the maritime climates of southeast China; the greatest concentration of storm development anywhere on Earth happens during springtime in the lee of the Mongolian Altai - these storms loft dust into the atmosphere and create the loess plateau and the associated environmental records; temperatures fall in India when the monsoon intensifies, breaking the link between precipitation and land-sea temperature contrasts; a springtime maximum in precipitation in western Asia occurs due to a storm track emanating from the Mediterranean; precipitation across central China maximizes in late summer due to a circulation feature known as the Meiyu front.

Recent studies of the dynamics of the monsoon have focussed on the moist entropy as the key driver of the south Asian monsoon, and have distinguished between the relative roles of the Himalaya and the plateau proper. While these advances have helped improved theoretical understanding of monsoon dynamics, complex land-atmosphere interactions and strong climate gradients means there remains great uncertainty over future regional climate changes.

Asia is also an important repository of paleoclimate information: striking connections are apparent between abrupt climate changes in the North Atlantic and isotopes in speleothems across China. However the dynamical connections remain elusive. Our confidence in the reconstruction and understanding of past climate variations rests on our accounting for, and understanding the cause of, modern variability. Toward that end, the recent incorporation of isotopes into global climate models represents an exciting development. Initial results from several groups suggest that the climatic controls on isotopic variations vary in different parts of Asia, with some places following the clear and theoretically predicted relationship between isotopic fractionation and precipitation intensity, whereas other regions appear to be controlled by variations in moisture source.

Cite as: Roe, G.H., 2010, The Climate of Asian and Tibet – Not Just a Simple Monsoon, in Leech, M.L., and others, eds., Proceedings for the 25th Himalaya-Karakoram-Tibet Workshop: U.S. Geological Survey, Open-File Report 2010-1099, 1 p. [http://pubs.usgs.gov/of/2010/1099/roe/].

Lower-Crustal Flow Beneath the Tibetan Plateau: Evidence from the 2001 Kokoxili Earthquake

Isabelle Ryder[1], Roland Bürgmann[2], Zheng-Kang Shen[3]

[1] School of Environmental Sciences, University of Liverpool, L69 3GP, UK, i.ryder@liv.ac.uk
[2] Berkeley Seismological Laboratory, UC Berkeley, CA 94704, U.S.A.
[3] Department of Earth and Space Sciences, UCLA, CA 90095, U.S.A.

In November 2001 a magnitude 7.8 earthquake ruptured a 400-km long portion of the Kunlun fault, northeastern Tibet. In this study we analyse over five years of postseismic geodetic data for the Kokoxili event and interpret the observed surface deformation in terms of viscoelastic relaxation in the lower crust. A combination of GPS (first year) and InSAR observations (2-5 years) allows us to place robust constraints on lower-crustal rheology. Asymmetry exists between surface displacements on the north and south side of the fault, with the latter showing a faster rate of deformation. Displacements on both sides of the fault are well explained by a Burgers rheology, which has two time constants and so can account for both the rapid early part of the postseismic transient and the subsequent slower phase. However, to account for the cross-fault asymmetry in rate, higher viscosities are required on the north side with respect to the south side; this is consistent with a more rigid Qaidam basin to the north, relative to the Qiangtang block to the south. This result is also consistent with independent geophysical studies, for example the inference of lower crustal high conductivity south of the Kunlun fault system (Unsworth and others, 2004). The pattern of surface displacement observed in the InSAR dataset on each side of the fault is matched well by the respective Burgers models. Furthermore, the spatially simple deformation field does not require viscoelastic stratification in the lower crust. To investigate regional variability in rheological structure, we apply the southern values of transient and steady-state viscosity obtained in this analysis to the postseismic phase of the 1997 Manyi earthquake, which occurred 250 km to the west of the Kokoxili rupture (Ryder and others, 2007). We also make comparisons with viscosity constraints inferred from postseismic deformation following several moderate-to-large normal-faulting events in the northwestern and central parts of the plateau during 2004 to 2008 (e.g., Ryder and others, 2010).

References

Ryder, I., Parsons, B., Wright, T.J. and Funning, G.J., 2007, Post-seismic motion following the 1997 Manyi (Tibet) earthquake: InSAR observations and modelling, Geophysical Journal International, 169, 1009-1027.

Ryder, I., Bürgmann, R. and Sun, J., 2010, Tandem afterslip on connected fault planes following the 2008 Nima Gaize (Tibet) earthquake, Journal of Geophysical Research, 115, B03404.

Unsworth, M., and others, 2004, Crustal and upper mantle structure of northern Tibet imaged with magnetotelluric data, Journal of Geophysical Research, 109, B02403.

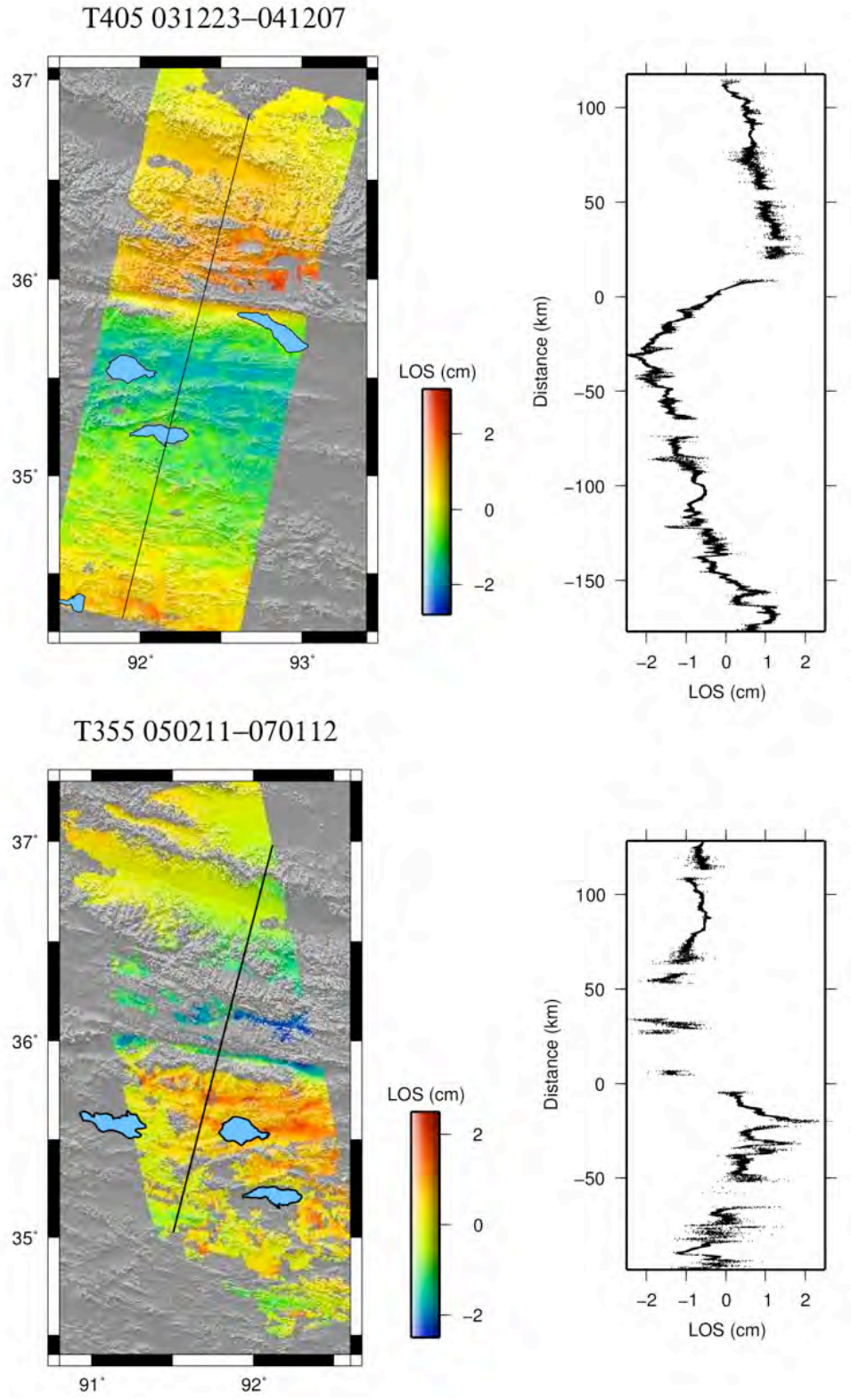

Figure 1. Postseismic interferograms for the 2001 Kokoxili earthquake, northeastern Tibetan Plateau. Black lines mark profile locations. Top: Envisat descending track 405; bottom: Envisat ascending track 355. To the right of each interferogram are line-of-sight displacement profiles. These show north-south asymmetry, which we attribute to a change in viscosity structure either across the Kunlun fault.

Cite as: Ryder, I., Bürgmann, R. and Shen, Z.K., 2010, Lower crustal flow beneath the Tibetan Plateau: evidence from the 2001 Kokoxili earthquake, *in* Leech, M.L., and others, eds., Proceedings for the 25th Himalaya-Karakoram-Tibet Workshop: U.S. Geological Survey, Open-File Report 2010-1099, 2 p. [http://pubs.usgs.gov/of/2010/1099/ryder/].

Seismic Velocity Structure From the ASCENT Seismic Array: Implications for Crustal and Mantle Deformation

Eric Sandvol[1], John Chen[2], James Ni[3], Frederik Tilmann[4], Shiyong Zhou[2], Yuhu Ma[5], Xiaoqing Zhang[4], Han Yue[2], Savas Ceylan[1], Bao Xueyang[1], Larry Brown[6]

[1] Department of Geological Sciences, University of Missouri-Columbia, Columbia, MO 65211, U.S.A.
[2] Institute for Theoretical and Applied Geophysics, Peking University, Beijing, China
[3] Department of Physics, New Mexico State University, Las Cruces, NM 88220, U.S.A.
[4] Bullard Laboratories, University of Cambridge, Cambridge, CB3 0EZ UK
[5] Earthquake Administration of Qinghai Province, China Earthquake Administration, Xining, Qinghai Province, China
[6] Earth and Atmospheric Sciences, Cornell University, Ithaca, NY 60602, U.S.A.

In order to study the evolution of the world's largest continental plateau, and the structure of the entire Himalayan-Tibet collision zone, Project INDEPTH (International Deep Profiling of Tibet and the Himalaya) was begun in 1992. The 4th phase of the INDEPTH project includes several key components including the deployment of a very large (600 km by 900 km) grid of seismometers covering nearly the entire northeastern corner of the Tibetan plateau (Figure 1). The northeastern boundary of the Tibetan Plateau is the location of several important tectonic boundaries within the Tibetan plateau including the Kunlun Fault Zone, Jinsha and Bangong-Nujiang sutures. In order to constrain various models for the evolution of the Tibetan lithosphere we have analyzed data from the ASCENT and surrounding arrays throughout the northeastern portion of the Tibetan plateau. Three-dimensional velocity structure derived from surface-wave tomography suggests there is strong heterogeneity within the Tibetan plateau including very slow seismic wave-speeds in the crust and mantle beneath the northernmost edge of the Tibetan plateau. Measurements of seismic attenuation are consistent with these low velocities as we observe much lower than average Lg and Pg Q values for most of the plateau with the exception of portions of the Qaidam basin crust. All these results strongly suggest that there can be little preserved anisotropic fabric in the crust or upper mantle beneath the northeastern corner of the plateau, with the exception of the Qaidam basin which seems to have a substantially thicker lithosphere.

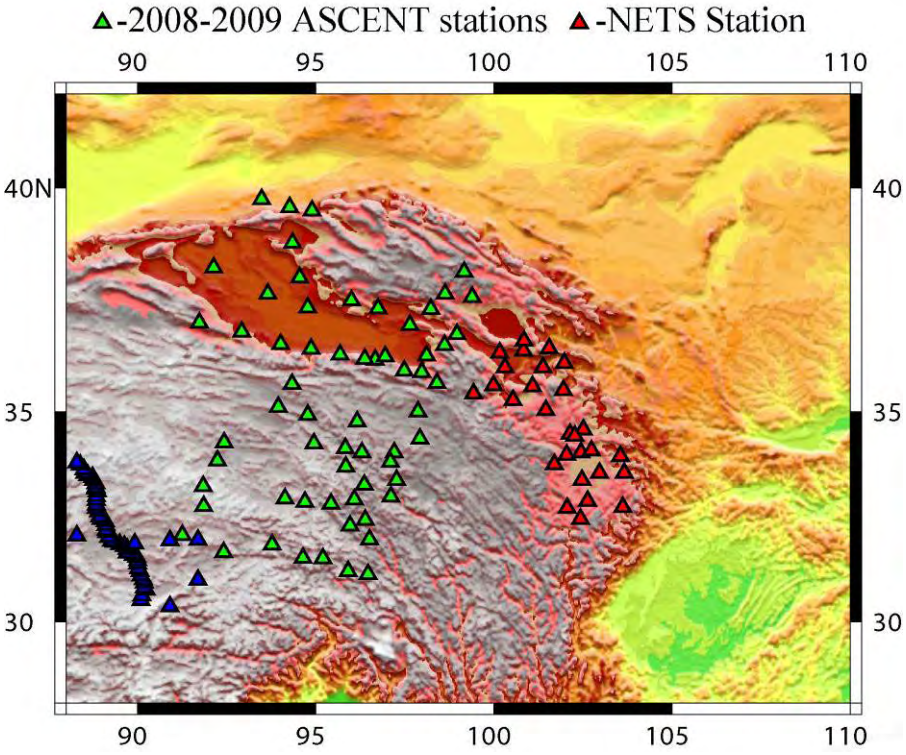

Figure 1. Map of recent temporary broadband seismic stations deployed in the northeastern corner of the Tibetan plateau. The blue stations are the stations deployed as a part of INDEPTH-III. All stations shown are broadband primarily composed of STS-2 and CMG-3T seismic stations. Approximately 50% of the stations, primarily in the north, were deployed for one year while the other half were deployed for two years.

We have combined both surface waves and body waves in order to estimate the three dimensional pattern of seismic anisotropy within the northeastern portion of the plateau. In general we observe a clockwise rotation in the fast directions of split SKS waves that is consistent with upper-mantle flow around the eastern Himalayan syntaxis. Azimuthal anisotropy from surface waves strongly indicates that this anisotropy is not confined to the lithosphere but extends into the asthenosphere. We observe significant azimuthal anisotropy (~2%) in the lower crust with fast directions that tend to follow the fast directions from the SKS measurements. We also observe evidence of asthenospheric flow along the eastern edge of the Tibetan plateau possibly affected by the lithospheric roots beneath the Sichuan basin and Ordos plateau.

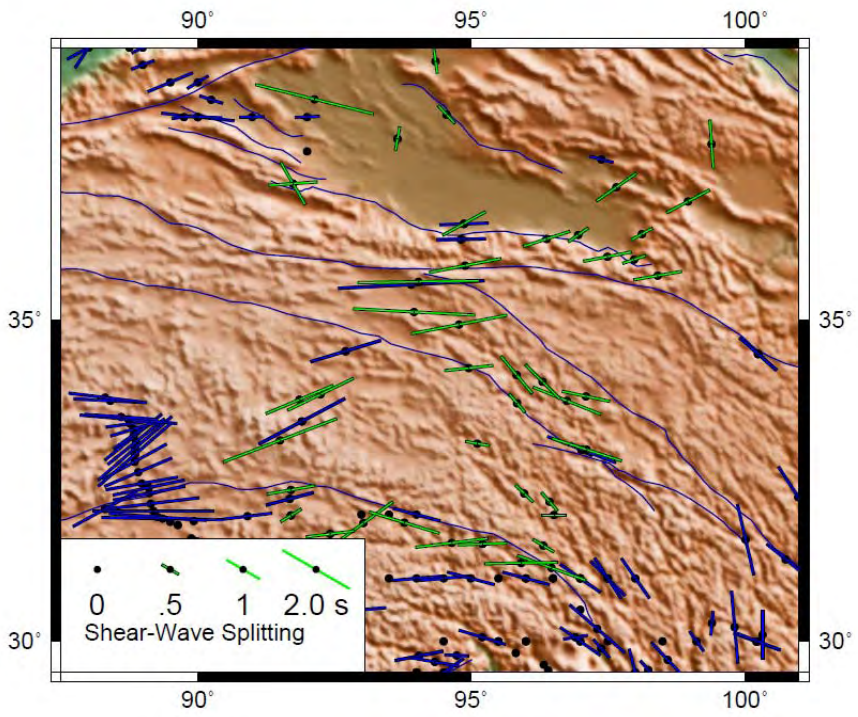

Figure 2. Map summarizing shear-wave splitting values for the Tibet plateau. The green (light) vectors are new unpublished results and the blue (dark) are previously published shear-wave splitting values. Note how most of the fast directions parallel the major fault zones and sutures.

We can interpret seismic anisotropic fast directions as indicative of present-day mantle strain patterns due to the observed low seismic wave-speeds throughout most of the northern Tibetan plateau excepting the Tarim and Qaidam basins. To first order we observe a fairly good agreement between our fast directions and the strike of the major fault zones outside of the Qaidam basin. This indicates a reasonable correlation between the strain fields of the Tibetan crust and the upper mantle. The geodynamic implications of this vertically coherent deformation (VCD) are currently being debated. Some have interpreted it as indicating a strong mechanical coupling between the crust and the mantle lithosphere, which is discordant with the evidence of a weak, flowing lower crust under Tibet. While the pattern of shear-wave splitting from this new and expanded datasets is in general agreement with previous results, we found important local variations, especially across the Bangong-Nujing suture zone, and significant azimuthal anisotropy in the lower crust. These variations indicate lithospheric heterogeneities between various terrains within the plateau. Recent numerical results show that the general coherence between crustal and mantle deformation can be attributed to the particular tectonic boundary conditions around the Tibetan Plateau which force both crustal and mantle material to flow coherently eastward as the consequence of the Indo-Asian collision. In this case the Tibetan VCD is consistent with a weak and flowing lower crust.

Cite as: Sandvol, E., and others, 2010, Seismic Velocity Structure From the ASCENT Seismic Array: Implications for Crustal and Mantle Deformation, *in* Leech, M.L., and others, eds., Proceedings for the 25th Himalaya-Karakoram-Tibet Workshop,: U.S. Geological Survey, Open-File Report 2010-1099, 2 p. [http://pubs.usgs.gov/of/2010/1099/sandvol.html].

Probing our understanding of the seismic cycle in the Himalayas of Nepal: Investigating mega-quakes with mega-trenches

Soma Nath Sapkota[1], Paul Tapponnier[2-3], Laurent Bollinger[4], Yann Klinger[2], Frederic Perrier[2], Dilli Ram Tiwari[1], Surendra Raj Panta[5], Indira Siwakoti[5]

[1] Department of Mines and Geology, National Seismological Centre Lainchaur Kathmandu, somanathsapkota@yahoo.com
[2] IPGP, Paris, France
[3] NTU, Singapore
[4] CEA/DIF/DASE France
[5] Tribhuwan University Central Department of Geology

Between Assam in the east and Kumaon in the west, the Himalayan range has experienced four catastrophic earthquakes since 1880, including the 1934 Bihar-Nepal earthquake. Results from geodetic and seismic monitoring show that elastic strain is rapidly accumulating along the locked part of the Main Himalayan Thrust (MHT), which is responsible for these events. Large earthquakes are therefore expected to devastate the Himalayan front again. The gap west of Kathmandu and east of Dehradun, India, for instance, which has not ruptured in at least the last 500 years, stands out as a potential site for a future great earthquake. Understanding of the seismic cycle in the Himalayas has greatly improved in the last decade, based in part on over 32 years of collaboration in seismic monitoring between Nepal and France (DASE). This was complemented by several collaborative research projects involving geodetic and geological investigations. Geodetic monitoring from 25 cGPS stations installed in collaboration with Caltech has emerged as one of the most useful complements to seismology. Together, the seismic and geodetic datasets show that the most active fault is the Main Frontal Thrust, which absorbs 15–18 mm/yr of roughly north-south convergence. Seismological, geodetic, geomorphic and paleo-seismological investigations imply that this fault is locked from the surface to beneath the High Himalayan peaks, over a distance of about 100 km, and slips mostly during great earthquakes with Mw $\geq$ 8.

The return periods of such earthquakes, or potential surface ruptures associated with the latest events, are uncertain or unknown. Although a paleo-seismological study of the Main Frontal Thrust was started in 2000, the two main trenches dug, within the 1934 maximum shaking area in central eastern Nepal (Mahra Khola) (Lavé and others, 2005), and in the far-western Nepal seismic gap (Mohana River) (Yule and others, 2006), brought evidence for only one, much more ancient earthquake (1100 AD, and 1505 AD, respectively).

To try to settle such issues, in collaboration with IPGP (France) and EOS (Singapore), we continued to look for a potential rupture of the 1934 Bihar-Nepal earthquake. We focussed our search between the Mahara Khola and Dharan, an area entirely within the 1934 isoseismal VIII. Two small trenches were dug in 2007-2008, and a natural river-cut section was refreshed. The Sir Khola river-cut provides exceptional exposure of offset terraces and shallow thrusting. Preliminary ^{14}C dating indicates the occurrence of two events more than 500 years apart, the last one postdating 1800. To confirm such results, we expanded the scale of our efforts and, in November 2009, opened a $\approx$ 60 m-long, >12 m-deep mega-trench across the 25 m-high cumulative scarp of the MFT near Charnath Khola. This trench, the largest in the Himalayas to date, exposes for the first time at least three thrust breaks of different ages. More than 300 charcoals were collected. We refreshed a nearby river-cut, revealing inverted and faulted Siwalik beds in the MFT hanging wall. Five smaller pits were also dug in terrace surfaces of different elevation to constrain their abandonment by ^{14}C dating. This large-scale paleo-seismological study was complemented by detailed topographic surveys, seismic profiles, and electrical-resistivity tomography. Such an integrated approach should help decide whether the 1934 event was blind or not, and provide a more definitive time sequence of catastrophic events in Nepal.

References

Lavé, J., and others, 2005, Evidence for a Great Medieval Earthquake (~1100 A.D.) in the Central Himalayas of Nepal, Science, 307, 1302-1305.

Yule, D., and others, 2006, Large surface ruptures of the Main Frontal Thrust in east-central and western Nepal: Evidence for an unprecedented type of Himalayan earthquake?, Abstract volume, International workshop on seismology, seismotectonics and seismic hazard in the Himalayan region, 28-29 November 2006, Kathmandu, 13-14,

Cite as: Sapkota, S.N., and others, 2010, Probing our understanding of the seismic cycle in the Himalayas of Nepal: Investigating mega-quakes with Mego-trenches, *in* Leech, M.L., and others, eds., Proceedings for the 25th Himalaya-Karakoram-Tibet Workshop: U.S. Geological Survey, Open-File Report 2010-1099, 2 p. [http://pubs.usgs.gov/of/2010/1099/sapkota/].

Origin of 'Millipede' and 'Rotational' Inclusion-Trail Microstructures in the NW Himalaya and their Tectonic Significance

Mohammad Sayab[1], Domingo Aerden[2], Syed Z. Shah[1], Mohammad Asif Khan[1]

[1]National Centre of Excellence in Geology, University of Peshawar-25120, NWFP, Pakistan, msayab@hotmail.com
[2]Departamento de Geodinamica, Universidad de Granada, C/ Fuentenueva s/n, 18002 Granada, Spain

Conflicting kinematic models have been postulated for the development of 'millipede' and 'rotational' microstructures preserved in porphyroblasts involving porphyroblast rotation (e.g. Jiang and Williams, 2004; Jessell and others, 2009), non-rotation (e.g. Aerden and Sayab, 2008; Bell and Hobbs, 2010) or little relative rotation (e.g. Johnson, 2009). These different interpretations of porphyroblast microstructures have important implications for the tectono-metamorphic growth of orogenic terrains. For this study, we applied advanced 3D microstructural techniques to examine the orientation of inclusion trail patterns preserved in porphyroblasts in medium- to high-grade rocks of the Swat region of the NW Himalaya in Pakistan. This area represents Indian-plate rocks that were deformed and metamorphosed during the Himalayan orogeny.

Previous workers in the Swat area and adjacent regions assumed 'rotational' porphyroblast models to calculate shear strain and kinematics of the thrust sheets. However, the timing of porphyroblasts preserving different types of inclusion trail patterns with respect to successive deformation regimes that affected the study area have remained poorly constrained. In order to investigate the growth sequence of porphyroblasts and their relationship with the orogenic evolution of the NW Himalaya, we applied two independent techniques for determining the orientation of inclusion trails in 3D developed by Hayward (1990) and Aerden, (2003). Both techniques are based on the measurements of porphyroblast inclusion-trail microstructures from multiple, differently-oriented thin sections of single samples. Axes of relative porphyroblast–matrix rotation (FIA: Foliation Intersection/Inflection Axes) previously determined via these methods in other orogens have systematically revealed regionally consistent orientations of these microstructures that appear to relate to (successive) crustal shortening directions that can, commonly, no longer be deduced from the study of matrix microstructures alone (e.g. Bell and others, 1995).

Fifty-five samples analyzed using both techniques yield coherent single- and multi-FIA results that demonstrate the existence of three principal sets of FIA in the study area. These FIA sets can be distinguished based on their specific relative timing, and geographic trends (Figure 1a). The FIA-trend succession, from old to young, is SE-NW (FIA set 1), E-W (FIA set 2) and NNE-SSW (FIA set 3). FIA set 2 can be further subdivided into set 2a (ESE-WNW) and set 2b (ENE-WSW). The FIA succession suggests an anticlockwise rotation of the bulk shortening directions through time, consistent with the collision history of the Indian plate, Kohistan-Ladakh Island Arc (KLIA) and the Eurasian plate since 55 Ma (Figure 1b-d). The orientation of FIA set 2 can be correlated with early-formed E-W trending thrust-related structures, whereas the trend of FIA set 3 is consistent with the younger regional-scale NNE-SSW trending folds and shear zones. FIA set 1 reflects the orientation of primitive structures that mark the trend of initial collision of the Indian plate with the KLIA. Regionally, relics of these primitive structures are barely preserved due to transposition by later deformation that caused for FIA sets 2 and 3.

The relative timing of E-W versus NNE-SSW trending regional structures in the Swat region was controversial (cf. Coward and others, 1988; Treloar and others, 1989; DiPietro and others, 2008), but is now resolved by the succession of FIA data and crustal shortening directions recorded by these microstructures (Figure 1d). In addition, two separate kyanite-grade metamorphic cycles have been identified associated with N-S (FIA set 2) and E-W (FIA set 3) shortening. Our combined data for both 'millipede' and 'rotational' types of inclusion trails indicate that all developed during a polyphase deformation history without having experienced significant relative rotations between them.

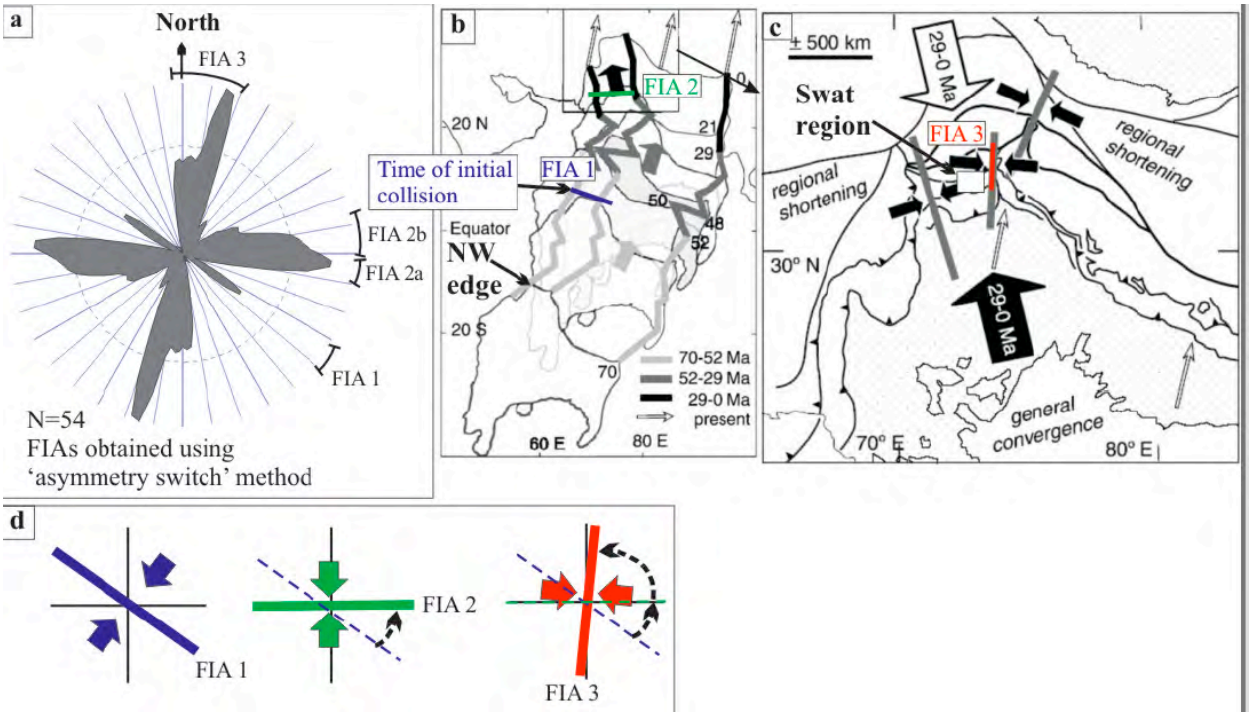

Figure 1. (a) Rose diagram showing FIA sets obtained with the 'asymmetry switch' method of Hayward (1990). (b) Movement trail of the Indian plate towards Eurasia after Patriat and Achache (1984). (c) Regional shortening directions inferred from fold orientations and plate convergence in the NW Himalaya (after Llana-Funez et al., and others, 2006). (d) Interpretation of the FIA sets (mean trends) with respect to the Indian plate (this study) convergence with the KLIA and Eurasian plate.

References

Aerden, D., and Sayab, M., 2008, From Adria- to Africa-driven orogenesis: Evidence from porphyroblasts in the Betic Cordillera, Spain, J. Struct. Geol. 30, 1272-1287.

Aerden, D.G.A.M., 2003, Preferred orientation of planar microstructures determined via statistical best-fit of measured intersection-lines: the 'FitPitch' computer program, J. Struct. Geol., 25, 923-934.

Bell, T.H. and Hobbs, B.E., 2010, Foliations and shear sense: a modern approach to an old problem, J. Geol. Soc. India, 75, 137-151.

Bell, T. H., Forde, A. and Wang, J., 1995, A new indicator of movement direction during orogenesis: measurement technique and application to the Alps, Terra Nova 7, 500-508.

Coward, M.P., and others, 1988, Folding and imbrications of the Indian crust during Himalayan collision, Phil. Trans. Roy. Soc. Lond. Ser. A, 326, 89-116.

Jiang, D. and Williams, P.F., 2004, Reference frame, angular momentum, and porphyroblast rotation, J. Struct. Geol., 26, 2211-2224.

DiPietro, J.A., Ahmad, I. and Hussain, A., 2008, Cenozoic kinematic history of the Kohistan fault in the Pakistan Himalaya. Geol. Soc. Am. Bull., 120, 1428-1440.

Hayward, N., 1990, Determination of early fold axis orientations in multiply deformed rocks using porphyroblast inclusion trails, Tectonophysics, 179, 353–369.

Jessell, M.W., Bons, P.D., Griera, A., Evans, L.A., and Wilson, C.J.L., 2009, A tale of two viscosities, J. Struct. Geol., 31, 719-736.

Johnson, S.E., 2009, Porphyroblast rotation and strain localization: Debate settled!, Geology, 37, 663-666.

Llana-Funez, S., Burg, J-P., Hussain, S.S., Dawood, H. and Chaudhry, M.N., 2006, Structural evolution of the footwall of the Indus Suture in Malakand (N Pakistan) during the Himalayan collision, J. Asian Earth Sci., 28, 691-706.

Patriat, P. and Achache, J., 1984, India-Eurasia collision chronology has implications for crustal shortening and driving mechanism of plates, Nature, 311, 615-621.

Treloar, P.J., Broughton, R.D., Williams, M.P., Coward, M.P. and Windley, B.F., 1989, Deformation, metamorphism and imbrication of the Indian plate, south of the Main Mantle thrust, north Pakistan, J. Metamorph. Geol., 7, 111–125.

Cite as: Sayab, M., Aerden, D., Shah, S.Z. and Khan, M.A., 2010, Origin of 'Millipede' and 'Rotational' Inclusion-Trail Microstructures in the NW Himalaya and their Tectonic Significance, *in* Leech, M.L., and others, eds., Proceedings for the 25th Himalaya-Karakoram-Tibet Workshop: U.S. Geological Survey, Open-File Report 2010-1099, 2 p. [http://pubs.usgs.gov/of/2010/1099/sayab/].

Cenozoic Emplacement Age of the Kangmar Granite in South Tibet

Chie Shirakawa[1], Simon R. Wallis[1], Kouki Kitajima[2], Yuji Sano[2]

[1] Department of Earth and Planetary Sciences, Graduate School of Environmental Studies, Nagoya University, Nagoya 464-8601, Japan, shirakawa.chie@f.mbox.nagoya-u.ac.jp
[2] Atmosphere and Ocean Reserch institute, The University of Tokyo, Kashiwa, Chiba 277-8568, Japan

The north Himalayan metamorphic domes have a deformed granite core that is mantled by metamorphic rocks. These domes are situated between the high Himalaya and the Yarlang Tsangpo suture zone and expose rocks formed at mid-crustal levels. Studies of these rocks are important for understanding the relationships between these two geological domains. The Kangmar dome is one of the best studied domes, and previous workers reported two U-Pb zircon ages of granite: 562±4 Ma (Shärer and others, 1986) and about 507 Ma (Lee and others, 2000). Based on these two ages, the Kangmar granite is regarded as a part of the pre-Himalayan Indian basement. However, the granitic core of another well-documented member of the north Himalayan metamorphic domes – the Malashan dome – yields Tertiary zircon ages and shows intrusive relationships with the surrounding Jurassic sediments suggesting it is best interpreted as a granite body related to the Himalayan orogeny (Aoya and others, 2005). Zircons from the Malashan granite show clear differences between old cores that commonly have ages of around 500 Ma and rims of around 20 Ma that represent intrusion age. The complications revealed in the Malashan area suggest that the formation age of the North Himalayan domes including the Kangmar granite may need to be revised. The purpose of this study is to re-evaluate the emplacement age of the Kangmar granite.

In the northwestern area of the Kangmar dome, field observation shows a granite dike cross-cutting pelitic schist that is correlated with Carboniferous (355–295 Ma) deposits. This observation constrains the age of the Kangmar granite to be younger than Lower Carboniferous and suggests, therefore, that the reported ages of around 500 Ma do not represent timing of granite intrusion. We interpret these old ages as probable xenocryst ages. This interpretation can account for the large difference in reported zircon ages of 50 million years.

In order to constrain timing of intrusion, we carried out U-Pb zircon dating for 44 grains of zircon. The zircon grains were separated from two-mica granites sampled from the dyke and core body. Backscattered electron images of zircons show a clear separation into core and brighter but narrow rim domains (Fig. 1). The narrow rims locally show both oscillatory and sector zoning, suggesting an igneous origin. For this study it was important to date the narrow rims and we used a Cameca NanoSIMS 50 instrument (at Ocean Research Institute, University of Tokyo) with which it is possible to analyze spots of less than 10 microns (Takahata and others, 2008). Because of the thickness of rim (about 5–20 μm) and low content of Pb, only a few Pb-Pb data were obtained. Core analyses yielded mainly fell in the range of about 500 Ma to 450 Ma (Fig. 2). Rim analyses show a wide scatter including Tertiary ages (Figs. 2 and 3).

Tertiary zircon age is consistent with the age of the Malashan granite and other young granite in the north Himalayan domes (Lee and Whitehouse, 2007). We propose, the Kangmar granite does not represent the Indian basement, as generally thought, but is a young granite body intruded during the Tertiary Himalayan orogeny. This implies it is necessary to reconsider the formation mechanism of the north Himalayan metamorphic domes.

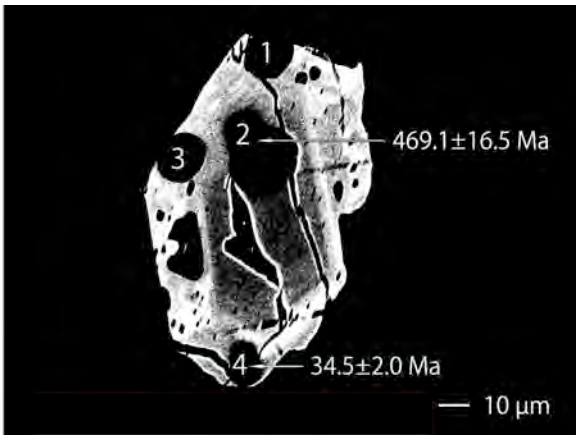

Figure 1. Backscattered electron image of a zircon grain from the Kangmar granite showing analyzed spots and corresponding $^{238}U/^{206}Pb$ ages. Analyses of spots 1&3 were excluded because of interferences of resin.

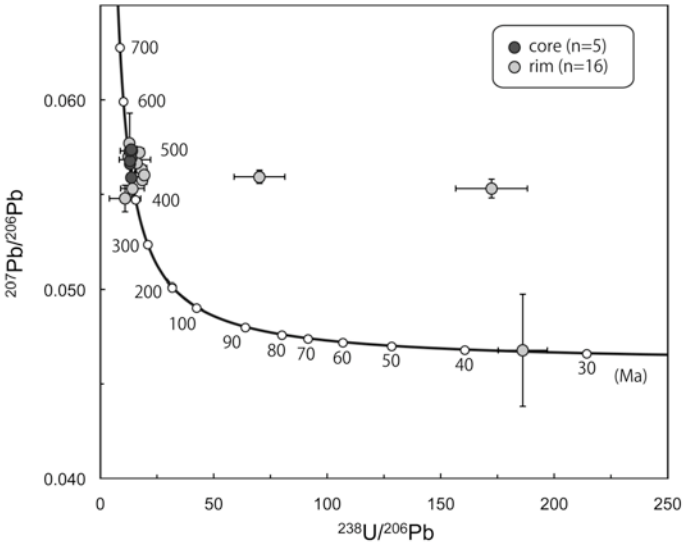

Figure 2. Tera-Wasserburg U-Pb concordia diagram for the Kangmar granite. Data are corrected for common Pb (±2 sigma).

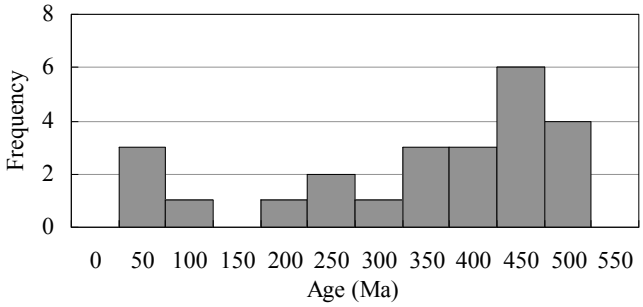

Figure 3. $^{238}U/^{206}Pb$ age distribution for 24 rim analyses.

References

Aoya, M., and others, 2005, North-south extension in the Tibetan crust triggered by granite emplacement, Geology, 33, 853-856.

Lee, J., and others, 2000, Evolution of the Kangmar Dome, southern Tibet: Structural, Petrologic, and thermochronologic constraints, Tectonics, 19, 872-895.

Lee, J. and Whitehouse, M. J., 2007, Onset of mid-crustal extensional flow in southern Tibet: Evidence from U-Pb zircon ages, Geology, 35, 45-48.

Shärer, U., Xu, R.-H. and Allégre, C.J., 1986, U-(Th)-Pb systematics and ages of Himalayan leucogranites, south Tibet, Earth and Planetary Science Letters, 77, 35-48.

Takahata, N., Tsutsumi, Y. and Sano, Y., 2008, Ion microprobe U-Pb dating of zircon with a 15 micrometer spatial resolution using NanoSIMS, Gondowana Research, 14, 587-596.

Cite as: Shirakawa, C., Wallis, S.R., Kitajima, K. and Sano, Y., 2010, Cenozoic Emplacement Age of the Kangmar Granite in South Tibet, *in* Leech, M.L., and others, eds., Proceedings for the 25th Himalaya-Karakoram-Tibet Workshop: U.S. Geological Survey, Open-File Report 2010-1099, 2 p. [http://pubs.usgs.gov/of/2010/1099/shirakawa/].

Geochemical Constraints on the Origin of the Ophiolites of the Indo-Myanmar Orogenic Belt, North East India

A. Krishnakanta Singh[1]

[1]Wadia Institute of Himalayan Geology, 33, General Mahadev Singh Road, Dehradun – 248001, India, aksingh_wihg@rediffmail.com

The Naga-Manipur Ophiolite (NMO), oceanic lithosphere of probable upper Cretaceous age, forms part of the NNE-SSW (~200 km in length, ~ 2-20 km in width, covers an area ~2000 sq. km.), trending Indo-Myanmar Orogenic Belt (IMOB). Further south in structural continuity with this belt, the Andaman and Nicobar Islands Arc has formed and the belt continues further southeast to the Mentawai Islands representing the outer Indonesian Island Arc (Moore and others, 1980). The IMOB is interpreted as representing the eastern suture of Indian plate formed due to the collision of the Indian plate with the Myanmar plate (Mitchell, 1981; Acharyya and others, 1989). The ophiolite sequence in this region is highly tectonised, dismembered and shows three phases of deformational events broadly comparable to the Himalayan orogeny and sea floor spreading of the Indian Ocean (Ghose and others, 1986). The ophiolites occur mainly as rootless subhorizontal bodies overlying Eocene-Oligocene flyschoid sediments.

Peridotites (harzburgite, lherzolite, wehrlite, dunite), mafic intrusives (gabbro, dolerite), mafic volcanics (massive basalt, pillow basalt, agglomeratic basalt), pelagic sediments (chert, cherty quartzite, marl, shale, phyllite, limestone) and podiform chromitites (massive, nodular, disseminated, granular) are the dominant lithologic units of this ophiolite. The absence of sheeted dykes together with the paucity of lavas in the ophiolites might be explained by formation in a slow-spreading environment where the magma budget was low and volcanism was episodic. Random distribution of chromitites suggests deep-mantle magmatic segregation and subsequent disruption of primary cumulate chromitites by deep-seated mantle subsolidus deformation (Coleman, 1977).

The Cr-spinel in peridotites of NMO is characterized by low Cr_2O_3 (10.03-41.12 wt.%) and high Al_2O_3 (25.34-55.86 wt.%), FeO (11.45–14.51 wt.%) and MgO (13.27–18.41 wt.%). Their chemistry is comparable to those of observed Cr-spinel of abyssal peridotites (Dick and Bullen, 1984; Arai, 1992). The mafic volcanics are represented by chemically two distinct groups of high-Ti and low-Ti mafic volcanics. The high-Ti type shows relatively uniform compositions and they have geochemical characteristics of Ti > 1 wt. %; Ti/V = 21-45; mild LREE depletion with flat HFSE patterns that are compatible with those of high-Ti basalts generated at mid-ocean ridges, whereas the low-Ti type shows Ti < 1 wt. %; Ti/V < 20; strong depletion of LREE with mild depletion of HFSE is consistent with the composition of magma generated in a supra-subduction zone setting from partial melting of refractory mantle source (Saccani and others, 2003).

The ophiolites containing both the high Al (Cr# = 30-60) and high-Cr chromite (Cr # = 75-80) chromitites, suggest a genetically separate process for these chromitites. Further it is suggested that high-Al chromite was modified by reaction with boninitic melts from which high-Cr chromite precipitated. These would typically be interpreted as chromites in equilibrium with tholeiitic melt and boninitic melts, indicating their genesis in mid-oceanic ridge and supra-subduction zone environment, respectively. Chromitites has higher concentrations of IPGE (Os, Ir, Ru) as compared to the PPGE (Rh, Pd, Pt) with concentration of PGE between 135 ppb and 551 ppb. The chondrite-normalized PGE patterns for these chromitites are comparable with typical podifom chromitites in ophiolite with enriched in IPGE and depleted in PPGE (Page and others, 1982; Zhou and others, 2005). Systematic study confirmed sulphide mineralization in these chromitites, and alloys were identified as argentite (Ag_2S), millerite (NiS), pentlandite (Fe, Ni)S etc. The sulphide mineral grains occur mainly as anhedral to subhedral (~ 5-20 mm in size) grains along the boundaries and fractures of chromites.

Evaluation of geochemical and petrogenetic data of the mantle sequence and cumulates reveals that the ophiolites of the Indo-Myanmar Orogenic Belt under investigation appear to have formed due to tectonic

dismemberment and accretion of material generated in an oceanic environment (i.e. MORB and OIB-type rocks) and after the process of accretion of the ophiolitic suite of rocks were affected by boninitic melts generated by partial melting of depleted peridotites in the fore-arc setting. This feature implies that tectonic incorporation into the accretionary wedge of MORB-type and OIB-type material occurred prior to the development of boninitic magmatism.

References

Acharyya, S.K., Ray, K.K. and Roy, D.K., 1989, Tectono-Stratigraphy and emplacement history of the Ophiolite assemblage from the Naga Hills and Andaman Island arc India. Journal of Geological Society of India. 33, 4-18.

Coleman, R.G., 1977, Ophiolites, Ancient oceanic lithosphere? Minerals and rocks series No.12, Springer-Verlag, Berlin, 229p.

Dick, H.J.B., Bullen, T., 1984, Cr-spinel as a petrogenetic indicator in abyssal and alpine-type peridotites and spatially associated lavas, Contribution to Mineralogy and Petrology, 86, 54-76.

Ghose, N.C., Agrawal, O.P. and Singh, R.N. 1986, Geochemistry of the ophiolite belt of Nagaland, N.E. India, In: Ghose, N.C. & Varadarajan, S. (eds.) Ophiolite and Indian plate margin. Sumna Publication, Patna, 241-293.

Moore, G.F., Curray, J.R, Moore, D.G. and Karig, D.E., 1980, Variations in geologic structure along the Sunda forearc, NE Indian ocean. In: The Tectonic and Geological Evolution of SE Asian Seas and Islands. Am. Geophys. Un., Geophys. Monog., 23, 145-160.

Mitchell, A.H.G., 1981, Phanerozoic plate boundaries in mainland SE Asia, the Himalayas and Tibet. Journal of Geological Society of London., 138, 109-122.

Page, N., Pallister, J., Brown, M., Smewing, J. and Haffty, J., 1982, Palladium, platinum, rhodium, ruthenium and iridium in Chromitite-rich rocks from the Samail Ophiolite, Oman, Canadian Mineralogist, 20, 537-548.

Saccani, E, Photiades, A. and Padoa, E., 2003, Geochemistry, petrogenesis and tectono-magmatic significance of volcanic and subvolcanic rocks from the Koziakas melange (Western Thessaly, Greece), Ofioliti, 28, 43-57.

Zhou, M.F., Robinson, P.T., Malpas, J. and Li, Z., 2005, Podifom chromitites in the Luobusa ophiolite (Southern Tibet): implications for melt-rock interaction and chromite segregation in the upper mantle, Journal of Petrology, 37, 3-21.

Cite as: Singh, A.K., 2010, Geochemical Constraints on the Origin of the Ophiolites of the Indo-Myanmar Orogenic Belt, North East India, *in* Leech, M.L., and others, eds., Proceedings for the 25th Himalaya-Karakoram-Tibet Workshop: U.S. Geological Survey, Open-File Report 2010-1099, 2 p. [http://pubs.usgs.gov/of/2010/1099/singh/].

Did the Late Miocene Phase of Himalayan Orogeny Drive a Major Shift in India's Climate and Vegetation?

S. Singh[1], B. Parkash[1], A. K. Awasthi[1], S. Kumar[2]

[1]Department of Earth Sciences, Indian Institute of Technology Roorkee, Roorkee-247667, India, geoseema05@yahoo.co.in
[2]National Institute of Hydrology, Roorkee-247667, India

Uplift of the Himalayan orogenic belt began as soon as the collision of the Indian and Eurasian plates took place at ~55 Ma ago. Since then, the Himalayan orogen has witnessed several phases of tectonic uplift, and the Himalaya attained a critical height to become a significant orographic barrier that set up an intense monsoonal climate, and consequently brought changes in flora and fauna of the Indian sub-continent. Besides changes in the sedimentological character of continental sediments, change in the photosynthetic pathway of plants on a large scale can reveal important information on the tectonic and climatic history of a region. In view of this, the objectives of the present work are (1) to reconstruct palaeovegetational and palaeoclimatic history from the isotopic study of Cenozoic Siwalik palaeosols in the Ramnagar sub-basin, (2) to examine observed similar palaeovegetational and palaeoclimatic changes, if any, in other parts of the Himalayan Foreland Basin (HFB) and (3) to correlate changes in palaeovegetation and palaeoclimate with the tectonic pulses in the late Cenozoic Himalayan orogeny.

We carried out carbon and oxygen isotope analyses of soil carbonate, largely nodules, from three Indian Siwalik sections: Jammu–Nandni, Purmandal-Uttarbehani and Samba-Mansar from Jammu & Kashmir state of India in the Ramnagar sub-basin covering a lateral stretch of ~40-50 km along strike (Figure 1a). The analysed samples cover a time range from mid-Miocene to late Pleistocene. In all the three studied sections, soil carbonate nodules were collected from the palaeosol horizons and their ages are assigned from ages of corresponding palaeosol beds, which are based on palaeomagnetic dating (Rao, 1993).

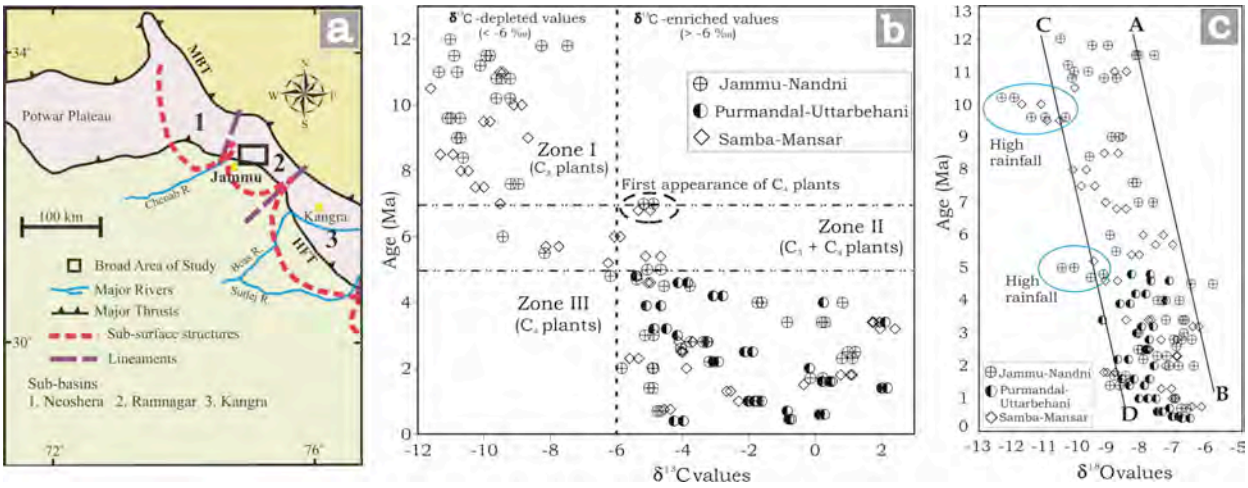

Figure 1 (a) Simplified geological map showing location of the present study in the Ramnagar sub-basin of the Himalayan Foreland Basin (modified after Raiverman, 2002). **(b)** Composite plot of $\delta^{13}C$ values against age from the studied sections. We divide the $\delta^{13}C$ values into two broad divisions; an older part characterized by $\delta^{13}C$ depleted isotopic values (< -6‰) and a younger part showing $\delta^{13}C$ enriched isotopic values (> -6‰) named Zone I and Zone III respectively. Zone I indicates the exclusive presence of C_3 plants whereas Zone III indicates the exclusive presence of C_4 plants. This change in vegetation with age from C_3 plants to C_4 plants spans a transition period, Zone II, in which both C_3 and C_4 plants have been found. Dotted ellipse marks the first appearance of C_4 plants at 7 Ma and 6.8 Ma in the Jammu-Nandni and Samba-Mansar sections respectively. **(c)** Composite plot of $\delta^{18}O$ values against age from the three studied sections. The $\delta^{18}O$ values are depleted from the normal AB-CD range at around 10 Ma and 5 Ma (marked by blue ellipses). These depleted values signify monsoon intensification during that time. The $\delta^{13}C$ and $\delta^{18}O$ values are expressed in per mil (‰).

Our results reveal that carbon isotopic record in the studied sections falls into two broad divisions, an older part (>7 Ma) characterized by $\delta^{13}C$-depleted isotopic values and a younger part (<5 Ma) consisting of $\delta^{13}C$-enriched values, respectively indicating exclusive presence of C_3 and C_4 plants (Figure 1b). This prominent change in vegetation from the primitive C_3 plants in mid-Miocene to C_4 plants in the late upper Miocene has also been reported in other parts of the HFB (Quade and others, 1989; Sanyal and others, 2004; and many more) and was first explained by Quade and others (1989) in the Pakistani and Nepali Siwaliks to be the result of intensification of Asian monsoon due to Himalayan uplift at ~10 Ma. Our oxygen isotope data also shows depleted $\delta^{18}O$ values from the normal AB-CD range at ~10 Ma and 5 Ma indicating an increase in rainfall or monsoon from the usual trend during that time (Fig. 1c). However, a time gap of ~5 Ma remains between complete vegetation change and monsoon intensification. Moreover, this late Miocene change in vegetation was a global phenomenon (Cerling and others, 1997; Selagen and others, 2007; and many more).

The Himalayan orogeny witnessed its greatest tectonic upheaval in the late Miocene (~10 Ma) as revealed by mean sediment accumulation rates in the HFB which have been derived from 56 magnetostratigraphic sections in the HFB (Sangode and Kumar, 2003), and this is well corroborated by much other geological evidence (Harrison and others, 1992; and many more). Even fluvial architecture changed markedly from minor to major multistoried sandstone bodies indicating an increase in channel dimension and discharge. Moreover, fossil evidence indicates that no significant physical barrier to migration of mammal faunas existed prior to the late Miocene (Wang and others, 1982). However, it seems monsoon intensification by this late Miocene tectonic uplift may not be a major cause for the prominent change in vegetation, but rather it seems more likely that increased chemical weathering due to late Miocene tectonic events resulted in a large-scale decrease in atmospheric CO_2 concentration (Raymo and Ruddiman, 1992) which finally prompted expansion of C_4 plants as they have a competitive advantage over C_3 plants when the ratio of atmospheric CO_2/O_2 concentration is low. Many workers have shown large-scale decline in atmospheric CO_2 concentration during the late Miocene (Spivack and others, 1993; and many more).

Hence the tectonic uplift of the Himalayan orogen during the late Miocene finally changed ancient tropical climate and C_3 vegetation of the Indian sub-continent to the present day monsoonal climate and C_4 vegetation.

References

Cerling, T.E., and others, 1997, Global vegetation change through the Miocene/Pliocene boundary, Nature, 389, 153-157.
Harrison, T.M., Copeland, P., Kidd, W.S.F. and Yin, A., 1992, Rising Tibet, Science, 255, 1663-1670.
Quade, J., Cerling, T.E. and Bowman, J.R., 1989, Development of Asian monsoon revealed by marked ecological shift during the latest Miocene in the northern Pakistan, Nature, 342, 163-166.
Raiverman, V. 2002, Foreland sedimentation: in Himalayan tectonic regime: A relook at the orogenic process, Bishen Singh Mahendra Pal Singh Publishers, Dehradun, India, 371.
Rao, R.A., 1993, Magentic polarity stratigraphy of Upper Siwalik of northwestern Himalayan foothills, Curr. Sc., 64, 863-872.
Raymo, M.E. and Ruddiman, W.F., 1992, Tectonic forcing of late Cenozoic climate, Nature, 359, 117-122.
Sangode, S.J. and Kumar, R., 2003, Magnetostratigraphic correlation of the Late Cenozoic fluvial sequences from NW Himalaya, India, Curr. Sci., 84, 1014-1024.
Sanyal, P., Bhattacharya, S.K., Kumar, R., Ghosh, S.K. and Sangode, S.J., 2004, Mio-Pliocene monsoonal record from Himalayan foreland basin (Indian Siwalik) and its relation to the vegetational change, Palaeo3, 205, 23-41.
Selagen, L., Lee Thorp, J.A. and Cerling, T.E., 2007, Timing of C_4 grass expansion across sub- Saharan Africa, Jour. of Human Evolution, 53, 549-559.
Spivack, A.J., You, C.F. and Smith, J.H., 1993, Foraminiferal Boron isotope ratios as a proxy for surface ocean pH over the past 21 Ma, Nature, 363, 149-151.
Wang, C.Y., Shi, Y.L. and Zhou, W.H., 1982, Dynamic uplift of the Himalayas, Nature, 289, 553-556.

Cite as: Singh, S., Parkash, B., Awasthi, A.K. and Kumar, S., 2010, Did the late Miocene phase of Himalayan orogeny drive a major shift in India's climate and vegetation?, *in* Leech, M.L., and others, eds., Proceedings for the 25th Himalaya-Karakoram-Tibet Workshop: U.S. Geological Survey, Open-File Report 2010-1099, 2 p. [http://pubs.usgs.gov/of/2010/1099/singh/].

Cooling and Exhumation Patterns associated with Tectonometamorphic Evolution of the Himalayan Metamorphic Belt in the Alaknanda and Dhauliganga valleys, Garhwal Himalaya, India

Sandeep Singh[1], Th. Nikunja Bihari Singha[1]

[1]Department of Earth Sciences, Indian Institute of Technology Roorkee, Roorkee-247 667, India, san662005@gmail.com

Two distinct packages of inverted metamorphic sequence of the Himalayan Metamorphic Belt (HMB) along the Alaknanda and Dhauliganga valleys of the Garhwal Himalaya are characterized by a basal package (Munsiari Formation) ranging from chlorite to staurolite zone, whereas the overlying package (Vaikrita Group) ranges from staurolite-kyanite to sillimanite-K-feldspar and migmatite zone, along with generation of insitu melt in the higher structural level.

The rates of cooling and exhumation of the HMB have been constrained using muscovite-biotite co-genetic pairs of Rb-Sr whole-rock mica ages (muscovite: 500±50°C and biotite: 300±50°C). In the present study we considered a simplified one-dimensional frame with the assumption that 30±10°C/km steady-state geothermal gradient persisted over the calculated age. The calculated data show that the rate of cooling or exhumation is higher at the central part of the thrust sheet indicating a concave upward geotherm or a reversal of the geotherm. Near the Vaikrita Thrust, mineral cooling ages give a higher exhumation rate of about 1.36 mm/yr between 8.61 Ma and 2 Ma, which is followed by an exceedingly high rate between 2 Ma and the present time within Munsiari Formation. The high cooling rate is associated with the measured shallow geothermal gradient in this area, which is related to the exceedingly high erosion rate observed in the dynamic and rugged terrain.

A total of 27 samples of metasediments, migmatites and leucosomes of the HMB along with Tethyan sedimentary rocks were also analysed for Nd-isotopic calculation for ε_{Nd} at the present time along with the corresponding values of $^{87}Sr/^{86}Sr$ ratios. The average value of $\varepsilon_{Nd\,(0)}$ and present-day $^{87}Sr/^{86}Sr$ ratios for the Vaikrita Group is ~ -16 (ranging between -7.0 and -21.4) and 0.78759 (ranging between 0.75152 and 0.86479) respectively. The samples mainly of leucosome yield anomalous values of ε_{Nd} probably due to high Sm/Nd ratio in the rocks and the corresponding $^{87}Sr/^{86}Sr$ ratio also has very high values indicating a disequilibrium melting of the crustal rocks. However, the Munsiari Formation values are ~ -25 (ranging between -24.0 and -25.8) and 0.90528 (ranging between 0.99398 and 0.81658). The ε_{Nd} and $^{87}Sr/^{86}Sr$ ratio values indicate that the source of the Munsiari Formation seems to be different that of the Vaikrita Group, whereas they appear to be part of same thrust sheets with similar tectonometamorphic history.

The migmatite zone gives a maximum temperature of metamorphism of about 700°C and a significantly lower pressure ranging from ~5 to ~7 kbar, whereas the lower part of the upper package also gives maximum temperature of about 700°C and pressure of about 12 kbar. The upper part of the Vaikrita Group clearly indicates total decompression of about 5-7 kbar and maintains near–isothermal conditions at about 700°C. On the contrary, the basal Munsiari Formation is characterized by lower pressure and temperature of about 7 kbar and 520°C. Garnet zoning profiles also indicate that the basal part of the Vaikrita Group displays progressive metamorphism. Between the basal Munsiari Formation and the upper Vaikrita Group, a sharp discontinuity in pressure and temperature is present across the Vaikrita Thrust (VT) where the contact between the staurolite zone and the staurolite-kyanite zone has been observed. However, no structural break has been encountered between these two packages. Samples from the basal part of the Vaikrita Group do not show the effect of the isothermal decompression, but seem to be overprinted by more recent localized metamorphism of short duration possibly related to thrusting along the VT.

Cite as: Singh, S. and Singha, T.N.B., 2010, Cooling and Exhumation Patterns associated with Tectonometamorphic Evolution of the Himalayan Metamorphic Belt in the Alaknanda and Dhauliganga valleys, Garhwal Himalaya, India, *in* Leech, M.L., and others, eds., Proceedings for the 25th Himalaya-Karakoram-Tibet Workshop: U.S. Geological Survey, Open-File Report 2010-1099, 1 p. [http://pubs.usgs.gov/of/2010/1099/singhsingha/].

Growth of drainage basins and sediment transport in the Dehradun Reentrant and Nahan Salient of the NW Sub-Himalaya: a comparative study

Tejpal Singh[1], A. K. Awasthi[2]

[1]Centre for Mathematical Modelling and Computer Simulation, NAL Belur Campus, Bangalore-560037, India
geotejpal@yahoo.co.in
[2]Department of Earth Sciences, Indian Institute of Technology Roorkee, Roorkee-247667, India

The kinematics of deformation within the foreland basins is realtively simple, but may be highly variable in space and time depending on the presence and orientation of pre-existing structures (DeCelles and Giles, 1996). We wish to understand how the variation in the kinematics of deformation and the geological structure effect the development of the surface topography, that in turn governs the evolution of the drainage network, basin geometries and related sediment transport processes.

The Sub-Himalayan belt is a classical example that has been sub-divided into a number of sub-basins based on the tectonic framework and basement geometry (Raiverman, 2002). The main structural entities present in the NW Sub-Himalayan belt include the areas of Kangra Reentrant, Nahan Salient and the Dehradun Reentrant (Figure 1).

Uplift within this belt has given rise to variable structural geometries in the abovementioned areas that manifest variable amount of shortening (Powers and others, 1998; Dubey and others, 2001) and convergence/slip/uplift rates in the NW Sub-Himalayan belt (Kumar and others, 2006). It varies a lot in space and time as demonstrated by the distribution of the topographic elevation (Figure 2). This uplift has given rise to a large number of drainage basins along the mountain front that exhibit variable geometries and surface topography. We integrate the morphometric data of these drainage basins with the field observations to characterize the geometry and surface topography of these basins (Figure 3). The most apparent and significant difference is in the form of basin areas. The basins present on the Mohand ridge

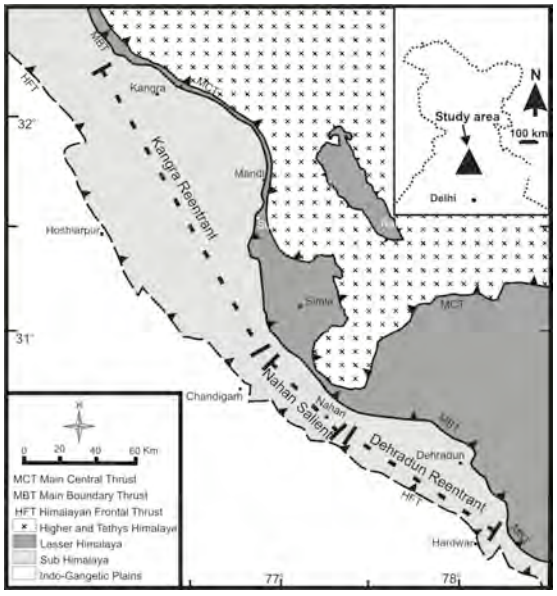

Figure 1. Tectonic sub-divisions of the NW Himalaya marked by the presence of the Kangra and Dehradun Reentrants and Nahan Salient. The study area is located in the Sub-Himalayan belt along the Himalayan front.

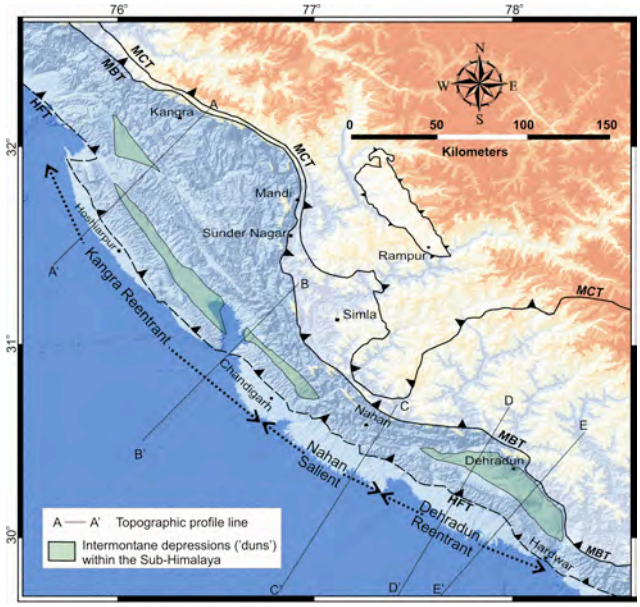

Figure 2. The topography of the NW Himalaya in India with special emphasis on the Sub-Himalayan belt present between the HFT and the MBT. This belt is broadly marked by the presence of the sinuous trace of the MBT giving rise to reentrants and salients.

of the Dehradun area are relatively much smaller (<35 km^2) and highly elongated, in comparison to the basins in the Morni Hills of Nahan area, which are much larger in area (>100 km^2) and poorly elongated. The stream profiles from the Mohand area conform to a second order curve that is relatively steeper towards the head region of the basin. No such distinct change in the gradient of the stream profiles from the Nahan-Morni area has been observed. The difference in the nature of stream profiles in these two areas with structural and topographic differences reflect distinctive differences in their respective stream powers. Stream power controls the sediment transport processes (Burbank and Verges, 1994).

Investigation of the sediment present within the basin bounds as well as their fans clearly indicates significant differences in the growth of basins, character of sediments and the related transport processes in the Dehradun and Nahan Morni areas. Stream profiles in the Dehradun area indicate that the basins grow by headward erosion; most of the sediment is sand size and is transported out of the basin by active streams. The slopes are mantled by a thin veneer of regolith and the structure of the underlying bedrock is clearly apparent. All the material is dumped at the towhead where it is consequently incised and forms terraces. The valleys are steep and narrow and mainly occupied by active channels. In contrast, in the Nahan-Morni area the basins grow by coalescence. They have broad valleys with very small active channels. The sediment are relatively coarser in nature mainly varying from sand to boulders larger than 50 cm. The slopes are covered by abundant loose regolith. Exposures of the bedrock are minor. These indicate that the main transport mechanism is debris flow during high discharge. Incision is dominant and broad flat terraces that completely cover the bedrock are prevalent all through the basins.

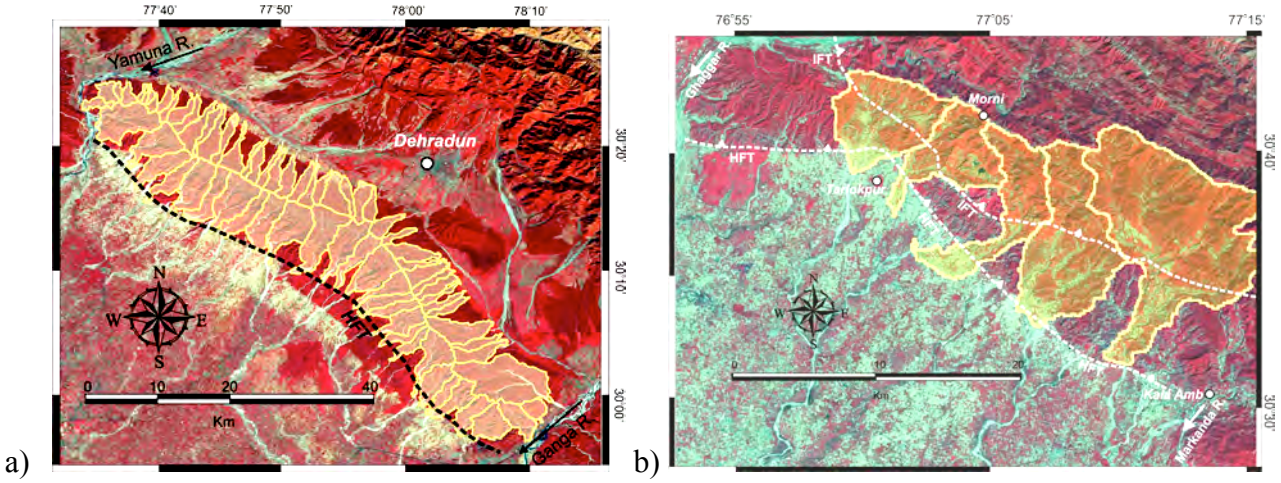

Figure 3. Drainage basins of (a) Dehradun Reentrant and (b) Nahan Salient.

References

Burbank, D.W., and Verges, J., 1994, Reconstruction of topography and related depositional systems during active thrusting, Journal of Geophysical Research, 99, 20281-20297.

DeCelles, P. G., and Giles, K. A., 1996, Foreland basin systems, Basin Research, 8, 105-123.

Dubey, A..K., Misra, R., and Bhakuni, S. S., 2001, Erratic shortening from balanced cross sections of the western Himalayan foreland basin: causes and implications for basin evolution, Journal of Asian Earth Sciences, 19, 765-775.

Kumar, S., Wesnousky, S.G., Rockwell, T.K., Briggs, R.W., Thakur, V.C., and Perumal, R.J., 2006, Paleoseismic evidence of great surface rupture earthquakes along the Indian Himalaya, Journal of Geophysical Research, 111, B03304, doi: 10.1029/2004JB003309.

Powers, P.M., Lille, R.J., and Yeats, R.S., 1998, Structure and shortening of the Kangra and Dehradun Reentrants, Sub-Himalaya, India. Geol. Soc. Am. Bull., 110, 1010-1027.

Raiverman, V. 2002, Foreland sedimentation in Himalayan tectonic regime: A relook at the orogenic process, Bishen Singh Mahendra Pal Singh Publishers, Dehradun, India, 371.

Cite as: Singh, T. and Awasthi, A.K., 2010, Growth of drainage basins and sediment transport in the Dehradun Reentrant and Nahan Salient of the NW Sub-Himalaya: a comparative study, *in* Leech, M.L., and others, eds., Proceedings for the 25th Himalaya-Karakoram-Tibet Workshop: U.S. Geological Survey, Open-File Report 2010-1099, 2 p. [http://pubs.usgs.gov/of/2010/1099/singhtejpal/].

Seismic Performance of the Rural Habitat on the Main Boundary Thrust

Amita Sinvhal[1], Ashok D. Pandey[1], S. M. Pore[1]

[1]Department of Earthquake Engineering, IIT Roorkee, Roorkee, Uttarakhand, India, amitafeq@iitr.ernet.in

Earthquake disasters and their accompanying human casualties are almost synonymous with destruction of the rural habitat. More than one million people were killed the world over, in the twentieth century alone, mostly due to collapse of stone houses. This is a particular problem within the seismo-tectonically active Alpine Himalayan belt. The Main Boundary Thrust (MBT) within the Himalayan collision zone has been repeatedly and frequently visited by disastrous earthquakes. Due to the known adverse seismic hazards on and around the MBT, the human habitat is vulnerable and large populations are at risk within the Himalayan arc. This situation intensifies in the western and in the eastern syntaxis. These syntaxes witness more frequent and larger earthquakes compared to the rest of the Himalayan arc. This exhibits an extreme seismic condition; in fact, it is the worst-case earthquake disaster scenario.

People who live in such adverse seismic conditions gradually learnt to live with earthquakes. After repeated disasters in stone houses, several practical methods were implemented to rectify the known deficiencies in stonewalls. The design of stone houses evolved over centuries, and used locally available material, expertise and masons. One such technology is known as *dhajji diwari*. It means "patch-work quilt wall". This kind of a house has a simple square plan. The super-structure of such a house consists of a judicious use of timber. This introduces several advantages, which become obvious in an earthquake. Timber is light, it is easy to work with, it is easily available in rural areas, and at affordable prices. It can be well seasoned, so that it does not shrink in dry weather and does not expand in wet weather. Each timber member is long and is continuous at corners, at junctions of walls and is also used as beams and columns. A very elaborate timber framework is used for the dhajji diwari kind of house.

The seismic advantage of this flexible and ductile inter-connected timber frame is manifold. The timber frame can sustain relatively large displacements without failure of individual timber members. As all timber members are meticulously interlinked, the frame behaves as one single unit during the strong ground shaking to resist the earthquake force. After the strong shaking is over, the entire frame comes back to rest in almost its original position, barring a few peripheral frayed timber joints. The most important aspect of introducing vertical timber members in walls is that these take the load off stiff, brittle and vulnerable stonewalls and become load-bearing elements in the house. It also introduces flexibility and strength to the stone walls. In addition, they restrain horizontal slip of stone. So the collapse of stonewalls is minimized in strong ground shaking.

In addition to the robust and larger timber frame a smaller timber frame work is embedded within the wall. These provide an additional framework that helps in minimizing the propagation of earthquake-induced diagonal shear cracks in stonewalls within the smaller panels. Thus, progressive destruction of interior walls is minimized. This propagation of cracks is what eventually leads to collapse of most stone houses. The large and small timber frame works are filled with partly dressed stone in the interior walls, and random rubble stone in the outer walls, in rural areas. In urban areas adobe, i.e. sun-dried clay bricks, or burnt bricks were used instead of random rubble. In addition to these earthquake resistant features in a dhajji diwari house, doors and windows are few and small, well-spaced out in the wall, are placed away from cross walls, and away from edges of walls. The space occupied by the wooden staircase is negligible in comparison with the overall size of the house. Therefore a dhajji diwari house can be three to four stories high and is still able to resist earthquake forces creditably.

The dhajji diwari style of construction has been observed to exhibit a desirable seismic response, and was ably implemented in the older houses of Kashmir, both in the rural and urban setting. It emerged as a time-tested earthquake resistant technique, indigenously developed through repeated earthquake disasters and several generations, that too in the rural setting. One such example is shown in Figure 1.

Today very few buildings exist in Kashmir whose construction is based on this system entirely. Long dormant periods between disastrous earthquakes probably led to abandoning robust and appropriate construction practices, in favor of newer construction technology, without any earthquake resistance, often with tragic consequences (Sinvhal, 2010). 86,000 people were killed in stone houses in the Kashmir earthquake of 2005.

In other parts of the world too, where destructive earthquakes are frequent, people have incorporated these critical elements of earthquake-resistant design in their traditional construction methods. These are include the Circum-Pacific belt (Peru and Chile) and the Alpine-Himalayan seismic belt (the Himalayan parts of India, Afghanistan, Iran, Pakistan and Turkey). The dhajji diwari style of construction has lived up to the lofty objectives of earthquake resistant design, mentioned in most earthquake codes, (ISI: 13828-1993). The principles on which dhajji diwari is based, are now being popularized as desirable measures of earthquake resistant design. There is an urgent need to revive this traditional form of construction practice.

(a) (b)

Figure 1. Seismic response of a *dhajji diwari* house in the Kashmir earthquake of October 8, 2006, magnitude, 7.6, epicentral distance 30 km. It survived the most adverse seismic conditions within the western syntaxis: on the MBT, perched on a steep slope near the mountain top, that was covered with weathered, jointed, fractured, sheared and faulted material. (a) The elaborate timber frame around the entire house, and (b) the smaller timber frame in the interior walls of this three-storey stone masonry house received extensive damage but saved all its occupants in the earthquake, unlike other houses in its neighborhood. Location: Sarai Bandi village, District Baramulla.

References

ISI: 13828-1993, Improving earthquake resistance of low strength masonry buildings---Guidelines, Bureau of Indian Standards, New Delhi, India, 11p.

Sinvhal A., Pandey, A.D. and Pore, S.M., 2005, Preliminary report on the 8th October 2005 Kashmir earthquake, Department of Earthquake Engineering, IIT Roorkee, 60 p.

Sinvhal, A., 2010, "Understanding Earthquake Disasters", Tata McGraw Hill, New Delhi, 285 p.

Cite as: Sinvhal, A., Pandey, A.D. and Pore, S.M., 2010, Seismic Performance of the Rural Habitiat on the Main Boundary Thrust, *in* Leech, M.L., and others, eds., Proceedings for the 25th Himalaya-Karakoram-Tibet Workshop: U.S. Geological Survey, Open-File Report 2010-1099, 2 p. [http://pubs.usgs.gov/of/2010/1099/sinvhal/].

Two Migmatite Zones within the Himalayan Metamorphic Belt (HMB) of the Sikkim Himalaya, India

H. Sinvhal[1], Maibam Rogibala[1], A.K. Choudhary[2], A.K. Jain[1], Sandeep Singh[1]

[1]Department of Earth Sciences, Indian Institute of Technology Roorkee, Roorkee-247 667, India, hsinvhal@gmail.com
[2]Institute Instrumentation Center, Indian Institute of Technology Roorkee, Roorkee-247 667, India

Migmatites characterise a zone of magma mobility with melt segregation within a narrow zone of the Himalayan Metamorphic Belt (HMB) across the Himalaya. The Sikkim Himalaya expose rocks in a arcuate regional doubly-plunging fold pattern with Lesser Himalayan Sedimentary Sequences (Daling Group) in the core. These Lesser Himalayan Sequences are overthrust by the Himalayan Metamorphic Belt (MBT) comprising two packages marked by two basal thrusts; the Main Central Thrust (MCT) and the Chungthang Thrust (CT). The rocks of these thrust sheets comprise metapelites with calc-silicate bands along with migmatites. Both the thrust sheets are marked by intense migmatization, partial melting, and *in situ* emplacement of various granitoids within sillimanite–K-feldspar bearing metapelite. In the middle of the package, sillimanite-kyanite-mica schist and gneiss pass gradually into stromatic- and diatexite-type migmatites. These have a melt fraction ranging from 20% to more than 50%, with clear presence of leucosomes containing a few garnet porphyroblasts. The rocks that develop migmatite are mica schist and gneisses and contain biotite, muscovite, quartz, k-feldspar, garnet, kyanite and a small amount of sillimanite. Migmatites in the basal formations are devoid of large tourmaline-bearing leucogranite bodies, whereas the overlying formations are characterised by sheet-like intrusions of tourmaline-bearing leucogranites in their upper reaches. Muscovites appears in smaller quantity than biotite, and kyanite is present along the main foliation as well as across it. Kyanite also shows extensive retrogression and sillimanite is present in needle form along the main foliation as well as along an extensional foliation. In the basal migmatite zones the pre-decompression garnet from basal migmatites has been dated to be around 23 Ma and near peak-metamorphic melting has been constrained as 16 Ma (Harris and others, 2004). However, the overlying widespread migmatites have not thus far been explored in the published literature.

Reference

Harris, N.B.W., and others, 2004, The pressure–temperature–time path of migmatites from the Sikkim Himalaya, Journal of Metamorphic Geology, 22, 249-264.

Cite as: Sinvhal, H., Rogibala, M., Choudhary, A.K., Jain, A.K. and Singh, S., 2010, Two migmatite zones within Himalayan Metamorphic Belt (HMB) of Sikkim Himalaya, India, *in* Leech, M.L., and others, eds., Proceedings for the 25th Himalaya-Karakoram-Tibet Workshop: U.S. Geological Survey, Open-File Report 2010-1099, 1 p. [http://pubs.usgs.gov/of/2010/1099/sinvhal/].

Stable and Clumped Isotope Analysis of Eocene Fenghuo Shan Group Sediments: Implications for Paleoelevation Estimates and Carbonate Diagenesis

Kathryn E. Snell[1], Peter C. Lippert[1], John M. Eiler[2]

[1] Earth and Planetary Sciences Department, University of California Santa Cruz, Santa Cruz, CA 95060, U.S.A., ksnell@pmc.ucsc.edu
[2] Division of Geological and Planetary Sciences, California Institute of Technology, Pasadena, CA, 91125, U.S.A.

The uplift history of the Tibetan Plateau is currently a subject of debate. Models of plateau growth vary in time, from pre-India-Asia collision (e.g., 100 Ma ago) to gradual uplift after the India-Asia collision (e.g., 55 Ma ago), to more recent abrupt uplift (<7 Ma ago). Models of plateau growth also vary in space, from northward stepwise growth of topography to simultaneous surface uplift across the plateau. Oxygen isotope paleoaltimetry studies have been used to estimate the elevation of the plateau in the past, but this technique requires assumptions about the temperature of mineral formation. Independent estimates of the temperature of mineral formation, available from the carbonate clumped-isotope (Δ_{47}) thermometer (Ghosh and others, 2006), may identify post-depositional recrystallization and/or isotopic exchange in carbonate samples. When plausible primary depositional temperatures are found, the Δ_{47} temperature estimates and the calcite $\delta^{18}O$ ($\delta^{18}O_c$) can be used to make more accurate estimates of $\delta^{18}O$ of the waters ($\delta^{18}O_w$) from which the calcite precipitated, assuming that the carbonates formed in equilibrium with clumped isotopes at the time of formation. This appears to be a reasonable approach for lacustrine carbonates and most soil carbonates, although some soil carbonates show disequilibrium effects that may be the result of rapid CO_2 degassing (Eiler and others, 2008).

Here we present preliminary clumped isotope (Δ_{47}) temperatures, calcite $\delta^{13}C$ and $\delta^{18}O$ ($\delta^{13}C_c$ and $\delta^{18}O_c$), and reconstructed water $\delta^{18}O$ ($\delta^{18}O_w$) values from paleosol carbonates and calcite cemented siliciclastic sediments of the early Eocene-aged Fenghuo Shan Group (FHSG). We collected samples from the TouTou He subbasin of the Hoh Xil Basin on the central Tibetan Plateau. This section contains fluvial deposits that comprise cross-bedded sandstones, muddy rip-up conglomerates and overbank successions with some incipient paleosol development. We collected paleosol carbonates from a limited number of horizons and carbonate-cemented siltstones and mudstones throughout the section. Both the paleosol carbonates and carbonate-cemented siliciclastic rocks contain additional secondary carbonates, typically in the form of vein-filling calcite. Lastly, for comparison with previous stable isotope studies on FHSG sediments (Cyr and others, 2006), we collected one lacustrine carbonate from a separate, nearby outcrop of FHSG deposits.

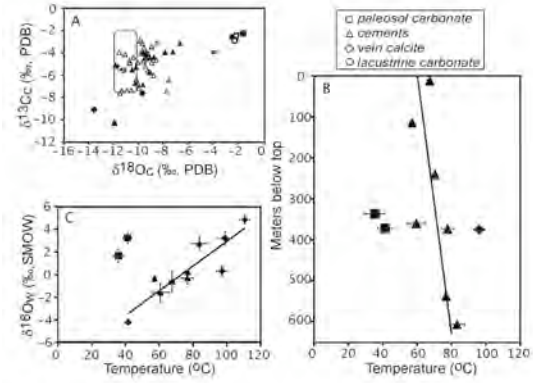

Figure 1. A: Plot of $\delta^{13}C_c$ versus $\delta^{18}O_c$. Filled symbols represent the subset of samples used for Δ_{47} analyses. Rectangle represents the range of $\delta^{13}C_c$ and $\delta^{18}O_c$ of the lacustrine carbonates from Cyr et al., 2005. B: stratigraphic level versus Δ_{47} temperature. C: $\delta^{18}O_w$ versus Δ_{47} temperature. Error bars shown represent 1σ standard errors. Data points without visible error bars have errors that are smaller than the size of the symbol.

$\delta^{13}C_c$ and $\delta^{18}O_c$ values for the secondary carbonates (cements and vein calcite) range from -3 to -10 ‰ (PDB) and -7 to -14 ‰ (PDB), respectively (Figure 1A). The limestone $\delta^{13}C_c$ and $\delta^{18}O_c$ values are similar to the secondary carbonate samples, and to the previously published $\delta^{13}C_c$ and $\delta^{18}O_c$ values from Fenghuo Shan Group lacustrine carbonates. The paleosol carbonates plot separately from these samples, and their $\delta^{13}C_c$ and $\delta^{18}O_c$ values range from -2 to -4 ‰ (PDB) and -1.6 to -4 ‰ (PDB), respectively. The Δ_{47} temperature estimates for a subset of the cements range from 57-83°C, and decrease up-section at a gradient of 30°C/km (Figure 1B). The vein calcite Δ_{47} temperature estimates range from 96 to 100°C.

These temperatures are all too high to represent earth-surface temperatures but are reasonable burial temperatures given estimates of the burial history of the region. The total thickness of Cenozoic basin sediments in this area are estimated to be between 3-5 km, with our section composing the base of this succession (Liu and Wang, 2001; Coward and others, 1988). Vitrinite reflectance data (personal communication, Haisheng Yi, CITS, Chengdu) from the overlying Yaxicuo Group suggest FHSG sediments have been exposed to maximum burial temperatures of up to 180°C, depending on actual thicknesses of the FHSG. Interestingly, the Δ_{47} temperature estimate from our limestone sample (111°C) is also too hot to represent the original depositional temperature. Rather, it appears to be reset to burial temperatures. This is consistent with the presence of significantly thermally altered organic biomarkers in these lacustrine carbonates (Polissar and others, 2009). Finally, the $\delta^{18}O_w$ values calculated for these samples range from -4 to 5‰ (SMOW), and change linearly with temperature by ~0.1‰/°C (Figure 1C).

Collectively, these data challenge the original assumption that because the primary (*ie*. lacustrine carbonate) and secondary carbonates had similar $\delta^{13}C_c$ and $\delta^{18}O_c$ values, the secondary carbonates precipitated from similar shallow, low-temperature waters as the lacustrine carbonates. Rather, these data suggest that, at minimum, diagenetic alteration reordered the isotopes within our lacustrine carbonate sample. Alteration under closed-system conditions could preserve the original bulk $\delta^{13}C_c$ and $\delta^{18}O_c$ values. Given the evidence for diagenetic isotopic reordering, however, the extent of alteration and possibility for open-system isotopic exchange should be re-evaluated for the FHSG lacustrine carbonates.

Although the lacustrine carbonates reflect isotopic reordering, the paleosol carbonates may preserve their primary isotopic signature. The distinction of their $\delta^{13}C_c$ and $\delta^{18}O_c$ values from the secondary carbonates and their lower Δ_{47} temperature estimates (35°C and 41°C) suggest, at minimum, that if these samples have been diagenetically altered, they have not been altered to the same extent as the lacustrine carbonates. These temperatures are warm for earth-surface temperatures, but are plausible considering that soil carbonate formation may be biased towards the summer months, and that soil temperatures can be increased with respect to surface air temperatures due to radiative heating. Additionally, as these sections were likely ~10° farther south than they are at present (Lippert and others, 2009), and were deposited during the early Eocene, the warmest time of the Cenozoic, the high calculated temperatures of the paleosol carbonates could possibly be the original formation temperatures. If these are primary temperatures, then the relatively ^{18}O-enriched signature of the soil water (>1 ‰) may reflect highly evaporated soil waters, implying relatively dry conditions. Because of the potential that the $\delta^{18}O_w$ has been affected by evaporation, and the limited number of primary temperature calculations, paleoelevation estimates based on this current dataset are extremely speculative. However, the relatively high temperatures and fairly ^{18}O-enriched soil water values are more consistent with a low elevation site than high elevations, suggesting that this region was uplifted to its current elevation later than ~40 Ma.

References

Coward, M.P., Kidd, W.S.F., Yun, P., Shackleton, R.M. and Hu, Z., 1988, The Structure of the 1985 Tibet Geotraverse, Lhasa to Golmud: Philos T Roy Soc A, 327, 307-336.

Cyr, A.J., Currie, B.S. and Rowley, D.B., 2005, Geochemical Evaluation of Fenghuoshan Group Lacustrine Carbonates, North-Central Tibet: Implications for the Paleoaltimetry of the Eocene Tibetan Plateau: J Geol, 113, 517-533.

Eiler, J.M., and others, 2008, Carbonate 'clumped isotope' thermometry: a status report: Geochim Cosmochim Ac, 72, A239.

Ghosh, P., and others, J.M., 2006, C-13-O-18 bonds in carbonate minerals: A new kind of paleothermometer: Geochim Cosmochim Ac, 70, 1439-1456.

Liu, Z.F. and Wang, C.S., 2001, Facies analysis and depositional systems of Cenozoic sediments in the Hoh Xil basin, northern Tibet: Sedimentary Geology, 140, 251-270.

Lippert, P. C., and others, 2009, Persistently shallow paleomagnetic inclinations from Central Tibet: Implications for Cenozoic tectonics and climate, EOS Trans AGU Fall Meet. Suppl., 90.

Polissar, P.J., Freeman, K.H., Rowley, D.B., McInerney, F.A. and Currie, B.S., 2009, Paleoaltimetry of the Tibetan Plateau from D/H ratios of lipid biomarkers, Earth Planet Sc Lett, 287, 64-76.

Cite as: Snell, K.E., Lippert, P.C., and Eiler, J.M., 2010, Stable and Clumped Isotope Analysis of Eocene Fenghuo Shan Group Sediments: Implications for Paleoelevation Estimates and Carbonate Diagenesis, *in* Leech, M.L., and others, eds., Proceedings for the 25th Himalaya-Karakoram-Tibet Workshop: U.S. Geological Survey, Open-File Report 2010-1099, 2 p. [http://pubs.usgs.gov/of/2010/1099/snell/].

$^{40}Ar/^{39}Ar$ Thermochronometry of Deformed Muscovite from the Zanskar Shear Zone, NW India

John W. Sommerfeld[1], Forrest M. Horton[1], William C. Hassett[1], and Mary L. Leech[1]

[1] Department of Geosciences, San Francisco State University, San Francisco, CA 94132, U.S.A., jsommerf@sfsu.edu

$^{40}Ar/^{39}Ar$ thermochronometry can provide time constraints for the ductile activity along the Zanskar Shear Zone (ZSZ), the western segment of the South Tibetan Detachment system that extends across the entire Himalayan orogen (Herren, 1987). This northeast-dipping lithotectonic contact separates the underlying high-grade metamorphic rocks of the Greater Himalayan Sequence (GHS) from the overlying low-grade metamorphic rocks of the Tethyan Himalayan Sequence (THS, Fig. 1). Patel and others (1993) show that the rocks exposed in the ZSZ possess multiple generations of fabric development that indicate a complex strain history for the ZSZ. A snowball garnet (Fig. 2a) from the ZSZ shows an earlier top-to-the-SW sense-of-shear indicating that the ZSZ initiated as a thrust fault, consistent with Patel and others (1993). A later top-to-the-NE sense-of-shear (Fig. 2b) overprints evidence of thrust motion, due to gravitational collapse along the ZSZ (Herren, 1987; Patel and others, 1993).

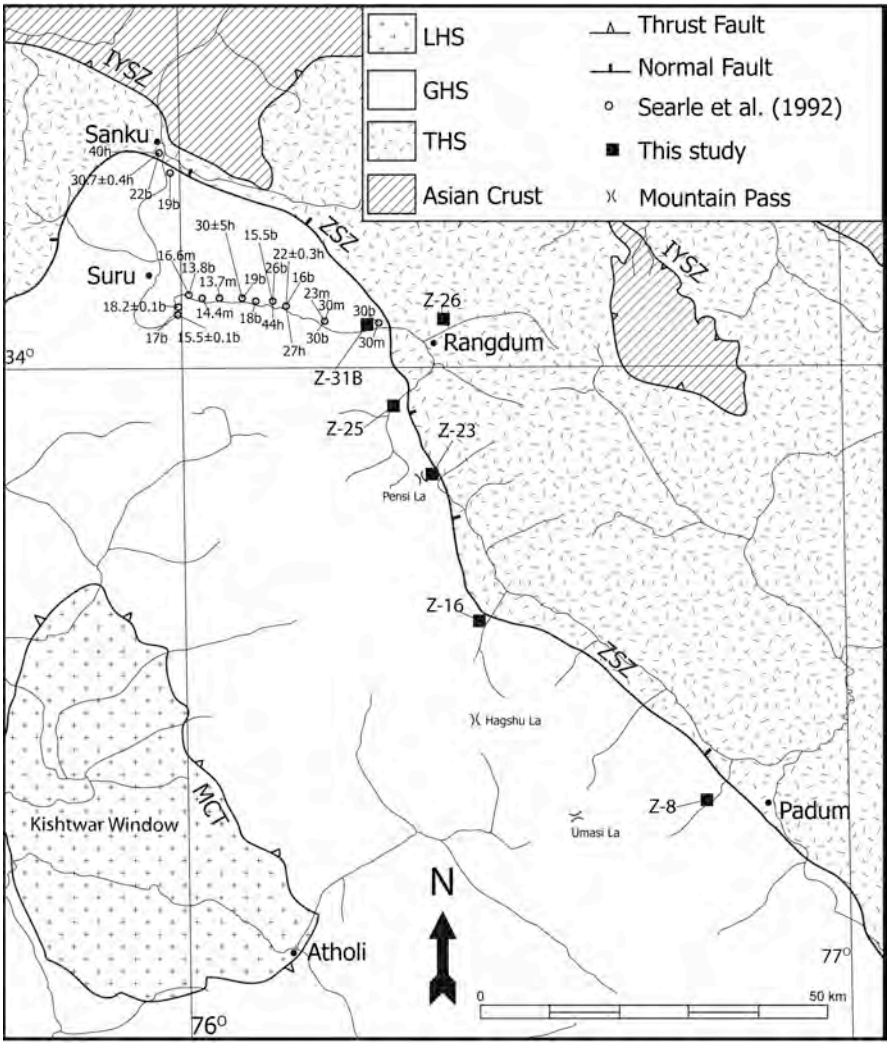

Fig. 1. Geologic map of NW Zanskar, India. Notice the widespread in K-Ar ages even from the same minerals and samples suggesting the presence of excess argon or argon loss. All ages are in Ma. Ages without 2σ errors are K-Ar; 2σ errors are approximately 1-3 Ma. Ages with 2σ error reported are $^{40}Ar/^{39}Ar$ ages. Dated minerals: hbl, hornblende; ms, muscovite; bt, biotite. Modified from Steck (2003).

100 km southeast of Padum, Dezes and others (1999) concluded that ductile extension along the ZSZ was active from 22.2 to 19.8 Ma, but the timing of ductile extension along the ZSZ in NW Zanskar is poorly constrained due to limited thermochronological data. Rb-Sr muscovite ages suggest that ductile extension started ~26 Ma (Inger, 1998). Kumar and others (1995) plotted the age of apatitie fission track ages vs. elevation from the ZSZ near Padum and concluded that the ZSZ was inactive by 11.7-8.0 Ma, and so ductile extension must have ended sometime prior to ~12 Ma. Searle and others (1992) reported 22 K-Ar dates from hornblende, muscovite, and biotite, and five $^{40}Ar/^{39}Ar$ dates from hornblende and biotite from the Suru and Nun-Kun Valleys. The spread in ages from K-Ar samples (e.g., 30-23 Ma for muscovite from one location) and the $^{40}Ar/^{39}Ar$ inverse isochron plot of their hornblende sample SVR 18 indicate the presence of excess argon. Lovera and others (2002) also reported five K-feldspar

$^{40}Ar/^{39}Ar$ spectra from the ZSZ that show the presence of both low-temperature and high-temperature excess argon. The presence of excess argon is an irresolvable problem for K-Ar dating, and any such dates are inherently unreliable. Muscovite $^{40}Ar/^{39}Ar$ dating has the potential to resolve this problem due to the $^{40}Ar/^{39}Ar$ technique advantages and because muscovite tends to incorporate less excess argon than biotite (McDougall and Harrison, 1999). In-situ $^{40}Ar/^{39}Ar$ dating of muscovite "fish" that show top-to-the-NE sense-of-shear (Fig. 2b) will constrain the timing of end-stage ductile deformation along the ZSZ (Mulch and others, 2005) providing valuable thermochronological data for NW Zanskar, and will be done at Stanford University in late 2010.

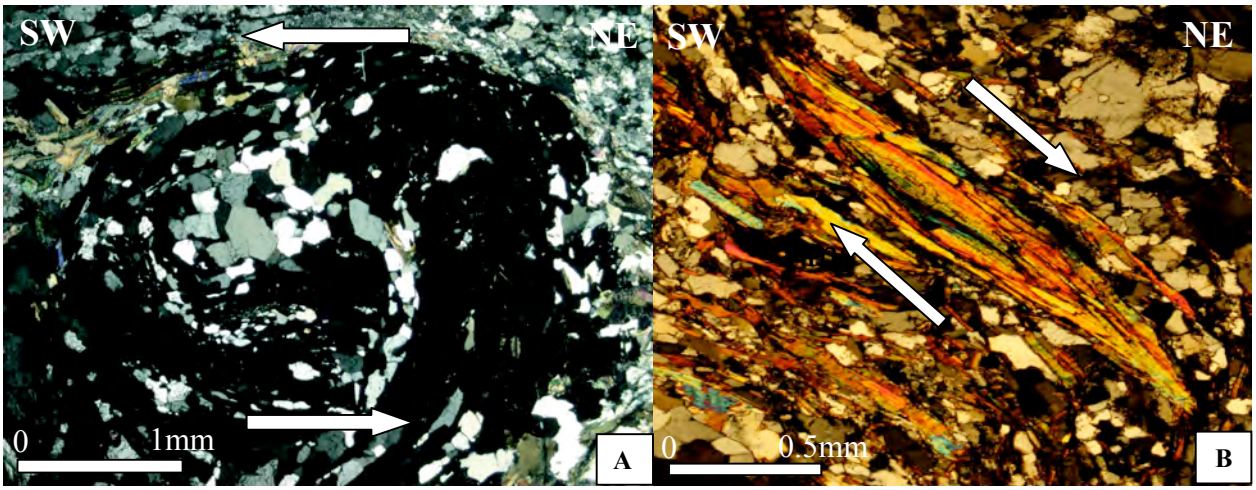

Figure 2. Photomicrographs of samples from the Zanskar Shear Zone. a) Snowball garnet in gneiss. The syn-tectonic garnet indicates a top-to-the-SW thrusting that preceded overprinting by top-to-the-NE shear in the Zanskar shear zone. XPL b) Deformed muscovite fish in gneiss. Muscovite shows top-to-the-NE sense-of-shear. XPL. Arrows show sense-of-shear direction.

References

Dezes, P.J., Vannay, J.-C., Steck, A., Bussy, F. and Cosca, M., 1999, Synorogenic extension: quantitative constraints on the age and displacement of the Zanskar shear zone (northwest Himalaya), GSA Bulletin, 111, 364-374.

Herren, E., 1987, Zanskar shear zone: northeast-southwest extension within the Higher Himalayas (Ladakh, India), Geology, 15, 409-413.

Inger, S., 1998, Timing of an extensional detachment during convergent orogeny: new Rb-Sr geochronological data from the Zanskar shear zone, northwestern Himalaya, Geology, 26, 223-226.

Kumar, A., Lal, N., Jain, A.K. and Sorkhabi, R.B., 1995, Late Cenozoic-Quaternary thermo-tectonic history of Higher Himalayan Crystalline (HHC) in Kishtwar-Padar-Zanskar region, NW Himalaya: evidence from fission track ages, Journal of the Geological Society of India, 45, 375-391.

Lovera, O.M., Grove, M. and Harrison, T.M., 2002, Systematic analysis of K-feldspar 40Ar/39Ar step heating results II: relevance of laboratory argon diffusion properties to nature, Geochim. Cosmochim. Acta, 66, 1,237-1,255.

McDougall, I. and Harrison, T.M., 1999, Geochronology and thermochronology by the $^{40}Ar/^{39}Ar$ method, Oxford University Press.

Mulch, A., Cosca, M., Andresen, A. and Fiebig, J., 2005, Time scales of deformation and exhumation in extensional detachment systems determined by high-spatial resolution in situ UV-laser 40Ar/39Ar dating, Earth and Planetary Science Letters, 233, 375-390.

Patel, R.C., Singh, S., Asokan, A., Manickavasagam, R.M. and Jain, A.K., Extensional tectonics in the Himalayan orogen, Zanskar, NW India, *in* Treloar, P.J. and Searle, M.P., eds., Himalayan Tectonics, Geological Society Special Publications, 74, 445-459.

Searle, M.P., Waters, D.J., Rex, D.C. and Wilson, R.N., 1992, Pressure, temperature and time constraints on Himalayan metamorphism from eastern Kashmir and western Zanskar, Journal of the Geol. Soc. London, 149, 753-773.

Steck, A., 2003, Geology of the NW Indian Himalaya, Eclogae Geologicae Helvetiae, 96, 147-196.

Cite as: Sommerfeld, J.W., Horton, F.M., Hassett, W.C. and Leech, M.L., 2010, $^{40}Ar/^{39}Ar$ thermochronometry of deformed muscovite from the Zanskar Shear Zone, NW India, *in* Leech, M.L., and others, eds., Proceedings for the 25th Himalaya-Karakoram-Tibet Workshop: U.S. Geological Survey, Open-File Report 2010-1099, 2 p.
[http://pubs.usgs.gov/of/2010/1099/sommerfeld/].

Deformation of the Greater Himalayan Sequence, Garhwal Himalaya via Sheath Folding and Late-Stage Brittle Extension: Implications for Channel Flow

Christopher J. Spencer[1], Ron A. Harris[1]

[1] Department of Geological Sciences, Brigham Young University, Provo, UT 84602, U.S.A., chrisspencer@byu.edu

Fold axes within the Greater Himalayan Sequence from the Garhwal region of India display nearly 150º of variability to the general assumed transport direction based on mineral stretching lineation and fold asymmetry data (Figure 1). Previous studies report fold axes that cluster in two distinct populations separated by 90º with an overall spread of 150º (Gairola and Srivastava, 1987; Vannay and Grasemann, 2001). This geometry was interpreted by these authors as evidence for two deformational events oriented ~90º apart. One of these deformational events would have a maximum stress oriented parallel to the current strike of the range. Because the major rivers of the Garhwal Himalaya cross the Greater Himalayan Sequence approximately perpendicular and parallel to the overall strike of the range, the majority of exposed outcrop is oriented in these two directions. This access and exposure bias may explain why previous measurements cluster in two distinct populations. Our investigation of structures throughout the region shows a spread of fold hinge-line trends ranging ~150º with axes trending from NW to SSE (Figure 1). The spread of fold hinge-line orientations is consistent with observations of sheath folds observed at several different scales. Sheath folds are characterised by curvilinear axes that are progressively rotated by general shear from high angles to the transport direction into parallelism with the transport direction (Figure 2). Stretching and/or mineral lineation is nearly parallel to the fold axes and reflects the direction of flow. This relationship is also documented in Himachal Pradesh (Vannay and Grasemann, 2001) and the Pakistani Himalaya (Treloar and others, 2007).

The Greater Himalayan Sequence is dominantly defined by top-to-the-south ductile flow and is bounded above by the South Tibetan Detachment and at the base by the Main Central Thrust. The antithetic shear sense of these bounding faults facilitate SW extrusion of the Greater Himalayan Sequence. Isoclinal to recumbent structures associated with sheath folding are found throughout the Greater Himalayan Sequence with the highest amount of strain localized at the Main Central Thrust. Most folds are top to the SW with the exception of folds those found near the South Tibetan Detachment, which are top to the NE. The opposite vergence directions of folds at the base and top of the Greater Himalayan Sequence are consistent with ductile extrusion of the Greater Himalayan Sequence while both the Main Central Thrust

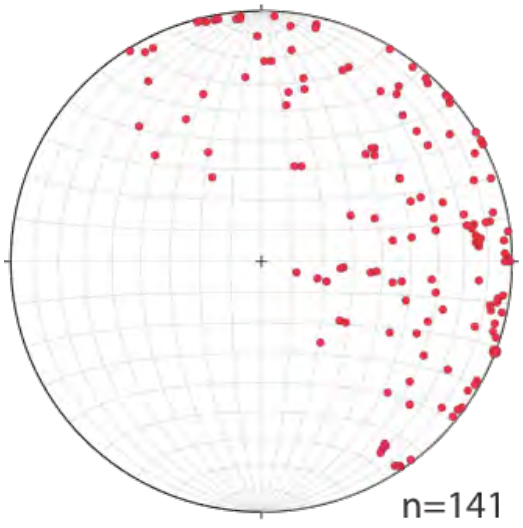

Figure 1: Stereographic plot of fold axes measured throughout the Greater Himalayan Sequence. Variation in fold axes is due to the curvilinear nature of fold axes within sheath folds.

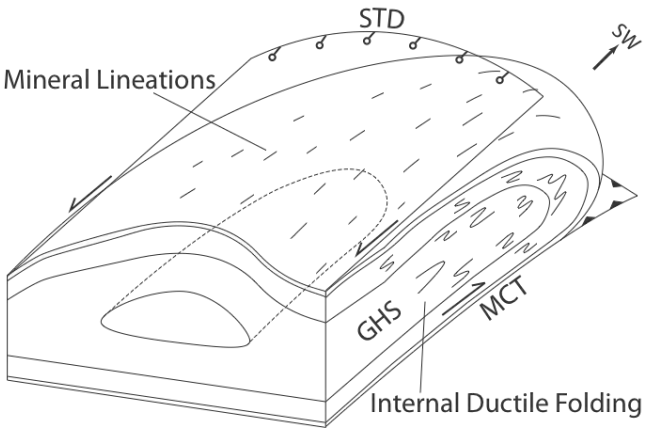

Figure 2: Idealized 3D cross section throught the Greater Himalayan Sequence showing the formation of sheath folding as the result of ductile shear along the Main Central Thrust and the South Tibetan Detachment. Dominant mineral lineation is oriented in the direction of flow (after Searle and Alsop, 2007)

and South Tibetan Detachment were active.

The ductile deformation of the Greater Himalayan Sequence was following by a brittle extensional phase. This extensional phase is expressed throughout the Greater Himalayan Sequence and into the Lesser Himalayan Sequence and Tethyan Himalayan Sequence as conjugate fractures and normal faults. The frequency of these features increases up structural section toward the South Tibetan Detachment. Conjugate fractures and en echelon fracture arrays exhibit a vertical σ1 and σ3 predominately toward the NE. Normal faults are mostly top down to the NE with minor normal faults with top down to the NW. Lesser amounts of conjugate fractures and normal faults are oriented north-south to northeast-southwest. These extensional features might represent orogen perpendicular extension resulting from the Indo-Asian collision as discussed by Kapp and Guynn (2004). The top of the Greater Himalayan Sequence is bounded by the brittle South Tibetan Detachment and juxtaposes unmetamorphosed Tethyan Himalayan Sequence with migmatitic grade Greater Himalayan Sequence.

Our study indicates that despite the similarities between a sheath-fold model and the channel-flow model, the uniform brittle structures that cross major tectonic boundaries can not be explained by channel flow. The most recent brittle exhumation appears to have been controlled by wedge-taper-adjustment normal faults. It also shows that the zone of hinterland extension in the Garhwal Himalaya is much broader than previously reported. This implies that the amount of extension across the range may be underestimated.

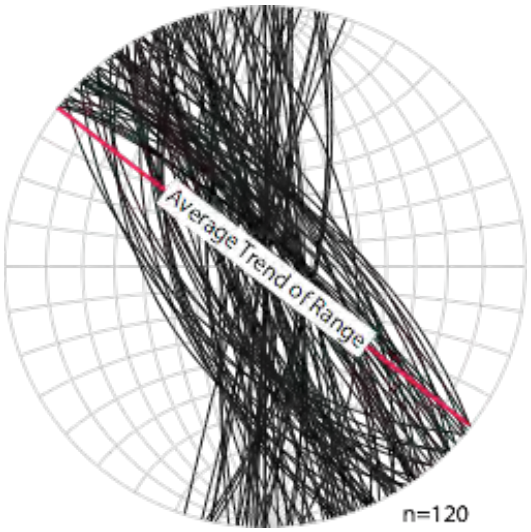

Figure 3: Stereographic plot of conjugate fractures trending nearly orogen parallel.

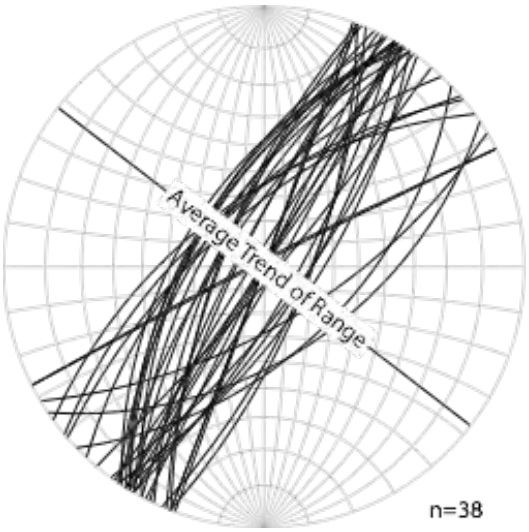

Figure 4: Stereographic plot of conjugate fractures trending nearly orogen perpendicular.

References

Gairola, V.K. and Srivastava, H.B., 1987, Deformational and metamorphic studies in the central crystallines around Joshimath, District Chamoli, U.P, Proceedings of the National Seminar of Tertiary Orogeny in Indian Subcontinent, 49-63.

Kapp, P. and Guynn, J.H., 2004, Indian punch rifts Tibet, Geology 32, 993-996.

Sealre, M.P. and Alsop, G.I., 2007, Eye-to-eye with a mega–sheath fold: A case study from Wadi Mayh, northern Oman Mountains, Geology 35, 1043-1046.

Treloar, P.J., Vince, K.J. and Law, R.D., 2007, Two-phase exhumation of ultra high-pressure and medium-pressure Indian Plate rocks from the Pakistan Himalaya, In: Ries, A.C., Butler, R.W.H, and Graham, R.H, (eds), Deformation of the Contiental Crust: The Legacy of Mike Coward, Geological Society, London, Special Publications 272, 155-185,

Vannay, J.C. and Grasemann, B., 2001, Himalayan inverted metamorphism and syn-convergence extension as a consequence of a general shear extrusion, Geological Magazine 138, 253–276.

Cite as: Spencer, C.J. and Harris, R.A., 2010, Deformation of the Greater Himalayan Sequence, Garhwal Himalaya via Sheath-Folding and Late-Stage Brittle Extension: Implications for Channel Flow, *in* Leech, M.L., and others, eds., Proceedings for the 25th Himalaya-Karakoram-Tibet Workshop: U.S. Geological Survey, Open-File Report 2010-1099, 2 p. [http://pubs.usgs.gov/of/2010/1099/spencer/].

Deformation Temperatures and Rapid Exhumation of the Greater Himalayan Series, Sutlej Valley, NW India

Donald W. Stahr, III[1], Richard D. Law[1], Clayton W. Loehn[1], Robert J. Tracy[1], Talat Ahmad[2], Santosh Kumar[2]

[1] Department of Geosciences, Virginia Tech., Blacksburg, VA 24061, U.S.A., dstahr@vt.edu
[2] Department of Geology, University of Delhi, Delhi, 110007, India

In the Sutlej Valley, NW India, late, high-amplitude NW-SE trending folding and subsequent erosion has resulted in the formation of several klippen comprised of Greater Himalayan Series (GHS) rocks bounded by the Main Central thrust (MCT). The Largi-Kulu-Rampur structural window exposes underlying Lesser Himalayan sedimentary rocks and metamorphosed Lesser Himalayan Crystalline Series rocks in the central region of the Sutlej Valley (see e.g., Vannay and others, 2004). Exposure of the MCT in several locations from more foreland to more hinterland (in the west and east, respectively) positions allowed us to examine multiple structural levels along a continuous crustal-scale structure. Rocks in the hanging wall of western exposures of the MCT attained peak temperatures at greenschist facies coonditions. Helicitic garnet porphyroblasts in rocks ≥1 km structurally above the MCT suggest deformation was ongoing during garnet growth (and therefore presumably during near-peak metamorphism), but temperatures were below that required for significant feldspar plasticity in MCT mylonites at the base of the section.

Assuming an ~25º dip on the MCT and that transport was parallel to the finite stretching lineation, the easternmost exposure of the MCT in the Sutlej Valley represents an ~3 km deeper crustal level than the more westerly MCT exposures described above. An approximately 10 km thick continuous section of the GHS is exposed between the MCT and Sangla Detachment, a part of the South Tibetan Detachment System of normal faults. Low thermodynamic variance pelitic assemblages (garnet ± staurolite + muscovite + biotite ± plagioclase + ilmenite ± rutile) are exposed <300 m structurally above the thrust suggesting metamorphism to mid-amphibolite facies. Microstructures observed in mylonitic granitoids and paragneisses adjacent to the MCT display evidence for high-temperature deformation. Large recrystallized quartz grains have lobate grain boundaries and occluded trails of aligned mica indicating exceptionally mobile grain boundaries during mylonitization and dynamic recrystallization. Thick mantles of recrystallized material surrounding large primary igneous feldspar grains in mylonitic footwall granitoids indicate that feldspar accommodated strain by crystal plastic processes. Semi-quantitative deformation temperatures obtained from the quartz c-axis fabric opening angle thermometer (~625 ºC; Kruhl, 1998, Law and others, 2004) are consistent with observed microstructure and are in excellent agreement with near-peak temperatures calculated by conventional garnet–biotite thermometry (~620 ºC) for pelitic samples in the immediate hanging wall of the MCT. In some samples, garnet X-ray compositional maps reveal euhedral Mn and oscillatory Ca zoning. Because Mn is the fastest-diffusing major divalent cation in garnet the presence of sharp zoning profiles indicates these rocks cannot have remained at near-peak temperatures for a significant period of time.

Lower calculated deformation and peak metamorphic temperatures and spatial position of western MCT exposures, versus those in the east, support the interpretation that western MCT mylonites represent shallower crustal levels. Identical results from multiple analytical techniques for temperature estimation, in addition to microstructural evidence of synkinematic porphyroblast growth, combined with chemical zoning evidence observed in garnet porphyroblasts all support the conclusion that post-peak exhumation of middle crustal GHS rocks was rapid.

References

Kruhl, J.H., 1998, Reply: Prism- and basal-plane parallel subgrain boundaries in quartz: a microstructural thermobarometer, Journal of Metamorphic Geology, 16, 142-146.

Law, R.D., Searle, M.P. and Simpson, R.L, 2004, Strain, deformation temperatures and vorticity of flow at the top of the greater Himalayan Slab, Everest Massif, Tibet, Journal of the Geological Society of London, 161, 305-320.

Vannay, J.-C., and others, 2004, Miocence to Holocene exhumation of metamorphic crustal wedges in the NW Himalaya: Evidence for tectonic extrusion coupled to fluvial erosion, Tectonics, 23, TC1014, doi:10.1029/2002TC001429.

Cite as: Stahr III, D.W., and others, 2010, Deformation Temperatures and Rapid Exhumation of the Greater Himalayan Series, Sutlej Valley, NW India, *in* Leech, M.L., and others, eds., Proceedings for the 25th Himalaya-Karakoram-Tibet Workshop: U.S. Geological Survey, Open-File Report 2010-1099, 1 p. [http://pubs.usgs.gov/of/2010/1099/stahr/].

Block Versus Continuum Descriptions of Continental Deformation: For Heaven's Sake, how are We Ever Going to Decide Which is Better?

Wayne Thatcher[1]

[1] Earthquake Science Center, U. S. Geological Survey, Menlo Park, CA 94025, U.S.A., thatcher@usgs.gov

After decades of research and partisan debate there is still no agreement on how best to describe the widespread deformation occurring in central Asia and elsewhere on the continents. Two alternative end-member models have been proposed. At one extreme, in analogy with the global tectonic model of rigid plates, it has been suggested that actively deforming regions are composed of blocks or microplates. Most deformation then occurs along major block-bounding faults, with minor faulting but little internal deformation of the blocks themselves. At the opposite extreme, continental deformation is viewed as quasi-continuous, governed by the fluid-like, solid-state flow of a viscous material. In this view, discrete slip in the brittle upper crust occurs on many faults with roughly equivalent slip rates. Global positioning system (GPS) and interferometric synthetic aperture radar (InSAR) data may ultimately be decisive in distinguishing between block and continuum models, at least for describing present-day deformation, but thus far there is no consensus. In this paper I discuss a possible resolution to this debate that focuses on the practical utility of both approaches rather than a decision about which is intrinsically "better."

First, it is generally agreed that at least upper-crustal deformation is discontinuous, occurs largely on faults, and is often block-like. There is also no disagreement that determining the sense and magnitude of fault slip is useful for characterizing active tectonic deformation and assessing earthquake hazard. The block/continuum debate then turns on whether the kinematics can be usefully described by a relatively small number of blocks or whether many are required. If slip rates on all active faults were well determined, upper-crustal kinematics would be known. The issue is then a practical one: how accurately can fault slip rates be determined in any region of interest? GPS data and continental block kinematics offer several advantages in providing useful constraints of fault slip rates. First, if the relative motions of the blocks can be constrained by data, the slip rates on block-bounding faults are specified, including any along-strike changes in rate and in the partitioning between fault-parallel and fault-normal motions. Second, the description is simple and feasible if only a small number of blocks are required to characterize any region of interest. And thirdly, the block modelling formalism permits inclusion of other Earth science constraints such as geologically determined, late Quaternary and Holocene slip rates and style of deformation, InSAR fault slip rate estimates, earthquake slip vectors, and current motions of major bounding plates. Block kinematics has several practical limitations. First, the description is cumbersome if many blocks are needed to match data. Second, even when GPS stations are densely distributed, block models cannot distinguish slip rates on closely spaced faults, and/or where blocks are small (characteristic dimension of ~50 km or less). However, good independent geologic slip-rate estimates will alleviate or resolve this indeterminacy (for example, the sub-parallel strike-slip faults of the San Andreas System in northern and southern California and the Marlborough faults of northern South Island, New Zealand). A kinematic description in terms of a spatially variable strain-rate field may well be preferable where many active faults occur, where numerous blocks are required, or where data constraints are limited. Candidate regions I believe currently fulfil these criteria include the southern California Transverse Ranges, western Anatolia, and southern Tibet. It is noteworthy that probabilistic seismic hazard assessment (PSHA) methodologies can be equally applied using either fault slip rates or locally averaged estimates of surface strain rate.

In many parts of central Asia it is hard to be sure how many blocks are needed to describe surface kinematics because of the incomplete and inhomogeneous distribution of existing GPS sites. This shortcoming is likely to be largely overcome during the next decade or so by new networks, especially in central and western Tibet, and by InSAR imagery from the new generation of radar satellites scheduled for launch between 2012 and 2017.

Cite as: Thatcher, W., 2010, Block Versus Continuum Descriptions of Continental Deformation: For Heaven's Sake, how are We Ever Going to Decide Which is Better?, *in* Leech, M.L., and others, eds., Proceedings for the 25th Himalaya-Karakoram-Tibet Workshop: U.S. Geological Survey, Open-File Report 2010-1099, 1 p. [http://pubs.usgs.gov/of/2010/1099/thatcher/].

Magnetic Fabrics, Microstructures and U-Pb Geochronology of the Kinnaur Kailash Granite and Associated leucogranites, Himachal Himalaya: Implications for Extensional Tectonics in the South Tibetan Detachment Zone

Kavita Tripathi[1]

[1]Wadia Institute of Himalayan Geology, 33, GMS Road, Dehradun 248001, India, kavi.tri@gmail.com

The South Tibetan Detachment (STD) is a system of low-angle normal faults that separates the High Himalayan Crystallines from metasedimentary rocks of the Tethyan Group. In the Himachal High Himalaya, the STD is characterized by presence of S-type per-aluminous Palaeozoic (~ 500 Ma) granite, called the Kinnaur Kailash Granite (KKG), in its hanging wall. This granite is also intruded by leucogranites in the vicinity of the STD zone. In the present work, an integrated magnetic-fabric analysis, microfabric analysis and U-Pb geochronology of zircons were carried out on the KKG and associated leucogranites in the Satluj and Baspa valleys of the Kinnaur region to understand the tectono-magmatic evolution of these granites with respect to the deformation history of the STD.

The magnetic susceptibility and thermal de-magnetization properties indicate that almost all the granite samples taken from this area are paramagnetic in nature with little or no magnetite. The degree of magnetic anisotropy (P′), which is an indicator of intensity of deformation, is higher for samples that lie in the vicinity of the STD as compared to samples away from the STD. The P′ value of granites varies from 1.025 (CS9/1) to 1.393 (CS11/5) and their corresponding Km value ranges from 18.2(10^{-6} SI) to 721(10^{-6} SI). The KKG and the leucogranites show no linear correlation between P′ and Km values suggesting that the magnetic anisotropy is controlled by intensity of deformation.

Strike of magnetic foliation of the granites in both the valleys shows a large variation, i.e. NW-SE close to the STD and E-W in the central part and then NW-SE again near the contact with the Tethyan rocks (Fig.1). Strike of magnetic foliation of leucogranites is sub-parallel to the STD with steep dips. The strike of magnetic foliation of the KKG develops a sigmoidal pattern on a regional scale indicating trans–tensional shearing related to deformation along the STD.

Microstructures in the KKG indicate superposition of a solid-state deformation fabric over a pre-existing magmatic fabric. Microstructures in granite near the STD show the signature of intense solid-state deformation. The intensity decreases away from the STD. The leucogranites show low temperature solid-state deformation fabrics. Shear criteria in the mylonites of the KKG and leucogranites suggest shearing related to eastward extension along the STD.

U-Pb geochronology of zircons of two samples of KKG yield crystallization age of ~475 Ma (CS11/2: 477±3.4Ma; MA4/5a: 472±4 Ma). The leucogranite gives a crystallization age of ~20 Ma (MA4/6B:18.5±0.6Ma). The zircons of MA4/5A also show the signature of a hydrothermal event (~20 Ma) at its rim.

From the present study, the following conclusions are made:
1) The regional sigmoidal pattern in the magnetic fabric of the KKG is caused by transtension due to eastward extension along the STD.
2) The microfabric indicates superposition of deformation features at various temperatures, indicating repeated activity along the STD.
3) Since the timing of the hydrothermal event in the KKG and the crystallization of the leucogranites are similar, it is proposed that the deformation in the KKG and crystallization of the leucogranites are synchronous and they are triggered by deformation along the STD.
4) Microstructures in the leucogranites suggest that deformation in the STD zone continued even after the crystallization of the leucogranites.

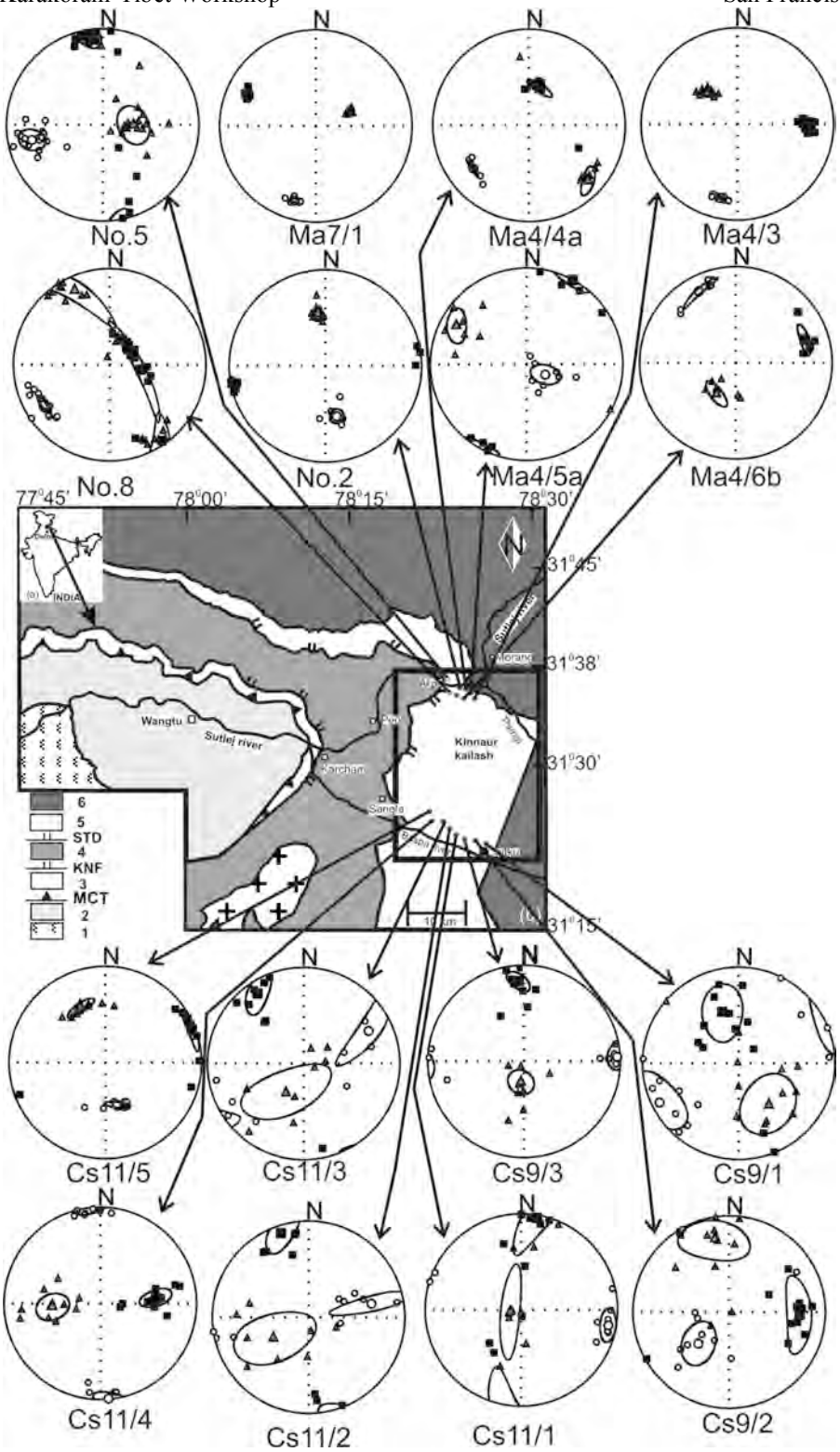

Figure 1. (a) Inset shows location of the area; (b) Geological map of the study area along with sample locations. Lower-hemisphere equal-area projections of AMS data of samples showing distribution of K1 (magnetic lineation; black squares), K2 (grey triangles), K3 (pole to magnetic foliation; open circles).

Cite as: Tripathi, K., 2010, Magnetic Fabrics, Microstructures and U-Pb Geochronology of the Kinnaur Kailash Granite and Associated Leucogranites, Himachal Himalaya: Implications for Extensional Tectonics in the South Tibetan Detachment Zone, *in* Leech, M.L., and others, eds., Proceedings for the 25th Himalaya-Karakoram-Tibet Workshop: U.S. Geological Survey, Open-File Report 2010-1099, 2 p. [http://pubs.usgs.gov/of/2010/1099/tripathi.html].

Constraining the timing and duration of backthrusting in the Indus Group: a detrital zircon (U-Th)/He approach

Alka K. Tripathy[1], Kip V. Hodges[2], Matthijs C. van Soest[2], Talat Ahmad[3]

[1] School of Earth and Space Exploration, Arizona State University, Tempe, AZ 85287, U.S.A., atrip@asu.edu
[2] School of Earth and Space Exploration, Arizona State University, Tempe, AZ 85287, U.S.A.
[3] Department of Geology, University of Delhi, New Delhi, India

For the past few years, we have been investigating the low-temperature exhumation history of the syncollisional Indus Group in Ladakh, India. The Indus Group represents the first continentally derived sediment deposited after initiation of the Indo-Eurasian collision in this part of the orogenic system. Spectacular exposures of the Indus Group basin south of Leh, India, display a complex pattern of north-verging fold-and-fault systems that represent an important phase of backthrusting. However, the age of this event remains poorly constrained. The most generally accepted estimate is that of Searle and others (1990), who postulated an Early Miocene age for backthrusting and interpreted it as coincident in time with termination of Indus basin sedimentation. Based on apatite fission-track thermochronology on samples from the Zanskar Gorge, Clift and others (2002) suggested that backthrusting is younger, ~13-14 Ma. More recently, Kirstein and others (2009) proposed that pre-20 Ma backthrusting might be responsible for an important rotation of the Ladakh batholith north of the outcrop trace of the Indus Group.

Clift and others (2002) used illite-crystallinity measurements of Zanskar Gorge samples to demonstrate that parts of the sequence have been heated to >200°C, which slightly exceeds the nominal closure temperature for radiogenic He diffusion in zircon (~170-190°C; Reiners and others, 2004). Here, we exploit this epizonal metamorphism and use detrital zircon (U-Th)/He thermochronometry to examine the low-temperature thermal evolution recorded in the sandstones in the Gorge to constrain the timing and duration of reheating. In the absence of any field evidence for alternative heating mechanisms, we relate this reheating event to backthrusting.

In theory, if the heating event were sufficiently long in duration, the reset (U-Th)/He dates would allow us to constrain the age of metamorphism, and, by inference, the timing of backthrusting. In practice, the single-grain (U-Th)/He dates we obtained for 93 detrital zircon grains from the Zanskar Gorge ranged from 7.8±0.4 Ma to 39.0±1.1 Ma (2σ), implying that many grains are only partially reset. These findings establish the ages of at least some of the N-vergent backthrusts as Late-Miocene or younger.

Moreover, if we assume that the variable resetting resulted from a single thermal pulse related to backthrusting, the zircon data also provide an opportunity to further constrain the timing, as well as the duration, of the heating event. We focus here on a single sample (ZG-O) for which we have the most data (n=32) because it was collected from one of the >200°C locations of Clift and others (2002) and it corresponds to the location of a major backthrust structure. The dates from ZG-O range from 10.3±0.4 Ma to 21.7±1.2 Ma (2σ).

To estimate the duration of reheating (t), we use the equation for fractional loss (f):

$$f = 1 - (6/\pi^2)\sum_{n=1}^{\infty}[(1/n^2)\exp(-n^2\,\pi^2 Dt/r^2)]$$

where D is the diffusivity at a specific temperature (diffusivity data from Reiners and others, 2004), and r is the measured radius of each grain (McDougall and Harrison, 1998).

We assume that the youngest grain is fully reset (f = 0.99), and calculate the duration (t) of the reheating event that would cause complete resetting at 200°C. A duration of 2 my would fully reset many of the grains in ZG-O. If grain size and age were correlated, that would imply that the sample cooled slowly enough such that each grain had a slightly different closure temperature, which could explain the range of ages that we see. However, there is no correlation between grain size and age, which implies that even

the youngest grain is not fully reset. As a consequence, we regard it as likely that the reheating event is younger than 10 Ma. Therefore, we postulate that the backthrusting responsible for reheating initiated at less than 10 Ma, and the duration of the event, or the maximum time that sample ZG-O was heated to 200°C, is less than 2 my. The lack of complete resetting of the (U-Th)/He zircon chronometer in these rocks implies a zircon resetting temperature, as defined by Gardés and Montel (2009), substantially in excess of 200°C for brief thermal events, consistent with our current understanding of He diffusion kinetics for zircon.

References

Clift, P.D., Carter, A., Krol, M. and Kirby, E., 2002, Constraints on India-Eurasia collision in the Arabian Sea region taken from the Indus Group, Ladakh Himalaya, India, in Clift, P.D., Kroon, D., Gaedicke, C., and Craig, J., eds., The Tectonic and Climatic Evolution of the Arabian Sea Region: London, Geological Society of London Special Publication 195, p. 97-116.

Gardés, F E. and Montel, J.-M., 2009, Opening and resetting temperatures in heating geochronological systems: Contributions to Mineralogy and Petrology, v. 158, p. 185-195.

Kirstein, L.A., Foeken, J.P.T., van der Beek, P., Stuart, F.M. and Phillips, R.J., 2009, Cenozoic unroofing history of the Ladakh Batholith, western Himalaya, constrained by thermochronology and numerical modelling: Journal of the Geological Society, London, v. 166, p. 667-678.

McDougall, I. and Harrison, T.M., 1998, Geochronology and Thermochronoogy by the Ar/ Ar Method: New York, Oxford University Press, 261 p.

Reiners, P.W., Spell, T.L., Nicoliescu, S. and Zanetti, K.A., 2004, Zircon (U-Th)/He thermochronometry: He diffusion and comparisons with $^{40}Ar/^{39}Ar$ dating: Geochimica et Cosmochimica Acta, v. 68, p. 1857-1887.

Searle, M. P., Pickering, K.T. and Cooper, D.J.W., 1990, Restoration and evolution of the intermontane molasse basin, Ladakh Himalaya, India: Tectonophysics, v. 174, p. 301–314.

Cite as: Tripathy, A.K., Hodges, K.V., van Soest, M.C. and Ahmad, T., 2010, Constraining the timing and duration of backthrusting in the Indus Group: a detrital zircon (U-Th)/He approach, *in* Leech, M.L., and others, eds., Proceedings for the 25th Himalaya-Karakoram-Tibet Workshop: U.S. Geological Survey, Open-File Report 2010-1099, 2 p. [http://pubs.usgs.gov/of/2010/1099/tripathy/].

Tertiary U-Pb Zircon Ages and Lower Paleozoic Signatures from Leucosomes of the Namche Migmatites, Everest Area, Nepal Himalaya

Bishal N. Upreti[1], George E. Gehrels[2], Santa M. Rai[1], Masaru Yoshida[3]

[1,3]Department of Geology, Tribhuvan University, Tri-Chandra Campus, Ghantaghar, Kathmandu, Nepal, bnupreti@wlink.com.np
[2]Department of Geosciences, University of Arizona, Tucson, AZ 85721, U.S.A.
[1]Department of Geology, Tribhuvan University,Tri-Chandra Campus, Ghantaghar, Kathmandu, Nepal
[3]Gondwana Institute for Geology and Environment, 147-2 Hashiramoto, Hashimoto 648-0091, Japan

Following Bordet (1961) and Lombardo and others (1993), from south to north, the Higher Himalayan Crystallines (HHC) of the Everest area can be broadly divided into: (1) Barun Gneiss, (2) Namche Migmatitic Orthogneiss and (3) Black gneiss. In this work, leucosome samples were collected for dating from two horizons of Namche migmatites – the lower one from a location about 1 km north of Phakdin Village lying on the left bank of the Dudhkoshi river (Sample No. 07EVT3). Another sample was collected from a stream east of Khumjun Village that lies to the north of Namche Bazaar (Sample No U1206). The Namche migmatite is a rock unit with upper amphibolite-granulite facies metamorphism and mainly composed of interlayered migmatitic ortho- to paragneisses with profusely developed leucosomes, biotite-sillimanite quartzo-feldspathic gneiss and minor calcsilicate rocks. These rocks were formed at high temperature (c. 700^0C) and at pressure of <5 kbar (Searle and others, 2003). A number of larger concordant bodies of Miocene leucogranites such as the Nuptse granite and granitic dyke networks intrude the overlying Black gneisses.

U-Pb geochronology of zircons was conducted by laser ablation-multicollector-inductively coupled plasma-mass spectrometry (LA-MC-ICP-MS) at the University of Arizona. The Concordia diagrams are shown in Figures 1A and 2A. Six overlapping analyses of the zircon grain from the leucosome sample No. 07EVT3 yielded an age of 20.9 ± 1.2 Ma (2σ) with early Paleozoic cores (Figure 1B). Similarly, the 12 overlapping analyses from Sample No. U1206 yielded the age of 24.8 ± 0.5 Ma (2σ) again with an older core (Figure 2B); bracketing the age of anatexis of the Namche Migmatites between 20.9 and 24.8 Ma. These data provide the age range of the peak Tertiary metamorphism in the Everest region. The data are comparable with the monazite and xenotime ^{207} U/^{235}Pb ages (25.4±0.11 and 22.11±0.22 Ma) reported by Viskupic and Hodges (2001) from the same area.

The analyzed zircon grains clearly show the inheritance of early Paleozoic cores surrounded by the Tertiary rims. Sample 07EVT3 shows the core age of 478±25 Ma whereas sample U1206 has a 515±20 Ma old core. Although a direct evidence of the origin of these relict zircon cores are not available, it is reasonable to infer that these grains may have derived from the granitoid protoliths of the Namche migmatites rather than representing the detrital grains from metasediments. This assumption further implies that these relict zircon grains must have formed during the Lower Paleozoic Pan-African orogeny producing the protoliths- granites and gneisses which in turn metamorphosed to produce, gneisses, migmatites and leucogranites during the much younger Himalayan orogeny during the Tertiary period. Thus, the Lower Paleozoic metamorphism during the Pan African orogeny seems to be nearly as strong as the Tertiary Himalayan orogeny to produce anatectic melts generating granites and migmatites. This interpretation confirms with the similar conclusions made by Gehrels et al. (2006a,b) for the Kathmandu and Dadeldhura thrust sheets in central and far western Nepal and Tonarini et al. (1994) and Pognante and Benna, (1993) for Everest-Makalu region. The high U/Th ratio (Fig. 3) found in the young Tertiary as well as the Lower Paleozoic zircons suggests that they grew in the presence of abundant metamorphic fluids.

References

Bordet, P., 1961, Recherches geoologiques dans l'Himalaya du Nepal, region du Makalu, Edition of CNRS, Paris, 275 pp.

Gehrels, G.E., DeCelles, P.G., Ojha, T.P. and Upreti, B.N., 2006a, Geologic and U-Pb geochronologic evidence for early Paleozoic tectonism in the Kathmandu thrust sheet, central Nepal Himalaya, GSA Bulletin, v. 118, No. ½, p. 185-198.

Gehrels, G.E., DeCelles, P.G., Ojha, T.P. and Upreti, B.N., 2006b, Geologic and U–Pb geochronologic evidence for early Paleozoic tectonism in the Dadeldhura thrust sheet, far-west Nepal Himalaya, Journal of Asian Earth Sciences 28, 385–408.

Lombardo, B., Pertusati, P. and Borgi, S., 1993, Geology and tectonomagmatic evolution of the eastern Himalaya along the Chomolungma-Makalu transect, Geological Society London, Special Publications, 74, 341–355.
Pognante, U., Benna, P., 1993, Metamorphic zonation, migmatization, and leucogranites along the Everest transect of Eastern valley, Everest region, Deformation features and geological implications, Journal of Asian Earth Sciences, 16, 299-311.
Searle, M. P., Simpson, R. L., Law, R. D., Parrish, R. R. and Waters, D J., 2003, The structural geometry, metamorphic and magmatic evolution of the Everest massif, High Himalaya of Nepal–South Tibet, Journal of the Geological Society, London, 160, 345–366.
Tonarini, S., Lombardo, B., Ferrara, G., and Marcassa, P., 1994, Partial melting in the Namche Migmatite of Khumbu Himal (Nepal Himalaya), Mineralogica Petrografica Acta, 37, 277-294.
Viskupic, K. and Hodges, K.V., 2001, Monazite–xenotime thermochronometry: methodology and an example from the Nepalese Himalaya, Contributions to Mineralogy and Petrology, 141, 233–247.

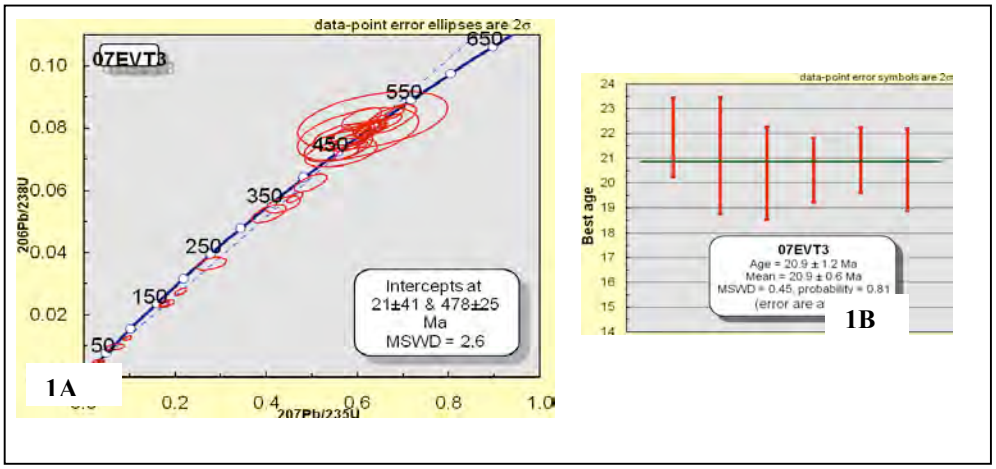

Figure 1A. Pb/U Concordia diagram of zircon analyses from north of Phakding Village Sample No. 07EVT3). **1B**: The weighted mean $^{206}Pb/^{238}U$ age of the concordant analyses is 20.9±0.6 Ma. MSWD - mean square of weighted derivatives.

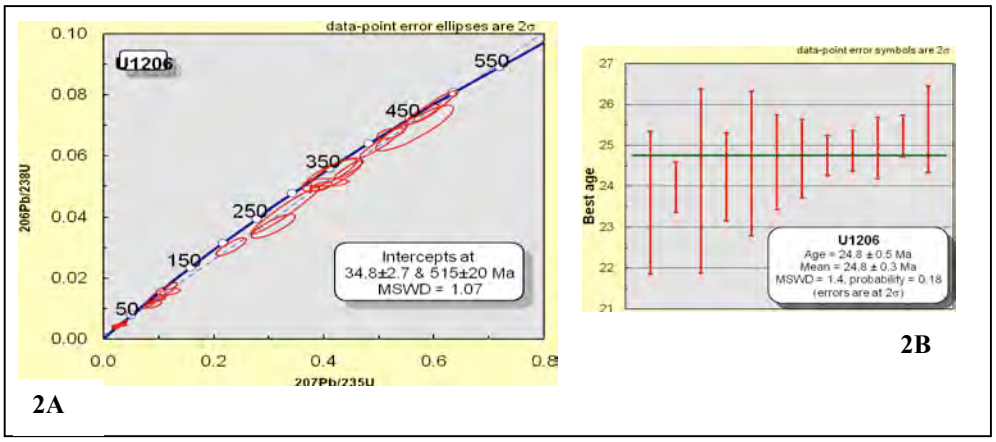

Figure 2A. Pb/U Concordia diagram of zircon analyses from east of Khumjun Village (Sample No. U1206). **2B:** The weighted mean $^{206}Pb/^{238}U$ age of the concordant analyses is 24.8±0.3 Ma. MSWD- mean square of weighted derivatives.

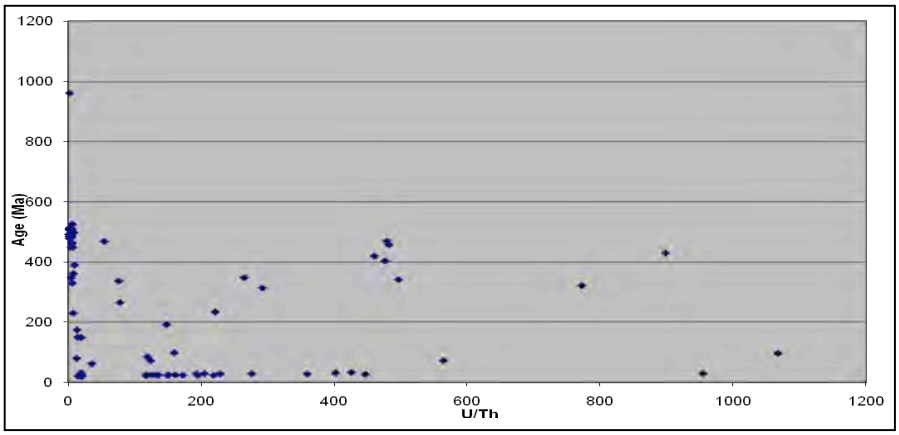

Figure 3. U/Th plot of the zircon samples

Cite as: Upreti, B.N., Gehrels, G.E., Rai, S.M. and Yoshida, M., 2010, Tertiary U-Pb Zircon Ages and Lower Paleozoic Signatures from Leucosomes of the Namche Migmatites, Everest Area, Nepal Himalaya, *in* Leech, M.L., and others, eds., Proceedings for the 25th Himalaya-Karakoram-Tibet Workshop: U.S. Geological Survey, Open-File Report 2010-1099, 2 p. [http://pubs.usgs.gov/of/2010/1099/upreti/].

Guidebook Series on the Himalayan Geology and Natural Hazards

B.N.Upreti[1,2], M. Yoshida[1,2], S.M. Rai1[1], T.N. Bhattarai[1] , P.D. Ulak[1], A.P. Gajurel[1], R.K. Dahal[1], S. Dhakal[1], M.P. Koirala[1]

[1]Department of Geology, Tribhuvan University, Trichandra Campus, Ghantaghar, Kathmandu, Nepal, bnupreti@wlink.com.np
[2]Gondwana Institute for Geology and Environment, 147-2 Hashiramoto, Hashimoto 648-0091 JAPAN

The Himalaya is the highest and one of the largest and still growing mountain ranges on our planet. It exhibits a distinct zonal arrangement of geology, geomorphology, climate, fauna and flora; and hence is an excellent laboratory to study nature and natural science of mountain ranges. However, there are almost no appropriate guidebooks for common people in the world market to introduce geology and natural hazards in the Himalaya. The present endeavor is to publish a series of such guidebooks along different transects of the Himalaya to bring out the much-admired geology and fantastic geomorphology, and the omnipresent natural hazards which are characteristic of the Himalaya.

Fig. 1. Guidebooks (3 Japanese and 1 English) published since 2005.

The first guidebook in this series – Guidebook for Himalayan Trekkers, Series No. 1: Geology and Natural Hazards along the Kaligandaki Valley, Nepal – was published in 2005 (Upreti and Yoshida, 2005, http://www.geocities.jp/gondwanainst/Yoshida/guidebookadv.pdf), and has been widely used by individuals and groups who are also interested to know these facets of the Himalaya. The guidebook Series No. 2, on the Everest area in the Khumbu region, No. 3 along the Langtang Valley of Nepal and No. 4 on the NW Indian Himalaya are in progress. Also, the provisional Japanese versions of these guidebooks were published in 2007, 2008 and 2009 as Miscellaneous Publications No. 19, 20 and 21 of the Gondwana Research Group/Gondwana Institute for Geology and Environment (Yoshida and others, 2007, 2008a; Yoshida and Upadhyay, 2009).

Many Japanese groups composed of engineers, scientists, teachers, students and common citizens, as well as many others, (Yoshida and others, 2008b; Yoshida and Upadhyay, 2010), have utilized these guidebooks to study geology and natural hazards during their field visits. The marketing of the guidebooks, as well as writing, editing and publication of new guidebooks for other parts of the Himalaya are in progress. It is expected that the incredible nature of Himalayan geology and environment described in these guidebooks will encourage a wide spectrum of people worldwide to visit and study the Himalaya which will also bring economic benefit to the local people. It will also help the people living in this beautiful mountain range to feel proud of their natural heritage. The guidebook series may work as a tool to popularize and highlight the importance of field-based geological studies of mountains, and also help in the advancement of geological sciences at large.

References

Upreti, B.N. and Yoshida, M., 2005 (eds.), Guidebook for Himalayan Trekkers, Ser. No. 1, Geology and Natural Hazards along the Kaligandaki Valley, Nepal., Special Publication No. 1, Department of Geology, Tribhuvan University, Trichandra Campus, Kathmandu, 1-165.

Yoshida, M., Upreti, B.N. and Rai, S.M., 2007, Geology and Natural Hazards along the Dudhukoshi Valley, Everest Area - Field excursion guidebook (in Japanese), GRG/GIGE Miscellaneous Publication No. 18, Field Science Publishers, Hashimoto, 41p.

Yoshida, M., Upreti, B.N., Rai, S.M. and Bhattarai, T.N., 2008(a), Geology and Natural Hazards along the Langtang Valley, Central Nepal Himalaya (in Japanese). GRG/GIGE Miscl. Pub. No. 19, Field Science Publishers, Gondwana Institute for Geology and Environment (GIGE), Hashimoto, Japan, 31p.

Yoshida, M., and others, 2008(b), Field excursion guidebook series on geology and natural hazards in Nepal Himalaya. Proc. Int. Conf. on Management of Landslide Hazard in the Asia-Pacific Region, the Japan Landslide Society, Sendai, 335-344.

Yoshida, M. and Upadhyay, R., 2009, Geology and Scenery of Northwest Indian Himalaya: Field Excursion Guidebook (In Japanese), GRG/GIGE Miscl. Pub. 20, Field Science Publishers, Hashimoto, 37p.

Yoshida, M. and Upadhyay, R., 2010, Geotraverse in the NW Indian Himalaya along the Delhi-Leh route (In Japanese)., Chigaku Kyoiku to Kagaku Undo (Education in Geoscience and Movement in Science), (in press).

http://www.geocities.jp/gondwanainst/ms2008/HimalayanGuidebook_Sendaicon f20081216.pdf.

Cite as: Upreti, B.N., and others, 2010, Guidebook Series on the Himalayan Geology and Natural Hazards, *in* Leech, M.L., and others, eds., Proceedings for the 25th Himalaya-Karakoram-Tibet Workshop: U.S. Geological Survey, Open-File Report 2010-1099, 2 p. [http://pubs.usgs.gov/of/2010/1099/upreti2/].

Electromagnetic Studies of Banggong-Nujiang Suture Architecture from INDEPTH Magnetotelluric Profiles and Magnetovariational Data

Jan Vozar[1], Alan G. Jones[1], Florian Le Pape[1], Wei Wenbo[2], Martyn J. Unsworth[3], INDEPTH MT Team

[1] Dublin Institute for Advanced Studies, Dublin 2, Ireland, vozar@cp.dias.ie
[2] China University of Geosciences Bejing, Beijing, 100083, China
[3] Department of Department of Physics, University of Alberta, Edmonton, AB T6G 2J1, Canada

During the years 1995 and 1999, broadband (BBMT) and long period (LMT) magnetotelluric data were collected and interpreted for two profiles crossing the Banggong-Nujiang Suture, as a part of the InterNational DEep Profiling of Tibet and the Himalaya project (INDEPTH). These profiles cross the Banggong-Nujiang suture, which separates the Qiangtang and Lhasa terranes, along approximately longitudes of 89°E (longer 500 line) and 92°E (shorter 400 line). These data have been combined with available magnetovariational data from permanent geomagnetic observatories situated within or close to the investigated area.

Strike and dimensionality analyses show the predominantly two-dimensionality of the regional geoelectrical structures with an approximately east-west direction. Both magnetotelluric TE and TM modes with the vertical field geomagnetic transfer functions (GTF) have been derived for the defined regional azimuth angle. We have derived he local geomagnetic depth soundings (GDS) responses and also responses from the generalized horizontal spatial gradient (gHSG) method for the mid-latitude INDEPTH region.

These input data have been inverted separately and simultaneously with different 2D inversion algorithms to obtain several two-dimensional geoelectrical models depending on the inversion parameters selected. The preferred model of the 500 profile confirms the previous observations of Wei and others (2001) and Solon and others (2005) that the region is characterized by resistive upper crust and conductive middle-to-lower crust that extends from the Lhasa terrain to the Qiangtang terrain with varying depth. The conductive layer is relatively uniform along whole profile except for two breaks in the region of the Banggong-Nujiang suture and 50 km south of it. Absence of highly conductive crustal layers in these short parts of the 500 line profile and the combination of long-period MT and magnetovariational responses allows us to obtain information about deeper structures and reveals the existence of a highly conductive layer localized at and below 100 km.

The same conductive structure setting is also present on the shorter 400 line. Other models show focused information about the Banggong-Nujiang suture and its changes in geoelectrical structure between the longitudes of 89°E and 92°E. The eastern profile (400 line) exhibits a shallower crustal conductive layer and a sharp horizontal jump in conductivity just below the surface trace of the Banggong-Nujiang suture in comparison with western 500 line. These along-strike differences represent varying conditions, such as temperature, partial-melt content and connectivity, and fluid content and connectivity, and/or varying rock types.

References

Solon, K. D., and others, 2005, Structure of the crust in the vicinity of the Banggong-Nujiang suture in central Tibet from INDEPTH magnetotelluric data, J. Geophys. Res., 110, B10102, doi: 10.1029/2003JB002405.

Wei, W., and others, 2001, Detection of widespread fluids in the Tibetan crust by magnetotelluric studies, Science, 292, 716-718.

Cite as: Vozar, J., and others, 2010, Electromagnetic Studies of Banggong-Nujiang Suture Architecture from INDEPTH Magnetotelluric Profiles and Magnetovariational Data, *in* Leech, M.L., and others, eds., Proceedings for the 25th Himalaya-Karakoram-Tibet Workshop: U.S. Geological Survey, Open-File Report 2010-1099, 1 p. [http://pubs.usgs.gov/of/2010/1099/vozar/].

Did the Lhasa Terrane Rift from the Indian Subcontinent?

Chengshan Wang[1], Bo Ran[2], Xixi Zhao[3]

[1]Research Center for Tibetan Plateau Geology, China University of Geosciences, Beijing 100083, China chshwang@cugb.edu.cn
[2]School of Earth Sciencess, Chengdu University of Technology, Chengdu 610059, China.
[3]Department of Earth and Planetary Sciences and the Institute of Geophysics and Planetary Physics, University of California, Santa Cruz, CA 95064, U.S.A.

In a generally believed tectonic model for the evolution of the Tibetan terranes, the Qiangtang, Lhasa, and Himalaya terranes were rifted and drifted from the northern ancient Indian subcontinent and sequentially added to Eurasia (Allègre and others, 1984; Metcalfe, 2002). Audley-Charles (1983, 1984), on the other hand, argued that the Lhasa Terrane has close affinity to the ancient Australian continent, instead of the Indian subcontinent, based on the sudden change of coexisting warm and cold water biota on the Lhasa terrane due to the mixing of the warmer Paleotethyan Ocean water rather than a quick change of paleoclimate. However, this interesting proposal has not been generally accepted scientifically due to the lack of evidence and remains the "Charles Puzzle" in Tibetan geology. Here, we present new paleomagnetic and geologic data from the Lhasa terrane. Coupled with other recently available data, our results support Audley-Charles's argument and suggest that Lhasa Terrane was rifted from the ancient north Australian, not the north Indian subcontinent. Our paleomagnetic data show that the Lhasa terrane occupied paleolatitudes of 25-35°S in the Late Carboniferous (Pennsylvanian), at 45-50°S in the Early-Middle Permian, and at 30-45°S in the Late Permian. After the Permian, the Lhasa terrane moved northward and did not return south again. The paleolatitude changes indicate a complicated displacement history of the Lhasa terrane, which does not fit with the swift northward-drifting model. Recent published lithochemical evidence suggests that volcanic islands were present in the southern edge of the Lhasa terrane in the Middle Permian (Zhu and others, 2010), but the coeval rocks were of rift-type volcanic rocks in the northern Indian margin (Zhu and others, 2010). Provenance analyses also indicate that the peak age of zircon U-Pb isotope is 1160 Ma (Zhu and others, 2009), which is similar to those from Northern Australia. Thus our new data reinvigorates the debate about the "Charles Puzzle".

References

Allègre, C.J., and others, 1984, Structure and evolution of the Himalayan-Tibet orogenic belt, Nature, 307, 17-22.
Audley-Charles, M.G., 1983, Reconstruction of eastern Gondwanaland, Nature, 306, 48-50.
Audley-Charles, M.G., 1984, Cold Gondwana, warm Tethys and the Tibetan Lhasa block, Nature, 310, 165.
Metcalfe, I., 2002, Permian tectonic framework and palaeogeography of SE Asia, Journal of Asian Earth Sciences, 20, 551-566.
Zhu, D.C., and others, 2009, Zircon U-Pb dating and in-situ Hf isotopic analysis of Permian peraluminous granite in the Lhasa terrane, southern Tibet: Implications for Permian collisional orogeny and paleogeography, Tectonophysics, 469, 48-60.
Zhu, D.C., and others, 2010, Presence of Permian extension- and arc-type magmatism in southern Tibet: Paleogeographic implications, GSA Bulletin, 122, 979-993.

Cite as: Wang, C., Ran, B., Zhao, X., 2010, Did the Lhasa Terrane Rift from the Indian Subcontinent?, *in* Leech, M.L., and others, eds., Proceedings for the 25th Himalaya-Karakoram-Tibet Workshop: U.S. Geological Survey, Open-File Report 2010-1099, 1 p. [http://pubs.usgs.gov/of/2010/1099/wangc/].

State of geological mapping in the Bhutan Himalaya

Ugyen Wangda[1]

[1] Geological Survey of Bhutan, Thimphu, Bhutan, uwangda@druknet.bt

The Geological Survey of Bhutan (GSB), the premier geoscientific organization in Bhutan, is mandated to carry out geologic mapping and exploration projects. Established only in 1981 under technical guidance from the Geological Survey of India (GSI), GSB has endeavored in its capacity to address geoscientific problems and bring geosciences to the forefront in Bhutan despite being a young evolving organization. Geology was virtually unknown in Bhutan until the pioneering work of the Swiss geologist Augusto Gansser between 1958 and 1977, who later published the first geologic map of Bhutan in 1983. This was followed by the publication of another map in 1995 by O.N. Bhargava. This map is the product of many years of mapping expeditions by GSI. These maps were and are the foundations upon which contemporary geologic research in Bhutan is mostly based. GSI left Bhutan in 2002 and since then GSB has been functioning as a fully-fledged geoscientific organization. In an effort to publish its own version of the geologic map of Bhutan, GSB has been systematically mapping the whole country on 50,000 scale even covering areas which remained unmapped due to rugged terrain. So far, GSB has only covered one-sixth of the total area. While trying to understand the geologic setting and tectonic framework of the Bhutan Himalaya, GSB has collaborated with researchers from foreign institutions particularly Princeton and Dalhousie. Besides establishing the regional tectonostratigraphy and mapping some of the complicated structures, introduction of a tectonic model to explain features inherent to the Himalayan orogenesis has taken center stage. The recognition of ductilely deformed rocks led to the inception of the channel-flow model which fundamentally changed our understanding of the role of ductile flow in mountain building processes in collision zones like the Himalaya. A study is underway in western Bhutan to figure out a package of rocks flanked by Greater Himalayan (GH) rocks and consisting of garnetiferous mica schist, quartzite, marble, calc-silicate, and slivers of orthogneiss, locally known as Paro Formation. Establishing the lithostratigraphy of Paro Formation is important because it has been correlated differently by different authors. Whether or not Paro Formation is equivalent to Greater Himalayan, Lesser Himalayan, or Tethyan rocks, has implications for the nature of its contact with the surrounding rocks. The mineral assemblage indicates that Paro rocks in general have attained upper-amphibolite facies metamorphism. This grade of metamorphism is higher than is observed in eastern Bhutan from the same structural level where rocks have attained only greenschist-facies metamorphism.

Cite as: Wangda, U., 2010, State of geological mapping in the Bhutan Himalaya, *in* Leech, M.L., and others, eds., Proceedings for the 25th Himalaya-Karakoram-Tibet Workshop: U.S. Geological Survey, Open-File Report 2010-1099, 1 p. [http://pubs.usgs.gov/of/2010/1099/wangda/].

When Did Shortening Cease Within the Tibetan plateau?

Erchie Wang[1], Dalai Zhong[1], Jiwen Teng[1], Eric Kirby[2]

[1] Institute of Geology and Geophysics, CAS, Beijing, 100029, China, erchie-wang@mail.iggcas.ac.cn
[2] Penn State University, University Park, PA 16802, U.S.A.

With an average elevation of near 5000 m in the west and 4000 m in the east, the low-relief surface of the Tibetan plateau is perhaps the most striking of geomorphic and geologic features within the Indo-Asian collision zone. Understanding how and when this surface developed is central to the geodynamic evolution of the plateau. Here, we undertake a regional synthesis of geologic constraints on the "age" of the plateau surface. Recognizing that even low-relief landscapes are dynamic features, evolving in response to erosion and/or deposition, we attempt to answer the question – when did shortening of Tibetan crust terminate?

By using simple stratigraphic arguments, we attempt to bracket the termination of deformation with strata beveled beneath the plateau surface and with undeformed strata deposited on the surface. Our preliminary compilation reveals that the oldest undeformed strata range in age from the Late Oligocene – Miocene. These strata are of Neogene age in the Hol Xil basin (northwest Tibet), Miocene age in the Wudaoliang area (northern Tibet), Oligocene-Miocene age along the southern slope of the Gangdise (southern Tibet), Oligocene through Pliocene age in the Langping-Simao basin (southeastern Tibet), and Miocene age in the Anduo region (central plateau). These results suggest that no significant shortening has occurred within the plateau since early Miocene time. This observation contrasts sharply with the peripherial regions of the plateau, most of which began to be active in the middle part of the Miocene.

The coincidence of the cessation of shortening within the high plateau with the onset of deformation around the margins and with widespread (yet small volume) alkalic volcanism is intriguing and suggests a potential genetic link. We suggest that these changes in the distribution of upper-crustal shortening and volcanism herald the onset of widespread flow of the lower crust, perhaps in response to changing mantle thermal structure. Outward flow of lower crust was associated with the disruption of the plateau surface by the north-south striking graben systems, by major strike-slip faults (Ganzi – Xianshuihe – Xiaojiang and Kunlun fault systems), and by the incision of the major rivers in eastern Tibet.

Cite as: Wang, E., Zhong, D., Teng, J. and Kirby, E., 2010, When Did Shortening Cease Within the Tibetan plateau?, *in* Leech, M.L., and others, eds., Proceedings for the 25th Himalaya-Karakoram-Tibet Workshop: U.S. Geological Survey, Open-File Report 2010-1099, 1 p. [http://pubs.usgs.gov/of/2010/1099/wangerchie/].

Discovery and Implications of the Qiangtang Indosinian Accretionary Complex Belt in Central Tibet, China

Genhou Wang[1,2], Xiao Liang[2]

[1] Institute of Geophysics, China Earthquake Administration, 100081, China, wgh@cugb.edu.cn
[2] Research Center for Tibetan Plateau Geology, China University of Geosciences, Beijing, 100083, China

The study area is located in the hinterland of the Qiangtang basin in the Tibetan plateau and situated between the Gondwana and Eurasian plates, whose north boundary is the Longmucuo-Shuanghu-Lancangjiang tectonic belt and south boundary is the Bangonghu-Nujiang tectonic belt (Figure 1). From northwest to southeast there exists a series of metamorphic complexes between the above two tectonic belts, including Gemuri, Nierong, Jiayuqiao, Jitang, Yunling, Ximeng-Mengtong, Changning-Menglian,and Jinghong, which were assembled during formation and linked together as an integrated tectonic zone. These metamorphic complexes are usually covered by Mesozoic strata and denudated by later intense extension, which caused ductile shear and transposition deformation. Detailed research on the Qiangtang accretionary complex is significant to understand the tectonic attributes of the complex aggregation, analyze the tectonic framework of the Qiangtang area, and study the evolution of Paleotethys.

The central Qiangtang area is mainly covered by Mesozoic and Cenozoic strata, complicating research on the metamorphic complexes that occurring across a very wide area. Although the study of these complexes relates to our understand of the evolution of the Qiangtang basin and even of the Tibetan plateau, there exist different views on their age, origin and tectonic attributes (Kapp and others, 2000; 2003). Based on our field work and data, it is found that the flysch and basalt-schist suites developed in the complexes experienced strong structural transposition. The complexes also include early-to-late Paleozoic marbles with rootless folds, blueschists in closed-isoclinal folds together with marbles, and blocks of eclogite in outcrop. Generally, they all occur as tectonic slices that experienced regional intense structural transposition and superimposition, and now exhibit a regular penetrative foliation. The original rocks interpreted from the metamorphic rocks include clastic rock, mudstone, siliceous rock, carbonatite, pillow basalt and gabbro. On the basis of the above characteristics, it is presumed that the central Qiangtang metamorphic complex should be classified as an accretionary complex. The construction of its lithology is described as follows:

1/ Terrigenous moderate- to deep-water flysch: the major rocks are silty slate, sericite-phyllite, and sericite quartz-schists, intercalated with yellowish gray medium-thick bedded quartzite, pebbly quartzite, muscovite quartzite, metamorphosed quartz sandstone, as well as occasionally intercalated with massive limestone, marble, greenish-gray epidote actinolite schists, phyllite, tuffaceous metamorphic siltstone, silty slate, and ophiolite blocks, etc. These rocks exhibit intense deformation, including tight folds, netted quartz vein and plenty of rootless folds.

2/ Seamount (ocean-island) blocks: these include massive basalt, limestone (formed in shallow water), and basaltic or limy conglomerate. In a few outcrops, the basalt and limestone are in direct contact. But in most cases, the basalt, limestone, and conglomerate blocks are dispersed through and incorporated in the flysch. Pillow structure is developed in the basalt, and sometimes basaltic columnar-joint structure is also observed as evidence of basalts erupting over the sea surface.

3/ Ocean-floor sedimentary rocks: they mainly include siliceous rock, argillite, so metimes including glacial-erratic blocks. Some thin-bedded limestone may also be ocean-floor sedimentary rock.

4/ Residual oceanic crust(ophiolite blocks): mainly found in the Jiaomuru area, including basalts, pillow basalt, diabase, gabbro, as well as ultrabasic rock and plagioclase granite.

5/ Ordovician-Devonian carbonate rocks: these are mainly include calcareous schists and low-grade metamorphic fine-grained clastic rock intercalated with crystalline limestone, etc. These rocks experienced complex structural deformation and tectonic transposition, to the extent that *Sinoceras* even exhibits boudinage due to ductile shear deformation.

6/ High-pressure metamorphic blocks: the rocks include grayish-white marble, white-mica marble, greenish-gray sericite quartz-schist, glaucophane-bearing epidote actinolite schist, garnet-bearing muscovite schists, glaucophane-bearing meta-basalts, meta-basalts, basalt schists and quartzite etc. The

main body of rocks consists of different kinds of crystalline limestone, marble, quartzite, and quartz-schist, which are intercalated with meta-basalts, basalt schists, and glaucophane-bearing schists. In addition, the basalts show the typical characteristic of ocean islands.

On the basis of regional contact relationships of the strata, isotopic dating and related magmatic rocks, we believe these accretionary complexes formed in the Indosinian Epoch.

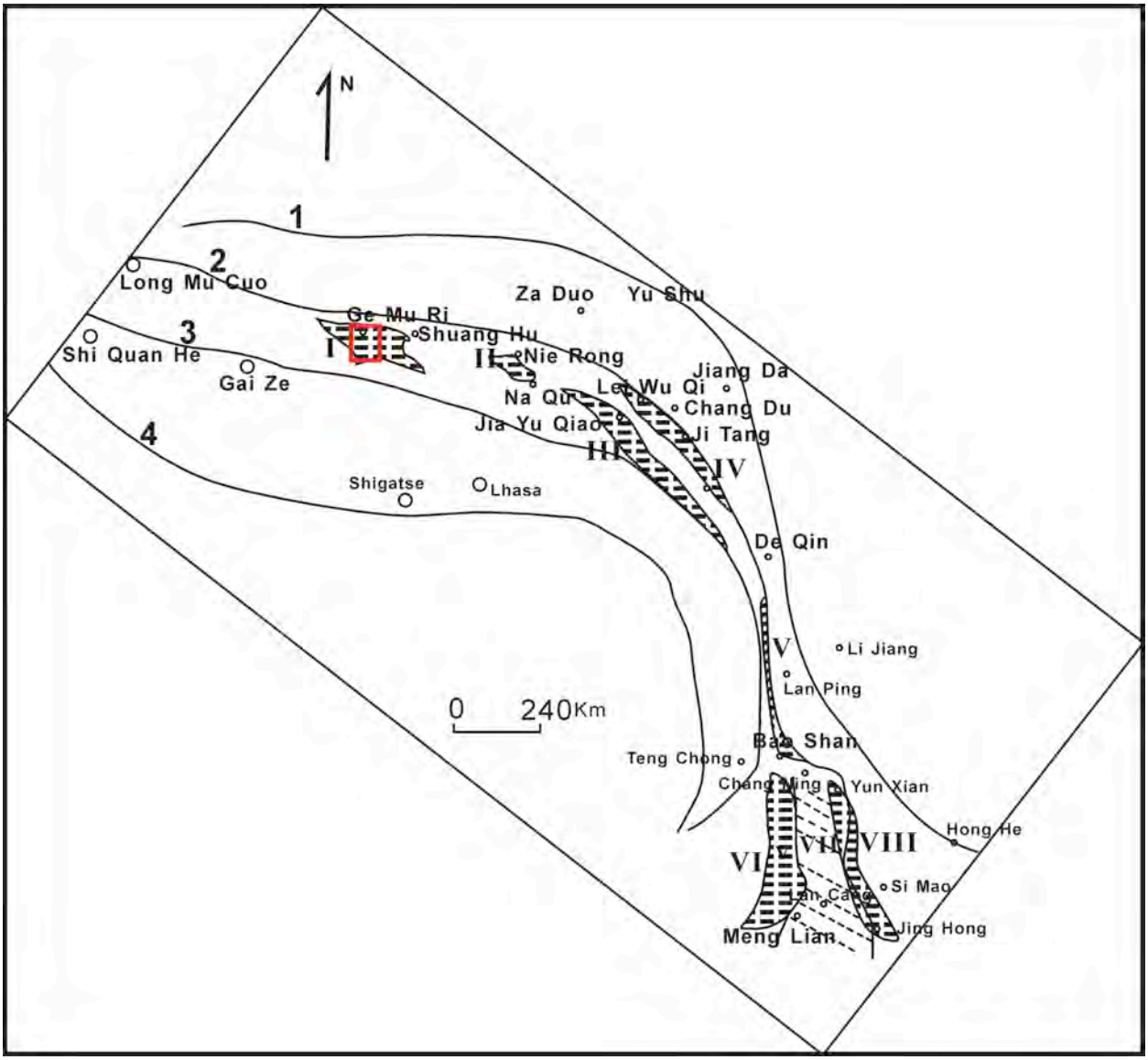

Figure 1. Tectonic map of the study area. Tectonic belts: 1. XijirUlan-Jinshajiang-honghe, 2. Longmucuo-Shuanghu-Lancangjiang, 3. Bangonghu-Nujiang, 4. Indus-Yarlung Zangbo. Metamorphic complexes: I. Gemuri, II. Nierong, III. Jiayuqiao, IV. Jitang, V. Yunling, VI. Ximeng-Mengtong, VII. Changning-Menglian, VIII. Jinghong.

References

Kapp, P., An,Y. and Manning, C.E., 2000, Blueschist-bearing metamorphic core complexes in the Qiangtang block reveal deep crustal structure of northern Tibet, Geology, 28, 19-22.

Kapp, P., An, Y. and Manning, C.E., 2003, Tectonic evolution of the early Mesozoic Blueschist-bearing Qiangtang metamorphic belt, central Tibet, Tectonics, 22, 1043.

Cite as: Wang, G. and Liang, X., 2010, Discovery and Implications of Qiangtang Indosinian Accretionary Complex Belt in Cenral Tibet, China, *in* Leech, M.L., and others, eds., Proceedings for the 25th Himalaya-Karakoram-Tibet Workshop: U.S. Geological Survey, Open File Report 2010-1099, 2 p. [http://pubs.usgs.gov/of/2010/1099/wang/].

Releasing a reservoir of shallow strain as a possible cause of the catastropic Wenchuan earthquake, China

Qi Wang[1,2*], Xuejun Qiao [2*], Qigui Lan[3*], Jeffrey Freymueller[4], Shaomin Yang[1,2], Caijun Xu[5]

[1] Centre of Space Research, Chinese University of Geosciences, Wuhan, 430074, China, wangqi@cug.edu.cn
[2] Institute of Seismology, Chinese Earthquake Administration & Hubei Earthquake Administration, Wuhan, 430071 China
[3] First Institution of Survey Engineering, Sichuan Bureau of Surveying & Mapping, Chengdu, 610100, China
[4] Geophysical Institute, University of Alaska, Fairbanks, Alaska, 99775, U.S.A.
[5] School of Geodesy and Geomatics, Wuhan University, Wuhan, 430072 China

Over the centuries, great earthquakes have occurred frequently in Asia, yet up-close, detailed geodetic observations of ground deformation are few. Here we present 484 ground-based measurements of surface displacement associated with the great Wenchuan earthquake of 12 May 2008. Analysis of the most comprehensive ground-based dataset and space-borne InSAR images reveal a minimum rupture length of 291 km, along which 5 shallow and 2 deep high-slip asperities are identified on two steeply-dipping ramp faults above a sub-horizontal décollement at 16-21 km depths under the Longmen Shan, and each produced moment release equivalent to a moment magnitude M_w6.9-7.4 earthquake. The rupture of those asperities with maximum slips of up to 14 meters in the uppermost 5-6 km of brittle crust may result from draining residual strain energy at shallow depths left over from previous earthquake cycles, or from cascading slip propagation across low-slip barriers either associated with past moderate earthquakes or with structure irregularities. The Wenchuan event therefore represents the latest culmination of the regional seismicity characterized by the rupture of multiple fault segments, and its atypical size that we estimate at M_w=7.96, if repeated, would occur much later than anticipated only from considerations of secular fault slip rate.

Cite as: Qi, W., and others, 2010, Releasing a reservoir of shallow strain as a possible cause of the catastrophic Wenchuan earthquake, China, *in* Leech, M.L., and others, eds., Proceedings for the 25th Himalaya-Karakoram-Tibet Workshop: U.S. Geological Survey, Open-File Report 2010-1099, 1 p. [http://pubs.usgs.gov/of/2010/1099/wangqi/].

Late Cenozoic Exhumation of the Eastern Margin of the Tibetan Plateau: New Constraints from Age-Elevation Transects in the Longmen Shan

Erchie Wang[1], Xuhua Shi[2], Eric Kirby[2], Kevin Furlong[2], Ganqing Xu[3], Peter Kamp[3], Peter Reiners[4]

[1] Institute of Geology and Geophysics, Chinese Academy of Sciences, Beijing 100029, China, erchie-wang@mail.iggcas.ac.cn
[2] Department of Geosciences, Pennsylvania State University, University Park, PA 16802, U.S.A.
[3] Department of Earth and Ocean Sciences, University of Waikato, Hamilton, New Zealand
[4] Department of Geosciences, University of Arizona, Tucson, AZ 85721, U.S.A.

The eastern margin of the Tibetan Plateau adjacent to the Sichuan Basin is characterized by one of the steepest escarpments on the continents – the Longmen Shan belt. Mean relief across this margin of the plateau exceeds ~ 4 km relief over a distance of ~ 50 km. The mechanisms by which this spectacular topography developed and is sustained is an ongoing debate and carries implications for the geodynamic evolution of the Tibetan Plateau (e.g., Royden and others, 1997; Clark and Royden, 2000; Kirby and others, 2002; Godard and others, 2009a). A number of recent studies used low-temperature thermochronology to decipher late Cenozoic thermal and exhumation evolution of the this region; collectively, these suggest that rapid cooling in the Late Cenozoic (e.g., 20 – 8 Ma; Arne and others, 1997; Kirby and others, 2002; Godard and others, 2009b) heralds the development of high topography. However, the rugged and inaccessible terrain has hindered attempts to collect dense age-elevation transects that cover the entire range of exposed rock.

Here we present preliminary results of low-temperature thermochronology (apatite fission-track and (U-Th)/He from zircon) from two age-elevation transects collected in the immediate hanging wall of the thrust that ruptured during the 2008 Sichuan Earthquake ($M_w = 7.9$). Both transects are from Proterozoic basement rocks of the Pengguan Massif; the apatite fission-track (AFT) transect spans the entire region of granitic rocks (1160 – 4174 m), whereas the zircon He data span a more limited range of relief (1100 – 2000 m). AFT ages are systematically younger at lower elevations and range from 15 – 56.5 Ma. In contrast, zircon (U-Th)/He ages range from 7.3 – 14.3 Ma. Thus, for samples with the same elevations, AFT ages are older than the zircon (U-Th)/He ages. This discrepancy may reflect spatial variability in the thermal structure beneath the Longmen Shan, perhaps as a consequence of: 1) topographic relief across the plateau margin; 2) lateral cooling across the range-bounding thrust; or 3) structural deformation (folding) of isotherms during shortening at the plateau margin. We are currently exploring these questions using simple thermal models, as well as collecting additional apatite and zircon (U-Th)/He data. Collectively, our results may suggest that exhumation began in Longmen Shan region somewhat earlier than previously thought (Kirby and others, 2002) but a definitive answer to this question awaits assessment of the effects of variations in the thermal structure beneath the eastern margin of the Tibetan Plateau.

References

Arne, D., and others, 1997, Differential exhumation in response to episodic thrusting along the eastern margin of the Tibetan Plateau, Tectonophysics, 280(3-4), 239-256.

Clark, M.K. and Royden, L.H., 2000, Topographic ooze: Building the eastern margin of Tibet by lower crustal flow, Geology, 28(8), 703-706.

Godard, V., Cattin, R. and Lavé J., 2009a, Erosional control on the dynamics of low-convergence rate continental plateau margins, Geophysical Journal International, 179, 763-777.

Godard, V., and others, 2009b, Late Cenozoic evolution of the central Longmen Shan, eastern Tibet: Insight from (U-Th)/He thermochronometry, Tectonics, 28. TC5009, doi:10.1029/2008TC002407.

Kirby, E., and others, 2002, Late Cenozoic evolution of the eastern margin of the Tibetan Plateau: Inferences from 40Ar/39Ar and (U-Th)/He thermochronology, Tectonics, 21(1): 1001, doi:10.1029/2000TC001246.

Royden, L.H., and others, 1997, Surface deformation and lower crustal flow in eastern Tibet, Science, 276(5313): 788-790.

Cite as: Wang, E., and others, 2010, Late Cenozoic Exhumation of the Eastern Margin of the Tibetan Plateau: New Constraints from Age-Elevation Transects in the Longmen Shan, *in* Leech, M.L., and others, eds., Proceedings for the 25th Himalaya-Karakoram-Tibet Workshop: U.S. Geological Survey, Open-File Report 2010-1099, 1 p. [http://pubs.usgs.gov/of/2010/1099/ewang/].

Post – 1991 Uttarkashi Earthquake Seismicity Pattern in the Garhwal Himalaya Region

H.R. Wason[1]

[1]Department of Earthquake Engineering, IIT Roorkee, Roorkee-247667, India, wasonfeq@iitr.ernet.in

The area under study falls in the Garhwal region of the Lesser Himalaya. The region lies between the Alaknanda River on the east and the Tons River on the west. This study area of the Lesser Himalayan sub-province encompasses a number of NW-trending transverse tectonic features (Valdiya, 1976; Fuchs and Sinha, 1978). The main tectonic elements of the region are shown in Figure 1. The major tectonic features have an average strike along NW-SE.

The aim of this paper is to present an analysis of local seismic activity of Garhwal Himalaya region recored since the Uttarkashi earthquake (m_b = 6.6; October 20, 1991). A total of 430 seismic events recorded by an analog micro-earthquake network during the two-year period from January, 1993 to January, 1995 are analyzed. Epicentral locations of the 430 seismic events recorded by the array are shown in Figure 1. About 70% of the events are found to lie in the aftershock zone of the Uttarkashi earthquake of October 20, 1991, in the vicinity of the Main Central Thrust. Some epicenters are also observed to the south of Main Central Thrust. The micro-earthquake activity is found to be concentrated in the region bounded by the Budhakedar, Bhatwari and Manpur stations.

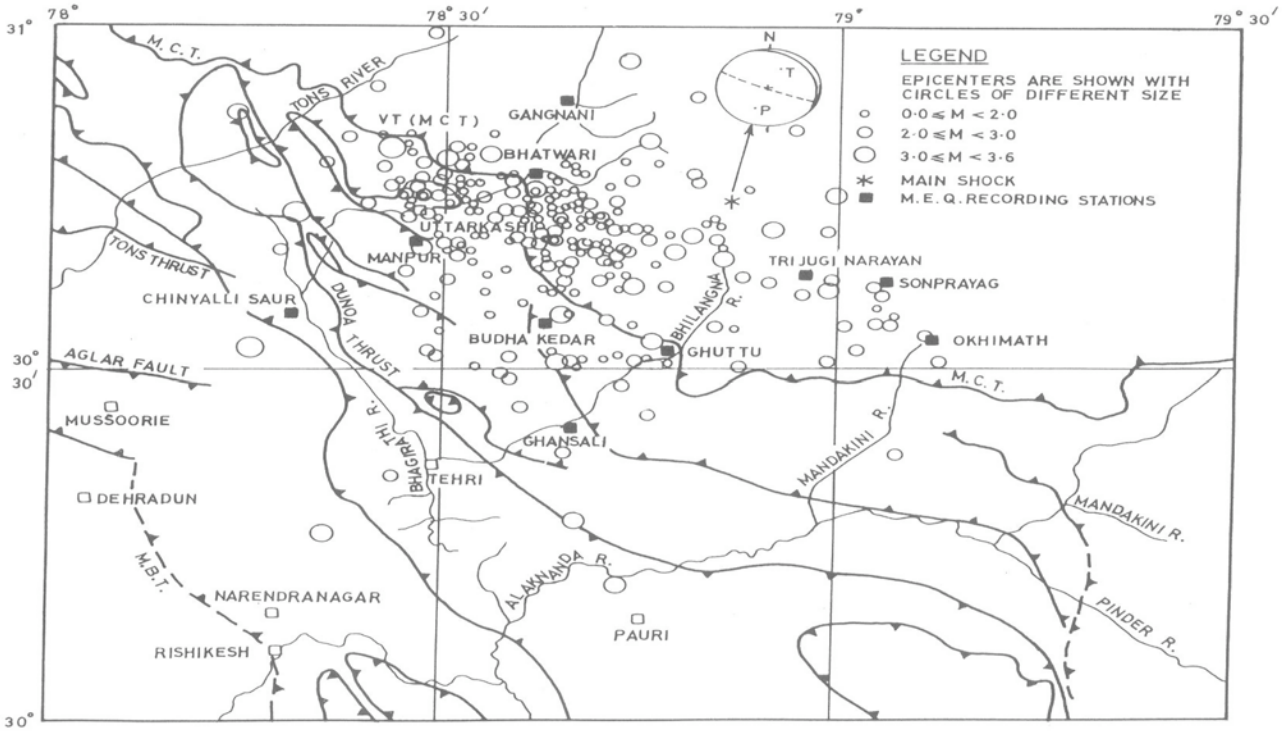

Figure 1. Tectonic map of Garhwal Himalaya region showing epicenters of local earthquakes recorded during January, 1993 to January, 1995, and focal mechanism of Uttarkashi earthquake of October 20, 1991.

Coda magnitudes of the events are calculated from the total signal duration using the relation given by Tsumura (1967) and Lee and others (1972). The coda lengths have been measured from the P onset to the point where the signal amplitude falls to the background noise level preceding the event. Out of a total of 430 events, 253 events are found to have coda magnitudes up to 2.0, 146 events have magnitudes between 2.1 and 3.0 and for 31 events the magnitudes are more than 3.0. The majority of the earthquakes are

observed to have their foci within the upper 15 km of the crust but a substantial number of events, 68 in number, have deeper focal depths between 15-28 km. The focal depth distribution along with coda magnitudes are given in Table 1. The focal depths of microearthquake events recorded prior to the Uttarkashi earthquake were also mostly above 15 km as reported by Agrawal and Kumar (1982), Khattri and others (1989), and Sharma and Wason (1994).

Table 1. Magnitude (M) and depth (H) distribution of epicenters

M	H≤10 Km	10<H≤15 Km	H>15 Km	Total
0.0-2.0	190	51	12	253
2.1-3.0	57	52	37	146
3.1-3.5	5	7	19	31
Total	252	110	68	430

Composite focal mechanism solutions have been determined for two clusters of microearthquake events. In doing this, we assume that all the events in each cluster have the same focal mechanism. In the first focal mechanism solution,18 microearthquake events which occurred within the region 30° 30' N to 30° 45' N & 78° 28' E to 78° 45' E are considered, whereas in the second solution, 20 events have been considered which occurred within 30° 40' N to 30° 50' N & 78° 26' E to 78° 45' E. The composite fault plane solutions for both the clusters of micro earthquake events are characterized by reverse faulting with a small strike-slip component. The main shock of the Uttarkashi earthquake was also characterized by reverse mechanism. However, in both the composite focal-mechanism solutions the pressure axes are observed to be sub-horizontal.

From depth sections oriented NW-SE and SW-NE, it can be seen that some of the events after the Uttarkashi earthquake of October 20, 1991, originated below the detachment surface. The distribution of focal depths of the events, the pattern of occurrence and composite focal-mechanism solutions of the clustered events, suggest that the local seismic activity during the period of investigation resulted from the ongoing readjustments in the area.

Acknowledgment

This study was undertaken under a research project funded by DST, Govt. of India, New Delhi under its Himalayan Seismicity Program.

References

Agrawal, P. N. and Kumar, A., 1982, Microearthquake recording for engineering applications, In Engineering geosciences, Sarita Prakashan, Meerut, India, 181-186.

Fuchs, G. and Sinha, A. K., 1978, The tectonics of the Garhwal-Kumaon Lesser Himalaya, J Geol. B. -A., BD., Heft 2, Wien, 121, 219-241

Khattri, K. N., Chander, R, Gaur, V. K., Sarkar, 1. and Kumar, S., 1989, New seismological results on the tectonics of the Garhwal Himalaya, Proc. Indian Acad. Sci. (Earth Planet Sci.), 98, 91-109.

Lee,W. H. K., Bennett, R E. and Meagher, K. L., 1972, A method of estimating magnitude of local earthquakes from signal duration, Geol. Surv. Open-File Rep. (U.S.), 28.

Sharma, M. L. and Wason, H. R., 1994, Occurrence of low stress drop earthquakes in the Garhwal Himalaya region, Phys. Earth Planet. Int., 85, 265-272.

Tsumura, K., 1967, Determination of Earthquake Magnitude from Total Duration of Oscillation, Bull. Earthquake Res. Inst., 15, 7-18.

Valdiya, K. S., 1976, Himalayan transverse faults and folds and their parallelism with subsurface structures of north Indian plains, Tectonophysics, 32, 353-386.

Cite as: Wason, H.R., 2010, Post-1991 Uttarkashi Earthquake Seismicity Pattern in the Garhwal Himalaya Region, *in* Leech, M.L., and others, eds., Proceedings for the 25th Himalaya-Karakoram-Tibet Workshop: U.S. Geological Survey, Open-File Report 2010-1099, 2 p. [http://pubs.usgs.gov/of/2010/1099/wason/].

Testing models for the kinematic evolution of the Lesser Himalayan Sequence by balanced reconstruction: Accretion dominant in northwestern India

A. Alexander G. Webb[1], Hongjiao Yu[1]

[1] Department of Geology and Geophysics, Louisiana State University, Baton Rouge, LA 70803, U.S.A., awebb@lsu.edu

Tectonic models of the Himalayan orogen may be categorized as critical taper (e.g., Kohn, 2008) or channel flow (e.g., Beaumont and others, 2004). These models explain the assembly of the three major Himalayan units (the Lesser Himalayan Sequence, Greater Himalayan Crystalline complex, and Tethyan Himalayan Sequence) by deformation concentrated on the two faults that limit the units (the Main Central thrust and South Tibet detachment). Both models accommodate a wide range of possible tectonic histories for the Lesser Himalayan Sequence, which represents the most recent bedrock addition to the growing orogenic wedge. Mechanisms proposed for the construction of the Lesser Himalayan Sequence include: (1) forward-propagating thrusting (e.g., Schelling and Arita, 1991); (2) accretion of thrust horses at upper crustal (e.g., Robinson, 2008) and/or middle crustal (e.g., Bollinger and others, 2004) depth; (3) out-of-sequence thrusting, which may be driven by focused precipitation and erosion (e.g., Thiede and others, 2004); and (4) thrusting both before and after Main Central thrust motion (Célérier and others, 2009a).

Detailed kinematic reconstructions are powerful tools for testing thermal and tectonic models of orogenic wedges (e.g., Célérier and others, 2009b; Malavieille, 2010). We test the Lesser Himalayan Sequence models by constructing and progressively retro-deforming a balanced cross section across the Lesser Himalaya and the foreland basin rocks of the Sub-Himalaya. We target the Shimla region of northwestern India because it contains the richest stratigraphic diversity in the orogen, thus allowing the highest resolution for constraining restoration [major units are the Cenozoic Sub-Himalaya, the Cretaceous-Eocene Subathu-Singtali rocks, the Late Proterozoic-Cambrian Outer Lesser Himalaya Group, the Early-Middle Proterozoic Deoban-Damtha Groups, the Early Proterozoic Berinag Group, and the Early Proterozoic Munsiari Group]. The section is informed by our regional geological map, which integrates literature mapping and analytical results with our own structural and analytical data (from >650 sites). Additional sketch cross sections were made to relate along-strike structural variations to the main section.

Our reconstruction shows a minimum shortening of ~268 km (~57%) across the Lesser Himalaya and Sub-Himalaya since ~14 Ma. We show the progressive evolution with sections representing ~14 Ma, ~5.4 Ma, ~1.9 Ma, and the present. Major thrusts accomplishing shortening via top-to-the-SW motion are the Main Frontal thrust, the Bilaspur thrust, the Krol thrust, the Tons thrust, the Berinag thrust, and the Munsiari thrust. We do not include a Main Boundary thrust, i.e., a structure defined to place the Lesser Himalayan Sequence atop the Sub-Himalaya, because the Bilaspur, Krol, and Tons thrusts all match this description. Shortening of the Deoban-Damtha rocks occurred within an upper crustal duplex; ongoing shortening of the Munsiari rocks occurs within a hinterland, middle crustal antiformal stack. Most shortening has been accomplished by accretion of footwall horses at both middle and upper crustal levels (roughly 75% of shortening) and foreward propagation of the thrust belt into the foreland (roughly 20% of shortening). Out-of-sequence shortening is limited to ~15 km along the Munsiari thrust and <3 km on other structures. The Munsiari thrust has been previously interpreted as an out-of-sequence structure having over 20 km of throw (e.g., Thiede and others, 2004). Our alternative model suggests that the vertical displacement accomplished by out-of-sequence Munsiari faulting may be limited to ~5 km, with remaining uplift accomplished by the Munsiari antiformal stack. The reconstruction does not require any Cenozoic deformation of exposed Lesser Himalayan Sequence rocks prior to Main Central thrust motion; we argue that such deformation is unlikely. The active basal thrust carries a leading fold-and-thrust belt in the south, an upper crustal duplex further north, and the growing Munsiari antiformal stack in the northern hinterland. This kinematic model is broadly similar to analog models featuring a main decollement and a zone of enhanced erosion over the hinterland (cf. Malavieille, 2010). Two possible causes for enhanced erosion over the Munsiari antiformal stack are a local precipitation maximum (e.g., Thiede and others, 2004) or the Sutlej River.

References

Beaumont, C., Jamieson, R.A., Nguyen, M.H. and Medvedev, S., 2004, Crustal channel flows: 1. Numerical models with applications to the tectonics of the Himalayan-Tibetan orogen: Journal of Geophysical Research, v. 109, B06406, doi:10.1029/2003JB002809.

Bollinger, L., and others, 2004, Thermal structure and exhumation history of the Lesser Himalaya in central Nepal: Tectonics v. 23, TC5015, doi:10.1029/2003TC001564.

Célérier, J., Harrison, T.M., Webb, A.A.G. and Yin, A., 2009a, The Kumaun and Garwhal Lesser Himalaya, India: Part 1. Structure and stratigraphy. Geological Society of America Bulletin, 121, 1262-1280.

Célérier, J., and others, 2009b, The Kumaun and Garwhal Lesser Himalaya, India: Part 2. Thermal and deformation histories. Geological Society of America Bulletin, 121, 1281-1297.

Kohn, M.J., 2008, P–T–t data from central Nepal support critical taper and repudiate large-scale channel flow of the Greater Himalayan sequence. Geological Society of America Bulletin, 120, 259–273.

Malavieille, J., 2010, Impact of erosion, sedimentation, and structural heritage on the structure and kinematics of orogenic wedges: Analog models and case studies. GSA Today, 20, 4-10.

Robinson, D.M., 2008, Forward modelling the kinematic evolution of the central Himalayan thrust belt, western Nepal. Geosphere, 4, 785-801.

Schelling, D. and Arita, K., 1991, Thrust tectonics, crustal shortening, and the structure of the far-eastern Nepal Himalaya. Tectonics, 10, 851-862.

Thiede, R.C., Bookhagen, B., Arrowsmith, J.R., Sobel, E.R. and Strecker, M.R., 2004, Climatic control on rapid exhumation along the Southern Himalayan Front: Earth and Planetary Science Letters 222 (3-4), 791-806.

Cite as: Webb, A.A.G. and Yu, H., 2010, Testing models for the kinematic evolution of the Lesser Himalayan Sequence by balanced reconstruction: Accretion dominant in northwestern India, *in* Leech, M.L., and others, eds., Proceedings for the 25th Himalaya-Karakoram-Tibet Workshop: U.S. Geological Survey, Open-File Report 2010-1099, 2 p. [http://pubs.usgs.gov/of/2010/1099/webb/].

The Impact of Mesozoic Tectonism on Eastern Tibet Plateau Crustal Infrastructure: Implications for Plateau Evolution

Amy L. Weislogel[1], Delores M. Robinson[1]

[1] Department of Geological Sciences, University of Alabama, Tuscaloosa, AL 35401, U.S.A., amy.weislogel@gmail.com

Often the impact of pre-Himalayan tectonic episodes is left largely unaddressed in plateau evolutionary models, which are primarily based on Cenozoic geological records. A legacy of Mesozoic collisional tectonics may be that no one mechanistic model is appropriate to explain wholesale elevation development of this region. Thus, constraining the architecture of pre-Himalayan Asian lithosphere is an integral element for an accurate model of Tibet plateau rise (Yin and Harrison, 2000; Kapp and others, 2003). The idea that the Qiangtang and Lhasa blocks formed an elevated proto-Tibet plateau, perhaps up to 3–4 km by Early Cretaceous time, prior to collision of India with Asia, has long been proposed (e.g., England and Searle, 1986; Murphy and others, 1997). High elevation (>2-3 km) may have persisted in the Qiangtang and Lhasa blocks since prior to the Late Eocene (Garzione and others, 2000; Spicer and others, 2003; Graham and others, 2005; Rowley and Currie, 2006; DeCelles and others, 2007). This elevation increase was likely caused by a series of Mesozoic collisional events that preceded Himalayan orogenesis and increased the thickness of the Asian lithosphere (e.g., Kapp and others, 2005, 2007). Models predicated upon geological evidence from western and central regions of Tibet support crustal thickening, and by association surface rise, during Early Cretaceous time. However, Reid and others (2005) concluded based on thermochronologic data that eastern Tibet experienced rapid uplift and denudation as early as Late Triassic, with <2 km of denudation across the high elevation, low relief areas of the Yidun arc since the India-Asia collision.

Analysis of well-preserved Mesozoic sediments in the Changdu basin (a.k.a., Qamdo or Markham basin) of eastern Tibet and adjacent fold belts offers geologic records with which to assess pre-Cenozoic plateau development. The Changdu basin is a 12,000 km^2, NW-SE elongate basin containing ~7000 m of well-exposed Upper Triassic-Lower Cretaceous basin-fill that rests on top of Precambrian and Paleozoic basement rocks of the Qiangtang block (Wang and others, 2008). Sedimentary evidence from the Changdu basin suggests subaerial terrestrial environments dominated since Early Jurassic time. The fossiliferous Tethyan marine carbonate Bolila Fm. is overlain by the Upper Triassic Bagong Group, a thick package of coal-bearing deposits representing the last marine-influenced deposition on the Qiangtang block. Overlying these marine-influenced deposits is the ≤5,000 m of interbedded siliciclastic fluvial, lacustrine and paleosol-bearing strata of the Lower-Upper Jurassic Chaya Group and Lower Cretaceous Xiangdui Fm. Thus, marine environments vacated the Qiangtang block ~75 Ma earlier than the Lhasa block.

The Changdu basin is bracketed by two suture zones: (1) the Jinshajiang suture to the NE, along which the Yidun arc collided with the Qiangtang block in latest Triassic time (Reid and others, 2005), and (2) the Bangong-Nujiang suture to the SW that formed due to collision between the Lhasa and Qiangtang blocks prior to Late Jurassic time (Kapp and others, 2003, 2005). The Jinshajiang suture may have marked the northern limit of the Tibetan plateau by 50 Ma (Roger and others, 2008; Tapponnier and others, 2001), but given the Mesozoic history of collisional tectonism along these sutures, perhaps surface elevation increase occurred even earlier. Determining provenance links between the rocks of the fold belts and Changdu basin deposits will permit deciphering Mesozoic structural evolution and crustal thickening from later overprinting coaxial Cenozoic deformation (e.g., Studnicki-Gizbert and others, 2008).

Preliminary detrital zircon U-Pb ages of the Upper Triassic Jiapeila mélange exposed along the western margin of the Jinshanjiang suture zone is compared with that of basal Chandu basin deposits (Fig. 1). Jiapeila zircon ages are more compatible with zircon ages reported from the Qiangtang block (Pullen and others, 2008), indicating a southerly affinity. However, the zircon age signature of the Upper Triassic Adula Fm. of the Bagong Group differs significantly from the adjacent Jiapeila mélange, suggesting Jiapeila melange rocks were not sources of sediment to the Changdu basin during Late Triassic time. Instead, the Bagong Group shares ages known from the SE Songpan-Ganzi complex, which was sourced

primarily by rocks of South China block-affinity, with minor input from the Yidun arc. Also, Changdu basin sandstone exhibits temporal compositional changes. Jiapeila mélange bears abundant poly- and monocrystalline quartz along with abundant sedimentary, low-grade metamorphic and volcanic lithic fragments. However, samples of Upper Triassic Bagong Group and Jurassic Chaya Group sandstone are primarily composed of monocrystalline quartz, implying a recycled orogen source, further rebutting any link between Jiapeila Fm. or its source as a contributor of sediment to basal Changdu basin siliciclastic deposits. In contrast, Lower Cretaceous Xiangdui Fm. sandstone contains abundant poly- and monocrystalline quartz along with abundant sedimentary, low-grade metamorphic and volcanic lithic fragments, potentially indicating a late-phase association with the Jiapeila Fm.

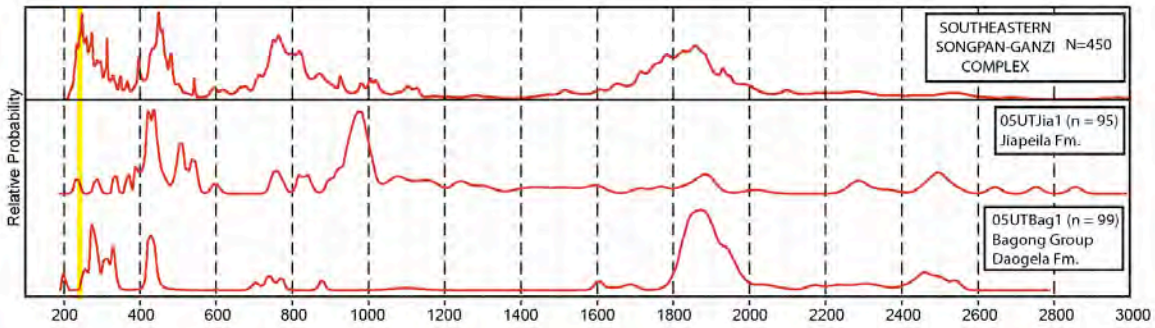

Figure 1. Detrital zircon ages from the Triassic Jiapeila Fm. and basal Changdu basin Bagong Group compared with detrital zircon ages of the SE Songpan Ganzi Complex. Yellow bar represents age of Yidun arc zircon ages.

References

DeCelles, P., and others, 2007, High and dry in central Tibet during the Late Oligocene. Earth Planet. Sci. Letts., 253, 389-401.

England, P. and Searle, M., 1986, The Cretaceous-Tertiary deformation of the Lhasa block and its implications for crustal thickening in Tibet. Tectonics, 5, 1-14.

Garzione, C., Quade, J., DeCelles, P. and English, N., 2000, Predicting paleoelevation of Tibet and the Himalaya from d18O vs. altitude gradients in meteoric water across the Nepal Himalaya. Earth Planet. Sci. Letts., 183, 215-229.

Graham, S., and others, 2005, Stable isotope records of Cenozoic climate and topography, Tibetan Plateau and Tarim Basin. Am. J. Sci., 305, 101-118.

Kapp, P., and others, 2003, Mesozoic and Cenozoic tectonic evolution of the Shiquanhe area of western Tibet. Tectonics, 22, 1029, doi:10.1029/2001TC001332.

Kapp, P., Yin, A., Harrison, T. and Ding, L., 2005, Cretaceous-Tertiary shortening, basin development, and volcanism in central Tibet. Geol. Soc. Am. Bull., 117, 865-878.

Kapp, P., DeCelles, P., Gehrels, G., Heizler, M. and Ding, L., 2007, Geological records of the Lhasa-Qiangtang and Indo-Asian collisions in the Nima area of central Tibet. Geol. Soc. Am. Bull., 119, 917-933.

Murphy, M., Yin, A., Harrison, T. and Durr, S., 1997, Did the Indo-Asian collision alone create the Tibetan plateau? Geology, 25, 719-722.

Pullen, A., Kapp, P., Gehrels, G., Vervoort, J. and Ding, L., 2008, Triassic continental subduction in central Tibet and Mediterranean-style closure of the Paleo-Tethys Ocean. Geology, v. 36, no. 5, 351-354.

Reid, A., Wilson, C., Phillips, D. and Liu, S., 2005, Mesozoic cooling across the Yidun Arc, central-eastern Tibetan Plateau: A reconnaissance 40Ar/39Ar study. Tectonophysics, v. 398, no. 1-2, p. 45-66.

Roger, F., Jolivet, M. and Malavieille, J., 2008, Tectonic evolution of the Triassic fold belts of Tibet. Comptes Rendus Geosciences, v. 340, no. 2-3, p. 180-189.

Rowley, D. and Currie, B., 2006, Palaeo-altimetry of the late Eocene to Miocene Lunpola basin, central Tibet. Nature, 439, 677-681.

Spicer, R., and others, 2003, Constant elevation of southern Tibet over the past 15 million years. Nature, 421, 622-624.

Studnicki-Gizbert, C., Burchfiel, B., Li, Z. and Chen, Z., 2008, Early Tertiary Gonjo basin, eastern Tibet: Sedimentary and structural record of the early history of India-Asia collision. Geosphere, 4, 713-735.

Tapponnier, P., and others, 2001, Oblique stepwise rise and growth of the Tibet Plateau. Science, 294, 1671-1677.

Wang, Q., and others, 2008, Eocene melting of subducting continental crust and early uplifting of central Tibet: Evidence from central-western Qiangtang high-K calc-alkaline andesites, dacites and rhyolites. Earth Planet. Sci. Letts., 272, 158-171.

Yin, A. and Harrison, T., 2000, Geologic evolution of the Himalayan-Tibetan orogen. Annual Review of Earth and Planetary Sciences, 28, 211-280.

Cite as: Weislogel, A.L. and Robinson, D.M., 2010, The Impact of Mesozoic Tectonism on Eastern Tibet Plateau Crustal Infrastructure: Implications for Plateau Evolution, *in* Leech, M.L., and others, eds., Proceedings for the 25th Himalaya-Karakoram-Tibet Workshop: U.S. Geological Survey, Open-File Report 2010-1099, 2 p. [http://pubs.usgs.gov/of/2010/1099/weislogel/].

The Himalayan Pile-Up: Revised Plate Reconstructions Provide Evidence of Multiple Accretion Events During the Himalayan Orogeny

Lloyd T. White[1], Gordon Lister[1]

[1]Research School of Earth Sciences, The Australian National University, Canberra, ACT, 0200, Australia, lloyd.white@anu.edu.au

The concept of "the collision" of India to Eurasia dominates the literature on the Himalaya. However, controversy surrounds the timing as to when this took place. One hypothesis suggests that this event occurred at ~50-55 Ma, whilst other hypotheses suggest that this event may have occurred earlier (~70 Ma) or later (~34 Ma) (Yin and Harrison 2000; Aitchison et al. 2007). This has led to a debate as to which time is the most appropriate age of "the collision". However, the logic that is adopted in this debate implies that there can only be one "main" collision. Yet, many workers also recognise that the Himalaya could have developed due to a number of accretion events (e.g. Searle and others, 1987). However, the problem remains that the accretion of India to Eurasia is deemed more important than any of the other accretion events that occurred during the closure of Tethys.

Perhaps this fixation with the idea of "the collision" is related to the results of past plate-tectonic reconstructions. All published plate reconstructions of India's motion relative to Eurasia show a single slow-down event at 45 Ma (Molnar and Tapponier 1975) or 50-55 Ma (Patriat and Achache, 1984; Dewey and others, 1989; Molnar and Stock, 2009). This rapid deceleration in the velocity of the Indian plate is usually taken to indicate the time of "the collision" between India and Eurasia. However, the same reconstructions also suggest that India is thousands of kilometres south of Eurasia at 45 Ma or 50-55 Ma. This in turn led to the concept of Greater India, an extension of the northern margin of the Indian continent that is invoked to "fill the gap" between India and Eurasia (Ali and Aitchison, 2005).

However, any individual tectonic reconstruction is based on a sequence of linked assumptions through space and time, and it is usually the resultant (regional or planetary) configuration that receives the greater emphasis when a reconstruction effort is reported. Whereas such configurations lend themselves to comparative analyses, the underlying assumptions (e.g. starting configurations and subsequent process) that lead to the different results are not easily appreciated or analysed. Too often, an individual tectonic reconstruction is difficult to assess in respect of its underlying, linked assumptions. Additionally, a change in the assumptions used in one reconstruction can lead the same processes to a different result. For example, suppose a well-accepted reconstruction has been incorporated into several subsequent reconstruction efforts. Revision of this reconstruction (e.g. by incorporation of additional or revised data) would flow through to affect all dependent reconstructions. This would necessitate revision of the configurations and their comparisons, possibly resolving conflicting results. Currently, because of the under-exposure of the assumptions and interpretation paths, revising a reconstruction with new information is extremely difficult.

Using the Indian plate as an example, we revised a number of widely accepted reconstructions of India relative to Eurasia. In doing so, we also noted the lineage of data, decisions and assumptions of each of these reconstructions. We then plotted all of this information graphically with a mind-map, which we refer to as The Didactic Tree. The aim of The Didactic Tree is to "teach" the reader about the lineage of data, decisions and assumptions that are made in any reconstruction. The reader can then use or modify any part of the tree to produce a new reconstruction, and a future reader can easily do the same, and so on.

Using this approach we identified that all previous reconstructions of the Indian plate are based on out-of-date geological timescales, or old data/reconstructions of the African or North American plates (to close the plate circuit with Eurasia). We therefore used more up-to-date motion histories for India relative to Africa, Africa relative to North America and North America relative to Eurasia. We also utilized the capabilities of the Pplates deformable reconstruction software (http://rses.anu.edu.au/tectonics/projects/p-plates/) to simulate the opening of the East African Rift.

The results of our reconstruction suggest that the Indian plate experienced several accelerations and decelerations over the past 100 Ma. If we follow the same line of logic as past reconstructions, each observed slow-down event could be interpreted as marking a discrete accretion event. Interestingly, each of the observed changes in velocity correspond with known tectonic episodes along the length of the Alpine-Himalayan orogen (Lister and others, 2001), including the proposed ages for "the collision", with slow-downs at 66 Ma, 57 Ma, 52 Ma and 34 Ma. In addition to this, our results also suggest that the final slow-down of the Indian plate began at 27 Ma. At this time there was also a major vertical-axis rotation from NE to N. This was followed by a period of slow, steady-state motion for 6-7 Ma before the plate again rapidly accelerated and rotated back from N to NE at 20 Ma. The Indian plate finally began to slow in interspersed bursts between 0-18 Ma.

The fluctuations in velocity profile of the Indian plate's motion between 0-100 Ma fit well with the idea that orogenesis consists of several episodes of crustal shortening and extension (Lister and Forster, 2009). However, our results do not fit with the idea that Barrovian metamorphism in the Himalaya is the result 20-30 Ma of prograde heating in a shortening regime and a slow, progressive evolution of a pressure-temperature path.

Our results also suggest that the northern margin of India was several thousands of kilometres south of Eurasia between 45-55 Ma. The slowest velocity of the Indian plate that we observe in the past 100 million years occurs between 18-25 Ma. At 25 Ma, our reconstruction suggests that there is approximately 750-1250 km between India and Eurasia. Interestingly, this distance is similar to the ~950 km maximum possible extent of Greater India that was defined by Ali and Aitchison (2005). In light of these results, we suggest that all tectonic models of the Himalaya require revision.

References

Aitchison, J.C., Ali, J.R. and Davis, A.M., 2007, When and where did India and Asia collide?, Journal of Geophysical Research, 112, BO5423, doi:10.1029/2006JB004706.

Ali, J.R. and Aitchison, J.C., 2005, Greater India, Earth Science Reviews, 72, 169-188.

Dewey, J.F., Cande, S. and Pitman, W.C., 1989, Tectonic evolution of the India/Eurasia Collision Zone, Eclogae Geologicae Helvetiae, 82, 717-734.

Lister, G.S. and Forster, M.A., 2009, Tectonic mode switches and the nature of orogenesis, Lithos, 113, 274-291.

Lister, G.S. and Forster, M.A., Rawling, T.J., 2001, Episodicity during orogenesis, Geological Society, London, Special Publications, 184, 89-113.

Molnar, P. and Tapponnier, P., 1975, Tectonics of Asia: Effects of a Continental Collision, Science, 189, 419-426.

Molnar, P. and Stock, J.M., 2009, Slowing of India's convergence with Eurasia since 20 Ma and its implications for Tibetan mantle dynamics, Tetonics, 28, TC3001, doi:10.1029/2008TC002271.

Patriat, P. and Achache, J., 1984, India–Eurasia collision chronology has implications for crustal shortening and driving mechanism of plates, Nature, 311, 615-621.

Searle, M.P., and others, 1987, The closing of Tethys and the tectonics of the Himalaya, Geological Society of America Bulletin, 98, 678-701.

Yin, A. and Harrison, T.M., 2000, Geologic evolution of the Himalayan-Tibetan orogen, Annual Review of Earth and Planetary Sciences, 28, 211-280.

Cite as: White, L.T. and Lister, G.S., 2010, The Himalayan-pile up: revised plate reconstructions provide evidence of multiple accretion events during the Himalayan orogeny, *in* Leech, M.L., and others, eds., Proceedings for the 25th Himalaya-Karakoram-Tibet Workshop: U.S. Geological Survey, Open-File Report 2010-1099, 2 p. [http://pubs.usgs.gov/of/2010/1099/white/].

Apparent Temperature Gradient across the Lesser Himalayan Sequence: Raman Spectroscopy on Carbonaceous Material in the Eastern Bhutan Himalaya

Nicholas Whynot[1], Djordje Grujic[1], Sean Long[2], Nadine McQuarrie[2]

[1] Department of Earth Sciences, Dalhousie University, Halifa, NS B3H 4J1, Canada, dgrujic@dal.ca
[2] Department of Geosciences, Princeton University, Princeton, NJ, 08544, U.S.A.

One of the important features of the Himalayan tectonics is the inverted apparent metamorphic field gradient across the Lesser Himalayan Sequence (LHS) and the Greater Himalayan Sequence (GHS). Several conceptual models have been put forward since the recognition of this phenomenon, but field testing of numerical and analytical models is constrained by the ability to precisely determine the peak metamorphic temperature in the LHS. Raman spectroscopy on carbonaceous material (RSCM) provides a means of determining peak metamorphic temperatures in rocks lacking metamorphic assemblages permitting standard thermobarometry. Here we present RSCM data on 16 slates samples collected along a transect across the LHS of eastern Bhutan.

RSCM data yield peak temperatures ranging from ~340 °C at the bottom of the sequence to ~ 510 °C at the top of it. The Shumar thrust, which may be equivalent to the Ramgarh thrust in the central and western Himalaya, separates this apparent temperature gradient in two parts. In the footwall, characterised by dominantly Paleozoic rocks (McQuarrie and others, 2008), the temperatures are nearly constant at ~350 °C. In the hanging wall, which is composed of Paleoproterozoic rocks (McQuarrie and others, 2008), temperatures progressively rise from ~450 °C to ~510 °C from the base (Shumar thrust) to the top (Main Central thrust). In the footwall there is therefore no apparent temperature gradient over a structural distance of ~12 km, whereas in the hanging wall there is an inverted apparent temperature gradient of 7-11 °C/km over a structural distance of ~8 km. Across the Shumar thrust there is thus a temperature jump on the order of 50 or 100 °C depending on the interpretation of the temperature in the highest sample in the footwall. Furthermore, we observe a temperature jump on the order of 140 °C between the highest sample in the LHS to the GHS where the temperatures were determined by standard thermobarometry (Daniel and others, 2003).

Finally, our data are consistent with equivalent data reported in central and western Himalaya (Beyssac and others, 2004; Célérier and others, 2009). However, the estimated thermal gradients are significantly different. We note that there are significant jumps in temperature across the first-order structures, and, therefore, only data between them should be taken into account to construct apparent temperature gradients.

We conclude that temperature distribution in the LHS of eastern Bhutan is compatible with the predictions of geodynamic models of Himalaya applying concepts of channel flow hypothesis (Jamieson and others, 2004) modified by discrete faulting.

References

Beyssac, O., Bollinger, L., Avouac, J.-P. and Goffe, B., 2004, Thermal metamorphism in the lesser Himalaya of Nepal determined from Raman spectroscopy of carbonaceous material, Earth and Planetary Science Letters 225, 233-241.

Célérier, J., and others, 2009, The Kumaun and Garwhal Lesser Himalaya, India: Part 2. Thermal and deformation histories, Geol. Soc. Am. Bulletin, 121, 1281–1297.

Daniel, C. G., Hollister, L. S., Parrish, R. R. and Grujic, D. 2003, Extrusion of the Main Central Thrust Zone from Lower Crustal Depths, Eastern Bhutan Himalaya, Journal of Metamorphic Geology. 21, 317-334.

McQuarrie, N., and others, M. 2008, Preliminary stratigraphic and structural architecture of Bhutan: Implications for the along strike architecture of the Himalayan system, Earth and Planetary Science Letters, 272, 105-117.

Jamieson, R. A., Beaumont, C., Medvedev, S. and Nguyen, M. H., 2004, Crustal channel flows: 2. Numerical models with implications for metamorphism in the Himalayan-Tibetan orogen, Journal of Geophysical Research, 109, 1–24.

Cite as: Whynot, N., Grujic, D., Long, S. and McQuarrie, N., 2010, Apparent Temperature Gradient across the Lesser Himalayan Sequence: Raman Spectroscopy on Carbonaceous Material in the Eastern Bhutan Himalaya, *in* Leech, M.L., and others, eds., Proceedings for the 25th Himalaya-Karakoram-Tibet Workshop: U.S. Geological Survey, Open-File Report 2010-1099, 1 p. [http://pubs.usgs.gov/of/2010/1099/whynot/].

Metamorphic and Structural Discontinuities in the Greater Himalayan Sequence, Karnali Valley, West Nepal

Chris Yakymchuk[1], Laurent Godin[1]

[1]Department of Geological Sciences and Geological Engineering, Queen's University, Kingston, ON, Canada, K7L 3N6, yakymchuk@geoladm.geol.queensu.ca

Tectonometamorphic domains along the Himalayan front should ideally be separated by distinctive and diagnostic structural and metamorphic discontinuities that can be quantitatively tested along the strike of the orogen. Although previous workers have mapped the Greater Himalayan sequence (GHS) in structural contact above the Lesser Himalayan sequence (LHS) along the Main Central thrust (MCT) in the Karnali valley of northwestern Nepal (Murphy and Copeland, 2005; Robinson and others, 2006), the region lacks comprehensive metamorphic, microstructural, and geochronological data that are essential to differentiate between the two tectonometamorphic packages.

We present new results of detailed mapping, quartz petrofabric data, vorticity estimates, and thermobarometric estimates that document two discontinuities in strain and metamorphism within the previously defined GHS and LHS. The lower 'structural' discontinuity juxtaposes a pervasively sheared sequence of mid- to high-grade metamorphic rocks that exhibit top-to-the-south shear sense above low-strain rocks that preserve polydeformational features and primary sedimentary structures. The structurally higher 'metamorphic' discontinuity is characterized by up section changes from: (1) increasing to decreasing metamorphic pressures at peak metamorphic temperature, (2) preservation to destruction of prograde garnet zonation, and (3) a single metamorphic event associated with top-to-the-south directed deformation into polymetamorphic and polydeformational assemblages. These two discontinuities separate three tectonometamorphic domains, which correspond from low to high structural levels to: (1) the Lesser Himalayan sequence, (2) the lower Greater Himalayan sequence (GHS_L), and (3) the pervasively migmatitic upper Greater Himalayan sequence (GHS_U).

The structural discontinuity is defined based on the change up structural section from low-strain units into high-strain pervasively sheared units that exhibit top-to-the-south directed deformation observed from field observations, microstructural analysis, quartz petrofabrics, and vorticity analysis. Asymmetric quartz c-axis petrofabrics between the structural and metamorphic discontinuities indicate top-to-the-south directed deformation. The opening angles of quartz c-axis girdles (e.g. Law and others, 2004) constrain temperatures to 430°C at lower structural levels just above the structural discontinuity to >630°C immediately beneath the metamorphic discontinuity. Chessboard extinction within quartz from most specimens above the metamorphic break indicate deformation temperatures >630°C.

Vorticity estimates using the rigid clast method (e.g. Law and others, 2004) suggest nearly equal contributions of pure and simple shear in the GHS_L. The simple shear component of deformation reaches a maximum of ~65 % in the vicinity of the metamorphic break and decreases structurally downwards to a minimum of 40% at the lowest structural levels just above the LHS. The simple shear component also decreases structurally upwards to a minimum of 45% approximately 4 km structurally above the metamorphic break. Beneath the structural break, the preservation of sedimentary features and polyphase deformation indicate the rocks are not pervasively sheared.

The GHS_L contains garnet- through kyanite-grade rocks. Peak metamorphic assemblages are developed during south-directed deformation as evidenced by spiral and sigmoidal inclusion trails in garnet and staurolite. The GHS_U preserves a polymetamorphic history with peak metamorphic assemblages that exhibit complex timing relationships with south-directed deformation. Sillimanite-grade specimens collected above the metamorphic break commonly contain leucosome pods with relict kyanite blades, indicative of crystallization in the kyanite field. These same specimens contain strongly developed north-plunging lineations defined by fibrolitic sillimanite that, in conjunction with sigma porphyroblasts, C-C'-S fabrics, and mica fish, suggest south-directed transport in the sillimanite stability field.

In the GHS_U, sillimanite-grade migmatitic paragneisses and orthogneisses preserve peak metamorphic temperatures of 650-720°C at 5-10 kbar (THERMOCALC, v. 3.30). Peak metamorphic temperatures remain constant and pressures at peak temperatures decrease gradually up structural section from 10 kbar to 5 kbar. In the GHS_L garnet- to kyanite-grade meta-pelitic schists record peak metamorphism temperatures of 570-640°C at 7.5-10.0 kbar. Peak metamorphic temperatures systematically increase up structural section coincident with an inverse Barrovian field gradient, ranging from biotite- through kyanite-grade. Calculated pressures at peak temperatures gradually increase up section from 6 kbar in the structurally lowest garnet zone, reaching a maximum of 10 kbar at the top of the GHS_L, which roughly coincides with the kyanite-in isograd. Peak metamorphic temperatures in the GHS_L overlap with deformation temperatures obtained from quartz c-axis opening angles and the operating temperatures of the observed dynamic recrystallization mechanisms of quartz and feldspar.

The integration of metamorphic and microstructural data indicate three distinct tectonometamorphic domains, from low to high structural levels: (1) a low-grade weakly strained unit (LHS), (2) a pervasively sheared mid-to-high grade package with top-to-the-south directed deformation and peak-metamorphic temperatures coinciding with calculated deformation temperatures (GHS_L), and (3) a pervasively sheared high-grade migmatitic unit with a polymetamorphic history (GHS_U). Observations from the GHS_U are consistent with the model of the southward ductile extrusion of the GHS from mid-crustal depths that is defined by early high-P (kyanite-bearing) assemblages overprinted by syn-deformational high-T and mid-P (sillimanite-bearing) assemblages. Structural and metamorphic data from the GHS_L are consistent with that from central Nepal (Larson and others, 2010). The GHS_L is interpreted to represent either a series of ductilely-deformed and accreted slices beneath a southward extruding channel, or alternatively, the incorporation of material into the channel as its lower boundary migrated structurally downwards with time. This regime is manifested metamorphically by peak assemblages temporally coinciding with simultaneous crustal thickening and south-directed deformation within the MCT zone. Below the structural discontinuity, primary structures and greenschist-facies metamorphism are preserved, along with an absence of pervasive shearing, consistent with the LHS below the MCT as defined by Searle and others (2008).

Microstructural and metamorphic data from this study present a temporal ‘snapshot’ of the complex interplay between deformation and metamorphism at the transition zone between the LHS and GHS and strongly negates the premise that a single discrete thrust fault separates the two in the Karnali valley of western Nepal. The characterization of three tectonometamorphic units separated by two discontinuities in strain and metamorphism in west Nepal indicates the need to reassess the LHG-GHS transition in regions where they are mapped as separated by a single discrete fault.

References

Larson, K.P., Godin, L. and Price, R.A., 2010, Relationships between displacement and distortion in orogens: Linking the Himalayan foreland and hinterland in central Nepal, Geol. Soc. Am. Bulletin, in press.

Law, R.D., Searle, M.P. and Simpson, R.L., 2004, Strain, deformation temperatures and vorticity of flow at the top of the Greater Himalayan Slab, Everest Massif, Tibet, Journal of the Geological Society of London, 161, 305-320.

Murphy, M. and Copeland, P., 2005, Transtensional deformation in the central Himalaya and its role in accommodating growth of the Himalayan orogen, Tectonics, 24, TC4012, doi:10.1029/2004TC001659.

Robinson, D.M., DeCelles, P.G. and Copeland, P., 2006, Tectonic evolution of the Himalayan thrust belt in western Nepal: Implications for channel flow models, Geol. Soc. Am. Bulletin, 118, 865-885.

Searle, M.P., and others, 2008, Defining the Himalayan Main Central Thrust in Nepal, Journal of the Geological Society of London, 165, 523-534.

Cite as: Yakymchuk, C. and Godin, L., 2010, Metamorphic and structural discontinuities in the Greater Himalayan sequence, Karnali valley, west Nepal, *in* Leech, M.L., and others, eds., Proceedings for the 25th Himalaya-Karakoram-Tibet Workshop: U.S. Geological Survey, Open-File Report 2010-1099, 2 p. [http://pubs.usgs.gov/of/2010/1099/yakymchuk/].

Rayleigh-Wave Phase Velocities and Azimuthal Anisotropy in Tibet and Surrounding Regions from Ambient Noise Tomography

Yingjie Yang[1,2], Yong Zheng[2], Michael H. Ritzwoller[1]

[1]Department of Physics, University of Colorado at Boulder, Boulder, CO 80309-0390, yingjieyang@gmail.com
[2]Institute of Geodesy and Geophysics, Chinese Academy of Sciences, Wuhan, Hubei, 430077, China

Tibet is our planet's natural laboratory for studying how continents interact and deform in response to the collision between the Indian and the Eurasian plates. Although numerous seismic studies of Tibet have been performed, there remain fundamental disagreements in first-order questions about crustal deformation; e.g., whether the crust deforms coherently vertically or is perhaps coupled to the mantle. The reason is that existing models either do not model the crust effectively or only model the crust beneath parts of Tibet due to limitations in the distribution of seismic stations.

In this study, we have applied ambient noise tomography, which provides new and pervasive constraints on crustal structure, to the significant data resources now available across all of Tibet and the surrounding regions. These resources include data from the permanent Federation of Digital Seismographic Networks (FDSN), several temporary US PASSCAL installations in and around Tibet, and the Chinese provincial networks surrounding Tibet. These networks comprise ~600 stations on which ambient noise cross-correlations are performed from 2003 to 2009. Inter-station Rayleigh wave dispersion curves are measured from cross correlations of vertical components. These dispersion measurements are used to invert for isotropic phase velocity maps and azimuthal anisotropy of Rayleigh waves. Phase velocity maps display features that correlate well with surface geology. Major basins, including Tarim, Qaidam and Sichuan, are all well delineated by slow phase velocities at short periods (8-15 sec). Crustal thinning from Tibet to the surrounding regions is manifest as a phase velocity increase at periods from 25 to 40 sec. Patterns of Rayleigh wave azimuthal anisotropy at periods from 10 to 30 sec differ only at small scales, meaning either that anisotropy in the shallow crust dominates both maps or that the mechanism of anisotropy extends from the shallow to the middle crust. In much of eastern Tibet, the fast directions of Rayleigh waves are similar to the strikes of left lateral planes of shear constrained from Quaternary fault slip rates and GPS measurements, consistent with the position that the azimuthal anisotropy from surface waves manifests upper-crustal shear. The fast directions of surface waves bifurcate around the Sichuan Basin, which may suggest a relation between anisotropy and crustal flow that has been proposed to explain the growth of the Tibetan Plateau and the variation of topography in eastern Tibet.

Cite as: Yang, Y., Zheng, Y. and Ritzwoller, M.H., 2010, Rayleigh-Wave Phase Velocities and Azimuthal Anisotropy in Tibet and Surrounding Regions from Ambient Noise Tomography, *in* Leech, M.L., and others, eds., Proceedings for the 25th Himalaya-Karakoram-Tibet Workshop: U.S. Geological Survey, Open-File Report 2010-1099, 1 p. [http://pubs.usgs.gov/of/2010/1099/yang/].

The Structure and Evolution of the Bangong-Nujiang Suture (Gaize, Central Tibet)

Yuxiu Zhang[1,2], Kaijun Zhang[2]

[1] School of Earth Sciences and Resources, China University of Geosciences, Beijing 100083, China, yushuzh@gmail.com
[2] Research for Tibetan Plateau Geology, China University of Geosciences, Beijing 100083, P.R. China
[3]Guangzhou Institute of Geochemistry, Key Laboratory of Geology of Marginal Sea, Chinese Academy of Sciences, Wushan, Guangzhou 510640, China

Systematic mapping of the Gaize area across the Bangong-Nujiang suture and the Lhasa and Qiangtang blocks was conducted, during which ophiolite overthrust sheets in both the northern Lhasa and southern Qiantang blocks were documented, and Late Jurassic rocks with magmatic-arc affinity and rocks with oceanic-plateau affinity were discovered in the northern Lhasa and southern Qiantang margins, and in the suture zone itself, respectively. This indicates that (Early Permian) mantle plume upwelling could have played a key role in the initiation of the Bangong-Nujiang mid-Tethys. Geochronological dating shows that these ophiolite sheets could have been transported bilaterally, both northward and southward, nearly simultaneously in the Late Jurassic (151-153 Ma). The obduction could have been driven by external forces, perhaps by shallow oceanic subduction of the Yarlung-Zangpo neo-Tethys. There is no definite evidence for Mid-Cretaceous shortening in central Tibet. In contrast, extensive distribution of Lower-Middle Cretaceous marine strata in central Tibet (including the Qiangtang terrain), along with the folded Mid-Cretaceous normal fault bounding the Qiangtang terrain and the Bagong suture zone, indicates there could be an extensive Mid-Cretaceous (back-arc) rifting event in central Tibet.

This research is supported by the Postdoctoral Science Foundation of China (20080430458, 200801100) and National Natural Science Foundation of China (40802048 and 4091014050).

Cite as: Zhang, Y. and Zhang, K., 2010, The structure and evolution of the Bangong-Nujiang Suture (Gaize, Central Tibet), *in* Leech, M.L., and others, eds., Proceedings for the 25th Himalaya-Karakoram-Tibet Workshop: U.S. Geological Survey, Open-File Report 2010-1099, 1 p., [http://pubs.usgs.gov/of/2010/1099/yuxiuzhang/].

Not Very Old but Not Too Young: Thermochronological Constraints on the Age of Low-Relief Surfaces in the Western Himalaya and Southeastern Tibet

Peter K. Zeitler[1]

[1] Department of Earth and Environmental Sciences, Lehigh University, Bethlehem, PA 18015, U.S.A., peter.zeitler@lehigh.edu

Low-relief high-elevation surfaces occur near the dissected fringes of the easternmost and westernmost Himalaya and Tibetan Plateau, and have been interpreted as remnants of an early and more extensive surface as old as Eocene. Alternatively, the Gamugah surface in the western Himalaya has also been interpreted as evidence for the glacial buzzsaw mechanism for trimming elevations. Cooling-age data from the Gamugah surface in northern Pakistan and from the high surface located west of Nyinchi in SE Tibet suggest that neither explanation is satisfactory for these two landscapes.

Samples from both surfaces have very similar low-temperature cooling histories marked by fairly rapid cooling to near-surface temperatures in the interval ~15 to 8 Ma, as constrained by U-Th/He dating of apatite and zircon and $^{40}Ar/^{39}Ar$ dating of k-feldspar and biotite. Assuming an orogenic thermal gradient of about 30˚C/km, higher-elevation samples at both localities were within one kilometer of the surface (or much shallower) by 7 Ma. On the one hand, this observation rules out these two surfaces as being old remnants (Eocene or older). On the other hand, particularly for the Gamugah surface, the data also do not support the notion of energetic cryogenically-driven erosion operative in the Quaternary. What is required is a mechanism to drive several kilometers of rock removal in the period 15 to 8 Ma.

Together with field relationships, the cooling ages also provide interesting constraints on the morphological evolution of the Indus and Tsang Po valleys in the hinterland. Both data sets are complicated by lateral heat flow from the rapidly advecting Nanga Parbat and Namche Barwa massifs, such that low-elevation ages close to the massifs are considerably younger due to the local steepening of the thermal gradient. For the Tsangpo, the best qualitative explanation for the data is that immediately following carving of topography that was close to the current relief, further relief development was arrested by pinning of the Tsang Po's local base level by initiation of extremely fast rock uplift within the Namche Barwa massif (the spatial magnitude of the lateral heat-flow anomaly is consistent with a duration of this uplift of at least several million years). This suggests that the current southeast Tibetan landscape may be on the order of 5-7 Ma in age, with very little incision occurring on the main river channels.

In the western Himalaya near Nanga Parbat, pending verification by additional thermal modeling, the cooling data and field relationships suggest that considerable relief must have been present in the Indus Valley at 7 to 9 Ma. Samples from atop the Gamugah surface fell below temperatures of 40˚C by 7 Ma. Given that samples located fully 3 km below these closed to helium diffusion at about the same time, relief of some 2 km must have been present, sufficient to warp isotherms and thus allow coeval cooling at widely spaced elevations. This implies that a proto-Indus River valley was present at that time. However, lateral heat flow can only explain the young ages obtained from a vertical transect adjacent to the massif if bedrock were available to transmit the lateral heat flow, suggesting removal of an additional 1-2 km of rock from the Indus Valley took place by about 4 Ma, but after initiation of the Nanga Parbat uplift. These data also suggest that incision of the middle Indus Valley between Nanga Parbat and the Gamugah surface has been relatively minor over the past few million years.

Cite as: Zeitler, P.K., 2010, Not very old but not too young: thermochronological constraints on the age of low-relief surfaces in the western Himalaya and southeastern Tibet, *in* Leech, M.L., and others, eds., Proceedings for the 25th Himalaya-Karakoram-Tibet Workshop: U.S. Geological Survey, Open-File Report 2010-1099, 1 p. [http://pubs.usgs.gov/of/2010/1099/zeitler/].

Late Eocene crustal thickening followed by Early-Late Oligocene Extension along the India-Asia suture zone: Evidence for cyclicity in the Himalayan orogen

Ran Zhang[1], Michael A. Murphy[1], Thomas J. Lapen[1], Veronica Sanchez[1], Matthew Heizler[2]

[1]Department of Earth and Atmospheric Sciences, University of Houston, Houston, TX 77204, U.S.A., mmurphy@mail.uh.edu
[2]New Mexico Geochronology Research Laboratory, New Mexico Institute of Mining and Technology, Socorro, NM 87801, U.S.A.

The timing of geologic events along the India-Asia suture zone remains poorly understood because exposures of structurally deep rocks are rare due to low amounts of denudation across much of the Himalayan orogen. In this study, we present geologic mapping across the India-Asia suture zone in southwestern Tibet of two structurally deep domes that are cored by mylonitic orthogneisses. This field study is complemented by U-Pb zircon geochronology from the orthogneisses as well as mylonitic leucocratic granite sills that intrude it. Our results indicate that the protolith of these orthogneisses are Gangdese arc rocks and that they experienced Late Eocene prograde metamorphism that we attribute to crustal thickening (Figure 1). Leucocratic granite sills have undergone top-to-southeast extension related to slip along a brittle-ductile shear zone referred to as the Ayi shan detachment. U-Pb zircon ages from synextensional granite bodies bracket the timing of extension between Early and Late Oligocene (Figure 1). A widespread siliciclastic unit, which is correlated to the Kailas Formation, lies in depositional contact across the Ayi shan detachment. A $^{40}Ar/^{39}Ar$ muscovite age from a rhyolitic dike cutting the Kailas Formation is 18.10 ± 0.05 Ma, thereby placing an upper age limit on slip along the Ayi shan detachment. The Kailas Formation is cut by the north-directed Great Counter thrust which defines the surface trace of the India-Asia suture zone. The Great Counter thrust, in turn is cut by the Karakoram fault which facilitates transtensional deformation. A $^{40}Ar/^{39}Ar$ muscovite age of 10.17 ± 0.04 Ma of a granite along its southside (footwall) is consistent with previously published thermochronologic data which suggest transtensional deformation along the Karakoram fault in southwest Tibet was active in the Late Miocene.

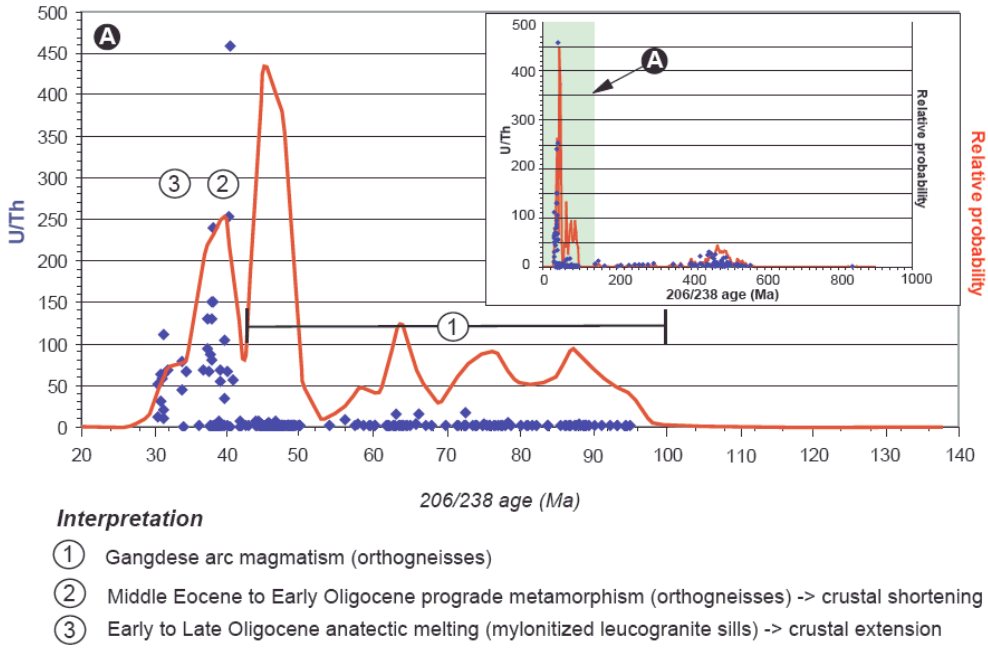

Figure 1. Plot of $^{206}Pb/^{238}U$ zircon ages versus U/Th values and their relative probability.

These results indicate two cycles of shortening and extension archived in the rocks along the India-Asia suture zone in southwest Tibet (Figure 2). The first cycle of shortening and extension, from Late Eocene to Late Oligocene, is recorded in Gangdese arc rocks. Previous results show that deformation of Gangdese arc rocks did not commence until the Late Oligocene, some 25 Ma after the initial collision between India and Asia. Structural interpretations of suture zone rocks that have undergone these two cycles of shortening and extension predict a complex structural configuration at depth, characterized by northward translation of the upper-crustal suture zone with respect to its position in the middle and lower crust.

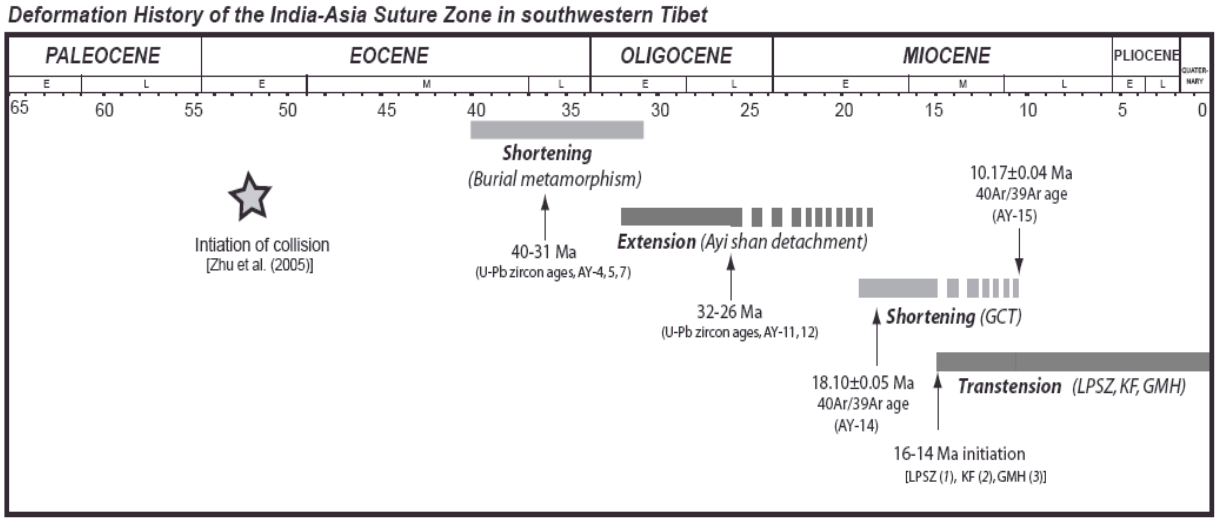

Figure 2. Table showing the history of geologic events along the IYS in southwest Tibet based on our geologic mapping and geochronologic studies of rocks exposed in the Ayi shan. Abbreviations: GCT-Great Counter thrust, LPSZ – Leo Pargil shear zone, GMH – Gurla Mandhata-Humla fault, KF – Karakoram fault. (1) Theide and others (2006, (2) Arnaud (1992), (3) Murphy and Copeland (2005).

References

Arnaud, N.O., 1992, Apports de la thermochronologie 40Ar/39Ar sur feldspath potassique a la connaisance de la tectoniique Cenozoique d'Asia: Ph.D. Dissertation: Universite Blaise Pascal; France, 160 p.

Murphy, M. A. and Copeland, P., 2005, Transtensional deformation in the central Himalaya and its role in accommodating growth of the Himalayan orogen, Tectonics, 24, doi: 10.1029/2004TC001659.

Thiede, R., and others, 2006, Dome formation and extension in the Tethyan Himalaya, Leo Pargil, northwest India, Geol. Soc. Am. Bull., 118, 635-650.

Cite as: Zhang, R., Murphy, M.A., Lapen, T.J., Sanchez, V. and Heizler, M., 2010, Late Eocene crustal thickening followed by Early-Late Oligocene Extension along the India-Asia suture zone: Evidence for cyclicity in the Himalayan orogen, *in* Leech, M.L., and others, eds., Proceedings for the 25th Himalaya-Karakoram-Tibet Workshop: U.S. Geological Survey, Open-File Report 2010-1099, 2 p. [http://pubs.usgs.gov/of/2010/1099/zhangmurphy/].

The Uplift of Mountain Chains along the Northern and Eastern Margins of the Tibetan Plateau

Peizhen Zhang[1]

[1] State Key Laboratory of Earthquake Dynamics, Institute of Geology, China Earthquake Administration, Beijing 100029, China, peizhen@ies.ac.cn

The first-order feature of the Tibetan Plateau is its relative flat interior and rugged margins. Mountain chains with elevation higher than the plateau interior constitute the plateau margins, including the Himalaya along its southern margin, the Karakorum along its western margin, the Altyn Tagh and Qilian Shan along its northern margin, and the Longmen Shan and Hengduan Shan along its eastern margin. Their rugged geomorphology and intense active tectonics show that these mountain chains have been actively deforming in late Cenozoic time, and are manifestations of the upward and outward growth of the Tibetan Plateau. Given their size and elevation, these mountain chains are important in environmental change and natural hazard occurrence in continental Asia.

Formation of high mountains is always associated with active deformation. The growth of the Altyn Tagh mountains is controlled by the Altyn Tagh fault, dominated by left-lateral strike-slip with a minor component of crustal shortening. Active tectonics in the Qilian Shan are characterized by partitioning of oblique convergence into left-lateral strike-slip faulting along the range-crest (the Haiyuan fault) and crustal shortening across the entire range especially along both its range-fronts. Shortening near the ends of major strike-slip faults also contributes to uplift in parts of the ranges in the northern margin of the Tibetan Plateau. The strike-slip faults in the northern margin of the plateau redistribute crustal thickness, accommodate regional oblique convergence, and reconcile inhomogeneous deformation. The Longmen Shan fault zone is predominantly a convergent boundary with a right-lateral strike-slip component. The co-seismic high-angle oblique reverse faulting and the uplift associated with the 2008 Wenchuan earthquake serve as a "snap-shot" of the style of late Cenozoic deformation of the Longmen Shan in the eastern margin of the Tibetan Plateau, and explain the presence of steep relief (>4000 m) with no coeval foreland subsidence. Formation of the north-south trending mountain ranges in Yun'nan Province (Hengduan Shan, or Longitudinal mountains) may be controlled by active north-south trending strike-slip faults. Outward flow of Tibet's crustal material and clockwise rotation around the Eastern Himalaya syntaxis may have caused north-south trending, left-lateral strike-slip motion in the Hengduan Shan region. The styles of late Cenozoic deformation in these mountain chains represent patterns of outward growth of the Tibetan Plateau and provide information on the geodynamics of continental deformation.

Although the onset of Cenozoic deformation in these mountain chains can be traced back to immediately after the collision between India and Eurasia, the late Cenozoic (14-6 Ma) appears to be the major period when uplift accelerated so that these mountains attained their current elevations to become significant geomorphic features. The initiation of mountain building differs from one mountain to another within this time period. Onset of uplift of the Altyn Tagh appears to be at 7-10 Ma. In the Qilian Shan and Qingling region, the exhumation started from 14 Ma to 6 Ma, and seems to propagate northeastward. Rapid exhumation in the Longmen Shan is reported to be from 5-12 Ma. Dating of rapid incisions of major rivers in the Hengduan Shan suggests major exhumation from 9-13 Ma. Thus, the northern and eastern margins of Tibetan Plateau appear to have grown outward and upward from 14-6 Ma.

The outward growth of the plateau, acceleration of tectonic deformation, and formation of mountain chains along the margins of Tibetan Plateau requires a change in the geodynamic framework that drives tectonic deformation of Asia. How this change is caused is not yet understood, but may relate to a slowing of relative motion between India and Eurasia, convective removal of Tibet's mantle lithosphere, and lower-crustal flow outward from the plateau interior. The change in driving forces may have triggered outward flow of the lower-crustal material of the Tibetan Plateau northward and eastward, that in turn caused outward growth and formation of mountain chains in the northern and eastern margins of the Tibetan Plateau.

Cite as: Zhang, P.-Z., 2010, The rising of mountain chains along the northern and eastern margins of the Tibetan Plateau, *in* Leech, M.L., and others, eds., Proceedings for the 25th Himalaya-Karakoram-Tibet Workshop: U.S. Geological Survey, Open-File Report 2010-1099, 1 p. [http://pubs.usgs.gov/of/2010/1099/pzzhang/].

Crustal Structure across the Qilian Orogenic Belt from In-line and Off-line Wide-angle Seismic Profiling in the North-eastern margin of Tibetan plateau

Zhongjie Zhang[1], Xiaobo Tian[1], Zhiming Bai[1], Xi Zhang[1], Bing Zhao[1], Jianli Zhang[1], Shaokun Shi[1], Tao Xu[1], Yun Chen[1], Jiwen Teng[1]

[1]State Key Laboratory of Lithospheric Evolution, Institute of Geology and Geophysics, Chinese Academy of Sciences, Beijing, China, zhangzj@mail.iggcas.ac.cn

The Qilian orogenic belt, located at the north-eastern edge of the Tibet, is a Caledonian orogenic belt reactivated by collision between India and Asia. GPS measurements indicate the Tibetan plateau is expanding to the northeast, and the Qilian tectonic block is an important place to understand this north-eastward expansion. In order to reconstruct crustal structure beneath the Qilian Shan tectonic block and to provide constraints on the Caledonian orogenic structure and lateral (N-E) expansion of the plateau, we carried out a wide-angle seismic experiment in 2008 and 2009 along a 430-km-long inline profile across the Qilian orogenic belt and along a 300-km-long cross-line profile, with support of SinoProbe-02-02. We present a crustal P-wave velocity structure model along the in-line wide-angle seismic profile, and find crustal thickness thins from about 52 km under the southwest end of the profile to about 49 km at the northeast end of the profile, which is consistent with the results from previous wide-angle seismic profiling by Liu and others (2006) and Zhang and others (2008). Notable features of the crustal velocity model include: (1) the Kunlun (or the western Qingling block) and the Qaidam block are clearly distinguished, with the northern margin fault of the western Qingling Mountains as the boundary between them; the crust of these two tectonic blocks is thickened both in the upper and lower crust, and their crusts can be divided into upper and lower crust with thickness about 27 km and 22-26 km, respectively; (2) P-wave velocity is very low for the whole crust, especially in the lower crust (6.3-6.6 km/s) beneath the Qilian terrain; (3) there is one lower-velocity layer (about 5.7 km/s) with thickness of 7-8 km in the upper crust beneath the south segment of the profile, and a 6.2-6.3 km/s higher-velocity layer with thickness of about 5 km in the upper crust beneath the north segment of the profile; (3) the Southern Qilian fault that bounds the early Paleozoic North Qaidam UHP metamorphic belt is of crustal scale, implying continental collision of the Qaidam block with the Qilian terrane that seems inconsistent with the paired subduction model of Yang and others (2002), but may support a transition from oceanic subduction (along the Northern Qilian fault) to continental collision (along the Southern Qilian fault belt) as suggested by Song and others(2006); (4) a lower-velocity zone in the depth range 25-30 km beneath the Qilian terrain is inferred to be a zone of partial melt that may be related to the thermomechanical evolution of UHP metamorphic rocks or diapiric flow of subducted continental crust (Yin and others, 2007). Analysis of individual seismic shots suggests that strong seismic reflections from the lower crust are weak or absent on in-line shot gathers, suggesting a transparent lower crust beneath the Qilian tectonic block, but in contrast well-developed reflections are seen on the off-line shot gathers. This discrepancy in the appearance of crustal reflections between NE-SW and NW-SE azimuths, and the very low crustal velocity, may suggest northeastern Tibet grows predominantly in the NW-SE direction, which matches with surface GPS measurements.

References

Liu, M.J., Mooney, W.D., Li, S.L., Okaya, N. and Detweiler, S., 2006, Crustal Structure of the Northeastern Margin of the Tibetan Plateau from the Songpan - Ganzi Terrane to the Ordos basin, Tectonophysics, 420, 253-266.

Song, S.G., and others , 2006, Evolution from oceanic subduction to continental collision: A case study from the northern Tibetan plateau based on geochemical and geochronological data, J. Petrol., 47, 435-455.

Yang, J.S., and others, 2002, Early Paleozoic North Qaidam UHP metamorphic belt on the north-eastern Tibetan plateau and a paired subduction model, Terra Nova, 14, 397-404.

Yin, A., and others 2007, Early Paleozoic Tectonic and Thermomechanical evolution of Ultrahigh-Pressure (UHP) metamorphic rocks in the Northern Tibetan Plateau, Northwest China, International Geology Review, 49, 681-716.

Zhang, X.K., and others, 2008, Crustal structures beneath West Qinling -East Kunlun orogen and its adjacent area –Results of wide-angle seismic reflection and refraction experiment, Chinese J. Geophys. (in Chinese), 51, 439-450.

Cite as: Zhang, Z., and others, 2010, Crustal Structure across the Qilian Orogenic Belt from In-line and Off-line Wide-angle Seismic Profiling in the North-eastern margin of Tibetan plateau, *in* Leech, M.L., and others, eds., Proceedings for the 25th Himalaya-Karakoram-Tibet Workshop: U.S. Geological Survey, Open-File Report 2010-1099, 1 p. [http://pubs.usgs.gov/of/2010/1099/zzhang/].

New Paleomagnetic Result on Tertiary Sediments From NW Qiangtang: Implications for the Cenozoic Tectonic History of the Tibetan Plateau

Xixi Zhao[1], David Finn[1], Chengshan Wang[2], Yalin Li[2], Lidong Zhu[3], Wenguang Yang[3], Jun Meng[2], Jingen Dai[2]

[1]Department of Earth Sciences and the Institute of Geophysics and Planetary Physics, 1156 High Street, University of California, Santa Cruz, CA 95064, USA, xzhao@ ucsc.edu
[2]China University of Geosciences, Xueyuan Lu 29, Beijing 100083, China
[3]Chengdu University of Technology, Chengdu 610059, P.R. China

The Qiangtang terrane of Tibet is a critical region for tectonic reconstruction of Asia. Here, we present new paleomagnetic results obtained from Tertiary sedimentary sessions of the Dead Yak Valley (located at ~36°N and ~88°E and named by ourselves in the field as we counted more than 100 dead yaks in the valley) of the northwestern Qiangtang terrane. The rocks are mainly red sedimentary rocks including siltstone, mudstone, sandstone, and conglomerate, offering opportunity of applying paleomagnetic fold and conglomerate tests to check the stability of the remanent magnetization. A total of 248 individual oriented paleomagnetic samples were collected from 60 measured stratigraphic levels. The samples were subjected to progressive thermal (mainly) and alternating field (AF) demagnetization. Progressive thermal demagnetization to 700°C revealed a high unblocking temperature component was isolated between 625 and 700°C in almost all sandstone samples. The high temperature component has both normal and reversed polarities and is interpreted as the characteristic remanent magnetization (ChRM) on the basis of linear trajectories of demagnetization towards the origin and a similar direction from sample to sample. The fold test results are positive at 95% confidence level. The paleomagnetic data clearly show that the Dead Yak Valley area (and by inference the northwestern Qiangtang terrane) occupied its current paleolatitude at the time when the redbeds were formed and imply a significant northward convergence of the Dead Yak Valley with respect to Eurasia (Siberia). Future work is needed to ascertain the influences of sedimentary inclination shallowing and tectonic shortening. Comparing these data from sections in the Dead Yak Valley to previously studied sections in the Fenghuo Shan region allows us to better define the western extent of the Hoh Xil basin and suggest that the Hoh Xil basin was a typical foreland basin in the Tertiary.

Cite as: Zhao, X., and others, 2010, New Paleomagnetic Result on Tertiary Sediments From NW Qiangtang: Implications for the Cenozoic Tectonic History of the Tibetan Plateau, *in* Leech, M.L., and others, eds., Proceedings for the 25th Himalaya-Karakoram-Tibet Workshop: U.S. Geological Survey, Open-File Report 2010-1099, 1 p. [http://pubs.usgs.gov/of/2010/1099/xxzhao/].

Post-Collisional Leucite Alnoite in South Tibet and its Significance

S. Zhou[1], X.X. Mo[1], Z.D. Zhao[1], Y.L. Niu[2], G.G. Xie, L. Qiu[3], K. Sun[1]

[1] China University of Geosciences, Beijing, 100083, China, zhousu@cugb.edu.cn
[2] Department of Earth Sciences, Durham University, Durham DH1 3LE, UK
[3] Hubei Land Resources Vocational College, Jingzou, China

Geological background

We report a preliminary study of newly recognized leucite alnoite dykes in the Lhasa Terrane in southern Tibet. The Lhasa terrane is the southernmost terrane of the Tibetan Plateau amalgamation immediately north of the India-Asia suture. Zhao and others (2009) have recently conducted a rather comprehensive petrological and geochemical study of the post-collisional ultrapotassic rocks throughout the Lhasa Terrane. The location (N 29°55'12", E 86°41'20") of our leucite alnoite samples is close to an outcrop of ultrapotassic rocks within the Dangreyougcuo-Xurucuo graben, one of the N-S-trending grabens.

Petrography and geochemistry

The specimens are dense and massive with yellowish-greenish ochreous colour and porphyritic texture. The phenocrysts include leucite, biotite, melilite and pyroxene with a microlitic matrix of the same mineralogy. Leucite is the major phenocryst and varies in size (~ 0.05 to 0.1mm) with apparent alteration and unidentified mineral inclusions. Small amounts of biotite occur as thin plates (up to 0.2 by 1 mm in size), mellilite appears as prisms (up to 0.02 by 0.3mm), and minor pyroxene (up to 0.02 by 0.3mm) as euhedral crystals.

The leucite alnoite is characterized by low SiO_2 (~52.86%) and high K_2O (~4.70%), P_2O_5 (~1.25%), MnO (~0.14%), CaO (~5.36%), and LiO (~6.22%), whereas TiO_2 (~1.56%), Al_2O_3 (~13.23%), Na_2O (~2.09%), MgO (~4.36%) and total Fe_2O_3 (~7.95%) are similar to high-K latites in the area (Zhao and others, 2009). The ultrapotassic nature of the leucite alnoite dykes are also manifested by high K_2O/Na_2O and $K_2O/A1_2O_3$ ratios as well illustrated in (Figures 1 and 2).

The samples are highly enriched in incompatible elements, e.g. very high Ba (3332 ppm), Rb (409 ppm), Sr (862 ppm), Th (233 ppm) and Zr (742 ppm) with high La_N/Yb_N (24.41), similar to the ultrapotassic volcanic rocks nearby. In comparison, leucite alnoite documents the weakest Eu anomaly (Eu/Eu^*=0.94).

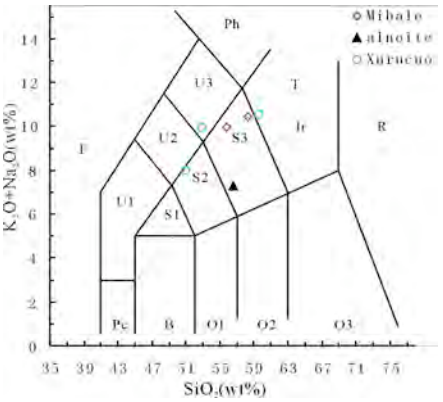

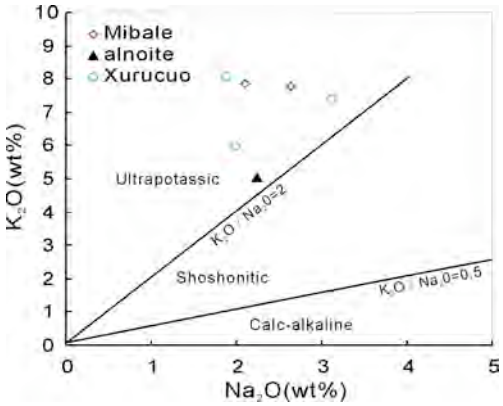

Figure 2. K2) vs. Na2O plots. Date for Mibale and Xurucuo are from Zhao and others (2009).

Figure 1 (above). K_2O+Na_2O vs. SiO_2 plot. Classification boundaries are from Le Bas and others (1986) and Le Maitre and others (1989). Mibale and Xurucuo are representative of adjacent post-collisional ultrapotassic rocks (Zhao and others, 2009). All data plotted have been recalculated to 100 wt.% on a volatile-free basis. Symbols are: Pc picrobasalt; B basalt; O1 basaltic andesite; O2 andesite; O3 dacite; R rhyolite; S1 trachybasalt; S2 basaltic trachyandesite; S3 trachy-andesite; T trachyte; U1 tephrite/basanite; U2 phono-tephrite; U3 tephri-phonolite; Ph phonolite; F foidite.

$^{40}Ar/^{39}Ar$ analysis and results

Incremental step-heating $^{40}Ar/^{39}Ar$ analysis of biotite separates was performed at the Geochronology Laboratory at China University of Geosciences (Beijing) using Macromass 5400 static vacuum mass spectrometry. The fluence monitor, ZBH-25, was an interlaboratory standard biotite with an age of 133.2 Ma and is typically used in Chinese argon-dating laboratories, calibrated by international standards (Standard analyses methods for isotopic samples, 1997). Twelve heating-increments were applied and the apparent age spectrums and isotope correlation (isochron) diagrams for $^{40}Ar/^{36}Ar$ versus $^{39}Ar/^{36}Ar$ are drawn through the results for plateau gas fractions (Figure 3). Both are calculated and displayed with 1σ uncertainties using the ISOPLOT software version 2.31 (Ludwig, 1993). Biotite separates yield $^{40}Ar/^{39}Ar$ released age spectra and isochron ages of 11.78±0.10 Ma. The plateau ages are essentially identical to the isochron ages with the intercept of the isochron giving an initial $^{40}Ar/^{36}Ar$ ratio not significantly different from 295.5, suggesting that the data are credible (Figure 3).

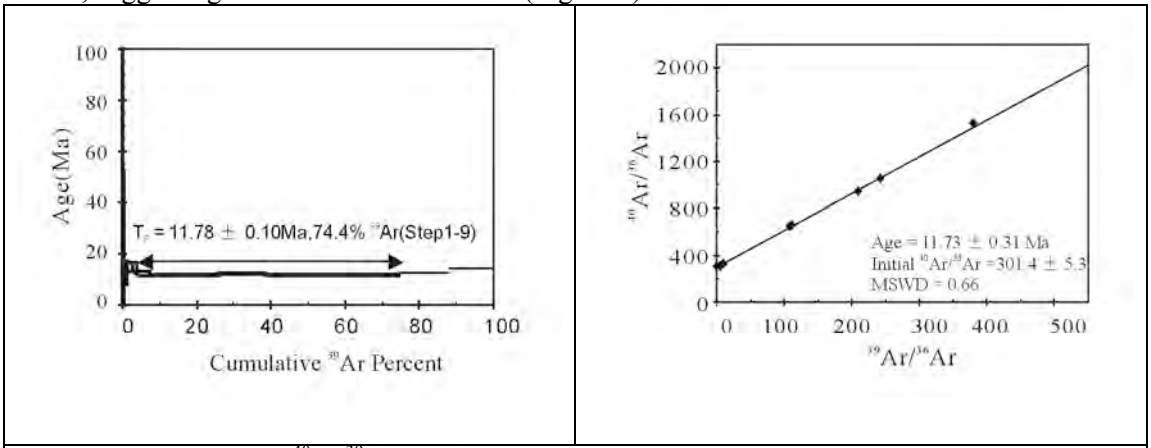

Fig 3. $^{40}Ar/^{39}Ar$ age spectra and an isochron plot of leucite alnoite

Significance

Lamprophyres occur widely on all of the continents in the form of dykes in extensional tectonic settings (Rock, 1987). Except for our study, a recent 1:250,000-scale regional geological survey has reported some N- or NW-trending minette dykes around the area, with a supposed Neogene formation age (XZBGMR, 2002). The radiometric dating of ultrapotassic volcanic rocks obtained in Dangreyougcuo-Xurucuo graben range from 11.5 Ma to 14.2 Ma (Zhao and others, 2009). Therefore, we infer that the latest magmatic episode in the study area is about 11 Ma and the Tibetan plateau may have reached its elevation by this time. Neal and Davidson (1989) proposed that the original alnoite magmas formed by decompression melting in a rising diapir of asthenospheric mantle, which could be the tectonic setting of our samples and also of ultrapotassic volcanic rocks in Dangreyougcuo-Xurucuo graben.

Acknowledgments: This research is supported by the National NSF of China (40572048, 40672044, 40830317 and 40873023), the National Key Project for Basic Research on the Tibetan Plateau 2009CB421000, and the Ministry of Science and Technology of the PRC, China Geology Survey Programs (1212010561502, 1212010561501).

References

Neal, C.R. and Davidson, J.P., 1989, An unmetasomatized source of the Malaitan alnoite (Solomon Islands): Petrogenesis involving zone refining, megacryst fractionation, and assimilation of oceanic lithosphere, Geochim. Cosmochim. Acta., 53, 1975-1990.

Rock, N.M.S., 1987, The nature and origin of lamprophyres: An overview. In: Fitton, J.G., and Upton, B.G.J., eds., Alkaline igneous rocks. Geol. Soc. London Spec. Pub. 30, 191-216.

XZBGMR (Xizang Bureau of Geology and Mineral Resources), 2002, Regional geological survey reports of Cuomai and Bangduo (scale 1:250,000).

Zhao, Z., and others, 2009, Geochemical and Sr − Nd − Pb − O isotopic compositions of the post-collisional ultrapotassic magmatism in SW Tibet: Petrogenesis and implications for India intra-continental subduction beneath southern Tibet, Lithos, 113, 190-212, doi:10.1016/j.lithos.2009.02.004

Cite as: Zhou, S., and others, 2010, Post-Collisional Leucite Alnoite in South Tibet and its Significance, *in* Leech, M.L., and others, eds., Proceedings for the 25th Himalaya-Karakoram-Tibet Workshop: U.S. Geological Survey, Open-File Report 2010-1099, 2 p. [http://pubs.usgs.gov/of/2010/1099/szhou/].

Late Triassic Tectonic-Sedimentary Paleogeography of the Northern Qiangtang Basin, Tibet Plateau, Western China

Tongxing Zhu[1], Dong Han[2], Cai Li[3], Xintao Feng[1], Zongliang Li[4], Yuanshan Yu[1], Canhai Jin[1], Banguo Zhou[1]

[1] Chengdu Institute of Geology and Mineral Resources, CGS, Chengdu 610082, Sichuan, China, ztongxing88@yahoo.com.cn
[2] Gansu Geological Survey, Lanzhou 730050, Gansu, China
[3] College of Earth Science, Jilin University, Changchun 130061, Jilin, China
[4]Yunnan Geological Survey,Yuxi 653100,Yunan, China

The late Triassic northern Qiangtang basin in the Tibet Plateau is located between the Lazhulong-Jinshajiang suture zone and the Shuanghu mélange belt. It is an important basin in the northern Qinghai-Tibet Plateau, and belongs to composite foreland basin type according to Jordan's classification of foreland basins. Based on rock-types and fossils, five sedimentary facies-belts or petro-stratigraphic units are recognized from north to south in the basin: a flysch nappe-arc volcanic rock-marble assemblage (the Ruolagangri Group); grey deep-water flysch sedimentary rocks (the Zangxiahe Formation); grey deep-water fine-clastic rocks (the Jieza Group); platform carbonates (the Juhuashang Formation); and deltaic coal-bearing clastic rocks (the Tumenggela Group). In transverse section, there is a wedge of sediments thicker in the north and thinner in the south, with dual provenance: the Ruolagangri thrust belt in the north and the Shuanghu mélange belt in the south. The late Triassic depocenter was located in the middle part of the basin, but subsidence was centered in the northern part of the basin. The foreland basin sedimentation and tectonic evolution are associated with collision of the Lazhulong-Jinshajiang orogenic zone. The basin is a typical symmetric foreland basin between suture belts. This kind of basin geometry allows very thick syn-sedimentary flysch and molasse sediments to be preserved and is related to the thrusts in the suture belt.

The detailed division and correlation of the late Triassic strata not only enriches our knowledge of the late Triassic stratigraphy and paleo-organisms and sedimentary facies, but also has important significance for understanding the sedimentary sequence and palaeogeographic and tectonic evolution of the late Triassic northern Qiangtang Basin.

Cite as: Tongxing, Z., and others, 2010, Late Triassic Tectonic-Sedimentary Paleogeography of the Northern Qiangtan Basin, Tibet Plateau, Western China, *in* Leech, M.L., and others, eds., Proceedings for the 25th Himalaya-Karakoram-Tibet Workshop: U.S. Geological Survey, Open-File Report 2010-1099, 1 p. [http://pubs.usgs.gov/of/2010/1099/zhu/].